



HAL
open science

Rôle de la protéine autophagique ATG9A dans la dynamique des protrusions cellulaires et la migration directionnelle

Daniele Campisi

► **To cite this version:**

Daniele Campisi. Rôle de la protéine autophagique ATG9A dans la dynamique des protrusions cellulaires et la migration directionnelle. Sciences agricoles. Normandie Université, 2021. Français. NNT : 2021NORMR110 . tel-03793819

HAL Id: tel-03793819

<https://theses.hal.science/tel-03793819>

Submitted on 2 Oct 2022

HAL is a multi-disciplinary open access archive for the deposit and dissemination of scientific research documents, whether they are published or not. The documents may come from teaching and research institutions in France or abroad, or from public or private research centers.

L'archive ouverte pluridisciplinaire **HAL**, est destinée au dépôt et à la diffusion de documents scientifiques de niveau recherche, publiés ou non, émanant des établissements d'enseignement et de recherche français ou étrangers, des laboratoires publics ou privés.

THÈSE

Pour obtenir le diplôme de doctorat

Spécialité Aspects Moléculaires et Cellulaires de la Biologie

Préparée au sein de l'Université de Rouen-Normandie

Role of the core autophagy protein ATG9A in the dynamics of cell protrusions and directed migration

Présentée et soutenue par
Daniele CAMPISI

Thèse soutenue publiquement le 01/10/2021
devant le jury composé de

M Philippe Deterre	Directeur de Recherche, Sorbonne Université	Rapporteur
Mme Monique Dontenwill	Directeur de Recherche, Université de Strasbourg	Rapporteur
M Etienne Morel	Directeur de Recherche, Université de Paris	Examineur
Mme Carole Brasse-Lagnel	Maître de conférences-HDR, Université de Rouen-Normandie	Examineur
M Pierrick Gandolfo	Professeur des Universités, Université de Rouen Normandie	Directeur de thèse
M Fabrice Morin	Maître de conférences, Université de Rouen Normandie	Co-Encadrant de thèse

Thèse dirigée par Fabrice Morin et Pierrick Gandolfo. Laboratoire DC2N – INSERM U1239



Remerciements

Le Docteur **Philippe Deterre**, Directeur de Recherche CNRS à la Sorbonne Université, a volontiers accepté de présider ce jury de thèse en tant que rapporteur. C'est un honneur pour moi que le travail présenté dans ce manuscrit soit jugé par un spécialiste des récepteurs chimiotactiques et de leurs voies de signalisation. Je tiens à le remercier chaleureusement pour sa présence.

Le Docteur **Monique Dontenwill**, Directrice de Recherche CNRS à l'Université de Strasbourg, a également accepté avec plaisir de faire partie de ce jury de thèse en tant que rapporteur. C'est un honneur pour moi de voir ma thèse évaluée et jugée par un expert des intégrines et du glioblastome, deux points centraux de mon travail au fil des ans. Pour cela, je la remercie sincèrement.

Le Docteur **Etienne Morel**, Directeur de Recherche Inserm à l'Université de Paris, me fait également l'honneur d'être examinateur dans ce jury. Je tiens particulièrement à le remercier de partager sa vaste expertise sur l'autophagie, qui est un point clé de mon travail. C'est pour cela que je lui en suis très reconnaissant.

Le Docteur **Carole Brasse-Lagnel**, Praticienne Hospitalière et Maître de Conférences à l'Université de Rouen Normandie, elle a également accepté, dans son rôle d'examinatrice de ce travail, d'apporter ses connaissances approfondies sur le processus autophagique et son expérience dans le domaine. Je tiens à lui exprimer ma sincère gratitude.

Je voudrais remercier en suivant mon cœur, l'organe de l'instinct, car il m'a fait rencontrer des personnes qui m'ont donné ou inspiré quelque chose. Ce "quelque chose", ce sont les adjectifs que j'ai associés à presque chacun d'entre eux et que je garderai toujours avec moi. Je voudrais remercier en suivant le temps, car ces 4 ans et demi ont été précieux et vitaux pour ce qu'il sera de moi. Enfin, je voudrais vous remercier en suivant le cerveau, mon cerveau, qui est un peu différent de celui des autres. Il est ma plus grande force et ma plus grande faiblesse en même temps. Mon cerveau qui écoute la moitié des choses, crée deux fois plus et pense mille fois plus.

Au Professeur **Pierrick Gandolfo**, Professeur à l'Université de Rouen Normandie. Je tiens à le remercier profondément pour ses précieux conseils et pour avoir toujours été disponible lorsque j'en avais besoin durant ces années de thèse et car il a été aussi un élément essentiel pendant ma période Erasmus, toujours prêt à m'aider dans les tâches administratives. Je le remercie ainsi parce qu'il a toujours été très compréhensif et pour son esprit toujours positif qui apportait de la joie durant les journées au laboratoire. Pour mon futur, je vais prendre avec moi, sa grande pédagogie et son dévouement à l'enseignement, à la formation et à la recherche.

Je tiens particulièrement à remercier le Docteur **Fabrice Morin**, Maître de Conférences à l'Université de Rouen Normandie ainsi que mon responsable depuis environ 4 ans. Depuis mon arrivée dans l'équipe pendant ma période Erasmus, j'ai admiré sa présence humaine et scientifique constante auprès des étudiants. Dès les premiers jours de mon début avec la thèse, il a été très proche de moi, humainement et scientifiquement, prêt à m'expliquer le projet en profondeur, à me clarifier les doutes, à me poser des questions pour me pousser à apprendre la science. Il a été compréhensif dans les moments difficiles, comme un père, et rigoureux dans les moments de formation. Je le remercie également pour les débats parfois « enflammés » que nous avons eus, qui m'ont quand même beaucoup aidé à voir les choses sous une perspective différente. Je le remercie chaleureusement pour sa présence constante pendant ces 4 ans, parfois « maniacale » (cela m'a aidé à ne pas faire d'erreurs pendant la rédaction de protocoles expérimentaux). Merci pour son énorme disponibilité et son dialogue scientifique de très très haute qualité qui, grâce à ses questions pointues, m'a permis de grandir, de comprendre, de critiquer et surtout de penser scientifiquement. Je le remercie pour tout le temps qu'il a passé à corriger mes résumés, mes discours écrits, notre article, et surtout la thèse, un travail qui a pris beaucoup de temps et dans lequel il m'a vraiment beaucoup aidé. Je le remercie pour toutes les fois où il m'a toujours poussé à produire des choses de ma propre main, sans jamais me donner les choses déjà toutes faites, en m'aidant à me former à l'écriture scientifique. Il a été pour moi un modèle unique, car il m'a appris la rigueur scientifique, technique et expérimentale, indispensable pour avancer dans ce domaine. Si un jour je réussis à atteindre mon objectif, je le lui devrai sûrement. Pour mon futur, je vais prendre avec moi, sa rigueur et sa patience.

Au Docteur **Hélène Castel**, Directrice de Recherche Inserm. La personne qui m'a permis d'être ici aujourd'hui. Bien que notre toute première rencontre n'ait pas été la meilleure, elle a immédiatement compris mon inexpérience et ma volonté de faire. Elle m'a accueilli dans son équipe avec beaucoup d'enthousiasme et m'a encouragé dès les premiers instants et me lancer dans les premières manips; quand j'avais peur de faire une erreur, elle me disait : "Essaie ! Ne t'inquiète pas, si tu fais une erreur, ce n'est pas grave ! nous sommes tous passés par là ». Je n'oublierai jamais la motivation qu'elle me donnait à chaque fois que j'obtenais des résultats intéressants, ce qui me poussait à rester jusqu'à tard dans le laboratoire à produire des dizaines de plaques de qPCR par jour, puis à rentrer chez moi pour analyser immédiatement les résultats obtenus afin que ne puisse ressentir la même énergie le lendemain lorsque je devais lui présenter mes nouveaux résultats. Je lui suis extrêmement reconnaissant, car elle s'est battue pour m'avoir dans son équipe, elle m'a aidé et surtout compris dans les moments difficiles, elle m'a conseillé et écouté comme une mère quand j'en avais besoin. Merci pour sa disponibilité sans limite de temps, toujours prête à m'accueillir dans son bureau même lorsqu'elle avait des dizaines de choses à faire, oubliant tout le reste pour un instant. Je ne peux qu'être infiniment reconnaissant pour tout ce qui m'a été donné, grâce à elle et à sa merveilleuse équipe qu'elle défend et protège si courageusement comme une grande famille. Pour mon futur, je vais prendre avec moi, son courage, sa force et sa ténacité, qui sont, je crois, incalculables dans son cas.

Au Docteur **Laurence Desrues**, Ingénieure de Recherche Inserm. La première personne que j'ai rencontrée dans ce laboratoire, qui m'a accueillie avec un grand sourire et m'a immédiatement mis à l'aise, alors que j'étais vraiment mal à l'aise ! Elle a été notre mère à tous, le cœur de l'équipe, l'enseignante qui nous a appris à utiliser une pipette, à passer les cellules, à trouver les produits alors que la plupart du temps, ils étaient simplement devant nos yeux. Je pense que c'est une des personnes la plus gentille, la plus disponible, positive et aimable que j'ai rencontré dans toute ma vie, qui m'a donné tellement de son temps, grâce à son énorme patience que je ne peux même pas quantifier (surtout devant à mes dizaines de questions par jour, ce qui, multiplié par 4 ans, fait beaucoup !). Les calculs et les techniques qu'elle m'a enseignés, je les garderai toujours avec moi. Dans ces mots, j'espère qu'elle trouvera ma profonde gratitude. Pour mon futur, je vais prendre avec moi, sa disponibilité et sa positivité infinie.

Je ne peux que remercier **Catherine Beau** pour sa gentillesse et sa disponibilité, elle m'a toujours aidé en cas de besoin et a pris en charge des choses que j'aurais pu faire très bien par moi-même. Pour cela, et pour ses sourires, je la remercie chaleureusement. Pour mon futur, je vais prendre avec moi, sa précision et sa solidarité pour les autres.

Je souhaite remercier le Docteur **Martine Dubois** pour son soutien général et durant les procédures d'expérimentation animale, ainsi que ses précieux conseils dans le domaine des statistiques. Bien qu'en apparence elle me semblait être une personne très sérieuse, elle est en fait très drôle!, il faut juste apprendre à la connaître mieux. Pour mon futur, je vais prendre avec moi, sa capacité de travailler en tranquillité et faire ressortir sa sympathie quand on s'y attend le moins.

Docteur **Marie-Christine Tonon**, Directrice de Recherche Inserm, je tiens à la remercier pour ses conseils et son aide au début et tout au long de mon Erasmus. J'ai fait mon premier western blot avec elle et je garde toujours son protocole, avec tendresse. Pour mon futur, je vais prendre avec moi sa sagesse.

Je remercie le Docteur **Youssef Anouar**, Directeur de Recherche Inserm pour m'avoir accueilli dans son unité pendant toutes ces années. Depuis mon Erasmus, il a été toujours si gentil avec moi.

Je voudrais remercier **Loubna**, qui a toujours été très aimable avec moi. Je tiens également à remercier tous les autres chefs et pour leur sympathie. Un merci spécial et sincère à **Maité, Christophe, Delphine, Olivier, Oana, Pascal, Dorthée, Magalie, Celine, Sylvie, Marie, Christine et Isabelle** (Boutelet). Ils ont été si chouette avec moi.

Je dois aussi remercier les jeunes, les jeunes du laboratoire (pas que les autres soient vieux, hein!).

Paul, le « boss », il a été mon enseignant dès le premier instant, il m'a expliqué et enseigné un grand nombre de techniques que je connais aujourd'hui, notamment la qPCR (pendant la période Erasmus) et les transwells, sa plus grande passion. J'ai un respect et une admiration inestimables pour sa capacité à garder son calme dans les

moments les plus difficiles en disant juste «Zut ! » pour retourner immédiatement à la normalité, alors que moi j'aurais crié du fond de mes poumons et risquer un AVC. Je ne pense pas avoir jamais rencontré une personne dotée de telles qualités comme lui. Avec cela, sa grande volonté de travailler dur et avec une énorme précision, il restera toujours un grand exemple pour moi. Pour mon futur, je vais prendre avec moi, sa résilience, son calme et sa capacité d'être un travailleur acharné.

Alex, je l'ai toujours admiré et observé avec l'espoir d'atteindre un jour sa maturité scientifique et sa connaissance théorique des choses. C'est vraiment un garçon spécial et grâce à son aide, j'ai réussi à résoudre tant de mes problèmes au cours de ma thèse. J'ai une profonde admiration pour son intelligence. Pour mon futur, je vais prendre avec moi, sa curiosité pour les choses et sa maturité scientifique.

Renaud, qui a été mon collègue de bureau depuis plusieurs années, prêt chaque matin à me dire « Bonjour » avec un grand sourire. Toujours positif face à des situations très chargées et difficiles sans jamais se décourager. Pour mon futur, je vais prendre avec moi, son courage et bonheur.

Je remercie également les autres membres de l'équipe pour ce qu'ils m'ont donné, **Lucie M. et Lucie P., Emmanuel, Quentin, Martin et Celeste**. Vous êtes des gars avec beaucoup envie de faire et de travailler. Je vous souhaite le meilleur, car vous le méritez. Pour mon futur, je vais prendre avec moi, son intelligence remarquable (Lucie M., merci pour ton aide !!), son organisation incomparable (Lucie P.), sa passion pour l'enseignement (Emmanuel), sa ponctualité (Quentin), l'efficacité dans la production de nombreuses données en très peu de temps (Martin) et son courage d'affronter ses peurs pour les souris (Celeste).

Même s'ils ne sont plus au laboratoire, je tiens à remercier ceux qui sont déjà partis: **Mélanie, Pierre-Michael, Jane, Karima, Julie et Valentina** qui ont fait de mon Erasmus (et le début de ma thèse) une expérience spéciale, qui se sont toujours occupés de moi et qui m'ont fait me sentir chez moi dans une expérience complètement nouvelle pour moi. De vous, je vais prendre avec moi, l'accueil et la folie totale (d'une équipe de jeunes très unis) !!!!

Au milieu de mon expérience dans ce laboratoire, j'ai rencontré d'autres personnes spéciales. **Inès**, mon point de référence dans les moments les plus difficiles (et pas seulement difficile hein !), toujours prête à m'écouter et à me prodiguer des conseils précieux. Elle a été ma valve de sortie qui me permettait de me défouler quand j'en avais besoin, de rire quand nous en avions tous les deux besoin. Je ne sais pas ce que j'aurais fait sans elle. D'elle, je vais prendre avec moi, le savoir écouter, capacité aujourd'hui très rare à trouver, et son remarquable intelligence.

Je remercie **Amine, Michael, Axel et Mouna** pour les moments agréables que nous avons passés ensemble pendant les pauses. De vous, je vais prendre avec moi, la légèreté et l'insouciance. Merci à **Lisa et Fanny**, pour leur aide pendant la période de l'enseignement. Merci à **Lina et Hussein**, qui sont été toujours si sympa et disponible avec moi.

Maria Del Mar, peparacita, elle a joué un rôle déterminant pendant sa permanence au laboratoire. J'ai trouvé en elle une amie formidable, capable d'écouter, d'aider, de s'amuser et de sourire. Elle a été ma source de vie pendant environ deux ans, sans elle il aurait été très difficile pour faire face à certaines situations. Je la remercie pour tout et j'espère que, dans ces mots, elle trouverait la plus profonde estime que je ressens pour elle. D'elle, je vais prendre avec moi sa spontanéité, sa joie et sa volonté de travailler dur.

Jonathan, baby impossible, pour pouvoir lui dire ce qu'il a été et ce qu'il est pour moi, il me faudrait une autre thèse, mais je vais malheureusement devoir résumer. Il a été fondamental dans mon parcours pour de nombreuses raisons. J'ai appris le français grâce à lui, j'ai appris à me connaître grâce à lui et j'ai aussi changé beaucoup de choses de moi que je n'aimais pas, grâce à lui. Je suis maintenant capable de mieux me gérer. Il est l'une des personnes en qui j'ai le plus confiance au monde, car il m'a donné l'occasion d'être une personne fidèle, toujours, et de ne jamais me décevoir. Merci pour son soutien continu pendant ces années, pour son immense aide et disponibilité à la maison pendant des périodes très chargées pour moi, pour les moments d'insouciance qu'il m'a donnés, pour toutes les fois où il m'a compris. Il est un frère spécial pour moi, parce qu'il m'a toujours tout donné,

sans rien demander en retour, ce qui est vraiment rare. De lui, je vais prendre la confiance et l'amour vers les autres.

Merci à **Arièle, Dominique, Grand-mémé, Gwenaelle, Rodrigue, Luna et Paul**. Vous étiez ma famille française. Je vous remercie profondément pour l'amour que vous m'avez manifesté, je vous en serai éternellement reconnaissant. De vous, je vais prendre avec moi l'union et l'accueil.

Merci à **Jimmy, Geoffrey et Meliton** pour leur compagnie sincère et très très chaleureuse. De vous, je vais prendre la spontanéité et l'légèreté.

Je tiens à remercier **Bertrand**, qui a été particulièrement proche de moi au cours de la dernière année de ce parcours. Je le remercie pour sa grande compréhension et de la situation que je vivais. Je le remercie pour ce qu'il m'a donné. Je vais prendre de lui sa grande capacité à maintenir l'ordre et l'organisation.

Merci **Biscuit**, tu m'as apporté tellement de joie depuis que je t'ai adopté, je n'ai jamais fait un meilleur choix. Tu es l'amour de ma vie.

Ringraziamenti

Grazie a **Naomi e Anna**, compagne e amiche di grandi risate, che hanno portato un'ondata di grande freschezza in questo laboratorio e alle mie giornate. È stato davvero bello poter condividere con voi una parte del mio percorso perché mi avete fatto sentire davvero a casa. Di voi porterò con me, la spensieratezza e la libertà.

Grazie a **Mattia**, con la quale ho condiviso una grossa parte del mio percorso. È stata una grande e piacevole compagnia con la quale ho riso, scherzato e con il quale mi sono confrontato. Di lui, mi porterò la sua resilienza, di fronte alle situazioni complesse.

Ringrazio **Giulia**, perché è stata sempre vicina a me, è stata il mio faro nei momenti più duri, la mia consigliera, il mio calmante naturale nei momenti in cui il mio cervello non riusciva più a ragionare. Nonostante la distanza è ancora qui, vicino a me, a sostenermi e a guardarmi con gli occhi di una ragazza solare e splendida. Di lei, mi porterò dietro la fiducia e l'ascolto.

Ringrazio **Maria C.**, perché durante questi 4 anni e mezzo è stata sempre presente, sebbene distante fisicamente. Mi ha ascoltato e consigliato in modo saggio quando ne avevo bisogno. Mi ha fatto ridere tanto ed è stata la valvola di sfogo quando volevo insultare qualcuno, cosa che ha pienamente ricambiato! Nonostante la distanza, anche lei è ancora qua a sostenermi con il suo sorriso. Di lei, mi porterò dietro i consigli e la leggerezza.

Grazie ad **Elena M.** che ha sempre fatto il tifo per me e che ha sempre condiviso i momenti più belli nelle sue storie, ricordandomi i momenti speciali che abbiamo passato assieme. Nonostante la distanza, anche lei è ancora qua a tifare per me con il suo concentrato di energia. Di lei, mi porterò la sincerità.

Grazie a **Calogero** per la sua presenza a distanza e la sua simpatia. Grazie ad **Egzon**, che mi è stato vicino quando ne avevo bisogno e per i momenti di profonda introspezione passati assieme. Grazie a **Valeria R.** con la quale ho mantenuto un bel rapporto a distanza sin dall'Università perché le vere amicizie non scompaiono. Di loro, mi porterò dietro l'umorismo, la riflessione e la simpatia, rispettivamente.

Il mio cuore mi porta alla mia famiglia, la cosa più grande che ho al mondo. Mia **Mamma**, mio **Papà**, **Luisa**, **Dalila** e i miei **Nonni** che sono la mia linfa vitale. Vi dedico completamente questo nuovo traguardo della mia vita perché senza di voi non ce l'avrei fatta. Luisa, mia sorella, la mia gemella diversa con la quale non serve molto parlare per capirsi. In particolare, Mamma e Papà, durante questi 4 anni siete stati la mia forza, il mio coraggio, il mio sostegno continuo senza mai mancare, mi avete sostenuto giorno dopo giorno e spinto a non mollare mai. Questa giornata non è solo mia, ma è anche la Vostra e ve ne sarò per sempre grato. Grazie dal profondo del mio cuore.

Summary

ABSTRACT	18
RESUMÉ	21
LIST OF FIGURES.....	24
LIST OF ABBREVIATIONS.....	28
CHAPTER I: CELL MIGRATION	33
1. Directional migration and cell polarization.....	33
1.1. Chemotactic migration	34
1.2. Cell polarization	34
2. Membrane protrusions and actin cytoskeleton.....	38
2.1. Lamellipodia.....	40
2.1.1. Mechanisms of lamellipodia formation and actin regulators	41
2.1.2. Rho GTPases and lamellipodium formation	44
2.2. Filopodia	44
2.2.1. Mechanisms of filopodia formation and actin regulators	44
2.2.2. Rho GTPases and filopodia formation	46
2.3. Formation of filopodia <i>versus</i> lamellipodia: the regulatory roles of Arp2/3 and profilin-1 ..	46
3. Cell adhesions	47
3.1. Extracellular matrix components	47
3.2. Different types of adhesions.....	49
3.2.1. Mechanisms of adhesions assembly	50
3.2.2. Maturation of adhesions	51
3.2.3. Mechanisms of adhesions disassembly.....	53
3.3. Endocytosis of integrins.....	55
3.4. Intracellular trafficking and recycling of integrins	57
4. Exocytosis and cell migration.....	59
4.1. Molecular mechanism of exocytosis: focus on SNARE proteins	60
4.2. Polarized exocytosis: Full-collapse fusion and Kiss-and-Run	62
5. Receptors-induced chemotactic migration.....	63
5.1. Receptor Tyrosine Kinases: focus on EGFR.....	63
5.2. G proteins-coupled receptors.....	66
5.2.1. C-X-C chemokine receptor type 4 (CXCR4).....	66

CHAPTER II: AUTOPHAGY	70
6. Generalities and historical overview.....	70
7. Different forms of autophagy	71
7.1. Microautophagy	71
7.2. Chaperone-mediated autophagy.....	72
7.3. Macroautophagy	75
8. Molecular mechanisms of the autophagic machinery.....	75
8.1. Initiation of autophagy	76
8.1.1. The Atg1/ULK complex: an initiator of autophagosome formation	77
8.1.2. Class III PI3K: a PI3P source at the initiation site	78
8.1.3. mTORC1 and AMPK: energy sentinels regulating autophagy initiation	80
8.2. Nucleation and elongation of the phagophore.....	80
8.2.1. Formation of ATG12-ATG5-ATG16L1.....	83
8.2.2. The LC3-PE conjugation system: synthesis of LC3-PE on the nascent autophagosome	83
8.2.3. Autophagosome closure.....	86
8.3. Maturation of autophagosomes and fusion with lysosomes.....	86
8.4. Different membrane sources for phagophore elongation.....	88
9. The core autophagy protein ATG9A	91
9.1. Topology and structural function of ATG9A	91
9.2. Biogenesis of ATG9A vesicles and their trafficking to the phagophore	93
9.2.1. ATG9A-positive vesicles emanating from different sources contribute to autophagosome biogenesis	93
9.2.2. ATG9A trafficking via AP complexes.....	93
9.2.3. ATG9A trafficking via BAR-domain proteins.....	95
9.2.4. Yeast Atg9, the central hub for the recruitment of the autophagic machinery	96
10. Signaling pathways regulating the autophagy machinery	99
10.1. Regulation by amino acids	99
10.2. Regulation by growth factors.....	100
10.3. Regulation by hypoxia.....	101
11. Other normal and pathophysiological roles of autophagy	102
11.1. Cellular homeostasis and quality control.....	102
11.2. Function in secretion and exocytosis (<i>ATG gene-dependent secretion</i>)	103
12. Autophagy and cancer.....	105
12.1. Anti-tumoral role of autophagy	105
12.2. Pro-tumoral role of autophagy	106
12.3. Autophagy modulation as a therapeutic cancer target	106
13. Autophagy and cell migration	107
13.1. Pro-migratory effects of autophagy.....	107

13.2. Anti-migratory effects of autophagy.....	108
13.3. Autophagy and epithelial-to-mesenchymal transition	109
AIM OF THE THESIS	113
RESULTS	114
PART I: THE CORE AUTOPHAGY PROTEIN ATG9A CONTROLS DYNAMICS OF CELL PROTRUSIONS AND DIRECTED MIGRATION	114
I. Abstract.....	116
II. Introduction	116
III. Results	118
III.1. Chemotactic migration depends on ATG9A protein	118
III.2. Depletion of ATG9A protein alters the formation of F-actin rich lamellipodia driving efficient cell migration	119
III.3. ATG9A-positive vesicles concentrate in F-actin rich protrusions and display anterograde trafficking toward the leading edge.....	120
III.4. Design and validation of ATG9A-pHluorin as a new probe to visualize ATG9A exocytosis	120
III.5. Exocytosis of ATG9A-positive vesicles is highly polarized toward the leading edge.....	122
III.6. Peripheral ATG9A-pHluorin signal correlates with protrusive activity.....	122
III.7. ATG9A regulates delivery of TGN46 and β 1 integrin to the leading edge through its N-terminal adaptor protein (AP) sorting signal	123
III.8. ATG9A protein controls the dynamics of adhesion complexes	124
IV. Discussion	125
V. Materials and Methods.....	128
V.1. Reagents and chemicals.....	128
V.2. Plasmid constructs and short interfering RNAs (siRNAs)	128
V.3. Cell culture and transfections	129
V.4. Reverse transcription quantitative polymerase chain reaction (RT-qPCR)	130
V.5. SDS-PAGE and Western blot	130
V.6. Autophagosome biogenesis.....	131
V.7. Migration assay.....	131
V.8. Immunocytochemistry and image analysis.....	131
V.9. Live-cell imaging	132
V.10. Statistical analysis	133

VI. Author's contributions.....	133
VII. Acknowledgments	133
VIII. Disclosure statement.....	134
IX. Main and supplementary figures.....	135
X. References	155

PART II: INTERACTION OF ATG9A WITH THE ACTIN-BINDING PROTEIN PROFILIN-1. POTENTIAL INVOLVEMENT IN ACTIN POLYMERIZATION OF THE CELL LEADING EDGE..... 166

I. Introduction	166
II. Materials and Methods.....	166
II.1. Reagents and chemicals.....	166
II.2. Test of protein-protein interactions in the yeast two-hybrid system.....	167
II.2.1. Yeast strains, culture media and co-transformation procedures.....	167
II.2.2. Plasmids and site-directed mutagenesis	167
II.2.3. Yeast two-hybrid assay and co-transformation procedures	167
II.3. Plasmid constructs and short interfering RNAs (siRNAs)	169
II.4. Cell cultures and transfections	169
II.5. Immunocytochemistry and image analysis.....	169
II.6. Live-cell imaging	170
III. Results	170
III.1. ATG9A interacts with profilin-1 through its C-terminal domain	170
III.2. ATG9A colocalizes with and promotes proper localization of profilin-1 at the migration front.....	172
IV. Discussion.....	173

GENERAL DISCUSSION AND PERSPECTIVES 179

14. Role of ATG9A in "Golgi-to-plasma membrane" trafficking during cell migration....	179
15. ATG9A protein: a master regulator of vesicle biogenesis from the TGN?.....	181
15.1. Interaction of ATG9A with the AP complexes.....	181
15.2. Interaction of ATG9A with the PI4KIII β	181
15.3. Trafficking of ATG9A-positive vesicles toward the migration front: role of microtubules.	183

Summary

16. ATG9A and cancer cell invasion..... 185

BIBLIOGRAPHICAL REFERENCES 189

SUPPLEMENTARY PUBLICATION..... 235

EUROPEAN
CURRICULUM
VITAE



PERSONAL
INFORMATIONS

Name **Daniele CAMPISI**
Personal Address 34, Rue du Lieu de Santé, 76000, Rouen (France)
Telephone +33 767297221
E-mail Job: daniele.campisi1@univ-rouen.fr Personal: daniele.campisi3@gmail.com
Nationality Italian
Date of birth 10/01/1992
Social Networks www.linkedin.com/in/daniele-campisi - Twitter: [@daniele_campisi](https://twitter.com/daniele_campisi)

WORK
EXPERIENCE

09/2020 – Present

Temporary Lecturer and Research Assistant (ATER)

Degree Course in Biology. University of Rouen-Normandy
INSERM U1239, Team: Astrocyte and Vascular Niche. Mont Saint Aignan (France)
Teaching: Seminars in **Animal Physiology** (SNA and heart control, L2, 52h) and **Introduction to Cell Biology** (L1, 26h).
Practical work in **Histology** (Muscle tissues, L1, 28h).

09/2017 – Present

PhD in Cellular and Molecular Biology

University of Rouen-Normandy
INSERM U1239, Team: Astrocyte and Vascular Niche. Mont Saint Aignan (France)
PI: Dr. Fabrice Morin
Project: Impact of autophagy in glioma chemotactic migration
Teaching ("Mission d'enseignement"): Practical work in **Histology** (Muscle tissues, L1, 32h).

03/2017 – 07/2017

ERASMUS TRAINEESHIP, POST-GRADUATE INTERNSHIP

University of Rouen-Normandy
INSERM U1239, Team: Astrocyte and Vascular Niche. Mont Saint Aignan (France)
PI: Dr. Helene Castel
Project: GPCRs and mesenchymal phenotype in high-grade glioma

15-17/09/2017

MASTERCLASS IN NEURO-ONCOLOGY, CHALLENGES IN RADIOTHERAPY FOR PATIENTS WITH GLIOMAS

European School of Oncology (ESO) and European Association of Neuro-Oncology (EANO)
Lugano, Switzerland

02/2016 – 07/2016

ERASMUS+, MASTER INTERNSHIP FOR EXPERIMENTAL THESIS

University of Rouen-Normandy
INSERM U1239, Team: Astrocyte and Vascular Niche. Mont Saint Aignan (France)
PI: Dr. Helene Castel
Project: GPCRs and mesenchymal phenotype in high-grade glioma

11/2015 – 01/2016

BACHELOR AND MASTER TRAINING

University of Turin
Neuroscience Institute Cavalieri Ottolenghi (NICO), Italy
PIs: Prof. Annalisa Buffo, Prof. Enrica Boda and Prof. Giancarlo Panzica

EDUCATION

09/2014 – 04/2017

MASTER DEGREE IN CELLULAR AND MOLECULAR BIOLOGY (SPECIALIZATION IN NEUROBIOLOGY)

University of Turin, (Turin, Italy)

Dissertation thesis's title: GPCRs and mesenchymal phenotype in high-grade gliomas

Pls: Dr. Helene Castel and Prof. Silvia De Marchis

Final Grade: **108/110**

09/2011 – 07/2014

BACHELOR DEGREE IN BIOLOGICAL SCIENCES (SPECIALIZATION IN MOLECULAR BIOLOGY)

University of Turin, Via Accademia Albertina 13 (Turin)

Dissertation Thesis's Title: Interhemispheric disconnection syndrome: Split brain in patients and murin models

Thesis Supervisors: Prof. Annalisa Buffo and Prof. Silvia De Marchis

Final Grade: **102/110**

10/2005 – 07/2011

SCIENTIFIC-TECHNOLOGICAL HIGH SCHOOL DEGREE

Michelangelo Bartolo Institute, Pachino (Syracuse, Sicily), Italy. Final Grade: **90/100**

PERSONAL SKILLS

MOTHER TONGUE

ITALIAN

OTHER LANGUAGES

ENGLISH - PROFESSIONAL

FRENCH - PROFESSIONAL

ORGANIZATIONAL SKILLS

03/2012 – 09/2016

STUDENT REPRESENTATIVES in

- Biological Science (Bsc) **Council at University of Turin**
- Cellular and Molecular Biology (Master) **Council at University of Turin**
- Department of Life Sciences and System Biology **Council at University of Turin**

As a Student Representatives my duties were to deal with students' problems, propose actions aimed to solve problems (e.g. modifications of the Academic rules) and promote the active student's participation during University daily life.

- Take part in Coordinamento Operativo di Supporto all'Accreditamento (C.O.S.A.) for annual accreditation of University of Turin by ANVUR (Agenzia Nazionale di Valutazione del Sistema Universitario e della Ricerca).
- Take part in Re-examination committee, Consultative parithetic committee (Bachelor and Master)
- Part of the project "Why study Biological Science?" concerning videos created to orient incoming students.
- Part of "Orient@mente" project with the aim to orient incoming students.
- Part of "Erasmus – Archivio Digitale" project to orient Erasmus incoming and outgoing students.
- Organization of "meeting students" to collect information about the classes to improve the quality.
- Part of "JobDay" organization, dedicated to graduated students.
- Tutor for new incoming students from Bachelor program to Master Program of University of Turin.
- Active member of different social network groups (facebook) to help and guide students with their doubts and difficulties.

TECHNICAL AND LAB SKILLS

CELL BIOLOGY

Human Cell cultures, Immunofluorescence, Cell transfection, Cell migration assay (Transwells and Ibidi), Bacterial protein expression, Mammalian cell protein expression, Protein-protein interaction: Yeast Two Hybrid Assay, Co-Immunoprecipitation, Biomolecular Fluorescence Complementation (BiFC).

MOLECULAR BIOLOGY

Development of recombinant plasmids, Plasmid preparation, Protein extraction/purification, SDS-PAGE, Western Blot, DNA and RNA extraction/purification, Primers design, RT-qPCR, RNA interference (siRNAs).

IMAGING

Confocal microscopy, Videomicroscopy, TIRF microscopy, Thunder microscopy, Conventional microscopy

INFORMATIC

ImageJ, Fiji, QuantStudio (Real-time PCR data analysis), BLAST, Primer-Blast, Primer Bank, ImageLab, GraphPad Prism, Adobe Premiere and Photoshop, Microsoft Office (Word, Excel and PowerPoint), Leica Las X.

FORMATIONS
01/2020

University Degree in “Applicateur de procédures expérimentales chez les rongeurs” (ex Niveau 2, corresponding to **FELASA function B**) – 45h, Mont Saint Aignan, France

10/2019

Image Analysis with ImageJ (Level 1) – 3 days (organized by PRIMACEN Platform a Mont Saint Aignan, France)

ORAL COMM. AND
POSTER

Oral Communications

- Campisi D., Coly PM., Castel H., Gandolfo P. and Morin F.: GPCR-induced repression of autophagy in glioblastoma cells: impact on lamellipodium expansion and chemotactic migration. 22th LARC NEUROSCIENCE, October 19th, 2018. Rouen. (**Award for the best oral communication**)
- Campisi D., Coly PM., Laurence D., Castel H., Gandolfo P. and Morin F.: GPCR-induced repression of autophagy in glioblastoma cells: critical role on chemotactic migration. 21th Journées de l'Ecole Doctorale Normande Biologie Intégrative, Santé, Environnement, March 21-22, 2019. Caen.
- Campisi D., Coly PM., Laurence D., Castel H., Gandolfo P. and Morin F.: GPCR-induced repression of autophagy in glioblastoma cells: critical role on chemotactic migration. CANCERPOLE NORD-OUEST, May 15-16-17, 2019. Deauville. (**Award for the best oral communication**)

Posters

- Campisi D., Guichet P.O., Dembele K.P., Mutel A., Desrues L., Ferracci F.X., Langlois O., Laquerrière A., Marguet F., Gandolfo P., Morin F. and Castel H.: Chemokine G protein-coupled receptors and mesenchymal phenotype in high-grade gliomas. 21th LARC NEUROSCIENCE, October 13th, 2017. Lille. (**Award for the best poster**).
- Campisi D., Coly PM., Castel H., Gandolfo P. and Morin F.: GPCR-induced repression of autophagy in glioblastoma cells: impact on lamellipodium expansion and chemotactic migration. 21th Journée de l'Ecole Doctorale Normande Biologie Intégrative, Santé, Environnement, March 22-23, 2018. Rouen.
- Campisi D., Coly PM., Castel H., Gandolfo P. and Morin F.: GPCR-induced repression of autophagy in glioblastoma cells: impact on lamellipodium expansion and chemotactic migration. CANCERPOLE NORD-OUEST, May 23-24-25, 2018. Deauville. (**Award for the best poster**).
- Campisi D., Coly PM., Castel H., Gandolfo P. and Morin F.: GPCR-induced repression of autophagy in glioblastoma cells: impact on lamellipodium expansion and chemotactic migration. Journée Normande de Recherche Biomédicale, September 20th, 2018. Rouen.
- Campisi D., Coly PM., Castel H., Gandolfo P. and Morin F.: GPCR-induced repression of autophagy in glioblastoma cells: impact on lamellipodium expansion and chemotactic migration. GDR3545, GPCR-PHYSIO-MED, October 29-31, 2018. Strasbourg.
- Campisi D., Coly PM., Desrues L., Castel H., Gandolfo P. and Morin F.: Endosomal recycling driving glioblastoma cell invasion depends on the core autophagy protein ATG9A. Journée Normande de Recherche Biomédicale, Novembre 19th, 2019. Caen.

OTHER AWARDS

- 2017 Scholarship by UNITO - “Erasmus Traineeship 2017” - University of Rouen (France)
- 2016 Scholarship by UNITO - “Erasmus – Archivio digitale” project (School of Science of Nature)
- 2016 Scholarship by UNITO - “Orient@mente” project (Depart. Life Science and System Biology)
- 2015 Scholarship by EDISU PIEMONTE - “Erasmus+ per Studio” University of Rouen (France)
- 2015 Scholarship by UNITO for “Erasmus+ per Studio” at the University of Rouen (France)
- 2015 Degree award fellowship by EDISU PIEMONTE
- 2014 Degree award fellowship by Cooperative Credit Bank of Pachino
- 2013 Scholarship by TRIESTE NEXT, Next WaterWise 2nd Edition
- 2012-17 Six Scholarships (one per year) by EDISU PIEMONTE

PUBLICATIONS

Campisi D., Laurence D., Gandolfo P., Castel H., and Morin F.: The core autophagy protein ATG9A controls dynamics of cell protrusions and directed migration. Under revision.

Le Joncour V., Guichet P.O., Dembele K.P., Mutel A., **Campisi D.**, Perzo N., Desrues L., Modzelevski R., Couraud P.O., Honnorat J., Ferracci F.X., Marguet F., Laquerrière A., Véra P., Bohn P., Langlois O., Morin F., Gandolfo P. and Castel H.: Targeting the uterotensin II/UT G protein-coupled receptor to counteract angiogenesis and mesenchymal hypoxia/necrosis in glioblastoma, 2021, *Frontiers in Cell and Developmental Biology* (IF 5.2) doi: 10.3389/fcell.2021.652544

ABSTRACT

Chemotactic migration is a fundamental cellular process generated by a concentration gradient of a specific mediator that allows cells to orient their movement in the surrounding space. Chemotactic migration represents a universal mechanism that affects several areas of study, such as embryogenesis, tissue regeneration, tissue repair following injury, inflammatory response, and cancer. This process is tightly regulated by the coordinated flux of lipids and cargo proteins to the migration front that allows the cell to develop cellular protrusions, such as lamellipodia and filopodia, to optimize their migration. The trafficking of lipids and proteins fluxes in the cell are also important for another fundamental mechanism, autophagy. Autophagy is a catabolic process in which various cellular components, proteins and organelles, are directed to the lysosomal compartment to be degraded. This process begins with the sequestration of cytoplasmic components in a double membrane structure called the phagophore. The closure of the phagophore gives rise to the autophagosome, which fuses to the lysosome to complete the degradation of its contents. It has now been widely accepted that autophagy is involved in cell migration, with the degradation of adhesion proteins (integrins and paxillin) or GTPases (RhoA and Src).

Vesicular trafficking is essential in both autophagy and cell migration and therefore must be finely regulated. In autophagy, many ATG proteins that play an essential role have been identified. These include ATG9A, the only transmembrane protein that cycles between the Golgi apparatus, the plasma membrane and the recycling compartment during autophagy induction. Extensive studies have demonstrated the critical role of ATG9A protein in autophagosome formation, proposedly by functioning in vesicular delivery to the phagophore initiation site, and by translocating lipids from the outer to the inner leaflet of the phagophore membrane in order to enable its expansion. In addition to this well-recognized function of ATG9A in phagophore expansion, recent studies point to the fact that it may have a wider role than anticipated and could be a general regulator of vesicular trafficking.

Based on these data, the objectives of my thesis work were *i)* to evaluate the role of ATG9A in chemotactic migration and *ii)* to study its role in the vesicular trafficking that supports the formation of cellular protrusions and adhesions to the extracellular matrix and *iii)* to evaluate if mammalian ATG9A may potentially control actin polymerization at the leading edge, by interacting with major actin regulators (profilin-1, Mena, VASP, Evl). To do so, we used the HeLa and HEK-293 cell lines and the highly invasive human glioblastoma cell lines U87 MG and 42 MG.

We first tested the role of the ATG9A protein in chemotactic migration induced by EGF, ligand of EGFR, and CXCL12, ligand of CXCR4, using the transwell assay in HeLa, HEK293, U87 MG, and 42 MG cell lines. We found that downregulation of ATG9A by siRNAs strongly decreased or abolished EGF- and CXCL12-induced chemotactic migration in the different cell lines. Because lamellipodia are the main structures mediating cell

Abstract

migration, we examined the impact of ATG9A deletion on the morphology of protrusions in U87 MG cells. Cells transfected with a control siRNA developed prominent lamellipodia, revealed by F-actin staining. In contrast, ATG9A-depleted cells exhibited abnormal protrusions. We then focused on the dynamics of these protrusions using time-lapse microscopy and found that ATG9A-depleted cells exhibited protrusions with normal velocity, but reduced distance and persistence. In order to test whether ATG9A can reach the plasma membrane, we next analyzed the localization of endogenous ATG9A and found that a fraction of ATG9A-positive vesicles localized in F-actin-labelled lamellipodia. EGF treatment induced an increase in the amount of endogenous ATG9A at the plasma membrane, as well as an increase in its co-localization with F-actin. To understand how ATG9A-positive vesicles are transported to the leading edge, we overexpressed ATG9A-mCherry in U87 MG cells and observed the movement of these vesicles by using live-cell TIRF microscopy. By tracking analyses, we found that about 80% of the ATG9A-positive vesicles located in protrusions were directed toward the migration front.

This led us to analyze whether these vesicles could perform exocytosis at the plasma membrane. For this, we created a construct encoding ATG9A, fused to the highly pH-sensitive GFP variant super-ecliptic pHluorin. The fluorescence of pHluorin is quenched at the acidic endosomal pH, but upon fusion with the plasma membrane, low luminal pH is immediately neutralized, resulting in a sudden increase in fluorescence intensity. We observed that ATG9A-pHluorin exocytosis was highly polarized toward the migration front in cells that exhibited an antero-posterior axis. In contrast, exocytosis was observed all over the cell surface of non-polarized cells. Furthermore, chemotactic stimulation of U87 MG cells with EGF increased the exocytosis frequency of ATG9A-pHluorin vesicles.

Delivery of cargo proteins, such as integrins, from the Golgi apparatus to the plasma membrane is critical for directional cell migration. We then performed co-localization experiments and found that ATG9A-mCherry partially co-localized with the *trans*-Golgi marker TGN46 and β 1 integrin in the perinuclear area and in puncta dispersed throughout the cytosol or near the cell membrane, likely representing *bona fide* post-Golgi carriers. Importantly, we found that depletion of ATG9A using siRNAs strongly inhibited EGF-induced redistribution of TGN46 and β 1 integrin toward cell protrusions, suggesting that ATG9A might be a constitutive component of vesicular trafficking from the Golgi apparatus.

ATG9A trafficking from the *trans*-Golgi has been shown to be tightly controlled by clathrin adaptor complexes, through a canonical AP sorting signal (⁸YXX Φ D/E¹²) located in its N-terminal domain. We demonstrated that, in cells depleted of endogenous ATG9A, overexpression of wild-type recombinant ATG9A-mCherry efficiently rescued EGF-induced delivery of TGN46 and β 1 integrin to the leading edge. A the contrary, a mutant form of ATG9A-mCherry, in which Tyrosine 8 of the AP sorting signal was replaced by a Phenylalanine, did not rescue TGN46 and β 1 integrin trafficking to the cell periphery. Based on the essential role of β 1 integrin in the formation/maturation of adhesion complexes, we next tested the impact of ATG9A protein on the

Abstract

formation and turnover of adhesion complexes, in cells expressing paxillin-eGFP. We demonstrated that depletion of ATG9A induced a marked reduction in the number of both assembling and disassembling adhesions. Finally, overexpression of ATG9A-pHluorin led us to observe that exocytosis occurred in close proximity of paxillin-containing adhesions, with an obvious clustering.

Altogether, data obtained in the first part of my thesis uncover a new function of ATG9A protein and indicate that ATG9A-positive vesicles originating from the Golgi apparatus are mobilized during chemotactic migration to facilitate the expansion of the lamellipodium and its anchorage to the extracellular matrix.

The second part of my thesis work was focused on the investigation of the ATG9A role in the actin polymerization at the leading edge, by studying possible molecular actin partners interacting with ATG9A. It has been recently shown that *Drosophila* Atg9 was able to interact with the well-known actin regulator Ena and profilin. This prompted us to investigate whether human ATG9A, similar to the *Drosophila* homolog, has the capacity to interact with Ena/VASP family members and/or profilin. Binary interactions, evaluated in the yeast two-hybrid system, allowed us to demonstrate that the C-terminal domain of ATG9A specifically interacts with profilin-1. By using site-directed mutagenesis, we further demonstrated that this interaction was partially mediated by several proline clusters located in the C-terminal domain of ATG9A. Interaction between ATG9A and profilin-1 suggested that these proteins function together in the regulation of the lamellipodial actin cytoskeleton. In support of this hypothesis, we found that ATG9A-myc and endogenous profilin-1 strongly colocalized at the migration front of U87 MG cells and that downregulation of ATG9A, by siRNAs or overexpression of the C-terminus of ATG9A (as a dominant negative), blocked the EGF-induced transport of profilin-1 to the cell periphery.

Collectively, data from the second part of my thesis suggest that regulation of the lamellipodial actin cytoskeleton constitutes another function of the transmembrane protein ATG9A. How the different interactions and regulatory functions of ATG9A are coordinated in migrating cells remains to be established.

RESUMÉ

La migration chimiotactique est un processus cellulaire fondamental généré par un gradient de concentration d'un médiateur spécifique, permettant aux cellules d'orienter leur mouvement dans l'espace environnant. Elle représente un mécanisme universel qui régule de nombreux processus physiologiques et physiopathologiques, tels que l'embryogenèse, la régénération des tissus, la réponse inflammatoire et le cancer. Ce processus est étroitement régulé par le flux coordonné de lipides et de protéines cargo vers le front de migration, permettant à la cellule de développer des protrusions cellulaires, telles que les lamellipodes et les filopodes.

De façon intéressante, le trafic intracellulaire des lipides et de protéines est également essentiel à un autre mécanisme fondamental, l'autophagie. L'autophagie est un processus catabolique par lequel certains composants cellulaires, protéines et organites, sont dirigés vers le compartiment lysosomal, afin d'y être dégradés. Ce processus débute par la séquestration de constituants cytoplasmiques par une structure précurseur appelée phagophore. La fermeture du phagophore donne naissance à une vésicule à double membrane nommée autophagosome, qui fusionne avec les lysosomes, conduisant à la dégradation du contenu de sa lumière. Alors que la plupart des protéines participant à la formation de l'autophagosome sont cytosoliques, la protéine ATG9A possède plusieurs domaines transmembranaires, et représente ainsi la seule protéine autophagique intégrée aux membranes cellulaires. Lors de l'induction de l'autophagie, les vésicules ATG9A-positives, émanant essentiellement du réseau *trans*-Golgien, sont alors dirigées vers le phagophore afin d'y apporter les protéines et phospholipides nécessaires à son expansion. En plus de cette fonction bien caractérisée de l'ATG9A, des études récentes indiquent qu'elle pourrait exercer un rôle bien plus étendu, en tant que régulateur intrinsèque du trafic vésiculaire. L'ensemble de ces informations nous ont conduits à émettre l'hypothèse selon laquelle la protéine ATG9A, en participant à la biogenèse des vésicules post-Golgiennes, pourrait jouer un rôle majeur dans l'expansion des lamellipodes et l'activité migratoire.

Les objectifs de mes travaux de thèse étaient donc d'évaluer, au sein de différentes lignées cellulaires, le rôle de la protéine ATG9A sur :

i) la migration chimiotactique, ainsi que le trafic vésiculaire sous-tendant la formation des protrusions cellulaires et leur ancrage à la matrice extracellulaire,

ii) la polymérisation de l'actine, au front de migration cellulaire.

Rôle de la protéine ATG9A sur la dynamique des protrusions cellulaires et la migration chimiotactique

Par une analyse en chambre de *Boyden* et l'utilisation d'ARN interférents, nous avons dans un premier temps démontré que la déplétion des pools de protéines ATG9A au sein de cellules de glioblastome humain (U87 MG et 42 MG), de cellules HeLa et de cellules HEK 293 abolit ou réduit fortement leur migration

Resumé

chimiotactique induite par l'EGF (ligand de l'EGFR) ou le CXCL12 (ligand du CXCR4). En accord avec le rôle déterminant des lamellipodes au cours de la migration cellulaire, nous démontrons par une analyse en microscopie *Time-Lapse* que la déplétion des pools d'ATG9A conduit à la formation de lamellipodes anormaux, dont la durée de la phase d'expansion ainsi que l'amplitude d'expansion sont altérées. De plus, une analyse des trajectoires cellulaires (*Cell Tracking*) indique que les cellules déplétées de l'ATG9A présentent une vitesse de migration réduite.

Par un immuno-marquage de l'ATG9A endogène, nous démontrons qu'une fraction de l'ATG9A est localisée dans les lamellipodes (co-marquage F-actine), à la membrane plasmique ou au sein de vésicules localisées sous la membrane plasmique. La stimulation chimiotactique des cellules par l'EGF augmente de façon significative l'intensité de l'immuno-marquage dans les protrusions cellulaires. La transfection des cellules par un construit permettant l'expression de la protéine de fusion ATG9A-mCherry nous a permis de constater que la plupart des vésicules ATG9A-positives localisées dans les protrusions cellulaires présentaient un trafic antérograde. Afin d'évaluer si les vésicules ATG9A s'orientant vers le front de migration fusionnent finalement avec la membrane plasmique, nous avons produit un construit permettant l'expression de la protéine ATG9A fusionnée à la pHluorine, un variant pH-sensible de la *Green Fluorescent Protein*. L'exocytose des vésicules ATG9A-positives est alors révélée par l'apparition de spots fluorescents suite à l'exposition de la pHluorine au pH neutre du milieu extracellulaire lors de l'ouverture du pore de fusion. L'analyse en microscopie TIRF (*Total Internal Reflection Fluorescence*) de cellules U87 MG ou HeLa transfectées avec ce construit indique que l'exocytose des vésicules ATG9A-positives est fortement polarisée et intense au front de migration. La stimulation chimiotactique des cellules par l'EGF augmente de manière significative le nombre d'évènements d'exocytose.

Des données récentes de la littérature ont permis de révéler un rôle essentiel du trafic polarisé de l'intégrine $\beta 1$, de l'appareil de Golgi vers la membrane plasmique, au cours de la migration cellulaire directionnelle. Dans ce contexte, nous avons constaté que la protéine de fusion ATG9A-mCherry co-localise partiellement avec le marqueur *trans*-Golgien TGN46 ainsi qu'avec l'intégrine $\beta 1$, dans la zone périnucléaire mais également au sein de vésicules périphériques localisées à proximité du front de migration. Par l'expression de formes mutées de l'ATG9A au sein de cellules U87 déplétées de l'ATG9A endogène, nous avons démontré que *i*) l'ATG9A est essentielle au transport de l'intégrine $\beta 1$ et du TGN46 au front de migration et que *ii*) cet effet de l'ATG9A est dépendant de sa capacité d'interagir avec les complexes adaptateurs de la clathrine (complexes AP). En accord avec un rôle essentiel de l'intégrine $\beta 1$ au cours de formation/maturation des complexes d'adhésion, nous démontrons finalement par microscopie *Time-Lapse* qu'une déplétion de l'ATG9A réduit fortement les activités d'assemblage et de désassemblage des complexes d'adhésion (marquage Paxilline-eGFP), et que la plupart des évènements d'exocytose des vésicules ATG9A-positives se situent à proximité de ces complexes d'adhésion.

Resumé

L'ensemble des résultats obtenus au cours du premier volet de ma thèse permettent de mettre en lumière une nouvelle fonction de la protéine ATG9A et indiquent que les vésicules ATG9A-positives en provenance de l'appareil de Golgi sont mobilisées au cours de la migration chimiotactique afin de faciliter l'expansion du lamellipode et son ancrage à la matrice extracellulaire.

Rôle potentiel de la protéine ATG9A au cours de la polymérisation de l'actine au front de migration

Le second objectif de ma thèse s'appuie sur une étude récente, ayant permis de mettre en évidence une fonction non-autophagique de la protéine Atg9 de Drosophile. Ces travaux ont en effet démontré que l'Atg9 de Drosophile est capable d'interagir avec deux protéines participant à la polymérisation de l'actine, Enabled (Ena) et Profiline. La déplétion de l'Atg9 bloque la localisation normale d'Ena et de la Profiline à la membrane plasmique, altérant ainsi le réseau cortical d'actine. Ces données de la littérature sont particulièrement pertinentes dans le cadre de mon travail de thèse puisque les protéines Mena, Vasp et Evl de vertébrés, homologues de la protéine Ena de Drosophile, ainsi que la profiline-1, constituent des acteurs essentiels à la machinerie de polymérisation de l'actine dendritique au sein du lamellipode.

Par l'utilisation du système double-hybride chez la levure, nous avons donc évalué la capacité de l'ATG9A humaine à interagir avec chacune de ces protéines. Nous démontrons ainsi qu'aucun des domaines cytosoliques de l'ATG9A n'est capable d'interagir avec les protéines Mena, Vasp et Evl. En revanche, cette stratégie nous a permis de mettre en évidence une interaction spécifique entre le domaine cytosolique C-terminal de l'ATG9A et la protéine profiline-1. La mutagenèse dirigée des vecteurs de double-hybride nous a permis de préciser que cette interaction est en partie relayée par des « clusters » de résidus proline localisés dans le domaine C-terminal de l'ATG9A.

En parallèle à ces résultats obtenus par la technique de double-hybride, des expériences réalisées sur des cellules U87 MG nous ont permis de démontrer que l'ATG9A et la profiline-1 présentent une forte co-localisation au niveau du front de migration cellulaire. La déplétion de l'ATG9A, par l'utilisation d'ARN interférents, ou la surexpression du domaine C-terminal de l'ATG9A (dominant-négatif), bloquent la redistribution EGF-dépendante de la profiline-1 vers les protrusions cellulaires.

De façon collective, les données obtenues au cours du second volet de ma thèse suggèrent que l'ATG9A participe également au transport dirigé de la profiline-1 vers le front de migration, afin d'y favoriser la formation du réseau d'actine nécessaire à l'expansion du lamellipode.

LIST OF FIGURES

INTRODUCTION

CHAPTER I

Figure 1. The different steps of chemotactic cell migration.....	35
Figure 2. The distribution of the main molecular actors of polarized cell migration.....	37
Figure 3. Regulation of actin treadmilling.....	39
Figure 4. Representation of the lamellipodium periodic regeneration model.....	40
Figure 5. Molecular actors involved in lamellipodium formation.....	42
Figure 6. Molecular actors involved in filopodium formation.....	45
Figure 7. The different forms of adhesions of a migrating cell.....	49
Figure 8. The integrin activation cycle.....	51
Figure 9. Structure of paxillin and adhesion assembly.....	53
Figure 10. The adhesion disassembly mechanisms.....	54
Figure 11. Clathrin-dependent endocytosis of integrins.....	56
Figure 12. Intracellular trafficking and recycling of integrins.....	58
Figure 13. Molecular mechanisms of exocytosis.....	61
Figure 14. Representation of EGFR activation and its signaling pathways.....	65
Figure 15. Representation of CXCR4 and its signaling pathways.....	68

CHAPTER II

Figure 16. Microautophagy.....	73
Figure 17. Chaperone-mediated autophagy.....	74
Figure 18. Macroautophagy.....	76
Figure 19. The ULK complex in mammals.....	77
Figure 20. The PI3KIII complex.....	78
Figure 21. Regulation of PI3KIII activity by beclin 1 partners.....	79
Figure 22. Regulation of the ULK complex by mTORC1 and AMPK.....	81
Figure 23. The key steps of initiation and phagophore nucleation.....	81
Figure 24. The Ubiquitylation system.....	82
Figure 25. The two ubiquitin-like conjugation systems essential for autophagy.....	84
Figure 26. The autophagic receptor p62 and selective autophagy.....	85

List of figures

Figure 27. Autophagosome closure.....	86
Figure 28. Autophagosome and autolysosome trafficking onto microtubules.....	87
Figure 29. The fusion between autophagosome and lysosome.....	88
Figure 30. Different membrane sources for phagophore elongation.....	90
Figure 31. Atg9/ATG9A topology and its internal pores system.....	92
Figure 32. ATG9A trafficking <i>via</i> AP complexes.....	94
Figure 33. ATG9A trafficking <i>via</i> BAR-domain proteins.....	96
Figure 34. Model for the initial steps of yeast Atg9-mediated phagophore generation.....	98
Figure 35. Model of the scramblase activity of Atg9/ATG9A.....	99
Figure 36. Regulation of autophagy by amino acid availability.....	100
Figure 37. Regulation of autophagy by growth factors.....	101
Figure 38. Hypoxia-dependent pathways regulating autophagy.....	102
Figure 39. The role of autophagy in exocytosis.....	104
Figure 40. Pro-migratory effects of autophagy.....	108
Figure 41. Compartmentalized regulation of autophagy by chemotactic GPCRs.....	110

RESULTS

PART I

Figure R1. Chemotactic migration depends on ATG9A protein.....	135
Figure R2. Depletion of ATG9A protein impairs formation of F-actin-rich protrusion and intrinsic cell speed.....	136
Figure R3. ATG9A-positive vesicles concentrate in F-actin-rich protrusions and display anterograde trafficking toward the leading edge.....	138
Figure R4. Structure and functional validation of ATG9A-pHluorin construct.....	140
Figure R5. Exocytosis of ATG9A-positive vesicles is polarized toward the cell front and induced by chemotactic stimulation.....	142
Figure R6. ATG9A-pHluorin signal at the cell periphery correlates with protrusive activity.....	144
Figure R7. ATG9A protein regulates delivery of $\beta 1$ integrin to cell protrusions.....	145
Figure R8. ATG9A regulates delivery of TGN46 and $\beta 1$ integrin to the leading edge through its N-terminal AP sorting signal.....	146
Figure R9. ATG9A protein regulates adhesion dynamics.....	147
Figure R10. ATG9A-positive vesicles target adhesion sites.....	148

List of figures

Supplementary Figure S1. Efficiency of siRNA knockdown of ATG9A and its effect on autophagosome biogenesis in U87 MG cells.....	149
Supplementary Figure S2. Depletion of ATG9A protein impairs the formation of cell protrusions.....	150
Supplementary Figure S3. ATG9A static puncta colocalize with the endocytic marker clathrin.....	150
Supplementary Figure S4. EGF stimulation increases the fusion activity of ATG9A vesicles in HeLa cells.....	151
Supplementary Figure S5. ATG9A protein regulates delivery of TGN46-positive post-Golgi carriers to cell protrusions.....	151
Supplementary Figure S6. Depletion of ATG9A protein inhibits EGF-induced formation of adhesion complexes in HeLa cells.....	152
Supplementary Figure S7. ATG9A-positive vesicles target adhesion sites in HeLa cells.....	153

PART II

Figure RR0. Schematic representation of the C-terminal domain of human ATGA and of the mutant forms produced by site-directed mutagenesis.....	168
Figure RR1. The C-terminal domain of ATG9A interacts with the actin regulator profilin-1.....	171
Figure RR2. ATG9A colocalizes with profilin-1 and governs its localization toward the leading edge.....	174
Figure RR3. ATG9A-EGFP and profilin-1-mCherry signals colocalize and correlate with protrusive activity...	176

DISCUSSION

Figure 42. Model of ATG9A-, PI4KIII β - and GOLPH3-mediated biogenesis of vesicles from the TGN network	182
Figure 43. Clinical data from <i>The Cancer Genome Atlas</i> (TCGA).....	187

List of movies

Movie 1. Depletion of ATG9A protein impairs the formation of cell protrusions.....154

Movie 2. ATG9A protein regulates adhesion dynamics.....154

Movie 3. “Spreading” ATG9A-pHluorin exocytotic events.....154

Movie 4. “Non-spreading” ATG9A-pHluorin exocytotic events.....154

Movie 5. ATG9A-pHluorinsignal appearance at the leading edge correlates with protrusive activity.....154

To access the online videos, click on the following link

<https://bit.ly/387qeKh>

LIST OF ABBREVIATIONS

AC:	<i>adenylate cyclase</i>
ALLN:	<i>N-acetyl-L-Leu-Leu-Norleu-al</i>
AMBRA1:	<i>autophagy and beclin 1 regulator 1</i>
AMPK:	<i>5'-adenosine-monophosphate-activated protein kinase</i>
AP:	<i>adaptor protein</i>
aPKC:	<i>Atypical PKC</i>
Arf:	<i>ADP-ribosylation factor</i>
ARF6:	<i>ADP-ribosylation factor 6</i>
ARH:	<i>autosomal recessive hypercholesterolemia</i>
Arp:	<i>actin-related protein</i>
At-Atg9:	<i>Arabidopsis thaliana Atg9</i>
ATCC:	<i>American Type Culture Collection</i>
Atg:	<i>autophagy-related</i>
Atg1:	<i>autophagy-related 1</i>
BAR:	<i>Bin/amphiphysin/Rvs</i>
BARA:	<i>β-α-repeated, autophagy-specific</i>
BH3:	<i>BCL2 homology 3</i>
Bif1:	<i>Bax-interacting factor 1</i>
BiFC	<i>Biomolecular Fluorescence Complementation</i>
BNIP3	<i>BCL2 interacting protein 3</i>
C5aR-GFP:	<i>C5a receptor fused to GFP</i>
cAMP:	<i>cyclic adenosine monophosphate</i>
CCD:	<i>coiled-coil domain</i>
Cdc42:	<i>cell division control protein 42</i>
CHMP:	<i>charged multivesicular body protein</i>
CMA:	<i>chaperone-mediated autophagy</i>
Co-IP	<i>Co-immunoprecipitation</i>
CPP:	<i>cell penetrating peptides</i>
CQ:	<i>chloroquine</i>
CRIB:	<i>Cdc42/Rac-interactive binding</i>
cryo-EM:	<i>cryo-electron microscopy</i>
Ctv:	<i>cytoplasm-to-vacuole</i>
CXCL12:	<i>C-X-C Motif Chemokine Ligand 12</i>
CXCR4:	<i>C-X-C chemokine receptor type 4</i>
DAB2:	<i>disabled homolog 2</i>
ddH ₂ O:	<i>doubled distilled water</i>
DDO:	<i>Double dropped out</i>
Dock180:	<i>dedicator of cytokinesis 180</i>
ECD:	<i>evolutionarily conserved domain</i>
ECM:	<i>extracellular matrix</i>
ED:	<i>extra domain</i>
EGF:	<i>epidermal growth factor</i>
EGFR:	<i>epidermal growth factor receptor</i>

List of abbreviations

ELMO:	<i>engulfment and cell motility protein</i>
eMA:	<i>endosomal microautophagy</i>
EMT:	<i>epithelial to mesenchymal transition</i>
Ena:	<i>Enabled</i>
EPG5:	<i>ectopic P-granules autophagy protein 5 homolog</i>
ER:	<i>endoplasmic reticulum</i>
ERES:	<i>Endoplasmic reticulum exit sites</i>
ERGIC:	<i>endoplasmic reticulum-Golgi intermediate compartment</i>
ERK:	<i>extracellular signal-regulated kinases</i>
ESCRT:	<i>endosomal sorting complexes required for transport</i>
Evh:	<i>Ena-VASP-homology</i>
Evl:	<i>Ena-VASP-like</i>
FA:	<i>focal adhesions</i>
FAB:	<i>F-actin binding</i>
F-actin:	<i>filamentous-actin</i>
FAK:	<i>focal adhesion kinase</i>
FGFR:	<i>fibroblast growth factor receptor</i>
FilGAP:	<i>Filamin A GTPase-activating protein</i>
FIP200:	<i>FAK family kinase-interacting protein of 200 kDa</i>
FLLME:	<i>flap-like lysosomal membrane extension</i>
FRET:	<i>fluorescent resonance energy transfer</i>
FX:	<i>focal complexes</i>
FYCO1:	<i>FYVE and coiled-coil domain autophagy adaptor 1</i>
GAB:	<i>G-actin binding</i>
GABARAP:	<i>gamma-aminobutyric acid receptor-associated protein</i>
G-actin:	<i>globular-actin</i>
GDP:	<i>guanosine diphosphate</i>
GEF:	<i>guanine nucleotide exchange factor</i>
GFP:	<i>green fluorescent protein</i>
GOLPH3:	<i>Golgi phosphoprotein 3</i>
GPCR:	<i>G proteins-coupled receptor</i>
Grb2:	<i>growth factor receptor-bound protein 2</i>
GTP:	<i>guanosine triphosphate</i>
HCQ:	<i>hydroxychloroquine</i>
HIF:	<i>hypoxia-inducible factor</i>
hsc70:	<i>heat shock cognate 70</i>
HSP:	<i>hereditary spastic paraplegia</i>
i.e.	<i>id est</i>
I-BAR:	<i>inverted-Bin-Amphiphysin-Rvs</i>
IQGAP:	<i>IQ-motif containing Ras GTPase-activating-like protein</i>
IRSp53:	<i>insulin receptor phosphotyrosine 53 kDa substrate</i>
Kif:	<i>kinesin family member</i>
KIR:	<i>Keap-interacting region</i>
KO:	<i>knockout</i>
LAMP2:	<i>lysosome-associated membrane protein type 2A</i>
LC3:	<i>microtubule-associated protein 1A/1B-light chain 3</i>
LDRL:	<i>low-density lipoprotein receptor</i>

List of abbreviations

LIM:	<i>Lin-11, Isl-1, Mec-3</i>
LIR:	<i>LC3-interacting region</i>
LW:	<i>lysosomal wrapping</i>
MACF1:	<i>microtubule-actin cross linking factor 1</i>
MCS:	<i>membrane contact sites</i>
mDia2:	<i>mammalian diaphanous 2</i>
MEK:	<i>mitogen-activated protein kinase/ERK kinase</i>
Mena:	<i>Mammalian Ena</i>
MLCK:	<i>myosin light-chain kinase</i>
MMP9:	<i>matrix metalloproteinase 9</i>
MT1-MMP:	<i>membrane-type 1 matrix metalloproteinase</i>
mTORC1:	<i>mammalian target of rapamycin complex 1</i>
NBR1:	<i>neighbor of BRCA1</i>
NPF:	<i>nucleation promoting factors</i>
nMDP:	<i>normalized mean deviation product</i>
Nvj1p:	<i>nucleus-vacuole junction protein 1</i>
ORP1L:	<i>oxysterol-binding protein-related protein 1L</i>
PAK1:	<i>P21 activated kinase 1</i>
PAS:	<i>pre-autophagosomal structure</i>
PB1:	<i>Phox and Bem1</i>
PDGFR:	<i>platelet derived growth factor receptor</i>
PI:	<i>phosphatidylinositol</i>
PI3K:	<i>phosphoinositide 3-kinase</i>
PI3KIII:	<i>class III phosphatidylinositol 3-kinase</i>
PI3P:	<i>phosphatidylinositol 3-phosphate</i>
PI4KIII β :	<i>class III phosphatidylinositol 4-kinase β</i>
PI4P:	<i>phosphatidylinositol 4-phosphate</i>
PIP:	<i>polyphosphoinositides</i>
PIP ₂ :	<i>phosphatidylinositol 4,5-biphosphate</i>
PIP ₃ :	<i>phosphatidylinositol 3,4,5-triphosphate</i>
PKA:	<i>protein kinase A</i>
PKC:	<i>protein kinase C</i>
PLC γ :	<i>phospholipase Cγ</i>
PTEN:	<i>phosphatase and TENsin homolog</i>
PTX:	<i>pertussis toxin</i>
QDO:	<i>Quadruple dropped out</i>
RAB11:	<i>Ras-related protein Rab 11</i>
RAB4:	<i>Ras-related protein Rab 4</i>
RAB5:	<i>Ras-related protein Rab 5</i>
RAB7:	<i>Ras-related protein Rab 7</i>
RGD:	<i>arginylglycylaspartic acid</i>
RHEB:	<i>Ras homolog enriched in brain</i>
RILP:	<i>rab-interacting lysosomal protein</i>
ROCK:	<i>Rho-associated, coiled-coil-containing protein kinase</i>
RTK:	<i>receptor tyrosine kinase</i>
RTK:	<i>receptors tyrosine kinase</i>
RUSC:	<i>RUN and SH3 domain containing</i>

List of abbreviations

RUSH:	<i>retention using selective hooks</i>
SBP:	<i>streptavidin-binding peptide</i>
SERP:	<i>secretory reticulophagy/ER-phagy</i>
SH2:	<i>Src homology 2</i>
siRNA:	<i>small interfering RNA</i>
SNAP:	<i>soluble NSF attachment protein</i>
SNARE:	<i>N-ethylmaleimide-sensitive factor attachment receptor</i>
SNX17:	<i>sortin nexin 17</i>
SNX31:	<i>sorting nexin 31</i>
Sos:	<i>son of sevenless</i>
STX:	<i>syntaxin</i>
TB:	<i>TRAF6-binding domain</i>
TGCA:	<i>The Cancer Genome Atlas</i>
TGN:	<i>trans-Golgi network</i>
TIRF:	<i>time-lapse total internal reflection fluorescence</i>
TM:	<i>transmembrane</i>
TSC1/2:	<i>tuberous sclerosis complex 1/2</i>
t-SNARE:	<i>target-SNARE</i>
UBA:	<i>Ubiquitin-associated domain</i>
ULK:	<i>uncoordinated 51-like Ser/Thr kinase</i>
UT:	<i>urotensin II receptor</i>
UVRAG:	<i>UV radiation resistance associated</i>
VAMP:	<i>vesicle associated membrane protein</i>
VASP:	<i>Vasodilatator-stimulated phosphoprotein</i>
VEGFR:	<i>vascular endothelial growth factor receptor</i>
VPS:	<i>vacuolar protein sorting-associated protein</i>
VPS34:	<i>vacuolar protein sorting 34</i>
v-SNARE:	<i>vesicle-SNARE</i>
WASH:	<i>Wiskott-Aldrich syndrome protein and scar homolog</i>
WASP:	<i>Wiskott-Aldrich syndrome protein</i>
WAVE:	<i>WASP-family verprolin-homologous protein</i>
WHAMM:	<i>WASP homolog-associated protein with actin, membranes, and microtubules</i>
WIPI:	<i>WD repeat domain phosphoinositide-interacting</i>
Y2H:	<i>yeast two-hybrid</i>
ZZ:	<i>Zinc finger</i>

CHAPTER I: CELL MIGRATION

Cell migration is a central physiological process during embryonic development, immune response and wound healing. It is likewise important in the survival of the species, by which organisms obtain nutrients, escape from toxic agents and predators. Cell migration is also important in pathological processes such as inflammatory diseases, *i.e.* multiple sclerosis, vascular diseases, cancer formation and development of metastases. Therefore, studying the fundamental mechanisms underlying cell migration is the key to better understand the physiology of the organisms as well as diseases, and thus, to find suitable therapeutic approaches.

Since the 17th century, more than 400 years ago, man has begun to study cell migration thanks to the advent of microscopy. In 1675, Antoni van Leeuwenhoek, a tailor by profession, published his observations about the movement of protozoa detected in different liquids in the journal "*Philosophical Transactions of the Royal Society*". In the following centuries, Theodor Engelmann (1881) and Wilhelm Pfeffer (1884) conducted experiments on bacteria and discovered that motility could be directed by external stimuli. It was only around the 1900s that the concept of cell migration became more consistent, when Il'ja Mečnikov described the phagocytic activity of neutrophils and their migration toward the site of infection (Mečnikov, 1905).

Around 1970s, Michael Abercrombie established modern theories on cell migration observing that cells move through the development of protrusions leading directed migration. This process included the formation of adhesions and collapsed protrusions when a nearby cell came into contact. At this point, the cell emitted a new protrusion in a different area and changed direction by retracting the back of the cell body (Abercrombie & Ambrose, 1958; Abercrombie & Dunn, 1975). These observations have given life to the new concept of "protrusion-contraction". These studies on cell migration, along with others, led to think that migration was first characterized by the alternation of a protrusion phase. They also led to the idea that this mechanism could be "directed" in response to local accumulation of molecules, hence the birth of directional migration.

1. Directional migration and cell polarization

Cell migration is a dynamic event and can be divided into individual and collective cell migration (Treat et al., 2012). Individual cell migration is typical of inflammatory processes and consists in the migration of immune cells at the site of infection, and fibroblasts in wound healing for *extracellular matrix* (ECM) secretion. Collective migration, on the other hand, is involved in the embryonic development and formation of metastases. It is defined as the migration of two or more cells using similar processes than individual cell migration (polarization, retraction and adhesions to the ECM) but in a set of cells that are joined together by adhesions, such as integrins and cadherins (Friedl & Gilmour, 2009). These junctions connect the actin cytoskeletons of the cells to create a "supracellular" structure that allows a dynamic and precise coordination

of migrating cells. The coordination of this process is ensured by a "leader" cell able to detect the molecular gradient and drive the migration of the cells with which it comes into contact (Vitorino & Meyer, 2008). By the use of *in vivo* imaging, Haas and Gilmour have shown that cells carrying a mutation in *C-X-C chemokine receptor type 4* (CXCR4), an important receptor acting in directional migration, were inhibited to be leaders in the Zebrafish lateral line primordium (Haas & Gilmour, 2006).

1.1. Chemotactic migration

It is important to distinguish disorderly or random migration from organized and directional migration. In contrast to random migration, directional migration is the persistent one-way movement of a cell in response to an external stimulus. Depending on the nature of the external stimulus, we can distinguish: *i)* the directional migration induced by a gradient of a soluble factor, *i.e.* chemotaxis or chemotactic migration, *ii)* the migration induced by a substrate-bound immobile factor, *i.e.* haptotaxis, *iii)* a mechanical cue exerted on the cell, *i.e.* mechanotaxis and *iv)* a mechanical gradient which arises from different properties of the extracellular matrix, *i.e.* durotaxis. From here on out, I will be focusing on chemotaxis, which is characterized by the activation of receptors located at the plasma membrane, that in turn activate intracellular pathways to keep this process active over time. It is nowadays accepted a model of chemotactic migration that is divided into five different cyclic steps (Lauffenburger & Horwitz, 1996). Following the recognition of a chemotactic stimulus, the *first step* is the polarization of the cell (Figure 1), with a clear distinction between a front (or leading edge) and a back (or retracting edge). This step involves the segregation of different molecular actors, such as actin. The consequence of polarization is the formation of a membrane protrusion (*second step*) called lamellum, made up of actomyosin fibres that end at the plasma membrane with an essential structure, called lamellipodium, consisting in a dense actin network. These protrusions are stabilized by the formation of adhesion complexes that serve as anchorage points to the ECM, and progressively mature and strengthen (*third step*). The protrusive force required to extend the lamellipodium forward is given by actin polymerization within this structure, while the contractile force is given by the actomyosin fibres present in the lamellum and at the back of the cell. The contraction of actomyosin filaments on mature adhesions allows the cell body to move forward (*fourth step*). The adhesions that no longer serve this process are demolished and/or recycled (*fifth step*) to generate a new cycle (Figure 1).

1.2. Cell polarization

The polarization of the cell is essential to direct its movement toward a chemotactic stimulus. The basic knowledge we have about this event comes mainly from studies conducted on the amoeba *Dictyostelium discoideum* (Weiner, 2002a) and neutrophils (Weiner et al., 2002). According to the Weiner's theory, also called the "chemotactic compass", the molecular actors of cell migration rapidly segregate in a front-to-back manner in response to a chemotactic gradient. This theory includes three different events: *i)* activation of chemotactic receptors, *ii)* accumulation of *phosphatidylinositol 3,4,5-triphosphate* (PIP₃) beneath the plasma

membrane and *iii*) stimulation of Rho small GTPases Rac1, Cdc42 and RhoA. The most characterized chemotactic receptors are the seven-domain transmembrane *G proteins-coupled receptors* (GPCR) and the *receptors tyrosine kinase* (RTK). Xiao and colleagues have demonstrated that the receptor of the *cyclic adenosine monophosphate* (cAMP), the GPCR cAR1, fused to a *green fluorescent protein* (GFP) is evenly distributed over the surface of the *Dictyostelium discoideum*, and this distribution is essential to allow this

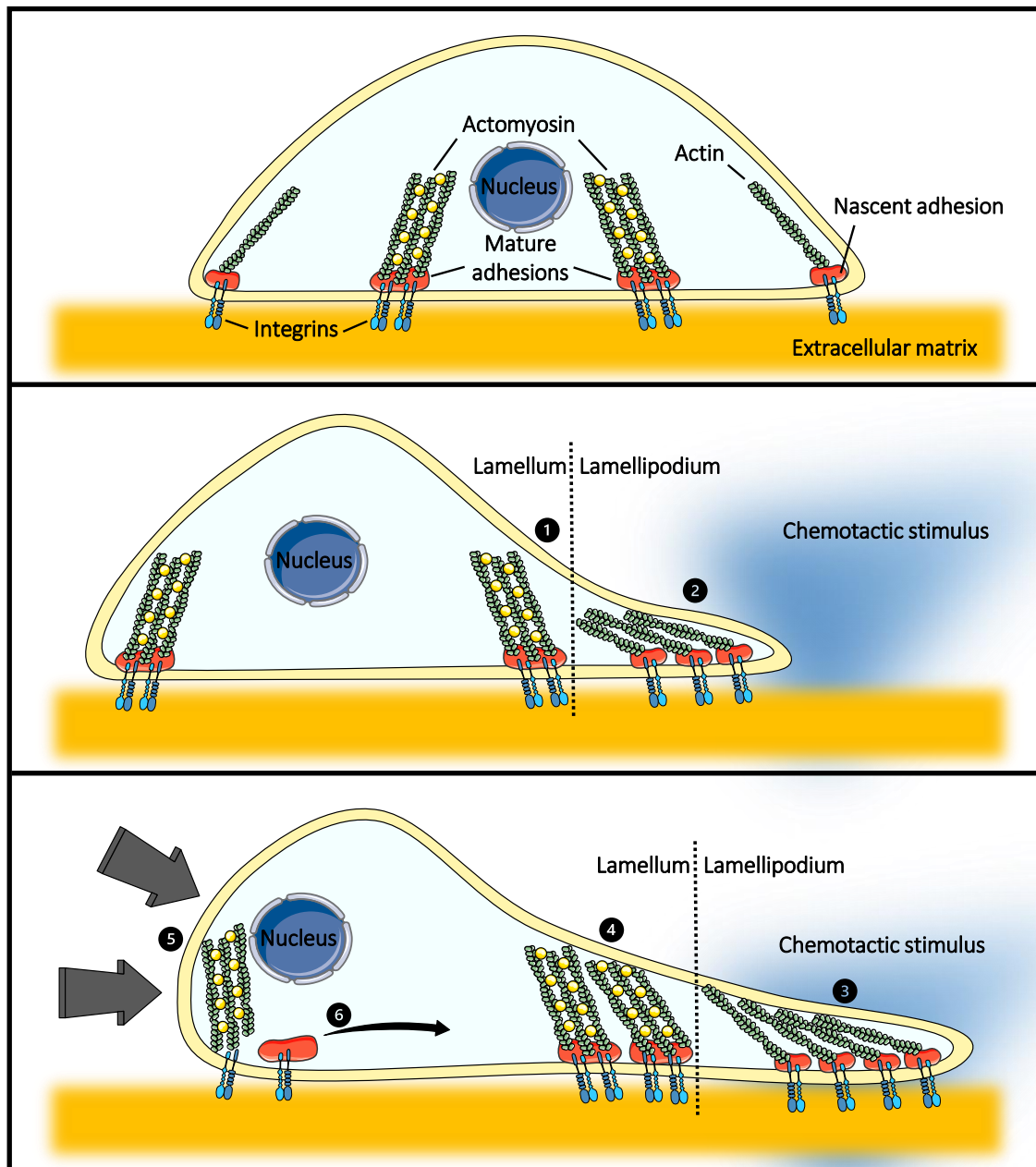


Figure 1. The different steps of chemotactic cell migration. In response to an extracellular chemotactic stimulus, intense actin polymerization induces the formation of a protrusion in the cell front, the lamellum (1), consisting of the lamellipodium (2) at its end. The cell polarizes and synthesizes nascent adhesions, consisting of integrins and other components, to stabilize the growing protrusion (3). During progression, these adhesions mature and serve as anchors to the extracellular matrix. Mature adhesions contact actomyosin contractile fibers in the lamellum (4). Contraction of these actomyosin fibers allows the cell body to retract (5) and allows the cell to advance toward the source of the chemotactic signal. Adhesions located at the back are disassembled and integrins are recycled to form new adhesions at the cell front (6).

organism to accurately detect external gradient changes. Furthermore, during chemotactic migration, these receptors are not re-distributed toward the migration pole but remain evenly distributed over the entire surface (Xiao et al., 1997). The demonstration that receptors are homogeneously distributed during directional migration has also been shown by expressing the *C5a receptor fused to GFP* (C5aR-GFP) in a neutrophil-like cell line (Servant et al., 1999). In fact, chemotactic stimulation of the cells induced polarization toward the gradient without changing the distribution of the C5aR-GFP over the surface (Servant et al., 1999). These data suggest that cell polarization is, in fact, driven by the activation of signaling cascades in a local and polarized manner beneath the membrane.

The signaling cascade, triggered by receptor stimulation, induces the accumulation of PIP₃ at the plasma membrane. This accumulation depends on the activation and asymmetric distribution of the enzyme *phosphoinositide 3-kinase* (PI3K), that processes *phosphatidylinositol 4,5-bisphosphate* (PIP₂) into PIP₃ at the leading edge (Weiner et al., 2002). PIP₃ can activate some *guanine nucleotide exchange factors* (GEF) which in turn stimulate Rho small GTPase, such as RhoA, Rac1 and *cell division control protein 42* (Cdc42). These GTPases act as a “molecular switch” shifting, under the control of specific GEF, from an “inactive” *guanosine diphosphate* (GDP)-bound form to an “active” *guanosine triphosphate* (GTP)-bound form (Weiner, 2002b) (Figure 2).

Cdc42 GTPase is a main actor of cell polarity and acts as a stabilizer of polarization. In budding yeast, Cdc42 localizes to the budding site (Adams et al., 1990) while, in neutrophils and other migrating mammalian cells, Cdc42 is found at the leading edge (Etienne-Manneville, 2008). Cdc42 inhibition strongly destabilizes cellular polarization in neutrophils (Srinivasan et al., 2003; Van Keymeulen et al., 2006), while its overexpression significantly improved HeLa cell migration by enhancing the formation of lamellipodia and filopodia (Huveneers & Danen, 2009; Ye et al., 2015). Cdc42 establishes this polarization by acting on the effector proteins *P21 activated kinase 1* (PAK1), along the cell protrusion structures, which in turn stabilizes the cytoskeleton (Parsons et al., 2005). In addition, PAK1 activates Cdc42 in a positive feedback loop, resulting in very high Cdc42 activity in the leading edge (Li et al., 2003) (Figure 2).

Another player of cell polarization is **Rac1**, which promotes actin polymerization in the migration front as well as lamellipodia development (Parri & Chiarugi, 2010). Rac1 is part of a positive loop involving the production of PIP₃ through the activation of PI3K. Srinivasan and colleagues have demonstrated that constitutive over-expression of Rac1 induces the accumulation of PIP₃ at the plasma membrane, as well as the formation of actin polymers. Accordingly, a dominant negative form of Rac1 inhibits the accumulation of actin

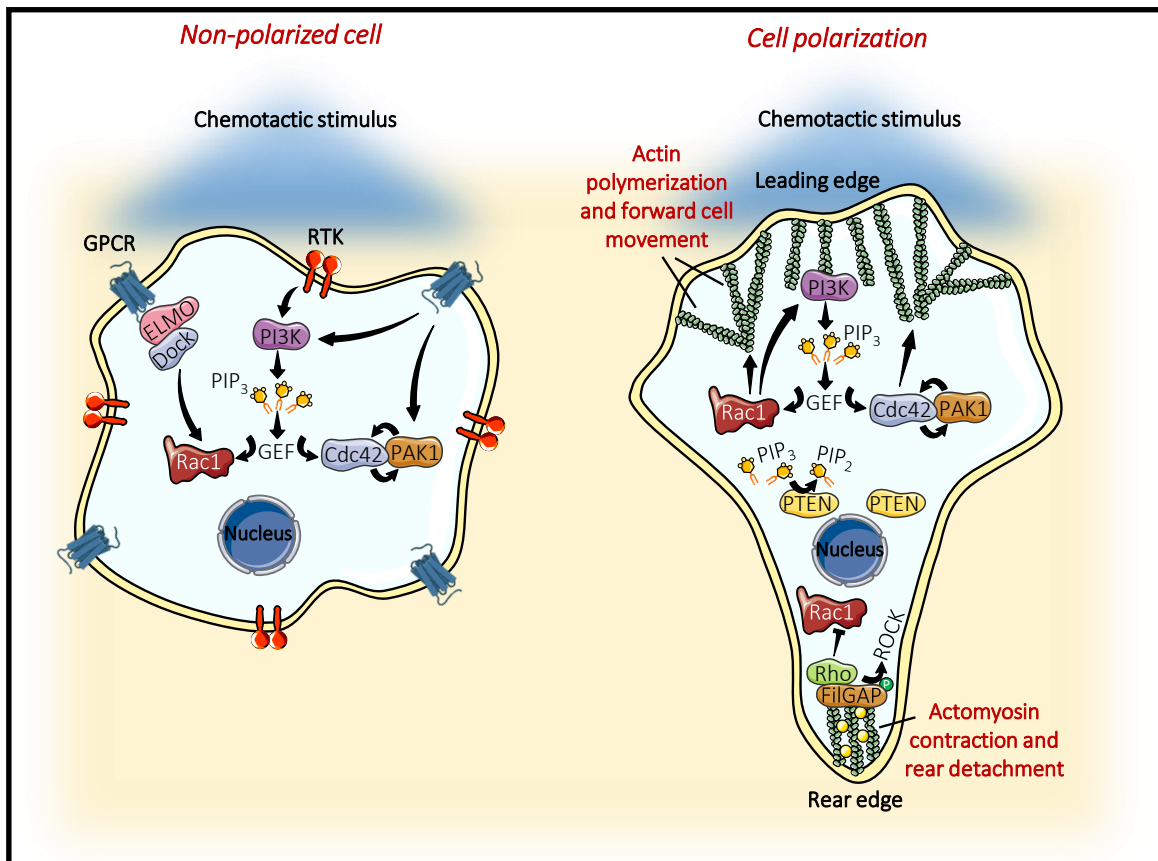


Figure 2. The distribution of the main molecular actors of polarized cell migration. At the origin of polarization (left), the GPCR and RTK membrane receptors are locally activated by a chemotactic gradient, capable of inducing simultaneous recruitment of PI3K and the ELMO1 and dock180 proteins. PI3K induces the accumulation of PIP₃, and continuous stimulation of GEF proteins translates with the recruitment of the active forms of the GTPases Rac1 and Cdc42. Cdc42, can also be stimulated by the PAK1 protein, one of the effector kinases of the signaling pathways of some membrane receptors. Activation of the Rho-GTPases Rac1 and Cdc42 allows the formation of a molecular gradient and polarization between the front and back of the cell (right). In fact, Rac1 catalyzes actin polymerization and the subsequent formation of protrusion and causes, through a positive feedback phenomenon on PI3K, the accumulation of PIP₃ in the cell front. Cdc42 establishes polarization by acting on PAK1. The accumulation of PIP₃ is tightly constrained in the cell front by the phosphatase PTEN, which is localized in the back of the cell, and which catalyzes the dephosphorylation of PIP₃ forming PIP₂. This mechanism fuels the formation of an antero-posterior PIP₃-PIP₂ gradient. In the back of the cell, the GTPase RhoA predominates and phosphorylates the Rac1 adaptor, FilGAP, inducing Rac1 inactivation in this area and promoting cell tail detachment.

polymers at the membrane as well as PIP₃ following chemotactic stimulation and prevents polarity from being achieved (Srinivasan et al., 2003). Interestingly, data indicate that receptor-induced activation of Rac1 can also operate independently of the classical PI3K/PIP₃ pathway. In this context, a more direct link between CXCR4 and Rac1 activation has been demonstrated. Indeed, Li and colleagues have shown that CXCR4 stimulation, by its ligand *C-X-C Motif Chemokine Ligand 12* (CXCL12), induces the translocation of *engulfment and cell motility protein* (ELMO) 1 at the plasma membrane and its interaction with the Gα₁₂ subunit. The Gα₁₂:ELMO1 complex, in turn, recruits the GEF *dedicator of cytokinesis 180* (Dock180), which activates Rac1 and promotes actin polymerization as well as migration of breast cancer cells (Li et al., 2013). Similarly, activated *epidermal growth factor receptor* (EGFR) also leads to the activation of Rac1, through the recruitment of a complex containing

the ELMO2 GEF protein, inducing actin remodelling and cell polarity in keratinocytes (Ho & Dagnino, 2012) (Figure 2).

If Cdc42 and Rac1 are involved in the early spreading steps of cell migration, **RhoA** is instead involved in later stages of the process. Cdc42 and Rac1 are gradually activated toward the leading edge where they control actin cytoskeleton rearrangements to promote protrusive activity, while RhoA is mainly active at the back of the cells where, by inducing actomyosin contractility, it controls the retraction of the rear (Etienne-Manneville, 2008; Nobes & Hall, 1995; Park & Bi, 2007) (Figure 2). Studies have shown that RhoA distribution is well polarized in migrating cells, as well as Rac1, with a cross-inhibition mechanism between these two GTPases. One of these studies has shown that the tail detachment depends on the activation of the RhoA downstream effector *Rho-associated, coiled-coil-containing protein kinase* (ROCK) which induces the phosphorylation of the Rac1 adapter *Filamin A GTPase-activating protein* (FilGAP) (Figure 2). This phosphorylation event finally promotes Rac1 inactivation at the rear of HEK293 cells (Ohta et al., 2006). In the same year, Van Keymeulen and colleagues demonstrated a more complex mechanism of mutual inhibition between these different GTPases. Expression of a constitutively active Cdc42 mutant increased RhoA activation in the back of the cell while the use of inhibitors for PIP₃ synthesis reduced both the activation of Cdc42 and RhoA suggesting a long-range inhibitory effect of PIP₃ and Cdc42 on RhoA activity (Van Keymeulen et al., 2006).

In addition to RhoA, the *phosphatase and tensin homolog* (PTEN) also acts as a “rear determinant”, by converting the PIP₃ pool into PIP₂ at the back of the cell (Funamoto et al., 2002; Worby & Dixon, 2014). The strict antero-posterior distribution of PI3K and PTEN, respectively, has been demonstrated (Merlot & Firtel, 2003). Recent studies have shown that loss of PTEN causes a constitutive enrichment of PIP₃ in the entire cell membrane, leading to the formation of multiples pseudopods toward different directions. Single-molecule measurements and kinetic analyses have demonstrated that local accumulation of PIP₃ at subdomains of the cell membrane inhibits the binding of PTEN, which may contribute to the exclusion of PTEN from the cell front following chemotactic stimulation (Matsuoka & Ueda, 2018). The exclusion of PTEN from the migration front also depends on the activation of Cdc42 *via* PAK1, which itself depends on PIP₃ (Li et al., 2003), as already discussed (Figure 2). All these data indicate that there is a precise control organization to maintain an antero-posterior axis that serves to establish cell polarity.

2. Membrane protrusions and actin cytoskeleton

The extension of the cell surface is essential in the early events of many processes such as phagocytosis, neurite growth and cell migration (Lauffenburger & Horwitz, 1996; Rogers et al., 1983). This event is the first step for the formation of the two main cell protrusions driving cell migration, called lamellipodia and filopodia. These two structures are guided by actin filaments that generate the intracellular force necessary for their formation as well as their disassembly. The distinction between lamellipodia and filopodia lies in the way actin polymerization takes place. In fact, lamellipodia are generated by an highly branched actin filament network

(Svitkina & Borisy, 1999) while filopodia are arranged as finger-like actin filaments forming bundled projections (Mattila & Lappalainen, 2008). Lamellipodia and filopodia are built at the outer edge of the plasma membrane and they constitute the protrusive module (Faix & Rottner, 2006; Gupton & Gertler, 2007; Pollard & Borisy, 2003). The contractile module is called lamellum, a structure consisting of a variety of *filamentous-actin* (F-actin)–myosin II structures located just behind the leading edge, formed by lamellipodia and filopodia (Ponti, 2004).

Each actin filament consists of two helices of *globular-actin* (G-actin) that are twisted together. Nucleation of an actin filament is stimulated by nucleating factors, which mimic a G-actin dimer and are important for this initial step. Once nucleation has started, G-actin is needed to continue the elongation of the filament. F-actin filaments are polarized with a fast-growing (+) end, called barbed-end, in which G-actin:ATP monomers are added and a slow-growing (-) end, called pointed end, in which G-actin:ADP monomers dissociate from the filament (Figure 3). The binding of ATP to G-actin (G-actin:ATP) reinforces the stability of the filament at the barbed end, while moving away toward the pointed end, ATP is hydrolyzed into ADP (G-actin:ADP), reducing its structural stability and increasing the chance of depolymerization, a mechanism called *treadmilling* (Figure 3).

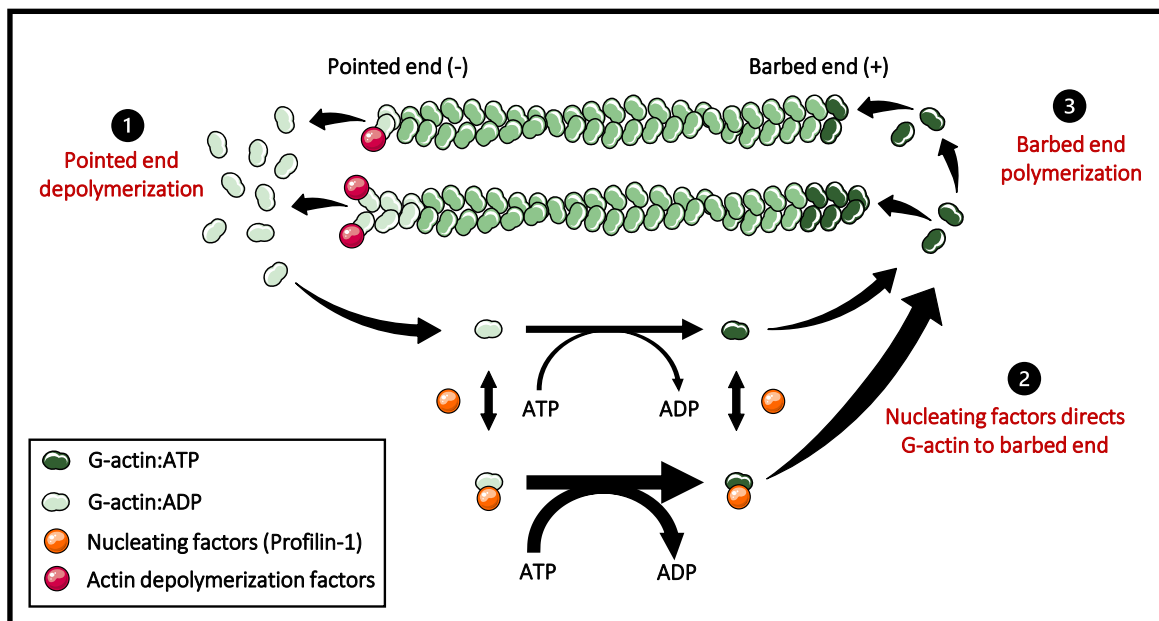


Figure 3. Regulation of actin treadmilling. Actin depolymerization factors bind to G-actin:ADP (steady state) at the pointed-end, inducing filament depolymerization (1). The concentration of G-actin at steady state increases. Nucleating factors, such as profilin-1, increase the likelihood of exchange of ADP for ATP to recycle G-actin at steady state. The profilin-1:G-actin:ATP complex is directed toward the barbed end of the actin filament (2), inducing its rapid polymerization (3).

2.1. Lamellipodia

The lamellipodium is a highly dynamic protrusion developed at the cell front and is the main actor leading mesenchymal cell migration. This structure has a thickness ranging from 0.1 to 0.3 μm and a length from 1 to 5 μm (Innocenti, 2018), and is built up of a dense branched network of F-actin (Svitkina & Borisy, 1999). To build the lamellipodium, the F-actin fast-growing end generates the necessary force to push the membrane outwards, allowing directional and persistent migration (Ridley et al., 2003). The formation of this protrusion depends on the synthesis of nascent adhesions at its growing edge and the stabilization of adhesions located more internally, in the lamellum, where myosin II resides. Once the nascent adhesion is formed, the continuous polymerization of actin filaments in the area between this adhesion and the more mature adhesion located in the lamellum induces an accumulation of actin filaments that deforms the plasma membrane. Myosin II, located in the mature adhesion, pushes the actin filaments of the lamellipodium forward generating enough tension to allow the protrusion to advance into the surrounding space. At this point, a new nascent adhesion is formed at the end of the lamellipodium and the cycle begins again (Giannone et al., 2007) (Figure 4).

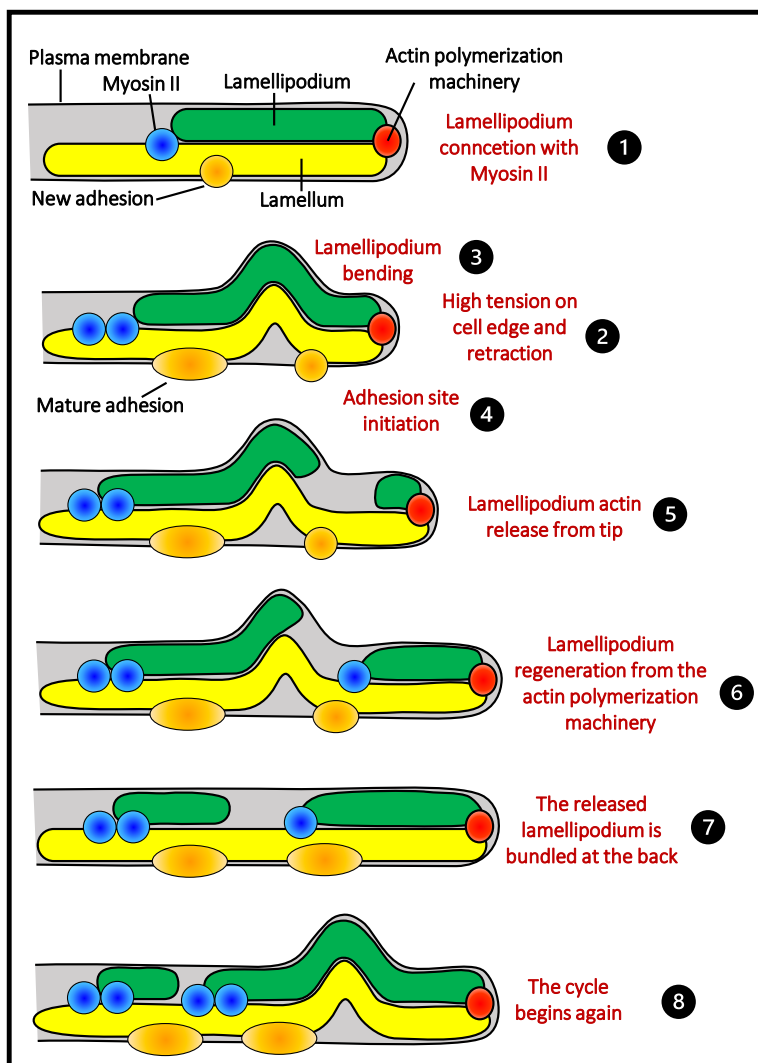


Figure 4. Representation of the lamellipodium periodic regeneration model. Polymerization of lamellipodium-associated actin (green) in the front induces its growth toward the back until it reaches a new adhesion site (dark yellow) where myosin II (blue) clusters (1). Myosin II pulls the growing lamellipodium, generating a strong tension in the cell front and thus its retraction (2). This induces deformation of the outward-pushing lamellipodium (3), and formation of a new adhesion (dark yellow) (4). The lamellipodium continues to be pulled until it is released from the tip (5), where it regenerates from the actin polymerization machinery (red) (6). The previously generated lamellipodium continues to be pulled by myosin II into a bundle, shrinking it to the level of the previous adhesion (7), while the new lamellipodium reaches the next adhesion and the cycle begins again (8). Cartoon adapted from Giannone et al., 2007.

2.1.1. Mechanisms of lamellipodia formation and actin regulators

The development of lamellipodia is controlled by the *actin-related protein* (Arp) 2/3 complex, constituted by the association of seven proteins: Arp2, Arp3 and Arpc1-5. This complex associates with actin filaments to induce actin polymerization. The Arp2/3 complex is not constitutively active and cannot induce nucleation of actin filaments alone. In fact, its activity is promoted by the *nucleation promoting factors* (NPF), such as proteins of the *Wiskott-Aldrich syndrome protein* (WASP) family, consisting in WASP itself, N-WASP, *WASP-family verprolin-homologous protein* (WAVE) 1-3, *WASP homolog-associated protein with actin, membranes, and microtubules* (WHAMM) and *Wiskott-Aldrich syndrome protein and scar homolog* (WASH). The exact functional role of each of these proteins is still unclear, but it would appear that they have similar functions, dependent on the cell type. These proteins essentially recruit Rho GTPases at the plasma membrane and organize the platform from which the actors of actin nucleation are recruited. For example, the WAVE complex is activated by Rac1 which induces its association with plasma membrane phospholipids at the leading edge (Chen et al., 2010) (Figure 5A). WAVE complex association with the plasma membrane leads the recruitment of Arp2/3 complex that binds the C-terminal WCA domain of the WAVE protein promoting Arp2/3 initial processivity. Arp2/3 complex can finally associate with pre-existing actin filaments where new “daughter” filaments develop from the “mother” ones, inducing branching. The resulting protrusion, formed by a branched and complex network of F-actin, constitutes the lamellipodium (Ridley, 2011; Rotty et al., 2013) (Figure 5A). The critical role of Arp2/3 in this process has been extensively studied and, accordingly, Arp2/3 accumulates at the barbed ends of the filaments following chemotactic stimulation (Bailly et al., 1999). Arp2/3 downregulation resulted in loss of lamellipodia and reduced directed migration induced by different cues in fibroblasts, epithelial cells, oligodendrocyte precursors and glioma cells (Beckham et al., 2014; Li et al., 2015; Liu et al., 2013; Suraneni et al., 2015; Wang et al., 2015; Wu et al., 2012). Interestingly, Arp2/3-deficient cells are still able to migrate but with reduced speed and the appearance of filopodia-like structures, instead of classical lamellipodia (Beckham et al., 2014; Li et al., 2015; Suraneni et al., 2012; Wu et al., 2012).

Other factors actively contribute to the ongoing polymerization, such as profilin-1 and proteins of the *Enabled* (Ena)/*Vasodilatator-stimulated phosphoprotein* (VASP) family. Profilin-1, by interacting with G-actin:ATP (Figure 3), constitutes an important source of actin monomers supplied at the barbed end of the filaments. Ena/VASP proteins improve F-actin elongation *i)* by inhibiting the association of “capping proteins” at the barbed ends of the growing filaments, and *ii)* by participating to the recruitment of the profilin-1:G-actin complex, as detailed below (Barzik et al., 2005) (Figure 5B). The Ena/VASP family consists of *Drosophila* Ena, *Caenorhabditis elegans* Unc-34, *Dictyostelium* DdVASP, and the three mammalian family members VASP,

mammalian *Ena* (Mena), and *Ena-VASP-like* (Evl). The specific roles of the mammalian proteins are still poorly understood, and mechanistic data mainly arise from studies performed on VASP from invertebrates.

All the members of the *Ena/VASP* family have conserved structural domains, consisting of a N-terminal domain defined *Ena-VASP-homology* (EVH)-1, a central proline-rich domain and a C-terminal domain, EVH2 (Figure 5B). The EVH1 domain interacts with adhesion proteins, such as zyxin and vinculin. The proline-rich domain binds and recruits profilin-1, while the EVH2 domain binds both G-actin and F-actin, through specific subdomains called *G-actin binding* (GAB) and *F-actin binding* (FAB), respectively (Brühmann et al., 2017).

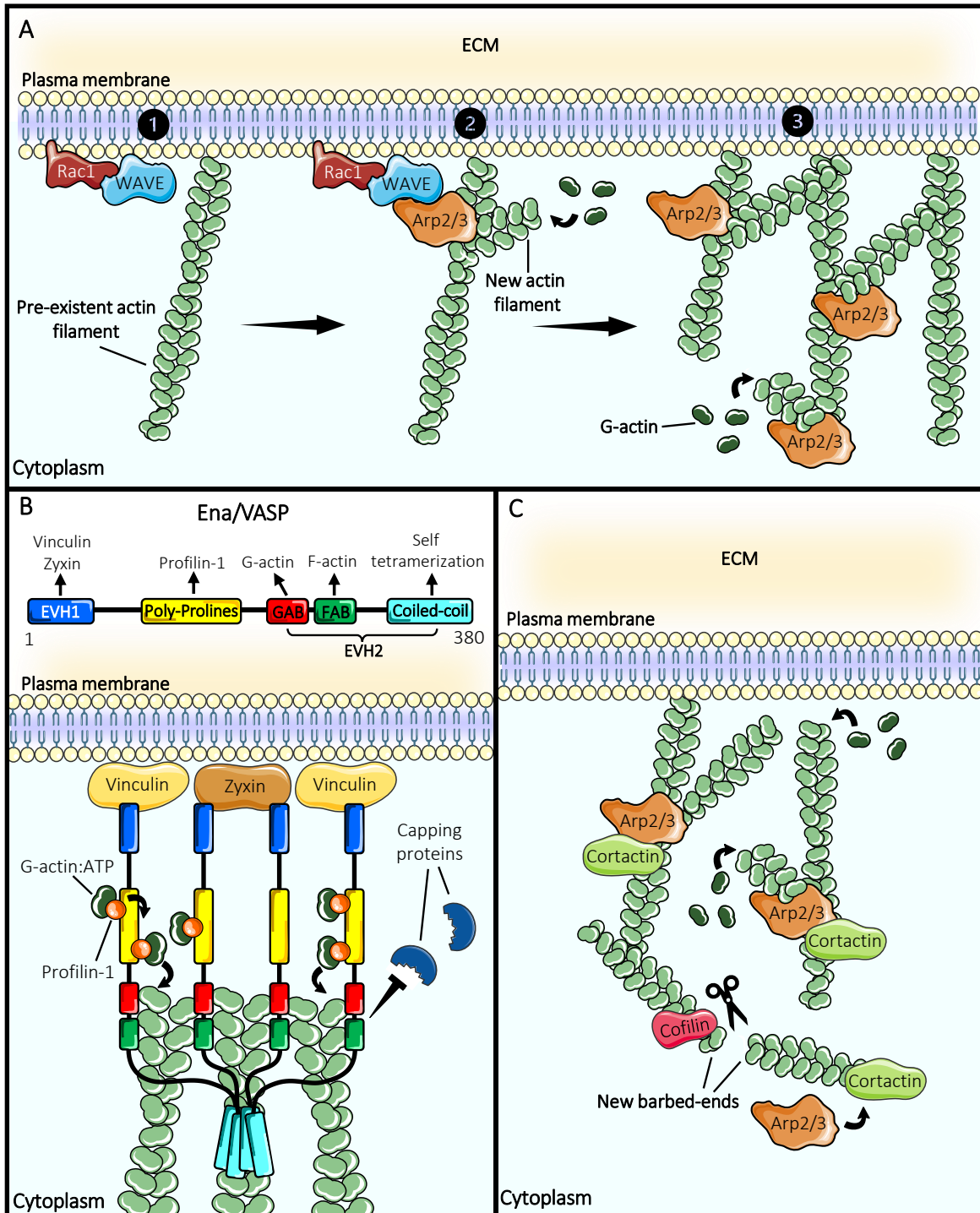


Figure 5. For caption see next page.

Figure 5. Molecular actors involved in lamellipodium formation. Lamellipodia formation and progression require the formation of an extensive dendritic network of actin filaments that pushes the plasma membrane outward. **A**| Following cell polarization, Rac1 is activated at the migration front and recruits the WAVE protein which binds the plasma membrane phospholipids (❶). Next, the WAVE protein induces the recruitment of the nucleation factor Arp2/3 that initiates branching and polymerization of a new actin filament from a pre-existing filament (❷). The Arp2/3 protein provides new spots for the formation of new barbed ends of actin filaments which ends in an extensive network of branched actin (❸). **B**| During actin polymerization Ena/VASP protein allows for fast synthesis and acts as an anti-capping agent. (Upper) The structure of the human Ena/VASP protein consists of an EVH1 domain at the N-terminal end, capable of interacting with the vinculin and zyxin adhesion proteins; a poly-prolines-rich domain, which gives the ability to interact with profilin-1; and an EVH2 domain at the C-terminal end, consisting of the GAB, FAB, and coiled-coil subdomains. The GAB subdomain interacts with G-actin while FAB interacts with F-actin. The coiled-coil subdomain allows homo-tetramerization with other Ena/VASP proteins. (Lower) A tetramer of Ena/VASP in association with actin filaments. Interaction between the EVH1 domain of Ena/VASP and adhesion proteins aid in the positioning of the Ena/VASP tetramer near the plasma membrane. The profilin-1:G-actin loading mechanism by which Ena/VASP is thought to supply actin monomers to the barbed end of actin filaments while antagonizing association of capping proteins that terminate filament elongation. Cartoon adapted from Bear and Gertler, 2009. **C**| Cofilin, by cutting pre-existing actin filaments, provides the Arp2/3 complex with new free barbed-ends. Finally, by binding to the Arp2/3 complex and actin filaments, cortactin stabilizes the actin network and thus the lamellipodium.

Ena/VASP proteins exert their actions immediately after initiation of the daughter filament, following dissociation of the WAVE complex from the Arp2/3 complex. They first anchor to the barbed end of the filament *via* their FAB domain, then induce the recruitment of profilin-1 *via* their proline-rich domain. Under this configuration, G-actin:ATP monomers are then transferred from profilin-1 to the GAB domain of Ena/VASP, and finally charged on the barbed end of F-actin (Hansen & Mullins, 2010; Pasic et al., 2008) (Figure 5B). Free profilin-1 moves away to be loaded with new G-actin:ATP, continuing to provide monomers to the GAB domain of Ena/VASP protein. Although, as stated above, the specific functions mammalian of Ena/VASP family members are still unclear, it has been shown that depletion of Evl, VASP or Mena proteins perturbs lamellipodial architecture with reduced F-actin assembly and an increased rate of capping activity, leading to reduced cell migration and lamellipodia persistence (Damiano-Guercio et al., 2020). Mutation of the poly-proline domain of Ena/VASP, implicated in profilin-1 binding, reduced the actin polymerization rate. Similar results were observed in a mutated form of profilin-1, that cannot bind G-actin (Hansen & Mullins, 2010).

Other proteins participate to lamellipodium formation, such as cofilin and cortactin. Cofilin mediates the cutting of existing cortical actin filaments, which generates new barbed ends to which the Arp2/3 complex can bind and stimulate polymerization (van Rheenen et al., 2009). Cortactin is a scaffold protein recruited to the Arp2/3 complex to stabilize the new synthesized branches and new filaments, giving stiffness to the whole structure. This allows the lamellipodium to be mechanically more rigid, increasing persistence during migration (Lai et al., 2009; Ren et al., 2009) (Figure 5C).

2.1.2. Rho GTPases and lamellipodium formation

Small GTPases of the Rho superfamily are particularly involved in actin network development. In particular, Rac1 and Cdc42 play a leading role in lamellipodia formation (Ridley, 2011). Rac1 mutants cells shown impaired lamellipodia formation while the development of a genetically-encoded photo-activatable of Rac1 could rescue lamellipodia formation and ruffling (Wu et al., 2009). Rac1 is able to activate the WAVE complex, normally sequestered and inactive, which in turn activates Arp2/3 (Chen et al., 2010). Furthermore, expression of a dominant negative form of Rac1 blocked lamellipodia spreading and generated a large number of filopodia (Guillou et al., 2008). Cdc42 can activate both WASP and N-WASP and induce their binding on PIP₂ located at the plasma membrane (Rohatgi et al., 2000). This mechanism is similar to that observed for Rac1-induced activation of the WAVE protein, which leads to the same result of recruiting Arp2/3 complex at the leading edge.

2.2. Filopodia

Filopodia are tiny (0.2 μm²) finger-like structures arising from the plasma membrane (Innocenti, 2018). They consist of 10 to 30 linear actin filaments arranged in parallel that push toward the tip (Yang & Svitkina, 2011). The role of the filopodia seems to be to function as "antennas" for the cell to probe the surrounding space during cell migration. It has been demonstrated that ErbB1 receptors localize within these structures and detect both the presence and concentration of effector molecules far from the cellular body to activate local signaling cascades (Lidke et al., 2005). Interestingly, filopodia are the scaffold structures for lamellipodia nucleation and can be dynamically converted into lamellipodia-like protrusions (Guillou et al., 2008). It is also accepted that filopodia control the persistence of cell migration by promoting the stabilization of focal adhesions at the cell front, stabilizing in turn the lamellipodium (Bornschlögl, 2013; Heckman & Plummer, 2013; Mattila & Lappalainen, 2008).

2.2.1. Mechanisms of filopodia formation and actin regulators

The development of filopodia is mainly controlled by proteins of the formin family, of which the most studied *mammalian diaphanous 2* (mDia2) protein belongs. mDia2 catalyzes the processive assembly of G-actin monomers at the tip of filopodia, promoting polymerization. Other NPFs sustain this process, such as the *insulin receptor phosphotyrosine 53 kDa substrate* (IRSp53), Ena/VASP and profilin-1 proteins (Campellone & Welch, 2010; Chhabra & Higgs, 2007; Mellor, 2010). The formation of filopodia can occur *de novo* from the plasma membrane or from barbed ends of actin filaments, generated by a Arp2/3-dependent mechanism, without branching out. *De novo* formation of filopodia occurs as follow: the mDia2 protein is activated by Cdc42 which induces its association with plasma membrane lipids at the leading edge (Goh et al., 2012). Cdc42 also binds and recruits the scaffolding protein IRSp53 (*via Cdc42/Rac-interactive binding* (CRIB) motif), a member of the *inverted-Bin-Amphiphysin-Rvs* (I-BAR) family protein, known for their ability to bend the

membranes *via* their N-terminal I-BAR domain. IRSp53 localized at the basis of the forming filopodia and then bends the plasma membrane outwards (Ahmed et al., 2010). The profilin-1:G-actin:ATP complex is finally recruited in order to allow the formation of actin filaments, which push the plasma membrane outwards and give shape to the filopodia (Le Clairche & Carrier, 2008; Ridley, 2011). Fascin, another actin-binding protein, is important in holding the actin filaments in a parallel direction along the filopodia, acting as a bridge and giving the characteristic shape of parallel bundles (Machesky & Li, 2010) (Figure 6). Loss- and gain-of-function approaches have shown that mDia2 depletion strongly inhibited filopodia formation, while a constitutively active form of mDia2 induced the accumulation of long and linear actin filaments in lamellipodia which subsequently exhibit high tendency to converge into filopodia (Yang et al., 2007). Moreover, mDia2 is highly-concentrated at the tip of cortical neurite filopodia (Dent et al., 2007; Yang et al., 2007). These results suggest that mDia2 protects the fast-growing (+) ends of actin filaments from capping and promotes their linear polymerization without branching, typical of filopodia.

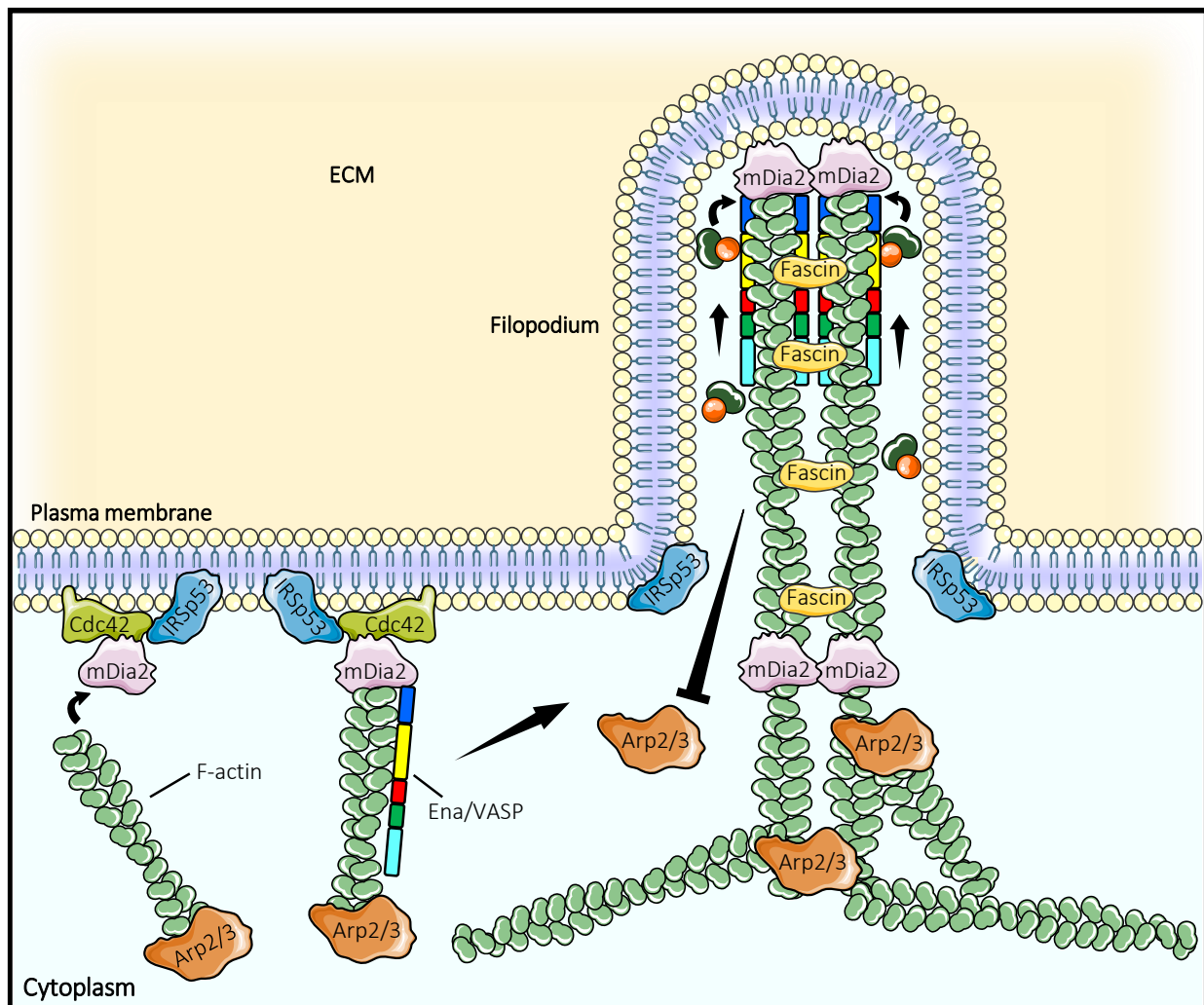


Figure 6. For caption see next page.

Figure 6. Molecular actors involved in filopodium formation. The action of the GTPase Cdc42 induces filopodia formation either from a pre-existing actin network or *de novo*. In the first case, Cdc42 activates mDia2 which polymerizes actin from a pre-existing network. In the second case, Cdc42 activates mDia2 which polymerizes actin and creates new filaments. Cdc42 can also recruit and activate the IRSp53 protein, which is responsible for membrane curvature at the base of the filopodium. Once the filopodium begins to grow from the plasma membrane, the filaments are bound together, forming actin bundles, by the fascin protein. At the tip of the filopodium, Ena/VASP proteins promote processivity and polymerization of the actin filaments also thanks to profilin-1, which supplies actin monomers to the growing end. In addition, mDia2 allows branching-free growth of actin filaments by excluding Arp2/3 from the filopodia growth zone.

2.2.2. Rho GTPases and filopodia formation

The Small GTPases of the Rho superfamily are involved in the development of the actin filaments during the formation of filopodia, and Cdc42 plays a crucial role (Nobes & Hall, 1995). Once Cdc42 is activated by GEFs, it recruits IRSp53 which leads membrane bending. This deformation acts as a platform for assembling the complex and once actin regulators are recruited the polymerization is started, generating the filopodium (Ahmed et al., 2010).

The role of Cdc42 in filopodia formation has been the focus of many studies. Expression of a dominant-negative form of Cdc42 impaired cell spreading and inhibited filopodia formation (Guillou et al., 2008). Moreover, by *fluorescent resonance energy transfer* (FRET), Peng and colleagues have shown that Cdc42 binds mDia2 and this interaction is essential for the recruitment of mDia2 at the tips of filopodia in migrating fibroblasts (Peng et al., 2003). Another strategy was to produce an engineered membrane receptor able to recruit activated Cdc42 at the plasma membrane. Inducible recruitment of Cdc42 to these receptors stimulated actin polymerization at the plasma membrane resulting in the formation of filopodia-like structure and recruitments of other proteins such as Ena/VASP (Castellano et al., 1999).

2.3. Formation of filopodia *versus* lamellipodia: the regulatory roles of Arp2/3 and profilin-1

As stated in the previous paragraphs, formation of lamellipodia and filopodia share common determinants. Indeed, extensive data indicate that proteins of the Ena/VASP family actively participate to both processes, using similar mechanisms, *i.e.* stimulation of actin polymerization and anti-capping activity. It therefore appears from the literature that the protrusive structure preferentially formed (lamellipodium or filopodia), tightly depends on Arp2/3 and profilin-1 availability. In cells that generally develop filopodia only, such as neurons, Arp2/3 might be excluded from the cell periphery, allowing mDia2 and Ena/VASP:profilin-1 to polymerize F-actin without branching. In fact, without any external influence, Ena/VASP promotes linear filament bundling *in vitro* (Barzik et al., 2005; Bear et al., 2002). A similar result was recently found for testis myotubes, in which filopodial-dependent migration was strongly stimulated by treatment with CK-666, an Arp2/3 inhibitor, supporting the notion that Arp2/3 has to be excluded for the development of filopodia (Bischoff et al., 2021).

Interestingly, Skrubber and colleagues have shown that profilin-1 expression level determines which leading-edge actin structure assemble from a common G-actin pool (Skruber et al., 2020). By introducing specific concentrations of profilin-1 in profilin-1 *knockout* (KO) cells, they have found that low levels of profilin-1 caused filopodia to form exclusively at the leading edge, while higher concentrations of profilin-1 inhibited filopodia and favored lamellipodia formation (Skruber et al., 2020).

3. Cell adhesions

During migration, the cell builds transient adhesions at the migration front to allow its anchorage on the substrate. The later maturation of these adhesions generates the force necessary for the contraction of actomyosin fibres. The force generated enables the cells to disassemble the adhesions in the back and pushes the entire cell body forward (Ridley et al., 2003). Focal adhesions contact the surrounding space through specific cell surface receptors, such as integrins, and interactions with the extracellular matrix (Giancotti, 1999). Adhesions also play a role in intracellular signalization and can control cell polarity through organization of the actin cytoskeleton (Giannone et al., 2007). In order for cell migration to be efficient, the assembly and disassembly of adhesions has to be tightly regulated. These events are connected to each other through a series of intracellular feedback loops that are spatially and temporally organized (Giannone et al., 2007; Machacek & Danuser, 2006; Totsukawa et al., 2004). This regulation takes place through the synergistic activity of the different Rho GTPases (Nobes & Hall, 1995; Rottner et al., 1999) already described in the previous paragraphs.

3.1. Extracellular matrix components

The ECM is a three-dimensional non-cellular structure present in the tissues of the organism and provides structural and biochemical support for the surrounding cells. The ECM is made up of proteoglycans, polysaccharides and proteins. The matrix is produced and secreted by specialized resident cells, *i.e.* fibroblasts, located in the connective tissues.

Proteoglycans are the major constituents of the matrix and act to fill most of the interstitial space. They give to the matrix a gel-like appearance (Järveläinen et al., 2009), hydration, buffering (Iozzo & Murdoch, 1996) or filtering (Morita et al., 2005) depending on the tissue in which they take part. A growing number of studies indicate that proteoglycans also play an important role in migration, adhesion and proliferation, acting as receptors for molecules or ligands contained in the surrounding space (Kirkpatrick & Selleck, 2007; Schaefer & Schaefer, 2010).

Hyaluronic acid is a polysaccharide that forms the ECM and gives tissues the ability to resist compressions thanks to its high capacity to absorb water. Its ability to bind the CD44 receptor makes it an important component during the formation of tumor metastases (Peach et al., 1993).

The ECM is mainly constituted of collagen, elastin, laminin and fibronectin. Collagen is the most abundant protein in the human body (Di Lullo et al., 2002). It provides traction strength to ECM and supports chemotactic cell migration (Rozario & DeSimone, 2010). Its function is to bridge other proteins, such as elastin, and to limit their stretching. Elastin fibres provide the rebound for tissues that undergo repeated stretching. This is the reason why collagen has the important role of protecting elastin by limiting its elongation, thanks to their close association (Wise & Weiss, 2009).

Last but not least, fibronectin is another ECM constituent protein that, through its binding with integrin receptors located on the cell surface of migrating cells, acts as the central player in the communication between the inner part of the cell and the surrounding space. Integrins belong to a large family of heterodimeric transmembrane adhesion receptors. They are synthesized as inactive monomers, and heterodimerization makes them functionally active. Fibronectin is recognized by heterodimer integrin receptors (α and β subunits) *via* a sequence consisting of *arginylglycylaspartic acid* (RGD) contained in fibronectin (Pytela et al., 1985). There are several α and β subunit isoforms and their combinations result in specific binding with ECM proteins. The $\alpha 5 \beta 1$ and $\alpha v \beta 3$ integrins specifically bind fibronectin, and are highly involved in tumor development, such as lung carcinoma, melanoma and glioblastoma (Adachi et al., 2000; Albelda et al., 1990; Bello et al., 2001). Two fibronectin isoforms exist, one containing the extra domain (ED)-A and one the ED-B, whose sequences are derived from alternative splicing. These two isoforms are synthesized during embryogenesis and their precise roles remain unclear. In adults, ED-A and ED-B fibronectins are only expressed under specific conditions such as tissue repair, angiogenesis and cell migration (Chauhan et al., 2004; Magnuson et al., 1991). Although the expression of isoform ED-B remains very restricted in healthy adult tissues, it is also highly expressed in breast cancer (Kaczmarek et al., 1994), brain tumors (Castellani et al., 1994) and prostate cancer (Locher et al., 2014). It has been shown that cancer cells can produce the ED-B fibronectin isoform independently of fibroblasts leading to its secretion in the stroma instead of being expressed at the plasma membrane (Midulla et al., 2000). The ED-A isoform was associated with an increase in $\alpha 5 \beta 1$ integrin expression in breast cancer cells cultured in matrigel and up-regulation of total fibronectin (Nam et al., 2010). Since fibronectin is an essential protein during *epithelial to mesenchymal transition* (EMT), a key mechanism for tumor progression (Petrini et al., 2017), the expression of these isoforms may increase tumor migration through the extracellular matrix. Also, these isoforms can be secreted instead of being expressed at the plasma membrane of cancer cells potentially impacting tumor therapy which requires direct binding of the therapeutic molecule at the tumor cell surface (Midulla et al., 2000).

3.2. Different types of adhesions

Chemotactic cell migration requires regulation of the adhesions cycle which consists in adhesion synthesis, adhesion stabilization and finally, adhesion degradation. During this process, adhesions differ in size, stability and molecular composition. Based on these characteristics, the level of adhesion maturation can be understood. The cycle of adhesion formation begins with the synthesis of the so-called *nascent adhesions*, small structures of about $0.2 \mu\text{m}^2$, appearing during the formation of the lamellipodium. Only a small population of nascent adhesions keeps maturing, while the others are disassembled within 76 seconds on average (Choi et al., 2008). The most stable adhesions continue to mature and give life to the *focal complexes* which are about $0.5 \mu\text{m}^2$ in size. These complexes mature definitively in very stable structures called *focal adhesions*, which are much larger ($1\text{-}5 \mu\text{m}$) (Choi et al., 2008). Focal adhesions can further develop into *fibrillar adhesions*, but these latter have a role in reshaping the ECM rather than promoting cell migration (Zaidel-Bar, 2003) (Figure 7).

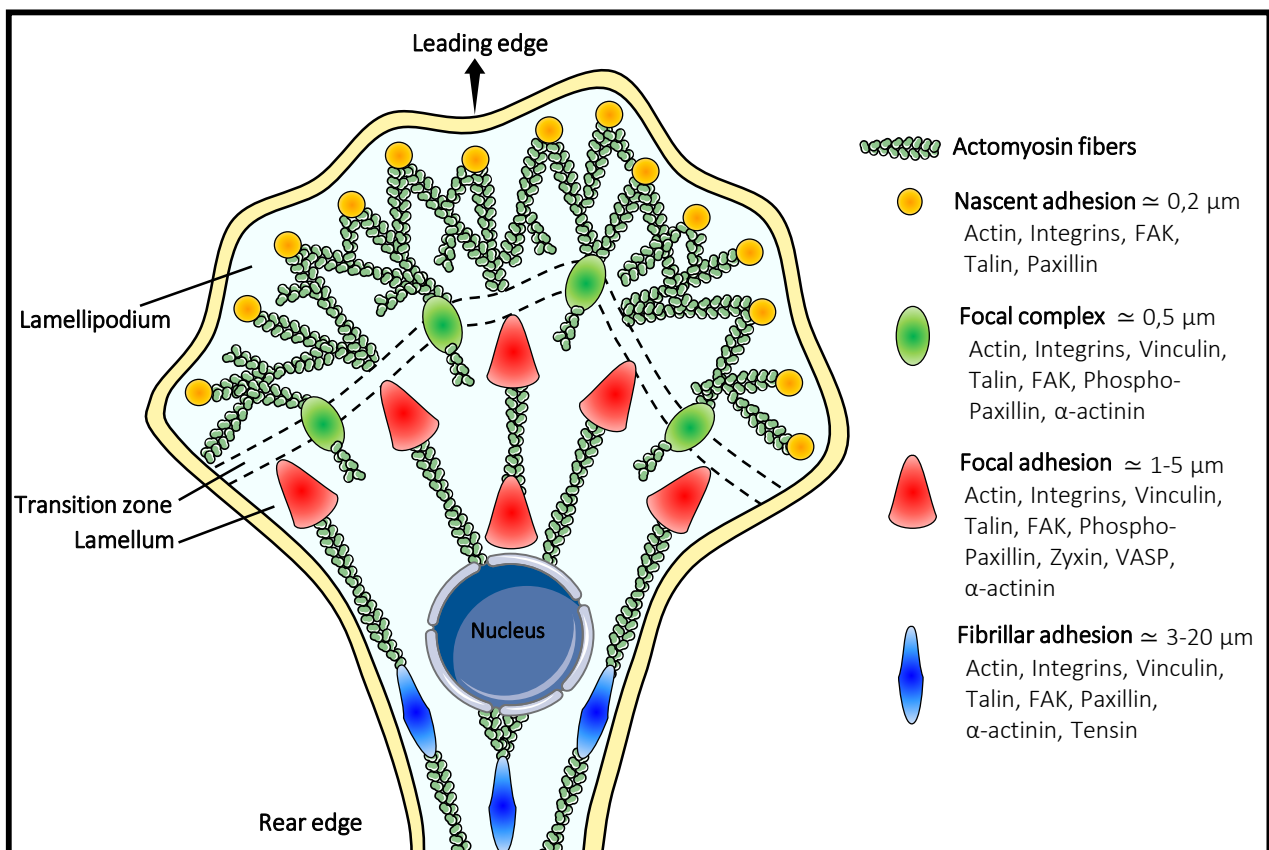


Figure 7. The different forms of adhesions of a migrating cell. Adhesions are tightly coupled to protrusions of the leading edge of the cell (lamellipodia and filopodia). Nascent adhesions form initially in the lamellipodium and their rate of formation correlates with the rate of protrusion. Nascent adhesions can be disassembled or mature to form focal complexes, located in the transition zone between the lamellipodium and lamellum. Maturation of focal complexes into focal adhesions is accompanied by the bundling and cross-bridging of actin filaments with myosin, forming actomyosin contractile fibers, which stabilizes adhesions and increases their size. Fibrillar adhesions form from maturation of focal adhesions and are mainly found at the rear of the cell.

Nascent adhesions are located at the edge of the nascent lamellipodium and are mainly made up of $\alpha 5\beta 1$ integrin, *focal adhesion kinase* (FAK), talin and paxillin (Bachir et al., 2014). Focal complexes begin to appear at the boundary between the lamellipodium and the lamellum and are constituted of $\alpha\beta 3$ integrins, FAK, phospho-paxillin, α -actinin (Laukaitis et al., 2001), vinculin (Rottner et al., 1999) and talin. Focal adhesions are located at the cellular periphery and are made of $\alpha\beta 3$ integrins, phospho-paxillin, vinculin, FAK, talin, zyxin and VASP (Gardel et al., 2010). In these adhesions, different tyrosine residues within paxillin are phosphorylated, regulating its activation status (Choi et al., 2008). Fibrillar adhesions are located in the central part of the cellular body and mainly contain $\alpha 5\beta 1$ integrin, vinculin, talin, FAK, paxillin, α -actinin and tensin (Zamir et al., 1999) (Figure 7).

3.2.1. Mechanisms of adhesions assembly

The genesis of nascent adhesions is induced by integrin activation. As already mentioned (paragraph 3), integrins are heterodimeric membrane receptors consisting of two distinct subunits, an α and a β subunit. These proteins consist of a long extracellular domain, a single transmembrane domain and a short cytoplasmic domain. The long extracellular domain is responsible for binding to many ligands of the ECM, such as fibronectin. Integrins generally have two conformational shapes: a *closed*, inactive form that does not allow interaction with other proteins and an *open*, active form, that can interact with molecular partners (Shattil et al., 2010). Integrin activation can be done by a signaling mechanism called “inside-out”, that starts from the integrin tails located in the cytoplasm (inside) toward the heads of the long domains placed in the extracellular space (out). Although a number of candidates have been studied (Liu et al., 2000) for triggering inside-out signaling, it is now accepted that talin is the first actor involved in integrin activation of the integrins and the formation of nascent adhesions. Talin acts as an intracellular activator by binding to the tail of the β integrin. This induces the dissociation between the α and β tails with the consequent conformational change that passes through the membrane and reaches the integrin-head on the extracellular side. This conformational change activates the integrins, increasing its affinity for extracellular ligands (Shattil et al., 2010) (Figure 8). Several *in vitro* studies have shown that talin 1 is able to bind and activate $\beta 1$, $\beta 2$ and $\beta 3$ integrin subunits (Simonson et al., 2006; Tadokoro, 2003). Accordingly, talin 1 depletion blocks the activation of $\beta 1$ and $\beta 3$ integrin subunits in platelets, *in vitro* and *in vivo* (Nieswandt et al., 2007).

Although less studied, it has been suggested that the activation of the integrins can also take place according to a mechanism called “outside-in” in which the signaling mechanism comes from the extracellular space (outside) as the ECM components, such as fibronectin, to the intracellular compartment (in), inducing the conformational changes described above (Figure 8). Whilst talin 1 is an essential component of integrin activation during the inside-out mechanism, it seems to play a secondary role in the outside-in mechanism. In fact, it has been demonstrated that the recruitment of talin takes place after the activation of the integrins in the CHO cells and is an essential process for cell spreading (Nieves et al., 2010). This result was supported by

in vivo studies in which the activation of the integrins was unaffected even upon talin KO in muscle development (Conti et al., 2009). This suggests that regardless of what signal the cell receives (from inside or outside), the result still leads to the activation of the integrins. Furthermore, it cannot be excluded that the inside-out and outside-in mechanisms are activated in parallel during the formation of adhesions for greater adhesion efficiency, depending on intracellular and/or extracellular conditions. In any case, integrin activation induces clustering with the adjacent integrins heterodimers, forming hetero-oligomers local clusters with further increased affinity for extracellular ligands (Shattil et al., 2010).

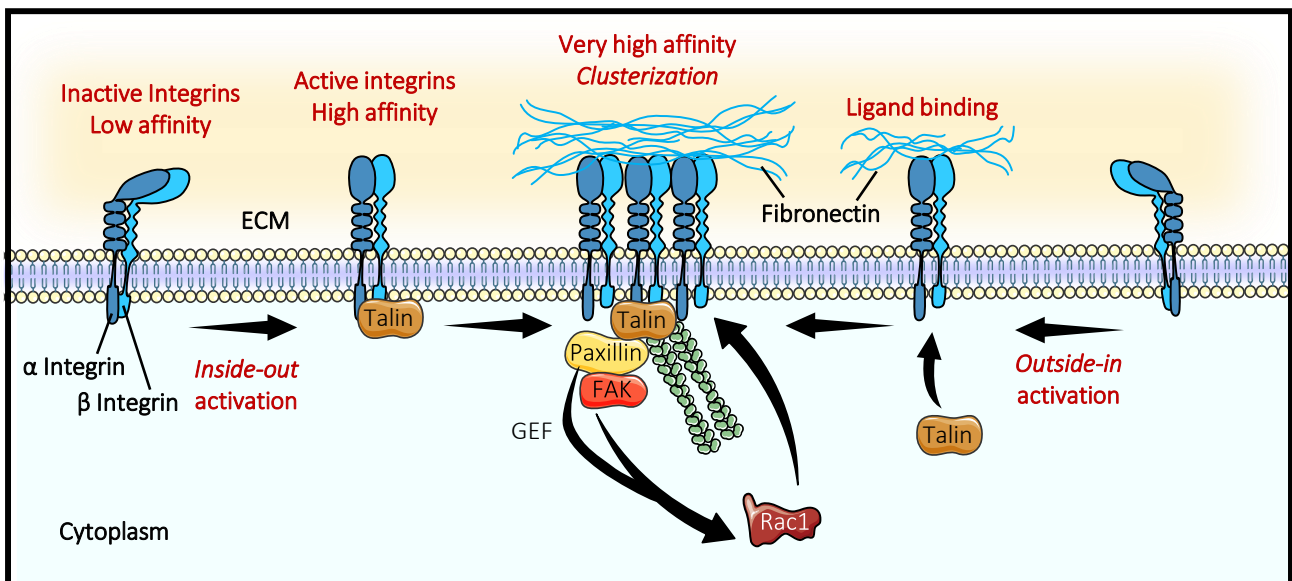


Figure 8. The integrin activation cycle. Integrin activation occurs by intracellular (*inside-out*) or extracellular (*outside-in*) pathways. In the first case, the activation of intracellular pathways result, in some cases, from the activation of a chemotactic receptor that induces the recruitment of talin to the cytoplasmic end of the β integrin. Talin induces a conformational change in integrins that acquire a high affinity for their ligand. In the second case, it is the binding of the ligand (e.g., fibronectin) to the integrins that causes the conformational change and their activation. Integrins with high-affinity for their ligand can form clusters, increasing their avidity for the substrates. Talin is then recruited and makes contact with F-actin and recruits paxillin, which in turn binds to FAK. These two proteins stimulate GEFs, which are responsible for local activation of Rac1, which in turn activates integrins, by a positive feedback mechanism.

3.2.2. Maturation of adhesions

The binding of talin is quickly followed by the recruitment of other proteins, such as paxillin, one of the first proteins present in nascent adhesions. Paxillin acts as a platform protein that regulates the interaction between the integrins and the actin cytoskeleton by modulating protein adhesion composition.

Paxillin contains four *Lin-11*, *Isl-1*, *Mec-3* (LIM) domains positioned in tandem. These domains are formed of double zinc-finger motifs and have the function of binding different proteins (Turner, 2000) (Figure 9A). Several reports have attempted to clarify the role of the different LIM domains in adhesion maturation and for example, beyond paxillin, proteins containing the LIM domain have the ability of binding the cytoplasmic tail of β integrins (Wixler et al., 2000). Although it is unclear which of these domains is involved,

paxillin also interact with $\beta 1$ integrins. In fact, it has been found that paxillin can bind to synthetic peptides mimicking the cytoplasmic tail of the $\beta 1$ integrin in chicken embryo cell lysate (Schaller et al., 1995) and, more recently, paxillin has been demonstrated to co-immunoprecipitate with $\beta 1$ integrin in neural cells (Chen et al., 2000). Recently, the LIM4 terminal domain of paxillin has been found to bind the plasma membrane and also interact with the cytoplasmic tail of $\beta 3$ integrin (Ripamonti et al., 2021). Specifically, the authors have shown that mutation of specific paxillin residues, capable to interact with $\beta 3$ integrin, blocks adhesion maturation and leads paxillin to slide on the substrate (Ripamonti et al., 2021).

The N-terminal region of paxillin controls most of its signaling activity and provides the specificity for interaction with individual partners, such as dock180, ELMO, vinculin and actopaxin. Furthermore, the N-terminal domain is the target for phosphorylation by tyrosine kinases. FAK phosphorylates paxillin at two main positions, tyrosine 31 and tyrosine 118 (Bellis et al., 1995; Schaller et al., 1995). The consequence of phosphorylation mainly consists in regulating the dynamics between the adhesion complex and the actin network (Nakamura et al., 2000). Although these phosphorylations are not necessary for the localization of paxillin in maturing adhesions, they are instead important for the recruitment of Crk and p130^{CAS} (Kiyokawa et al., 1998) which in turn promotes the recruitment of dock180 and ELMO proteins for the formation of an active Rac1 GEF complex. This complex finally activates Rac1 to promote cell migration (Brugnera et al., 2002) (Figure 9A).

While paxillin has a scaffold function to spatially and temporally integrate the action of the complexes in the adhesion sites (Deakin & Turner, 2008), vinculin has a structural role through direct interaction with the actin cytoskeleton (Galbraith et al., 2002). Once vinculin has been recruited by paxillin (Turner et al., 1990) it binds the actin filaments *via* its C-terminus and talin *via* its N-terminus (Humphries et al., 2007). This dual interaction is necessary for vinculin activation (Chen et al., 2006; Gilmore & Burridge, 1996). Once this complex has been formed, the focal adhesions are finally mature and can resist very intense forces (Hirata et al., 2014) (Figure 9B).

The maturation and stabilization of adhesion complexes enable the cells to exert the force necessary for their movement. The contraction of the actin fibres depends on non-muscle myosin IIA (Cai et al., 2006) which allows the actin filaments to slide over each other, generating the force needed to move the cell forward. Reversible phosphorylation of myosin IIA by kinases regulates its continuous activity on contraction of actin filaments (Parsons et al., 2010) (Figure 9B).

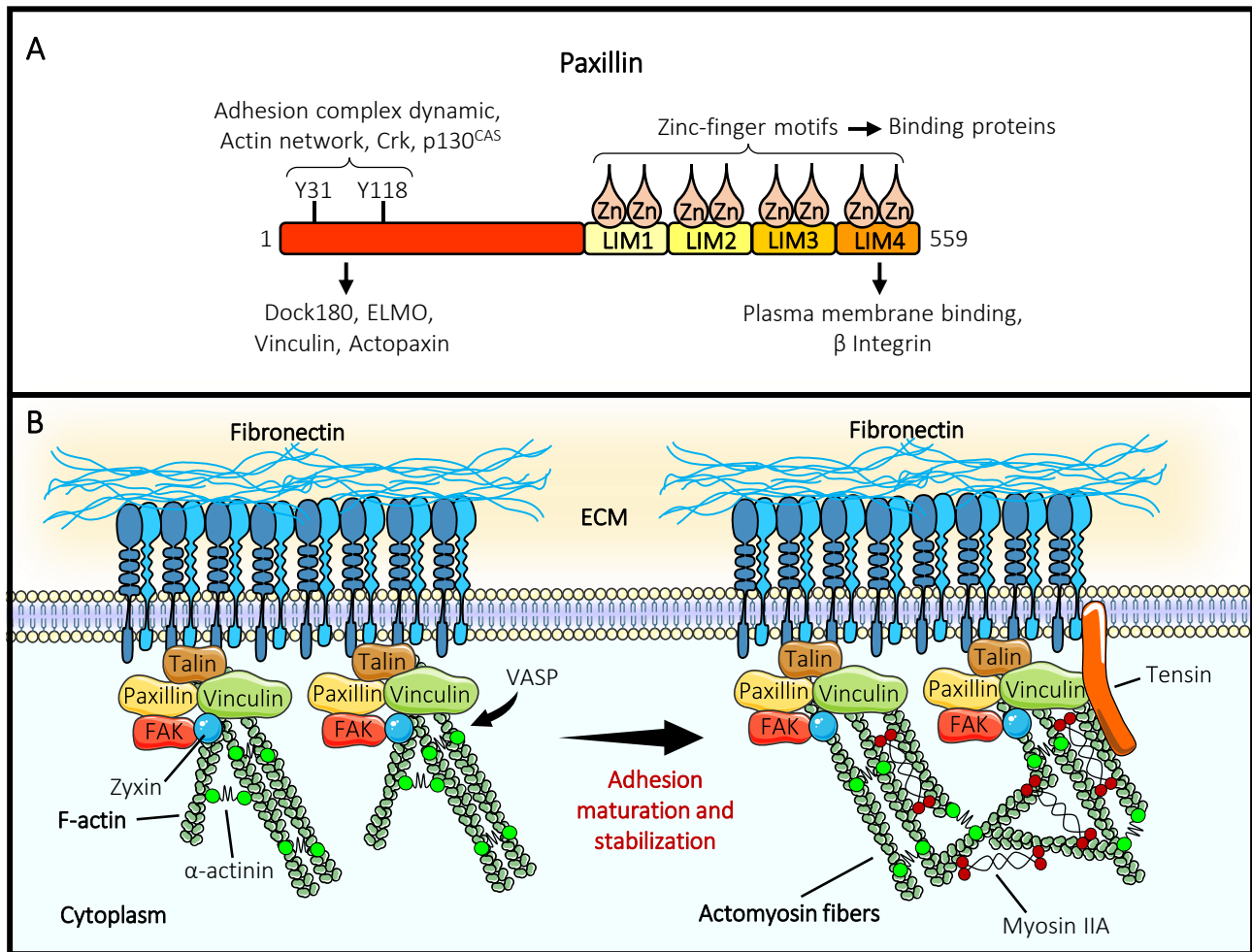


Figure 9. Structure of paxillin and adhesion assembly. **A** | Paxillin is a scaffold for the recruitment of several signaling proteins to the plasma membrane. Paxillin contains specific tyrosine residues that can be phosphorylated at positions 31 and 118, which specifically relates to induction of adhesion complex organization, actin network dynamics and recruitment of Crk and p130^{CAS} proteins. The N-terminal end of Paxillin also recruits ELMO1 and its GEF dock180, as well as adhesion proteins such as Vinculin and Actopaxin. Paxillin contains four LIM domains, capable of binding other proteins (*via* zinc-finger motifs) and plasma membrane, as well as β integrins (*via* the LIM4 domain). **B** | During the assembly of adhesions and their maturation, additional proteins are recruited, such as zyxin and vinculin, the latter of which binds to talin and establishes actin binding. α-actinin and myosin IIA allow actin filaments to bind together, be stabilized, and contract. During the late stage of adhesion maturation (fibrillar adhesion), tensin allows further stabilization by connecting integrins to actin filaments.

3.2.3. Mechanisms of adhesions disassembly

The disassembly of adhesions is an essential step for the cell to move forward and takes place both at the migration front (lamella-lamellipodium interface) and at the rear of the cell. Adhesion disassembly occurs *via* a protease-dependent cleavage mechanism and/or *via* endocytosis. Cleavage of specific adhesion proteins by the calpain proteases is a main determinant of adhesion disassembly (Franco et al., 2004). In fact, the inhibition of calpains either by inhibitors or pharmacologically active molecules, such as calpastatin or *N*-acetyl-L-Leu-Leu-Norleu-al (ALLN) respectively, blocks the adhesion disassembly process (Bhatt et al., 2002). Among the proteins identified as sensitive substrates for calpain activity, we find β integrins, FAK, paxillin, talin 1 and vinculin. Furthermore, the existence of two different isoforms, calpain 1 and 2, induces the proteolytic

cleavage of different adhesion molecules (Du et al., 1995; Franco et al., 2004; Pfaff et al., 1999; Serrano & Devine, 2004) (Figure 10). In fact, the production of a calpain-resistant talin 1 mutant strongly reduces the disassembly rate of adhesions and the use of *small interfering RNA* (siRNA) against calpain 2 inhibits the cleavage of paxillin, FAK and talin 1 (Franco et al., 2004).

The disassembly of adhesions is also regulated by endocytosis mechanisms. Ezratty and colleagues have demonstrated that dynamin, a protein that mediates plasma membrane fission during clathrin-mediated endocytosis, contributes to focal adhesion disassembly by removing integrins and other components from adhesion sites (Ezratty et al., 2005). Indeed, the authors have found that dynamin strongly co-localizes with focal adhesions during disassembly induction, and expression of a dominant negative form of the protein, mutated within the GTP-binding site, totally blocked directed cell migration in a wound healing assay (Ezratty et al., 2005). The importance of clathrin-dependent endocytosis of integrins in focal adhesion disassembly was also described by Chao and Kunz, showing that depletion of dynamin 2 and *adaptor protein* (AP) 2 blocked $\beta 1$ integrin internalization (Chao & Kunz, 2009) (Figure 10).

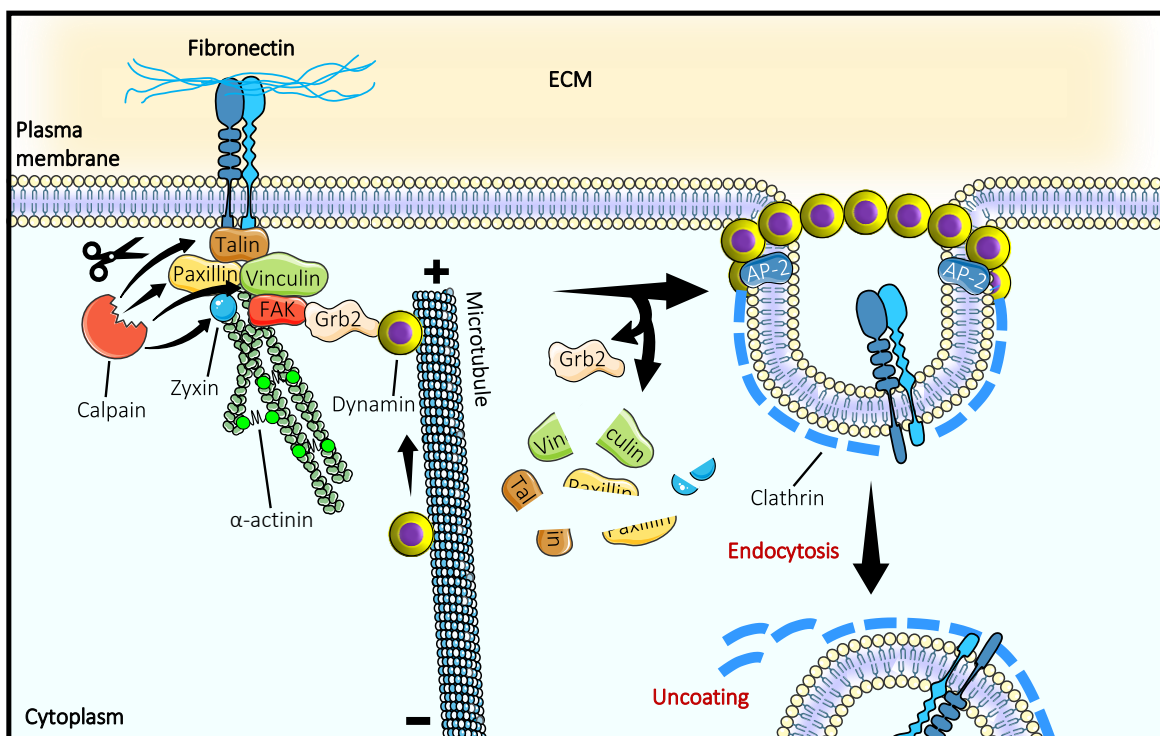


Figure 10. The adhesion disassembly mechanisms. The proposed model for the disassembly of adhesions describes that different destabilizing signals reach the adhesion sites. These signals arrive *via* microtubules or directly from the cytoplasm in the case of calpains. Calpain, can cleave vinculin, paxillin, zyxin and talin. Microtubules reach and interact with adhesions, in part through association *via* dynamin 2 and FAK. This interaction is mediated by the adaptor protein Grb2, which binds, on the one hand, to phosphorylated tyrosines of FAK and, on the other hand, to the proline-rich domains of dynamin 2. In addition, dynamin 2 can promote endocytosis of adhesions *via* clathrin adaptor proteins, such as AP-2. Dynamin 2 generates a collar in the forming vesicle where it pinches off from the plasma membrane.

Microtubules have been recognized as candidates for the stimulation of focal adhesion disassembly (Small et al., 2002) (Figure 10). The first findings came from Kaverina and colleagues which have shown that adhesions sites are specifically targeted by microtubules at the retracting edges of living fibroblasts (Kaverina et al., 1999) for their disassembly. Incubation of cells with nocodazole, a depolymerizing agent of microtubules, induced a lower adhesion turnover and a keep going elongation outwards of adhesion complexes already formed. Following nocodazole washout, microtubules regrew and localized again within disassembling focal adhesions (Kaverina et al., 1999).

3.3. Endocytosis of integrins

As already mentioned in the previous paragraph, endocytosis of integrins is the final step that allows the degradation or disassembly of adhesions. Integrins are also internalized to be recycled to new adhesions sites (Margadant et al., 2011). This mechanism takes place *via* a clathrin-dependent or clathrin-independent mechanism, the latter involving caveolins. Among these two mechanisms of internalization, clathrin-dependent endocytosis is the best-characterized. The initial phase consists in the formation of specific areas of the inner face of the plasma membrane in which the structures to be internalized are clustered. Slight membrane depressions are formed, called “coated pits” because surrounded by clathrin proteins. As the icosahedron structure forms, the invagination of the membrane becomes more evident. The closure and scission of the vesicle is due to dynamin, a protein that is arranged in a ring around the neck of budding vesicle (Kaksonen & Roux, 2018). Dynamin is a GTPase that exploits the hydrolysis of GTP in GDP for final scission of the vesicle from the plasma membrane (Mousavi et al., 2004). Once the coated vesicle has formed, clathrin is released and returns to the plasma membrane to form new coated pits (Figure 11).

During the disassembly of adhesions, different proteins are quickly recruited, together with clathrin, for integrin internalization, such as the adaptors *disabled homolog 2* (DAB2), *autosomal recessive hypercholesterolemia* (ARH) and NUMB (Ezratty et al., 2009; Nishimura & Kaibuchi, 2007). These proteins recognize the NP-xY-motif in the β integrin cytoplasmic tails and then interact with clathrin and dynamin to regulate integrin endocytosis. Depletion of NUMB by siRNAs impaired both integrin endocytosis and cell migration (Nishimura & Kaibuchi, 2007) while ARH and DAB2 downregulation prevented microtubule-induced focal adhesions disassembly, also resulting in impaired cell migration (Ezratty et al., 2009). It has recently been demonstrated that AP-2, the most abundant clathrin adaptor, is also implicated in endocytosis of integrins. In fact, AP-2 binds to the cytoplasmic tail of $\alpha 2$ and $\alpha 4$ integrins inducing their endocytosis (De Franceschi et al., 2016) (Figure 11).

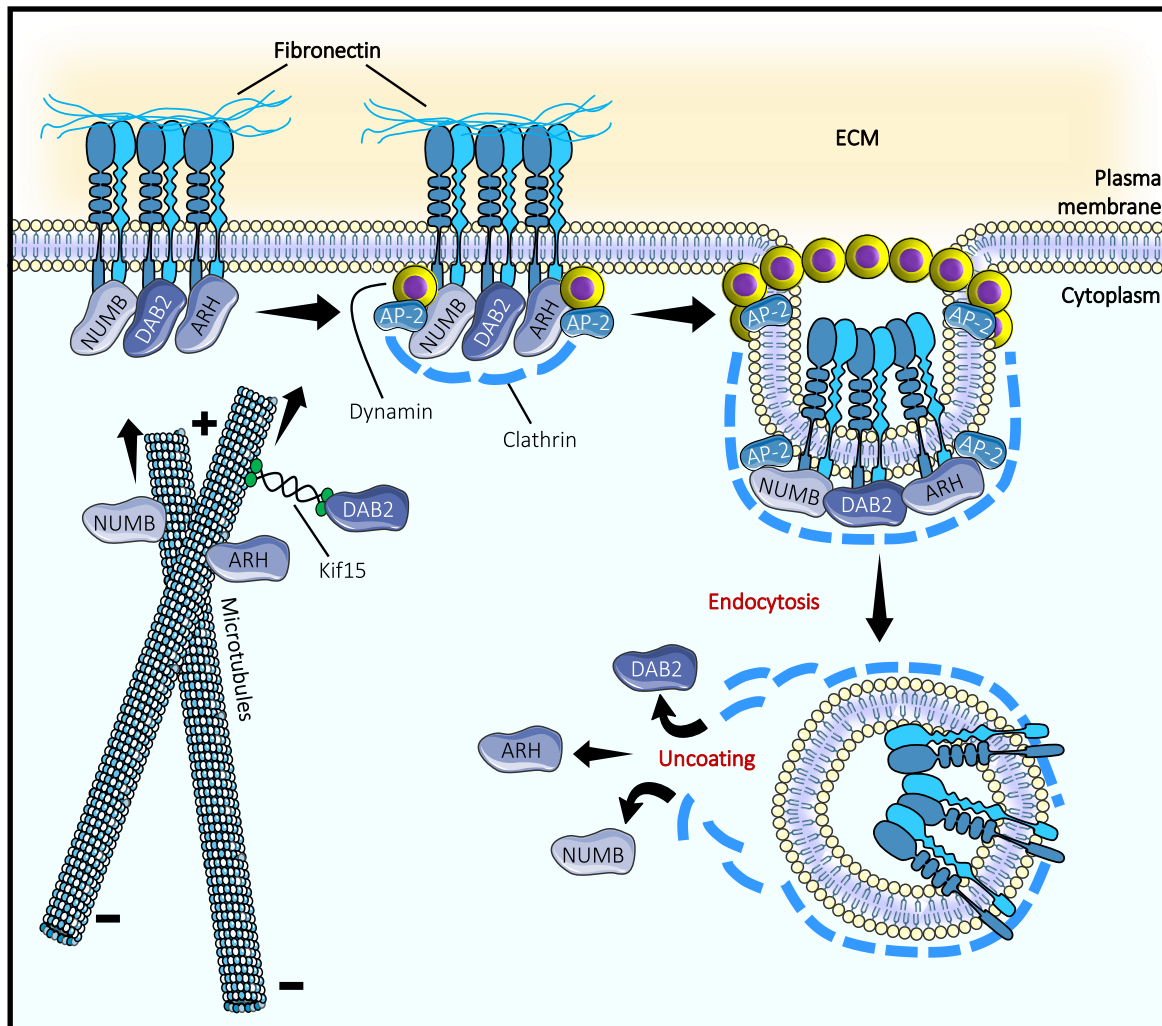


Figure 11. Clathrin-dependent endocytosis of integrins. Integrins to be endocytosed are recognized by clathrin adaptor proteins, such as AP-2, DAB2, ARH, and NUMB, which arrive *via* the microtubule pathway, also due to the transport employed by the kinesin Kif15. Clathrin and dynamin 2 assemble around the cargo, along with other accessory proteins to form the plasma membrane invagination. Again, dynamin 2 allows the vesicle to detach from the cell membrane and be endocytosed. Finally, the vesicle loses its clathrin coat, as well as the other adaptor proteins and integrins are recycled.

For a long time, it has been thought that the internalization of integrins occurs only in the rear of the cell during migration, to allow the detachment of the retraction zone from the ECM (Bretscher, 1996). Today, we know that endocytosis actually occurs throughout the entire cell surface, even at the migration front, with no specific compartmentalization (Rappoport & Simon, 2003). The peculiarity lies in the different molecular actors involved during the endocytosis processes in the migration front and in the rear of the cell. In fact, in the migration front of polarized cells, the internalization of integrins takes place *via* processes involving the interaction between clathrin and NUMB (Nishimura & Kaibuchi, 2007).

At the cell rear, where the disassembly of adhesions becomes massive, *kinesin family member* (Kif) 15 promotes the recruitment of DAB2 to trigger FAK- and dynamin-dependent vesicle scission (Eskova et al., 2014; Ezratty et al., 2005, 2009). Noteworthy is the different distribution of AP-2 during cell migration of

glioblastoma cells. By the use of spinning-disk confocal and light-sheet microscopy, Kural and colleagues have shown that AP-2-coated pits initiated on the dorsal surface of the cell, at the leading edge, and continued to grow as they moved toward the back of the cell. Interestingly, these coated pits were absent from the corresponding ventral part of the cell, revealing a clear dorsal/ventral asymmetry (Kural et al., 2015) (Figure 11).

3.4. Intracellular trafficking and recycling of integrins

Vesicular trafficking is essential during cell migration because it regulates the localization of the different actors located at the plasma membrane, such as integrins and other receptors, and is closely coordinated from a spatio-temporal point of view. Although some integrins are degraded *via* the lysosomal pathway, many studies suggest that the largest pool is recycled back to the plasma membrane (Caswell & Norman, 2006; Morgan et al., 2009; Scita & Di Fiore, 2010). This direct route to the plasma membrane is controlled by *sortin nexin 17* (SNX17) and *sorting nexin 31* (SNX31). These proteins are found in *Ras-related protein Rab 5* (RAB5) early endosomes and by binding to the cytoplasmic tail of β integrins, they can divert traffic to the recycling route (Böttcher et al., 2012; Tseng et al., 2014) (Figure 12). From here the integrins return to the membrane *via* a slow recycling mechanism, driven by *Ras-related protein Rab 11* (RAB11) and *ADP-ribosylation factor 6* (ARF6) passing through the perinuclear recycling compartment. The alternative is the *Ras-related protein Rab 4* (RAB4)-dependent fast recycling mechanism that does not pass through the recycling compartment (Bridgewater et al., 2012). The option of one of these two mechanisms seems to be due to the activation status of the integrins. In fact, although active and inactive integrins are endocytosed via clathrin- and dynamin-dependent early endosomes routes, inactive $\beta 1$ integrins are rapidly recycled via the actin- and RAB4-dependent route at the plasma membrane, while active $\beta 1$ integrins pass through the RAB11-dependent recycling route close the perinuclear compartment before returning to the plasma membrane (Arjonen et al., 2012) (Figure 12). The consequence of this process is that the inactive forms of the β integrin are localized mostly to the membrane, while the active forms are more cytosolic. This could be due to the fact that the active forms are still bound to their ligands, such as fibronectin, and before being routed to the plasma membrane they undergo a proteolysis process that leads to the detachment of the ligand and makes the inactive integrin ready for a new activation cycle (Lobert & Stenmark, 2012). It has also been observed that only the inactive form of the integrins can be diverted to an extra *Ras-related protein Rab 7* (RAB7) positive compartment, called late endosomes (Arjonen et al., 2012) (Figure 12).

Although cellular trafficking of integrins has been extensively studied, little is known about anterograde transport from the site of synthesis, the *endoplasmic reticulum* (ER), to the site of maturation, the Golgi apparatus, for their secretion at the plasma membrane. The *endoplasmic reticulum-Golgi intermediate compartment* (ERGIC) is involved in ER-to-Golgi apparatus transport to facilitate the sorting of several cargos (Appenzeller-Herzog & Hauri, 2006), including integrins. An early report has shown that the cytosolic tail of $\beta 1$

integrin overlapped with the ERGIC 58K marker and partially with the ER KDEL marker (Martel et al., 2000). Another study showed that the rat homologue of TGN46, a protein involved in regulation of membrane traffic from and to *trans*-Golgi network (TGN), interacts with $\beta 1$ integrin and also colocalized with $\alpha 5$ integrin (Wang & Howell, 2000) (Figure 12).

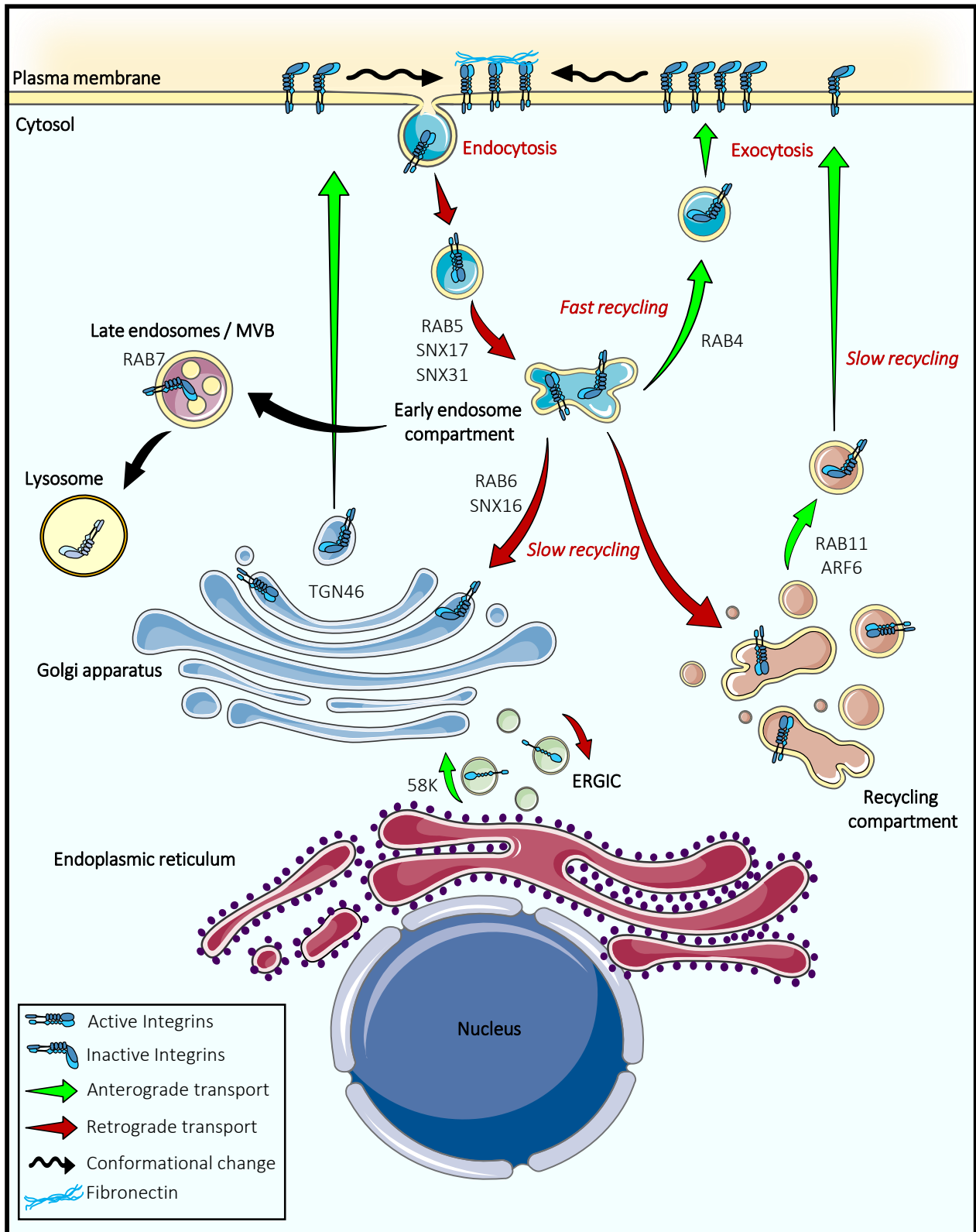


Figure 12. For caption see next page.

Figure 12. Intracellular trafficking and recycling of integrins. Internalized active integrins are directed to the early endosomal compartment (markers: RAB5, SNX17, SNX31). From here, they can undertake a *fast recycling* route and return to the plasma membrane (marker: RAB4) or follow a longer pathway (*slow recycling*) that can pass either from the perinuclear recycling compartment (markers: RAB11, ARF6) or to the Golgi apparatus (markers: RAB6, SNX16, TGN46) where, in all cases, integrins are inactivated, and then return to the plasma membrane through mechanisms of exocytosis. From the early endosomal compartment, integrins can be degraded through late endosomes (marker: RAB7) to end up in lysosomes. Integrins can also traffic into the ERGIC compartment (marker: 58K), which connects the endoplasmic reticulum and the Golgi apparatus.

In addition, overexpression of the wild-type form of TGN46 induced the retention of both $\alpha 5$ and $\beta 1$ integrins in the Golgi. Whilst, mutation of a TGN46 residue, which induces blockage of endocytosis and thus its accumulation at the plasma membrane, also induced the accumulation of the $\alpha 5$ and $\beta 1$ integrins at the plasma membrane (Wang & Howell, 2000). This shows that altering the trafficking of TGN46 also has an impact on the integrin trafficking to the periphery and this occurs through a direct interaction.

More recently, several studies have also shown that integrins are transported *via* the Golgi network by retrograde transport (Riggs et al., 2012; Shafaq-Zadah et al., 2016). This is an alternative mechanism complementary to the slow recycling pathway described above. Retrograde transport to the Golgi is then followed by anterograde transport toward the migration front for integrin secretion in a polarized manner, which is important in the process of adhesion formation and thus cell migration. The authors propose a specific function for these two different “slow” pathways, the one involving the recycling compartment and the one involving the Golgi apparatus. It would appear that recycling of $\beta 1$ integrins through the RAB11-recycling compartment is important for random migration (White et al., 2007), whereas recycling of $\beta 1$ integrins through the Golgi apparatus is useful for persistent migration (Shafaq-Zadah et al., 2016) (Figure 12). These results demonstrated that the Golgi-to-plasma membrane route of $\beta 1$ integrins is essential for persistent migration.

4. Exocytosis and cell migration

Many studies have indicated that biased vesicle trafficking toward the leading edge is crucial for the different steps of directed migration (Fletcher & Rappoport, 2010). Focal exocytosis of vesicles at the cell front can indeed accomplish several tasks, such as the recycling of integrins (Huet-Calderwood et al., 2017; Lawson & Maxfield, 1995; Paul et al., 2015), the delivery of bulk membrane for efficient lamellipodium expansion (Bretscher, 1996), and the supply of matrix metalloproteinases for enhanced matrix degradation (Kean et al., 2009; Sneeggen et al., 2019). Other molecules trafficked in a migrating cell include receptors for chemotactic stimuli (Coombs et al., 2019; Maisel et al., 2018) and GTPases of the Rho family (RhoA, Rac1, Cdc42) participating in actin dynamics (Osmani et al., 2010; Williamson & Bass, 2015; Wu et al., 2011). Although focal exocytosis is well described during cell migration, the origin and diversity of the vesicles, as well as their modes of transport to the cell front are still unclear. Data obtained from several cell types indicate that recycling endosomes constitute an important source of membrane and cargo proteins that are incorporated at the

leading edge during cell migration (Kean et al., 2009; Proux-Gillardeaux et al., 2005; Riggs et al., 2012; Sneeggen et al., 2019; Tayeb et al., 2005; Veale et al., 2010, 2011). Using *time-lapse total internal reflection fluorescence* (TIRF) microscopy, post-Golgi vesicles of the constitutive secretory pathway were also found to exhibit polarized exocytosis toward the cell front of migrating fibroblasts and astrocytes (Letinic et al., 2009a; Schmoranzler, 2003).

4.1. Molecular mechanism of exocytosis: focus on SNARE proteins

Phospholipids coming from an internal source have to be incorporated into the plasma membrane. The two membranes have to fuse by a mechanism involving proteins called soluble *N-ethylmaleimide-sensitive factor attachment receptor* (SNARE) (Bonifacino & Glick, 2004). The carrier vesicles of the internal source contain the *vesicle-SNARE* (v-SNARE) membrane protein that recognizes and binds the *target-SNARE* (t-SNARE) membrane protein. The most characterized SNARE complex is involved in the exocytosis of neuronal synaptic vesicles constituted of *vesicle associated membrane protein* (VAMP), also called synaptobrevin, *syntaxin* (STX) 1 and *soluble NSF attachment protein* (SNAP) 25. During vesicle docking, the first step consists in the interaction between VAMP (v-SNARE) and STX1 (t-SNARE) cytosolic domains. Together with SNAP25, the structure become a tight coiled-coil motif characterized by four-helix bundles. To counteract the repulsive forces of the two approaching membranes, the mechanism requires energy. The progressive folding of the SNARE complex results in the conversion from a *trans*- to *cis*- configuration in which SNAREs are firmly anchored to the membrane. The interaction forms the *trans*-SNARE complex, and the vesicles are in a docked state. Then, a bridge is formed and the first phospholipids of the two membranes begin to interact and mix. The fusion of the two membranes ends with the formation of a pore and the vesicular membrane melts completely into the cell membrane (Han et al., 2017) (Figure 13).

SNARE proteins can modulate cell migration by organizing the localization of the molecular actors involved. Experiments done in macrophages have established that recycling endosomes, expressing the v-SNARE VAMP3, constitute an important source of internal membrane incorporated at the cell front (Veale et al., 2010, 2011). Along with the addition of extra membrane, VAMP3-positive endosomes were also found to participate in the recycling of integrins in macrophages, HeLa, CHO and epithelial cells (Proux-Gillardeaux et al., 2005; Riggs et al., 2012; Tayeb et al., 2005; Veale et al., 2010), and in the secretion of the matrix metalloproteinases, for enhanced degradation of the extracellular matrix and increased cancer cell invasion (Kean et al., 2009; Sneeggen et al., 2019). The use of siRNAs against SNAP23 or VAMP3 reduces the localization of integrins at the migration front by inhibiting lamellipodium development (Veale et al., 2010). Botulinum and tetanus neurotoxins carry a proteolytic activity which selectively cleaves SNAREs. These neurotoxins are zinc proteases that have been studied to demonstrate the involvement of SNAREs proteins during cellular trafficking as they inhibit synaptic vesicles fusion to the plasma membrane (Galli et al., 1998).

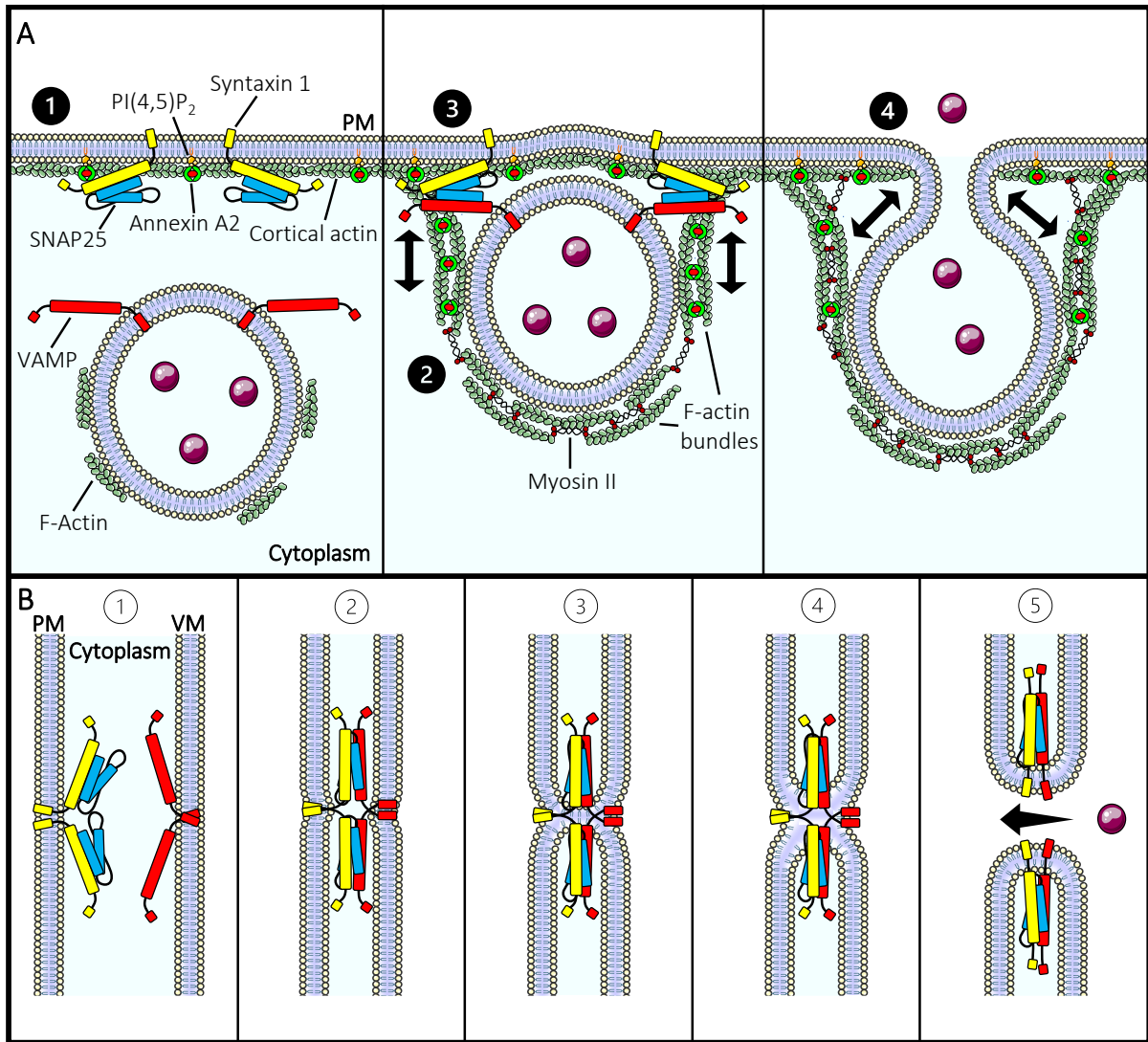


Figure 13. Molecular mechanisms of exocytosis. **A** | The vesicle is transported close to the plasma membrane, a process operated by microtubules and actin filaments (1). The SNARE molecular machine used for fusion is constituted by VAMP (red), anchored to the vesicle membrane, syntaxin 1 (yellow) and SNAP25 (blue) complex which is instead anchored to the plasma membrane. Vesicle is docked at the fusion site by bundles actin filaments (2) where SNARE complexes interact and the plasma membrane bends (3). The bundling of actin filaments surrounding the vesicle links the vesicle to the plasma membrane by recruiting several proteins, such as annexin A2, which interacts with both membrane lipid (PIP₂), actin bundles and myosin II. Membrane fusion is mediated by the formation of the SNARE four-helix bundle which pulls the vesicle membrane against the plasma membrane. A lipidic fusion pore is formed (4) and the vesicle membrane collapses into the target membrane and the content is exocytosed. Contraction of the actin coat, *via* myosin II, around the vesicle promote the expulsion of cargo. **B** | The membrane hemifusion model consists of the targeting of the vesicles toward the plasma membrane (PM) in which VAMP (red) and syntaxin 1 (yellow) are in a trans conformation (1). Initial interaction between VAMP and the cytosolic domains of syntaxin 1 (yellow) and SNAP25 (blue) occurs (2) and the energy released after the formation of the SNARE complex in trans conformation is used to bring the membranes into close proximity, this overcomes the repulsive force between the negative charges contained in the two membranes. After formation of the SNARE complex, the vesicle is docked. Hydrophobic contacts begin to form between the vesicle membrane (VM) and the plasma membrane (3). Subsequently, outer wall lipids begin to mix (4). The stalk continues to elongate until the inner walls of the membranes begin to mix, forming the fusion pore, and all lipids are incorporated into the plasma membrane (5).

Exocytosis involves cortical actin network beneath the plasma membrane. The role of a dense actin filaments is mostly to form a platform that drives exocytic vesicles to the fusion hot spot, regulates the fusion pore opening and provides the necessary strength for final fusion (Li et al., 2018). It has been proposed that the early steps of exocytosis consist in the polymerization of G-actin monomers to form an actin coated structure around the vesicles beneath the plasma membrane. Together with myosin proteins, this coated structure can then contract to squeeze the vesicles against the plasma membrane promoting the fusion process (Miklavc et al., 2012; Nightingale et al., 2011, 2012). This process is sustained by pre-existing actin filaments which scaffold and stabilize the vesicles onto the hotspot. Interaction between cortical actin and plasma membrane is sustained by the actin-nucleating factor, annexin A2, which is recruited at the plasma membrane upon cell stimulation and interact with SNAP23 (Gabel & Chasserot-Golaz, 2016; Umbrecht-Jenck et al., 2010). A recent study has shown that annexin A2 provides membrane bridges during exocytosis (Grill et al., 2018) facilitating both the docking and fusion steps (Figure 13).

4.2. Polarized exocytosis: Full-collapse fusion and Kiss-and-Run

Over the last 50 years, the debate on the nature and the role of the molecular machinery involved in the exocytosis event remained open. Nowadays, two different mechanisms of exocytosis have been proposed: a mechanism in which the secretory vesicle is completely fused to the plasma membrane and retrieved by a clathrin-coat-dependent mechanism, *i.e.* full-collapse fusion event, or a mechanism in which the vesicle is partially fused to the membrane and then endocytosed, *i.e.* kiss-and-run fusion event. Although exocytosis has been described extensively in neurons or in other cellular systems, such as adrenal cells and astrocytes (Bowser & Khakh, 2007; He et al., 2006; Ryan, 2003), exocytosis during cell migration is less characterized.

During chemotactic migration, the cell must produce a lamellipodium which is sufficiently developed to advance. In this context, the cell membrane at the front needs a source of phospholipids to develop properly and the coupled mechanism of exocytosis-endocytosis is essential (Bretscher, 2008; Schmoranzer, 2003). Whilst it remains a hypothesis, the following is the most credited model to explain how the exo-endocytosis mechanism sustain migration. By using photobleached experiments, Tanaka and colleagues have shown that the portion of the exocytosed membrane totally fuse (full spreading event) at the migration front of Dictyostelium and is moved dorsally and ventrally toward the back of the cell. Then it is internalized in the form of endosomes which are redirected, within the cell, toward the migration front for a new cycle of exocytosis (Tanaka et al., 2017). Interestingly, by using isotope-labelled surface, it has been calculated that it takes about 45 minutes to completely regenerate the cell membrane in Dictyostelium fast-migrating cells (Vogel et al., 1980). In support of this model of full-fusion polarized exocytosis, Schmoranzer and colleagues have shown that post-Golgi vesicles, loaded with the *low-density lipoprotein receptor* (LDLR)-GFP cargo, was polarized toward the leading edge of migrating fibroblasts (Schmoranzer, 2003) in a full spreading fashion. In polarized astrocytes, post-Golgi vesicles carrying the YFP-tagged vesicular stomatitis virus glycoprotein

exhibited biased exocytosis toward the cell front, while exocytotic events appeared uniformly distributed in non-polarized cells (Letinic et al., 2009).

The mechanism of kiss-and-run seems to be instead predominant in cells that secrete neurotransmitters, such as neurons and endocrine cells (MacDonald et al., 2006; Stevens & Williams, 2000). Little is known as to why the exocytic mechanism of full spreading is preferred over the kiss-and-run mechanism, and *vice versa*. It is likely that full spreading provides an important membrane source for the proper development of the leading edge. Moreover, this fusion mechanism is supported by dynamic F-actin assembly at the front, where lamellipodia are built, which provides sufficient membrane tension turning into a full spreading fusion (Wen et al., 2016). Otherwise, advantages of kiss-and-run events are that they can limit how much neurotransmitter is released due to a smaller fusion pore and they can recycle vesicles economically (Rizzoli & Jahn, 2007). A role of kiss-and-run events during cell migration is not yet established.

5. Receptors-induced chemotactic migration

As already introduced in paragraph 1.2, the main players of cell migration are chemotactic receptors that respond to the gradient by interacting with their own ligand. The most characterized receptors involved in cell migration are the seven-domain transmembrane GPCR and the RTK, which have been shown to mediate chemotactic response to chemokines and growth factors, respectively (SenGupta et al., 2021).

5.1. Receptor Tyrosine Kinases: focus on EGFR

There are 58 genes coding for RTKs in humans, which in turn are classified into 20 families according to the nature of their ligands and the molecular composition of their extracellular domain. These master regulators control several processes such as cell migration, invasion, proliferation and survival (Schlessinger, 2000) and numerous signaling cascades involving RTKs have a relevant impact on the development of human malignancies (Ségaly et al., 2015). Among the RTKs, the most involved in cell migration are EGFR, the *platelet derived growth factor receptor* (PDGFR), the *fibroblast growth factor receptor* (FGFR) and the *vascular endothelial growth factor receptor* (VEGFR) (Glen et al., 2011; Taeger et al., 2011).

The RTKs are plasma membrane receptors, characterized by a single α -helix transmembrane domain, a large extracellular N-terminal domain and an intracellular C-terminal domain. The C-tail harbors a specific domain with tyrosine kinase activity that catalyzes autophosphorylation (Ullrich & Schlessinger, 1990). The extracellular domain is involved in the homodimerization process of the receptor to make it active. Once the receptor is conformationally in the open state, EGFR dimers without its ligands. This homodimer is however unstable and may uncouple unless *epidermal growth factor* (EGF) is present. When EGF binds to the EGFR binding domain, it becomes stabilized triggering further changes within the transmembrane domain (Moriki et al., 2001). Rotation of the transmembrane domain transduces the conformational change to the intracellular C-terminal kinase domain resulting in a cross-phosphorylation of the cytoplasmic tails (Honegger

et al., 1989; Kourouniotis et al., 2016; Moriki et al., 2001) (Figure 14A). The phosphorylated residues are then recognized by adaptor proteins. Among them, *phospholipase C* (PLC γ) is the first to have been identified (Meisenhelder et al., 1989). Thanks to its *Src homology 2* (SH2) domain, PLC γ binds the phosphorylated tyrosines of the receptor, resulting in an increase in the turnover of *polyphosphoinositides* (PIPs), elevation of cytosolic calcium concentration and activation of *protein kinase C* (PKC). The second adaptor protein, the *growth factor receptor-bound protein 2* (Grb2) (Lowenstein et al., 1992) which is capable of activating a GEF called *son of sevenless* (Sos), identified for its ability to exchange GDP from the Ras protein for a GTP (Wolfman & Macara, 1990). The Ras protein can then bind the serine/threonine kinase Raf (Hallberg et al., 1994), which in turn recruits the *mitogen-activated protein kinase/ERK kinase* (MEK) which phosphorylates *extracellular signal-regulated kinases* (ERK) 1/2 (Kolch, 2000). All this work has made it possible to characterize this RTK-induced activation of the Ras/Raf/MEK/MAPK pathway (Cook & McCormick, 1993) (Figure 14B).

The PI3K/Akt is another major pathway activated by RTKs (Bjorge et al., 1990; Franke et al., 1995). PI3K activation phosphorylates and activates Akt, which is then recruited at the plasma membrane to exert several downstream effects, such as proliferation, cellular quiescence, cancer and aging (Díaz et al., 2012; King et al., 2015). Both the Ras/Raf/MEK/MAPK and PI3K/Akt pathways have been shown to be important for EGFR-induced cell migration. Indeed, overexpression of EGFR in breast cancer cell lines induces migration/metastasis via an MEK-dependent pathway (Verbeek et al., 1998), while inhibition of EGFR activation blocks migration of a breast cancer cell line (Hsieh et al., 2013). In this study, the use of inhibitors demonstrated that the effects of EGFR on migration via the PI3K/Akt pathway and the expression of the *matrix metalloproteinase 9* (MMP9) (Hsieh et al., 2013). It has been shown that EGFR activation induces FAK phosphorylation via its binding to integrin (Schlaepfer et al., 2004). Subsequently, c-Src is recruited into the FAK complex and different tyrosine residues are phosphorylated. This multiple phosphorylation is critical for FAK-mediated cell migration (Schlaepfer et al., 2004; Westhoff et al., 2004) by building up a bridge interaction between EGFR and FAK, which recruit FAK at the plasma membrane (Long et al., 2010). Mutation of EGFR are common in cancer and, in fact, EGFR amplification or expression of the constitutively active mutant EGFRvIII are found in many glioblastoma (Shinojima et al., 2003; Smith et al., 2001) (Figure 14B).

During chemotactic migration, the cell must continuously maintain a certain "sensitivity" thanks to the receptors at the membrane in response to their ligands. This mechanism helps the cell to protect itself in case of an excessive activation of the receptor and therefore an exaggerated intracellular response. In the absence of stimulation, the EGFR is continuously recycled via RAB11 recycling endosomes. The dynamics of this event leads to a slower mechanism of endocytosis and a faster mechanism of exocytosis, which results in an accumulation of EGFR at the membrane. If EGFR is activated by EGF binding the equilibrium is changed (Burke & Wiley, 1999; Herbst, 2004; Steven Wiley, 2003) and EGFR is rapidly internalized after triggering the intracellular response, spending more time into the recycling pathway.

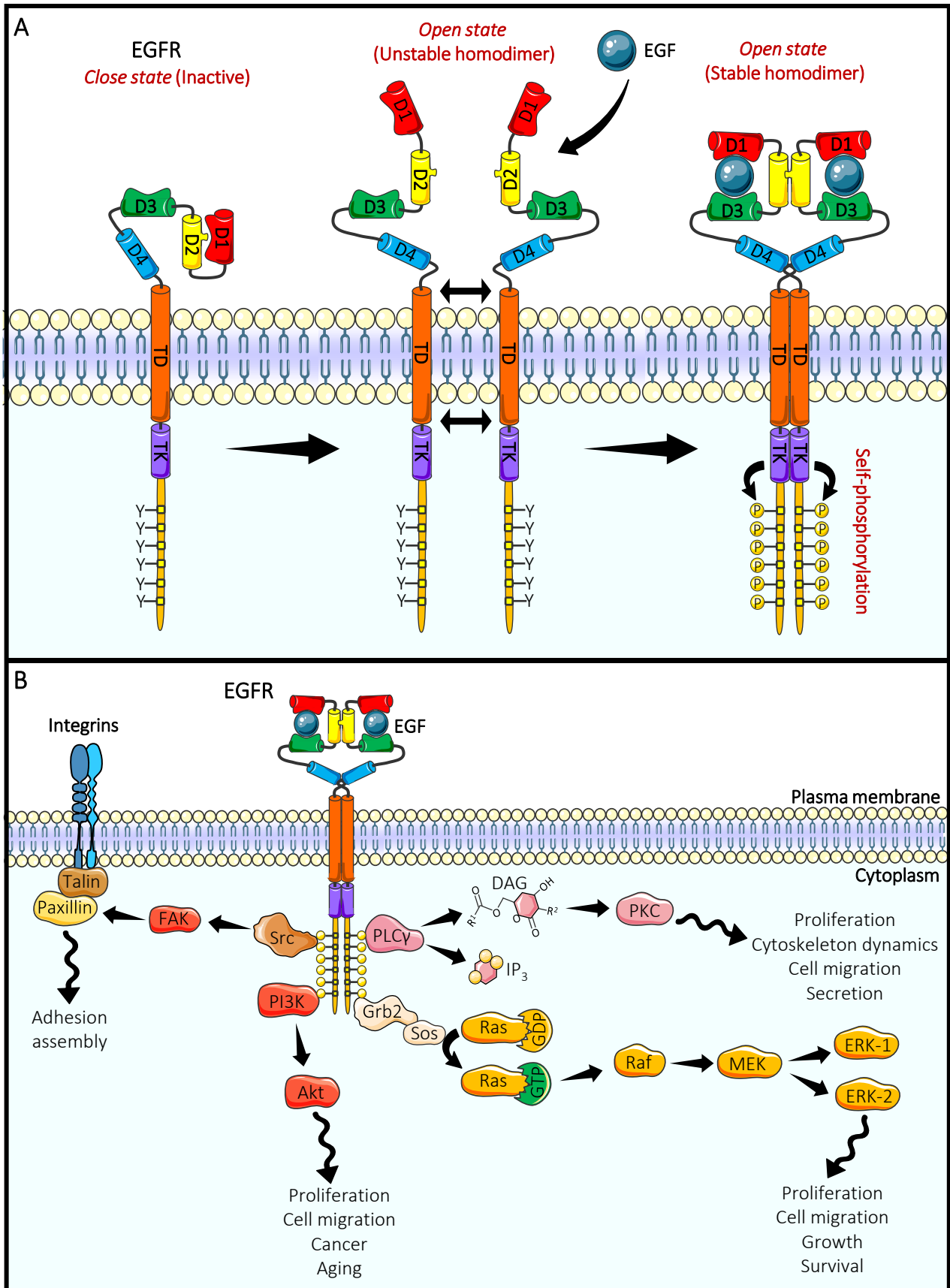


Figure 14. For caption see next page.

Figure 14. Representation of EGFR activation and its signaling pathways. A| Schematic representation of the EGFR and EGF-induced receptor activation. The extracellular region of EGFR consists of domains 1, 2, 3 and 4 (D1-D4); followed by a transmembrane domain (TD) and an intracellular region made up of a tyrosine kinase (TK) domain and a carboxy-terminal tail, rich in tyrosine residues. In the absence of EGF, EGFR can be in an inactive, closed state in which D1 and D2 interact or in an open and unstable state in which D1 and D2 do not interact revealing the pocket in which EGF can bind. Binding of EGF to the receptor (D1 and D3) induces dimerization with another receptor. This triggers a conformational change to the intracellular tail that leads the TK domain to autophosphorylate tyrosine residues within the carboxyl terminus. The receptor is then fully active triggering an intracellular signaling cascade. **B|** Signaling pathways of EGFR. After EGFR activation, several proteins are recruited at the carboxyl terminal tail of the receptor. Phospholipase C γ (PLC γ) binds directly to the receptor tail where it associates to plasma membrane PIP $_3$ and hydrolyze PIP $_2$ to produce 1,2-diaclyglycerol (DAG) and inositol (1,3,5)-triphosphate (IP $_3$). DAG remains localized at the membrane, so as to mediate the association of protein kinase C (PKC) to the cell membrane, followed by its activation, initiating a chain of phosphorylations, which will contribute to the functional responses of the cell. IP $_3$ is an intracellular cytoplasmic messenger, causing the release of stored Ca $^{2+}$ into the smooth endoplasmic reticulum and, therefore, the elevation of cytosolic Ca $^{2+}$ concentration (contraction and secretion). PI3K can also bind directly to EGFR tail and activates the Akt pathway leading to proliferation and tumor growth. The reduction of membrane PIP $_2$ concentration by PLC γ is in itself a signal for the modulation of PI3K activity, which modulates actin filament polymerization by interacting with various actin-binding proteins (profilin-1, cofilin, etc). EGFR activation also leads to Grb2 and Sos association which in turns promotes the removal of GDP with GTP on Ras that become active. Activated Ras activates Raf kinase which phosphorylates and activates MEK. MEK phosphorylates ERK1/2 triggering proliferation, cell migration, cancer growth and survival. Finally, EGFR activation induces Src-signaling which phosphorylates FAK and regulates integrin and adhesion assembly.

The degree of EGFR stimulation by its ligand defines its fate. If the stimulation is weak, the EGFR recruits and phosphorylates the AP-2 β 2 subunit and is endocytosed by clathrin-dependent mechanism (Rappoport & Simon, 2009; Robinson, 2015; Sigismund et al., 2005) and is transferred into RAB5 early endosomes to the perinuclear compartment where phosphatases will deactivate the receptor. Once the EGFR became inactive, it is recycled to the plasma membrane via RAB11 recycling endosomes. If, on the other hand, stimulation has been strong, EGFR is endocytosed by a clathrin-independent mechanism and is directly transported via RAB7-late endosomes to the lysosomes to be degraded (Bakker et al., 2017; Sigismund et al., 2005).

5.2. G proteins-coupled receptors

5.2.1. C-X-C chemokine receptor type 4 (CXCR4)

We now know that GPCRs and their chemokines are involved in physiological processes requiring cell migration, such as wound healing, angiogenesis and cancer progression (Rahmeh et al., 2012). One of the best characterized chemokine receptors is CXCR4, because of its role in the internalization of the human immunodeficiency virus as well as for its involvement in the progression of cancer (Chatterjee et al., 2014). The endogenous ligand of this receptor is CXCL12 (Lazarini et al., 2003). CXCR4 can trigger several signaling cascades regulating a range of biological processes. Following CXCL12 binding, conformational changes occur at the receptor level leading to the activation of heterotrimeric G proteins. Dissociation of the G α subunit from the G $\beta\gamma$ will be able to activate downstream signaling pathways that will orchestrate actin cytoskeleton reorganisation and cell migration. In fact, we can distinguish between the *i*) pro-migratory pathway dependent of the G $\beta\gamma$ subunits and PI3K activation, and *ii*) the pro-migratory pathway dependent of the G α subunits (Figure 15).

Although CXCR4 activates several classes of G α subunits, it is mostly coupled to the G α_i and G α_q (Teicher & Fricker, 2010). Maghazachi and colleagues were one of the first to demonstrate that CXCR4 could be coupled to several isoforms of the G α . By treating lymphocytes with blocking antibodies directed against specific subunits, they showed that G α_q was necessary for the induction of chemotaxis by CXCL12 (Maghazachi, 1997). Most of the functions of the CXCR4, including chemotaxis, are however sensitive to treatment with *pertussis toxin* (PTX), suggesting an essential role for the G α_i family (Rubin, 2009). Through the ADP-ribosylation of a cysteine residue located at the C-terminal end of the α_i subunit, this bacterial toxin inhibits the entire signaling cascade downstream of the G protein (Kaslow & Burns, 1992). The G α_i protein is a direct inhibitor of *adenylate cyclase* (AC) and it is able to reduce the production of cAMPs. Generally, cAMP can inhibit cell migration by increasing the activity of *protein kinase A* (PKA). Although its effects seem to vary from one cell type to another, PKA can inhibit *myosin light-chain kinase* (MLCK), which is essential for the activation of myosin II, and therefore for the maturation of adhesions. Furthermore, in a breast cancer cell line, it has recently been shown that the G α_{i2} subunit is capable of interacting with one of the Rac1 GEFs, ELMO1, in response to stimulation by CXCL12. This interaction seems to be essential for the activation of Rac1 as well as for the CXCR4-mediated chemotactic migration (Li et al., 2013) (Figure 15).

GPCRs are also endocytosed after their activation, inducing desensitization. Following the binding of the agonist, phosphorylation of the cytosolic C-terminal end of the GPCR induces the recruitment of β arrestin, thus initiating the endocytosis process (Krupnick & Benovic, 1998). β arrestin induces receptor internalization by interacting with endocytosis proteins such as AP-2 and ARF6 (Lefkowitz et al., 2006). It has thus been shown that a reduction in β arrestin levels in lymphocytes decreases the desensitization phenomenon and increases the coupling of CXCR4 to G proteins. However, these cells also show a loss of chemotactic response to CXCL12, suggesting that GPCR internalization is required for its chemotactic properties (Fong et al., 2002). In fact, CXCR4/ β arrestin coupling constitutes an intracellular platform that can induce activation of MAPK p38 and ERK1/2 (Luttrell et al., 2001; Rubin, 2009). These kinases induce chemotactic migration by activating/recruiting paxillin, MLCK, calpains and FAK (Huang et al., 2004) (Figure 15). Similar results were obtained in HEK293 cells overexpressing CXCR4. In these cells, siRNA against β arrestin blocks the activation of p38 and ERK, as well as chemotactic migration induced by CXCL12 (Cheng et al., 2000; Sun et al., 2002). As already described for EGFR, GPCR is internalized and dephosphorylated in order to be re-directed toward the plasma membrane (Krueger et al., 1997).

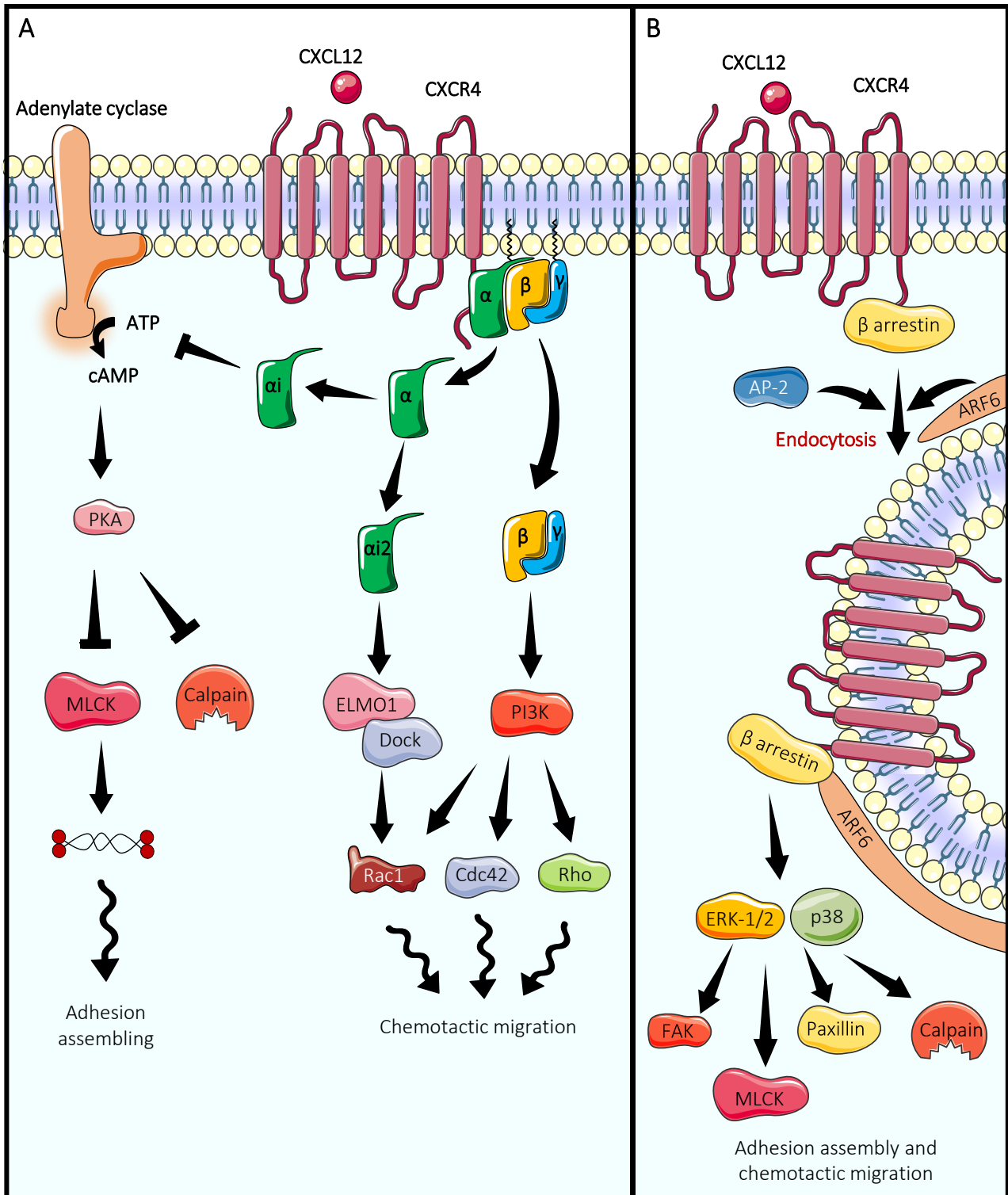


Figure 15. Representation of CXCR4 and its signaling pathways. A | CXCR4 activation induces the release of G α_i subunits that inhibit adenylate cyclase and stimulate adhesion formation. The G α_{i2} subunit has specifically been shown to allow the recruitment of ELMO1 and dock180 to the membrane, for subsequent activation of GTPase proteins, such as Rac1. The G $\beta\gamma$ subunits activate PI3K which results in the activation of other GTPases, Cdc42 and Rho, that together promote directional migration. B | CXCR4 signaling is rapidly desensitized after CXCL12 binding and the receptor is internalized. The intracellular C-terminus of CXCR4 is rapidly phosphorylated after ligand binding and this process is followed by recruitment of β arrestin, AP-2 and ARF6, allowing clathrin-mediated endocytosis. Although CXCR4 is internalized, β arrestin can still trigger different effects, such as ERK activation, thereby promoting cell migration.

CHAPTER II: AUTOPHAGY

6. Generalities and historical overview

The term "autophagy" derives from the Greek "auto" and "phagy", meaning to eat itself. It is a catabolic process characteristic of eukaryotes, in which a cell digests and recycles parts of itself, organelles and molecules, such as damaged mitochondria, aggregates, incorrectly conformed or long-lived proteins and other components in a regulated manner within the autophagic machinery pathway. Its recycling function allows the cell to reuse non-essential cytoplasmic elements for the synthesis of other molecules. Autophagy is essential to maintain energy levels, to help the cell to survive low-nutrient conditions, protect it against various stresses or get rid of intracellular waste which would compromise its proper functioning. For example, non-mitotic cells, such as neurons and muscle cells, rely heavily on autophagy to eliminate protein aggregates or defective organelles due to the fact that they are not able to dilute the accumulation of harmful substances in the cytoplasm through cell division (Damme et al., 2015). Defective autophagy leads to major neurodegenerative diseases such as Alzheimer's, Parkinson's, Huntington's, multiple sclerosis or other pathologies such as tumours, metabolic and immune alteration (Eskelinen, 2019). Clearly, autophagy is also involved in other cellular functions such as development, differentiation, inflammation and elimination of intracellular pathogens (Eskelinen, 2019). For these reasons, autophagy is a homeostatic cellular process which must be continuously balanced.

Historically, the first discoveries closely related to autophagy date back to the 1950s when Clark looked through his electron microscope at kidneys of newborn mice and noticed something he had never seen before. He later described this as membrane-bound structures within the cytoplasm of the kidney cells, in which altered mitochondria were contained (Clark, 1957). The discovery of autophagy also begins with that of the lysosome. De Duve succeeded in detecting the lysosomal activity in vesicle-like fractions by separation of cellular compartments through centrifugation. In 1955, de Duve named these compartments lysosomes, reflecting their digestive activity (de Duve et al., 1955). The same year, Novikoff and de Duda obtained confirmation of the presence of hydrolytic enzymes in lysosomes through the use of electron microscopy (Novikoff et al., 1956). For these discoveries, de Duda will receive the Nobel Prize for medicine in 1974. In 1962, Ashford and Porter observed that liver cells exposed to glucagon had an increased number of lysosomes, as well as the cytoplasmic components into them (Ashford & Porter, 1962). Furthermore, Novikoff and Essner have found that these structures contained damaged mitochondria (Novikoff & Essner, 1962). One year later, in 1963, de Duda coined the term "autophagy" during the Ciba Foundation symposium on lysosomes to describe the presence of double-membrane vesicles containing parts of cytoplasm or entire organelles. Pursuing his studies, de Duda observed with electron microscopy that another type of vesicle contained cytoplasm as well as mitochondria at different stages of digestion within the cells, suggesting that something

else contributed to cellular degradation together with lysosomes. De Duve named these vesicles “autophagosomes” (de Duve, 1967). It was then demonstrated that autophagy was stimulated by glucagon (Ashford & Porter, 1962; Deter et al., 1967) while insulin could inhibit it (Pfeifer, 1977). It became therefore evident that cellular starvation promotes and enhances this process. In the 1980s, the use of radioactive probes to examine the different steps of autophagy provided a key by identifying new components of this mechanism, 1) the phagophore, an early sequestering vesicle that gives rise to the autophagosome and 2) the amphisome, a non-lysosomal structure formed by the fusion of an autophagosome with an endosome (Gordon & Seglen, 1988). Although studies on autophagy originate from mammalian organisms, an extensive amount of work and discoveries come from analyses in the yeast thanks to the pioneering work of Pr. Yoshinori Ohsumi. His work defined how the autophagic mechanisms observed in yeast were similar to those heretofore studied in mammals (Takeshige et al., 1992). Placing a culture of mutated yeast, *i.e.* lacking lysosomal enzymes, under starvation conditions, Ohsumi noticed an accumulation of autophagosomes in their vacuoles that would not form if yeasts were not mutated, because autophagosome would be readily degraded (Takeshige et al., 1992). These findings were followed by elucidation of several other mechanisms such as the degradation of peroxisomes (pexophagy) (Titorenko et al., 1995) and the *cytoplasm-to-vacuole* (Ctv) targeting pathway (Umekawa & Klionsky, 2012). In the mid-1990s, the discovery of *autophagy-related* (Atg) genes in the yeast *Saccharomyces cerevisiae* has led to a better understanding of the functioning. *Autophagy-related 1* (Atg1) was the first identified autophagy gene in *Saccharomyces cerevisiae* (Matsuura et al., 1997; Tsukada & Ohsumi, 1993) encoding for a protein kinase involved in phosphorylation that leads the regulation of the autophagic process. These discoveries have led Pr. Yoshinori Ohsumi to win the Nobel Prize for the Physiology or Medicine in 2016. Over the past 20 years, significant progress has been made in understanding the autophagic machinery with the discovery of its regulation and effects during physiological and pathological processes (Dikic & Elazar, 2018; Galluzzi et al., 2014; Mizushima, 2018).

7. Different forms of autophagy

To date, there are several cellular pathways by which material to be discarded or recycled can be directed to lysosomes. According to these pathways, we distinguish three forms of autophagy: microautophagy, chaperone-mediated autophagy and macroautophagy.

7.1. Microautophagy

Microautophagy is either a selective or non-selective degradation process in which the cytoplasmic material to be degraded is directly incorporated by the lysosome or the vacuole (the lysosome equivalent in yeast), through random tubular invaginations and evaginations of the membrane. This mechanism is better characterized in yeasts where, under nutrient deficiency, invaginations increase dramatically to form the so-called “autophagic tubes”. The formation of the tube occurs spontaneously thanks to a lateral sorting mechanism which consists of a change in the distribution of membrane components with a strong

accumulation of lipids at the expense of proteins that are eliminated in the tip of the forming-autophagic tube (Müller et al., 2000). During the maturation of this tube, that gradually gives rise to a vesicle, enzymes and molecules to be discarded are engulfed and bind to the inner leaflet of the membrane budding vesicle. The vesicle then buds off into the lumen of the lysosome and its content is thus degraded by hydrolases (Li et al., 2012). Finally, the degraded contents are recycled by the permease Atg22p that recycles back the degradation products into the cytosol (Li et al., 2012). Regarding the selectivity of this mechanism, digestion of entire organelles has been described, for instance mitochondria (micromitophagy) in yeast and mammals (Lemasters, 2014; Sakai et al., 1989), and both peroxisomes (micropexophagy) (Farré & Subramani, 2004; Yuan et al., 1999) and nuclei (micronucleophagy) (Krick et al., 2008) in yeast only. Selectivity of yeast microautophagy has been further supported by the identification of specific cargo receptors, such as *nucleus-vacuole junction protein 1* (Nvj1p) during micronucleophagy (Kvam, 2004).

At first, research on microautophagy in mammals was slowed down by the impossibility of demonstrating the mechanism of lysosome invagination already observed in yeast. Moreover, the genes responsible for microautophagy in yeast are not conserved in mammals. For these reasons, it remains less studied although two types of mechanisms have been described by using electron microscopy: the **flap-like lysosomal membrane extension** (FLLME) and the **wrapping lysosome** (WL) mechanisms (Mijaljica et al., 2011). The FLLME mechanism consists in the formation of a lysosomal extension encompassing a portion of the cytoplasm leading to the formation of an intra-lysosomal vesicle (Marzella et al., 1980). The WL mechanism instead consists in the direct engulfment of cytoplasmic components by lysosomes completely changing their structures, from spherical to elongated forms, with an arm-like extension. However, the mechanism by which these two processes occurs remains to be elucidated. A somewhat better-known variant of microautophagy in mammals is the so-called **endosomal microautophagy** (eMA), which consists in the digestion of proteins and organelles targeted to late endosomes instead of lysosomes. In non-selective eMA, cargos are randomly trapped by the late endosome membranes *via* the coordinated action of *endosomal sorting complexes required for transport* (ESCRT)-dependent mechanism, a dedicated machinery for membrane invagination. In selective eMA, instead, *heat shock cognate 70* (hsc70) binds to a KFERQ pentapeptide motif contained in some substrates targeted to the late endosome, which will then be engulfed and digested by an ESCRT-dependent mechanism (Tekirdag & Cuervo, 2018) (Figure 16).

7.2. Chaperone-mediated autophagy

Chaperone-mediated autophagy (CMA) is a selective form of lysosomal degradation uniquely described in eukaryotes. This form of autophagy is mediated by chaperones that recognize protein substrates and transport them directly to the lysosome, without passing through intermediary vesicles. Substrate recognition is mediated by hsc70, already mentioned in paragraph 7.1, a chaperone protein that binds the specific KFERQ pentapeptide motif expressed by the substrate (Chiang et al., 1989; Chiang & Dice, 1988).

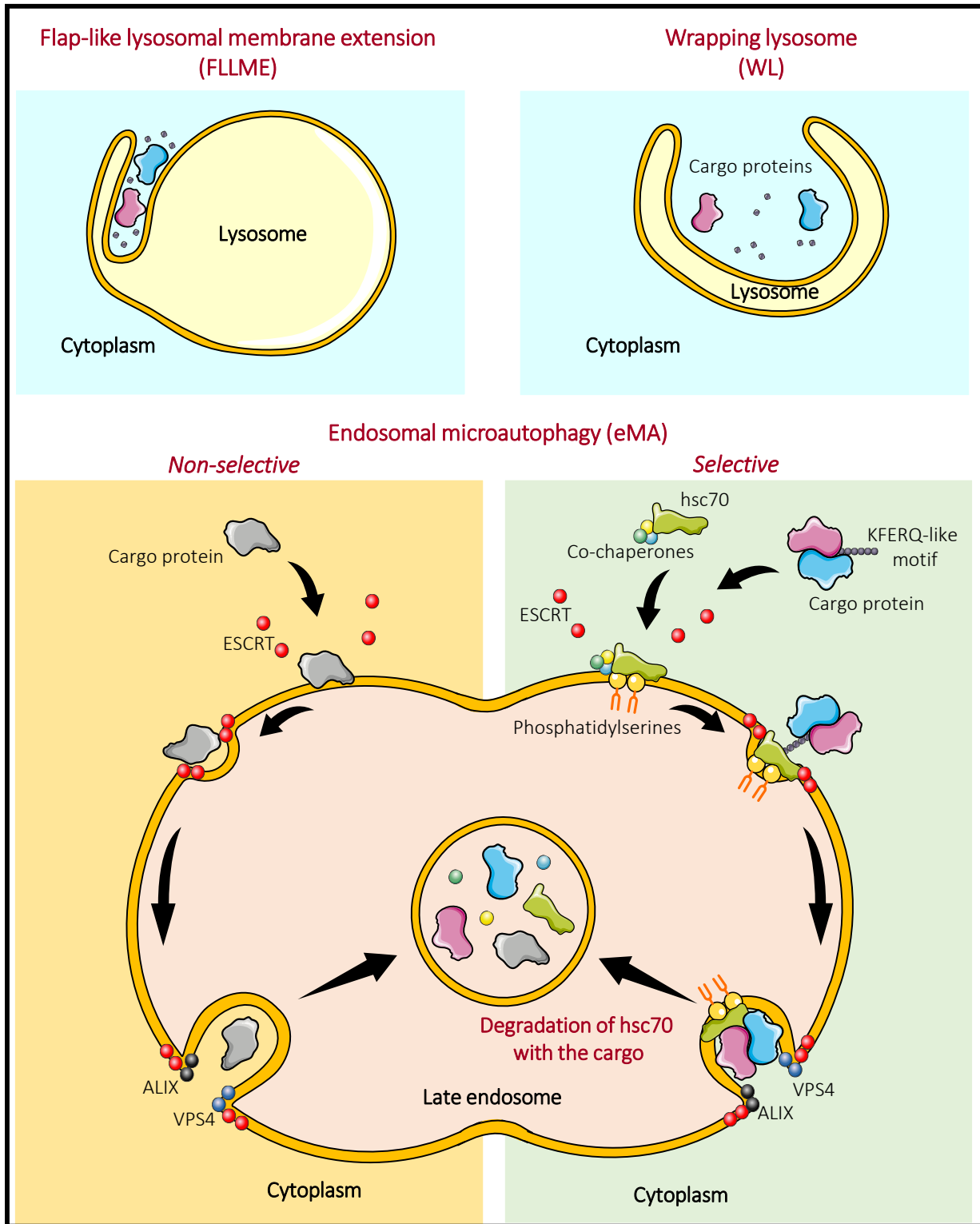


Figure 16. Microautophagy. (Upper left) Flap-like lysosomal membrane extension (FLLME) involves the engulfment of particles by an extension of the lysosomal membrane. (Upper right) Wrapping lysosome (WL) mechanism concerns the engulfment of parts of cytoplasm by the conformational change of the entire structure of the lysosomal membranes. (Lower left) Non-selective endosomal microautophagy consists of sequestering of cytosolic cargo proteins by an invagination that forms at the surface of the late endosome through the coordinated function of ESCRT (VPS4) and accessory proteins (ALIX). (Lower right) Selective endosomal microautophagy consists in a selective targeting of cargo proteins containing a KFERQ-like motif to late endosomes. This mechanism is mediated by hsc70 and co-chaperones. Hsc70 interacts directly with the endosomal membrane phosphatidylserine and is internalized along with the cargo protein in a process depending on VPS4 and ALIX. Hsc70 and parts of others accessory proteins are degraded with the cargo.

Recognition of the KFERQ pentapeptide motif is necessary and sufficient to drive the hsc70:substrate complex to the lysosomal membrane, which is not the case for eMA (Tekirdag & Cuervo, 2018). Indeed, it has been shown that generation of a peptide containing the KFERQ motif fused to a fluorescent probe was only targeted toward lysosomes, and not toward late endosomes (Koga et al., 2011). Once hsc70 has recognized the substrate, the complex is directed to the cytosolic tail of the *lysosome-associated membrane protein type 2A* (LAMP2) protein (Cuervo & Dice, 1996) which triggers multimerization of LAMP2, forming a complex of 700 kDa, and then unfolds and linearizes the substrate that will be finally translocated into the lysosomal lumen for degradation (Tekirdag & Cuervo, 2018). CMA is essentially regulated by the LAMP2A protein level at the lysosomal membrane. In fact, an increase in CMA activity by oxidative stress or starvation induces the upregulation of the LAMP2A protein by preventing its degradation (Cuervo & Dice, 2000) (Figure 17).

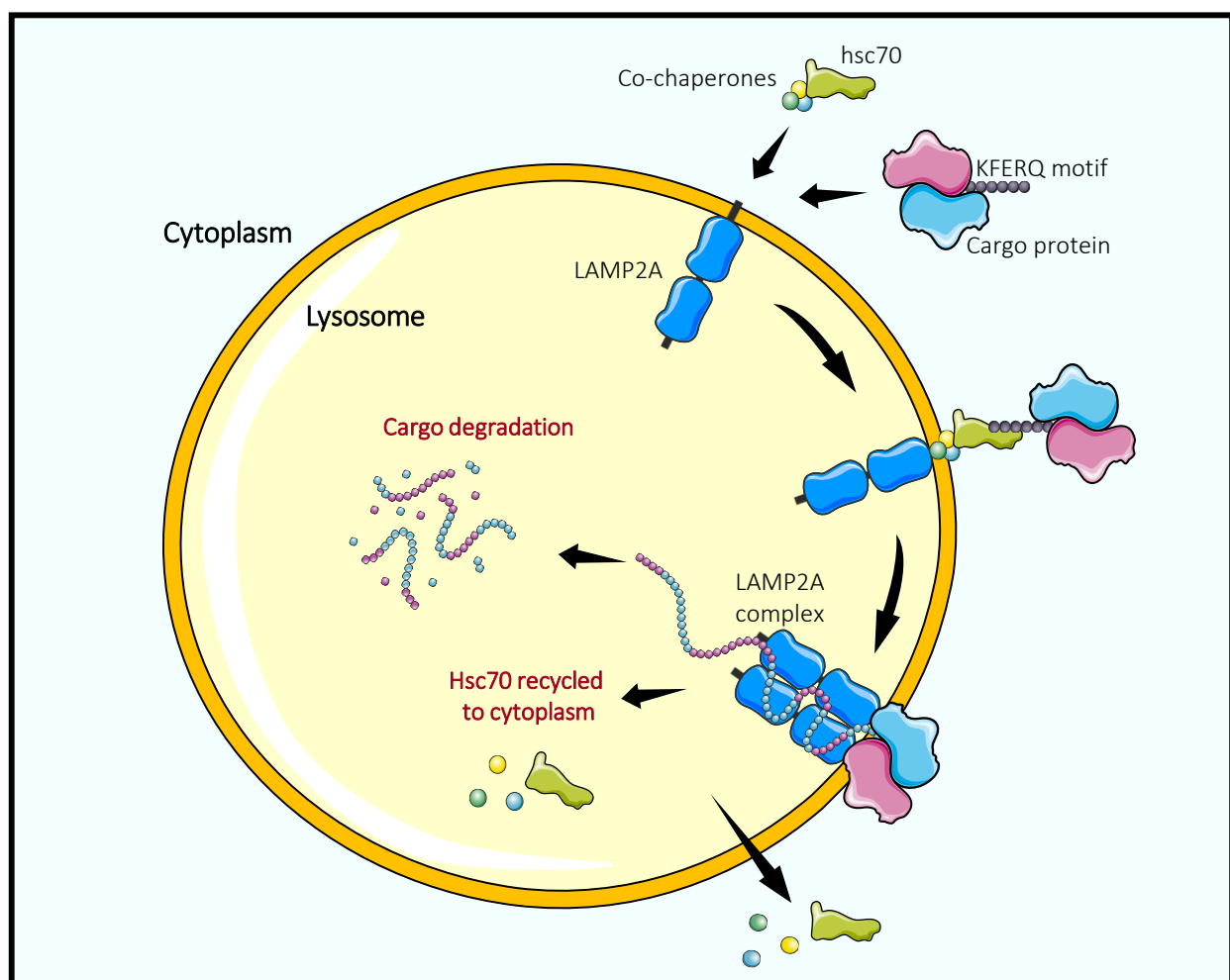


Figure 17. Chaperone-mediated autophagy. During chaperone-mediated autophagy (CMA) all cargo proteins, containing the KFERQ motif, are selectively targeted to lysosomes upon recognition by hsc70 and co-chaperones. The cargo complex then binds the lysosomal membrane through the LAMP2A protein which dimerizes. The cargo protein is then unfolded and internalizes into the lumen for degradation. LAMP2A dimer dissociates and hsc70 is recycled back to the cytoplasm.

Nutritional condition of the cell also influences whether this form of autophagy is upregulated/activated or not, although, in all cells CMA has minimal detectable activity. Intensive CMA upregulation takes place during prolonged nutrient deprivation, oxidative stress, hypoxia or exposure to toxic substances. Generally, macroautophagy is activated in the first line, switching from proteins to lipid degradation after five hours of starvation, then the CMA takes over to supply the cell with recycled amino acids essential for protein synthesis up to three days of starvation (Tekirdag & Cuervo, 2018).

7.3. Macroautophagy

Macroautophagy is the most widely known and studied form of lysosomal degradation in the scientific literature. Macroautophagy is commonly referred to as autophagy (herein referred to as autophagy) during which large portions of cytosol, containing different substrates, are sequestered in the inner leaflet of a double-membrane structure called the **phagophore**, which later matures to form an **autophagosome**. The autophagosome then fuses with the lysosome to form an **autolysosome**, in which substrates are degraded. At last, the degraded components are released into the cytoplasm and recycled by the cell. The difference with the other forms of lysosomal degradation described in the previous sections is that in autophagy, the substrates to be degraded are sequestered in structures located away from the lysosome, such as the phagophore. Furthermore, autophagy is both a selective and non-selective degradation mechanism in which entire damaged organelles, large protein complexes, long-lived proteins, nucleic acid complexes or invasive microbes can be degraded simultaneously (Feng et al., 2014). It is necessary to specify that, between selective and non-selective autophagy, the general mechanism is the same but with the difference that the forming autophagosome targets specific cargos in selective autophagy rather than random cytoplasm during non-selective autophagy. Different types of selective autophagy are largely studied, such as mitophagy (degradation of mitochondria), pexophagy (degradation of peroxisomes), reticulophagy (degradation of portions of the endoplasmic reticulum), glycophagy (degradation of glycogen), lysophagy (degradation of lysosomes), nucleophagy (degradation of nuclei), aggrephagy (degradation of protein aggregates) and xenophagy (degradation of pathogens, such as bacteria or viruses) (Feng et al., 2014; Ke, 2018).

8. Molecular mechanisms of the autophagic machinery

The different steps involved in autophagy are as follow: initiation, nucleation, elongation of the phagophore, fusion of the autophagosome with the lysosome and finally the digestion of the content and nutrient recycling. **Initiation** consists in the activation of autophagy by initiator protein complexes in the perinuclear area near the ER, where the **nucleation** of the phagophore takes place. In yeast, this phagophore derives from a single membrane called *pre-autophagosomal structure* (PAS) (Suzuki et al., 2001). The phagophore continues to elongate and curves on itself during the **elongation** step, sequestering parts of cytoplasm inside it until it closes completely on itself. Once the closure of the double membrane vesicle is complete, the phagophore becomes an autophagosome. Finally, the autophagosome **fuses** with the lysosome

to form the autolysosome where the contents are degraded (**digestion**) by lysosomal hydrolases in an acidic environment for **nutrient recycling** (Figure 18).

As already stated in paragraph 6, autophagy is orchestrated by Atg proteins that operate during the different steps of the process, from the formation of the phagophore to that of the autolysosome. Genetic screens for autophagy-defective mutants in yeast have so far identified more than 40 genes encoding Atg proteins (Ohsumi, 2014), many of which have one or more mammalian orthologues. In addition, about 15 Atg genes are conserved in mammals, indicating that autophagy is an evolutionarily conserved process in all eukaryotes (Klionsky et al., 2003; Nakatogawa et al., 2009).

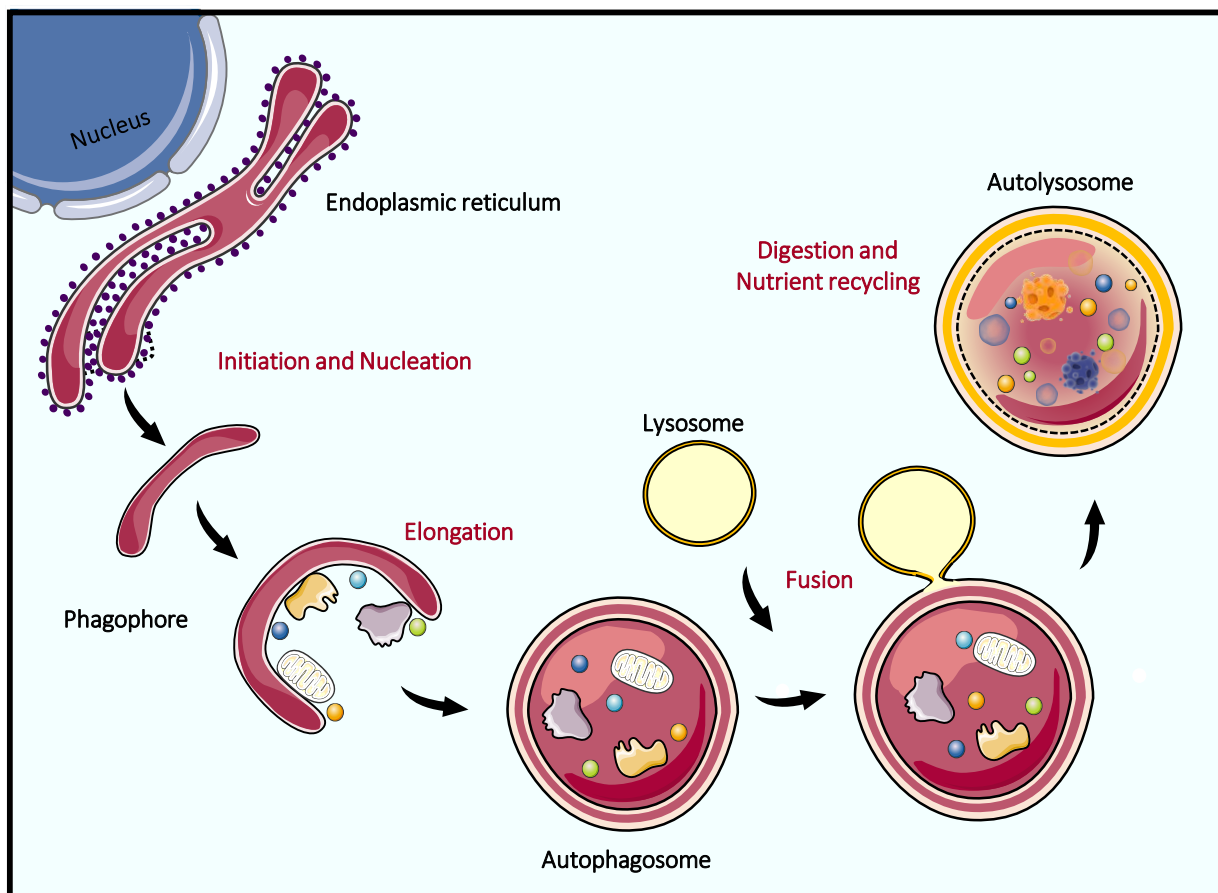


Figure 18. Macroautophagy. The first step in macroautophagy is the formation of a double-membrane structure, called the phagophore, which is formed in specific domains of the endoplasmic reticulum (Initiation and Nucleation). The membranes of the phagophore elongate (Elongation) and incorporate cytoplasmic material until it fully matures, which forms the autophagosome. This autophagosome fuses with the lysosome (Fusion), giving rise to the autolysosome, in which the contents are degraded and recycled for nutritional purposes (Digestion and Nutrient recycling).

8.1. Initiation of autophagy

The initiation of autophagy is driven by two molecular actors: Atg1/*uncoordinated 51-like Ser/Thr kinase* (ULK) complex and the *class III phosphatidylinositol 3-kinase* (PI3KIII). Besides, other factors determine the initiation of autophagy, such as the energy status of the cell, and in this view the energy sentinels *mammalian target of rapamycin complex 1* (mTORC1) and *5'-adenosine-monophosphate-activated protein kinase* (AMPK)

determine whether or not the cell needs to induce autophagy. The cross action of these actors induces the recruitment of the molecular machinery that will subsequently start with the nucleation of the phagophore.

8.1.1. The Atg1/ULK complex: an initiator of autophagosome formation

The ULK complex, homologue of yeast Atg1, consists of one of two kinases ULK1 or ULK2, ATG13 (homologue of yeast Atg13), *FAK family kinase-interacting protein of 200 kDa* (FIP200) (homologue of yeast Atg17) and ATG101 (not conserved in yeast) (Hosokawa et al., 2009; Mercer et al., 2009). Until a while ago, the precise roles of ULK1 and ULK2 were not well defined, and it was thought that these two kinases had a redundant and even interchangeable function during autophagy induction. In fact, Tooze's group has identified ULK1, but not ULK2, as responsible for initiating starvation-induced autophagy, by measuring the lipidation of *microtubule-associated protein 1A/1B-light chain 3* (LC3) in HEK293 cells (Chan et al., 2007). A similar result in the critical role of ULK1, rather than ULK2, was also obtained in cerebellar granule neurons pointing out that the function of ULK2 may be to compensate the lack of ULK1 in a tissue-specific manner (Lee & Tournier, 2011). This later speculation on tissue-specific regulation of these two kinases has been recently supported by other studies (Demeter et al., 2020; Fuqua et al., 2019). A computational analysis based on interactions and structure predictions has shown that ULK1 and ULK2 molecular interactors were implicated in different types of selective autophagy, such as mitophagy, aggrephagy and xenophagy (Demeter et al., 2020). ULK alone is unable to initiate autophagy, in fact the involvement of ATG13, FIP200 and ATG101 is critical to properly position ULK from the cytoplasm toward the initiation site and to induce its maximum kinase activity (Ganley et al., 2009). ATG13 protein is essential for autophagy induction in mammalian cells and mediates the interaction between ULK1 and FIP200 (Figure 19). The ULK binding of ATG13 has been shown to stabilize and activate ULK, leading to increased phosphorylation of both ATG13 and FIP200 by ULK (Jung et al., 2009). ULK has a putative lipid-binding region located in its C-terminus which associates with cell membranes (Chan et al., 2009) and liposomes with a preference for small, highly curved vesicles (Ragusa et al., 2012; Rao et al., 2016). ATG13 also has a lipid-binding region at its N-terminus (Karanasios et al., 2013). The lipid affinity of these two proteins probably facilitates their recruitments to ER subdomains in order to activate phagophore initiation and nucleation. Studies focusing on the newly discovered ATG101 protein suggest that it is important to protect ATG13 from degradation, thus stabilizing its levels in the cytosol (Hosokawa et al., 2009; Mercer et al., 2009).

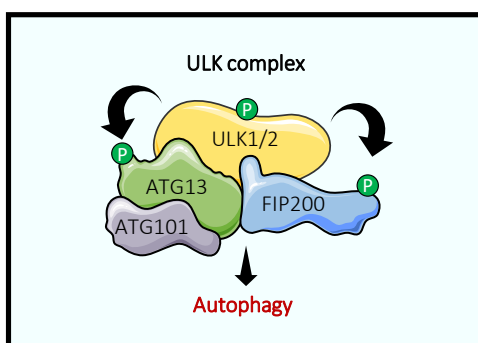


Figure 19. The ULK complex in mammals. Overview of the suggested ULK complex structure, made up of ULK1 or ULK2, ATG13, FIP200 and ATG101. Upon autophagy induction, ULK1/2 phosphorylates itself, *via* a kinase domain located at its N-terminus, and also phosphorylates ATG13 and FIP200, with which it interacts directly *via* its C-terminal domain. ATG101, an accessory protein, associates with ATG13 in order to improve the overall activity of the complex.

8.1.2. Class III PI3K: a PI3P source at the initiation site

Among the various forms of lipids that can be found in cell membranes of eukaryotic cells, crucial for the initiation/nucleation of the phagophore is *phosphatidylinositol 3-phosphate* (PI3P). PI3P production occurs at the level of the ER domains, via PI3KIII. PI3KIII consists of *vacuolar protein sorting 34* (VPS34), VPS15/p150, Atg6/beclin 1 and ATG14L (Nishimura & Tooze, 2020). This complex forms a V-shaped structure (Figure 20) with one arm containing the lipid kinase VPS34, and VPS15/p150, that strongly influences the scaffolding of the complex and kinase activity. The other arm includes beclin 1, a modulator of Vps34 catalytic activity and ATG14L, thought to recruit the autophagy machinery to the ER and to sense membrane curvature (Matsunaga et al., 2010; Nishimura & Tooze, 2020). Once ULK1 has been activated by the ATG13:FIP200:ATG101 complex, it phosphorylates beclin 1 at Ser14 which in turn activates VPS34 (Russell et al., 2013) (Figure 20). The C-terminus of VPS34 has a dual function, that of to determine the orientation of the PI3KIII complex at the membrane and to recognize, with high affinity, *phosphatidylinositol* (PI) which is phosphorylated at the position three of the inositol ring to form PI3P (Jaber & Zong, 2013; Su et al., 2017) (Figure 20).

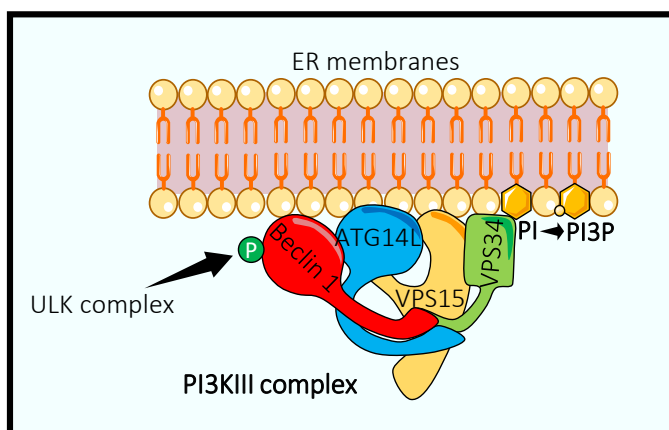


Figure 20. The PI3KIII complex. Representation of the proposed structural arrangement of the subunits of mammalian class-III PI3K complex. The V-shaped structure is formed by VPS34 and VPS15, in the right branch, which extends and forms contacts with the left branch of the complex, consisting of beclin 1 and ATG14L1. ULK phosphorylates beclin 1, thus increasing the activity of VPS34 that catalyzes the phosphorylation of PI at position 3 of the inositol ring, to produce PI3P.

Beclin 1 is a multi-domain protein consisting in a *BCL2 homology 3* (BH3) domain, a *coiled-coil domain* (CCD), an *evolutionarily conserved domain* (ECD) followed by a *β - α -repeated, autophagy-specific* (BARA) domain (Figure 21A). Beclin 1 can therefore bind different partners *via* these specific domains, resulting in pro-autophagic or anti-autophagic effects (Menon & Dhamija, 2018). Under normal conditions, beclin 1 is anchored to the cytoskeleton, preventing its pro-autophagic activity. This localization is mediated by *autophagy and Beclin 1 regulator 1* (**AMBRA1**), one of the beclin 1 partners, which keeps beclin 1 bound to microtubules. Upon autophagy induction, phosphorylation of AMBRA1 by ULK1 releases beclin 1 from microtubules facilitating its translocation to the ER for autophagy induction (Di Bartolomeo et al., 2010) (Figure 21B). By interacting with the CDD domain of beclin 1, *UV radiation resistance associated* (**UVRAG**) enhances the kinase activity of VPS34 and therefore exerts pro-autophagic functions (Liang et al., 2008) (Figure 21C). The effect of UVRAG seems to be independent from ATG14L, since both proteins compete for the same binding

site in the CDD domain of beclin 1. It is interesting to note that, in addition to its function during autophagy initiation, UVRAG is also critical during the late steps of autophagy, by promoting the fusion between mature autophagosomes and lysosomes (Liang et al., 2008). By interacting with the BH3 domain of beclin 1, **BCL2** and **BCL-XL** proteins inhibit the association of beclin 1 with VPS34, resulting in the inhibition of autophagosome biogenesis (Pattingre et al., 2005). Finally, the protein **RUBICON** also exerts an anti-autophagic function by interacting with UVRAG and thus inhibiting a specific subpopulation of PI3KIII complexes (Matsunaga et al., 2009; Sun et al., 2015) (Figure 21C).

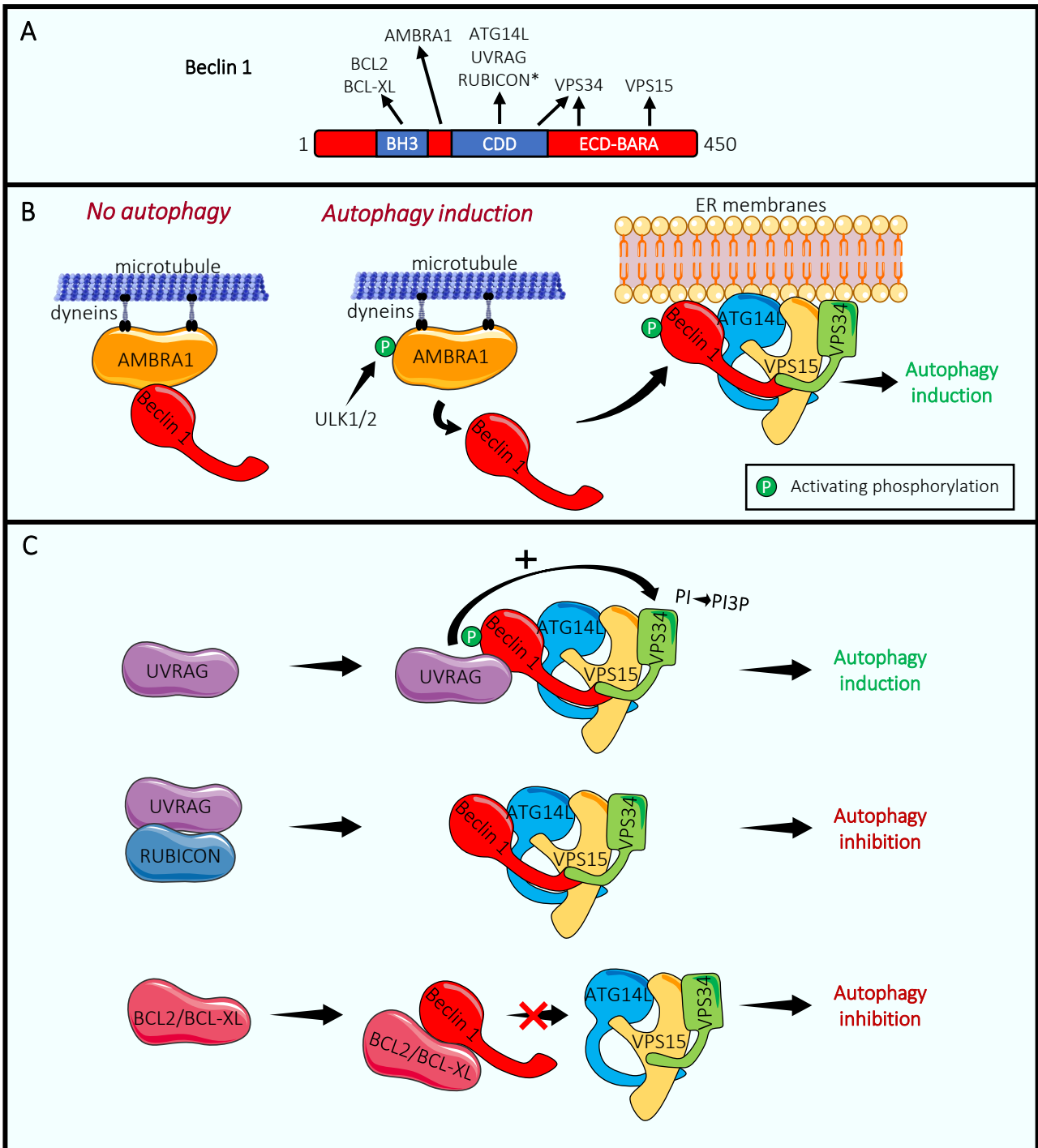


Figure 21. For caption see next page.

Figure 21. Regulation of PI3KIII activity by beclin 1 partners. **A|** Structure of beclin 1 showing the BH3 domain, responsible for binding with BCL2/BCL-XL, a flexible helical domain that interacts with AMBRA1, a central coiled coil domain (CDD), which binds ATG14L, VPS34, UVRAG and RUBICON (*via* UVRAG) and a ECD-BARA domain for VPS34 and VPS15 proteins binding. **B|** (*Left*) In the presence of nutrients, the ULK complex is inhibited. In this scenario, a pool of AMBRA1:beclin 1 is associated, in an inactive form, with the molecular motor dynein. (*Right*) Upon nutrient deficiency, autophagy is induced and ULK1 is active to phosphorylate AMBRA1. This phosphorylation allows beclin 1 to dissociate from the complex with dynein and associate with the endoplasmic reticulum membranes, where VPS34 phosphorylates the PI to produce PI3P. **C|** UVRAG associates with beclin 1 and increase its ability to stimulate VPS34, thus promoting autophagy. RUBICON sequesters UVRAG, which is no longer available to stimulate beclin 1, strongly reducing autophagy activity. BCL2/BCL-XL interacts with beclin 1, inducing its dimerization with another beclin 1 protein, blocking beclin 1 association with the other PI3K complex partners and inhibiting autophagy.

To conclude, the initiation of autophagy first requires the activation of ULK complex which, *via* a cascade mechanism, phosphorylates beclin 1 and thus activates the PI3KIII complex (Russell et al., 2013). Essential to the understanding of these mechanisms was the use of different pharmacological inhibitors of PI3KIII, such as wortmannin, LYS294002 and 3-methyladenine (Blommaert et al., 1997; Petiot et al., 2000) which have then shown to block autophagy in mammalian cells, and are thus commonly used in this field.

8.1.3. mTORC1 and AMPK: energy sentinels regulating autophagy initiation

The activity of the ULK complex and thus autophagic activity also depends on its phosphorylation status. Several phosphorylation sites have been identified on ULK1 and ATG13. In this context, the kinase activities of mTORC1 complex and AMPK are able to finely regulate autophagy initiation as a function of the cell energy status (Wong et al., 2013). The mTORC1 complex is formed by the kinase mTOR, Raptor, mLST8, Deptor and PRAS40. In nutrient-rich conditions, the mTORC1 complex interacts with and phosphorylates ULK1 and ATG13, thus suppressing ULK1 activity and autophagy. In contrast, under nutritional-deficiency conditions or rapamycin treatment, mTORC1 is released from the ULK complex, resulting in ULK1 and ATG13 inhibitory dephosphorylations. The kinase activity of ULK1 is thus restored leading to efficient autophagy initiation (Hosokawa et al., 2009; Jung et al., 2009) (Figure 22).

AMPK is the cell's other energy sensing kinase, activated when the concentration of AMP reaches low levels that are inadequate for the cell energetic support. It has been shown that AMPK acts either by phosphorylating Raptor, thus decreasing the inhibitory impact of mTORC1 on ULK complex (Gwinn et al., 2008), or by direct phosphorylation/inhibition of ULK1 protein (Egan et al., 2011; Mack et al., 2012) (Figure 22).

8.2. Nucleation and elongation of the phagophore

Phagophore nucleation is enabled by the production of PI3P by the PI3KIII complex at specific ER subdomains. Here the autophagic platform takes place and where autophagic proteins are recruited. The PI3P-rich ER region in which the phagophore nucleates is called the *omegasome*, due to its shape resembling the Greek letter “Ω”. In fact, it has been demonstrated that starvation by amino acid deficiency induced PI3P accumulation at ER subdomains, followed by the extension of ER membrane to generate the omegasome (Axe et al., 2008).

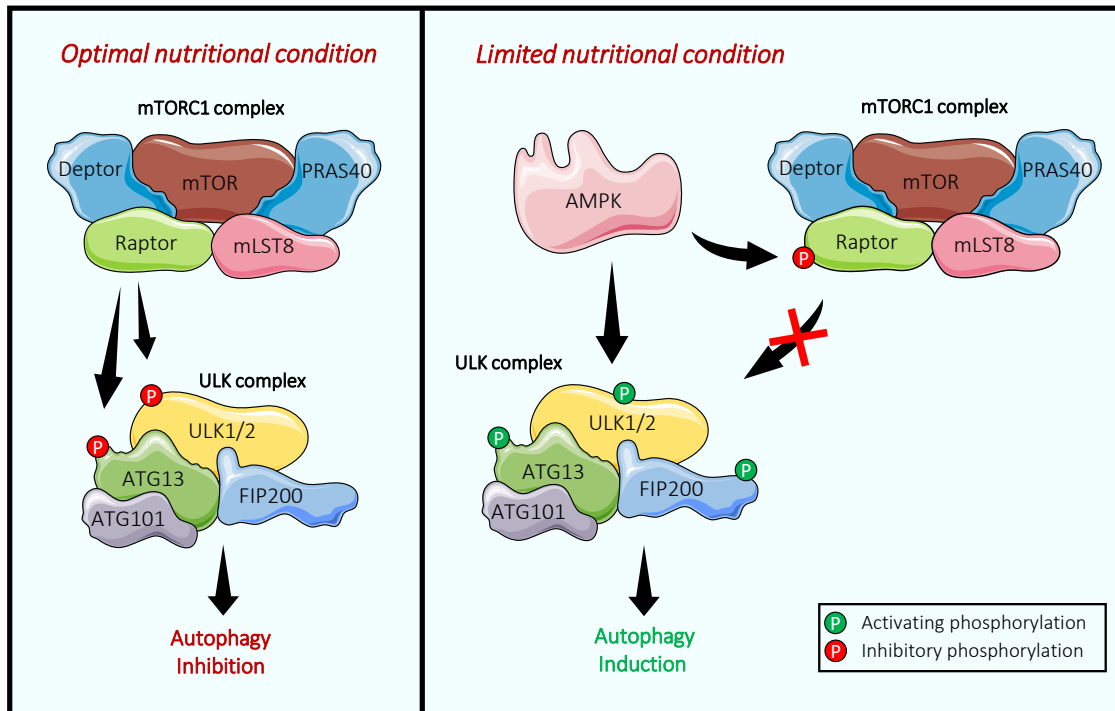


Figure 22. Regulation of the ULK complex by mTORC1 and AMPK. (Left) Under optimal nutritional conditions, the ULK complex is inhibited by phosphorylation of ULK1/2 and ATG13 proteins by mTORC1. (Right) When nutritional conditions worsen, AMPK can remove this inhibition by blocking mTORC1 activity through Raptor phosphorylation. AMPK can also directly act by phosphorylating ULK1/2 at specific residues in order to stimulate its activity. The activated ULK complex can then reach the initiation site for phagophore formation.

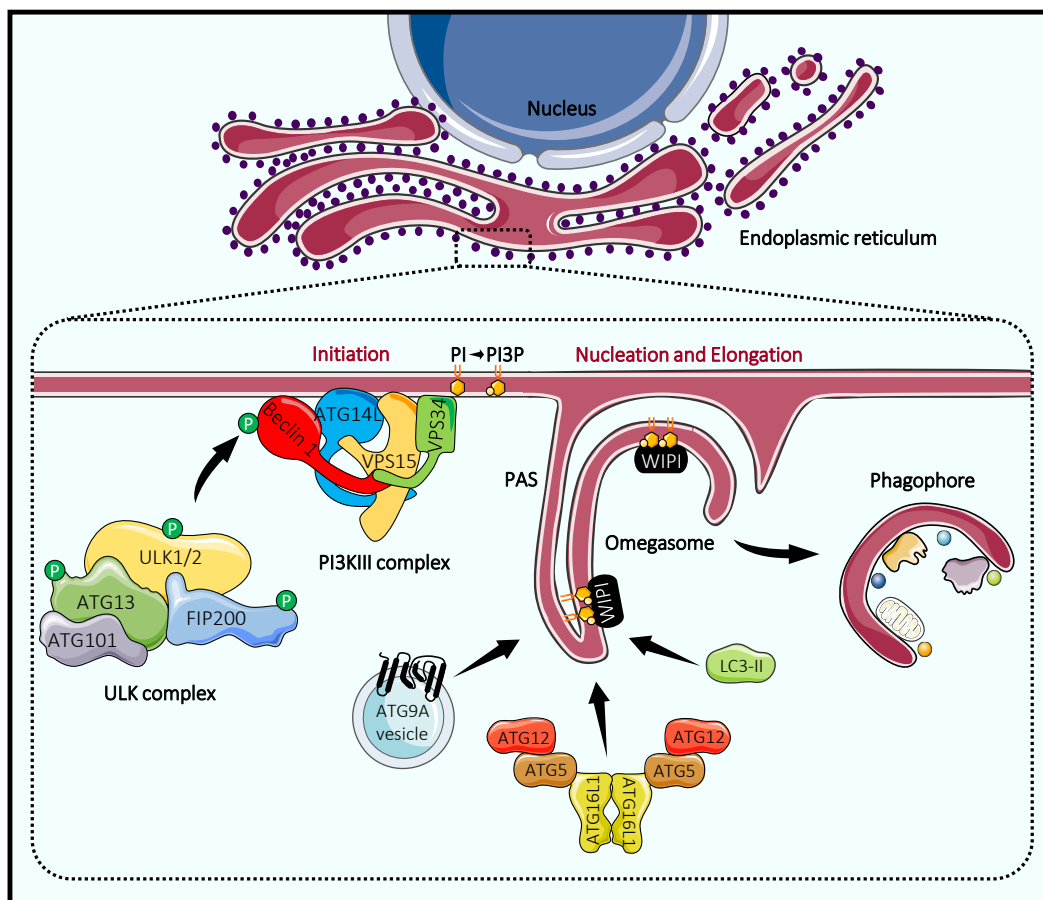


Figure 23. For caption see next page.

Figure 23. The key steps of initiation and phagophore nucleation. Representation that highlights, in a sequential manner, the most important moments in the formation of the phagophore. The ULK complex stimulates and activates the PI3KIII complex, which induces the accumulation of PI3P at specific domains of the endoplasmic reticulum. The PI3P-rich zones are hot spots where the omegasome is formed and where the numerous autophagy proteins are recruited for its nucleation and elongation. WIPI proteins, by binding to PI3P within the omegasome, acts as a platform for the recruitment of the ATG12-ATG5-ATG16L1 complex with which it interacts directly. ATG9A vesicles contribute to supply phospholipids to the omegasome for its elongation while LC3-II allows the fast elongation of the phagophore until its complete maturation into an autophagosome.

Once PI3P has been produced, chain recruitment of several proteins induces nucleation of the phagophore. In particular, proteins from the WIPI family are the first to localize on these PI3P-rich domains. They, in turn, induce the recruitment of other proteins such as Atg9, the ATG12-ATG5-ATG16L1 ternary complex, and the LC3 protein conjugated to phosphatidylethanolamine (PE), that will support the expansion of the phagophore until its complete maturation into an autophagosome (Figure 23). Synthesis of the ATG12-ATG5-ATG16L1 ternary complex and of LC3-PE involves two conjugation systems, called “ubiquitin-like”, from the similarities they share with the ubiquitin system involved in the proteasomal degradation of proteins. The ubiquitination system requires three enzymes, called E1, E2 and E3 ligases, that sequentially act to induce the transfer of a ubiquitin residue on the target protein (Figure 24). In the context on autophagosome biogenesis, the mechanism does not involve the transfer of ubiquitin, but that of ATG12 and LC3 proteins.

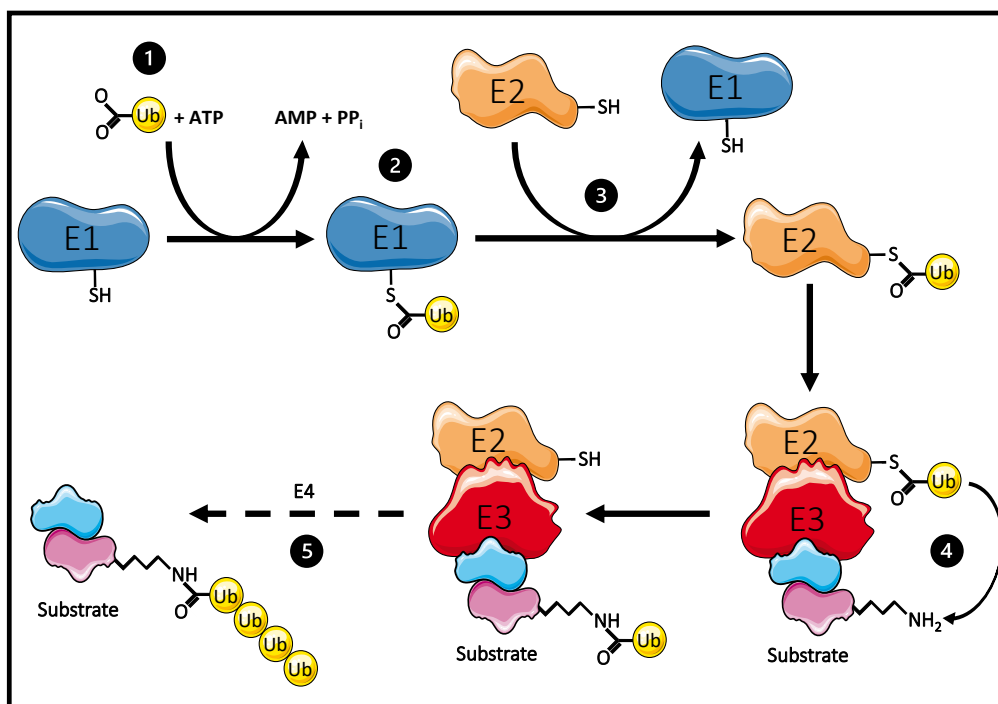


Figure 24. The Ubiquitination system. The ubiquitination of a substrate requires three enzymes: ubiquitin-activating enzyme (E1), ubiquitin-conjugation enzyme (E2) and ubiquitin ligase (E3). The process consists of three main steps: activation, conjugation and ligation. The activation step starts with ubiquitin activation *via* the E1. E1 binds ubiquitin and ATP and forms an ubiquitin-adenylate intermediate (1). Then, the intermediate is transferred to an active site cysteine residue of E1, with the release of AMP (2). The conjugation step involves the E2 enzyme which catalyzes the transfer of ubiquitin from E1 to its cysteine active site (3). The ligation step requires E3 enzyme, able to interact with both E2 and the substrate, and catalyzes the direct transfer of the ubiquitin from E2 to the substrate (4). Other enzymes, such as E4 (ubiquitin-chain elongation enzyme) can eventually add pre-formed polyubiquitin chains to the substrate (5).

8.2.1. Formation of ATG12-ATG5-ATG16L1

The first conjugation system allows the conjugation of the C-terminal glycine residue of ATG12 to the lysine-130 residue of ATG5, through the generation of an isopeptide bond. For this to occur, the C-terminal glycine of ATG12 is first activated by the E1-like activating enzyme ATG7. This mechanism requires ATP, and a thioester intermediate ATG12-ATG7 is formed. ATG12 is then transferred to the ATG10 E2-like conjugating enzyme, forming a second intermediate. Finally, the glycine at the C-terminal position of ATG12 is irreversibly conjugated on the lysine-130 residue of ATG5 (Mizushima et al., 1998) forming the ATG12-ATG5 complex. ATG12-ATG5 complex then interacts non-covalently with ATG16L1 forming the ATG12-ATG5-ATG16L1 ternary complex (Mizushima et al., 1999). As detailed in the next paragraph, this ternary complex will act as a E3-like ligase enzyme in the second conjugation system represented by LC3, facilitating the transfer of LC3 to phosphatidylethanolamine (PE) (Figure 25).

It is interesting to note that ATG16L1 has been shown to homodimerize through its N-terminal domain. This leads to the formation of a large complex of approximately 800 kDa, consisting of two ATG16L1 proteins bound together with an ATG5-ATG12 complex associated to each of them (Mizushima et al., 2003) (Figure 25). Once the phagophore is formed, this large complex dissociates from the phagophore membrane.

8.2.2. The LC3-PE conjugation system: synthesis of LC3-PE on the nascent autophagosome

The conjugation of LC3 to PE, a mechanism called LC3 lipidation, is essential for the elongation of the phagophore (Dooley et al., 2014). The process starts with the synthesis of a precursor form of LC3, called pro-LC3. Cleavage of arginine at the C-terminus of pro-LC3 by the protease ATG4 leaves exposed a glycine residue, resulting in LC3-I. The E1-like ATG7 enzyme, shared with the ATG12-ATG5 conjugation system, processes LC3-I to form the thioester intermediate LC3-I-ATG7. This intermediate enables LC3-I to be transferred to the E2-like enzyme Atg3, to form the intermediate LC3-I-ATG3. The final step, catalyzed by the ATG12-ATG5-ATG16L1 complex, acting as E3-like ligase, consists in the conjugation of LC3-I from ATG3 to the amino-group of PE, resulting in the formation of LC3-PE or LC3-II (Hanada et al., 2007; Ichimura et al., 2000). Incorporation of LC3-PE at the membrane of the phagophore is critical for the next steps of the autophagic process, including elongation of the phagophore, its closure, and fusion of the mature autophagosome with the lysosomal compartment (Kawabata & Yoshimori, 2020). Besides LC3 conversions, the protease ATG4 can cleave LC3-PE, in a process called LC3 delipidation, to recycle LC3 for another round of conjugation (Nakatogawa et al., 2012) (Figure 25). The critical role of LC3 has been extensively demonstrated by knockout experiments, in both yeast and mammals (Abeliovich et al., 2000; Kirisako et al., 2000; Weidberg et al., 2010; Xie et al., 2008). In fact, Atg8/LC3 downregulation induced the formation of autophagosomes with reduced size, and a delay in degradation of the inner part of the autophagosomal membrane and cargoes (Tsuboyama et al., 2016). Interestingly, while other Atg proteins are located outside the forming autophagosome and then released from

the membrane after autophagosome formation, LC3 is located both at the outer and inner part of this membrane, thus staying within autophagosomes. This characteristic arrangement of LC3 and therefore the fact that LC3 itself is degraded by autophagy makes this substrate extremely useful for studying autophagy. Increased conversion of LC3-I to LC3-II is used as a marker of increased autophagy activity (Klionsky et al., 2021). In fact, fluorescent-tagged LC3 is the best-known marker used to monitor autophagosomes both in fixed and in living cells, as well as, its use in SDS-page since the LC3-I and LC3-II can be easily separated each other and be detected in a western blot (Klionsky et al., 2021).

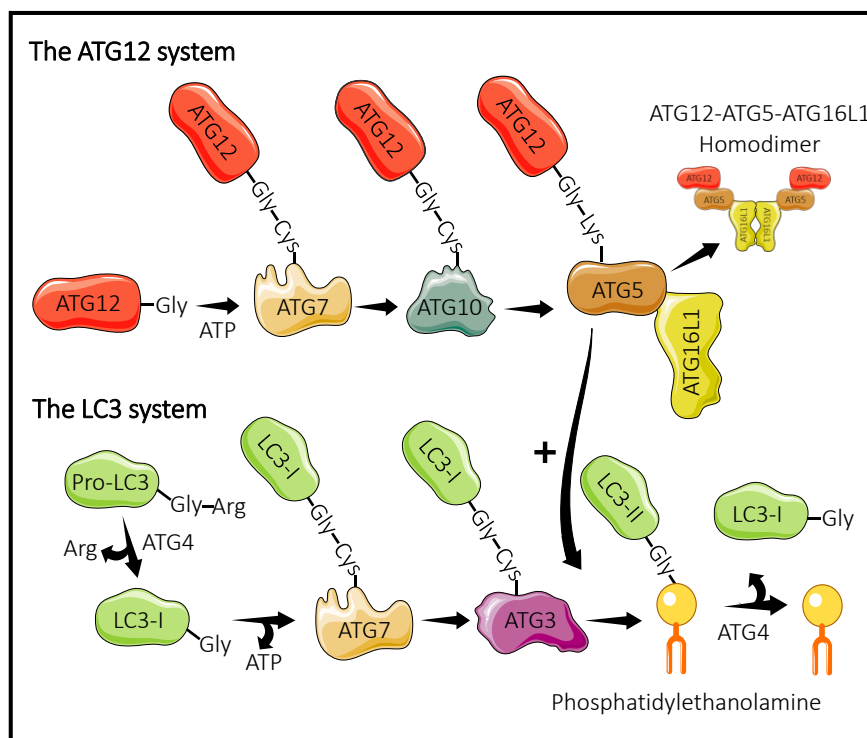


Figure 25. The two ubiquitin-like conjugation systems essential for autophagy. During phagophore elongation, two ubiquitin-like conjugation systems allow to form the ATG12-ATG5-ATG16L1 complex and the LC3-II protein. (*Upper*) Sequential reactions by the E1-like protein ATG7 and the E2-like protein ATG10 conjugate ATG12 to a lysine residue of ATG5, and the resulting ATG12-ATG5 complex then interacts non-covalently with ATG16L1. The ATG12-ATG5-ATG16L1 ternary complex can form a homodimer with another complex. (*Lower*) After post-translational modifications, pro-LC3 is cleaved into LC3-I by ATG4. LC3-I is activated by the E1-like protein ATG7, then transferred to the E2-like protein ATG3 and finally conjugated to phosphatidylethanolamine with the support of the E3-like ATG12-ATG5-ATG16L1 complex. Membrane-localized LC3-II can be delipidated by ATG4 to recycle LC3-I.

In mammals, there are at least eight different Atg8 orthologues involved in the biogenesis of autophagosomes. They can be classified under two families: the LC3 family consisting of LC3A, LC3B and LC3C and the *gamma-aminobutyric acid receptor-associated protein* (GABARAP) family consisting of GABARAP1, GABARAP2, GABARAPL1, GABARAPL2 and GABARAPL3. The most studied and best characterized is LC3B. Although all these proteins are similarly lipidated by the conjugation system described above, proteins of the LC3 family seem to be mainly involved in the elongation of the phagophore, whereas proteins of the GABARAP subfamily participate in later stages of autophagy, *i.e.* phagophore closure and fusion with the lysosomes (Lee & Lee, 2016; Weidberg et al., 2010). In addition to their roles in autophagosome biogenesis, proteins of the

LC3 family have an important role in the recognition and specific recruitment of substrates to be degraded. This mechanism involves autophagic receptors containing an *LC3-interacting region* (LIR). This domain allows the autophagic receptors to bind the LC3-II conjugates present at the phagophore membrane and to sequester the elements to be degraded (Birgisdottir et al., 2013; Padman et al., 2019). A classic example of autophagic receptors is p62, also called sequestosome 1, used as an indirect indicator of autophagic activity as it accumulates within the cytosol when autophagy is impaired (Klionsky et al., 2021) (Figure 26).

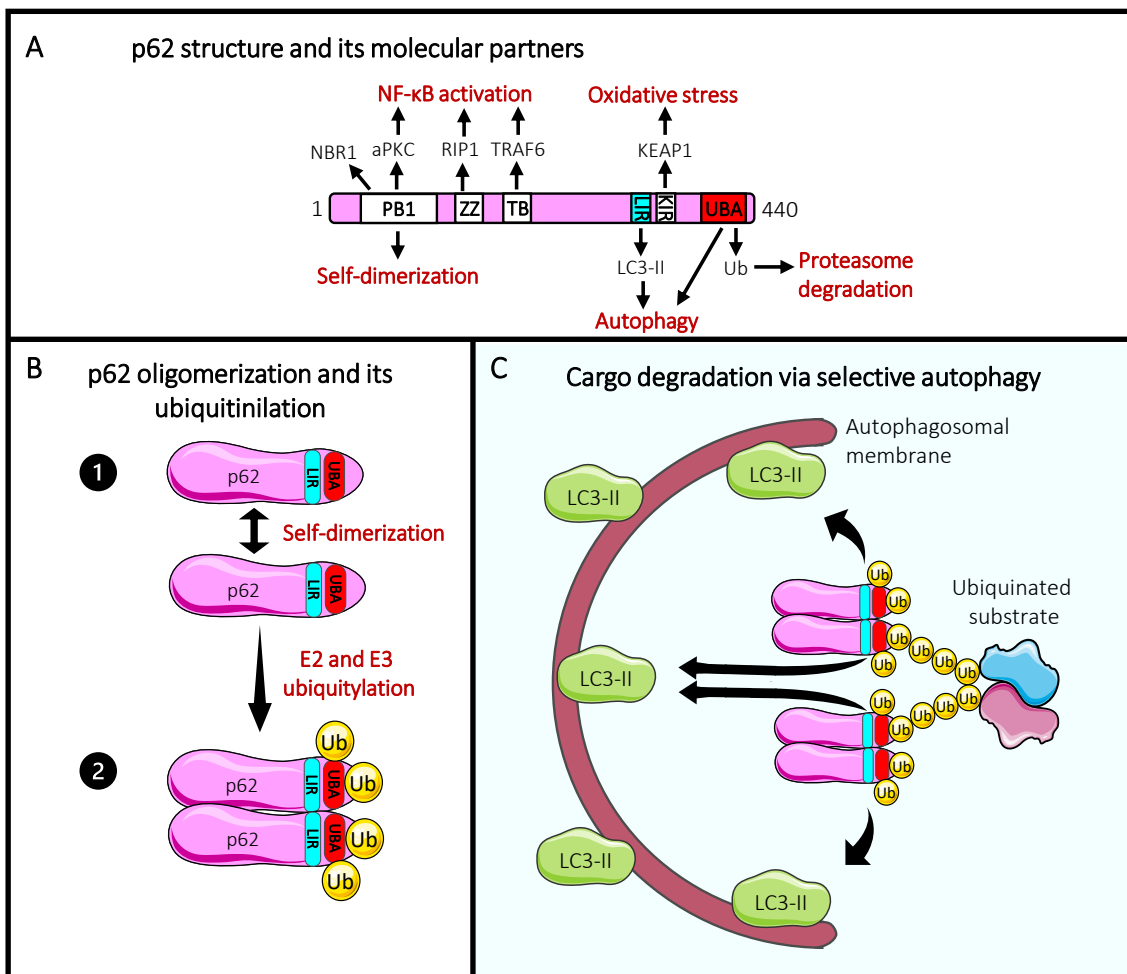


Figure 26. The autophagic receptor p62 and selective autophagy. **A** | The structure of the human p62 protein and its interacting partners. p62 consists in six domains: the *Phox and Bem1* (PB1) domain is involved in self-oligomerization of p62 or heterodimerization with NBR1 (another autophagic receptor, similar to p62) and binding to *atypical PKC* (aPKC). The central *zinc finger* (ZZ) domain and the *TRAF6-binding domain* (TB) interact with the RIP1 and TRAF6 proteins, respectively in order to regulate NF- κ B pathway. The *LC3-interacting region* (LIR) motif is involved in binding LC3-II protein, while the *ubiquitin-associated domain* (UBA) binds ubiquitinated proteins to promote their selective degradation *via* autophagy. Finally, the *Keap-interacting region* (KIR) which binds Keap1 leading to the stabilization of transcription factors involved in oxidative stress. **B** | Model for the Ub-driven formation of the scaffold for selective autophagy. After self-dimerization (1), p62 protein can be mono- and polyubiquitinated by the E2 and E3 enzymes (2). **C** | Model of cargo degradation *via* selective autophagy. After the substrate has been ubiquitinated, it associates with p62 dimers which then contact LC3-II, *via* their LIR domains. The cargo is then engulfed by the LC3-II-containing autophagosomal membranes and will be finally degraded *via* selective autophagy.

8.2.3. Autophagosome closure

The use of specific markers for closed autophagosomes, such as STX17, has made possible the identification of the determinants of phagophore closure (Itakura et al., 2012). Many studies suggest an important role of the ESCRT machinery in this final step. For example, ESCRT depletion induced the accumulation of autophagosomes (Lee et al., 2007), although it is difficult to identify between those that are completely closed and those that have holes in ESCRT-depleted cells. Recent data revealed that components of ESCRT-I are primarily recruited to the phagophore by a yet unknown mechanism. The recruitment of *charged multivesicular body protein* (CHMP) 2A and CHMP4B then induces the polymerization of ESCRT-III filaments that bring the two membrane flaps close to each other, allowing membrane fission. The last step seems to be mediated by *vacuolar protein sorting-associated protein* (VPS) 4, an ATPase that resolves the fission process by facilitating ESCRT-III depolymerization (Melia et al., 2020; Takahashi et al., 2019; Zhou et al., 2019) (Figure 27).

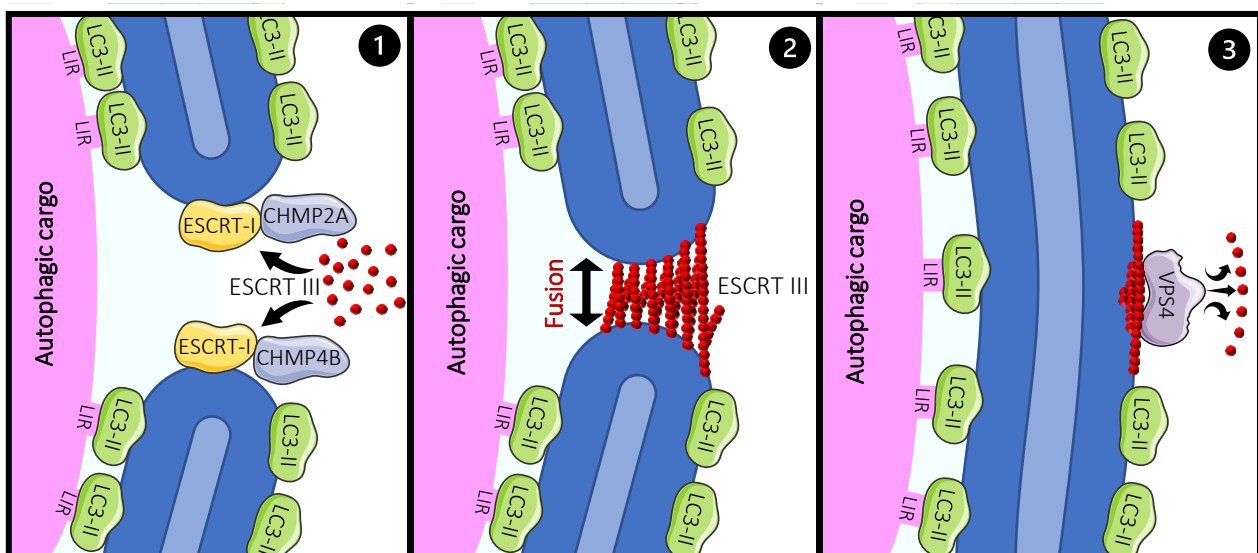


Figure 27. Autophagosome closure. ESCRT-I proteins are first recruited to the phagophore edge membranes and then followed by the recruitment of ESCRT-III proteins and the filament-forming components CHMP2A and CHMP4B (1). ESCRT-III proteins polymerize leading to the formation of a spiral-like filament that brings the leading edge of the phagophore membranes into close proximity and allowing membrane fusion (2). The last step is facilitated by the ATPase VPS4 which resolves the fusion and facilitates depolymerization of the ESCRT-III spiral-like filament structure (3). LC3-II is also involved in this process, but its mechanism has not yet been clarified. Cartoon adapted from Melia et al., 2020.

8.3. Maturation of autophagosomes and fusion with lysosomes

The maturation stage occurs immediately after autophagosome closure (paragraph 8.2.3) and consists of the fusion of the autophagosome with the lysosome to form the autolysosome, for its content degradation by lysosomal hydrolases. The autophagosome and lysosome originate from different parts of the cell and although autophagosomes originate randomly in the cytosol, lysosomes are specifically produced in the perinuclear area, close the microtubule organizing centre (Kawabata & Yoshimori, 2020). Autophagosome and

lysosome must be in close contact in order to fuse, and therefore both vesicles must travel onto microtubules to meet in the perinuclear area of the cell, where the fusion occurs. Autophagosome movement toward the minus-end of microtubules, or perinuclear area, is dictated by its binding with dynactin and dynein via Rab7, *rab-interacting lysosomal protein* (RILP) and *oxysterol-binding protein-related protein 1L* (ORP1L) (Jordens et al., 2001; Pankiv et al., 2010; Wijdeven et al., 2016). Whilst, Rab7 and its effector *FYVE and coiled-coil domain autophagy adaptor 1* (FYCO1) drive the movement of the autophagosome toward the plus-end of microtubules, the periphery (Pankiv et al., 2010) (Figure 28). About the movement of lysosomes, inhibition of kinesins, such as Kif1B and Kif2A, has been shown to induce increased fusion with autophagosomes. Overexpression of kinesin 5B, on the other hand, causes lysosomes to disperse toward the periphery, reducing the rate of fusion as well as the accumulation of autophagosomes in the perinuclear zone (Cardoso et al., 2009; Korolchuk et al., 2011). These results suggest that lysosome positioning determinate whether autophagosome-lysosome fusion occur.

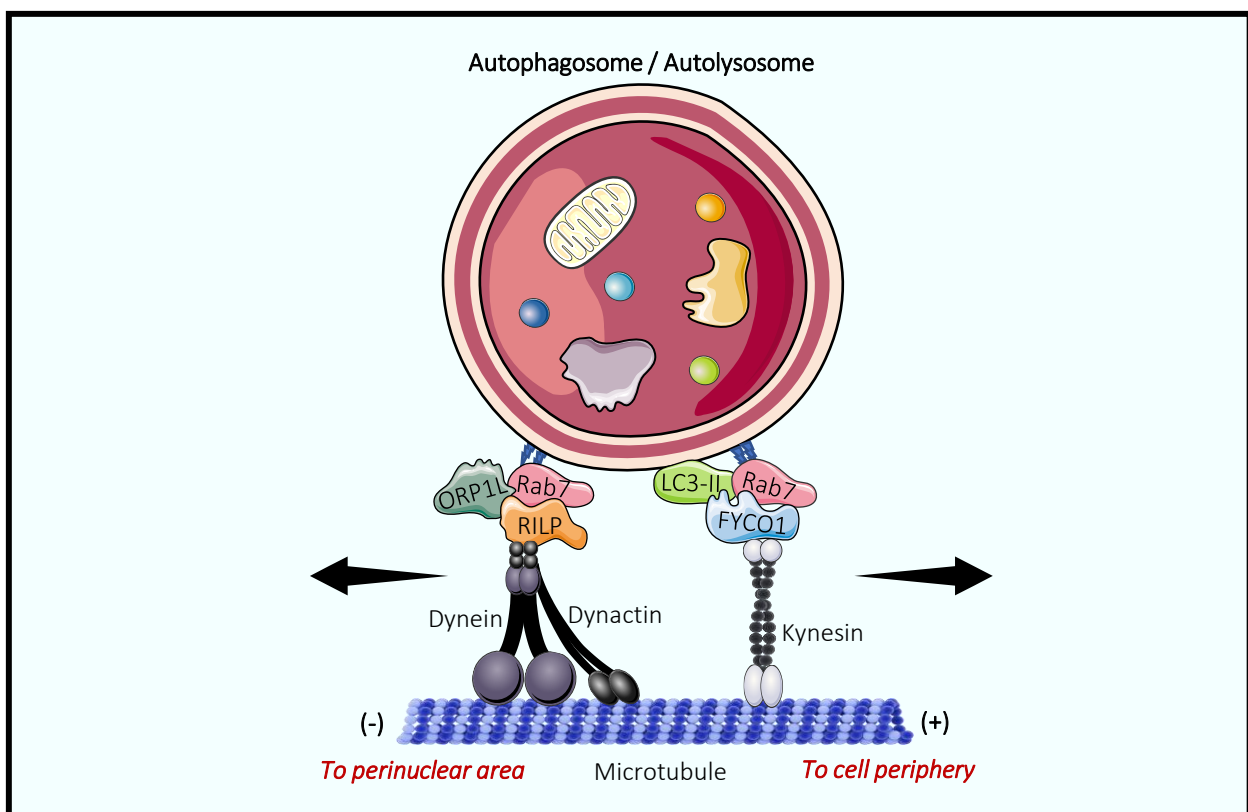


Figure 28. Autophagosome and autolysosome trafficking onto microtubules. Proposed mechanism of autophagosome/autolysosome bidirectional migration on microtubules *via* Rab7. Rab7 links autophagosomes to the molecular motor kinesin through FYCO1 and facilitates the microtubule-dependent trafficking toward the plus end (cell periphery). The microtubule-dependent trafficking toward the minus end (perinuclear area) is also governed by Rab7, but Rab7 instead interacts with the effectors ORP1L and RILP, the latter which binds to the dynein:dynein complex. Cartoon adapted from Kuchitsu and Fukuda, 2018.

Once the lysosome and autophagosome are in proximity, the high-energy barrier between the two membrane vesicles must be by-passed by the formation of a complex involving SNARE proteins. Autophagosomes are built by two lipid bilayer membranes whereas lysosomes are delimited by a single bilayer membrane. During the fusion between autophagosome and lysosome, the outer lipid bilayer membrane of autophagosomes fuses with the lipid bilayer membrane of lysosomes and here SNAREs take place. STX17, a SNARE protein located on autophagosomes form a complex with the cytosolic protein SNAP29 and with another SNARE protein, VAMP7/8, located on the lysosome membrane (Hikita et al., 2018). Assembly and stability of the STX17:SNAP29:VAMP7/8 complex is improved by the concomitant recruitment of a tethering modulator, called *ectopic P-granules autophagy protein 5 homolog* (EPG5), which interacts with both Rab7 and VAMP7/8 located in the lysosome surface, and with LC3 and STX17:SNAP29 located on the autophagosomal surface (Figure 29). The critical role of EPG5 has been demonstrated in knockdown experiments, showing that its depletion strongly reduces autophagosome-lysosome fusion (Wang et al., 2016)

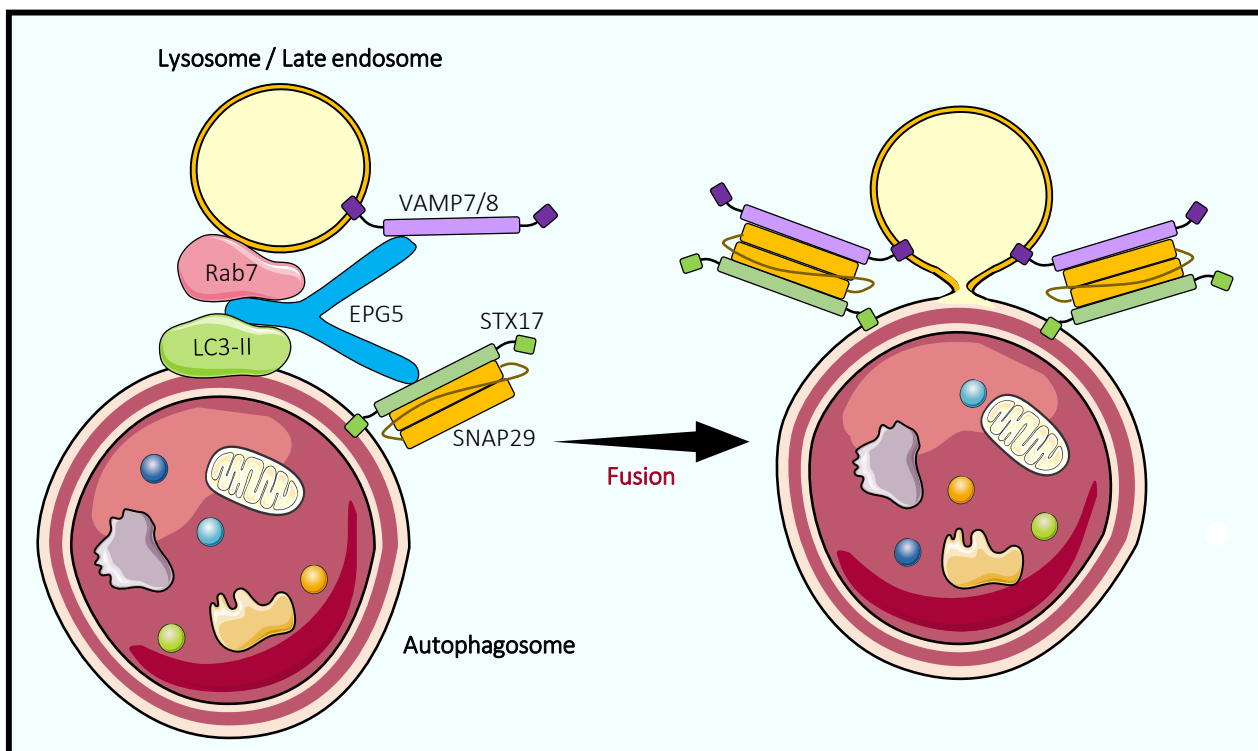


Figure 29. The fusion between autophagosome and lysosome. Proposed mechanism showing the role of EPG5 protein mediating the fusion between an autophagosome and a lysosome/late endosome. EPG5 is recruited to lysosome/late endosome membranes by binding with Rab7 and VAMP7/8 proteins. EPG5 also binds the autophagosome membranes by associating with LC3-II and STX17:SNAP29 and facilitates the organization of the *trans*-SNARE complex involved in the fusion between the two organelles. Cartoon adapted from Wang et al., 2016.

8.4. Different membrane sources for phagophore elongation

To date, the description of the molecular mechanism leading to the initiation of the phagophore has been based on a well-studied structure, the ER. In fact, it was generally accepted that the phagophore was generated *de novo* from the ER compartment (Axe et al., 2008; Ylä-Anttila et al., 2009). However, the origin of

the membrane that contributes to the formation of the phagophore has been a much-debated topic in recent years. During the last years several studies have shown that other cell compartments, such as the plasma membrane (Moreau et al., 2012; Ravikumar et al., 2010), the Golgi apparatus (Ge et al., 2013; Orsi et al., 2012), mitochondria (Hailey et al., 2010) and recycling endosomes (Puri et al., 2013, 2018), contribute significantly to the expansion of the phagophore. In support of the view of ER as a major source of lipids, a recent study published by Schütter and colleagues has highlighted that *de novo* synthesized phospholipids from the ER are likely the main membrane sources for phagophore expansion rather than other organelles membranes (Schütter et al., 2020). Noteworthy, ER exhibits the most extensive membrane platform and forms the so-called *membrane contact sites* (MCS) with almost every membrane-bound organelle in the cell (Helle et al., 2013). Studies based on electron tomography revealed that the ER membrane was found in the inner and outer membranes of the phagophore, owning multiples MCSs (Hayashi-Nishino et al., 2010).

Concerning the contribution from other cell compartments, the involvement of mitochondria in the biogenesis of the phagophore has been demonstrated (Hailey et al., 2010). Disruption of the MCS between mitochondria and the ER inhibited the recruitment of both ATG14 and LC3 and thus autophagosome biogenesis. This result makes possible to speculate on the fact that autophagosomes are produced from phospholipids originated from the ER that are then transferred to the mitochondrion to support the phagophore initiation process (Hailey et al., 2010; Hamasaki et al., 2013). The Golgi apparatus has been recognized as another source of lipids for the phagophore. In fact, it has been demonstrated that autophagy induction leads the redistribution of ATG9A-positive vesicles from the Golgi to the initiation site (Mari et al., 2010; Young et al., 2006), interacting transiently with the phagophore (Orsi et al., 2012). The plasma membrane has been found to be the source of production of so called “pre-autophagic endosomes”, a sub-population of endosomes marked by ATG16L1 or ATG9 proteins which contribute to the autophagosome formation (Ravikumar et al., 2010). This mechanism also involves the recycling compartment, where the pre-autophagic endosomes fuse (providing ATGs proteins) leading the recruitment of *WD repeat domain phosphoinositide-interacting* (WIPI) proteins and the machinery involved in the LC3 lipidation (Puri et al., 2018). Since the recycling compartment and the ER are very close is likely that these compartments contribute at different steps of the phagophore formation, putting forward the idea of the difference between membranes that contribute to the phagophore initiation and the platform where the ATG16-ternary complex and LC3 lipidation take place (Figure 30).

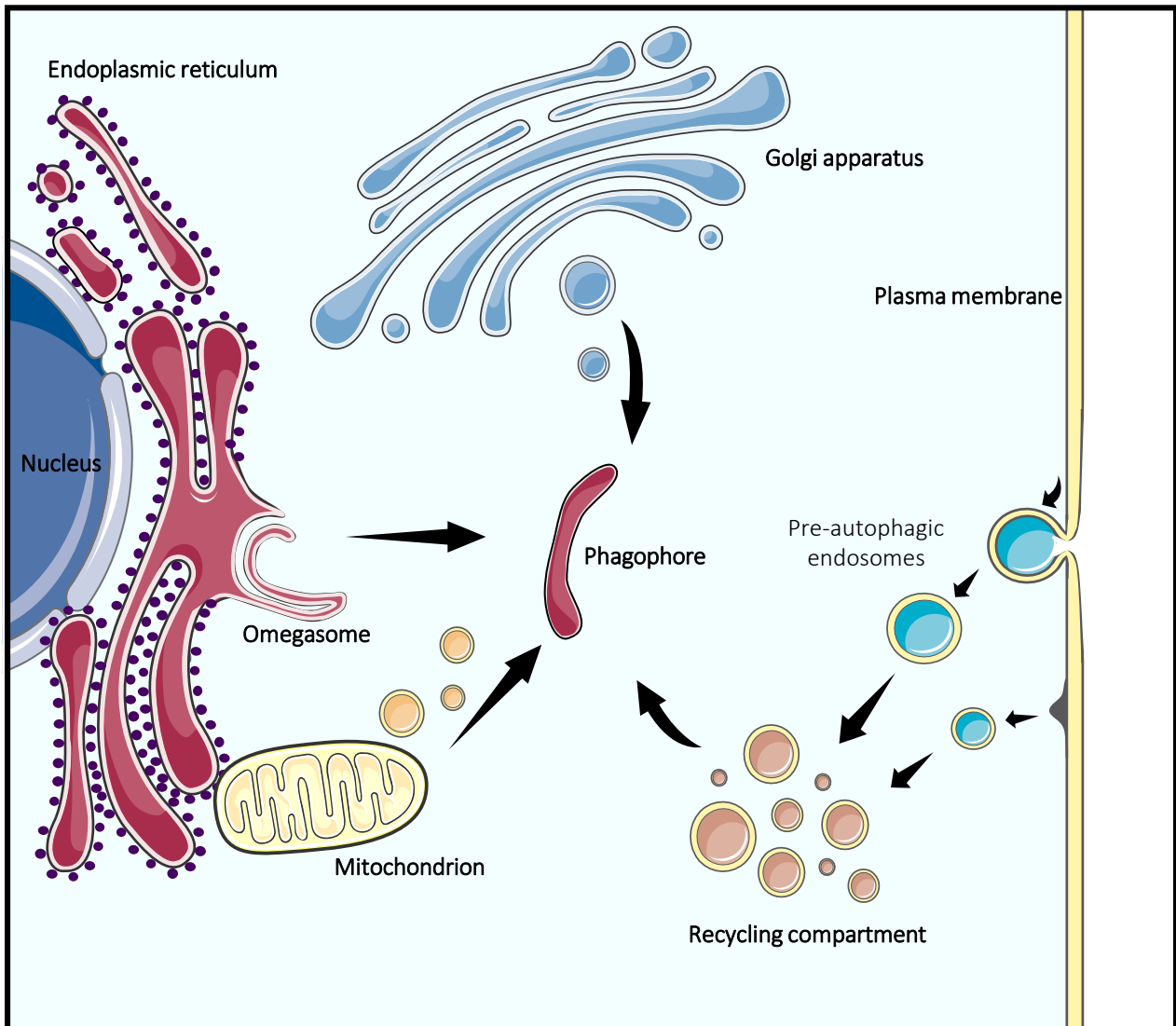


Figure 30. Different membrane sources for phagophore elongation. It has been accepted that different cellular compartments are involved in the autophagosome formation. The endoplasmic reticulum, the mitochondria, the Golgi apparatus, the recycling compartment and the plasma membrane with its pre-autophagic endosomes, are considered as different sources contributing to the omegasome/phagophore expansion.

9. The core autophagy protein ATG9A

As already introduced previously, ATG9A is an important regulator of the autophagy machinery, involved in the early steps of autophagosome biogenesis. Nevertheless, its precise function for phagophore expansion is still a matter of debate. Latest studies done on both mammalian ATG9A and yeast Atg9 are bringing to light new evidence on its precise function, described later in this thesis manuscript.

9.1. Topology and structural function of ATG9A

ATG9A is the only multi-spanning transmembrane protein among the core Atg proteins. It was first characterized as an integral membrane protein about twenty years ago, and it was then believed that the protein consists of six transmembrane domains, with both N- and C-termini oriented toward the cytosolic side of the cell. The first 3D structure of the protein came from *Arabidopsis thaliana* (At-Atg9) with a 7.8-Å-resolution, using single-particle *cryo-electron microscopy* (cryo-EM) (Lai et al., 2019). By combining predictive data from sequence co-evolution together with cryo-EM results, Lai and colleagues found that At-Atg9 organizes into a homotrimer, with each protomer containing at least six *transmembrane* (TM) α -helices (TM1-6) flanked by disordered N- and C-termini cytoplasmic regions. The homotrimer forms a central pore in which each protomer interacts, *via* its C-terminal region, with the other protomers in order to stabilize the entire complex (Lai et al., 2019) (Figure 31A). Although Lai and colleagues raised here important information, the cryo-EM “low” resolution did not allow to discern the arrangement of the transmembrane helices, as well as other structural details. Guardia and colleagues came to fill this gap by using cryo-EM at 2.9-Å-resolution on human ATG9A. They found that each homotrimer does not have six transmembrane helices, unlike At-Atg9, but only four (α 2, α 6, α 14, and α 15) and two more helices (α 11 and α 19) that are partially embedded in the membrane, without completely crossing it (Guardia et al., 2020). Juxtaposition between protomers is allowed by α 14 and α 15 that are stacked in a parallel fashion with α 2 and α 6 from neighbouring protomer, with specific interactions mainly observed between α 2 and α 14 (Guardia et al., 2020) (Figure 31B-C). An extensive domain located at the C-terminal of ATG9A, of about 250 amino acids, forms a platform presumably involved in protein-protein interactions with other partners. Interestingly, the ATG9A trimer displays an important network of internal cavities with a large central pore (Figure 31D) that was also observed in the plant Atg9. A lateral branch, extending from the central pore to the membrane-cytoplasm interface, is made of hydrophilic residues, suggesting a possible role of the protein in the transport of polar molecules such as lipids residing at the membrane. The critical role of these cavities was confirmed by mutating specific residues (Tryptophan) located at the lateral branch-central pore junction, or at the lateral branch-cytoplasmic interface (Figure 31D). In fact, expression of recombinant ATG9A proteins carrying these mutations was unable to rescue the normal size of LC3B puncta in ATG9A-KO cells, suggesting that the mutation-induced occlusion of the lateral branch impairs the possible transport of molecules for correct phagophore expansion (Guardia et al., 2020).

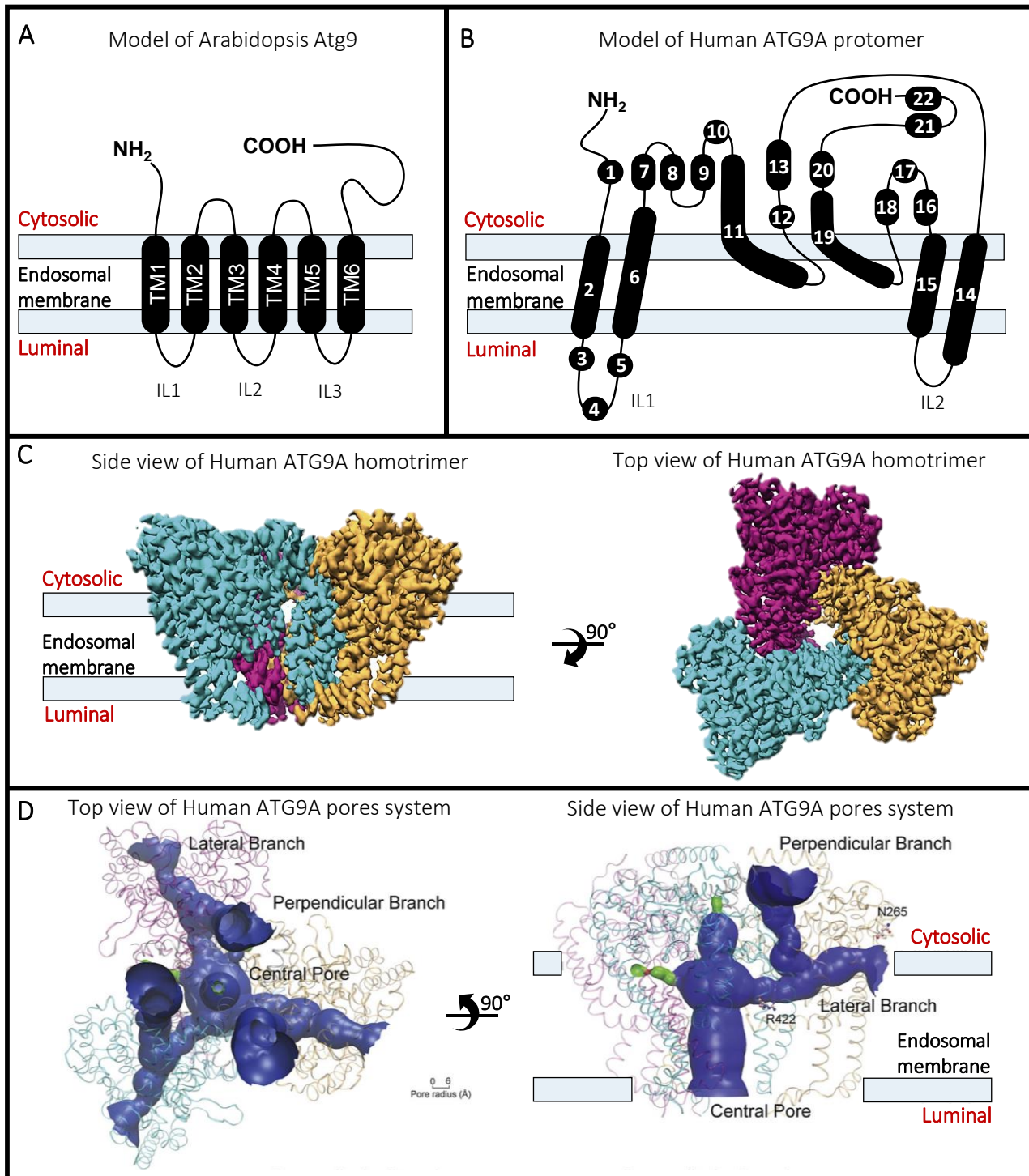


Figure 31. Atg9/ATG9A topology and its internal pores system. **A** | Cartoon illustrating the predicted topology of Atg9 from Arabidopsis, determined by using ultra-deep learning model from cryo-EM data at 7.8 Å resolution. Atg9 presents a disordered N-terminal tail, six transmembrane helices, three intra-luminal domains (IL1 to IL3) and a long-disordered C-terminal tail. The edges of the membrane are shown as soft blue rectangles. Cartoon adapted from Lia et al., 2020. **B** | Cartoon illustrating the topology of human ATG9A protomer obtained by cryo-EM at 2.9 Å resolution showing 22 α -helices (although β -strands are contained in the structure, they are not shown in the cartoon) and two intra-luminal domains (IL1 and IL2). The edges of the membrane are shown as soft blue rectangles. Cartoon adapted from Guardia et al., 2020. **C** | Cryo-EM density map of human ATG9A homotrimer in conformation B is shown in side (*Left*) and top views (*Right*) and colored in cyan, magenta and dark yellow. The edges of the membrane are shown as soft blue rectangles. **D** | Branched network of internal pores of ATG9A trimer shown in **C** | in top (*Left*) and in side views (*Right*). The internal pore network is shown with blue color. Three lateral branches and three perpendicular branches are shown on the *Left* and only one lateral and one perpendicular branch is shown on the *Right*. The edges of the membrane are shown as soft blue rectangles. Images shown in **C** | and **D** | are adapted from Guardia et al., 2020.

9.2. Biogenesis of ATG9A vesicles and their trafficking to the phagophore

ATG9A protein cycles between different cellular compartments, *via* vesicular transport, in order to deliver different sources of membrane to the forming autophagosome. It resides within highly dynamic vesicles with a diameter of 30 to 60 nm. In this section, I will detail the mechanism and protein complexes, emphasizing that ATG9A vesicles are synthesized and targeted to the phagophore during autophagy induction.

9.2.1. ATG9A-positive vesicles emanating from different sources contribute to autophagosome biogenesis

ATG9A-containing vesicles originate from the *trans*-Golgi, the plasma membrane, or the endosomal compartment and are an essential source for the formation of the phagophore. The Golgi apparatus was the first compartment to be recognized as a primary source of phospholipids and ATG9A vesicles for phagophore biogenesis (Mari et al., 2010; van der Vaart et al., 2010; Young et al., 2006). In fact, upon amino acid deprivation, a fraction of ATG9A redistributes to the omegasome (Mari et al., 2010; Young et al., 2006) where it transiently interacts with the phagophore, without being totally incorporated into its membrane (Orsi et al., 2012). The plasma membrane has been also found to be the source of production of so called “pre-autophagic endosomes”, a sub-population of endosomes marked by ATG9A and ATG16L1 proteins which contribute to the autophagosome formation (Ravikumar et al., 2010). This mechanism also involves the recycling compartment, where the pre-autophagic endosomes fuse (providing ATGs proteins) leading to the recruitment of WIPI proteins and the machinery involved in the LC3 lipidation (Puri et al., 2018).

9.2.2. ATG9A trafficking via AP complexes

Members of the AP family are heterotetrameric cytosolic complexes that are involved in the intracellular trafficking of cargo proteins between different organelles. Five AP complexes are nowadays known, from AP-1 to AP-5 (Park & Guo, 2014). These complexes can be incorporated into clathrin-containing vesicles or not. Intracellular clathrin-coated vesicles contain AP-1 or AP-2, whilst biogenesis of AP-3-containing vesicles can be partially dependent of clathrin. Formation of AP-4- or AP-5-containing vesicles is instead totally independent of clathrin. The N-terminus of ATG9A contains specific tyrosine- and dileucine-based sorting motifs, $^8\text{YQRLE}^{12}$ ($^8\text{YXX}\Phi\text{D}/\text{E}^{12}$) and $^{22}\text{EEDLL}^{26}$ ($^{22}\text{E}/\text{DxxLL}^{26}$) that allow its sorting from the TGN (AP-1 and AP-4) or its sorting in pre-autophagic endosomes emanating from the plasma membrane (AP-2) (Imai et al., 2016; Zhou et al., 2017; Mattera et al., 2017) (Figure 32). ATG9A mutations within these motifs inhibit redistribution of the protein by keeping it blocked at the *trans*-Golgi or at the plasma membrane due to a severe endocytosis defect (Zhou et al., 2017). Interestingly, cell stimulation with EGF can induce Src kinase-dependent phosphorylation of Y_8 into the N-terminus sorting motif of ATG9A, thereby promoting ATG9A-AP-1/2 interaction and ATG9A trafficking between compartments (Imai et al., 2016; Zhou et al., 2017). Although AP-1 and AP-2 sorting of ATG9A have been largely described, less is known about AP-4. AP-4 has recently been described in neuronal deficiencies,

in which AP-4 mutations lead to a form of *hereditary spastic paraplegia* (HSP) called the *AP-4 deficiency syndrome*. Purkinje and hippocampal neurones of HSP patients exhibit a missorting of the AMPA receptor which accumulates in abnormal LC3B structures (Matsuda et al., 2008). Later, Mattera and colleagues provided a direct link between *AP-4 deficiency syndrome* and autophagy, by demonstrating that AP-4 mutations induce the retention of ATG9A within the TGN, leading to autophagy impairment (Mattera et al., 2017). A work from Davies and colleagues provided additional mechanistic information by demonstrating that AP-4-dependent sorting and trafficking of ATG9A from the TGN is *RUN and SH3 domain containing* (RUSC)-dependent (Davies et al., 2018). RUSC1 and 2 are indeed accessory protein of AP-4, and mutations in RUSC2 cause a neurological disorder similar to the *AP-4 deficiency syndrome* (Alwadei et al., 2016) (Figure 32).

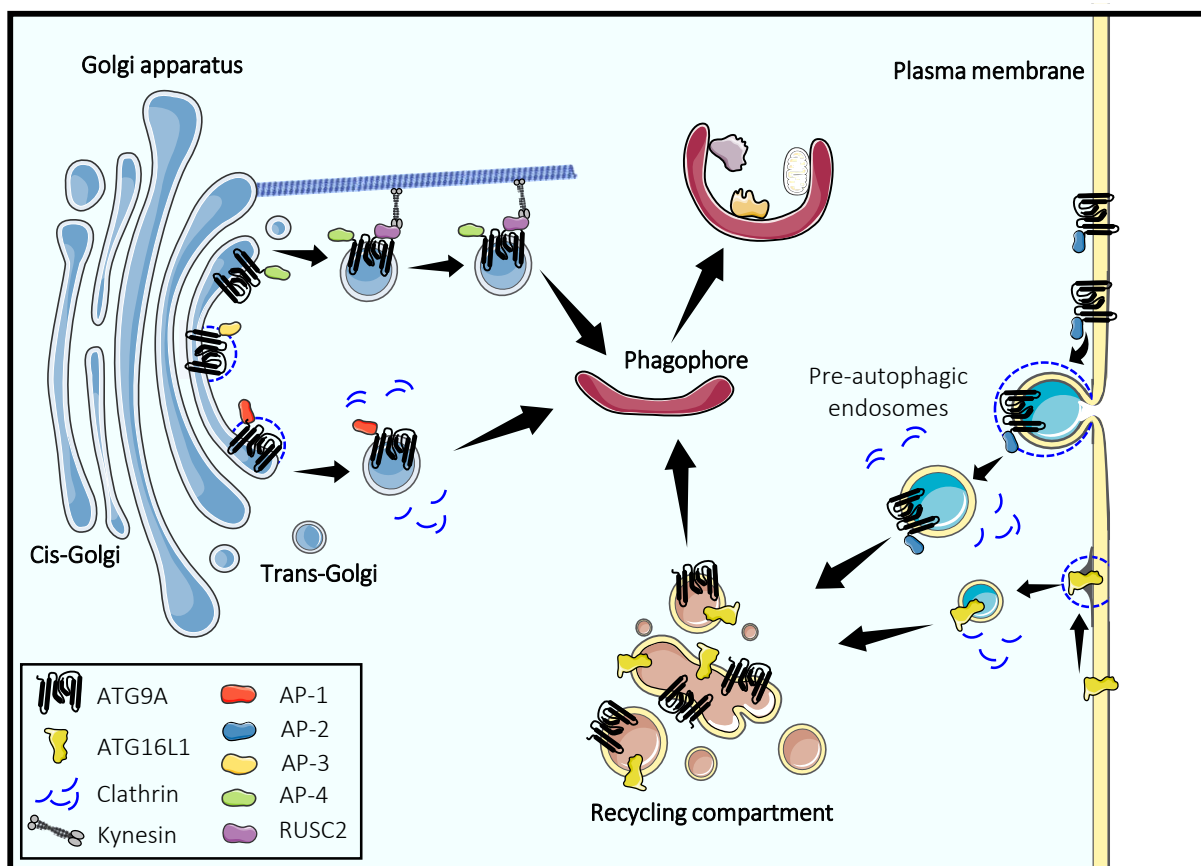


Figure 32. ATG9A trafficking via AP complexes. Representation of ATG9A trafficking between different cellular membrane compartments governed by AP complexes. ATG9A vesicles traffic from the Golgi apparatus toward the phagophore *via* AP-1, charged into clathrin-coated pits, and/or AP-4 complexes. Moreover, AP-4-containing vesicles are directed to the phagophore *via* RUSC2, which connects the cytosolic side of ATG9A with the molecular motor kinesin onto microtubules. ATG9A can be transported to the phagophore *via* AP-3-containing clathrin-coated pits, but this mechanism has not yet been clarified. In addition, ATG9A vesicles can come from the plasma membrane *via* AP-2-derived vesicles (also called pre-autophagic endosomes). ATG16L1-pre-autophagic endosomes are also internalized from the plasma membrane and meet ATG9A into the recycling compartment, which is another platform for phagophore elongation.

9.2.3. ATG9A trafficking via BAR-domain proteins

Traffic of ATG9A protein has been described to be also regulated by *Bin/amphiphysin/Rvs* (BAR)-domain containing proteins. BAR proteins are the best-known regulators of cell membrane curvature, and each BAR protein contains one of several BAR domains which differ in length, intrinsic curvature and binding affinity to the membrane. Combination of these features defines the specific cellular localization (Golgi, ER, plasma membrane, endosomes, filopodia etc) of BAR proteins into the cell (Simunovic et al., 2015). Three different classes of BAR proteins have been described: *Bax-interacting factor 1* (**Bif1**), **SNX18** and *ADP-ribosylation factor* (**Arf**) 2.

Bif1, also known as endophilin B, participates to the sorting of ATG9A-positive vesicles from the TGN or the RAB11-positive perinuclear recycling compartment. Consistently, Bif1 downregulation suppresses fission of Golgi membranes as well as redistribution of ATG9A toward periphery (Takahashi et al., 2011). During autophagy induction, Bif1 cooperates with dynamin 2, a protein which, by forming a bottleneck, participates to the final steps of the vesicle fission. It has been proposed that recruitment of Bif1 at the membrane budding site of ATG9A reservoirs initiates membrane tubulation, and then promotes the subsequent recruitment of dynamin 2 for final membrane fission and generation of ATG9A-positive vesicles (Takahashi et al., 2016) (Figure 33).

The second class of BAR proteins comprises **SNX18**, responsible for the binding of SNXs to PIs. SNX18, has been reported to be involved in the biogenesis of ATG16L1-ATG9A-positive vesicles from the RAB11-positive perinuclear recycling compartment. Depletion of SNX18 induces the accumulation of ATG9A proteins in RAB11-recycling endosomes. Similar to Bif1, SNX18 binds and recruits dynamin 2 to trigger the biogenesis of autophagic vesicles from the RAB11 compartment, and it is still unclear whether SNX18 and Bif1 compete or cooperate in this process (Sørensen et al., 2018) (Figure 33).

Last but not least is **Arf**, the third BAR family protein which localizes at the TGN *via* interaction between Arf1 motif and *phosphatidylinositol 4-phosphate* (PI4P). Arf1 is likely involved in the formation of secretory granules while Arf2 has been shown to regulate exocytosis of metalloproteinases and trafficking of ATG9A (De Tito et al., 2020). Interestingly, ATG9A vesicles contain and deliver *class III phosphatidylinositol 4-kinase β* (PI4KIII β) to the growing phagophore by a direct interaction between ATG9A and PI4KIII β to control PI4P production, which then recruits ULK1/2 to nascent autophagosomes (Judith et al., 2019). Downregulation of Arf2 protein or blocking its binding to PI4P induces an important dispersal of ATG9A vesicles from the perinuclear region as well as reduces ULK1-containing autophagic membranes and LC3B-positive autophagosome biogenesis (Judith et al., 2019) (Figure 33).

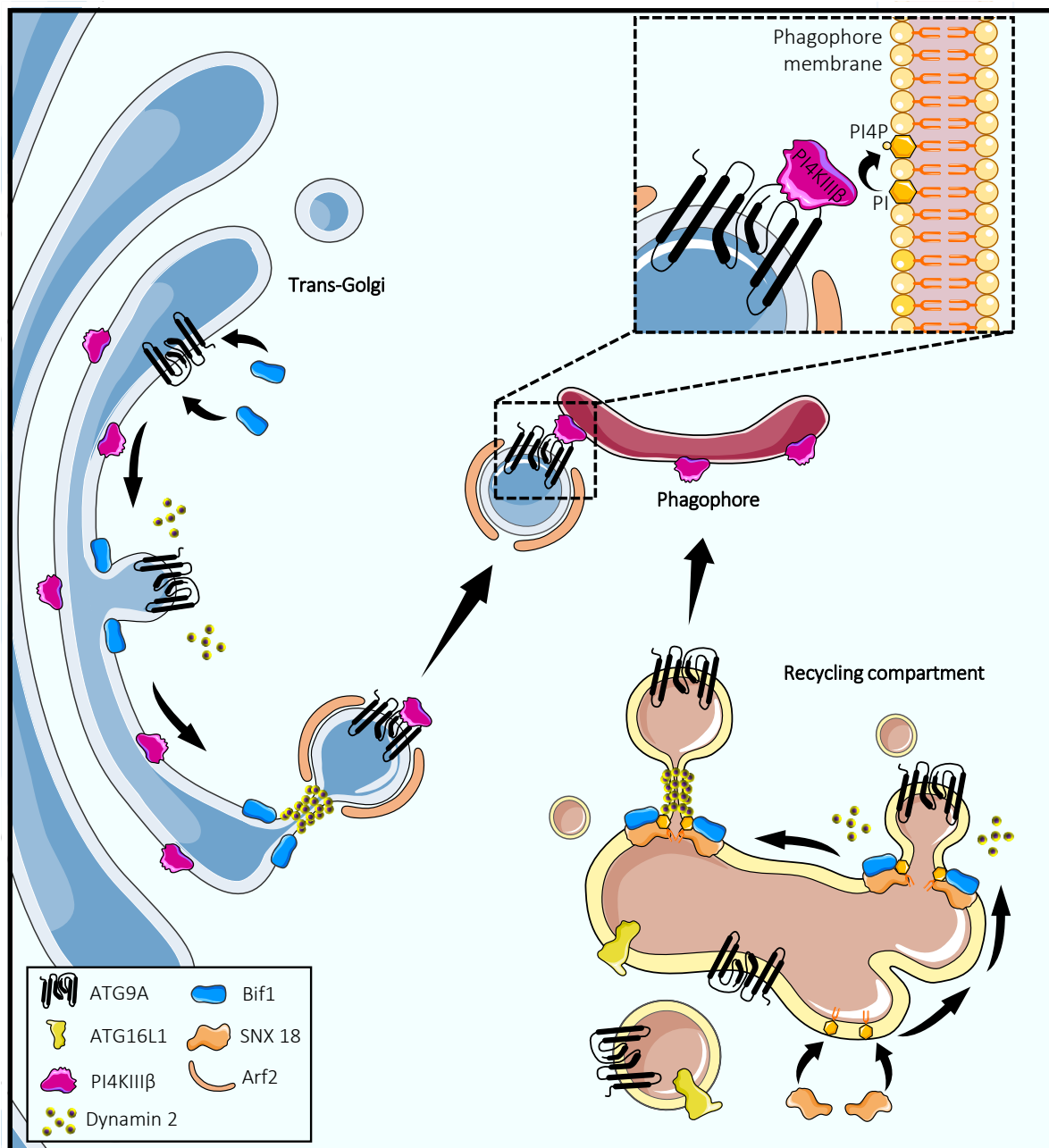


Figure 33. ATG9A trafficking via BAR-domain proteins. Representation of ATG9A trafficking between the Golgi apparatus and the recycling compartment regulated by BAR-domain proteins. ATG9A transport between the Golgi apparatus is mediated by Bif1 and Arf2, which also controls the correct delivery of PI4KIIIβ to the phagophore via an interaction with ATG9A cytosolic side. PI4KIIIβ mediates the phosphorylation of PI to produce PI4P at the phagophore membrane. The biogenesis of ATG9A vesicles from the recycling compartment is controlled by SNX18. The activity of dynamin 2 pinches off the vesicles from both the recycling compartment and the Golgi apparatus.

9.2.4. Yeast Atg9, the central hub for the recruitment of the autophagic machinery

The first of the latest major report on Atg9 was recently published in *Science*, in which a more defined role of Atg9 was studied in yeast for the first time. By using an *in vitro* reconstituted system, including 21 polypeptides and membrane platforms, Sawa-Makarska and colleagues built the entire yeast core autophagy machinery to better control the different reactions of the early steps of autophagy (Sawa-Makarska et al., 2020). They have found that Atg9 vesicles are the substrates of PI3KIII and that PI3P production at their

surfaces mediates the recruitment of the autophagy machinery, including the Atg2-Atg18 “lipid transfer module”, and Atg12-Atg5-Atg16 ternary complex for Atg8 lipidation. Most importantly, since autophagosomes are generated in close proximity of ER, data from Sawa-Makarska and colleagues suggest that Atg9 vesicles may actually be the seeds of the phagophore. Atg9 vesicles would progressively expand and mature into autophagosomes thanks to the lipid transfer activity of Atg2, that would control the flux of lipids from the ER toward the outer leaflet of the Atg9 vesicle.

According to this model, if Atg2 inserts lipids only into the outer leaflet of the vesicle, a mechanism must then exist to transport half of the absorbed lipid into the inner leaflet of the phagophore, in order to allow the two leaflets of the membrane to grow evenly over time. Two key reports, published almost at the same time than the work of Sawa-Makarska and colleagues, designated Atg9 as a prime candidate for playing this role (Figure 34).

They indeed shed light on the scramblase activity of Atg9, *i.e.* the enzymatic-like ability to redistribute phospholipids from the outside to the inside of a lipid bilayer and vice versa with no use of ATP (Maeda et al., 2020; Matoba et al., 2020). By using the dithionite assay, a molecule that quenches the fluorophores on the outer leaflet, they have found that Atg9 transports different types of fluorescent phospholipids (such as phosphatidylcholine, phosphatidylserine and phosphatidylethanolamine), from the inner to the outer leaflet of liposomes, in a non-selective manner (Maeda et al., 2020; Matoba et al., 2020). Taken together, these results propose a very attractive model by which lipids insert their head groups into the vertical pore and then are flipped laterally (Maeda et al., 2020). Although the mechanism by which Atg9 uses its pores to transport lipids has not yet been elucidated, these reports have uncovered an unexpected and appealing role for this protein (Figure 35).

Could ATG9A-positive vesicles also be the seeds of autophagosomes in mammals? Although human ATG9A also possesses scramblase activity (Maeda et al., 2020; Matoba et al., 2020) and ATG9A trimers contain internal cavities that may allow the transfer of lipids (Guardia et al., 2020), this scenario is not consistent with earlier observations. Indeed, in mammals, retention of ATG9A in mature autophagosomes and prolonged colocalization of the protein with the conjugation systems have never been observed. Several studies have instead proposed that ATG9A-positive vesicles emanating from different sources establish dynamic and transient contacts with the phagophore to deliver lipids and important components for its expansion (Orsi et al., 2012). In this alternative scenario, the specific roles of mammalian ATG9A scramblase and ATG2 lipid transfer activities deserve further investigations.

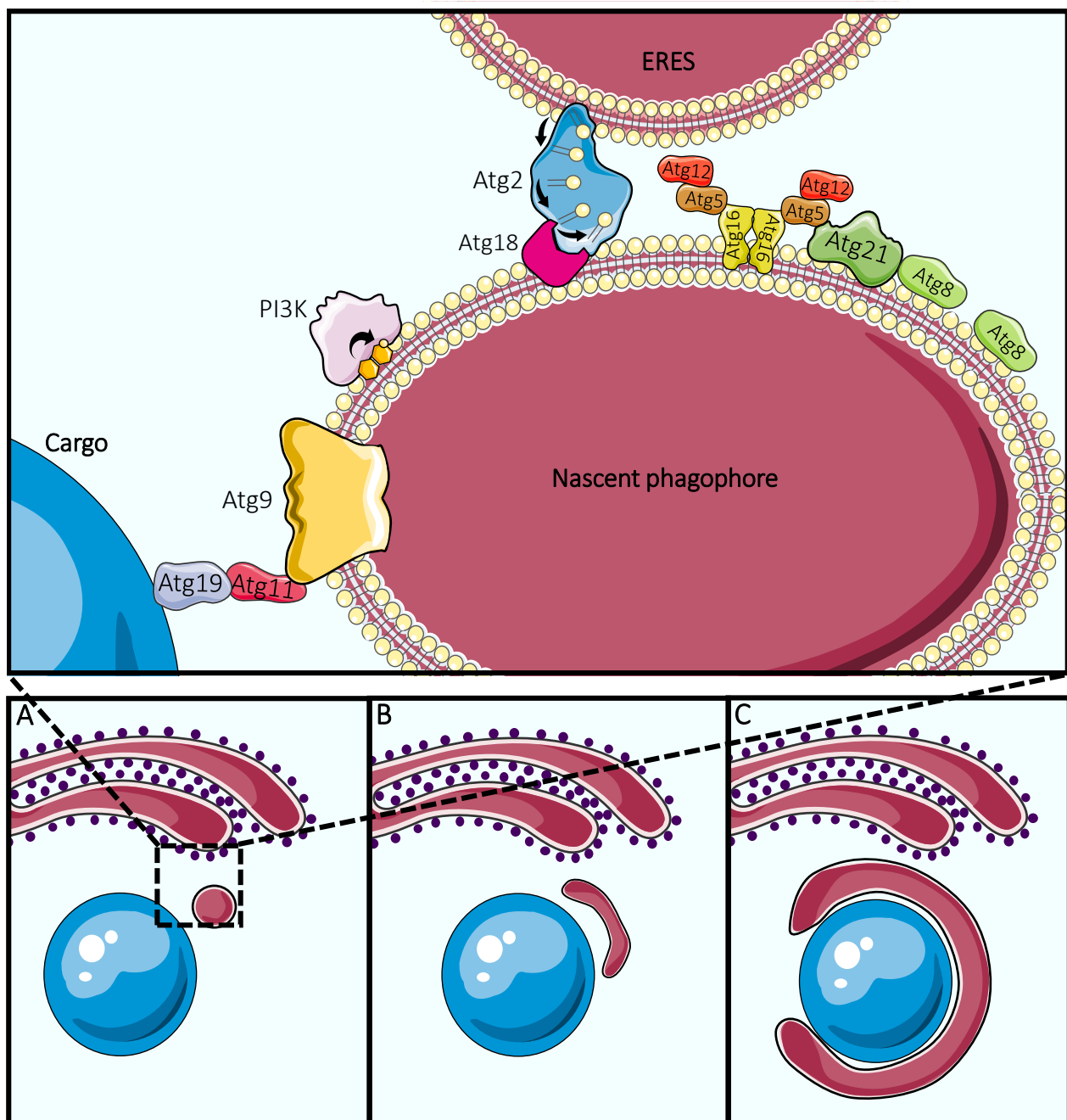


Figure 34. Model for the initial steps of yeast Atg9-mediated phagophore generation. **A** | Atg9 vesicles are recruited to the cargo *via* the Atg19:Atg11 scaffold complex. Then, Atg9 vesicles recruit Atg2:Atg18 lipid transfer complex and PI3K in order to transfer phospholipids from the donor compartment (*endoplasmic reticulum exit sites*, ERES) to the nascent phagophore and to produce PI3P, respectively. Production of PI3P by PI3K induces the recruitment of Atg21 and the E3-like Atg12-Atg5-Atg16 complex which control the Atg8 conjugation to the membrane. **B** | Lipid influx from the donor compartment, *via* the lipid transfer machinery favors expansion of nascent phagophore membranes and **C** | supplies component for Atg8 lipidation, until the autophagosome matures. Cartoon adapted from Sawa-Makarska et al., 2020.

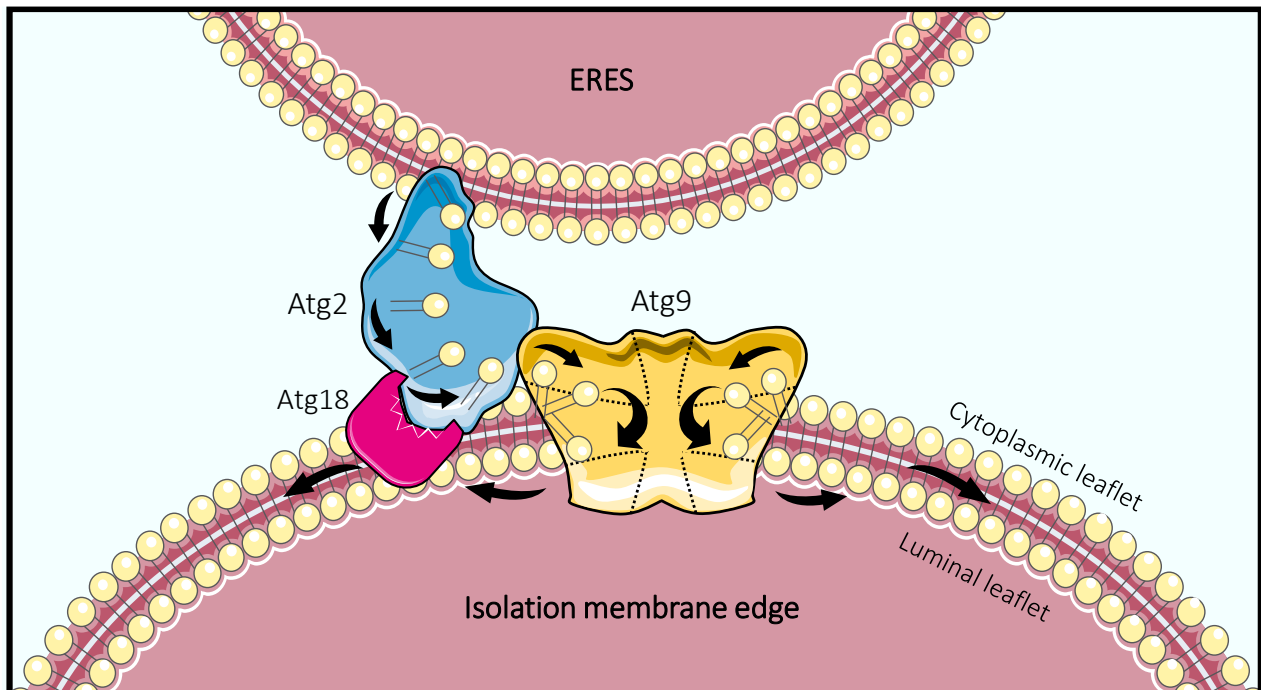


Figure 35. Model of the scramblase activity of Atg9/ATG9A. During membrane isolation, the lipid transfer enzyme Atg2 transport lipids from the donor compartment (*endoplasmic reticulum exit sites*, ERES) to the nascent phagophore, with the support of the Atg18 scaffold protein. Atg9/ATG9A redistributes the phospholipids from the cytoplasmic leaflet of the isolation membrane to the luminal leaflet, *via* its scramblase activity, enabling the expansion of the phagophore. A vesicle lacking Atg9/ATG9A is unable to expand because phospholipids are distributed in the cytoplasmic leaflet only, inhibiting the luminal leaflet to grow. Cartoon adapted from Maeda et al., 2020 and Matoba et al., 2020.

10. Signaling pathways regulating the autophagy machinery

Eucaryotes have developed different strategies for maintenance of the normal physiological status and homeostasis of nutrient metabolism is critical for this purpose. Signaling pathways, including transcription, translation and post-translation modifications are necessary for cell adaptation in an environment that is constantly changing and subject to nutrient deficiencies or excesses. Generally, when nutritional stress deficiency occurs, cells respond by activating autophagy, whereas nutrition excess inhibits this mechanism. Autophagy regulation is then crucial for both cell survival and death. Next paragraphs are going to describe how different energy sources have an impact on autophagy.

10.1. Regulation by amino acids

The main key factor of amino acid-mediated regulation of autophagy is mTORC1 that is sensitive to amino acids levels as well as growth factors. As already mentioned (paraphaph 8.1.3), mTOR activation inhibits autophagy by acting on the ULK complex. The clearer mechanism for mTORC1 activation by amino acids came from the identification of the Rag GTPase complexes that interact with mTORC1 at the membrane of lysosomes (Kim et al., 2008; Sancak et al., 2008). Amino acid levels are detected by the Rag family proteins, that include four members (Rag A, Rag B, Rag C and Rag D) able to form heterodimers. In the presence of amino-acids, Rag A-B-GTP and Rag C-D-GDP heterodimers recruit mTORC1 at the lysosomal membrane (Sancak et al., 2008)

through another complex called regulator (Sancak et al., 2010). There, another small GTPase, named *Ras homolog enriched in brain* (RHEB), can finally activate mTORC1 and autophagy is then inhibited (Russell et al., 2014). Amino acid deficiency, instead, switches the Rag heterodimer into an inactive form containing GDP-bound Rag A-B, hence releasing inactivated mTORC1 from the lysosomal membrane (Rabanal-Ruiz et al., 2017) (Figure 36).

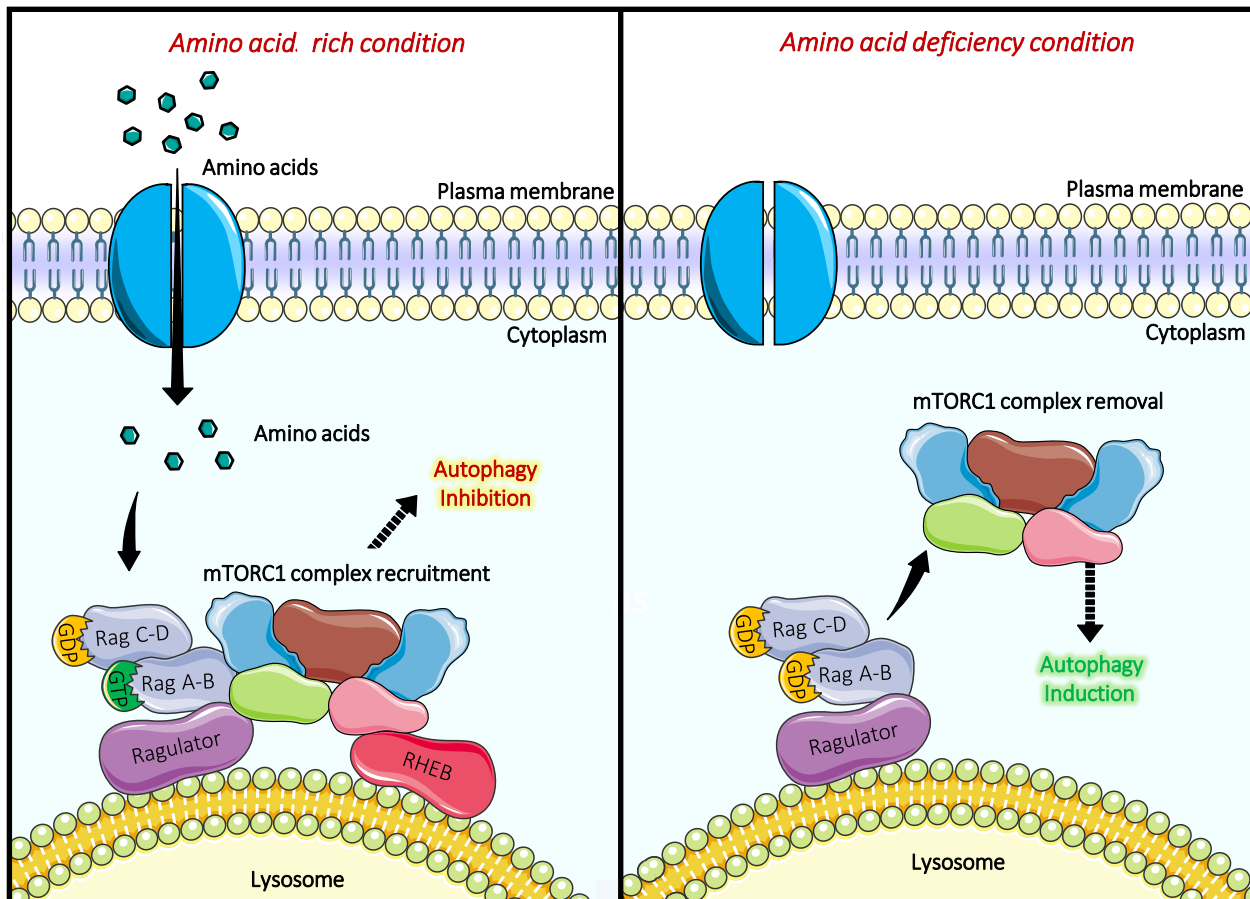


Figure 36. Regulation of autophagy by amino-acid availability. (Left) Under optimal amino acids conditions, amino acids activate Rag GTPases which associate with Ragulator on the lysosomal membrane. This induces Rag A-B to exchange GDP for GTP and causes the recruitment of mTORC1 and its interaction with RHEB protein. RHEB finally activates mTORC1, leading to autophagy inhibition. (Right) Upon amino acid deficiency, Rag A-B does not exchange GDP with GTP and mTORC1 cannot be recruited and remains inactive, leading to autophagy induction.

10.2. Regulation by growth factors

The control of autophagy is also exerted by growth factors. In the presence of growth factors, such as EGF, PI3K signaling pathway is activated and induces the inhibition of *tuberous sclerosis complex 1/2* (TSC1/2) which, by acting as a GTPase protein, in turn inactivates RHEB (Russell et al., 2014). As already mentioned above, RHEB activates mTORC1 and autophagy is inhibited. Conversely, withdrawal of growth factors from the extracellular medium is sufficient to stimulate autophagy despite the presence of other nutrients (Lum et al., 2005). The action of growth factors can also be independent of mTOR, as it has been shown that activated EGFR can directly phosphorylate beclin 1 on different tyrosine residues. In fact, phospho-beclin 1 owns a higher

affinity for Rubicon and a moderate affinity for Vps34, two proteins already addressed in paragraph 8.1.2., the outcome will be a reduction of PI3KIII activity and thus, of autophagic activity (Wei et al., 2013) (Figure 37).

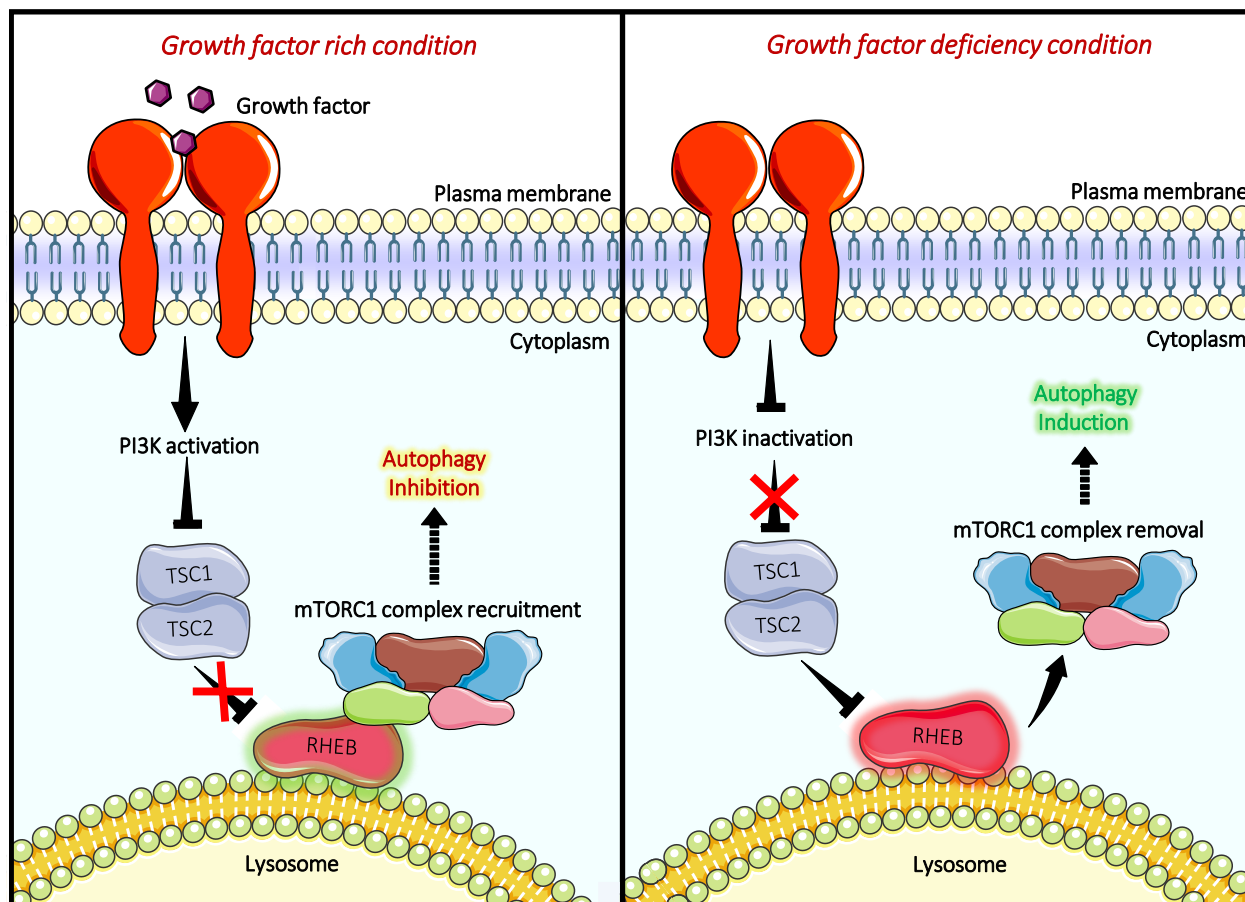


Figure 37. Regulation of autophagy by growth factors. (Left) Under optimal growth factor conditions, growth factor receptors (such as EGFR) activate the downstream pathway involving PI3K/Akt axis. PI3K/Akt cascade inhibits TSC1/2 proteins, removing the inhibitory brake they had on RHEB. RHEB can activate mTORC1 to mediate signaling for autophagy inhibition. (Right) Upon growth factor deficiency, PI3K/Akt axis is not triggered, leading to activation of TSC1/2 proteins which inhibit RHEB protein. mTORC1 is then removed and inhibited, resulting in autophagy induction.

10.3. Regulation by hypoxia

Low oxygen availability, or hypoxia, represents a feature that can be encountered in both pathological and normal conditions. Together with nutrient deprivation, hypoxia is the most powerful factor relaying autophagy induction. Under hypoxic conditions, the transcription factor *hypoxia-inducible factor* (HIF)-1 α is stabilized and induces the expression of key genes involved in autophagosomes biogenesis, including *BCL2 interacting protein 3* (BNIP3), beclin 1, PI3KIII, ATG7, ATG5 and ATG9A (Zaarour et al., 2021). Although not a core protein of the autophagy machinery, BNIP3 is a pivotal protein for hypoxia-induced autophagy. Its increased expression indeed induces the formation of a BNIP3:BCL2 complex, which releases the inhibitory tone exerted by BCL2 on beclin 1. Sequestration of BCL2 away from beclin 1 then makes beclin 1 available to interact with VPS34, thereby initiating the autophagic process (Zhang et al., 2008). Consistent with this model, depletion of BNIP3 totally abrogates hypoxia-induced autophagy (Bellot et al., 2009) (Figure 38).

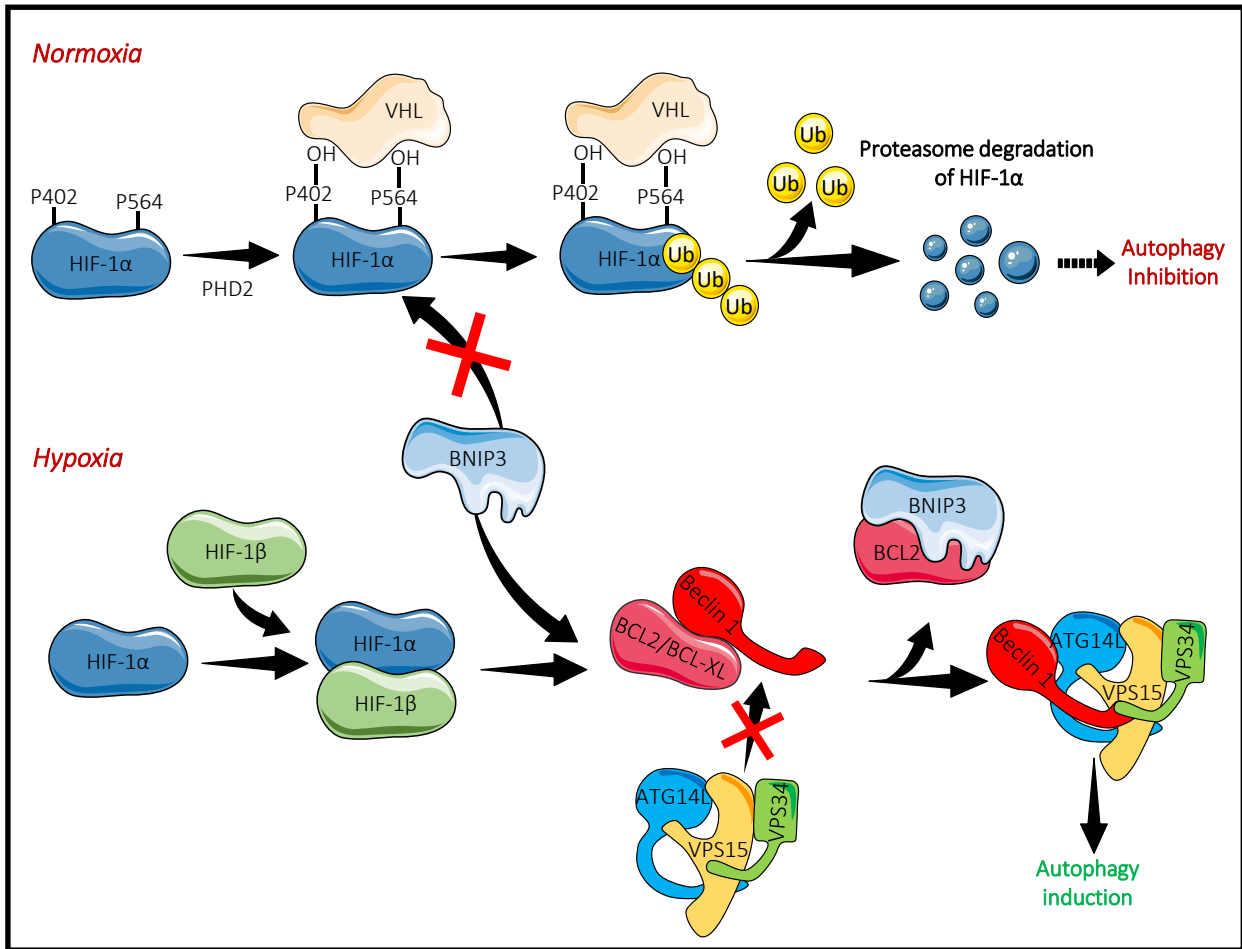


Figure 38. Hypoxia-dependent pathways regulating autophagy. (Upper) HIF-1 α regulation under normoxia. In the presence of oxygen, HIF-1 α subunits are hydroxylated on proline residues (P402 and P564) by *prolyl hydroxylase 2* (PHD2). Hydroxylation is important for *Von Hippel-Lindau protein* (VHL) binding to HIF-1 α , which recruits the E3 (ubiquitin ligase) enzyme that ubiquitinates HIF-1 α . Ubiquitination of HIF-1 α directs it for degradation via the proteasomal machinery, and autophagy is thus inhibited. (Lower) HIF-1 α regulation under hypoxia. Upon hypoxia induction, HIF-1 α becomes stable and dimerizes with HIF-1 β . In these conditions, BNIP3 is overexpressed, leading to sequestration of BCL2/BCL-XL which normally inhibits Beclin-1. Beclin-1 is then free to associate with the other components of the PI3K complex and favors autophagy induction.

11. Other normal and pathophysiological roles of autophagy

11.1. Cellular homeostasis and quality control

The activation of autophagy is not only induced by nutritional deficiency or cellular stress but is constantly active at basal levels. Basal activation of autophagy is not necessarily linked to the energy status of the cell but mostly in maintaining cellular homeostasis by controlling clearance of aggregate-prone proteins, misfolded proteins, or damaged organelles. This role has been deeply investigated during the last decade in the context of neurodegenerative diseases, as a selective autophagy mechanism called aggrephagy. The brain needs to be protected under nutrients withdrawal by constant supply from other organs and autophagy does not cooperate in response to nutritional starvation, suggesting that autophagy occurs at basal rate in the brain and is not enhanced during starvation. It is also admitted that autophagy activity decreases over the age, making it more difficult to treat neurodegenerative diseases in which protein aggregates accumulate and

induce neuronal death (Komatsu et al., 2007). To investigate the pathophysiological roles of basal autophagy in the brain, autophagy-deficient mice have been generated. Atg7-deficient mice exhibited several neurological and behavioural deficits and died within 28 weeks after birth. Furthermore, Atg7-KO mice have shown neuronal loss in both cerebellar and cerebral cortex as well as accumulation of polyubiquitylated proteins which increased in size and number with aging (Komatsu et al., 2006). Similar results were obtained in Atg5-deficient mice (Hara et al., 2006). Although aggregation of proteins induced cell death in neurons and hepatocytes (Hara et al., 2006; Komatsu et al., 2005, 2006) deficient for autophagy genes, this did not occur in fast growing cells such as mouse embryonic fibroblasts or astroglia cells with the same deficient-gene battery (Komatsu et al., 2007). This leads the scientific community to suggest that fast and dividing cells often manage to resist very efficiently the accumulation of these protein aggregates because cell division allows dilution of these waste in daughter cells. On the other hand, cells that do not undergo mitosis, such as neurons and hepatocytes, are much more susceptible to the accumulation of these aggregates because they cannot dilute the waste, making the accumulation phenomenon toxic and irreversible.

11.2. Function in secretion and exocytosis (*ATG gene-dependent secretion*)

Autophagy genes are not involved in autophagy process only but also in targeting intracellular cargo to the plasma membrane or extracellular environment, putting forward the new paradigm of “secretory autophagy” or ATG gene-dependent secretion in which the part of the term “phagy” is not really involved. In mammalian cells, the mechanism of exocytosis of the pro-inflammatory cytokine IL-1 β , driven by Atg5, has been described. Dupont and colleagues have shown that autophagy induction cooperates with GTPase proteins, such as Rab8a, controlling post-Golgi polarized trafficking and exocytosis of IL-1 β , uncovering how the autophagy machinery is employed for unconventional secretion (Dupont et al., 2011). *How can these secretory vesicles bypass the autophagic pathway to be directed to the plasma membrane?* Kimura and colleagues have shown that autophagosome-like vesicles containing IL-1 β are directed toward the plasma membrane thanks to the residence of SNARE proteins, such as SEC22B, instead of STX17 which normally directs the autophagosome-like vesicles toward the degradative pathway and support the fusion with lysosomes (Kimura et al., 2017). Although this mechanism has been proposed *in vitro*, it remains difficult to verify *in vivo*, as deletion of Atg5, Atg7 and Atg16L1 is instead associated with increased level of IL-1 β secretion (Kimmey et al., 2015; Saitoh et al., 2008) (Figure 39). In Alzheimer disease, Atg7-KO neurons have a diminished amyloid β secretion and the Atg7 rescue restores its secretion (Nilsson et al., 2013) (Figure 39). Recent work from Galli’s lab has shown a new mechanism called *secretory reticulophagy/ER-phagy* (SERP) that consists in the incorporation of ER components into late endosomes targeted to the secretory pathway, instead of an incorporation in forming autophagosomes during “regular” ER-phagy. They have found that Atg5 KO induced a more efficient SERP mechanism leading to an increased secretion of LC3B-II as well as LC3-interacting region-

containing proteins of the ER. This mechanism is VAMP7-dependent and is particularly active and important during neurite growth (Vats & Galli, 2021; Wojnacki et al., 2020) (Figure 39).

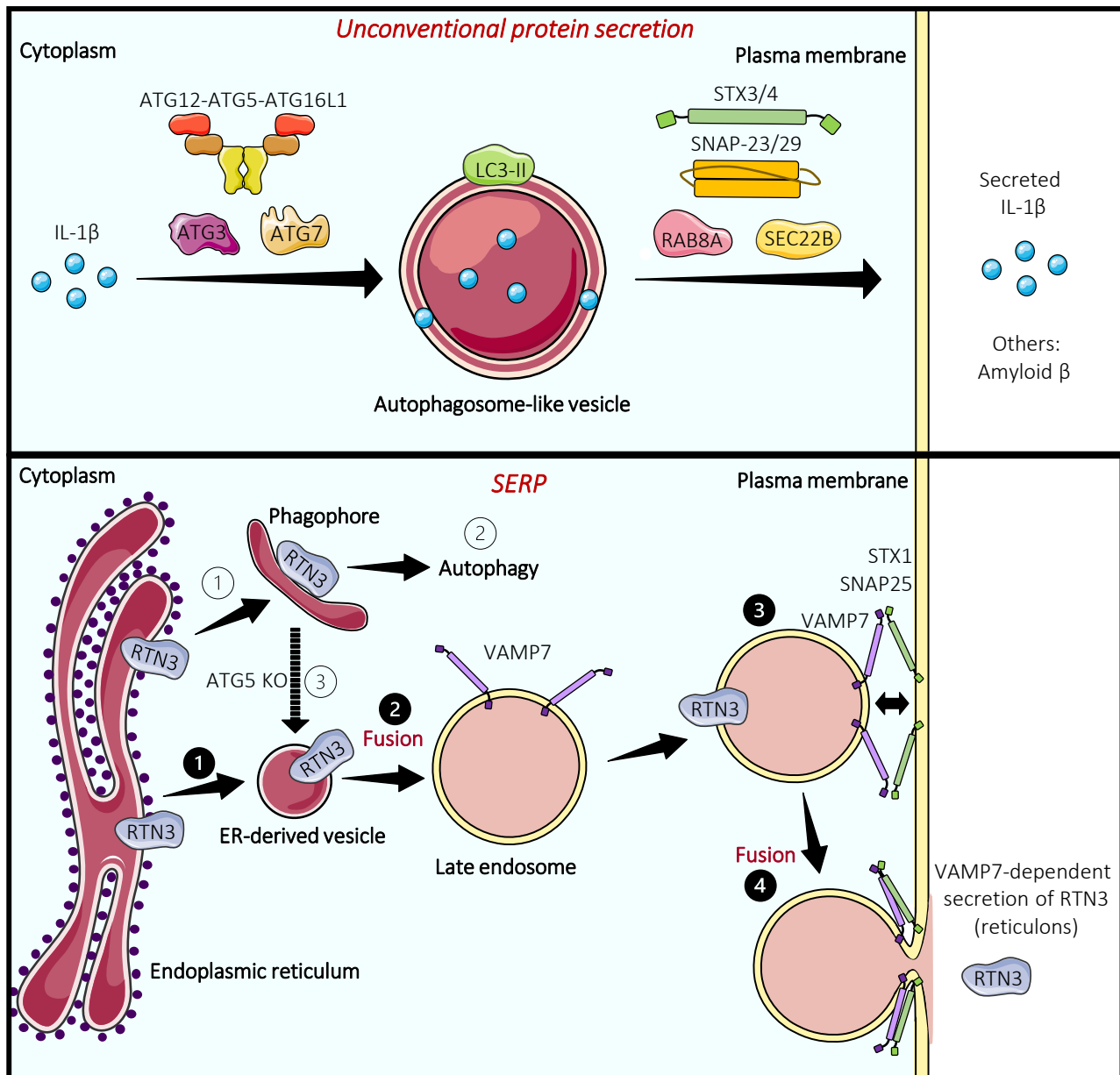


Figure 39. The role of autophagy in exocytosis. (Upper) Unconventional protein secretion of pro-inflammatory cytokines, such as IL-1 β , or amyloid β requires ATG12-ATG5-ATG16L1 complex, ATG3 and ATG7 proteins. Autophagosome-like vesicles containing LC3-II protein are then target toward the plasma membrane and secretion is facilitated by a mechanism involving RAB8A, SEC22B and the SNARE proteins STX3/4 and SNAP-23/29. (Lower) Model of VAMP7-dependent *secretory reticulophagy/ER-phagy* (SERP). The ER adaptor protein, RTN3L contains a LIR motif, and is then capable to interact with LC3-II protein and packed ER fragments into nascent phagophore (1). This led to degradation *via* autophagy (2). Eventually, ATG5 KO moves RTN3 traffic to a SERP mechanism (3), rather than autophagy. Alternatively, ER fragments containing RTN3 protein can be associated to ER-derived vesicles (1) and then fuse with late endosomes which contain VAMP7 (2). This late endosome fuses with the plasma membrane *via* a mechanism involving the SNARE proteins VAMP7, STX1 and SNAP25, thereby secreting ER cargo called reticulons in the extracellular space (3) (4). This mechanism is important during membrane expansion and neurite growth. Cartoon adapted from Vats and Galli, 2021.

12. Autophagy and cancer

The relationship between autophagy and cancer is now increasingly well researched. However, the exact connection of these two processes remains elusive. In the biology of cancer, autophagy plays two different roles, an anti-tumour or pro-tumour role. In this context some antitumoral drugs can regulate autophagy but this can act by inducing either expression of cancer suppressor proteins or oncogenes. The pro- or anti-tumoral activity of autophagy then strictly depends on the context in which the tumour develops.

12.1. Anti-tumoral role of autophagy

Many studies have shown that autophagy has an anti-tumour role. This tumour-protective role is already inherent in the meaning of the term 'autophagy' because it acts by decreasing various stresses (nutrient deprivation and oxidative stress), eliminating damaged cellular compartments, including organelles, misfolded and long-lived proteins, that may finally interfere with cellular homeostasis. When homeostasis is no longer balanced, the formation of malignancies is thus favored (Yun & Lee, 2018). Early studies have shown that monoallelic deletion of the BECN1 gene, encoding beclin 1, is frequent in several types of breast, ovarian and prostate cancers (40 to 75% of cases) (Liang et al., 1999). Loss of beclin 1 in both cancer cell lines and mouse models has shown a reduction of autophagy activity and an increase of cell proliferation. Instead, beclin 1 overexpression is linked to inhibition of proliferation in the MCF7 breast cancer cell line and tumorigenesis in nude mice. Moreover, beclin 1 protein is endogenously weakly expressed in human breast carcinoma, whereas it is highly expressed in normal breast epithelium (Liang et al., 1999; Qu et al., 2003). These data show that beclin 1 acts as an oncosuppressor gene.

Other autophagy genes have been shown to be associated with tumour growth. For example, loss of Atg5 and Atg7 in hepatocytes induces the formation of liver cancer due to the accumulation of p62, damaged DNA, mitochondria alteration and thus oxidative stress (Takamura et al., 2011). The mono-allelic loss of ATG5 is a factor of poor prognosis in patients suffering from melanoma, and this alteration, reproduced in mice, increases the metastatic potential of cancer cells as well as their resistance to treatments (García-Fernández et al., 2016). In glioma, previous work has demonstrated that autophagic activity was inversely correlated to the tumoral grade. Specifically, downregulation of beclin 1 and LC3B-II was associated with glioblastoma (Huang et al., 2010). Also correlative, these data suggest that alteration in autophagy genes may constitute a key event during glial tumorigenesis. Also, autophagy may inhibit the early stages of tumorigenesis by limiting inflammation, tissue and genome damages. This suggests that stimulation of autophagy might prevent some forms of cancer. Indeed, it has been widely demonstrated that low-calorie diets combined with physical activity have a positive effect in aging as well as cancer prevention that could be attributed to autophagy (Blagosklonny, 2010; He et al., 2012).

12.2. Pro-tumoral role of autophagy

Many studies indicate that autophagy acts as a tumour inducer in advanced cancers. In some cancers, cells are exposed to extreme stressful conditions, such as low nutrients and hypoxia due to abnormal vascularisation. In this view, autophagy is an important source for drawing energy from its constituents and maintaining a satisfactory energy need (Yun & Lee, 2018), allowing cell survival. For example, loss of beclin 1 and thus inhibition of autophagy induces cell death in solid tumours, especially in highly hypoxic regions (Degenhardt et al., 2006). Autophagy is also upregulated in cells carrying mutation of Ras, a GTPase involved in cell proliferation and tumour survival. The accumulation of altered mitochondria is observed in these cells as well as a decrease in cell growth (Guo et al., 2013; Guo & White, 2013). Collectively, the extensive literature on autophagy and cancer leads to the view that autophagy has several functions during cancer development. It is thought that autophagy slows the early stages of tumour progression by limiting the toxic effects of substance accumulation and DNA damage. In the later stages, autophagy would promote cancer cell survival in an environment where cells are deprived of oxygen and nutrients.

12.3. Autophagy modulation as a therapeutic cancer target

Autophagy is a protective mechanism in many types of tumours undergoing drug therapy and modulation of autophagy is a potential strategy to enhance patient outcome. Chemotherapy is a common treatment for cancer, but it is often limited by induction of chemoresistance. Furthermore, chemotherapy enhances autophagy inducing failure of cell death and thus cancer-cell survival. Different autophagy regulators are used in cancer therapy which act at different steps of the autophagic process, such as rapamycin, *chloroquine* (CQ) and *hydroxychloroquine* (HCQ) (Mulcahy Levy & Thorburn, 2020). The most used approach to inhibit autophagy in cancer therapy is the use of chloroquine and hydroxychloroquine, a well-known drug that prevent and treat malaria acting as lysosomal inhibitors (by altering lysosomal pH) and then inhibiting autophagic flux. It has been shown that these molecules are effective *in vitro* to inhibit tumour growth by blocking autophagy and inducing apoptosis in bladder, colon and pancreatic cancer cells (Frieboes et al., 2014; Jiang et al., 2018; Lin et al., 2017). Several clinical trials have been carried out to test CQ and HCQ and, although relatively safe when used for short periods, the effective doses to have a clinical response were often toxic for some patients, notably in kidney cancer. Moreover CQ/HCQ have to be used for a longer time to be effective, which can result in cardiotoxicity (Kimura et al., 2013). Some studies have used combination therapies, including HCQ with other classical anti-tumour drugs, showing surprising efficacy in patients with melanoma, renal carcinoma and colon cancer, highlighting that certain types of tumours are more susceptible to this type of treatment strategy (Mahalingam et al., 2014; Rebecca & Amaravadi, 2016). HCQ in combination with temozolomide and radiation in glioblastoma multiforme required a smaller daily dose showing to be two-fold effective in doubling the median survival of patients (Rosenfeld et al., 2014; Sotelo et al., 2006). Some *in vivo* studies have shown that the use of Lys05, a CQ analogue and a more potent and selective lysosomal inhibitor,

exhibited a more efficient activity result at lower doses compared to CQ in xenograft murine model of melanoma, colon and breast cancer (McAfee et al., 2012; Rebecca et al., 2017). Recent studies are uncovering other and more potent derivatives of CQ, such as DC661. DC661 has shown impressive activity in vivo, in melanoma and colorectal cancer (Rebecca et al., 2019). Other drugs have been developed for tumour therapy blocking the early stages of autophagy, such as VPS34 and ULK1. Since ULK1 is the only serine/threonine kinase in the autophagy machinery, it has been found that its inhibition efficiently induced a cytotoxic apoptotic response in lung cancer (Egan et al., 2015). Similarly, VPS34 inhibitors have been shown to efficiently act on brain tumour cells by inhibiting autophagy (Zahedi et al., 2019), and to reduce tumour growth in xenograft models of breast cancer (Dyczynski et al., 2018). Ultimately, it is very complex to control autophagy in cancer and achieve a beneficial effect in patients. The strategy remains to find the right way to modulate autophagy in order to maximize benefits and extend the survival of patients.

13. Autophagy and cell migration

An increasing number of studies are highlighting the role of autophagy in cell migration and the greatest efforts have been made in the field of oncology. Unfortunately, the functional link between these two important processes is still not well understood. As mentioned above, the role of autophagy in tumour processes is sometimes contradictory, assuming that autophagy acts at different steps of tumorigenesis. Cell migration in this context is extremely important because it allows tumour cells to move away from the primary mass and to form secondary masses or metastases. Several studies conflict on whether autophagy supports the metastatic process or not. The role of autophagy appears to be multifactorial depending on cell type, microenvironment, tumour stage and other factors. Autophagy would act at different levels of cell migration: dynamics of focal adhesions, integrin trafficking, cytoskeleton remodelling, EMT and ECM remodelling.

13.1. Pro-migratory effects of autophagy

Autophagy has emerged as an important machinery in focal adhesion turnover, in particular in regulating the disassembling of adhesion complexes. Loss of ATG7 or ATG12 proteins impaired cell migration as well as increased FA size and FA accumulation in epithelial cells (Kenific et al., 2016). Interestingly, co-localization of LC3 and *neighbor of BRCA1* (NBR1) has been found in FAs concomitantly of their disassembling. This leads to the assumption that during cell migration, FAs have to be disassembled and/or recycled so as to enable the cell to move forward. In fact, LC3-positive structure found in FAs are likely forming autophagosomes responsible of their degradation. Moreover, NBR1 is a cargo receptor which mediates selective autophagy by targeting the autophagy machinery in FAs regions. NBR1 biochemically interacts with several FA proteins, such as paxillin, vinculin and FAK and its downregulation significantly attenuates the targeting of autophagosomes to the FAs at the leading edge (Kenific et al., 2016). Furthermore, after recruitment of LC3 in a NBR1-mediated mechanism, NBR1 binds LC3 via its LIR motif. Generation of a mutant form of NBR1, without the LIR motif, renders null the binding with LC3 and thus its recruitment (Kenific et al.,

2016). A recent study indicates that phosphorylation of paxillin by Src induced its interaction with LC3 protein via the N-terminal of paxillin which also contains a LIR motif. This interaction promotes autophagic degradation of paxillin and thus FA disassembly. Loss of LC3 by siRNAs induced paxillin accumulation and reduced cell migration (Sharifi et al., 2016). These data suggest that autophagy is actively involved during cell migration for efficient FA degradation which allows the cell to detach and advance more efficiently (Figure 40).

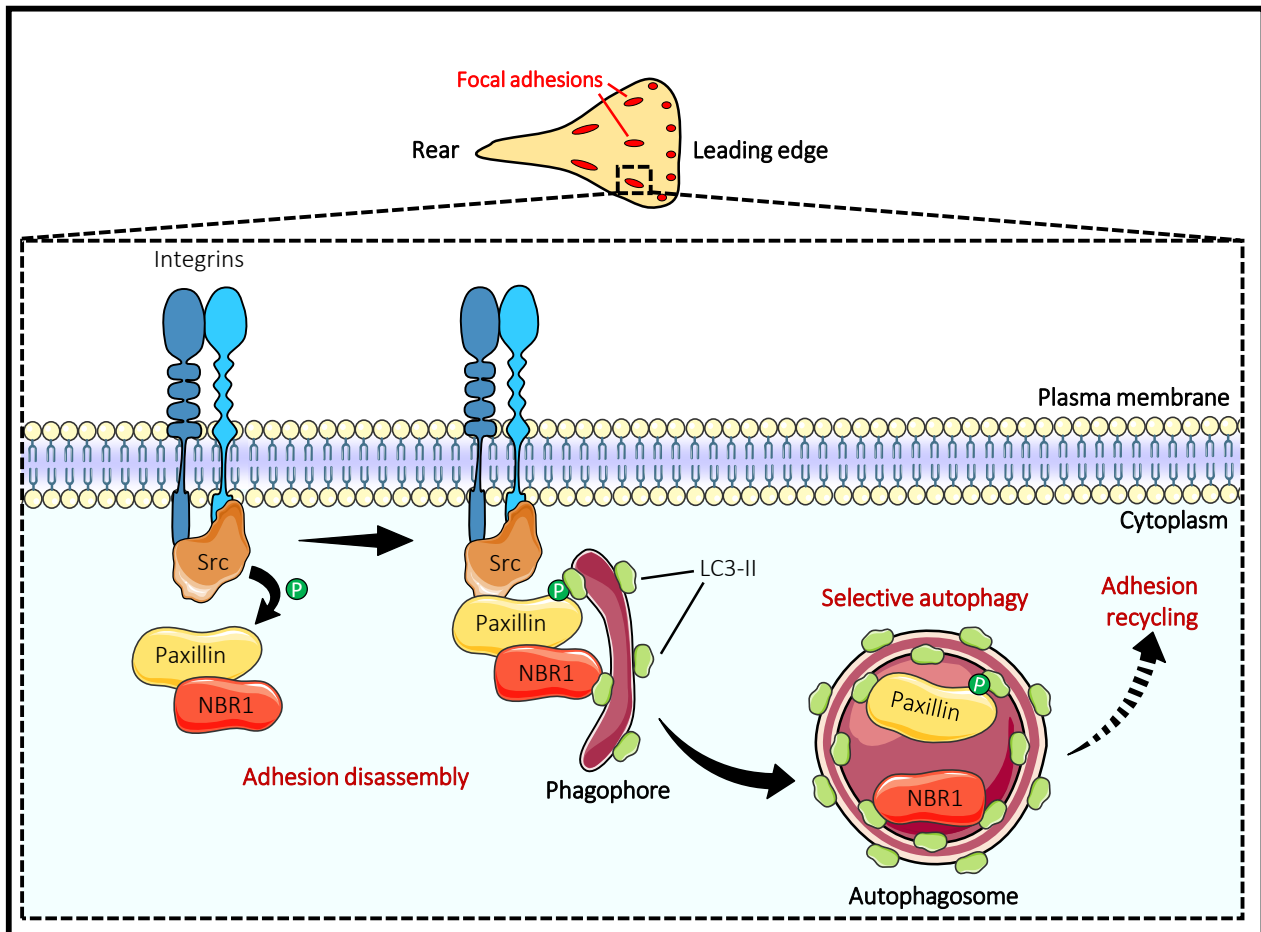


Figure 40. Pro-migratory effects of autophagy. Paxillin contains a LIR motif and can then be bound to LC3-II after its phosphorylation by Src enzyme. This induces the disassembly of the adhesion complex and degradation *via* selective autophagy. The autophagy cargo receptor NBR1 can bind to both LC3-II (*via* its LIR motif) and adhesion proteins, which also induces the formation of a phagophore around the adhesion to be selectively degraded by autophagy. Within the autophagosome, adhesion components can be recycled back to the plasma membrane in order to form nascent adhesions.

13.2. Anti-migratory effects of autophagy

Several studies have shown that autophagy is involved in the inhibition of cell migration. In particular, endosomal trafficking and autophagy play an important role in integrin transport as autophagy has been found to modulate integrin recycling. For example, starvation-induced autophagy increases the colocalization between LC3-containing autophagosomes and $\beta 1$ integrin and correlates with reduction of cell migration (Tuloup-Minguez et al., 2013). It has been also shown that during autophagy induction, migration of

glioblastoma cells was impaired and the two-master regulators of EMT, SNAIL and SLUG, were downregulated. Conversely, depletion of beclin 1 was sufficient to increase migration of glioblastoma cells resulting in the up-regulation of the SNAIL and SLUG proteins in these cells (Catalano et al., 2015). The loss of other autophagic proteins, such as ULK1, has been demonstrated to be important in cell migration. In fact, ULK1 KO increased fibronectin deposition to the ECM and promoted metastasis in breast cancer cell lines (Dower et al., 2017). A work from our team has shown that activation of the two GPCRs *urotensin II receptor* (UT) and CXCR4, receptors of the urotensin II and CXCL12 ligands, respectively, leads to inhibition of autophagy in glioma cells (Coly et al., 2016). In fact, UII or CXCL12 chemotactic stimulation induced both accumulation of p62 and reduction of LC3B accumulation in the cytosol. They further demonstrated that calpain activation, induced by CXCR4 or UT, reduces the pool of ATG5 at the plasma membrane and inhibits the recruitment of ATG16L1 protein to endocytic vesicles, thereby limiting the formation of pre-autophagic endosomes required for the expansion of the phagophore (Coly et al., 2016). Coly and colleagues have then proposed a new paradigm in which a competition between lamellipodium expansion and autophagosome biogenesis for a common source of membrane may exist, resulting in the compartmentalization of autophagy following GPCR activation (Coly et al., 2017). Specifically, activation of GPCRs at the cell front locally inhibits the formation of pre-autophagic endosomes with the subsequent reduction of ATG proteins pool in the recycling compartment. This reduction may then induce a “targeting switch” which reduces the flux of membrane toward the phagophore to favor endosomal recycling to the plasma membrane. The source of phospholipids coming from these endosomes would be critical for lamellipodium expansion as well as exocytosis of integrins-containing endosomes within nascent adhesions (Coly et al., 2017). Inhibition of autophagy at the leading edge would also protect from degradation several proteins involved in remodelling of the actin cytoskeleton. Nevertheless, autophagy may be still activated at the rear of the cell, at distance from chemotactic GPCRs, to participate in adhesion disassembly of large adhesions (Coly et al., 2017) (Figure 41).

13.3. Autophagy and epithelial-to-mesenchymal transition

The EMT is a process in which the phenotype of an epithelial cell changes completely, losing its polarity and cell-cell adhesions to become a mesenchymal cell with migratory and highly invasive properties. This mechanism is important in many physiological processes, from embryonic development with the formation of embryonic leaflets, to wound healing repair, tumour progression and metastasis. In order to migrate, epithelial cells must activate a series of morphological changes and transcribe certain key transcription factors that enable phenotypic transformation. The regulators of this transformation are SNAIL, SLUG, ZEB1/2 and TWIST1/2 because they induce the transcription of some proteins important for migration such as vimentin, fibronectin and N-cadherin, which are characteristic of the mesenchymal phenotype. Conversely, they must silence other genes that induce the production of E-cadherin, occludin and claudin, which are characteristic of epithelial cells (Colella et al., 2019).

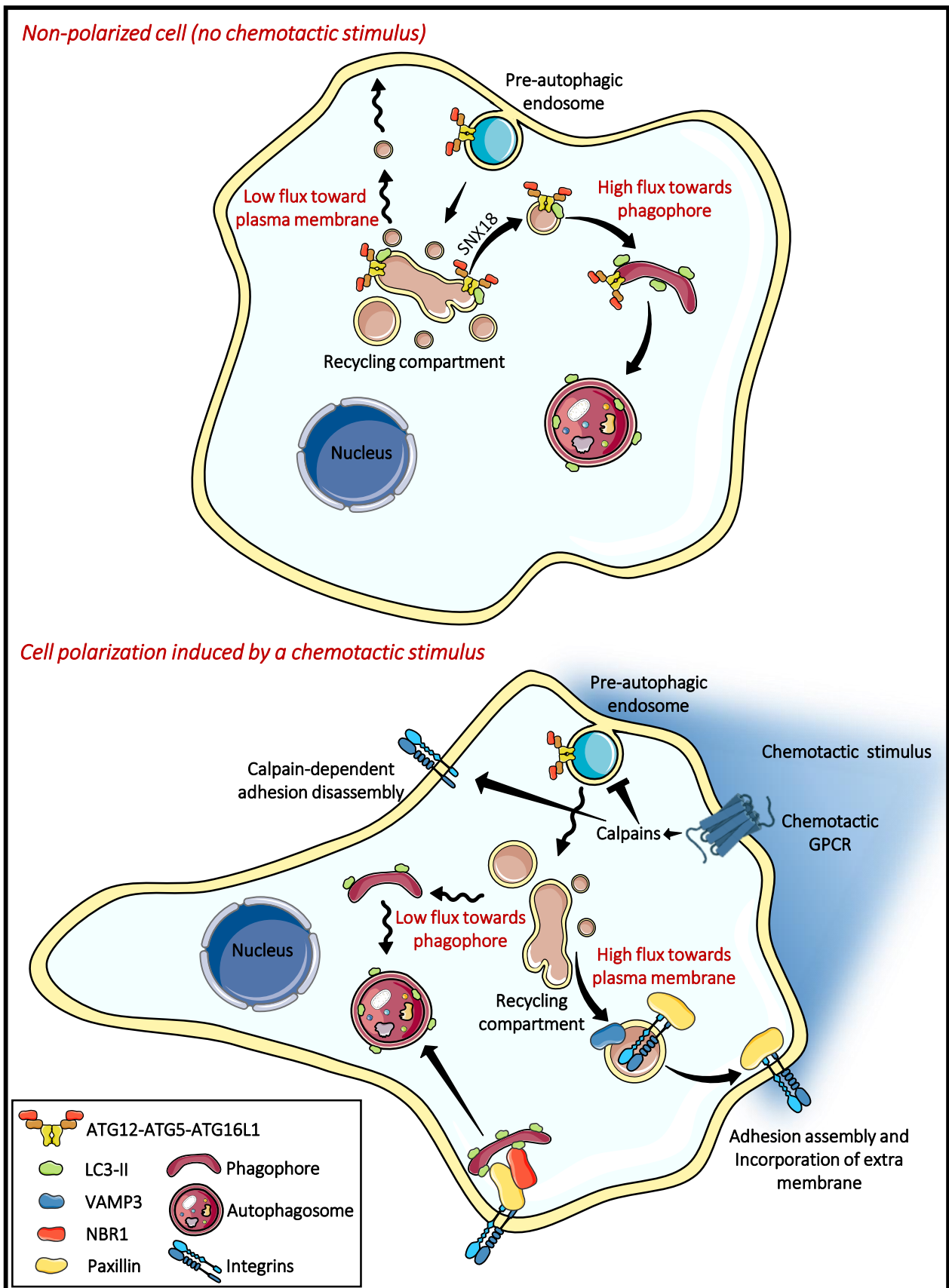


Figure 41. For caption see next page.

Figure 41. Compartmentalized regulation of autophagy by chemotactic GPCRs. **A|** Under basal conditions, ATG5-ATG16L1-positive pre-autophagic endosomes bud from the plasma membrane and are directed to the recycling endosome compartment. From there, SNX18-dependent tubules target vesicles containing ATG5-ATG16L1 and LC3 to the expanding phagophore. **B|** Upon activation by chemoattractant stimuli, chemotactic GPCRs locally inhibit the formation of pre-autophagic endosomes. The subsequent reduction of ATG proteins in the recycling compartment may trigger a “targeting switch” which reduces membrane flux toward the phagophore to favor VAMP3-enabled recycling to the plasma membrane. Exocytosis allows integrins to be recycled to nascent adhesions, while phospholipids are incorporated into the lamellipodium and contribute to its expansion. Autophagy inhibition at the leading edge may also locally protect proteins involved in actin remodelling and adhesion assembly, which would otherwise be sequestered and degraded. Autophagy could remain active at distance from chemotactic GPCRs in order to participate in the disassembly of large focal adhesions.

EMT has been well characterized in carcinoma cells and its role in glioma development has been recently investigated (Iser et al., 2017). Gliomas do not undergo classical EMT but a sort of glial-to-mesenchymal transition or EMT-like since the cell phenotype is not really epithelial and different genetic subtypes have been classified by *The Cancer Genome Atlas* (TCGA): mesenchymal, classical, neural and proneural (Colella et al., 2019). It has been shown that autophagy directly affects the regulation of the transcription factors mentioned above during EMT. For example, TWIST1 is responsible for the loss of E-cadherin-mediated cell-cell adhesion and the loss of ATG3, ATG5, ATG9 or ATG12 *in vivo* induces p62 accumulation, which determines the stabilisation of TWIST1 by preventing its degradation in both autophagosomes and proteasomes. This increase in TWIST1 levels then participates to tumoral growth and metastasis in mice (Qiang et al., 2014). In a similar way, it has been shown that ATG7 KO reduces the expression of epithelial markers and increases the levels of mesenchymal markers in hepatocytes (Grassi et al., 2015). It should be however noted that even in the context of EMT, the literature is contradictory, as modulation of autophagy leads to different outputs depending on the cell type.

AIM OF THE THESIS

Work done in our team aims at better understanding the intracellular mechanisms engaged by chemotactic receptors during migration, with a special focus on the mechanisms of glioblastoma cell invasion (Coly et al., 2016; Lecointre et al., 2015). According to the information presented in the introduction section, there are increasing evidences for a critical role of autophagy during cell migration and cancer invasion. The functional connection between these processes is, however, incompletely understood and constitutes the topic of extensive research.

In addition to the well-recognized function of ATG9A in phagophore expansion (Mari et al., 2010; Orsi et al., 2012; Puri et al., 2018; van der Vaart et al., 2010; Young et al., 2006), recent data point to the fact that this core autophagy protein may have a wider role than anticipated (Claude-Taupin et al., 2021; Yamaguchi et al., 2018) and could be a general regulator of vesicular trafficking (Jia et al., 2017). In addition, studies done in *Drosophila* indicated that Atg9 was able to interact with the well-known actin-regulators Ena and profilin, thereby regulating the cortical actin network of the cells (Kiss et al., 2020).

Based on these data, the objectives of this study were therefore:

- 1) to test the impact of human ATG9A on the chemotactic migration of several cell lines, including highly invasive glioblastoma cells
- 2) to define, in this context, the role of human ATG9A on the dynamics of cell protrusions and on the polarized transport/exocytosis of adhesions proteins at the migration front
- 3) to evaluate whether human ATG9A, similar to *Drosophila* Atg9, has the ability to interact with actin regulators controlling the lamellipodial actin network

RESULTS

Part I: The core autophagy protein ATG9A controls dynamics of cell protrusions and directed migration

Daniele Campisi, Laurence Desrues, Renaud Parment, Pierrick Gandolfo, H el ene Castel and Fabrice Morin

Data presented in this section uncover a new function of mammalian ATG9A, involved in directed cell migration. We showed that ATG9A controls dynamics of F-actin-rich lamellipodia and regulates the anterograde transport of β 1 integrin to focal adhesions located in the lamellipodium. This transport is essential for the dynamics of nascent focal adhesions and lamellipodia stabilization during chemotactic migration.

Journal of Cell Biology (under revision)

The core autophagy protein ATG9A controls dynamics of cell protrusions and directed migration

Daniele Campisi^{1,2}, Laurence Desrues^{1,2}, Renaud Parment^{1,2}, Pierrick Gandolfo^{1,2},
Hélène Castel^{1,2} and Fabrice Morin^{1,2}

¹Normandie University, UNIROUEN, INSERM U1239, DC2N, 76000 Rouen, France.

²Institute for Research and Innovation in Biomedicine (IRIB), 76000 Rouen, France.

Running title: ATG9A and cell migration.

Corresponding author:

Dr Fabrice Morin, Normandie University, UNIROUEN, INSERM U1239, DC2N, Team Astrocyte and Vascular Niche, 25 Rue Lucien Tesnière, CURIB, 76821 Mont-Saint-Aignan Cedex, France.

Email: fabrice.morin@univ-rouen.fr

Tel: (+33)235-146-630.

Main Figures: 10

Supplementary Figures: 7

Movies: 5

I. Abstract

Chemotactic migration is a fundamental cellular behaviour relying on the coordinated flux of lipids and cargo proteins toward the leading edge. We found here that the core autophagy protein ATG9A plays a critical role in the chemotactic migration of several human cell lines, including highly invasive glioma cells. Depletion of ATG9A protein altered the formation of large and persistent filamentous actin (F-actin)-rich lamellipodia that normally drive directional migration. Using live-cell TIRF microscopy, we demonstrated that ATG9A-positive vesicles are targeted toward the migration front of polarized cells, where their exocytosis correlates with protrusive activity. Finally, we found that ATG9A was critical for efficient delivery of β 1 integrin to the leading edge and normal adhesion dynamics. Collectively, our data uncover a new function for ATG9A protein, and indicate that ATG9A-positive vesicles are mobilized during chemotactic stimulation to facilitate expansion of the lamellipodium and its anchorage to the extracellular matrix.

Keywords: ATG9A, autophagy, cell adhesion, chemotactic migration, exocytosis, lamellipodium.

Abbreviations: ATG, autophagy-related; BafA1, bafilomycin A1; CQ, chloroquine; CXCL12, C-X-C motif chemokine ligand 12; EGF, epidermal growth factor; EGFP, enhanced green fluorescent protein; FAAS, Focal Adhesion Analysis Server, F-actin, filamentous actin; IL, intraluminal loop; LC3B, microtubule-associated protein 1 light chain 3 beta; pHluorin, pH-sensitive GFP variant superecliptic pHluorin; PXN, paxillin; ROI, region of interest; siRNA, short interfering RNA; TIRF, total internal reflection fluorescence; TGN, *trans*-Golgi network

II. Introduction

Chemotactic cell migration is critical for a variety of cellular processes, including cell movement during normal development, immune responses, as well as pathological processes such as tumor cell invasion and metastasis (Keller, 2005; Bravo-Cordero *et al*, 2012). It is a highly coordinated and dynamic process that involves polarization of the cell, followed by the extension of an actin-dependent membrane protrusion, the lamellipodium, toward the chemotactic stimulus. Formation of adhesions to the extracellular matrix, *via* the integrin family of transmembrane receptors, then stabilizes the lamellipodium and acts as a molecular clutch allowing the cell body to pull itself forward (Ridley *et al.*, 2003).

Many studies have indicated that biased vesicle trafficking toward the leading edge is crucial for the different steps of directed migration (Fletcher & Rappoport, 2010). Focal exocytosis of vesicles at the cell front can indeed accomplish several tasks, such as the recycling of integrins (Lawson & Maxfield, 1995; Paul *et al*, 2015; Huet-Calderwood *et al*, 2017), the delivery of bulk membrane for efficient lamellipodium expansion (Bretscher,

1996), and the supply of matrix metalloproteinases for enhanced matrix degradation (Kean *et al*, 2009; Sneeggen *et al*, 2019). Other molecules trafficked in a migrating cell include receptors for chemotactic stimuli (Maisel *et al*, 2018; Coombs *et al*, 2019) and GTPases of the Rho family (RHOA, RAC1, CDC42) participating in actin dynamics (Osmani *et al*, 2010; Williamson *et al*, 2015).

Although focal exocytosis is well described during cell migration, the origin and diversity of the vesicles, as well as their modes of transport to the cell front are still unclear. Mounting evidence suggests a prominent role of the secretory pathway in cell migration. Disruption of Golgi integrity and failure of the Golgi to re-orient toward the leading edge of migrating cells have been shown to block directional cell movement (Bisel *et al*, 2008; Millarte & Farhan, 2012; Pallesi-Pocachard *et al*, 2016). Accordingly, using time-lapse total internal reflection fluorescence (TIRF) microscopy, post-Golgi vesicles were found to exhibit polarized exocytosis toward the cell front of migrating fibroblasts and astrocytes (Schmoranzner *et al*, 2003; Letinic *et al*, 2009). Data obtained from several cell types also indicate that recycling endosomes constitute an important source of internal membrane and cargo proteins that are incorporated at the leading edge during cell migration (Kean *et al*, 2009; Sneeggen *et al*, 2019) (Proux-Gillardeaux *et al*, 2005; Riggs *et al*, 2012; Tayeb *et al*, 2005; Veale *et al*, 2011; Veale *et al*, 2010).

Macroautophagy (hereafter referred to as autophagy) is an evolutionarily conserved lysosomal pathway involved in the degradation of long-lived proteins and cytoplasmic organelles. This process, which is essential for normal turnover of cellular compartments, is upregulated in response to nutrient starvation. One of the first events in autophagy is the formation of the phagophore. The edges of the phagophore membranes elongate and thereby engulf portions of cytoplasm. After the scission of the membrane edges, the structure becomes a completed autophagosome, which later fuses with lysosomes, resulting in the degradation of its luminal content (Dikic & Elazar, 2018). Several highly conserved autophagy-related (ATG) proteins that function at key steps in the autophagy process have been identified. Among them, ATG9A is the only transmembrane protein. In mammalian cells, ATG9A cycles primarily between the *trans*-Golgi network (TGN), the plasma membrane and endosomal compartments (Young *et al*, 2006; Ravikumar *et al*, 2010; Puri *et al*, 2013; Sørensen *et al*, 2018; Longatti & Tooze, 2012). Extensive studies have demonstrated the critical role of ATG9A protein in autophagosome formation, proposedly by functioning in vesicular delivery to the phagophore initiation site, and by translocating lipids from the outer to the inner leaflet of the phagophore membrane in order to enable its expansion (Orsi *et al*, 2012; Maeda *et al*, 2020; Matoba *et al*, 2020). In addition to this well-recognized function of ATG9A in phagophore expansion, recent studies point to the fact that it may have a wider role than anticipated, and could act as a general regulator of vesicular trafficking. Hence, Jia and coll. found that ATG9A was required for the post-Golgi transport and the maturation of lysosomal hydrolases (Jia *et al.*, 2017a). In cortical neurons, the loss of ATG9A, but not that of other autophagy genes (ATG7 or ATG16L1), markedly reduced neurite extension (Yamaguchi *et al.*, 2018), a process that strongly relies on intracellular membrane trafficking (Sann *et al.*, 2009).

In this framework, we found here that ATG9A-containing vesicles are essential components of directed cell migration. ATG9A-depleted cells were unable to form large and stable F-actin rich lamellipodia. By the design of a pH-sensitive fluorescently tagged ATG9A, together with live-cell TIRF imaging, we established that exocytosis of ATG9A-containing vesicles is highly polarized toward the cell front, induced by chemotactic stimuli and synchronized with protrusive activity. Finally, we further demonstrated that ATG9A is critical for the delivery of $\beta 1$ integrin to the leading edge and normal adhesion dynamics.

III. Results

III.1. Chemotactic migration depends on ATG9A protein

We tested the role of ATG9A during chemotactic migration by targeting the ATG9A transcript by short interfering RNA (siRNA) in several human cell lines, *i.e.* HeLa, HEK 293 and the highly invasive U87 MG and 42 MG glioma cells. These cell lines were chosen due to their well-described responsiveness to various chemotactic stimuli (Dillenburg-Pilla *et al*, 2015; Lecointre *et al*, 2015; Coly *et al*, 2016), and the already characterized localization and trafficking of ATG9A during autophagy induction in both HeLa and HEK 293 cells (Takahashi *et al*, 2016; Zhou *et al*, 2017; Kakuta *et al*, 2017; Davies *et al*, 2018). In order to make sure that siRNA effects would not be due to off-target effects, we performed experiments with two independent siRNAs interacting with different regions of the ATG9A transcript. Effectiveness of each siRNA was verified in HeLa (Fig. R1A) and U87 MG cells (Fig. S1A). As a control, we also tested the effect of each siRNA on autophagic activity. In agreement with the well-documented role of ATG9A in phagophore expansion, the knockdown of ATG9A strongly reduced autophagosome biogenesis in HeLa cells (Fig. R1B) and U87 MG cells (Fig. S1B), as evaluated by the accumulation of EGFP-microtubule associated protein 1 light chain 3 β (LC3B) puncta under chloroquine (CQ) treatment (see Materials and Methods). We next assessed the role of ATG9A in chemotactic migration using a transwell chemotaxis assay, in which cells loaded in the upper chamber of the transwell migrate toward the bottom chamber containing the chemoattractant. We first examined the effects of epidermal growth factor (EGF), a potent factor that has been shown to be critical for normal and cancer cell chemotaxis (Adelmann-Grill *et al*, 1990; Segall *et al*, 1996; Kim *et al*, 2008; Mendoza *et al*, 2011; Biswenger *et al*, 2018). A chemotactic gradient elicited by EGF stimulated the migration of HeLa, U87 MG and 42 MG cells (Fig. R1C). EGF produced no effect when added in both chambers of the transwell, stressing the fact that it stimulates chemotaxis rather than chemokinesis (random motility). Transfection of cells with each siRNA targeting the ATG9A transcript abrogated or markedly reduced chemotactic cell migration induced by EGF (Fig. R1C). The experiments were repeated using C-X-C motif chemokine ligand 12 (CXCL12), the ligand of the prototypical chemokine receptor C-X-C motif chemokine receptor 4 (Chatterjee *et al.*, 2014b). Similar to data obtained with EGF, ATG9A depletion abolished or markedly reduced CXCL12-induced chemotactic migration

of HeLa, HEK 293 and 42 MG cells (Fig. R1D). Together, these data suggest that, regardless of the cell type and the nature of the stimulus, ATG9A protein is a critical component of directed cell migration.

III.2. Depletion of ATG9A protein alters the formation of F-actin rich lamellipodia driving efficient cell migration

Since lamellipodia/lamella are considered the main drivers of chemotactic migration, we carefully examined the impact of ATG9A depletion on the morphology of cell protrusions. Experiments were done in U87 MG cells, since they consistently develop well-defined protrusions, even in the absence of chemotactic stimulation. Rhodamine phalloidin labelling of U87 MG cells transfected with irrelevant siRNA indeed revealed prominent lamellipodia, with intense F-actin staining (Fig. R2A). In ATG9A-depleted cells, most of the protrusions exhibited an abnormal morphology, as they were narrow and often resembled small ruffles (Fig. R2A), and broad F-actin-rich lamellipodia were rarely observed. Quantitative analysis of the rhodamine phalloidin fluorescence signal was then used to measure relative amounts of peripheral F-actin. Filament levels in protrusions of ATG9A-depleted cells were reduced more than 38% in comparison to control cells (Fig. R2B). Moreover, we estimated that F-actin-rich protrusions occupied about 14% of the cell perimeter in ATG9A-depleted cells, as compared to approximately 30% in control cells (Fig. R2C). In agreement with their inability to form large lamellipodia, we noticed that most ATG9A-depleted cells ($\approx 80\%$) displayed a non-polarized phenotype, with no clear front-rear axis (Fig. R2D).

The altered morphology of protrusions on fixed ATG9A-depleted cells led us to evaluate their dynamics, using phase contrast time-lapse microscopy. Live-cell movies of U87 MG cells transfected with irrelevant siRNA indicated that cells developed large protrusions associated with typical ruffles (Innocenti, 2018), accounting for 31% of the cell perimeter (Fig. S2). In agreement with experiments done on fixed cells, siATG9A-transfected cells displayed smaller protrusions, developing on about 18% of the cell perimeter (Fig. S2). Analyses of the live-cell movies (Movie 1) using kymographs indicated that, although the protrusion velocities were similar in both groups (Fig. R2E), siATG9A-transfected cells displayed protrusions with reduced distance and persistence (Fig. R2E). We next monitored the intrinsic movement of cells transfected with siRNAs against ATG9A or irrelevant siRNA over a 3-hour period. The single cell trajectories are shown in Fig. R2F. Quantitative analysis revealed that, whereas control cells migrated with a speed of $0.85 \mu\text{m}/\text{min}$, the velocity of ATG9A-depleted cells was reduced to about $0.40 \mu\text{m}/\text{min}$ (Fig. R2G). Accordingly, depletion of ATG9A also markedly reduced the mean square displacement (Fig. R2H), which is a measure of the surface area explored by the cell over time. Collectively, our data indicate that ATG9A protein is necessary for the formation of large and polarized F-actin-rich protrusions and efficient cell migration.

III.3. ATG9A-positive vesicles concentrate in F-actin rich protrusions and display anterograde trafficking toward the leading edge

In order to evaluate whether ATG9A-positive vesicles could potentially deliver bulk membrane or essential proteins for the formation/anchorage of cell protrusions, we first examined the subcellular distribution of endogenous ATG9A. The ATG9A signal, whose specificity was verified using siRNAs (data not shown), displayed a punctuated pattern, and vesicles mainly localized in the perinuclear area (Fig. R3A). Importantly, a significant fraction of ATG9A signal was also concentrated in F-actin rich protrusions, at the cell membrane and in small vesicles localized beneath the plasma membrane (Fig. R3A). Chemotactic stimulation of cells with EGF increased the fraction of ATG9A signal localized in protrusions (+ 156 %), as well as the colocalization score (Pearson correlation coefficient) of peripheral ATG9A with F-actin (Fig. R3B-D). In order to examine the dynamics of ATG9A-positive vesicles, we next used live-cell TIRF microscopy on cells expressing the ATG9A-mCherry fusion protein (De Pace et al., 2018). Live-cell movies of U87 MG cells revealed that many small (<500 nm) motile or non-motile ATG9A-positive puncta were located into the evanescent field of the TIRF microscope (110-nm penetration depth), in the perinuclear region or at the tips of cell protrusions. Tracking experiments revealed that most of the motile vesicles ($\approx 80\%$) located in protrusions displayed an anterograde movement toward the cell edge (Fig. R3E). This prompted us to evaluate whether ATG9A-positive vesicles could indeed reach the plasma membrane and accomplish polarized exocytosis at the migration front.

III.4. Design and validation of ATG9A-pHluorin as a new probe to visualize ATG9A exocytosis

To record exocytosis of ATG9A-positive vesicles, we designed an ATG9A construct containing the highly pH-sensitive GFP variant superecliptic pHluorin (pHluorin) (Fig. R4A, left panel). The fluorescence of pHluorin is quenched at the acidic endosomal pH, but upon fusion with the plasma membrane, low luminal pH is immediately neutralized, resulting in a sudden increase in fluorescent intensity (Fig. R4A, right panel) (Miesenböck *et al*, 1998; Sankaranarayanan *et al*, 2000). We designed the ATG9A-pHluorin based on the predicted topology of mammalian ATG9A, displaying six transmembrane domains, with both N- and C-termini located in the cytosol (Young et al., 2006). Based on these preliminary data, we tentatively inserted the pHluorin sequence into the intraluminal loop (IL) 1 of ATG9A, since alignment of mammalian ATG9A and yeast ATG9 sequences indicated significantly lower conservation in IL1 than IL2 or IL3 predicted domains. During the course of our study, Guardia and coll. solved the structure of human ATG9A to a 2.9-Å resolution using cryoelectron microscopy (Guardia et al., 2020). Unlike the predicted structure, they showed that ATG9A displayed in fact four transmembrane helices (α_2 , α_6 , α_{14} , α_{15} ; Fig. R4A), with an IL1 identical to that predicted but devoid of the predicted IL2 and IL3 (Fig. R4A). Reinforcing the rational of our strategy, the solved

structure of ATG9A further indicated that the selected intraluminal insertion site for pHluorin (between amino-acids *Leu102* and *His103*) has no defined secondary structures (Fig. R4A).

To validate our construct, we first assessed whether the ATG9A-pHluorin fusion protein retains autophagic activity, by evaluating its ability to rescue the siRNA-induced knockdown of endogenous ATG9A. For this goal, we used a siRNA that specifically targets endogenous ATG9A, without affecting the expression of recombinant ATG9A-pHluorin, due to the codon-optimization procedure of the recombinant sequence introducing several siRNA/target mRNA mismatches. In cells transfected with irrelevant siRNA, overexpression of ATG9A-pHluorin did not stimulate autophagosome biogenesis (as evaluated by the accumulation of mCherry-LC3B puncta under CQ treatment), suggesting that endogenous ATG9A does not constitute a limiting factor under these conditions (Fig. R4B). More importantly, the marked reduction of autophagosome biogenesis induced by the knockdown of endogenous ATG9A was totally rescued by overexpression of recombinant ATG9A-pHluorin (Fig. R4B), indicating that insertion of the pHluorin sequence within the IL1 loop of ATG9A does not preclude its pro-autophagic function.

We next verified that the ATG9A-pHluorin protein has the expected topology, with the pHluorin facing the vesicular lumen. We then performed live-cell epifluorescence imaging of U87 MG cells co-expressing ATG9A-pHluorin and the pH-insensitive ATG9A-mCherry. Co-transfected cells were treated with bafilomycin A1 (BafA1), a selective inhibitor of the vacuolar-type ATPase, an essential proton pump for maintaining vesicular acidic pH (Bowman et al., 1988). As expected, the ATG9A-mCherry fluorescence, mainly localized in perinuclear vesicles, did not significantly change following BafA1 treatment (Fig. R4C). In contrast, the ATG9A-pHluorin signal in the perinuclear region gradually increased upon BafA1 treatment, to reach a plateau at about 30-min post-treatment (Fig. R4C). At this time point, most perinuclear vesicles appeared co-labelled with mCherry and pHluorin signals (Fig. R4C). The progressive de-quenching of pHluorin fluorescence during vesicular pH change induced by BafA1 strongly suggests that the ATG9A fusion protein has the expected topology in perinuclear endosomes, with the pHluorin sequence oriented toward the lumen.

To record individual ATG9A-pHluorin exocytotic events, we then used TIRF microscopy, at a high frame rate (one frame every 390 millise). Besides exocytotic events, we first noticed that, under TIRF configuration, most of the ATG9A-pHluorin signal appears scattered in small and relatively static puncta decorating the bottom surface of the cell (Fig. R4D). These puncta likely represent ATG9A-pHluorin proteins trapped in endocytic structures since *i*) they rapidly dimmed following extracellular acidification (Fig. R4D), indicating that the protein is at the plasma membrane, with the pHluorin facing the extracellular medium, and *ii*) they frequently localized with the endocytic marker clathrin (Fig. S3). We next focused on exocytotic events, which were monitored as bright and suddenly (within a frame) appearing spots. Interestingly, visual examination of the events suggested heterogeneity. The majority ($\approx 70\%$) of the events showed a clear signature of full fusion exocytosis, *i.e.* *i*) a rapid increase (< 0.390 sec) of the pHluorin signal in a central region of interest (ROI), likely due to fusion pore opening, and *ii*) diffusion of the ATG9A-pHluorin cargo into the plasma membrane, revealed

by the delayed increase of fluorescence in a distant ROI (Fig. R5A; Movie 2). The average profile of these fusion events ($n = 68$), which were time-aligned to fusion, allowed the estimation of a half-life of about 2.8 sec (Fig. R5A). The remaining events were characterized by the absence of significant diffusion of the fluorescence signal in areas of the plasma membrane surrounding the insertion site, and generally displayed a slower intensity decay (mean decay half-life 4 sec) (Fig. R5B; Movie 3). Although in depth analysis would be required to definitely conclude, these latter events likely represent fusion of ATG9A-loaded vesicles with the plasma membrane according to a kiss-and-run mechanism (Alabi & Tsien, 2013). Such a mechanism has been described for the delivery of lipids and/or cargo proteins from ATG9A-positive vesicles to the expanding phagophores, without retention of ATG9A protein in mature autophagosomes (Orsi et al., 2012).

III.5. Exocytosis of ATG9A-positive vesicles is highly polarized toward the leading edge

We next evaluated the spatial distribution of ATG9A-pHluorin fusion events. We first focused on cells displaying a clear rear-front axis, with a unique and well-developed protrusion. Moreover, since uneven adherence within a single cell might bias the TIRF analysis, which relies on the plasma membrane being in close contact with the coverslip, we selected cells that showed a uniform adherence pattern, as evaluated by the static ATG9A-pHluorin puncta decorating the plasma membrane at the beginning of the acquisitions. We found that ATG9A-pHluorin exocytotic events were highly polarized, with a clear clustering near the cell front (Fig. 5C). Quantitative analysis indicated that the frequency of events, after normalization by the areas of the regions of interest, was about 5-fold higher at the cell front ($< 10 \mu\text{m}$ from the leading edge) than the other parts of the cell (Fig. R5D). In sharp contrast, TIRF analysis of non-polarized cells, devoid of large lamellipodia, showed that fusion events were relatively uniformly distributed, with no obvious hotspot (Fig. R5E).

We next tested the impact of chemotactic stimulation with EGF. For each cell, fusion events were recorded over 1-min periods, just before and 2-min after EGF treatment. Analyses of the time-lapse movies indicated that EGF exposure significantly increases the fusion activity ATG9A-positive vesicles, in U87 MG cells (Fig. R5F) or HeLa cells (Fig. S4). Altogether, our data suggest that ATG9A endosomes are targeted toward the leading edge for exocytosis, in order to deliver lipids and/or cargo proteins for cell expansion.

III.6. Peripheral ATG9A-pHluorin signal correlates with protrusive activity

Cells expressing ATG9A-pHluorin were recorded at a low frame rate (one frame every minute) using TIRF, during the spontaneous formation of protrusions. The formation of broad protrusions was systematically marked by the appearance of a bright ATG9A-pHluorin signal close to the leading edge (Fig. R6A; Movie 4). The vesicular pattern of the signal likely represents ATG9A-pHluorin proteins which rapidly relocalize in endocytic structures following focal bursts of exocytosis. Notably, analyses of the movies using kymographs indicated that the ATG9A-pHluorin signal is sustained at the edges of expanding protrusions, but sharply

decreased during protrusion collapse (Fig. R6B). To precisely define the cell edges and establish a temporal correlation between edge advance and appearance of ATG9A signal, we used mKate2, a red fluorescent protein diffusely expressed in the cytosol. A representative time-lapse sequence (Fig. R6C-E) shows that appearance of ATG9A-pHluorin signal near the cell edge was synchronized with protrusive activity.

III.7. ATG9A regulates delivery of TGN46 and β 1 integrin to the leading edge through its N-terminal adaptor protein (AP) sorting signal

Delivery of cargoes from the TGN to the leading edge is critical for directional migration (Millarte & Farhan, 2012; Riggs *et al*, 2012; Shafaq-Zadah *et al*, 2016; Mana *et al*, 2016; Hao *et al*, 2020), and several studies, using live-cell TIRF microscopy, indeed demonstrated polarized exocytosis of post-Golgi carriers at the cell front (Schmoranzler *et al*, 2003; Letinic *et al*, 2009). This led us to evaluate whether ATG9A proteins transported toward cell protrusions essentially emanate from the TGN. We then performed colocalization experiments with the Golgi marker TGN46, an integral membrane protein mainly residing in the TGN, that has been shown to cycle between the TGN and the plasma membrane (Banting & Ponnambalam, 1997). In agreement with previous studies (Orsi *et al.*, 2012), we found that ATG9A-mCherry and TGN46 strongly co-localize in typical TGN cisternae, as well as in more peripheral post-Golgi carriers (Fig. S5A). Importantly, TGN46 and ATG9A-mCherry also displayed a marked co-localization in cell protrusions, near or at the cell membrane (Fig. S5A). A 30-min chemotactic stimulation of cells with EGF increased the fractions of ATG9A and TGN46 signals localized in protrusions (TGN46: + 74.3 % ; ATG9A-mCherry: + 104.4 %), with a concomitant decrease of their signals in the perinuclear area (Fig. S5B-E).

ATG9A protein, through its interaction with the adaptor protein (AP) complex AP-1, plays an active role in the TGN-to-lysosome transport of hydrolases (Jia *et al.*, 2017), putting forward the idea that ATG9A could be a constitutive component of cargo sorting/trafficking from the TGN. We therefore investigated the impact of ATG9A on TGN46 trafficking and found that depletion of ATG9A protein levels using two independent siRNAs markedly reduces EGF-induced redistribution of TGN46 toward the cell periphery (Fig. S5F-H).

Through its luminal domain, the rat homologue of TGN46 interacts with β 1 integrin, thereby regulating the sorting of this major adhesion molecule from the TGN to the plasma membrane (J. Wang & Howell, 2000b). Notably, several reports demonstrated that retrograde transport of β 1 integrin to the TGN, followed by its polarized reshuffling from the TGN to the leading edge, is essential for the establishment of nascent adhesions and directional cell migration (Riggs *et al*, 2012; Shafaq-Zadah *et al*, 2016; Mana *et al*, 2016). This prompted us to assess whether ATG9A also regulates EGF-induced delivery of β 1 integrin to the cell protrusions. Fluorescently immunostained endogenous β 1 integrin partially co-localized with TGN46 and ATG9A in the perinuclear area and in puncta dispersed throughout the cytosol or near the cell membrane, likely representing *bona fide* post-Golgi carriers (Fig. R7A). In cells transfected with control siRNAs, a 30-min

incubation with EGF induced a marked redistribution of $\beta 1$ integrin toward the periphery, with a concomitant decrease of its relative amounts in the cytosol (Fig. R7B). Similar to data obtained with TGN46, depletion of ATG9A using each siRNA strongly inhibits EGF-induced redistribution of $\beta 1$ integrin toward cell protrusions (Fig. R7B).

ATG9A trafficking from the TGN, recycling endosomes or the plasma membrane is tightly controlled by clathrin adaptor complexes (AP). Hence, ATG9A contains a canonical AP sorting signal ($^8\text{YXX}\Phi\text{D}/\text{E}^{12}$) within its N-terminal domain (Fig. R8A), which confers binding to AP-1 (endosome- and TGN-localized), AP-2 (plasma membrane-localized) and AP-4 (TGN-localized) complexes (Imai *et al*, 2016; Zhou *et al*, 2017; Jia *et al*, 2017; Mattera *et al*, 2017; Ivankovic *et al*, 2020). Within this motif, Tyrosine 8 residue is critical since its mutation abolishes AP binding, resulting in altered ATG9A trafficking (Zhou *et al*, 2017; Mattera *et al*, 2017). We demonstrated that, in cells depleted of endogenous ATG9A, overexpression of wild-type recombinant ATG9A-mCherry efficiently rescued EGF-induced delivery of $\beta 1$ integrin and TGN46 to the leading edge (Fig. R8B-E). As expected, mutant ATG9A-mCherry, in which Tyrosine 8 was replaced by a Phenylalanine, did not show increased localization in cell protrusions following EGF stimulation, nor did it rescue $\beta 1$ integrin and TGN46 trafficking to the cell periphery (Fig. R8B-E). Together, our data indicate that ATG9A, through its interaction with AP, is critical for EGF-induced delivery of $\beta 1$ integrin and TGN46 toward cell protrusions.

III.8. ATG9A protein controls the dynamics of adhesion complexes

Clustering of $\beta 1$ integrin at the plasma membrane triggers the recruitment of several cytoplasmic proteins, including paxillin (PXN), that participates to the formation and maturation of adhesion complexes (Deakin & Turner, 2008). We then tested the impact of ATG9A protein on the formation and turnover of adhesion complexes, in cells expressing PXN-EGFP (Stehbens *et al*, 2014; Stehbens & Wittmann, 2014). Live-cell TIRF imaging of cells transfected with irrelevant siRNA revealed a dynamic adhesion turnover. Automated analysis using the Focal Adhesion Analysis Server (FAAS) allowed the detection of a mean of about 100 assembling adhesions and a mean of 139 disassembling adhesions during the 40-min recording period (Fig. R9A-D, Movie 5). In ATG9A-depleted cells, adhesions appeared much more static (Fig. R9A-D, Movie 5), and automated analysis of the live-cell movies revealed a marked reduction in the number of both assembling and disassembling adhesions (Fig. R9A-D). We next tested whether ATG9A is also involved in the formation of adhesions induced by EGF treatment. As expected, a 1-hour incubation with EGF induced an increase in the number of PXN-positive adhesion complexes, in U87 MG cells (+ 46%, Fig. R9E) and HeLa cells (+ 66%, Fig. S6). Knockdown of ATG9A using each siRNA targeting the ATG9A transcript totally abolished the effects of EGF, in both cell lines (Fig. R9E, Fig. S6).

To further support a role of ATG9 protein in adhesion dynamics, we next assessed whether the exocytosis of ATG9A-positive vesicles occurs in close proximity to focal adhesions. Live-cell TIRF imaging of cells expressing

both ATG9A-pHluorin and PXN-mCherry allowed us to generate spatial maps of exocytotic events, overlaid on a focal adhesion map (Fig. R10A, Fig. S7A). To statistically test our data, a parallel analysis was performed by producing simulated events randomly scattered on the ventral surface of the cell (Fig. R10B, Fig. S7B). An algorithm was then used to compute the distance of each fusion event, real or simulated, to the closest focal adhesion. Experiments done in U87 MG (Fig. R10C-D) or HeLa cells (Fig. S7C-D) revealed an obvious clustering, with a mean distance between real ATG9A-pHluorin events and focal adhesions of 1.3 μm (365 events from eight U87 MG cells) and 1.9 μm (1297 events from eight HeLa cells), respectively. Randomly simulated events occurred further away from focal adhesions (Fig. R10C-D; Fig. S7C-D).

IV. Discussion

Using complementary approaches, we have provided here extensive evidence that the core autophagy protein ATG9A constitutes an essential component of chemotactic cell migration. Knockdown of ATG9A abolished or markedly reduced chemotactic movement of human cells induced by EGF or CXCL12. Accordingly, ATG9A-depleted cells were unable to form large and polarized F-actin-rich protrusions, which normally drive efficient mesenchymal cell migration. By the design of an ATG9A-pHluorin construct and live-cell TIRF imaging, we further found that ATG9A-positive vesicles exhibited biased exocytosis toward the migration front, thereby participating to the local delivery of $\beta 1$ integrin and the formation/maturation of adhesions.

Accumulating reports indicate that several components of the autophagy machinery mediate one or multiple cellular functions, which may not directly depend on autophagosome biogenesis (Subramani & Malhotra, 2013). Among studies specifically related to cell shape dynamics, it was demonstrated that Atg1 and Ref(2)P, the *Drosophila* homologs of mammalian ULK 1/2 and SQSTM1, respectively, were essential for the extension of protrusions in blood cells (Kadandale et al., 2010). Depletion of the autophagy proteins ULK1 and beclin 1 severely reduced the ability of mouse macrophages to spread and elongate (Kadandale et al., 2010). A recent report pointed to a non-autophagic function of *Drosophila* ATG9, indicating that loss of ATG9 caused aberrant cortical actin network organization in nurse cells surrounding the oocyte and female sterility (Kiss et al., 2020a). Another study demonstrated that ATG9A was required for the post-Golgi transport and the maturation of lysosomal hydrolases (Jia et al., 2017). The present work adds to these data, and stresses the fact that, in addition to its well documented role during phagophore expansion, ATG9A should also be viewed as an essential component of vesicular trafficking driving cell migration.

We found that ATG9A signal localizes in cell protrusions, at the plasma membrane or in small vesicles located beneath the plasma membrane, displayed a marked co-localization with TGN46, suggesting that peripheral ATG9A mainly originates from the TGN. The Golgi apparatus plays a well-appreciated role during cell migration and invasion (Millarte & Farhan, 2012). In polarized cells, the TGN faces the leading edge and represents as such an optimally positioned sorting platform to ensure efficient delivery of pro-migratory proteins. Hence,

Golgi-associated microtubules, as a special subgroup of microtubules, have been found to serve as fast tracks to support anterograde trafficking of post-Golgi cargoes to the leading edge (Hao et al., 2020a). It should be noted that only few reports monitored polarized exocytosis of post-Golgi vesicles at the single vesicle level, using live-cell TIRF microscopy. This includes data from Schmoranzer and coll., showing that exocytosis of post-Golgi vesicles, loaded with low-density lipoprotein receptor-GFP, was polarized toward the leading edge of migrating fibroblasts (Schmoranzer et al., 2003). In polarized astrocytes, post-Golgi vesicles carrying the YFP-tagged vesicular stomatitis virus glycoprotein exhibited biased exocytosis toward the cell front, while exocytotic events appeared uniformly distributed in non-polarized cells (Letinic et al., 2009). In line with these observations, spatial maps from our live-cell TIRF experiments demonstrated that most ATG9A-pHluorin events were clustered near ($< 10 \mu\text{m}$) the leading edge of polarized cells, while fusion events did not display obvious hotspot in non-polarized cells. Critically, most of the recorded events were characterized by the dispersal of ATG9A-pHluorin into the plasma membrane, in a manner that shows a clear signature of full vesicle fusion. This raises the possibility that, in addition to the delivery of specific cargoes, ATG9A-positive vesicles may primarily act as a reservoir which dynamically delivers bulk lipids for lamellipodial expansion.

Integrins receptors are $\alpha\beta$ heterodimers, in which 8 β subunits can assort with 18 α subunits to form 24 distinct heterodimers with varied affinities for extracellular matrix proteins (Hynes, 2002; Fu *et al.*, 2012). By far the most commonly found subunit in integrin heterodimers is $\beta 1$ integrin, which has been shown to pair with a variety of α subunits to form 12 different heterodimers. Several studies have focused on the recycling of specific heterodimers, leading to the demonstration of an antagonistic relationship between the recycling of $\alpha v\beta 3$ and $\alpha 5\beta 1$ during cell migration. Hence, the $\alpha v\beta 3$ integrin heterodimer was found to be implicated in persistent cell migration, through a « short-loop » endosomal recycling pathway involving the small GTPase Rab4 (Danen et al., 2005). Endosomal recycling of the $\alpha 5\beta 1$ heterodimer through a Rab11-dependent, « long-loop » pathway, promotes random cell migration (White et al., 2007b). Shafaq-Zadah and coll. established a new paradigm by demonstrating that retrograde trafficking of $\beta 1$ integrin, followed by its polarized re-secretion from the TGN, also supports directional cell migration (Shafaq-Zadah et al., 2016). Using a transwell chemotaxis assay, we demonstrated here that depletion of ATG9A abolished or markedly reduced EGF-induced directional migration. We also found that ATG9A is essential for EGF-induced trafficking of $\beta 1$ integrin toward the cell protrusions. Although a fraction of $\beta 1$ integrin may recycle through the endosomal pathway under this latter protocol, it is likely that the critical role of ATG9A observed in our chemotactic assays essentially relies on its ability to control $\beta 1$ integrin trafficking from the TGN. Interestingly, we noticed that most ATG9A-depleted cells did not have a polarized shape, with a clear front-rear axis and a leading lamellipodium, and analyses from our live-cell movies indicated that membrane protrusions of siATG9A-transfected cells, although displaying normal velocities, showed reduced elongation and persistence. This phenotype has already been observed in $\alpha 3\beta 1$ -deficient keratinocytes, which retained the ability to form initial actin-containing protrusions rapidly extending and retracting along the circumference of the cell (Choma et

al., 2004). Deficient keratinocytes, however, did not have the ability to form stable lamellipodia and become polarized, leading to random migration. Collectively, our data support the view that ATG9A-dependent trafficking of $\beta 1$ integrin toward the leading edge, by establishing nascent adhesions, directs the stabilization of a unique lamellipodium required for chemotactic migration.

Could ATG9A protein be an intrinsic regulator of vesicle biogenesis from the secretory pathway? A specific role of ATG9A in the budding of clathrin-coated pits from the TGN has been recently reported (Jia et al., 2017). It was demonstrated that ATG9A, through its interaction with the clathrin adaptor complex AP-1, was required for the transport of cathepsins from the TGN to lysosomes (Jia et al., 2017). Mechanistically, the authors found that the association of ATG9A with AP-1 facilitated subsequent interaction of AP-1 with the cathepsin receptor CIMPR, resulting in the polymerization of AP-1 and vesicle budding. We found from our rescue experiments that the N-terminal AP-binding site of ATG9A was critical for the transport of $\beta 1$ integrin and TGN46 to the cell protrusions. These data are in agreement with the reported role of AP-1 in delivering $\beta 1$ integrin to the cell membrane (Mana et al., 2016), and support the idea that association of ATG9A with AP-1 is a priming event allowing the sorting/trafficking of a variety of cargoes. In addition to AP-1, it was found that ATG9A interacts with phosphatidylinositol 4-kinase III beta (PI4KIII β), a phosphatidylinositol 4-phosphate (PI4P)-producing enzyme that is required for the budding of ATG9A-containing vesicles from the Golgi during autophagy induction (Judith et al., 2019b). Interestingly, Golgi-localized PI4KIII β and PI4P, well-known regulators of membrane dynamics, have also been recognized as essential components of cell adhesion and migration (Tokuda *et al*, 2014; Bilodeau *et al*, 2020). Hence, functional studies established that PI4P produced at TGN microdomains triggers the recruitment of GOLPH3 protein which, by inducing local curvature of the TGN membrane, promotes the biogenesis of post-Golgi carriers and their transport to the leading edge (Xing *et al*, 2016; Rahajeng *et al*, 2019). In this framework, in depth identification of the molecular mechanisms driven by ATG9A and GOLPH3 for the biogenesis of particular post-Golgi carriers, during chemotactic stimulation or autophagy induction, is a critical subject for further studies.

In summary, our work sheds light on a previously unappreciated role for ATG9A during chemotactic migration. This constitutes an additional mechanism linking Atg proteins and cell migration (Coly *et al*, 2016; Kenific *et al*, 2016a; Kenific *et al*, 2016b; Coly *et al*, 2017), and may help to fully characterize the pro-tumoral functions of ATG9A already reported in triple negative breast cancer (Claude-Taupin et al., 2018a) and glioblastoma (Abdul Rahim et al., 2017a). According to our model, we suspect that ATG9A may, in addition to $\beta 1$ integrin, drive the delivery of an ensemble of cargoes to the leading edge of migrating cells. Future work is required to identify these critical cargoes.

V. Materials and Methods

V.1. Reagents and chemicals

Antibodies were as follow: rabbit monoclonal anti-paxillin (Y31) (Abcam, Ab32115), mouse monoclonal anti-c-myc (Santa Cruz, sc-40), sheep polyclonal TGN46 (Bio-rad AHP500GT), rabbit monoclonal ATG9A (Abcam, Ab108338), mouse monoclonal β 1 Integrin (Abcam, Ab24693). Secondary antibodies used were Alexa Fluor 488-conjugated antibody against rabbit IgG (Invitrogen, A21206), Alexa Fluor 594-conjugated antibody against mouse IgG (Invitrogen, A21203), Alexa Fluor 647-conjugated antibody against sheep IgG (Abcam, Ab150179). Other reagents in this study were recombinant human EGF (Gibco, PHG0314), human CXCL12 (R&D System, 350-NS), chloroquine (CQ, Sigma-Aldrich, C6628), bafilomycin A1 (BafA1, Sigma-Aldrich, B1793), 4',6-diamidino-2-phenylindole (DAPI, Sigma-Aldrich, D8417), rhodamine phalloidin (Fisher Scientific, R415), hematoxylin (Sigma-Aldrich, HHS32), fibronectin (FN1, Sigma-Aldrich, F0895), mowiol (Merck Millipore, 475904), normal donkey serum (Sigma-Aldrich, D9663), formaldehyde (Sigma-Aldrich, F8775), Dulbecco's phosphate-buffered saline without salts (DPBS, Sigma-Aldrich, D8537), triton X-100 (Fisher Scientific, T3751/08), bovine serum albumin fraction V (BSA, Roche, 10735108001) and methanol (Fisher Scientific, M4056/17).

V.2. Plasmid constructs and short interfering RNAs (siRNAs)

The expression vectors encoding the fusion protein EGFP-LC3B (#24920, deposited by Toren Finkel) and mCherry-Clathrin LC-15 (#55019, deposited by Michael Davidson) are available from Addgene. The *pmKate2-N* vector was purchased from Evrogen (#FP182). All the following expression vectors were purchased from GenScript. The expression vector encoding *ATG9A-pHluorin* was obtained by inserting codon-optimized human *ATG9A* (Uniprot, Q7Z3C6) and superecliptic pHluorin sequences into a pcDNA3.1(+) plasmid. The pHluorin sequence was fused in-frame into the first luminal domain of human *ATG9A* protein, between the amino acids *Leu102* and *His103*. The expression vector encoding wild-type *ATG9A-mCherry* used in Fig. R7, Fig. R8 and Fig. S5 was obtained by inserting codon-optimized human *ATG9A* sequence (Uniprot, Q7Z3C6) and mCherry sequence (GenBank, MK160997.1) into a pcDNA3.1(+) plasmid. The mCherry sequence was fused in-frame into the first luminal domain of human *ATG9A* protein, between the amino acids *Leu102* and *His103*. The *ATG9A-mCherry* Y8F mutant was obtained by replacing the TAC codon specifying tyrosine at the position 8 by a TTT codon specifying a phenylalanine. An alternative expression vector encoding *ATG9A-mCherry* was used in Fig. R3E and Fig. R4C; it was generated by inserting a codon-optimized human *ATG9A* sequence, fused in-frame with the mCherry sequence (GenBank, MK160997.1) at its C-terminus, into a pcDNA3.1(+) plasmid, using *HindIII* and *EcoRI* cloning sites. The expression vector encoding *ATG9A-myc* was obtained by inserting

the sequence of human *ATG9A* (GenScript clone ID OHu04028C; GenBank, NM_001077198.2) into a pcDNA3.1(+)-C-myc plasmid, using *XhoI* and *Apal* cloning sites; the myc epitope is located at the C-terminus of the *ATG9A* protein. The expression vector encoding *mCherry-LC3B* was generated by inserting the human *LC3B* sequence (GenScript clone ID OHu18146C; GenBank, NM_022818.5), fused in-frame with the mCherry sequence at its N-terminus, into a pcDNA3.1(+) plasmid. The expression vector encoding *PXN-EGFP* was obtained by inserting the sequence of human *PXN* (GenScript clone ID OHu13990C; GenBank, NM_002859.3) into a pcDNA3.1(+)-N-EGFP plasmid, using *KpnI* and *BamHI* cloning sites; the EGFP sequence is located at the N-terminus of the *PXN* protein. The expression vector encoding *PXN-mCherry* was obtained by inserting the sequence of human *PXN* (GenScript clone ID OHu13990C; GenBank, NM_002859.3) into a pcDNA3.1(+) plasmid, using *KpnI* and *BamHI* cloning sites; the mCherry sequence is located at the N-terminus of the *PXN* protein. For *ATG9A* knockdown experiments, control (D-001810-03, 5'-UCAGAAAACAUGUAAACCA-3'), *ATG9A* #1 (J-014294-09, 5'-UUCUGCGUCUGCAGAUCC-3') and *ATG9A* #2 (J-014294-10, 5'-UUUCGGAAGAAGUCUAUAA-3') siRNAs were purchased from Dharmacon Horizon Discovery. Cells were subject to 2 rounds of transfection in order to ensure adequate knockdown of the long-lived *ATG9A* protein.

V.3. Cell culture and transfections

The glioblastoma multiform cell line U87 MG (WHO grade IV) was purchased from *American Type Culture Collection* (ATCC, HTB-14™) and the glioblastoma multiform cell line 42 MG (WHO grade IV) from *German Collection of Microorganisms and Cell Cultures GmbH* (DSMZ, ACC 431) was generously provided by Pr. J. Honnorat (CNRL, Lyon, France). HeLa (ATCC, CCL-2) cell line was generously provided by Dr. P. Gaildrat (University of Rouen-Normandy, France). HEK 293 (ATCC, CRL1573) cell line was generously provided by Dr. L. Prézeau, C. Barrère and I. Bidaud (IGF, Montpellier, France). These cells were routinely maintained in our laboratory according to the instructions from ATCC and cultured in DMEM (Gibco, 41965-039), supplemented with 10% fetal bovine serum (Dutscher, S181H-500), 1% of antibiotic-antimycotic solution (Sigma-Aldrich, A5955) and 1% of sodium pyruvate (Sigma-Aldrich, S8636). For all experiments, cells were placed in either serum-free DMEM, supplemented with 1% of antibiotic-antimycotic solution and 1% of sodium pyruvate or serum- and phenol red-free Leibovitz's L-15 medium (Gibco, 21083027), supplemented with 1% D-Glucose (Sigma-Aldrich, G8644), 1% of antibiotic-antimycotic solution and 1% of sodium pyruvate. Transient transfections were performed using the Amaxa Cell Line Nucleofector Kit V (Lonza, VCA-1003) according to the manufacturer's protocol, using the A-023 program for U87 MG and 42 MG cells, the I-003 program for HeLa cells and the Q-001 program for HEK 293 cells.

V.4. Reverse transcription quantitative polymerase chain reaction (RT-qPCR)

Total RNA was extracted using Trizol Reagent (Sigma-Aldrich, T9424) and purified on NucleoSpin RNA II columns (Macherey-Nagel, 740955-250) according to the manufacturer's instructions. An amount of 0.3 µg of total RNA was used for cDNA synthesis using the ImProm-II Reverse Transcription System (Promega, A3800). Real-time PCR was performed in a FAST SYBR green master mix (Applied Biosystems, 4385612) using the QuantStudio 3 Real-Time PCR System (Fisher Scientific, France). The fold change in expression of *ATG9A* mRNA relative to Glyceraldehyde 3-phosphate dehydrogenase (*GAPDH*) mRNA was calculated based on the threshold cycle (*Ct*) as $2^{-\Delta Ct}$, where $\Delta Ct = Ct_{ATG9A} - Ct_{GAPDH}$. *ATG9A* sense and antisense primers: 5'-CTGCCCTCCGTATTGCAC-3' and 5'-CTCACGTTTGTGGATGCAGAT-3'; *GAPDH* sense and antisense primers: 5'-CTGGGCTACACTGAGCACC-3' and 5'-AAGTGGTCGTTGAGGGCAATG -3'.

V.5. SDS-PAGE and Western blot

Cell lysis was performed in ice-cold lysis buffer (25 mM Tris HCl pH 7.6 [Fisher Scientific, BP153-1], 150 mM NaCl [Fisher Scientific, S3160/60], 1% Nonidet P40 [Sigma-Aldrich, 74385], 1% sodium deoxycholate [Sigma-Aldrich, 30970], 0.1% sodium dodecyl sulfate [SDS, Fisher Scientific, BP2436], 0.6 mM dithiothreitol [DTT, ALX-280-001-G050], 1X protease inhibitor cocktail [Sigma-Aldrich, S8340], 1X phosphates inhibitor cocktail 2 [Sigma-Aldrich, P5726] and 3 [Sigma-Aldrich, P0044]) on ice for 10 minutes, and was completed by passing cells through a syringe tip. After centrifugation (16.000 g, 20 min, 4 °C), cytoplasmic proteins were collected. Equal amounts of proteins (30 µg) were mixed with a volume of laemmli buffer containing 2-Mercaptoethanol (Gibco, 21985-023) and loaded onto a precast 4-20% gradient SDS polyacrylamide gel (NuSep, NB17-420). Prestained protein ladder (Thermofisher, 26619) was loaded onto the gel along with protein samples. After separation, proteins were transferred onto a polyvinylidene difluoride membrane within a transfer buffer using the Trans-blot Turbo RTA Transfer Kit (BioRad, #1704272) and the Trans-blot turbo system (BioRad, #1704150) according to the manufacturer's protocol. Membranes were blocked with 5% nonfat milk [Sigma-Aldrich, 70166] (1 h, room temperature) and incubated (overnight, 4 °C) with the primary antibody (rabbit monoclonal anti-*ATG9A* [Abcam, Ab108338] or mouse monoclonal anti- β -actin [Santa Cruz Biotechnology, sc-47778] as equal loading control). Membranes were then incubated (2 h, room temperature) with horseradish peroxidase-conjugated secondary antibodies raised against rabbit (Thermofisher, #31460) or mouse (Thermofisher, #31430) IgG. Immunoreactive bands were visualized with the enhanced chemiluminescence Western blotting substrate (GE Healthcare, RPN2236).

V.6. Autophagosome biogenesis

Autophagic activity was evaluated in cells expressing EGFP-LC3B or mCherry-LC3B fusion proteins. LC3B protein is a well-established effector of autophagy and a *bona fide* marker for autophagosomes (Klionsky et al., 2021a). Punctate EGFP-LC3B or mCherry-LC3B staining provides a measure of ongoing autophagy, because it marks the successful processing of the cytosolic form LC3B-I to LC3B-II, a phospholipid-conjugated form that is targeted to phagophore membranes. Cells were transfected and placed in complete DMEM. At 24 h post-transfection, cells were rinsed twice with warm DPBS and placed for 6 h in serum-free DMEM in absence or presence of CQ (10^{-5} M). After the incubation time cells were rinsed with warm DPBS, fixed (4% formaldehyde), mounted in glass slides with mowiol and randomly photographed using the Leica DMI6000 B inverted microscope. The number of autophagosomes was calculated using the ComDet plug-in of the ImageJ software.

V.7. Migration assay

HEK 293 cells (80,000/insert), U87 MG, 42 MG, HeLa cells (20,000/insert) were seeded on FN1-coated transwell inserts (8- μ m pores, 24 wells; Corning, 3422). The gradient of ligands was generated by addition of EGF or CXCL12 in the lower chamber. After 24 h, cells on the upper surface of the insert were removed using a cotton swab. Cells that migrated onto the lower surface were fixed with four successive baths of methanol (50%, 70%, 90% diluted in DPBS and 100% methanol) and then stained with hematoxylin. Insert membranes were cut out and mounted on glass slides with mowiol and randomly photographed with a Nikon inverted microscope (Nikon France, Champigny-sur-Marne, France; 10 random fields/membrane). Cells in the photographic fields were counted by using the Cell counter plug-in of the ImageJ software.

V.8. Immunocytochemistry and image analysis

Cells were fixed with formaldehyde (4%, 10 min), permeabilized with Triton X-100 (0.05%, 5 min) and blocked for 1 h with a mixture of normal donkey serum (2%) and fetal bovine serum (10%) diluted in DPBS. Cells were incubated overnight with the adequate primary antibody at 4°C followed by incubation for 2 h at room temperature with the adequate secondary antibody. Cells were counterstained with DAPI (1 μ g/mL, 10 min) to label nuclei, and imaged using the Leica DMI6000 B inverted microscope, the Leica SP8 MP confocal multiphoton microscope or the Leica THUNDER Imager 3D Tissue. In PXN-labelled cells (Fig. R8, Fig. S10), the number of focal adhesion complexes was calculated using the function Find Maxima after successive image treatment with the ImageJ software. Radial intensity profile of the β 1 integrin signal (Fig. R6) was produced using the Clock-scan plug-in (Dobretsov & Romanovsky, 2006).

V.9. Live-cell imaging

Transfected cells were seeded on FN1-coated 35-mm glass dishes (P35G-1.5-14-C, MatTek Corporation) for TIRF and epifluorescence experiments, or on FN1-coated 24 multi-well glass plate (P24G-1.5-13-F, MatTek Corporation) for phase contrast experiments. At 24 h post-transfection, live-cell imaging was performed in serum-free Leibovitz's L-15 medium supplemented with 1% D-Glucose, 1% of antibiotic-antimycotic and 1% of sodium pyruvate (TIRF and epifluorescence), or in serum-free DMEM supplemented with 1% of antibiotic-antimycotic and 1% of sodium pyruvate (phase contrast).

TIRF: TIRF images were acquired using a system that was built around a Leica DMI6000 B inverted microscope equipped with a $\times 100$ oil objective with a numerical aperture of 1.46 (HCX PL APO, Leica), a Hamamatsu Orca-Flash 4.0 camera, and 488-nm and 561-nm lasers. The TIRF angle was set for the 488-nm and 561-nm lasers to achieve an evanescent field with a characteristic penetration depth of 110nm. In the experiments involving dual channel recording, 488-nm and 561-nm lasers were used consecutively for each image of the time series. Time intervals were recorded as follow. *ATG9A-mCherry vesicle tracking experiments (Fig. R3E)*: time series of images at 500-millisecond intervals; *ATG9A-pHluorin exocytosis experiments (Fig. R5, Fig. R10)*: time series of images at 390-millisecond intervals; *ATG9A-pHluorin and mKate2 dual channel experiments (Fig. R6C-E)*: time series of images at 1-min intervals (having a time delay of 2.2 seconds between the two channels); *ATG9A-pHluorin experiments for kymograph analyses (Fig. R6B)*: time series of images at 30-sec intervals; *ATG9A-pHluorin and Clathrin-mCherry dual channel experiments (Fig. S3)*: time series of images at 3.4-sec intervals (having a time delay of 1.6 second between the two channels). *PXN-EGFP experiments (Fig. R9A-D)*: time series of images at 30-sec intervals. All TIRF live-cell movies provided with this manuscript are shown at a frame rate of 15 frames per second.

Tracking of moving ATG9A-mCherry vesicles was performed using the Manual Tracking tool of the ImageJ software. In PXN-EGFP transfected cells, the number of assembling and disassembling adhesions during a 40-min imaging session was determined using the Focal Adhesion Analysis Server (Berginski et al., 2011). The results only include focal adhesions with a minimum size of 2 pixels (0.25 μm), and with assembly or disassembly phase lengths of at least 10 images (5 min). Simulated fusion events for uniform distributions were performed with R software (v.4.0.5.). The function `runif()` was used to generate uniformly spaced points within the cell whose ROI coordinates defined the minimum and maximum xy interval for the position of the random points. For each cell, the number of simulated fusion events produced by the algorithm was identical to the number of real ATG9A-pHluorin events.

Epifluorescence: Images were acquired using a Leica DMI6000 B inverted microscope equipped with a $\times 63$ oil objective with a numerical aperture of 1.32 (HCX PL APO CS, Leica), a Hamamatsu Orca-Flash 4.0 camera, and 488-nm and 561-nm lasers. *ATG9A-pHluorin and ATG9A-mCherry dual channel experiments (Fig. R4C)*:

time series of images at 30-sec intervals were recorded (having a time delay of 1.7 second between the two channels).

Phase contrast: Cells were placed in a temperature- and CO₂-controlled (37°C, 5% CO₂) environment of a Zeiss Cell Discoverer 7 microscope system. Live-cell phase contrast images of the individual field regions inside each well were automatically acquired using the ZEN Blue 2.6 software with a time series of images at 40-sec intervals. Kymographs of the cell protrusions were generated using the Multi Kymograph tool of Fiji software from one-pixel wide lines manually traced perpendicularly to the ruffling cell edges, and the protrusion distances (Δx), persistences (Δy) and velocities ($\Delta x/\Delta y$) were evaluated. Cell trajectories (Fig. R2F) were obtained using a semi-automatic tracking macro of the ImageJ software, generously provided by Federico Saltarin (Theodor Kocher Institute, Bern, Switzerland) and trajectories plots were rendered using the DiPer excel macro (Gorelik & Gautreau, 2014). Average speeds (Fig. R2G, average of the instantaneous speed) and Mean Square Displacements (Fig. R2H) were calculated using the DiPer excel macro (Gorelik & Gautreau, 2014). Representative figure images were selected and additional image post-processing steps (contrast adjustment, field selection, and scale bar addition) were performed using the ImageJ software. Phase contrast live-cell movie 1 provided with this manuscript is shown at a frame rate of 25 frames per second.

V.10. Statistical analysis

Data are presented as the mean \pm SEM for each group of samples. Statistical analyses were performed using the GraphPad Prism 8 software (GraphPad Software). Details of the individual tests are included in the figure legends.

VI. Author's contributions

D.C. conducted all the experiments, designed the work, analyzed, interpreted data and wrote the manuscript. L.D. contributed providing materials, reagents, support during experiments and revised the manuscript. R.P. analysed data and edited the manuscript. P.G. contributed to discussion, reviewed and edited the manuscript. H.C. contributed to discussion, reviewed and edited the manuscript. F.M. designed, validated the work, analyzed, interpreted data and wrote the manuscript.

VII. Acknowledgments

This work was supported by Inserm, GEFLUC, TC2N network, the Ligue contre le Cancer Normandie, the french Agence Nationale de la Recherche and the University of Rouen Normandy. D.C. is recipient of a fellowship

from Normandy. We grateful the PRIMACEN team (<http://www.primacen.fr>, the Cell Imaging Platform of Normandy, IRIB, Faculty of Sciences, University of Rouen-Normandy, 76821, Mont-Saint Aignan) for technical support on imaging experiments. We thank Inès Drissa (INSERM 1239, Mont Saint Aignan, France) for her generous technical support to ImageJ software and Federico Saltarin (Theodor Kocher Institute, Bern, Switzerland) for kindly providing us the ImageJ macro for semi-automatic cell tracking.

VIII. Disclosure statement

The authors declare no competing interests.

IX. Main and supplementary figures

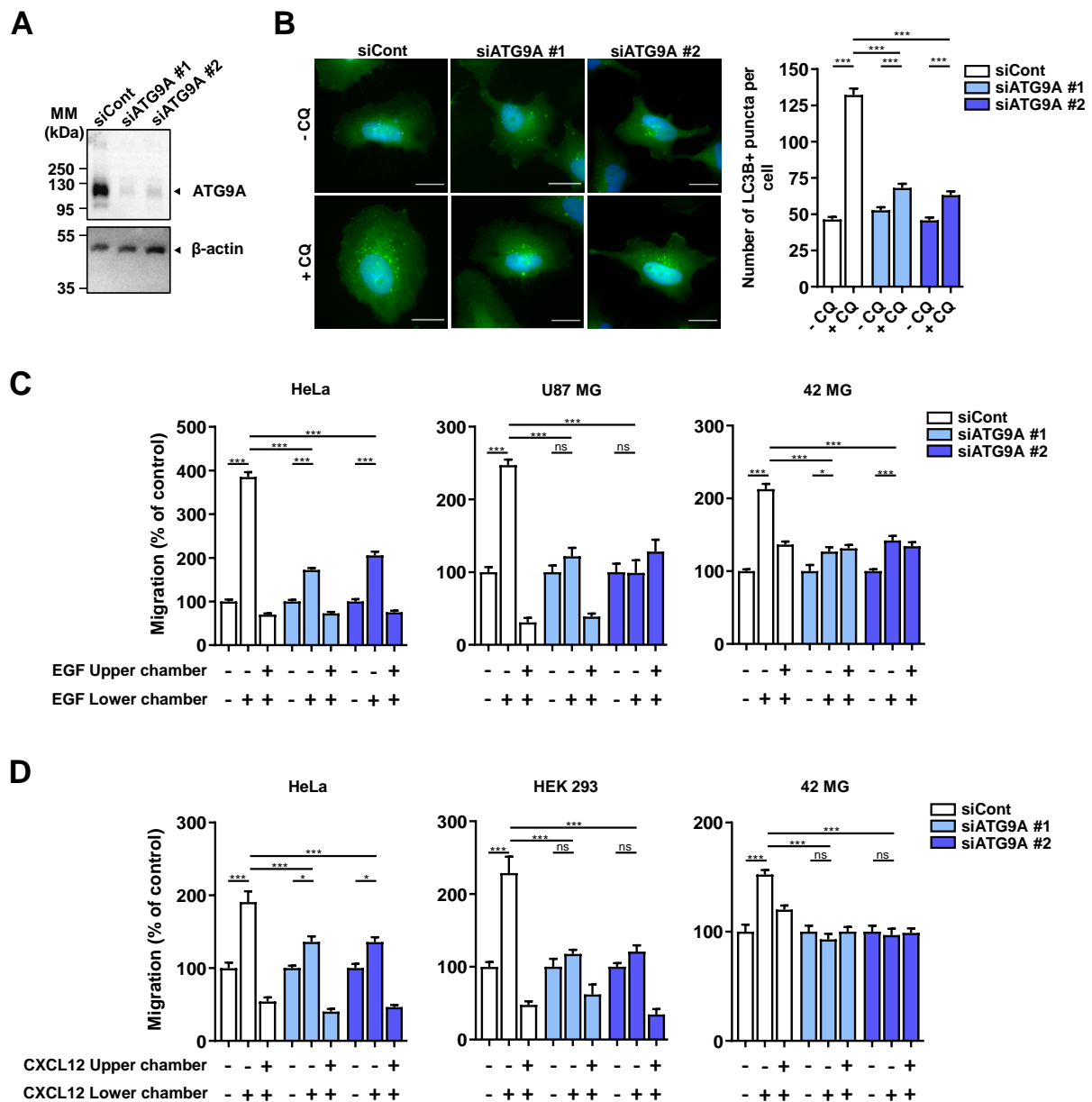


Figure R1. Chemotactic migration depends on ATG9A protein. (A) Efficiency of siRNA knockdown of ATG9A. HeLa cells were transfected with nontargeting siRNA (*siCont*) or one of the two siRNAs targeting ATG9A (*siATG9A #1*, *siATG9A #2*). Shown is a representative Western blot analysis of ATG9A protein levels. The lower part of the blot was probed with an anti-β-actin antibody. MM, molecular mass. (B) Effect of siRNA knockdown of ATG9A on autophagosome biogenesis. HeLa cells were transfected with nontargeting siRNA (*siCont*) or one of the two siRNAs targeting ATG9A (*siATG9A #1*, *siATG9A #2*), together with a construct encoding the EGFP-LC3B protein (marker of autophagosomes). Transfected cells were placed in serum-free DMEM for 6 h, in the presence or absence of chloroquine (CQ, 5×10^{-5} M), as indicated. Cells were fixed and the number of autophagosomes (EGFP-LC3B fluorescent dots) per cell was quantified. Data represent means and SEM (*siCont*, $n = 424$ cells; *siATG9A #1*, $n = 414$ cells; *siATG9A #2*, $n = 421$ cells; from 3 independent experiments). Scale bar 20 μ m. (C) Effect of siRNA knockdown of ATG9A on chemotactic migration induced by EGF. HeLa cells (*left*), U87 MG cells (*middle*) and 42 MG cells (*right*) were transfected with nontargeting siRNA (*siCont*) or one of the two siRNAs targeting ATG9A (*siATG9A #1*, *siATG9A #2*). Transfected cells were loaded in the upper chamber of transwells, containing or not EGF (50 ng/mL) in the upper or lower chamber, as indicated. After 24 h, cells that migrated onto the lower surface of the membrane were fixed, stained and counted. Data represent means and SEM ($n = 6$ transwells). (D) Effect of siRNA knockdown of ATG9A on chemotactic migration induced by CXCL12. HeLa cells (*left*), HEK 293 cells (*middle*) and 42 MG cells (*right*) were transfected with nontargeting siRNA (*siCont*) or one of the two siRNAs targeting ATG9A (*siATG9A #1*, *siATG9A #2*). Transfected cells were loaded in the upper chamber of transwells, containing or not CXCL12 (10^{-8} M) in the upper or lower chamber, as indicated. After 24 h, cell migration was quantified following the protocol described in (C). Data represent means and SEM ($n = 6$ transwells). Statistical significance was evaluated using a one-way ANOVA followed by Sidak post-hoc test (B), or a one-way ANOVA followed by Turkey post-hoc test (C, D). * $P < 0.05$; *** $P < 0.001$; ns, not statistically different.

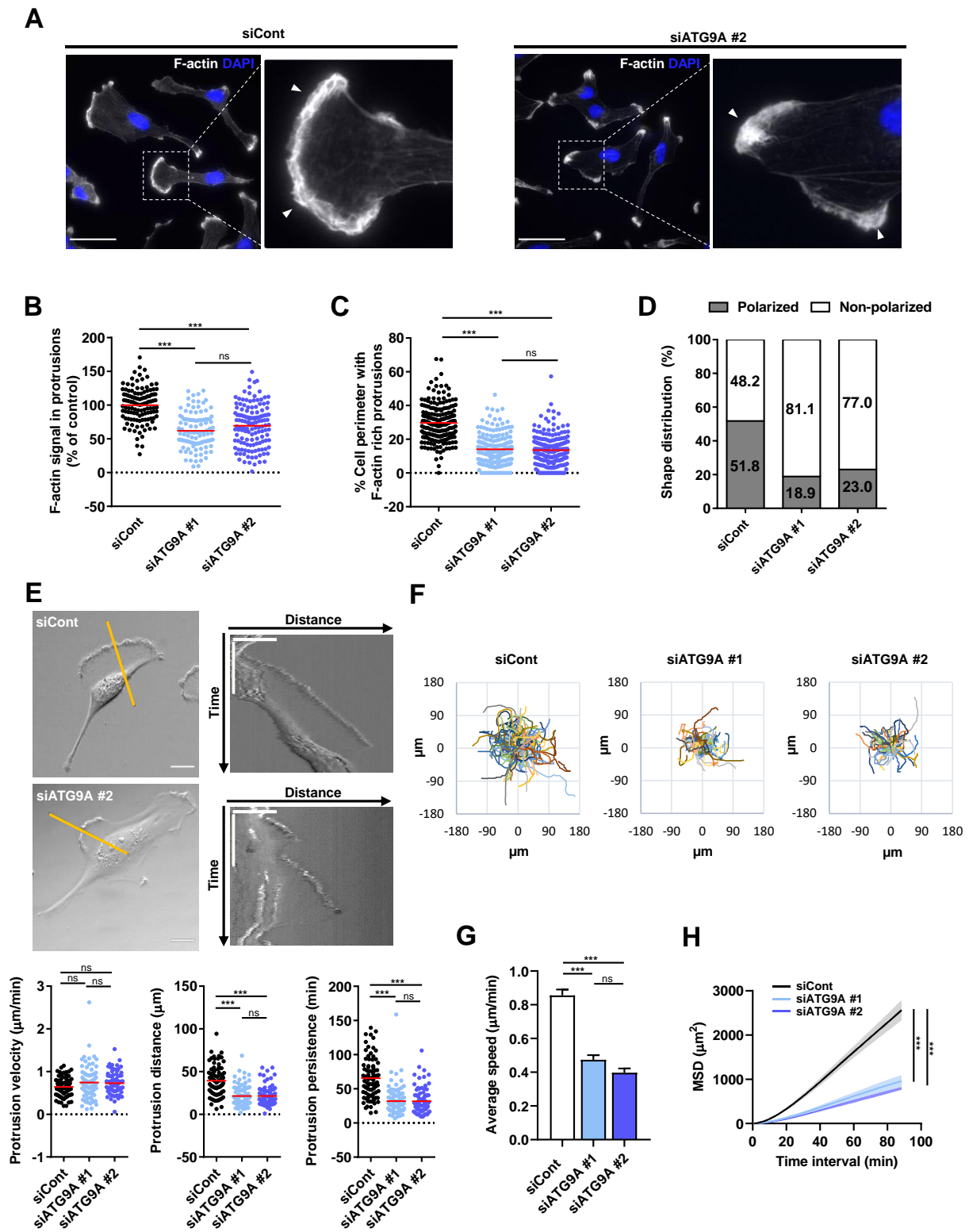


Figure R2. For caption see next page.

Figure R2. Depletion of ATG9A protein impairs the formation of F-actin-rich protrusions and intrinsic cell speed. (A) Representative epifluorescence images showing F-actin (rhodamine phalloidin labelling; *grey levels*) and nuclei (DAPI labelling; *blue*) of U87 MG cells transfected with nontargeting siRNA (*siCont*, *left panel*) or siRNA targeting ATG9A (*siATG9A #2*, *right panel*). Control cells generally develop large F-actin-rich lamellipodia (*arrowheads*), while ATG9A-depleted cells display smaller and irregular protrusions (*arrowheads*). Scale bar, 20 μm . (B) Quantification of F-actin intensities, after background subtraction, in protrusions of U87 MG cells transfected with nontargeting siRNA (*siCont*) or one of the two siRNAs targeting ATG9A (*siATG9A #1*, *siATG9A #2*). For each cell, values correspond to cumulated signal of all protrusions (*siCont*, $n = 117$ cells; *siATG9A #1*, $n = 106$ cells; *siATG9A #2*, $n = 135$ cells; from 3 independent experiments). (C) Percentage of the cell perimeter containing F-actin-rich protrusions, in U87 MG cells transfected with nontargeting siRNA (*siCont*) or one of the two siRNAs targeting ATG9A (*siATG9A #1*, *siATG9A #2*); (*siCont*, $n = 210$ cells; *siATG9A #1*, $n = 209$ cells; *siATG9A #2*, $n = 219$ cells; from 3 independent experiments). (D) Effect of siRNA knockdown of ATG9A on cell polarization of U87 MG cells. The quantitative analysis was performed by establishing that polarized cells have a clear front-back axis with the presence of a single lamellipodium at the front, while non-polarized cells do not have a front-back axis and display several lamellipodia or small ruffles scattered at the cell periphery. Data represent the percentage of polarized or non-polarized cells (*siCont*, $n = 222$ cells; *siATG9A #1*, $n = 212$ cells; *siATG9A #2*, $n = 226$ cells; from 3 independent experiments). (E) Phase contrast time-lapse sequences acquired from U87 MG cells transfected with nontargeting siRNA (*siCont*) or one of the two siRNAs targeting ATG9A (*siATG9A #1* or *siATG9A #2*). *Upper panels*: single images from representative sequences of U87 MG cells transfected with nontargeting siRNA (*siCont*) and *siATG9A #1* (*upper left*; scale bar, 20 μm), and kymographs (*upper right*) generated from one-pixel wide lines drawn on the cell edges. The scale bars in the kymographs are 20 μm (horizontal) and 40 min (vertical). *Lower panels*: quantification, from kymographs, of protrusion velocity (*left*), protrusion distance (*middle*) and protrusion persistence (*right*) (*siCont*, $n = 84$ protrusions; *siATG9A #1*, $n = 86$ protrusions; *siATG9A #2*, $n = 87$ protrusions; from 3 independent experiments). (F) Cell trajectories over a 3-hour period (one frame every 40 sec) of randomly migrating U87 MG cells transfected with nontargeting siRNA (*siCont*, $n = 101$ cells) or siRNA targeting ATG9A (*siATG9A #1*, $n = 88$ cells; *siATG9A #2*, $n = 97$ cells). (G) Analysis of average cell speed and (H) Mean Square Displacement, calculated from the cell trajectories presented in (F). Data represent means and SEM. Statistical significance was evaluated using a one-way ANOVA followed by Turkey post-hoc test (B, C, E, G), or a two-way ANOVA followed by Dunnett post-hoc test (H). *** $P < 0.001$; ns, not statistically different

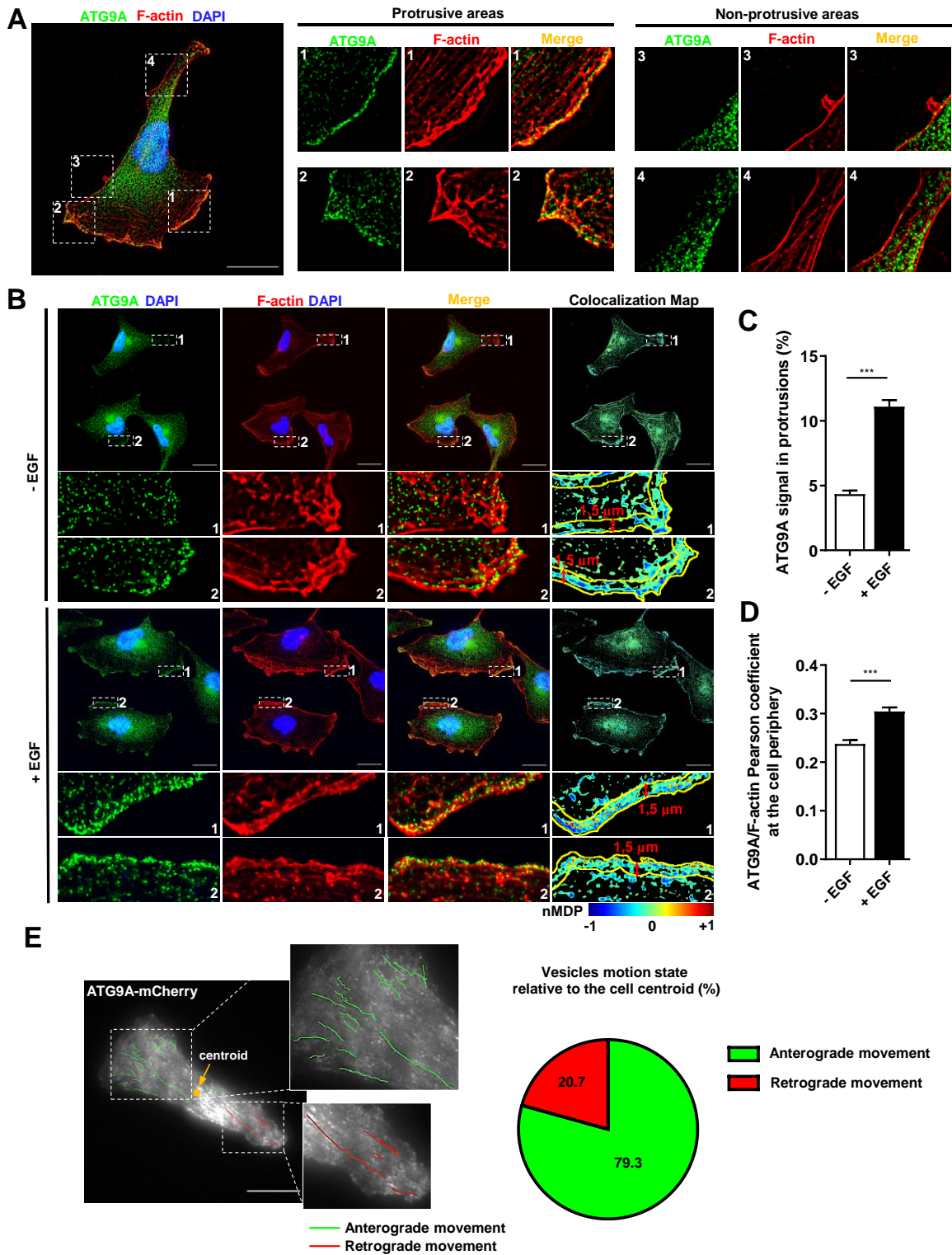


Figure R3. For caption see next page.

Figure R3. ATG9A-positive vesicles concentrate in F-actin rich protrusions and display anterograde trafficking toward the leading edge. (A) Endogenous ATG9A localizes in F-actin rich cell protrusions. *Left*: U87 MG cells co-labelled for endogenous ATG9A (*green*), F-actin (rhodamine phalloidin, *red*) and nuclei (DAPI labelling; *blue*). *Middle and right*: magnified views of cell presented on the left panel, showing protrusive (*middle*) and non-protrusive (*right*) areas. Note that endogenous ATG9A puncta frequently colocalize with F-actin in protrusive areas. Scale bar, 20 μm . (B) Chemotactic stimulation with EGF increases peripheral localization of ATG9A. U87 MG cells were starved (30 min) in serum-free medium and incubated (30 min) with or without EGF (50 ng/mL), as indicated. Cells were fixed and labelled for endogenous ATG9A (*green*), F-actin (rhodamine phalloidin, *red*) and DAPI (nuclei, *blue*). For each condition, a merged image and a ATG9A/F-actin colocalization map is shown. The association of ATG9A with F-actin was representatively shown with Colocalization Colormap tool, where normalized mean deviation product (nMDP) shows the correlation between intensities of corresponding pixels (values are ranging from -1 to 1). Negative nMDP values are represented by cold colors (segregation) whilst values above 0 are represented by hot colors (colocalization). Scale bar, 20 μm . (C) Quantification from images shown in (B) of the fraction of the ATG9A signal (after background subtraction) located in F-actin rich protrusions. For each cell, values correspond to the cumulated signal of all protrusions (- EGF, n = 88 cells; + EGF, n = 89 cells; from 2 independent experiments). (D) Quantification from images shown in (B) of the ATG9A/F-actin colocalization score (Pearson coefficient) at the cell periphery, in a region of interest of 1.5 μm width from the cell membrane. Data represent means \pm SEM (- EGF, n = 73 cells; + EGF, n = 74 cells; from 2 independent experiments). (E) ATG9A-mCherry positive vesicles display anterograde trafficking toward the leading edge. *Left*: map of all observed (5-min period) ATG9A-mCherry vesicle trajectories from a representative, polarized U87 MG cell. Trajectories were color-coded and defined as anterograde (*green*) or retrograde (*red*), as a function of vesicle displacement relative to the cell centroid. Scale bar, 20 μm . *Right*: pie chart showing the percentage of ATG9A-mCherry vesicles displaying anterograde or retrograde movement in cell protrusions (total number of 87 trajectories, recorded from four U87 MG polarized cells). Statistical significance was evaluated using a Mann and Whitney test. ***P < 0.001.

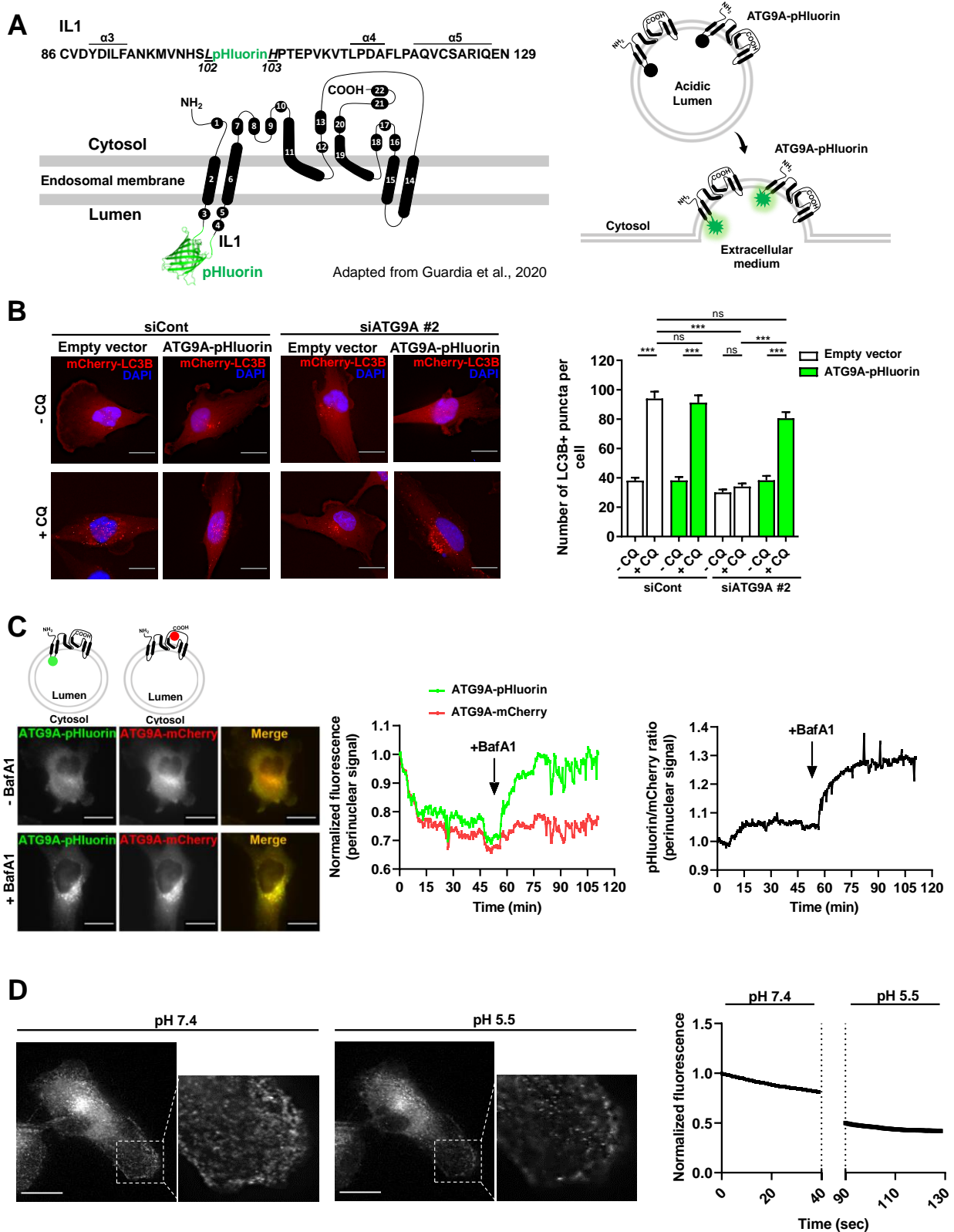


Figure R4. For caption see next page.

Figure R4. Structure and functional validation of ATG9A-pHluorin construct. (A) *Left*: topology of human ATG9A protein, adapted from Guardia and Coll. (Guardia *et al*, 2020), displaying four transmembrane domains ($\alpha 2$, $\alpha 6$, $\alpha 14$ and $\alpha 15$) and two domains ($\alpha 11$ and $\alpha 19$) that are partially embedded in the membrane but do not cross it completely. The ATG9A-pHluorin fusion protein was produced by inserting the pHluorin sequence (depicted by a cartoon of GFP) into the first luminal domain, between amino-acids *Leu102* and *His103* of the human sequence. *Right*: the pHluorin fluorescence is expected to be quenched at the acidic endosomal pH. Upon fusion of ATG9A-containing endosomes with the plasma membrane, pHluorin fluorescence will sharply increase at the contact of extracellular physiological pH. (B) *Left*: validation of functional activity of ATG9A-pHluorin on autophagosome biogenesis. U87 MG cells were transfected with nontargeting siRNA (*siCont*) or siRNA targeting ATG9A (*siATG9A #2*), together with an empty vector or the ATG9A-pHluorin construct and a construct encoding the mCherry-LC3B protein (marker of autophagosomes). Transfected cells were placed in serum-free DMEM for 6 h, in the presence or absence of chloroquine (CQ, 5×10^{-5} M), as indicated. Cells were fixed and the number of autophagosomes (mCherry-LC3B fluorescent dots) per cell was quantified. Data represent means and SEM (*siCont* + Empty vector, $n = 192$ cells; *siCont* + ATG9A-pHluorin, $n = 204$ cells; *siATG9A #2* + Empty vector, $n = 205$ cells; *siATG9A #2* + ATG9A-pHluorin, $n = 202$ cells; from 2 independent experiments). Scale bar, 20 μm . (C) Validation of ATG9A-pHluorin topology. Representative U87 MG cell co-expressing ATG9A-pHluorin and ATG9A-mCherry was imaged by epifluorescence (one frame every 30 sec) before and after bafilomycin A1 (*BafA1*, 100 nM) treatment. *Left*: images, extracted from the time-lapse sequence, before (*-BafA1*) and at the end (*+BafA1*; 1-hour incubation) of the *BafA1* treatment. Scale bar, 20 μm . *Middle*: mCherry and pHluorin fluorescence signal intensities measured in the perinuclear area and plotted against time. *Right*: analysis of the pHluorin/mCherry fluorescence intensity ratio, plotted against time. The increased ratio value following *BafA1* treatment indicates de-quenching of the pHluorin signal in endosomes, suggesting that the ATG9A-pHluorin fusion protein has the expected topology, with the pHluorin facing the vesicular lumen. (D) *Left*: representative U87 MG cell expressing ATG9A-pHluorin recorded using TIRF microscopy (one frame every 390 millisecc), before (pH 7.4) and after (pH 5.5) acidification of the extracellular medium. Note that most ATG9A-pHluorin puncta rapidly dimmed following extracellular acidification, indicating that ATG9A-pHluorin proteins concentrating in these puncta are located at the plasma membrane, with the pHluorin facing the extracellular medium. *Right*: pHluorin fluorescence signal intensity measured before and after extracellular acidification and plotted against time. Scale bar, 20 μm .

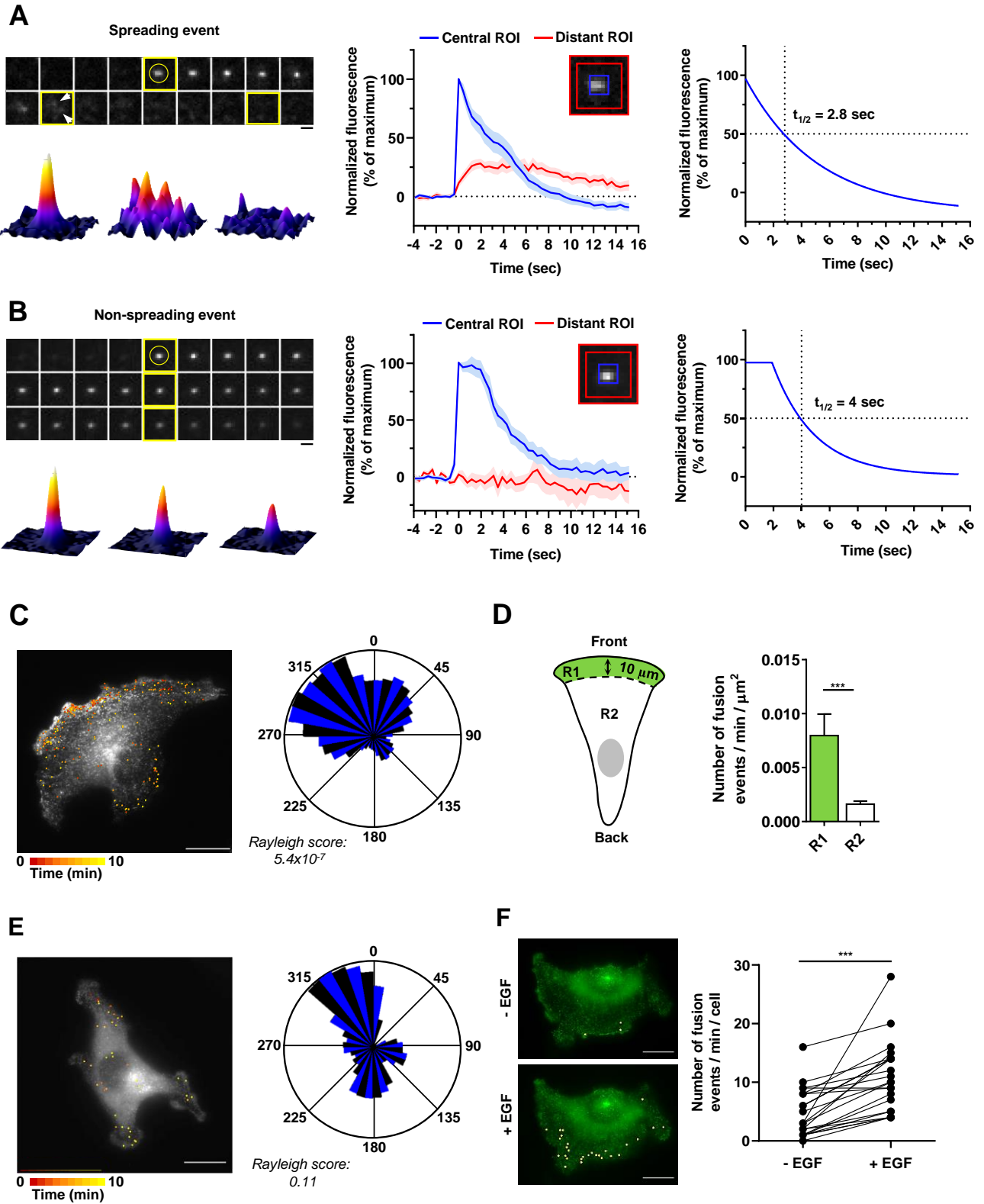


Figure R5. For caption see next page.

Figure R5. Exocytosis of ATG9A-positive vesicles is polarized toward the cell front and induced by chemotactic stimulation. (A) U87 MG cells expressing ATG9A-pHluorin were recorded (one frame every 390 millisecond) using TIRF microscopy. *Upper left*: time-lapse sequence of a representative “spreading event”. *Yellow circle* indicates the rapid appearance of the pHluorin signal, likely due to de-acidification upon fusion pore opening. *Arrows* indicate diffusion of the fluorescence signal in areas of the plasma membrane surrounding the insertion sites. Scale bar, 1 μm . *Bottom left*: 3D fusion profiles of the indicated images (*framed in yellow*) from the time-lapse sequence. *Middle*: normalized fluorescence intensities, from the analysis of 68 spreading events. For each event, measurements were performed in parallel into a central ROI (5x5 pixels; 0.64 x 0.64 μm), and a distant ROI (delimited by 13x13 pixel and 17x17 pixel squares). Note the delayed fluorescence increase in the distant ROI, due to full fusion of the vesicles and radial diffusion of the pHluorin signal into the plasma membrane. Data represent means and SEM. *Right*: nonlinear regression analysis (single exponential decay) from the profile obtained in the central ROI, for the determination of spreading event half-life (2.8 sec). (B) U87 MG cells expressing ATG9A-pHluorin were recorded as in (A). *Upper left*: time-lapse sequence of a representative “non-spreading” event. *Yellow circle* indicates the rapid appearance of the pHluorin signal, likely due to de-acidification upon fusion pore opening. Scale bar, 1 μm . *Bottom left*: 3D fusion profiles of the indicated images (*framed in yellow*) from the time-lapse sequence. *Middle*: Normalized fluorescence intensities, from the analysis of 13 non-spreading events. For each event, measurements were performed in a central ROI and a distant ROI, as in (A). Note the absence of increased fluorescence in the distant ROI following fusion pore opening. Data represent means and SEM. *Right*: nonlinear regression analysis (plateau followed by single exponential decay) from the profile obtained in the central ROI, for the determination of non-spreading event half-life (4 sec). (C) *Left*: map of all observed ($n = 248$) ATG9A-pHluorin fusion events from a representative, polarized U87 MG cell, during a 10-min time-lapse sequence. Scale bar, 20 μm . *Right*: rose plot (interior angle: 66°; interval: 10°) from the cell shown on the *left*, depicting the angular distribution of the fusion events relative to the cell centroid. (D) Quantification, from U87 MG cells displaying clear polarization with unique and large lamellipodia ($n = 11$ cells), of the number of fusion events occurring at a distance inferior (*R1* region) or superior (*R2* region) to 10 μm from the leading edge. For each cell, data were normalized to the areas of the respective regions. Data represent means and SEM. (E) *Left*: map of all observed ($n = 40$) ATG9A-pHluorin fusion events from a representative, non-polarized U87 MG cell, during a 10-min time-lapse sequence. Scale bar, 20 μm . *Right*: rose plot (interior angle: 66°; interval: 10°) from the cell shown on the *left*, depicting the angular distribution of the fusion events relative to the cell centroid. (F) *Left*: representative U87 MG cell with projections of all observed ATG9A-pHluorin fusion events, during 1-min time-lapse sequences, before (*-EGF*) and 2-min after (*+EGF*) treatment with EGF (50 ng/mL). Scale bar, 20 μm . *Right*: quantification of the effect of EGF, as depicted on the left, on the number ATG9A-pHluorin fusion events ($n = 23$ cells; from 3 independent experiments). Statistical significance was evaluated using a Mann and Whitney test (D), a Paired t-test (F) and a Rayleigh test for fusion events distribution (C, E). *** $P < 0.001$.

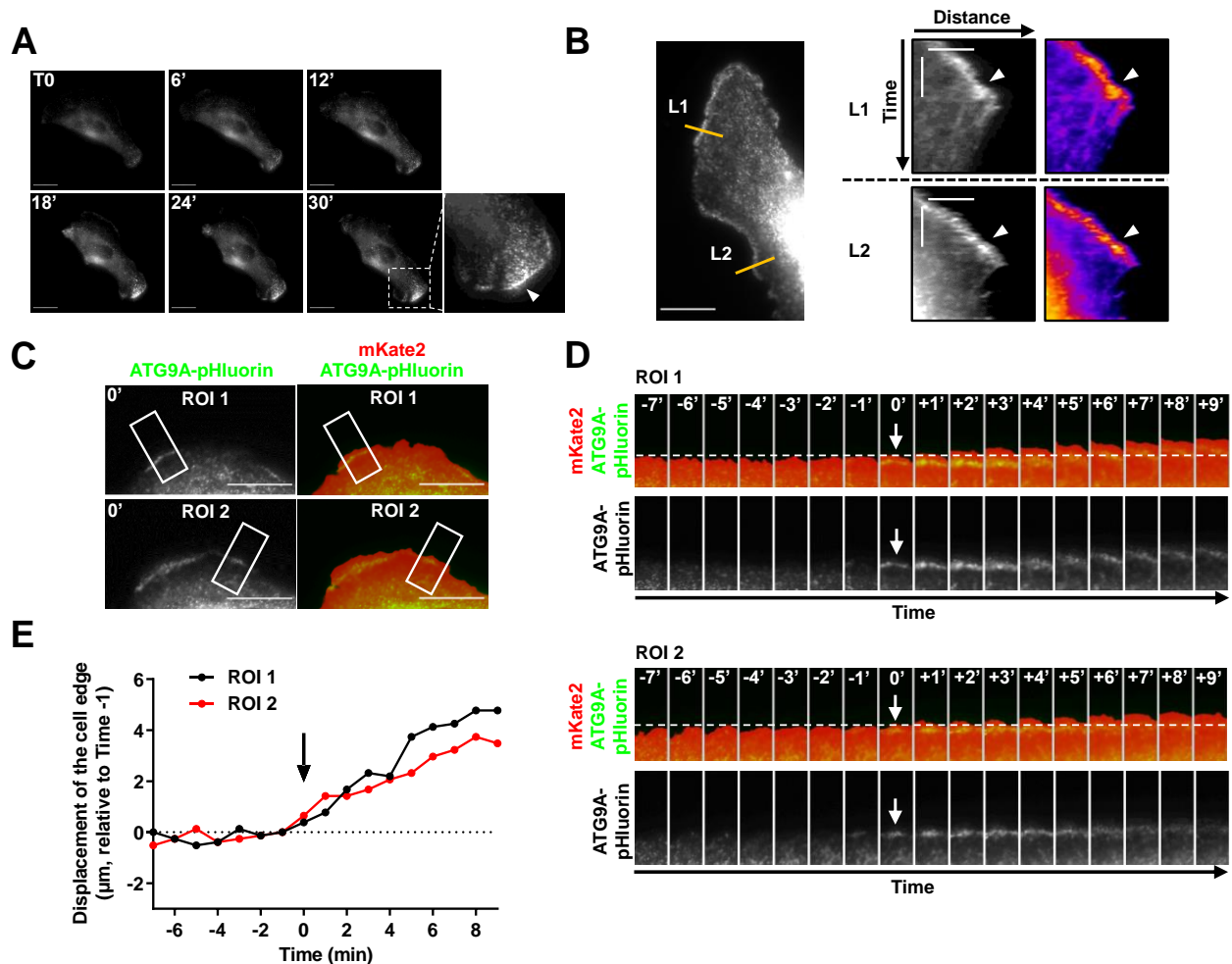
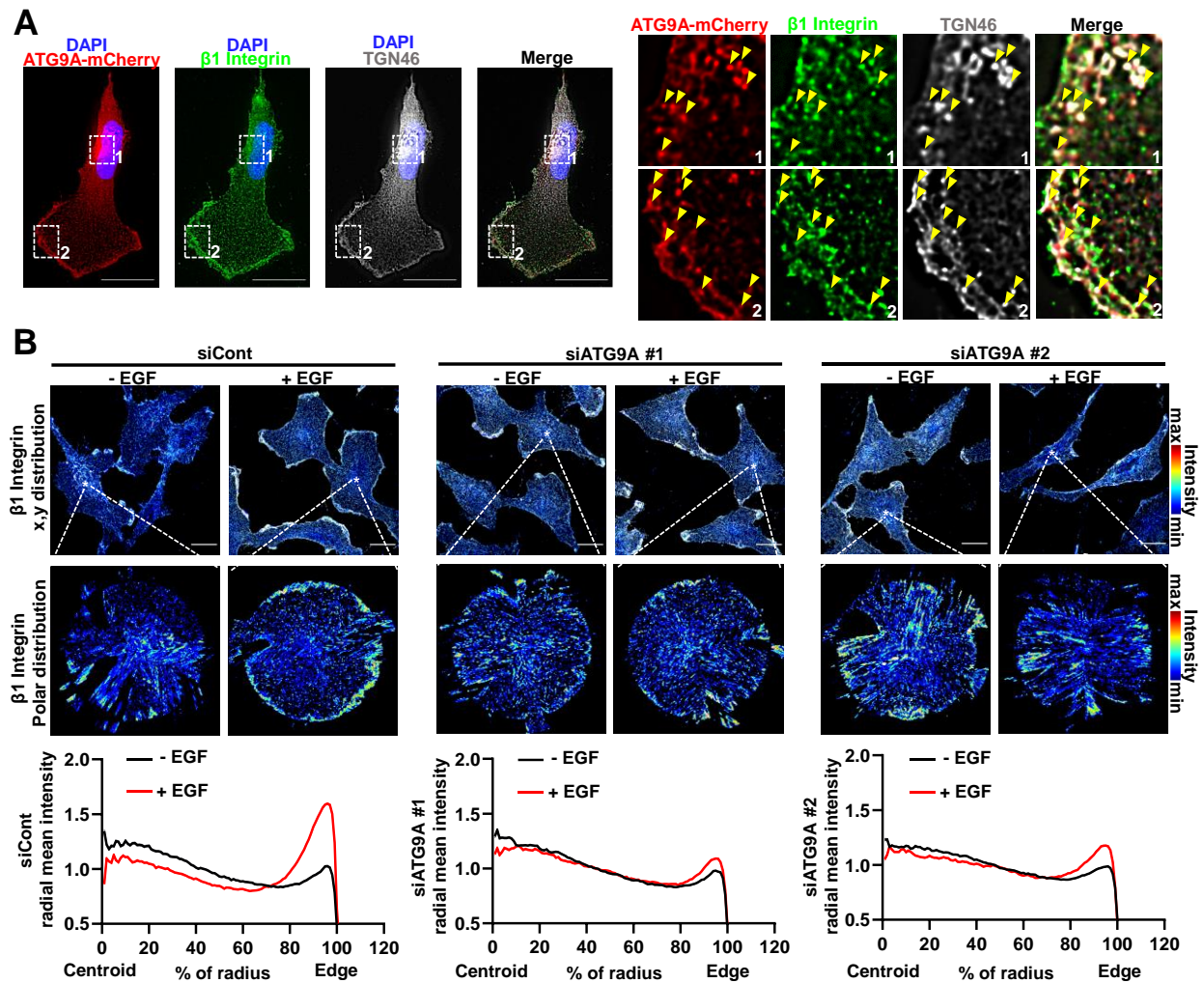


Figure R6. ATG9A-pHluorin signal at the cell periphery correlates with protrusive activity. (A) Time-lapse TIRF images of a U87 MG cell expressing ATG9A-pHluorin. The development of a large cell protrusion correlates with the appearance of a marked pHluorin signal at the leading edge. A magnified image of the leading edge (*dashed rectangle*) is presented in the *lower right* and shows numerous ATG9A-pHluorin positive vesicles (*arrowhead*). Scale bar, 20 μm . (B) *Left*: TIRF image, extracted from a time-lapse sequence, of a U87 MG cell expressing ATG9A-pHluorin. Scale bar, 20 μm . *Right*: kymographs were made from 10-pixel wide lines (L1 and L2) indicated in the left image. The scale bars in the kymograph are: 5 μm (horizontal) and 10 min (vertical). A clear ATG9A-pHluorin signal was observed near the cell edge during the formation of protrusions (*arrowheads*). The signal sharply decreased during protrusion collapses. (C) TIRF image of a U87 MG cell expressing mKate2 (*red*) and ATG9A-pHluorin (*green*). The mKate2 protein, diffusely expressed in the cytosol, was used to precisely delineate the cell edges. Scale bar, 20 μm . (D) Time-lapse montage of ROI 1 and ROI 2 shown in (C). For each time-lapse, time 0 represents the time of appearance of ATG9A-pHluorin positive vesicles (*arrows*) near to the cell edge. The position of the cell edge before the appearance of the ATG9A-pHluorin signal is marked by a dashed line. (E) Displacements of the cell edges shown in ROI 1 and 2 were plotted against the time. The position of the cell edge one minute before the appearance of the ATG9A-pHluorin signal was set at zero and positive values in the y-axis represent cell protrusion.



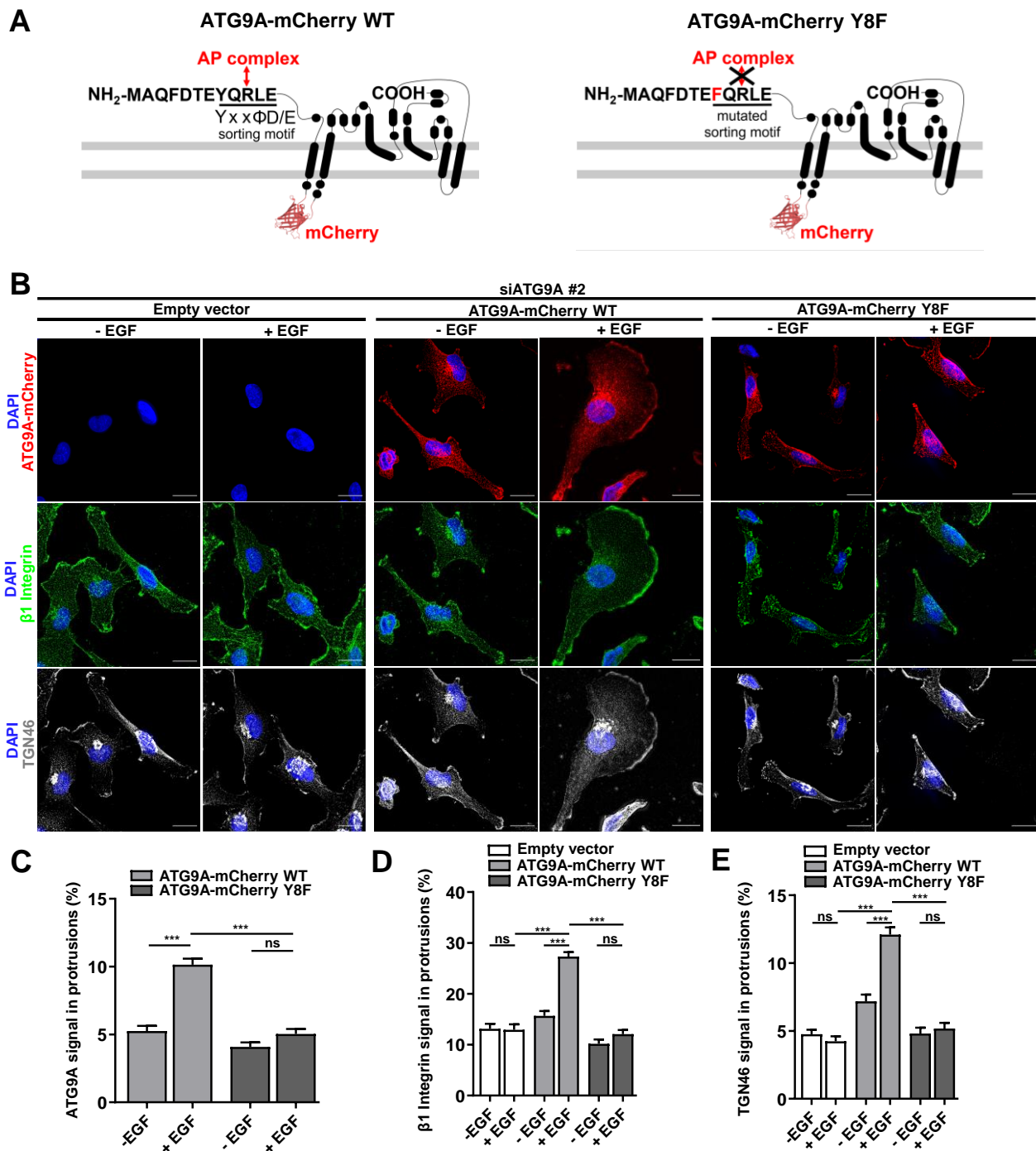


Figure R8. ATG9A regulates delivery of TGN46 and $\beta 1$ integrin to the leading edge through its N-terminal AP sorting signal. **(A) Left:** scheme depicting the topology of the ATG9A-mCherry fusion protein and the canonical AP sorting signal (8 YQRLE 12) located in the N-terminal cytosolic domain. **Right:** scheme depicting the mutant ATG9A-mCherry protein, for which replacement of the critical Tyrosine residue at position 8 by a Phenylalanine abolishes AP binding (Zhou *et al*, 2017) (Mattera *et al*, 2017). **(B-E)** Rescue experiments with wild-type and mutant ATG9A-mCherry proteins. **(B)** Following depletion of endogenous ATG9A using interfering RNA (*siATG9A #2*), U87 MG cells were transfected with an empty vector, a vector encoding wild-type ATG9A-mCherry or a vector encoding mutant ATG9A-mCherry Y8F. Transfected cells were starved (30 min) in serum-free medium and incubated (30 min) with or without EGF (50 ng/mL), as indicated. Cells were fixed and labelled for $\beta 1$ integrin (green), TGN46 (white) and nuclei (DAPI labelling, blue). Scale bar, 20 μ m. **(C)** Quantification from images shown in (B) of the ATG9A-mCherry (wild-type or mutant) signal located in protrusions. Note that, as previously observed (Zhou *et al*, 2017) (Mattera *et al*, 2017), the ATG9A-mCherry Y8F mutant demonstrates altered trafficking and does not redistribute to cell protrusions following chemotactic stimulation. **(D)** Quantification from images shown in (B) of the $\beta 1$ integrin signal located in protrusions. **(E)** Quantification from images shown in (B) of the TGN46 signal located in protrusions. Data represent means SEM (Empty vector, $n = 122$ cells; Wild-type ATG9A-mCherry vector, $n = 124$ cells; mutant ATG9A-mCherry Y8F vector, $n = 122$ cells; from 2 independent experiments). Statistical significance was evaluated using a one-way ANOVA followed by Turkey post-hoc test. *** $P < 0.001$; ns, not statistically different.

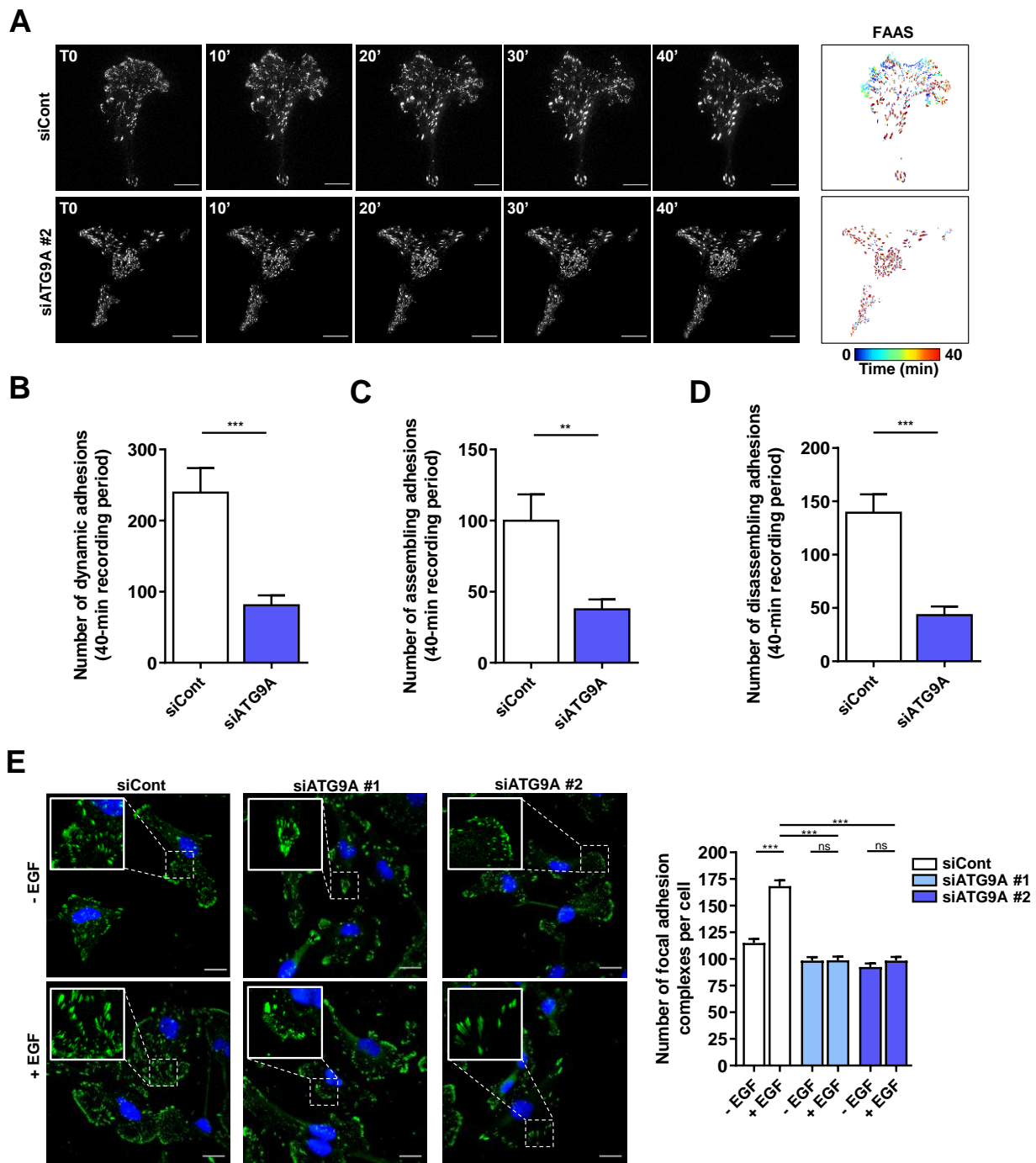


Figure R9. ATG9A protein regulates adhesion dynamics. (A-D) ATG9A depletion reduces intrinsic adhesion dynamics. (A) Representative live-cell TIRF images of U87 MG cells expressing PXN-EGFP together with nontargeting siRNA (*siCont*) or siRNA targeting ATG9A (*siATG9A #2*). Image sequences show adhesion changes over a 40-min period. *Right-hand panels*: color scale output generated from the *Focal Adhesion Analysis Server (FAAS)*, representing early (*blue*) to late (*red*) adhesions. Scale bar, 20 μ m. (B-D) FAAS output of the number of dynamic adhesions (B), assembling adhesions (C) and disassembling adhesions (D). Data represent means and SEM (*siCont*, $n = 13$ cells; *siATG9A #2*, $n = 13$ cells; from 5 independent experiments). (E) ATG9A depletion inhibits EGF-induced formation of adhesion complexes. U87 MG cells were transfected with nontargeting siRNA (*siCont*) or one of the two siRNAs targeting ATG9A (*siATG9A #1*, *siATG9A #2*). After starvation (1 h) in serum-free DMEM, cells were treated (1 h) with or without EGF (50 ng/mL), fixed and labelled with an anti-PXN antibody (*green*) and DAPI (nuclei, *blue*). The number of adhesion complexes was quantified for each cell. Data represent means and SEM (*siCont*, $n = 309$ cells; *siATG9A #1*, $n = 301$ cells; *siATG9A #2*, $n = 288$ cells; from 2 independent experiments). Scale bar, 20 μ m. Statistical significance was evaluated using a Mann and Whitney test (B, C, D), or a one-way ANOVA followed by Sidak post-hoc test (E). ** $P < 0.01$; *** $P < 0.001$; ns, not statistically different.

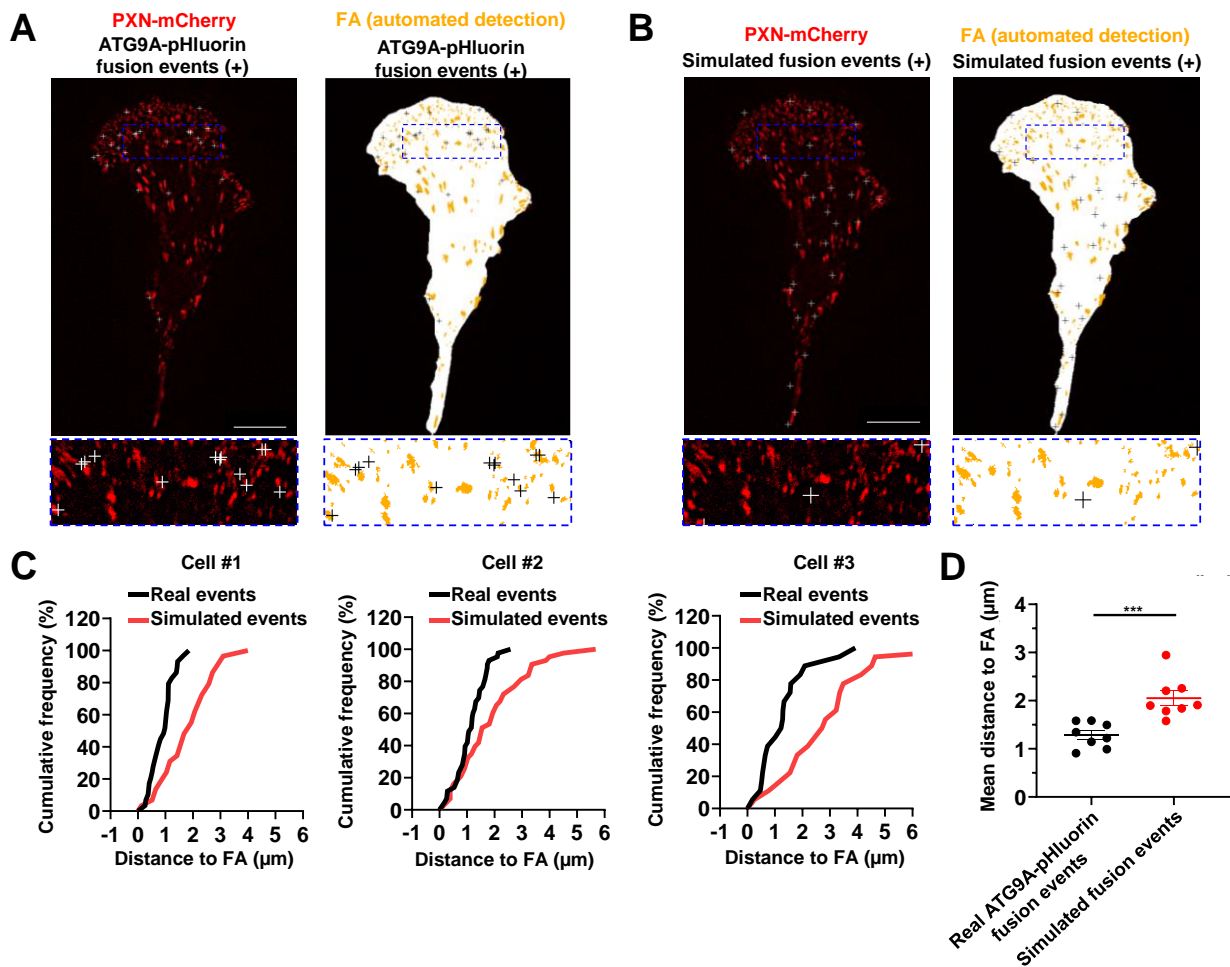
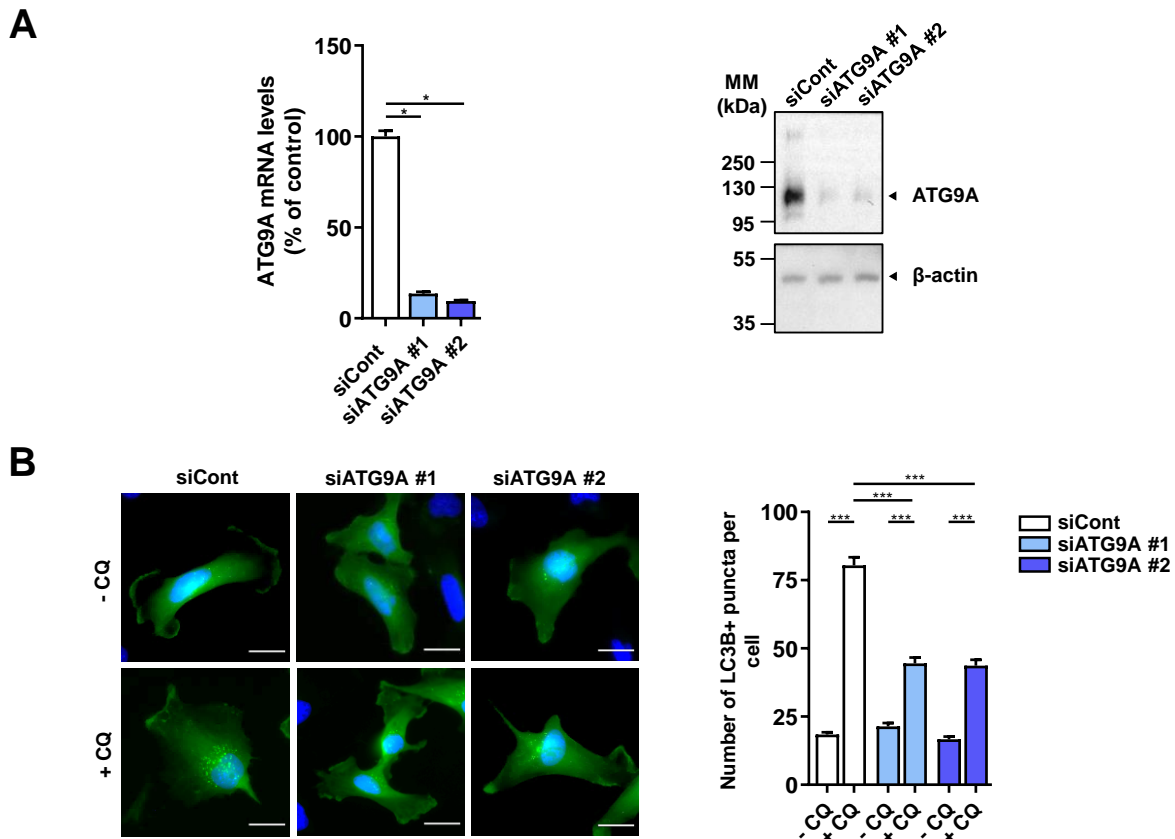
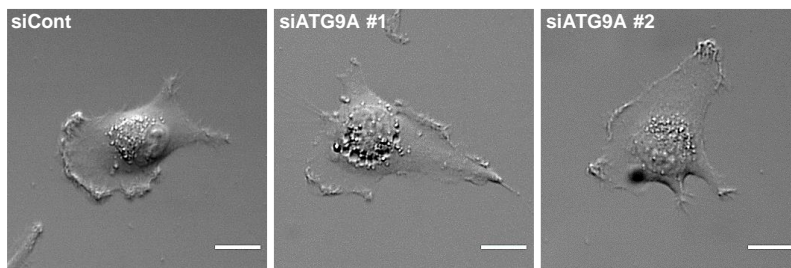


Figure R10. ATG9A-positive vesicles target adhesion sites. U87 MG cells expressing PXN-mCherry and ATG9A-pHluorin were recorded using live-cell TIRF microscopy. **(A)** *Left*: distribution of all observed ATG9A-pHluorin fusion events during the recording period (*crosses*), overlaid on the PXN-mCherry signal (*red*). *Right*: derived synthetic image depicting the ventral cell surface area (*white*), the PXN-positive adhesion complexes (*orange*, automated detection using ImageJ) and the ATG9A-pHluorin fusion events (*crosses*). Note the promiscuity between the adhesion complexes and the fusion events in the magnified view. Scale bar, 20 μm . **(B)** *Left*: map of randomly simulated fusion events (*crosses*), overlaid on the PXN-mCherry signal (*red*). *Right*: derived synthetic image depicting the ventral cell surface area (*white*), the PXN-positive adhesion complexes (*orange*) and the simulated fusion events (*crosses*). Scale bar, 20 μm . **(C)** Cumulative frequency charts, from the cell shown in **(A)** (cell #1) and two other representative cells (cell #2 and cell #3), demonstrating the difference in distance to focal adhesions (FA) between real ATG9A-pHluorin fusion events (*black line*) and simulated events (*red line*). **(D)** Quantification of the mean distance to the centroid of closest focal adhesion for real ATG9A-pHluorin events or simulated events ($n = 8$ cells, for a total number of 365 events). Statistical significance was evaluated using a Mann and Whitney test. *** $P < 0.001$.

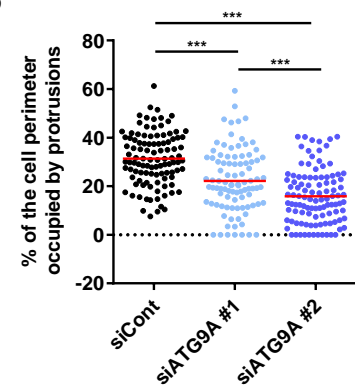


Supplementary Figure S1. Efficiency of siRNA knockdown of ATG9A and its effect on autophagosome biogenesis in U87 MG cells. **(A)** U87 MG cells were transfected with a nontargeting siRNA (*siCont*) or one of the two siRNAs targeting ATG9A (*siATG9A #1*, *siATG9A #2*). *Left*: RT-qPCR analysis of ATG9A mRNA levels. Data show means \pm SEM (n=4). *Right*: Western blot analysis of ATG9A protein levels. The blot was cut and the upper and the lower parts were probed with antibodies against ATG9A and β -actin, respectively. MM, molecular mass. **(B)** U87 MG cells were transfected with nontargeting siRNA (*siCont*) or one of the two siRNAs targeting ATG9A (*siATG9A #1*, *siATG9A #2*), together with a construct encoding the EGFP-LC3B protein (marker of autophagosomes). Transfected cells were placed in serum-free medium for 6 h, in the presence or absence of chloroquine (CQ, 5×10^{-5} M), as indicated. Cells were fixed and the number of autophagosomes (EGFP-LC3B fluorescent dots) per cell was quantified. Data represent means \pm SEM (siCont, n = 298 cells; siATG9A #1, n = 315 cells; siATG9A #2, n = 316 cells; from 2 independent experiments). Scale bar, 20 μ m. Statistical significance was evaluated using a Mann and Whitney test **(A)** or a one-way ANOVA followed by Sidak post-hoc test **(B)**. * $P < 0.05$; *** $P < 0.001$.

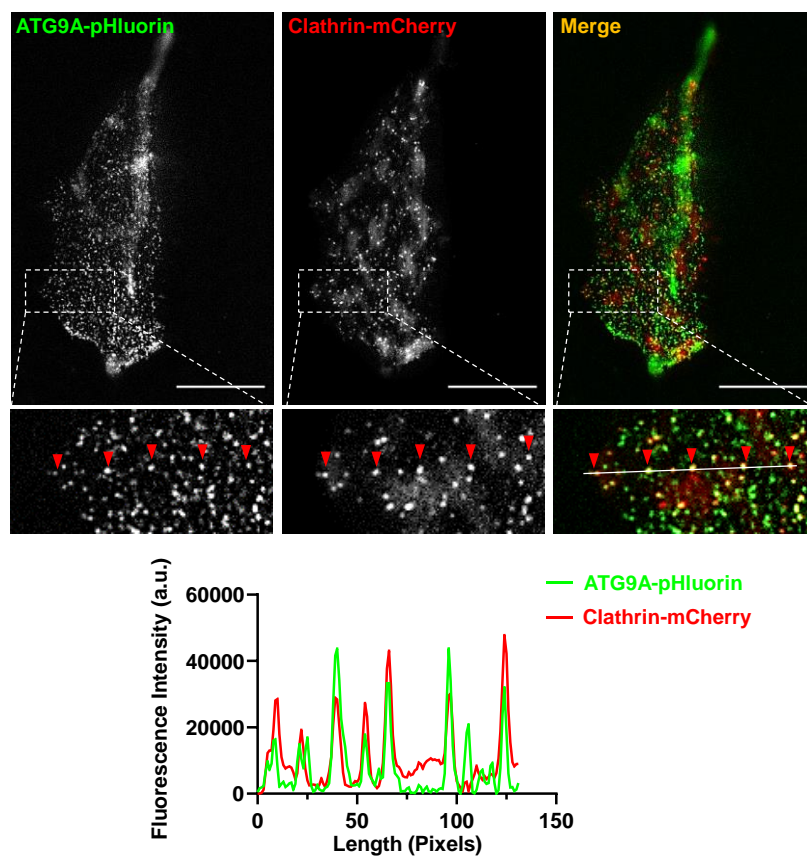
A



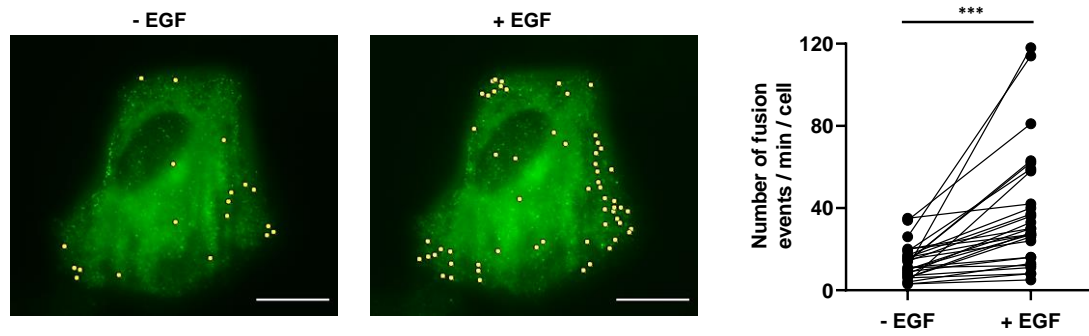
B



Supplementary Figure S2. Depletion of ATG9A protein impairs the formation of cell protrusions. (A) Representative images from phase contrast time-lapse sequences acquired from U87 MG cells transfected with nontargeting siRNA (*siCont*) or one of the two siRNAs targeting ATG9A (*siATG9A #1*, *siATG9A #2*). (B) Percentage of the cell perimeter occupied by ruffling protrusions. Data represent means \pm SEM (*siCont*, $n = 105$ cells; *siATG9A #1*, $n = 94$ cells; *siATG9A #2*, $n = 106$ cells; from 3 independent experiments). Scale bar, 20 μm . Statistical significance was evaluated using a one-way ANOVA followed by Turkey post-hoc test. *** $P < 0.001$.



Supplementary Figure S3. ATG9A static puncta colocalize with the endocytic marker clathrin. *Upper*: Representative TIRF images, extracted from a time-lapse sequence, showing a U87 MG cell co-expressing ATG9A-pHluorin (*green*) and clathrin-mCherry (*red*). Note on the magnified images that ATG9A-pHluorin puncta frequently localize with clathrin (*red arrowheads*), suggesting that they likely represent ATG9A-pHluorin proteins trapped in forming endocytic structures. *Lower*: line profile plot indicates the fluorescence intensity distribution of green and red channels, through the white line shown in the magnified view of the merged image. Scale bar, 20 μm .



Supplementary Figure S4. EGF stimulation increases the fusion activity of ATG9A vesicles in HeLa cells. Representative HeLa cell with projections of all observed ATG9A-pHluorin fusion events, during 1-min time-lapse TIRF recording, before (-EGF) and 2-min after (+EGF) treatment with EGF (50 ng/mL). Scale bar, 20 μ m. *Right:* quantification of the effect of EGF, as depicted on the left, on the number ATG9A-pHluorin fusion events ($n = 28$ cells; from 3 independent experiments). Statistical significance was evaluated using a Paired t-test. *** $P < 0.001$.

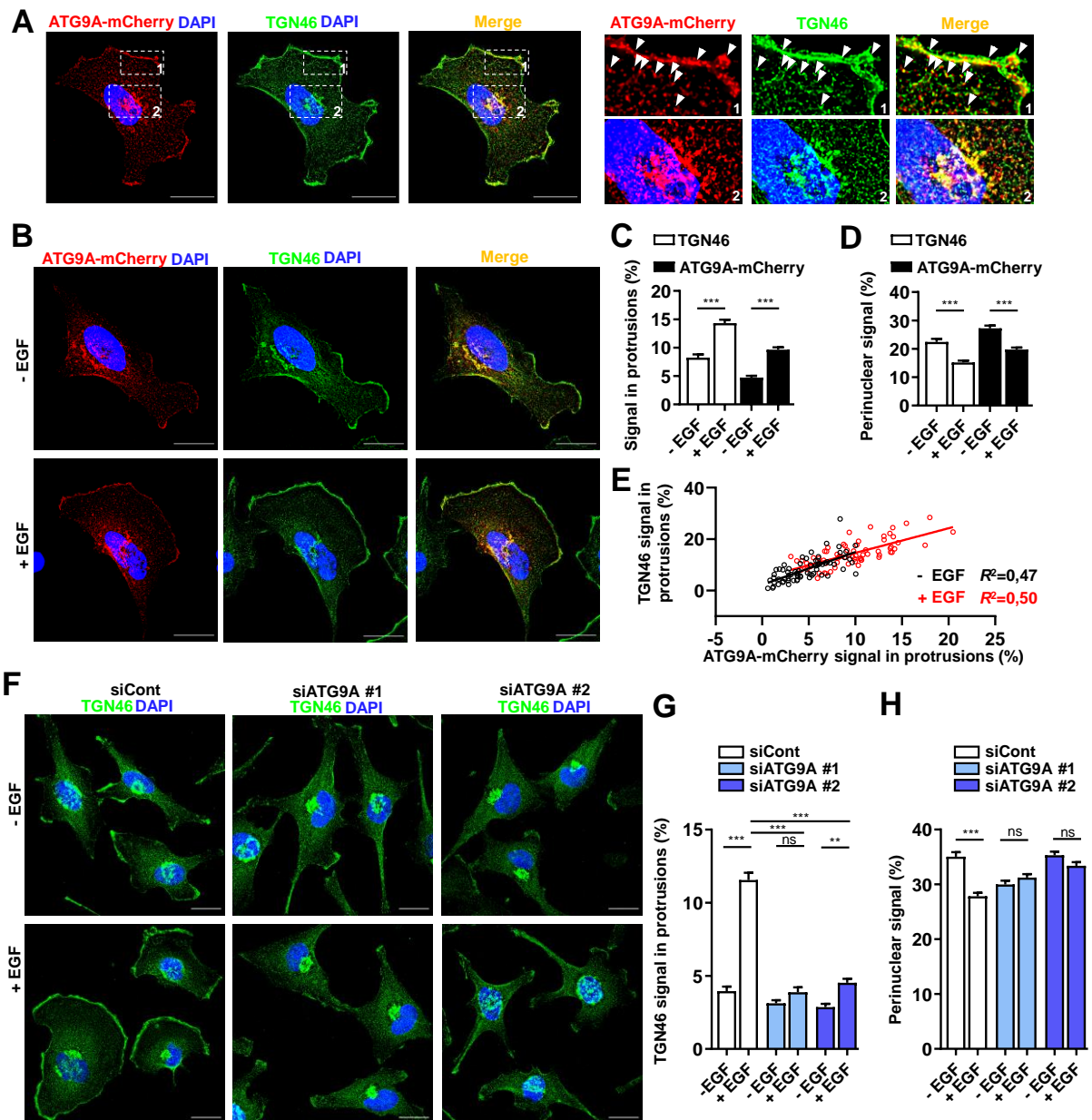
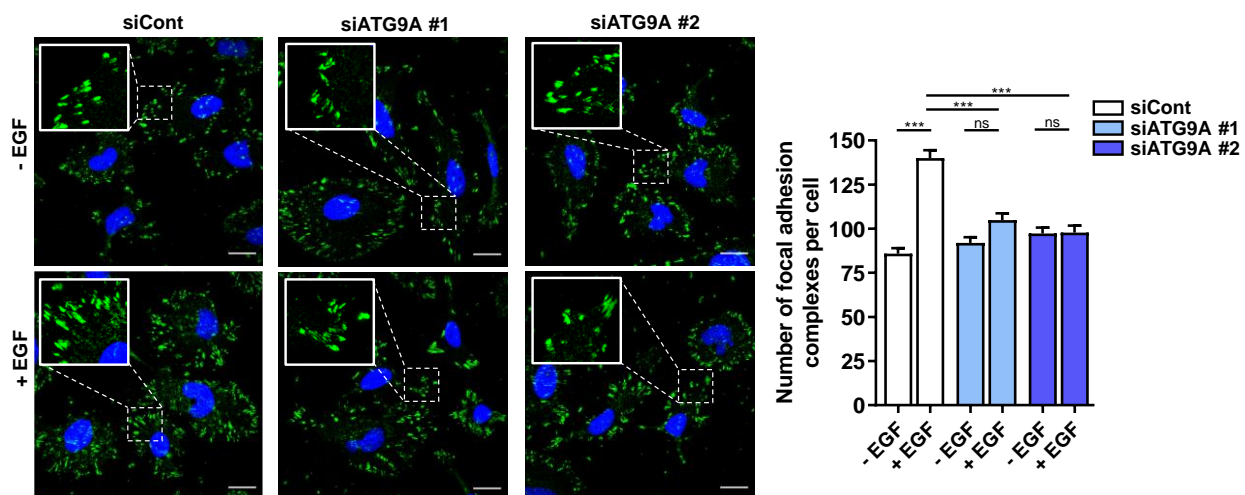
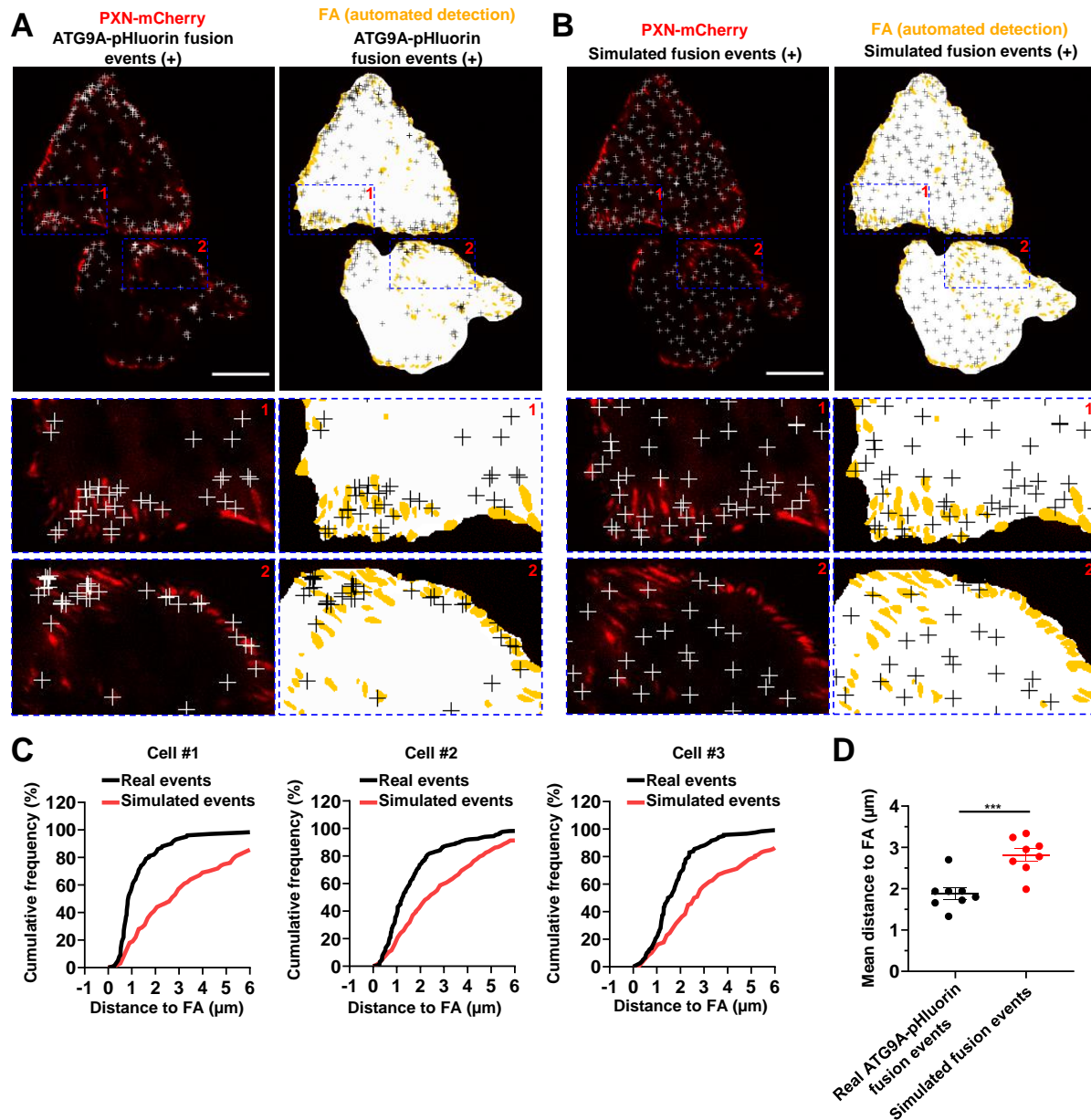


Figure S5. For caption see next page.

Supplementary Figure S5. ATG9A protein regulates delivery of TGN46-positive post-Golgi carriers to cell protrusions. **(A)** *Left:* representative U87 MG cell expressing ATG9A-mCherry (*red*), co-labelled for TGN46 (*green*) and nuclei (DAPI labelling; *blue*). Scale bar, 20 μ m. *Right:* magnified views of the cell presented on the left. Note that ATG9A co-localizes with TGN46 in typical TGN cisternae (*upper panels*) and at the cell membrane or vesicles close to the cell membrane (*lower panels*). **(B-E)** Chemotactic stimulation induces redistribution of TGN46 and ATG9A-mCherry toward the cell membrane. **(B)** U87 MG cells expressing ATG9A-mCherry were starved (30 min) in serum-free medium and incubated (30 min) with or without EGF (50 ng/mL), as indicated. Cells were fixed and labelled for TGN46 (*green*) and nuclei (DAPI labelling, *blue*). Scale bar, 20 μ m. **(C)** Quantification from images shown in (B) of the TGN46 and ATG9A-mCherry signals located in protrusions. For each cell, values correspond to the cumulated signal of all protrusions. **(D)** Quantification from images shown in (B) of the TGN46 and ATG9A-mCherry signals located in the perinuclear area. Data represent means \pm SEM (- EGF, n = 68 cells; + EGF, n = 68 cells; from 2 independent experiments). **(E)** Cell-to-cell correlation between TGN46 and ATG9A-mCherry signals located in cell protrusions, in both untreated (*black dots*) and EGF-treated (*red dots*) cells. **(F-H)** EGF-induced redistribution of TGN46 to the cell protrusions depends on ATG9A. **(F)** U87 MG cells were transfected with nontargeting siRNA (*siCont*) or one of the two siRNA targeting ATG9A (*siATG9A #1*, *siATG9A #2*). Transfected cells were starved (30 min) in serum-free medium and incubated (30 min) with or without EGF (50 ng/mL), as indicated. Cells were fixed and labelled for TGN46 (*green*) and nuclei (DAPI labelling, *blue*). Scale bar, 20 μ m. **(G)** Quantification from images shown in (F) of the TGN46 signal located in protrusions. **(H)** Quantification from images shown in (F) of the TGN46 signal located in the perinuclear area. Data represent means \pm SEM (*siCont*, n = 204 cells; *siATG9A #1*, n = 200 cells; *siATG9A #2*, n = 192 cells; from 3 independent experiments). Statistical significance was evaluated using a Mann and Whitney test (**C, D**), or a one-way ANOVA followed by Turkey post-hoc test (**G**), or a one-way ANOVA followed by Sidak post-hoc test (**H**), $^{**}P < 0.01$; $^{***}P < 0.001$; ns, not statistically different.



Supplementary Figure S6. Depletion of ATG9A protein inhibits EGF-induced formation of adhesion complexes in HeLa cells. HeLa cells were transfected with nontargeting siRNA (*siCont*) or one of the two siRNAs targeting ATG9A (*siATG9A #1*, *siATG9A #2*). After starvation (1 h) in serum-free medium, cells were treated (1 h) with or without EGF (50 ng/mL), fixed and labelled with an anti-PXN antibody (*green*) and nuclei (DAPI labelling, *blue*). The number of adhesion complexes was quantified for each cell. Data represent means \pm SEM (*siCont*, n = 254 cells; *siATG9A #1*, n = 256 cells; *siATG9A #2*, n = 251 cells; from 2 independent experiments). Scale bar, 20 μ m. Statistical significance was evaluated using a one-way ANOVA followed by Sidak post-hoc test. $^{***}P < 0.001$; ns, not statistically different.



Supplementary Figure S7. ATG9A-positive vesicles target adhesion sites in HeLa cells. HeLa cells expressing PXN-mCherry and ATG9A-pHluorin were recorded using live-cell TIRF microscopy. **(A)** *Left:* distribution of all observed ATG9A-pHluorin fusion events during the recording period (*crosses*), overlaid on the PXN-mCherry signal (*red*). *Right:* derived synthetic image depicting the ventral cell surface area (*white*), the PXN-positive adhesion complexes (*orange*, automated detection using ImageJ) and the ATG9A-pHluorin fusion events (*crosses*). Note the promiscuity between the adhesion complexes and the fusion events in the magnified view. Scale bar, 20 μm . **(B)** *Left:* map of randomly simulated fusion events (*crosses*), overlaid on the PXN-mCherry signal (*red*). *Right:* derived synthetic image depicting the ventral cell surface area (*white*), the PXN-positive adhesion complexes (*orange*) and the simulated fusion events (*crosses*). Scale bar, 20 μm . **(C)** Cumulative frequency charts, from the cells shown in **(A)** (*cell #1* and *cell #2*) and one other representative cell (*cell #3*), demonstrating the difference in distance to focal adhesions (FA) between real ATG9A-pHluorin fusion events (*black line*) and simulated events (*red line*). **(D)** Quantification of the mean distance to the centroid of closest focal adhesion for real ATG9A-pHluorin events or simulated events ($n = 8$ cells, for a total number of 1297 events). Statistical significance was evaluated using a Mann and Whitney test. *** $P < 0.001$.

To access the online videos, click on the following link

<https://bit.ly/387qeKh>

Movie 1. Depletion of ATG9A protein impairs the formation of cell protrusions. Representative live-cell phase contrast images showing U87 MG cells transfected with nontargeting siRNA (*siCont*, *left*) or siRNA targeting ATG9A (*siATG9A #1*, *right*). Control cells develop large and stable protrusions, while ATG9A-depleted cells display smaller and unstable protrusions. Movies plays at 25 frames per second. Scale bar, 20 μm .

Movie 2. ATG9A protein regulates adhesion dynamics. Representative live-cell TIRF images of U87 MG cells expressing PXN-EGFP together with nontargeting siRNA (*siCont*, *left*) or siRNA targeting ATG9A (*siATG9A #2*, *right*). Image sequences show adhesions changes over a 40-min period. Movies plays at 15 frames per second. Scale bar, 20 μm .

Movie 3. “Spreading” ATG9A-pHluorin exocytotic events. Time-lapse TIRF images of U87 MG cells expressing ATG9A-pHluorin. Arrows indicate the rapid appearance of the pHluorin signal upon fusion pore opening followed by signal diffusion into the plasma membrane. Movies plays at 15 frames per second. Scale bar, 1 μm .

Movie 4. “Non-spreading” ATG9A-pHluorin exocytotic events. Time-lapse TIRF images of U87 MG cells expressing ATG9A-pHluorin. Arrows indicate the rapid appearance of the pHluorin signal upon fusion pore opening, followed by signal decay without diffusion into the plasma membrane. Movies plays at 15 frames per second. Scale bar, 1 μm .

Movie 5. ATG9A-pHluorin signal appearance at the leading edge correlates with protrusive activity. Time-lapse TIRF images of a U87 MG cell expressing ATG9A-pHluorin. Movies plays at 15 frames per second. Scale bar, 20 μm .

X. References

- Abdul Rahim, S.A., A. Dirkse, A. Oudin, A. Schuster, J. Bohler, V. Barthelemy, A. Muller, L. Vallar, B. Janji, A. Golebiewska, and S.P. Niclou. 2017. Regulation of hypoxia-induced autophagy in glioblastoma involves ATG9A. *Br. J. Cancer.* 117:813–825. doi:10.1038/bjc.2017.263.
- Adelmann-Grill, B.C., F. Wach, Z. Cully, R. Hein, and T. Krieg. 1990. Chemotactic migration of normal dermal fibroblasts towards epidermal growth factor and its modulation by platelet-derived growth factor and transforming growth factor-beta. *Eur. J. Cell Biol.* 51:322–326.
- Alabi, A.A., and R.W. Tsien. 2013. Perspectives on kiss-and-run: role in exocytosis, endocytosis, and neurotransmission. *Annu. Rev. Physiol.* 75:393–422. doi:10.1146/annurev-physiol-020911-153305.
- Banting, G., and S. Ponnambalam. 1997. TGN38 and its orthologues: roles in post-TGN vesicle formation and maintenance of TGN morphology. *Biochim. Biophys. Acta BBA - Mol. Cell Res.* 1355:209–217. doi:10.1016/S0167-4889(96)00146-2.
- Berginski, M.E., E.A. Vitriol, K.M. Hahn, and S.M. Gomez. 2011. High-resolution quantification of focal adhesion spatiotemporal dynamics in living cells. *PLoS ONE.* 6:e22025. doi:10.1371/journal.pone.0022025.
- Bilodeau, P., D. Jacobsen, D. Law-Vinh, and J.M. Lee. 2020. Phosphatidylinositol 4-kinase III beta regulates cell shape, migration, and focal adhesion number. *Mol. Biol. Cell.* 31:1904–1916. doi:10.1091/mbc.E19-11-0600.
- Bisel, B., Y. Wang, J-H. Wei, Y. Xiang, D. Tang, M. Miron-Mendoza, S. Yoshimura, N. Nakamura and J. and Seemann. 2008. ERK regulates Golgi and centrosome orientation towards the leading edge through GRASP65. *J. Cell Biol.* 182: 837–843. doi:10.1083/jcb.200805045.
- Biswenger, V., N. Baumann, J. Jürschick, M. Häckl, C. Battle, J. Schwarz, E. Horn, and R. Zantl. 2018. Characterization of EGF-guided MDA-MB-231 cell chemotaxis in vitro using a physiological and highly sensitive assay system. *PLoS ONE.* 13:e0203040. doi:10.1371/journal.pone.0203040.
- Bowman, E.J., A. Siebers, and K. Altendorf. 1988. Bafilomycins: a class of inhibitors of membrane ATPases from microorganisms, animal cells, and plant cells. *Proc. Natl. Acad. Sci.* 85:7972–7976. doi:10.1073/pnas.85.21.7972.
- Bravo-Cordero, J.J., L. Hodgson, and J. Condeelis. 2012. Directed cell invasion and migration during metastasis. *Curr. Opin. Cell Biol.* 24:277–283. doi:10.1016/j.ceb.2011.12.004.
- Bretscher, M.S. 1996. Moving membrane up to the front of migrating cells. *Cell.* 85:465–467. doi:10.1016/S0092-8674(00)81246-5.

- Chatterjee, S., B. Behnam Azad, and S. Nimmagadda. 2014. The intricate role of CXCR4 in cancer. *Adv. Cancer Res.* 124:31–82. doi:10.1016/B978-0-12-411638-2.00002-1.
- Choma, D.P., K. Pumiglia, and C.M. DiPersio. 2004. Integrin $\alpha 3\beta 1$ directs the stabilization of a polarized lamellipodium in epithelial cells through activation of Rac1. *J. Cell Sci.* 117:3947–3959. doi:10.1242/jcs.01251.
- Claude-Taupin, A., L. Fonderflick, T. Gauthier, L. Mansi, J.-R. Pallandre, C. Borg, V. Perez, F. Monnier, M.-P. Algos, M. Vigneron, P. Adami, R. Delage-Mourroux, P. Peixoto, M. Herfs, M. Boyer-Guittaut, and E. Hervouet. 2018. ATG9A is overexpressed in triple negative breast cancer and its in vitro extinction leads to the inhibition of pro-cancer phenotypes. *Cells.* 7:248. doi:10.3390/cells7120248.
- Coly, P.-M., P. Gandolfo, H. Castel and F. Morin. 2017. The autophagy machinery: a new player in chemotactic cell migration. *Front. Neurosci.* 11. doi:10.3389/fnins.2017.00078.
- Coly, P.-M., N. Perzo, V. Le Joncour, C. Lecointre, M.-T. Schouft, L. Desrues, M.-C. Tonon, O. Wurtz, P. Gandolfo, H. Castel, and F. Morin. 2016. Chemotactic G protein-coupled receptors control cell migration by repressing autophagosome biogenesis. *Autophagy.* 12:2344–2362. doi:10.1080/15548627.2016.1235125.
- Coombs, C., A. Georgantzoglou, H.A. Walker, J. Patt, N. Merten, H. Poplimont, E.M. Busch-Nentwich, S. Williams, C. Kotsi, E. Kostenis, and M. Sarris. 2019. Chemokine receptor trafficking coordinates neutrophil clustering and dispersal at wounds in zebrafish. *Nat. Commun.* 10:5166. doi:10.1038/s41467-019-13107-3.
- Danen, E.H.J., J. van Rheenen, W. Franken, S. Huvneers, P. Sonneveld, K. Jalink, and A. Sonnenberg. 2005. Integrins control motile strategy through a Rho–cofilin pathway. *J. Cell Biol.* 169:515–526. doi:10.1083/jcb.200412081.
- Davies, A.K., D.N. Itzhak, J.R. Edgar, T.L. Archuleta, J. Hirst, L.P. Jackson, M.S. Robinson, and G.H.H. Borner. 2018. AP-4 vesicles contribute to spatial control of autophagy via RUSC-dependent peripheral delivery of ATG9A. *Nat. Commun.* 9:3958. doi:10.1038/s41467-018-06172-7.
- De Pace, R., M. Skirzewski, M. Damme, R. Mattera, J. Mercurio, A.M. Foster, L. Cuitino, M. Jarnik, V. Hoffmann, H.D. Morris, T.-U. Han, G.M.S. Mancini, A. Buonanno, and J.S. Bonifacino. 2018. Altered distribution of ATG9A and accumulation of axonal aggregates in neurons from a mouse model of AP-4 deficiency syndrome. *PLOS Genet.* 14:e1007363. doi:10.1371/journal.pgen.1007363.
- Deakin, N.O., and C.E. Turner. 2008. Paxillin comes of age. *J. Cell Sci.* 121:2435–2444. doi:10.1242/jcs.018044.
- Dikic, I., and Z. Elazar. 2018. Mechanism and medical implications of mammalian autophagy. *Nat. Rev. Mol. Cell Biol.* 19:349–364. doi:10.1038/s41580-018-0003-4.

- Dillenburg-Pilla, P., V. Patel, C.M. Mikelis, C.R. Zárate-Bladés, C.L. Doçi, P. Amornphimoltham, Z. Wang, D. Martin, K. Leelahavanichkul, R.T. Dorsam, A. Masedunskas, R. Weigert, A.A. Molinolo, and J.S. Gutkind. 2015. SDF-1/CXCL12 induces directional cell migration and spontaneous metastasis via a CXCR4/Gai/mTORC1 axis. *FASEB J.* 29:1056–1068. doi:10.1096/fj.14-260083.
- Dobretsov, M., and D. Romanovsky. 2006. “Clock-scan” protocol for image analysis. *Am. J. Physiol.-Cell Physiol.* 291:C869–C879. doi:10.1152/ajpcell.00182.2006.
- Fletcher, S.J., and J.Z. Rappoport. 2010. Moving forward: polarised trafficking in cell migration. *Trends Cell Biol.* 20:71–78. doi:10.1016/j.tcb.2009.11.006.
- Fu, G., W. Wang, and B.-H. Luo. 2011. Overview: Structural Biology of Integrins. In *Integrin and Cell Adhesion Molecules*. M. Shimaoka, editor. Humana Press, Totowa, NJ. 81–99.
- Gorelik, R., and A. Gautreau. 2014. Quantitative and unbiased analysis of directional persistence in cell migration. *Nat. Protoc.* 9:1931–1943. doi:10.1038/nprot.2014.131.
- Guardia, C.M., X.-F. Tan, T. Lian, M.S. Rana, W. Zhou, E.T. Christenson, A.J. Lowry, J.D. Faraldo-Gómez, J.S. Bonifacino, J. Jiang, and A. Banerjee. 2020. Structure of human ATG9A, the only transmembrane protein of the core autophagy machinery. *Cell Rep.* 31:107837. doi:10.1016/j.celrep.2020.107837.
- Hao, H., J. Niu, B. Xue, Q.P. Su, M. Liu, J. Yang, J. Qin, S. Zhao, C. Wu, and Y. Sun. 2020. Golgi-associated microtubules are fast cargo tracks and required for persistent cell migration. *EMBO Rep.* 21:e48385. doi:10.15252/embr.201948385.
- Huet-Calderwood, C., F. Rivera-Molina, D.V. Iwamoto, E.B. Kromann, D. Toomre and D.A. Calderwood. 2017. Novel ecto-tagged integrins reveal their trafficking in live cells. *Nat. Commun.* 8: 570. doi: 10.1038/s41467-017-00646-w.
- Hynes, R.O. 2002. Integrins: bidirectional, allosteric signaling machines. *Cell.* 110:673–687. doi:10.1016/S0092-8674(02)00971-6.
- Imai, K., F. Hao, N. Fujita, Y. Tsuji, Y. Oe, Y. Araki, M. Hamasaki, T. Noda, and T. Yoshimori. 2016. Atg9A trafficking through the recycling endosomes is required for autophagosome formation. *J. Cell Sci.* 129:3781–3791. doi:10.1242/jcs.196196.
- Innocenti, M. 2018. New insights into the formation and the function of lamellipodia and ruffles in mesenchymal cell migration. *Cell Adhes. Migr.* 12:401–416. doi:10.1080/19336918.2018.1448352.
- Ivankovic, D., J. Drew, F. Lesept, I.J. White, G. López Doménech, S.A. Tooze, and J.T. Kittler. 2020. Axonal autophagosome maturation defect through failure of ATG9A sorting underpins pathology in AP-4 deficiency syndrome. *Autophagy.* 16:391–407. doi:10.1080/15548627.2019.1615302.

- Jia, S., Y. Wang, Z. You, B. Liu, J. Gao, and W. Liu. 2017. Mammalian Atg9 contributes to the post-Golgi transport of lysosomal hydrolases by interacting with adaptor protein-1. *FEBS Lett.* 591:4027–4038. doi:10.1002/1873-3468.12916.
- Judith, D., H.B.J. Jefferies, S. Boeing, D. Frith, A.P. Snijders, and S.A. Tooze. 2019. ATG9A shapes the forming autophagosome through Arfaptin 2 and phosphatidylinositol 4-kinase III β . *J. Cell Biol.* 218:1634–1652. doi:10.1083/jcb.201901115.
- Kadandale, P., J.D. Stender, C.K. Glass, and A.A. Kiger. 2010. Conserved role for autophagy in Rho1-mediated cortical remodeling and blood cell recruitment. *Proc. Natl. Acad. Sci.* 107:10502–10507. doi:10.1073/pnas.0914168107.
- Kakuta, S., J. Yamaguchi, C. Suzuki, M. Sasaki, S. Kazuno, and Y. Uchiyama. 2017. Small GTPase Rab1B is associated with ATG9A vesicles and regulates autophagosome formation. *FASEB J.* 31:3757–3773. doi:10.1096/fj.201601052R.
- Kean, M.J., K.C. Williams, M. Skalski, D. Myers, A. Burtnik, D. Foster, and M.G. Coppelino. 2009. VAMP3, syntaxin-13 and SNAP23 are involved in secretion of matrix metalloproteinases, degradation of the extracellular matrix and cell invasion. *J. Cell Sci.* 122:4089–4098. doi:10.1242/jcs.052761.
- Keller, R. 2005. Cell migration during gastrulation. *Curr. Opin. Cell Biol.* 17:533–541. doi:10.1016/j.ceb.2005.08.006.
- Kenific, C.M., S.J. Stehbens, J. Goldsmith, A.M. Leidal, N. Faure, J. Ye, T. Wittmann, and J. Debnath. 2016a. NBR1 enables autophagy-dependent focal adhesion turnover. *J. Cell Biol.* 212:577–590. doi:10.1083/jcb.201503075.
- Kenific, C.M., Wittmann, and J. Debnath. 2016b. Autophagy in adhesion and migration. *J. Cell Sci.* 129:3685–3693. doi:10.1242/jcs.188490.
- Kim, H-D., T.W. Guo, A.P. Wu, A. Wells, F.B. Gertler and D.A. Lauffenburger. 2008. Epidermal growth factor-induced enhancement of glioblastoma cell migration in 3D arises from an intrinsic increase in speed but an extrinsic matrix- and proteolysis-dependent increase in persistence. *Mol. Biol. Cell.* 19: 4249–4259. doi:10.1091/mbc.e08-05-0501.
- Kiss, V., A. Jipa, K. Varga, S. Takáts, T. Maruzs, P. Lőrincz, Z. Simon-Vecsei, S. Szikora, I. Földi, C. Bajusz, D. Tóth, P. Vilmos, I. Gáspár, P. Ronchi, J. Mihály, and G. Juhász. 2020. *Drosophila* Atg9 regulates the actin cytoskeleton via interactions with profilin and Ena. *Cell Death Differ.* 27:1677–1692. doi:10.1038/s41418-019-0452-0.

Klionsky, D.J., A.K. Abdel-Aziz, S. Abdelfatah, M. Abdellatif, A. Abdoli, S. Abel, H. Abeliovich, M.H. Abildgaard, Y.P. Abudu, A. Acevedo-Arozena, I.E. Adamopoulos, K. Adeli, T.E. Adolph, A. Adornetto, E. Aflaki, G. Agam, A. Agarwal, B.B. Aggarwal, M. Agnello, P. Agostinis, J.N. Agrewala, A. Agrotis, P.V. Aguilar, S.T. Ahmad, Z.M. Ahmed, U. Ahumada-Castro, S. Aits, S. Aizawa, Y. Akkoc, T. Akoumianaki, H.A. Akpinar, A.M. Al-Abd, L. Al-Akra, A. Al-Gharaibeh, M.A. Alaoui-Jamali, S. Alberti, E. Alcocer-Gómez, C. Alessandri, M. Ali, M.A. Alim Al-Bari, S. Aliwaini, J. Alizadeh, E. Almacellas, A. Almasan, A. Alonso, G.D. Alonso, N. Altan-Bonnet, D.C. Altieri, É.M.C. Álvarez, S. Alves, C. Alves da Costa, M.M. Alzaharna, M. Amadio, C. Amantini, C. Amaral, S. Ambrosio, A.O. Amer, V. Ammanathan, Z. An, S.U. Andersen, S.A. Andrabi, M. Andrade-Silva, A.M. Andres, S. Angelini, D. Ann, U.C. Anozie, M.Y. Ansari, P. Antas, A. Antebi, Z. Antón, T. Anwar, L. Apetoh, N. Apostolova, T. Araki, Y. Araki, K. Arasaki, W.L. Araújo, J. Araya, C. Arden, M.-A. Arévalo, S. Arguelles, E. Arias, J. Arikath, H. Arimoto, A.R. Ariosa, D. Armstrong-James, L. Arnauné-Pelloquin, A. Aroca, D.S. Arroyo, I. Arsov, R. Artero, D.M.L. Asaro, M. Aschner, M. Ashrafizadeh, O. Ashur-Fabian, A.G. Atanasov, A.K. Au, P. Auberger, et al. 2021. Guidelines for the use and interpretation of assays for monitoring autophagy (4th edition). *Autophagy*. 17:1–382. doi:10.1080/15548627.2020.1797280.

Lawson, M.A., and F.R. Maxfield. 1995. Ca²⁺- and calcineurin-dependent recycling of an integrin to the front of migrating neutrophils. *Nature*. 377:75–79. doi:10.1038/377075a0.

Lecointre, C., L. Desrues, J.E. Joubert, N. Perzo, P.-O. Guichet, V. Le Joncour, C. Brulé, M. Chabbert, R. Leduc, L. Prézeau, A. Laquerrière, F. Proust, P. Gandolfo, F. Morin, and H. Castel. 2015. Signaling switch of the urotensin II vasosactive peptide GPCR: prototypic chemotaxic mechanism in glioma. *Oncogene*. 34:5080–5094. doi:10.1038/onc.2014.433.

Letinic, K., R. Sebastian, D. Toomre, and P. Rakic. 2009. Exocyst is involved in polarized cell migration and cerebral cortical development. *Proc. Natl. Acad. Sci.* 106:11342–11347. doi:10.1073/pnas.0904244106.

Longatti, A., and S.A. Tooze. 2012. Recycling endosomes contribute to autophagosome formation. *Autophagy*. 8:1682–1683. doi:10.4161/auto.21486.

Maeda, S., H. Yamamoto, L.N. Kinch, C.M. Garza, S. Takahashi, C. Otomo, N.V. Grishin, S. Forli, N. Mizushima, and T. Otomo. 2020. Structure, lipid scrambling activity and role in autophagosome formation of ATG9A. *Nat. Struct. Mol. Biol.* 27:1194–1201. doi:10.1038/s41594-020-00520-2.

Maisel, S., D. Broka and J. Schroeder. 2018. Intravesicular epidermal growth factor receptor subject to retrograde trafficking drives epidermal growth factor-dependent migration. *Oncotarget*. 9: 6463–6477. doi:10.18632/oncotarget.23766.

Mana, G., F. Clapero, E. Panieri, V. Panero, R.T. Böttcher, H.-Y. Tseng, F. Saltarin, E. Astanina, K.I. Wolanska, M.R. Morgan, M.J. Humphries, M.M. Santoro, G. Serini, and D. Valdembrì. 2016. PPF1A1 drives active $\alpha 5\beta 1$

integrin recycling and controls fibronectin fibrillogenesis and vascular morphogenesis. *Nat. Commun.* 7:13546. doi:10.1038/ncomms13546.

Matoba, K., T. Kotani, A. Tsutsumi, T. Tsuji, T. Mori, D. Noshiro, Y. Sugita, N. Nomura, S. Iwata, Y. Ohsumi, T. Fujimoto, H. Nakatogawa, M. Kikkawa, and N.N. Noda. 2020. Atg9 is a lipid scramblase that mediates autophagosomal membrane expansion. *Nat. Struct. Mol. Biol.* 27:1185–1193. doi:10.1038/s41594-020-00518-w.

Mattera, R., S.Y. Park, R. De Pace, C.M. Guardia, and J.S. Bonifacino. 2017. AP-4 mediates export of ATG9A from the trans -Golgi network to promote autophagosome formation. *Proc. Natl. Acad. Sci.* 114:E10697–E10706. doi:10.1073/pnas.1717327114.

Mendoza, M.C., E.E. Er, W. Zhang, B.A. Ballif, H.L. Elliott, G. Danuser and J. Blenis. 2011. ERK-MAPK drives lamellipodia protrusion by activating the WAVE2 regulatory complex. *Mol. Cell.* 41: 661–671. doi:10.1016/j.molcel.2011.02.031.

Miesenböck, G., D.A. De Angelis, and J.E. Rothman. 1998. Visualizing secretion and synaptic transmission with pH-sensitive green fluorescent proteins. *Nature.* 394:192–195. doi:10.1038/28190.

Millarte, V., and H. Farhan. 2012. The Golgi in cell migration: regulation by signal transduction and its implications for cancer cell metastasis. *Sci. World J.* 2012:1–11. doi:10.1100/2012/498278.

Orsi, A., M. Razi, H.C. Dooley, D. Robinson, A.E. Weston, L.M. Collinson, and S.A. Tooze. 2012. Dynamic and transient interactions of Atg9 with autophagosomes, but not membrane integration, are required for autophagy. *Mol. Biol. Cell.* 23:1860–1873. doi:10.1091/mbc.e11-09-0746.

Osmani, N., F. Peglion, P. Chavrier, and S. Etienne-Manneville. 2010. Cdc42 localization and cell polarity depend on membrane traffic. *J. Cell Biol.* 191:1261–1269. doi:10.1083/jcb.201003091.

Pallesi-Pocachard, E., E. Bazellieres, A. Viallat-Lieutaud, M.-H. Delgrossi, M. Barthelemy-Requin, A. Le Bivic, and D. Massey-Harroche. 2016. Hook2, a microtubule-binding protein, interacts with Par6 α and controls centrosome orientation during polarized cell migration. *Sci. Rep.* 6:33259. doi:10.1038/srep33259.

Paul, N.R., G. Jacquemet, and P.T. Caswell. 2015. Endocytic Trafficking of Integrins in Cell Migration. *Curr. Biol.* 25:R1092-1105. doi:10.1016/j.cub.2015.09.049.

Proux-Gillardeaux, V., J. Gavard, T. Irinopoulou, R.-M. Mege, and T. Galli. 2005. Tetanus neurotoxin-mediated cleavage of cellubrevin impairs epithelial cell migration and integrin-dependent cell adhesion. *Proc. Natl. Acad. Sci.* 102:6362–6367. doi:10.1073/pnas.0409613102.

Puri, C., M. Renna, C.F. Bento, K. Moreau, and D.C. Rubinsztein. 2013. Diverse autophagosome membrane sources coalesce in recycling endosomes. *Cell.* 154:1285–1299. doi:10.1016/j.cell.2013.08.044.

- Rahajeng, J., R.S. Kuna, S.L. Makowski, T.T.T. Tran, M.D. Buschman, S. Li, N. Cheng, M.M. Ng, and S.J. Field. 2019. Efficient Golgi forward trafficking requires GOLPH3-driven, PI4P-dependent membrane curvature. *Dev. Cell.* 50:573-585.e5. doi:10.1016/j.devcel.2019.05.038.
- Ravikumar, B., K. Moreau, L. Jahreiss, C. Puri, and D.C. Rubinsztein. 2010. Plasma membrane contributes to the formation of pre-autophagosomal structures. *Nat. Cell Biol.* 12:747–757. doi:10.1038/ncb2078.
- Ridley, A.J., M.A. Schwartz, K. Burridge, R.A. Firtel, M.H. Ginsberg, G. Borisy, J.T. Parsons, and A.R. Horwitz. 2003. Cell migration: integrating signals from front to back. *Science.* 302:1704–1709. doi:10.1126/science.1092053.
- Riggs, K.A., N. Hasan, D. Humphrey, C. Raleigh, C. Nevitt, D. Corbin, and C. Hu. 2012. Regulation of integrin endocytic recycling and chemotactic cell migration by syntaxin 6 and VAMP3 interaction. *J. Cell Sci.* 125:3827–3839. doi:10.1242/jcs.102566.
- Sankaranarayanan, S., D. De Angelis, J.E. Rothman, and T.A. Ryan. 2000. The use of pHluorins for optical measurements of presynaptic activity. *Biophys. J.* 79:2199–2208. doi:10.1016/S0006-3495(00)76468-X.
- Sann, S., Z. Wang, H. Brown, and Y. Jin. 2009. Roles of endosomal trafficking in neurite outgrowth and guidance. *Trends Cell Biol.* 19:317–324. doi:10.1016/j.tcb.2009.05.001.
- Schmoranzner, J., G. Kreitzer, and S.M. Simon. 2003. Migrating fibroblasts perform polarized, microtubule-dependent exocytosis towards the leading edge. *J. Cell Sci.* 116:4513–4519. doi:10.1242/jcs.00748.
- Segall, J.E., S. Tyerech, L. Boselli, S. Masseling, J. Helft, A. Chan, J. Jones and J. Condeelis. 1996. EGF stimulates lamellipod extension in metastatic mammary adenocarcinoma cells by an actin-dependent mechanism. *Clin. Exp. Metastasis.* 14: 61–72. doi:10.1007/BF00157687.
- Shafaq-Zadah, M., C.S. Gomes-Santos, S. Bardin, P. Maiuri, M. Maurin, J. Irazzo, A. Gautreau, C. Lamaze, P. Caswell, B. Goud, and L. Johannes. 2016. Persistent cell migration and adhesion rely on retrograde transport of $\beta 1$ integrin. *Nat. Cell Biol.* 18:54–64. doi:10.1038/ncb3287.
- Sneeggen, M., N.M. Pedersen, C. Campsteijn, E.M. Haugsten, H. Stenmark, and K.O. Schink. 2019. WDFY2 restrains matrix metalloproteinase secretion and cell invasion by controlling VAMP3-dependent recycling. *Nat. Commun.* 10:2850. doi:10.1038/s41467-019-10794-w.
- Sørensen, K., M.J. Munson, C.A. Lamb, G.T. Bjørndal, S. Pankiv, S.R. Carlsson, S.A. Tooze, and A. Simonsen. 2018. SNX18 regulates ATG9A trafficking from recycling endosomes by recruiting Dynamin-2. *EMBO Rep.* 19. doi:10.15252/embr.201744837.

- Stehbens, S.J., M. Paszek, H. Pemble, A. Ettinger, S. Gierke, and T. Wittmann. 2014. CLASPs link focal-adhesion-associated microtubule capture to localized exocytosis and adhesion site turnover. *Nat. Cell Biol.* 16:558–570. doi:10.1038/ncb2975.
- Stehbens, S.J., and T. Wittmann. 2014. Analysis of focal adhesion turnover. In *Methods in Cell Biology*. Elsevier. 335–346.
- Subramani, S., and V. Malhotra. 2013. Non-autophagic roles of autophagy-related proteins. *EMBO Rep.* 14:143–151. doi:10.1038/embor.2012.220.
- Takahashi, Y., N. Tsotakos, Y. Liu, M.M. Young, J. Serfass, Z. Tang, T. Abraham and H-G. Wang. 2016. The Bif-1-Dynamin 2 membrane fission machinery regulates Atg9-containing vesicle generation at the Rab11-positive reservoirs. *Oncotarget.* 7: 20855–20868. doi:10.18632/oncotarget.8028.
- Tayeb, M., M. Skalski, M. Cha, M. Kean, M. Scaife, and M. Coppolino. 2005. Inhibition of SNARE-mediated membrane traffic impairs cell migration. *Exp. Cell Res.* 305:63–73. doi:10.1016/j.yexcr.2004.12.004.
- Tokuda, E., T. Itoh, J. Hasegawa, T. Ijuin, Y. Takeuchi, Y. Irino, M. Fukumoto and T. Takenawa. 2014. Phosphatidylinositol 4-phosphate in the golgi apparatus regulates cell–cell adhesion and invasive cell migration in human breast cancer. *Cancer Res.* 74: 3054–3066. doi:10.1158/0008-5472.CAN-13-2441.
- Veale, K.J., C. Offenhäuser, and R.Z. Murray. 2011. The role of the recycling endosome in regulating lamellipodia formation and macrophage migration. *Commun. Integr. Biol.* 4:44–47. doi:10.4161/cib.4.1.13569.
- Veale, K.J., C. Offenhäuser, S.P. Whittaker, R.P. Estrella, and R.Z. Murray. 2010. Recycling endosome membrane incorporation into the leading edge regulates lamellipodia formation and macrophage migration. *Traffic.* 11:1370–1379. doi:10.1111/j.1600-0854.2010.01094.x.
- Wang, J., and K.E. Howell. 2000. The Luminal Domain of TGN38 Interacts with Integrin β 1 and is Involved in its Trafficking. *Traffic.* 1:713–723. doi:10.1034/j.1600-0854.2000.010904.x.
- White, D.P., P.T. Caswell, and J.C. Norman. 2007. α v β 3 and α 5 β 1 integrin recycling pathways dictate downstream Rho kinase signaling to regulate persistent cell migration. *J. Cell Biol.* 177:515–525. doi:10.1083/jcb.200609004.
- Williamson, R.C., C.A.M. Cowell, T. Reville, J.A. Roper, T.C.S. Rendall, and M.D. Bass. 2015. Coronin-1C protein and caveolin protein provide constitutive and inducible mechanisms of Rac1 protein trafficking. *J. Biol. Chem.* 290:15437–15449. doi:10.1074/jbc.M115.640367.

Xing M., M.C. Peterman, R.L Davis, K. Oegema, A.K. Shiau and S.J. Field. 2016. GOLPH3 drives cell migration by promoting Golgi reorientation and directional trafficking to the leading edge. *Mol. Biol. Cell.* 27: 3828–3840. doi:10.1091/mbc.E16-01-0005.

Yamaguchi, J., C. Suzuki, T. Nanao, S. Kakuta, K. Ozawa, I. Tanida, T. Saitoh, T. Sunabori, M. Komatsu, K. Tanaka, S. Aoki, K. Sakimura, and Y. Uchiyama. 2018. Atg9a deficiency causes axon-specific lesions including neuronal circuit dysgenesis. *Autophagy.* 14:764–777. doi:10.1080/15548627.2017.1314897.

Young, A.R.J., E.Y.W. Chan, X.W. Hu, R. Köchl, J. Lippincott-Schwartz, and S.A. Tooze. 2006. Starvation and ULK1-dependent cycling of mammalian Atg9 between the TGN and endosomes. *J. Cell Sci.* 119:3888–3900. doi:10.1242/jcs.03172.

Zhou, C., K. Ma, R. Gao, C. Mu, L. Chen, Q. Liu, Q. Luo, D. Feng, Y. Zhu, and Q. Chen. 2017. Regulation of mATG9 trafficking by Src- and ULK1-mediated phosphorylation in basal and starvation-induced autophagy. *Cell Res.* 27:184–201. doi:10.1038/cr.2016.146.

Part II: Interaction of ATG9A with the actin-binding protein profilin-1. Potential involvement in actin polymerization of the cell leading edge

I. Introduction

Recent reports have highlighted the autophagy-independent role of the Atg9 protein. One of these studies has shown that KO of *Drosophila* Atg9 induces severe locomotor problems in fruit flies and a malformation during midgut development (Wen et al., 2017). These resulting defects were due to a major disruption of the actin network caused by loss of Atg9. In fact, phalloidin staining of actin filaments in visceral muscles revealed a severe discontinuity of the layers surrounding the gut as well as enlarged cells and protrusions with abnormal apical membranes, unlike wild-type Atg9 fruit flies owning, instead, a tight and polarized intestinal epithelium monolayer. The authors pointed out that polarization in these cells is due to the simultaneous interaction of Atg9 with partners involved in apical cell polarity, such as Patj and TSC2. Without Atg9, these two factors fail to regulate these processes, inducing a disorganization of the cytoskeleton (Wen et al., 2017). Recently, another report has demonstrated a more direct involvement of Atg9 on actin cytoskeleton, pointing out that *Drosophila* Atg9 binds actin cables at the plasma membrane, and this is essential for cortical actin organization in nurse cells surrounding the oocyte (Kiss et al., 2020). Specifically, Atg9 loss leads to a severe alteration of the cortical actin network in the ovary cells and enhances filopodia formation in neurons (Kiss et al., 2020). This specific function does not depend on the autophagic activity of Atg9, since other Atg mutants did not show such phenotype. From a mechanistic point of view, the authors of this study demonstrated that *Drosophila* Atg9 can interact with the actin NPFs Ena/VASP and profilin, and that Atg9 depletion alters the localization of these two regulators at the plasma membrane (Kiss et al., 2020). These studies propose an alternative role for Atg9, as a *i*) contributor of cell polarity and *ii*) a carrier of NPFs at the plasma membrane for the organization of actin network. As already described in paragraph 2.1.1., extensive literature has demonstrated that profilin-1, a major actin-monomer-binding protein, and the three Ena-related family members Mena, VASP and Evl play critical roles in F-actin elongation and lamellipodial architecture in vertebrates (Damiano-Guercio et al., 2020; Rotty, 2020; Skruber et al., 2020). This prompted us to investigate whether human ATG9A, similar to its *Drosophila* homolog, has the capacity to interact with Ena/VASP family members and/or profilin, and whether such interactions could regulate protrusion dynamics.

II. Materials and Methods

II.1. Reagents and chemicals

Antibodies were as follow: rabbit monoclonal anti-profilin-1 (Abcam ab124904), mouse monoclonal anti-c-myc (Santa Cruz, sc-40), rabbit monoclonal anti-ATG9A (Abcam, Ab108338). Secondary antibodies used were Alexa Fluor 488-conjugated antibody against rabbit IgG (Invitrogen, A21206), Alexa Fluor 594-conjugated antibody against mouse IgG (Invitrogen, A21203). Other reagents in this study were recombinant human EGF

(Gibco, PHG0314), 4',6-diamidino-2-phenylindole (DAPI, Sigma-Aldrich, D8417), rhodamine phalloidin (Fisher Scientific, R415), fibronectin (FN1, Sigma-Aldrich, F0895), normal donkey serum (Sigma-Aldrich, D9663), formaldehyde (Sigma-Aldrich, F8775), Dulbecco's phosphate-buffered saline without salts (DPBS, Sigma-Aldrich, D8537), triton X-100 (Fisher Scientific, T3751/08) and bovine serum albumin fraction V (BSA, Roche, 10735108001).

II.2. Test of protein-protein interactions in the yeast two-hybrid system

II.2.1. Yeast strains, culture media and co-transformation procedures

Yeast-two-hybrid assays were performed using the Gal4-based Matchmaker system in the *Saccharomyces cerevisiae* AH109 yeast strain, containing *Ade2*, *His3*, *LacZ* and *Mel1* reporter genes under the control of the activation sequence of the Gal4 transcription factor located upstream these genes. The AH109 cells were grown and maintained on full YPDA (Takara, #630307) agar plates at 30 °C.

II.2.2. Plasmids and site-directed mutagenesis

All the following expression vectors used for Y2H assay were generated by GenScript. The expression vectors encoding the human Mena (clone ID: OHu15865), VASP (clone ID: OHu30167), Evi (clone ID: OHu29478) and profilin-1 (clone ID: OHu24169) were inserted into pGBKT7 vector, using the EcoRI/BamHI sites, so that the inserts are in frame with the DNA-binding domain (BD) of Gal4. These proteins have been used as "bait" since they are fused to Gal4-BD. The expression vectors encoding the cytosolic fragments (ATG9A₁₋₆₆, ATG9A₁₅₃₋₂₈₉ and ATG9A₄₉₅₋₈₃₉) of the human ATG9A were inserted in the EcoRI/BamHI cloning sites of the pGADT7 vector, so that the sequences are in frame with the activating domain (AD) of Gal4. These protein fragments have been used as "prey" since they are fused to Gal4-AD.

Site-directed mutagenesis of the wild-type ATG9A₄₉₅₋₈₃₉ sequence to obtain the eight vectors encoding for different ATG9A₄₉₅₋₈₃₉-mut (ATG9A₄₉₅₋₈₃₉-mutP569A, ATG9A₄₉₅₋₈₃₉-mutP633A, ATG9A₄₉₅₋₈₃₉-mutP657A, ATG9A₄₉₅₋₈₃₉-mutP767A, ATG9A₄₉₅₋₈₃₉-mutP795A, ATG9A₄₉₅₋₈₃₉-mutP820A, ATG9A₄₉₅₋₈₃₉-mutP833A and ATG9A₄₉₅₋₈₃₉-mutD503A; Figure. RR0) was performed by Genscript.

II.2.3. Yeast two-hybrid assay and co-transformation procedures

Co-transformation of the yeast strain AH109 with pGBKT7-prey and pGADT7-bait vectors was performed using the "Quick and Easy Yeast Transformation Mix" (Takara, #631851) and according to the manufacturer's instructions ("Protocol-At-A-Glance"; Clontech). The co-transformants were then grown on

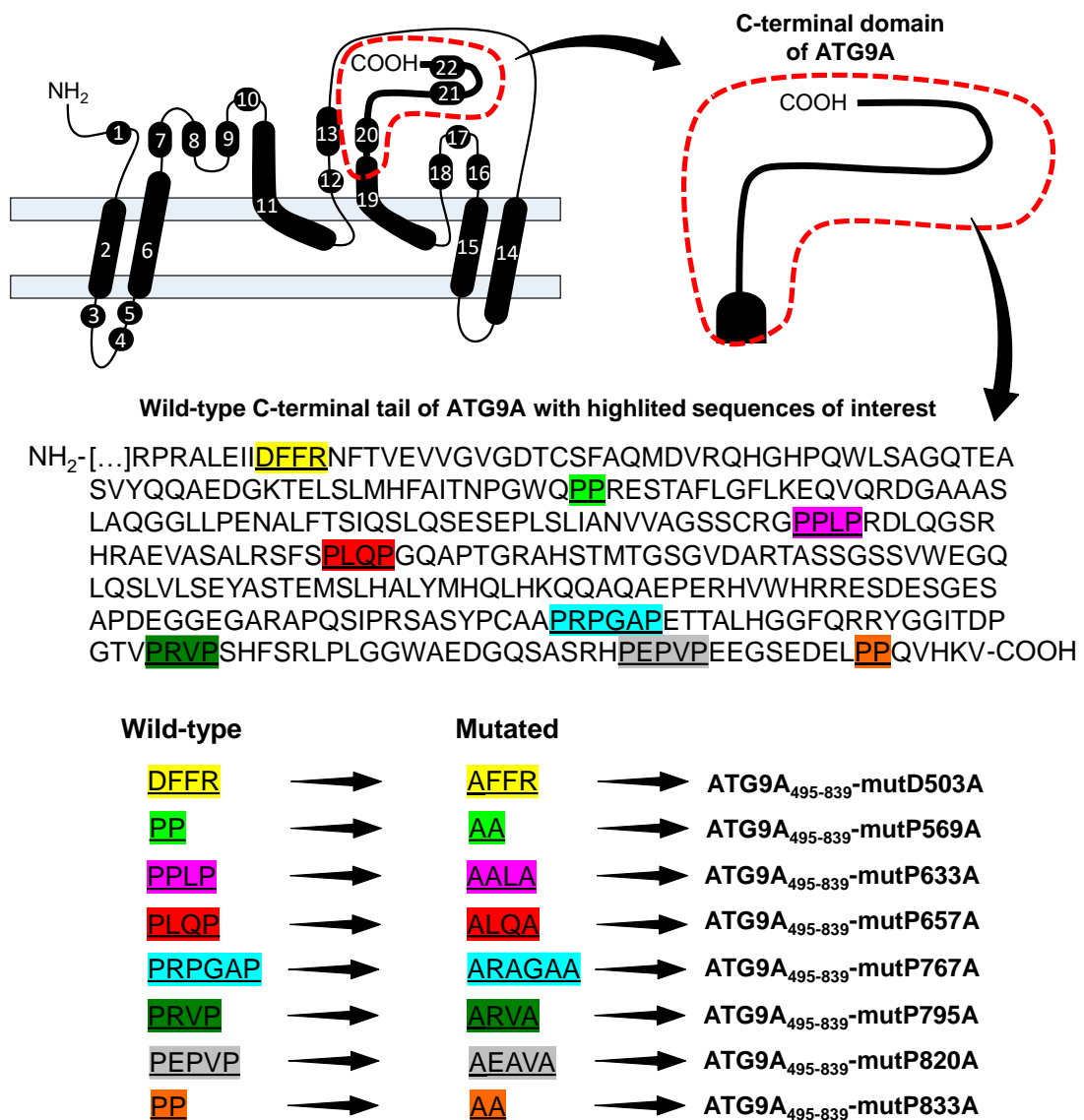


Figure RR0. Schematic representation of the C-terminal domain of human ATGA and of the mutant forms produced by site-directed mutagenesis.

double "dropped out" (DDO) agar plates lacking Leucine and Tryptophan (SD/-Trp/-Leu) at 30 °C for about five days. Interaction of fusion proteins was then evaluated by the activation of ADE2 and HIS3 reporter genes in a drop-test assay. For this purpose, three individual colonies from each co-transformation were suspended in *doubled distilled water* (ddH₂O) and 20 μL of each suspension was dropped onto a *quadruple "dropped out"* (QDO) agar plate lacking Histidine, Adenine, Leucine and Tryptophan (SD/-Trp/-Leu/-His/-Ade) and grown at 30 °C for five to seven days. Two controls were included for each Y2H assay: p53 (murine p53 protein, fused to the Gal4 DNA-BD) and T-antigen (SV40 large T-antigen, fused to Gal4-AD) are known to interact and used as a positive control; Lamin (human Lamin C, fused to the Gal4 DNA-BD) and T-antigen were used as a negative control.

II.3. Plasmid constructs and short interfering RNAs (siRNAs)

The expression vector encoding *ATG9A-myc* was obtained by inserting the sequence of human ATG9A (GenScript clone ID OHu04028C; GenBank, NM_001077198.2) into a pcDNA3.1(+)-C-myc plasmid, using XhoI and ApaI cloning sites; the myc epitope is located at the C-terminus of the ATG9A protein. The expression vector encoding C-terminal domain of ATG9A (named *ATG9A₄₉₅₋₈₃₉-DN*) was obtained by inserting the codon-optimized sequence of wild type ATG9A₄₉₅₋₈₃₉ into a pcDNA3.1(+) plasmid. The expression vector encoding *ATG9A-EGFP* was obtained by inserting codon-optimized human ATG9A (Uniprot, Q7Z3C6) and EGFP (GenBank, U55761.1) sequences into a pcDNA3.1(+) plasmid. The EGFP sequence was fused in-frame into the first luminal domain of human ATG9A protein, between the amino acids Leu102 and His103. The expression vector encoding profilin-1-mCherry was obtained by inserting codon-optimized human profilin-1 (clone ID: OHu24169; NM_005022) and mCherry sequence into a pcDNA3.1(+) plasmid. The mCherry sequence was inserted between the amino acids Gln80 and Asp81 and flanked by two “SGSSGS” and “GGSLQ” linkers (from Nejedla et al. 2016). For ATG9A knockdown experiments, control (D-001810-03, 5'-UCAGAAAACAUGUAAACCA-3'), ATG9A #1 (J-014294-09, 5'-UUCUGCGUCUGCAGAUCC-3') and ATG9A #2 (J-014294-10, 5'-UUUCGGAAGAAGUCUAUAA-3') siRNAs were purchased from Dharmacon Horizon Discovery. Cells were subject to 2 rounds of transfection in order to ensure adequate knockdown of the long-lived ATG9A protein.

II.4. Cell cultures and transfections

The glioblastoma multiform cell line U87 MG (WHO grade IV) was purchased from *American Type Culture Collection* (ATCC, HTB-14™). These cells were routinely maintained in our laboratory according to the instructions from ATCC and cultured in DMEM (Gibco, 41965-039), supplemented with 10% fetal bovine serum (Dutscher, S181H-500), 1% of antibiotic-antimycotic solution (Sigma-Aldrich, A5955) and 1% of sodium pyruvate (Sigma-Aldrich, S8636). For all experiments, cells were placed in either serum-free DMEM, supplemented with 1% of antibiotic-antimycotic solution and 1% of sodium pyruvate or serum- and phenol red-free Leibovitz's L-15 medium (Gibco, 21083027), supplemented with 1% D-Glucose (Sigma-Aldrich, G8644), 1% of antibiotic-antimycotic solution and 1% of sodium pyruvate. Transient transfections were performed using the Amaxa Cell Line Nucleofector Kit V (Lonza, VCA-1003) according to the manufacturer's protocol, using the A-023 program for U87 MG.

II.5. Immunocytochemistry and image analysis

Cells were fixed with formaldehyde (4%, 10 min), permeabilized with Triton X-100 (0.05%, 5 min) and blocked for 1 h with a mixture of normal donkey serum (2%) and fetal bovine serum (10%) diluted in DPBS. Cells were incubated overnight with the adequate primary antibody at 4°C followed by incubation for 2 h at room temperature with the adequate secondary antibody. Cells were counterstained with DAPI (1 µg/mL, 10 min) to label nuclei, and imaged using the Leica THUNDER Imager 3D Tissue.

II.6. Live-cell imaging

Transfected cells were seeded on FN1-coated 35-mm glass dishes (P35G-1.5-14-C, MatTek Corporation) for epifluorescence experiments. At 24 h post-transfection, epifluorescence live-cell imaging was performed in serum-free Leibovitz's L-15 medium supplemented with 1% D-Glucose, 1% of antibiotic-antimycotic and 1% of sodium pyruvate. Epifluorescence images were acquired using a system that was built around a Leica DMI6000 B inverted microscope equipped with a $\times 63$ oil objective with a numerical aperture of 1.46 (HCX PL APO, Leica), a Hamamatsu Orca-Flash 4.0 camera, and 488-nm and 561-nm lasers. During dual channel recording, 488-nm and 561-nm lasers were used consecutively for each image of the time series. Time interval for *ATG9A-EGFP and profilin-1-mCherry* dual channel experiment was of 30 sec (having a time delay of 1.5 second between the two channels).

III. Results

III.1. ATG9A interacts with profilin-1 through its C-terminal domain

Polymerization of actin filaments to form lamellipodia occurs through the cooperation of the NPFs Ena/VASP family proteins and profilin-1 at the plasma membrane where they localize (Applewhite et al., 2007; Hartwig et al., 1989). This specific localization is similar to what we saw in case of ATG9A, since it localizes and accumulates in F-actin-rich lamellipodia (Campisi et al., under revision). Results from Kiss and colleagues, showing a direct interaction between *Drosophila* Atg9 with Ena and profilin (Kiss et al., 2020), prompted us to determine whether mammalian ATG9A also interact with Mena, VASP, Evl and profilin-1. For this purpose, we carried out protein-protein interaction tests by using the *yeast two-hybrid* (Y2H) assay, with the AH109 reporter strain. Since ATG9A is a multi-spanning membrane protein (Figure RR1A), AH109 yeast cells were co-transformed with pGADT7 constructs encoding the cytosolic domains of human ATG9A (ATG9A₁₋₆₆: N-terminal cytosolic domain encompassing amino-acids 1 to 66; ATG9A₁₅₃₋₂₈₉: cytosolic domain encompassing amino-acids 153 to 289; ATG9A₄₉₅₋₈₃₉: C-terminal cytosolic domain encompassing amino-acids 495 to 839; Figure RR1A), together with pGBKT7 constructs encoding full-length Mena, VASP, Evl or profilin-1 proteins. The cytosolic domains of ATG9A of only a few amino acids long were not taken into account for a Y2H assay. Our drop-test experiments on yeast co-transformants indicated that activation of *Ade2* and *His3* reporter genes, allowing cells to grow on medium lacking adenine and histidine, was found in cells harboring both ATG9A₄₉₅₋₈₃₉ and profilin-1, or the positive control partners p53 and T-antigen (Figure RR1B). The expression of ATG9A₄₉₅₋₈₃₉ with Mena, VASP or Evl did not yield a positive result under identical conditions, and ATG9A₁₋₆₆ and ATG9A₁₅₃₋₂₈₉ did not display any interaction with the tested proteins, indicating that the interaction of ATG9A₄₉₅₋₈₃₉ with profilin-1 is specific (Figure RR1B).

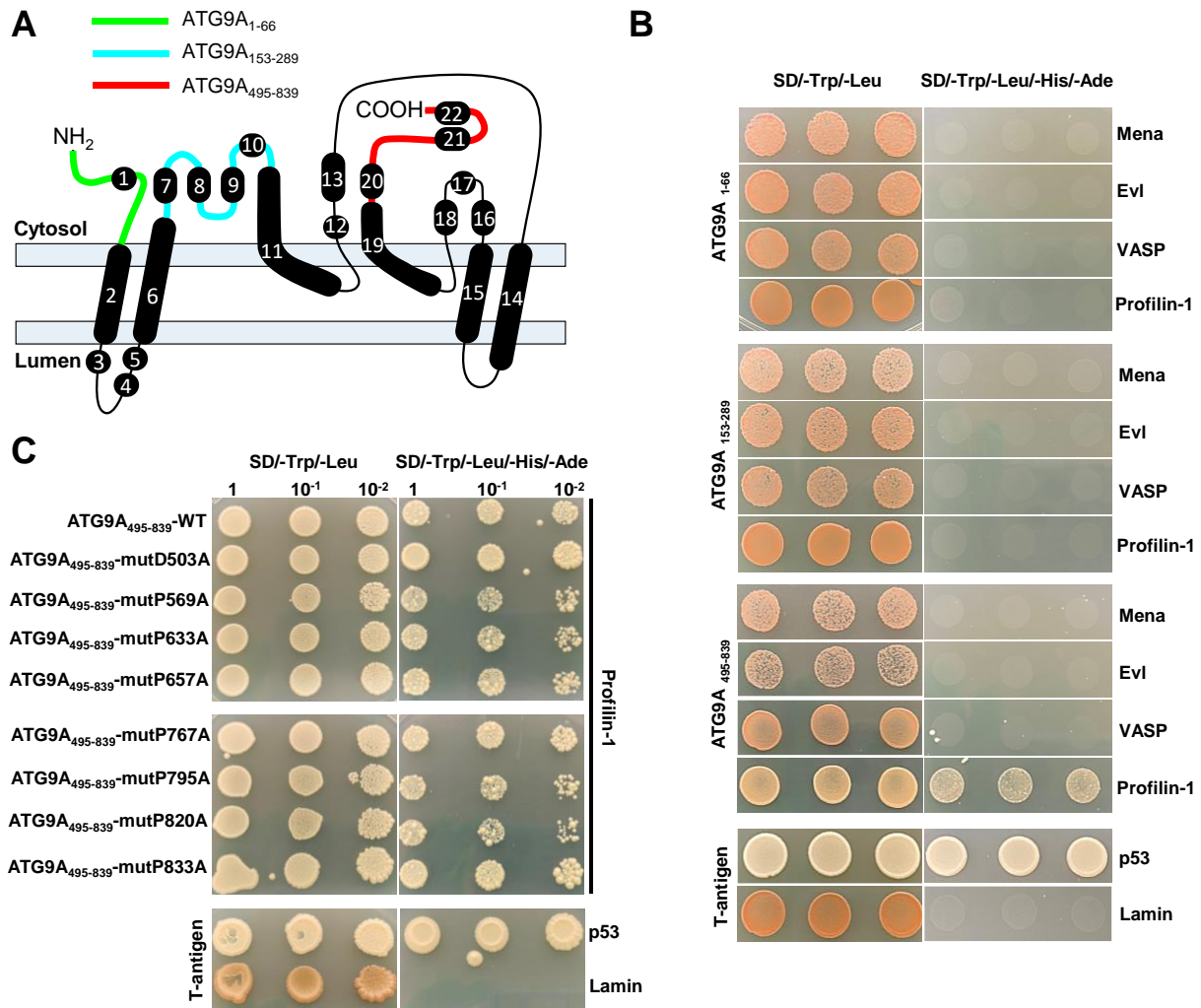


Figure RR1. The C-terminal domain of ATG9A interacts with the actin regulator profilin-1. **A** | Scheme presenting the three cytosolic domains of human ATG9A used in the yeast two-hybrid assay ($ATG9A_{1-66}$: N-terminal cytosolic domain encompassing amino-acids 1 to 66, green; $ATG9A_{153-289}$: cytosolic domain encompassing amino-acids 153 to 289, blue; $ATG9A_{495-839}$: C-terminal cytosolic domain encompassing amino-acids 495 to 839, red). **B** | AH109 yeast cells were co-transformed with pGBKT7 vectors encoding Gal4 DNA-binding domain (*Gal4-BD*) fused in frame with full-length Mena, VASP, Evl or profilin-1 sequences, together with pGADT7 vectors encoding Gal4 activating domain (*Gal4-AD*) fused in frame with $ATG9A_{1-66}$, $ATG9A_{153-289}$ or $ATG9A_{495-839}$ sequences. A positive control (p53 and T-antigen) and a negative control (Lamin and T-antigen) were included. Co-transformants were tested for activation of *Ade2* and *His3* reporter genes by plating triplicate drops on medium lacking adenine and histidine (SD/-Trp/-Leu/-His/-Ade). As a loading control, drops were plated in parallel on medium containing adenine and histidine (SD/-Trp/-Leu). **C** | AH109 yeast cells were co-transformed with pGBKT7 vectors encoding Gal4 DNA-binding domain (*Gal4-BD*) fused in frame with full-length profilin-1 sequence, together with pGADT7 vectors encoding Gal4 activating domain (*Gal4-AD*) fused in frame with either $ATG9A_{495-839}$ -WT or one of the vector encoding $ATG9A_{495-839}$ mutated in proline-rich motifs ($ATG9A_{495-839}$ -mutP569A, $ATG9A_{495-839}$ -mutP633A, $ATG9A_{495-839}$ -mutP657A, $ATG9A_{495-839}$ -mutP767A, $ATG9A_{495-839}$ -mutP795A, $ATG9A_{495-839}$ -mutP820A or $ATG9A_{495-839}$ -mutP833A). An additional form of mutated ATG9A was used $ATG9A_{495-839}$ -mutD503A. A positive control (p53 and T-antigen) and a negative control (Lamin and T-antigen) were included. Co-transformants were tested for activation of *Ade2* and *His3* reporter genes by plating triplicate drops at 10-fold decreasing concentrations compared to the previous one, on medium lacking adenine and histidine (SD/-Trp/-Leu/-His/-Ade). As a loading control, drops were plated in parallel on medium containing adenine and histidine (SD/-Trp/-Leu).

Most of the profilin-1 protein partners described in the literature have proline-rich regions in their sequence that are essential for this interaction (Krishnan & Moens, 2009). In accordance with this notion, we analyzed the amino acid sequence of the C-terminal tail of ATG9A, and identified several proline clusters, which may be responsible for profilin-1 binding. We thus induced the disruption of each of these clusters by directed mutagenesis, by exchanging the prolines within each cluster for alanines obtaining seven mutant forms of the C-terminal domain of ATG9A, *i.e.* ATG9A₄₉₅₋₈₃₉-mutP (ATG9A₄₉₅₋₈₃₉-mutP569A, ATG9A₄₉₅₋₈₃₉-mutP633A, ATG9A₄₉₅₋₈₃₉-mutP657A, ATG9A₄₉₅₋₈₃₉-mutP767A, ATG9A₄₉₅₋₈₃₉-mutP795A, ATG9A₄₉₅₋₈₃₉-mutP820A and ATG9A₄₉₅₋₈₃₉-mutP833A; Figure RR1C and Figure RR0). An additional sequence at the beginning of the C-terminal domain of ATG9A containing an aspartic acid at position 503 was also identified as a potential motif for profilin-1 binding, as it is a highly conserved region between *Drosophila* and vertebrate Atg9. This aspartic acid 503 was then exchanged for an alanine, obtaining an additional mutant, named ATG9A₄₉₅₋₈₃₉-mutD503A (Figure RR1C). Drop-test experiments on yeast co-transformants revealed that cells expressing either ATG9A₄₉₅₋₈₃₉-mutP569A, ATG9A₄₉₅₋₈₃₉-mutP633A, ATG9A₄₉₅₋₈₃₉-mutP795A or ATG9A₄₉₅₋₈₃₉-mutP820A displayed a delayed growth on a medium lacking adenine and histidine, indicating that four proline clusters are involved in the interaction with profilin-1 (Figure RR1C). Surprisingly, AH109 cells harboring ATG9A₄₉₅₋₈₃₉-mutD503A colonies grew faster on the selective medium, which may indicate a strengthened interaction between profilin-1 and this specific mutant. In a first attempt to confirm the ATG9A-profilin-1 interaction observed in the Y2H system, we next performed a co-immunoprecipitation (Co-IP) assay by overexpressing recombinant ATG9A-myc protein in U87 MG cells and by conjugating an anti-myc to the resin as bait for myc-ATG9A. Unfortunately, endogenous profilin-1 did not co-precipitate with ATG9A-myc (data not shown), suggesting that the interaction between profilin-1 and ATG9A might be transient.

III.2. ATG9A colocalizes with and promotes proper localization of profilin-1 at the migration front

Interaction between ATG9A and profilin-1 suggested that these proteins function together in the regulation of the actin cytoskeleton. Indeed, we found that recombinant ATG9A-myc and immunolabeled endogenous profilin-1 strongly colocalized at the leading edge of U87 MG cells (Figure RR2A). Furthermore, chemotactic stimulation induced by EGF increased colocalization (Pearson Coefficient) of the two proteins (Figure RR2A). This led us to evaluate whether ATG9A protein governs the distribution of profilin-1 at the cell periphery. We found that depletion of ATG9A protein levels using two independent siRNAs markedly reduced EGF-induced redistribution of profilin-1 toward the cell periphery (Figure RR2B). To further investigate whether ATG9A protein is critical for the delivery of profilin-1 at the cell periphery, we produced a vector encoding the wild-type C-terminal domain of ATG9A in U87 MG cells. We expected that this fragment, named ATG9A₄₉₅₋₈₃₉-DN, could act as a dominant negative by interfering with the functional assembly of endogenous ATG9A protein with profilin-1. Profilin-1, sequestered by the dominant negative, would no longer be able to reach the plasma membrane, thus altering the formation of lamellipodia. As a control, U87 MG cells were transfected in parallel with an empty vector. As expected, chemotactic stimulation of control U87 MG cells

with EGF induced a marked increase of endogenous profilin-1 levels at the cell periphery, within F-actin-rich protrusions (Figure RR2C). Instead, overexpression of the ATG9A₄₉₅₋₈₃₉-DN totally abolished the EGF-induced distribution of endogenous profilin-1 at the cell periphery, with a concomitantly reduction of F-actin-rich protrusions (Figure RR2C). Together, these results suggest that ATG9A protein, through its C-terminal domain, is critical for the transport of profilin-1 to the migration front.

In order to examine whether ATG9A and profilin-1 appearance at the leading edge correlates with protrusive activity, we next used epifluorescence live-cell microscopy on U87 MG cells expressing both the ATG9A-EGFP and profilin-1-mCherry fusion proteins during the spontaneous formation of protrusions. We followed the formation of protrusions at low frame rate (one image every 30 sec) and we observed that newly formed protrusions were systematically marked by the appearance of both ATG9A-EGFP and profilin-1-mCherry signals close to the leading edge. Notably, analyses of the movies using kymographs indicated that the ATG9A-EGFP and profilin-1-mCherry signals were sustained at the edges of expanding protrusions, but sharply decreased during protrusion collapse (Figure RR3).

IV. Discussion

Preliminary results obtained in this pilot study shed light on a new link between autophagy and cell migration. Experiments conducted on highly invasive glioblastoma multiforme cells, U87 MG, suggest that ATG9A and profilin-1 interact for the formation of lamellipodia. These *in vitro* results were sustained by our Y2H approach, showing that the C-terminal domain of ATG9A interacts with profilin-1, the latter as the best-known protein able to bind monomeric G-actin. Moreover, we depleted ATG9A protein pools to test its functional impact on profilin-1 localization and found that, under these conditions, endogenous profilin-1 was not capable to localize in F-actin-rich protrusions following chemotactic stimulation. These data were supported by experiments done with the ATG9A₄₉₅₋₈₃₉-DN fragment, whose overexpression in U87 MG cells also interfered with the proper localization of profilin-1 at the cell periphery. A recent paper revealed a non-autophagic function of *Drosophila* Atg9 showing that its loss induces a severe alteration of the cortical actin network in nourishing cells surrounding the oocyte. Mechanistically, the authors found that *Drosophila* Atg9 was capable to interact with the actin regulators Ena and profilin, and that its loss disrupts the normal localization of these two proteins at the plasma membrane (Kiss et al., 2020). They further found that mutation of the proline-rich motif "PPRPPAAP" located within the C-terminal domain of Atg9 strongly reduces its ability to bind profilin (Kiss et al., 2020). These data are particularly relevant to our work since *i)* we have already found that mammalian ATG9A is critical for the formation of F-actin-rich protrusions during directed migration (Campisi et al., under revision) and *ii)* profilin-1 is a key protein for the transport and release G-actin to the migration front, in order to fuel actin polymerization within protrusions (Damiano-Guercio et al., 2020; Rotty, 2020; Skrubber et al., 2020). Similar to *Drosophila* Atg9, we have also demonstrated, using the Y2H system that

mammalian ATG9A interacts with profilin-1 through its cytosolic C-terminal domain. It should be noted that the PRRPPAAP motif located in the C-terminal domain of yeast Atg9 is not conserved in vertebrate homologues.

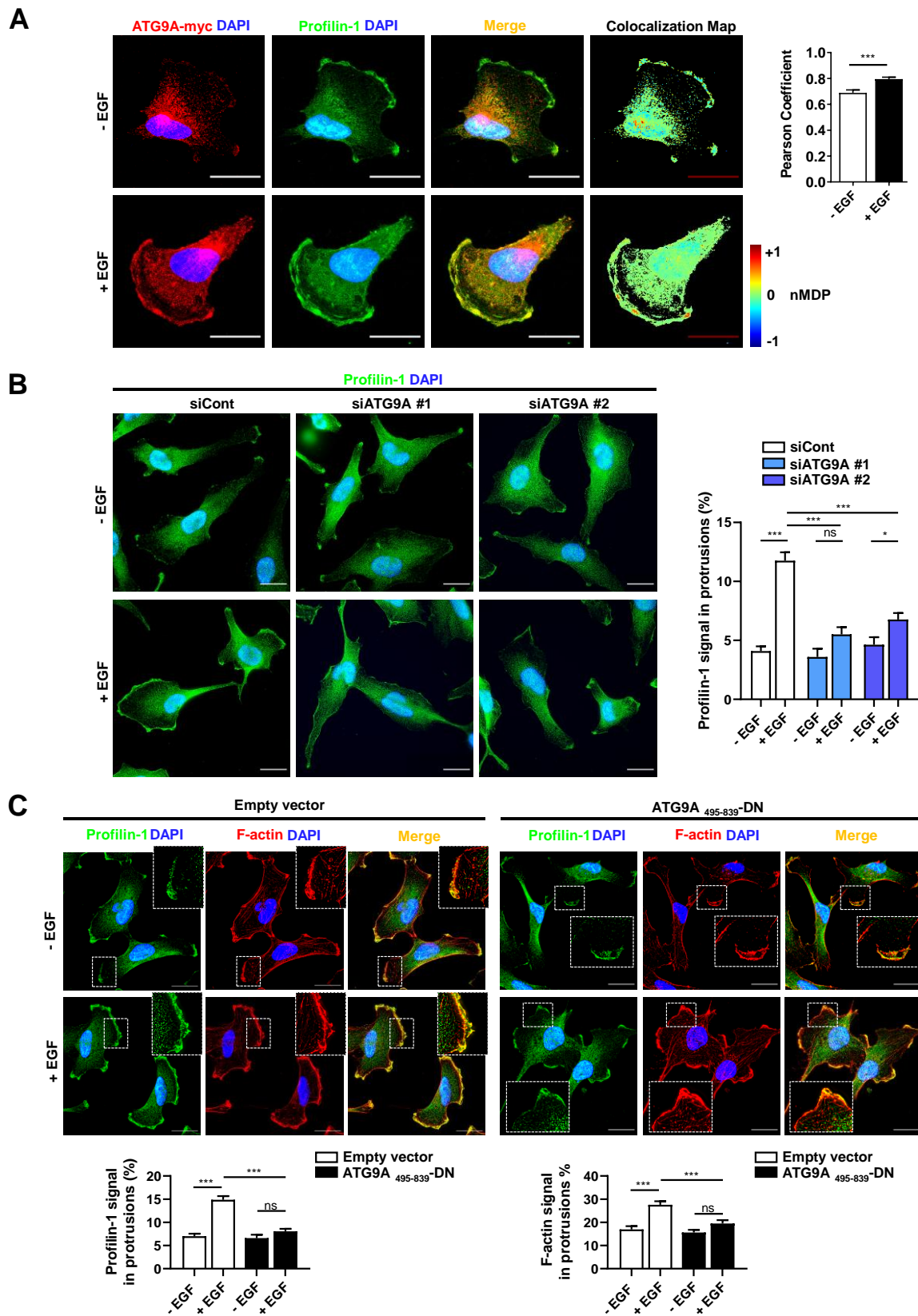


Figure RR2. For caption see next page.

Figure RR2. ATG9A colocalizes with profilin-1 and governs its localization toward the leading edge. **A|** U87 MG cells were transfected with ATG9A-myc. Cells were starved (30 min) in serum-free medium, treated (30 min) with or without EGF (50 ng/mL), fixed and labelled with an anti-myc antibody (red), endogenous profilin-1 (green) and DAPI (nuclei, blue). The association of ATG9A with profilin-1 was representatively shown with Colocalization Colormap tool, where *normalized mean deviation product* (nMDP) shows the correlation between intensities of corresponding pixels (values are ranging from -1 to 1). Negative nMDP values are represented by cold colors (segregation) while values above 0 are represented by hot colors (colocalization). Histogram shows Pearson's coefficient between ATG9A and profilin-1 from cells represented above. Colocalization values were calculated on a 1.5 micrometers cellular portion from the plasma membrane inwards. Data represent means \pm SEM (- EGF, n=13 cells; + EGF, n=13 cells; from 1 experiment). Scale bar, 20 μ m. **B|** (Left) U87 MG cells were transfected with nontargeting siRNA (siCont) or one of the two siRNA targeting ATG9A (siATG9A #1, siATG9A #2). Transfected cells were starved (30 min) in serum-free medium and incubated (30 min) with or without EGF (50 ng/mL), as indicated. Cells were fixed and labelled for endogenous profilin-1 (green) and nuclei (DAPI labelling, blue). Scale bar, 20 μ m. (Right) Quantification from images shown in (Left) of the profilin-1 signal located in protrusions. Data represent means \pm SEM (siCont, n = 59 cells; siATG9A #1, n = 48 cells; siATG9A #2, n = 65 cells; from 1 experiment). **C|** (Upper) U87 MG cells were transfected with a vector encoding the cytosolic domain of ATG9A (ATG9A₄₉₅₋₈₃₉-DN) or an empty vector, as control. Transfected cells were starved (30 min) in serum-free medium and incubated (30 min) with or without EGF (50 ng/mL), as indicated. Cells were fixed and labelled for endogenous profilin-1 (green), F-actin (red) and nuclei (DAPI labelling, blue). Scale bar, 20 μ m. (Lower) Quantification from images shown in (Upper) of the profilin-1 and F-actin signals located in protrusions. Data represent means \pm SEM (empty vector, n = 83 cells; ATG9A₄₉₅₋₈₃₉-DN, n = 91 cells; from 1 experiment).

However, we demonstrated that mutation of proline residues within four proline clusters of human ATG9A (xPPx, xPPxP, xPxxPx and xPxPxPx, see Figure RR0) significantly reduced the growth of AH109 cells in our drop-test experiments. Although the three-dimensional structure of the human ATG9A C-terminal domain is still not available, we can speculate that several proline clusters may interact together in order to form of recruitment platform for profilin-1. An additional way to confirm that the interaction between ATG9A and profilin-1 occurs *via* poly-proline motifs is to generate a poly-proline binding defective mutant form of profilin-1 (Kiss et al., 2020). In fact, Tryptophan in position 3 of human profilin-1 has been shown to be essential for the binding proline-rich domains (Lambrechts et al., 2002), and replacing this amino acid to an Alanine not only eliminated the interaction between *Drosophila* profilin and Ena, but also that between profilin and the C-terminal domain of Atg9 (Kiss et al., 2020).

The interaction between ATG9A and profilin-1 needs to be confirmed by another method, beside the Y2H assay. Our first attempts, using co-IP, did not yield a positive result, suggesting that the ATG9A:profilin-1 complex formation might be transient and may not resist to the successive washing steps of the co-IP protocol. We therefore envisage to evaluate this interaction in living cells, by the use of the *Biomolecular Fluorescence Complementation* (BiFC) technique (Kodama & Hu, 2012). This technique is based on the expression, in the same cell, of N- and C-terminal portions of a fluorescent protein, fused to the sequences of the potential protein partners of interest. If an interaction between the two proteins of interest indeed occurs, the N- and C-terminal portions of the fluorescent protein will come close from each other and will finally reconstitute a functional protein emitting a visible BiFC signal. The BiFC protocol based on the fluorescent protein *Venus* being largely described in the literature (Kodama & Hu, 2012), we will induce the expression of ATG9A and

profilin-1 fused to the N- and C-terminal domains of *Venus*, respectively. The BiFC signal, generated under control conditions or following chemotactic stimulation, will then be monitored using time-lapse microscopy.

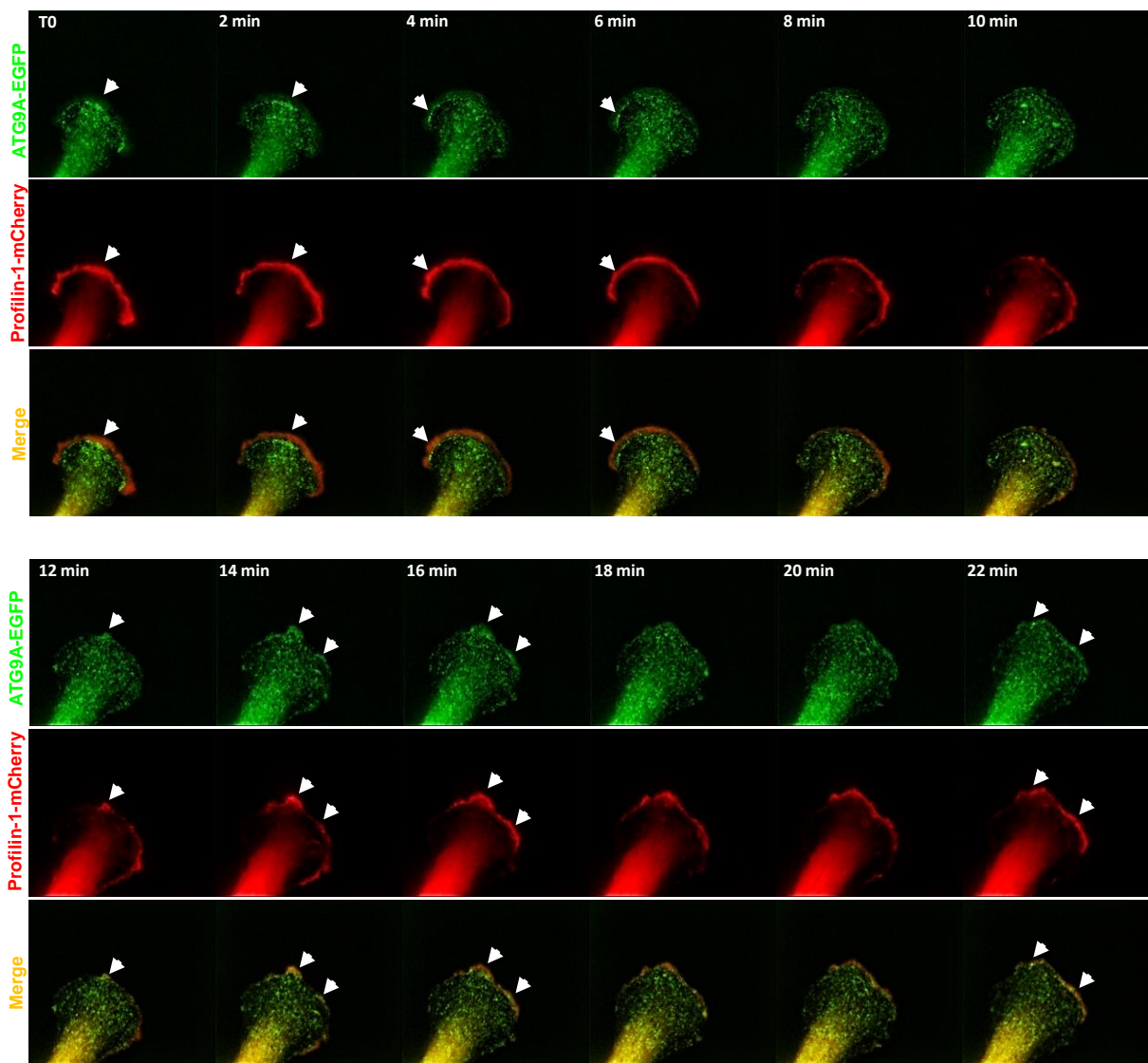
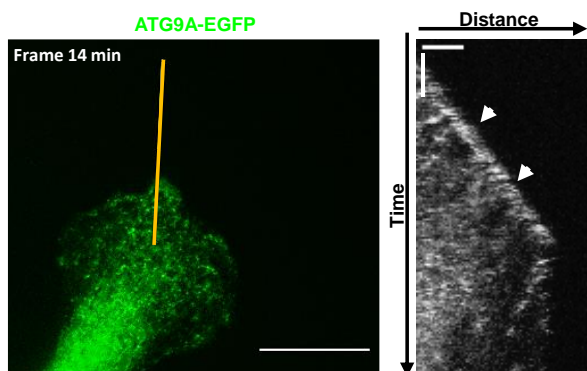
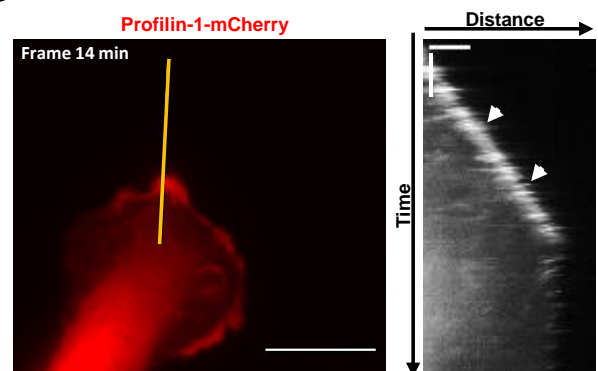
A**B****C**

Figure RR3. For caption see next page.

Figure RR3. ATG9A-EGFP and profilin-1-mCherry signals colocalize and correlate with protrusive activity. **A|** Time-lapse epifluorescence images of a spontaneous large protrusion from a U87 MG cell expressing both ATG9A-EGFP and profilin-1-mCherry. The development of protrusions over time correlates with the appearance of a marked EGFP and mCherry signals at the leading edge. Some images show numerous ATG9A-EGFP positive vesicles (*arrow*) appearing concomitantly of profilin-1-mCherry signal (*arrow*). **B|** (Left) Epifluorescence images extracted from the time-lapse sequence shown in **A|** of a protrusion from a U87 MG cell, expressing both ATG9A-EGFP and profilin-1-mCherry, marked with ATG9A-EGFP signal. Scale bar, 20 μm . (Right) The kymograph was generated from a one-pixel wide line drawn in the left image. The scale bars in the kymograph are 4 μm (horizontal) and 20 min (vertical), respectively. A clear ATG9A-EGFP signal was observed near the cell edge during the formation of the protrusion (*arrow*). The signal sharply decreased during protrusion collapse. **C|** (Left) Epifluorescence images extracted from the time-lapse sequence shown in **A|** of a protrusion from a U87 MG cell, expressing both ATG9A-EGFP and profilin-1-mCherry, marked with profilin-1-mCherry signal. Scale bar, 20 μm . (Right) The kymograph was generated as indicated above. The scale bars in the kymograph are 4 μm (horizontal) and 20 min (vertical), respectively. A clear profilin-1-mCherry signal was observed near the cell edge during the formation of protrusions (*arrow*).

What is the functional role of the ATG9A-profilin-1 interaction? A recent report has supported the idea that ATG9A may work as a “trafficking shuttle” for different cargo proteins. In fact, it has been shown that ATG9A controls Golgi-to-lysosome trafficking of hydrolases by interacting with AP-1 (Jia et al., 2017). This report was important to us since our results, presented in the first chapter of this manuscript (Campisi et al., under revision), have shown that ATG9A-containing vesicles govern anterograde trafficking of $\beta 1$ integrin, in order to stabilize and anchor the lamellipodium to the ECM (Campisi et al., under revision). In this view, the function of ATG9A in the anterograde transport of various cargoes may also involve profilin-1. In support of this hypothesis, we have already demonstrated that ATG9A knockdown or overexpression of the C-terminal fragment of ATG9A abrogated the accumulation of profilin-1 at the cell periphery following chemotactic stimulation. At this point, data obtained following overexpression of ATG9A₄₉₅₋₈₃₉ have however to be interpreted with caution, since this large region of ATG9A may likely interact with other proteins than profilin-1. A more detailed analysis of the structural determinants involved in ATG9A:profilin-1 complex formation needs to be done in order to design small and specific interfering peptides.

From a mechanistic point of view, it is now important to understand how the dynamics of interaction between profilin-1, G-actin and ATG9A take place. Structurally, profilin-1 can bind proline-rich motifs *via* its N-terminal domain and G-actin *via* its C-terminal domain (Pimm et al., 2020), supporting the idea that interaction of ATG9A with profilin-1 does not preclude the association of profilin-1 with G-actin. If so, ATG9A-positive vesicles may participate to the delivery of a ATG9A:profilin-1:G-actin ternary complex toward the leading edge. From here, profilin-1:G-actin may dissociate from ATG9A in order to be loaded on Ena/VASP proteins, thereby enhancing processivity of F-actin polymerization in the lamellipodium. Several experiments need to be done in order to validate this model, still very speculative. For example, it will be important to test the impact of ATG9A knockdown on the transport of monomeric G-actin from the perinuclear area to the leading edge, by the use of a construct encoding photoactivable GFP fused to actin, as previously described (Vitriol et al., 2015).

In this framework, the use of small peptides specifically interfering with the ATG9A:profilin-1 interaction will also give valuable data.

The recent report of Jia and colleagues (Jia et al., 2017) together with data presented in the “Part I – Results” section of this manuscript led us to speculate that ATG9A protein could be an intrinsic regulator of vesicle biogenesis from the secretory pathway. Interestingly, a previous study has demonstrated that profilin-1 co-localized with Golgi markers and was required for the formation of constitutive transport vesicles at the TGN network (Dong et al., 2000). Moreover, it has been reported that short actin filaments are found in close proximity of the Golgi apparatus, and that the actin cytoskeleton contributes to the budding of vesicles from the TGN (Carreno et al., 2004). It can therefore be envisaged that the ATG9A:profilin-1 interaction may tightly control actin polymerization at TGN subdomains, for efficient vesicle budding. Experiments based on ATG9A knockdown or the use of small interfering peptides will also help to test this hypothesis.

GENERAL DISCUSSION AND PERSPECTIVES

The results obtained during this study revealed a direct link between the core autophagy protein ATG9A, a well-known actor involved in the autophagy machinery, and directional cell migration. The experiments carried out on different cell lines, but mainly in highly invasive U87 MG glioblastoma cells, revealed that the ATG9A protein is critical for the formation of protrusions and their stability. In fact, siRNA-induced downregulation of ATG9A protein strongly reduced or completely abolished chemotactic movements induced by several stimuli, *i.e.* EGF and CXCL12. Furthermore, cells in which ATG9A expression was repressed were not capable of forming large and polarized F-actin rich protrusions, recognized as essential structures driving chemotactic cell migration. The design of an ATG9A-pHluorin construct, encoding the ATG9A protein fused with a pH-sensitive GFP variant, allowed us to demonstrate that ATG9A-containing vesicles displayed exocytosis toward the leading edge, thus participating to the local delivery of β 1 integrin required for adhesion formation and/or maturation.

14. Role of ATG9A in “Golgi-to-plasma membrane” trafficking during cell migration

Several studies indicate that ATG9A-containing vesicles are formed at the TGN and cycle between the TGN, endosomes and the plasma membrane (Orsi et al., 2012; Reggiori et al., 2005). After autophagy induction, ATG9A protein displays reduced localization at the TGN, and its targeting to the phagophore is supposed to deliver lipids and/or specific proteins for its expansion. We have shown that ATG9A protein strongly colocalized with the TGN46 marker at the TGN or in cell protrusions, at the plasma membrane or in small vesicles located beneath the plasma membrane. This suggests that ATG9A-positive vesicles emanating from the TGN can, in addition of being targeted to the phagophore, also be transported toward the cell periphery to support chemotactic migration.

The Golgi apparatus was shown to be essential in cell migration about three decades ago (Kupfer et al., 1983), and its orientation seems to be critical in this process. In fact, wound-healing experiments have demonstrated that cells far from the wound exhibited a random orientation of the Golgi relative to the nucleus. In contrast, cells located close the wound edge and capable to migrate toward the surrounding space exhibited the Golgi apparatus facing the leading edge (Kupfer et al., 1983). Orientation of the Golgi apparatus to the leading edge was coupled to the movement of the centrosome, which is the platform where microtubules are generated and where vesicular trafficking toward the cell periphery occurs (Bisel et al., 2008; Hao et al., 2020). Another study has also shown that disruption of the Golgi apparatus architecture, *via* knockdown of the golgin-160 protein, strongly inhibited cell migration (Yadav et al., 2009). Despite this recognized role of the Golgi apparatus in cell migration, only few reports have evaluated polarized exocytosis of post-Golgi carriers at the single vesicle level, by using live-cell TIRF microscopy. This includes data from Schmoranzler and colleagues, showing that exocytosis of post-Golgi vesicles, loaded with low-density lipoprotein receptor-GFP, was

polarized toward the leading edge of migrating fibroblast (Schmoranzner, 2003). In polarized astrocytes, post-Golgi vesicles exhibited exocytosis toward the leading edge whereas, in non-polarized cells, exocytotic events appeared uniformly distributed (Letinic et al., 2009). In agreement with these observations, our live-cell TIRF experiments have shown that most of ATG9A-pHluorin events were clustered near the leading edge of polarized U87 MG cells, in non-polarized cells, while these fusion events did not show any obvious clustering and were uniformly distributed over the plasma membrane. Moreover, U87 MG cells were characterized by a high percentage of full spreading events, in which ATG9A-pHluorin proteins are totally dispersed over the plasma membrane. In contrast, HeLa cells mostly displayed non-spreading events, likely representing kiss-and-run events, where vesicles do not fuse with the plasma membrane but are recycled back. This raises the possibility that, in addition to the delivery of specific cargoes, U87 MG cells may need a more consistent reservoir of lipids in order to build and develop large lamellipodia. In this view, full spreading events may primarily deliver bulk lipids in these cells. HeLa cells do not develop such large lamellipodia and non-spreading events may be mainly useful for the delivery of specific cargo proteins rather than bulk lipids.

We found that siRNA knockdown of ATG9A markedly reduced peripheral localization of both TGN46 and $\beta 1$ integrin following chemotactic stimulation, suggesting that ATG9A protein is a general regulator of the “Golgi-to plasma membrane” trafficking. One way to address this point would be to use a method based on the expression of a temperature-sensitive mutant of the viral glycoprotein VSVG, the VSVGts045. The mutated protein, retained in the endoplasmic reticulum at a “restrictive” temperature (40 °C), can again circulate toward the plasma membrane, through the Golgi apparatus, at a “permissive” temperature (32 °C) (Presley et al., 1997). U87 MG cells, depleted or not of endogenous ATG9A, could then be transfected by a construct encoding VSVGts045 fused to eGFP and then maintained at a restrictive temperature. After transfer to the permissive temperature, we will evaluate the transport efficiency of the VSVGts045-eGFP from the ER to the Golgi, and from the Golgi to the plasma membrane, under basal conditions or following chemotactic stimulation.

The specific role of ATG9A in the polarized transport of $\beta 1$ integrin from the Golgi toward the migration front could be assessed using the *retention using selective hooks* (RUSH) system. The RUSH system is based on the reversible interaction between two proteins (Zhao et al., 2018), *i.e.* *i)* the hook, which consists in a streptavidin molecule fused to a resident protein of a specific cellular compartment and *ii)* the protein of interest fused to a *streptavidin-binding peptide* (SBP). In normal conditions, the protein of interest fused to SBP interacts with streptavidin, resulting in its retention into the specific compartment. Upon addition of biotin, which binds to streptavidin with high affinity, the protein of interest is released from the hook, allowing its synchronized re-trafficking within the cell. In our model, expression of the Golgi-resident protein GM130 fused with streptavidin could be used to “hook” an ATG9A-SBP fusion protein within the Golgi apparatus. The impact of retention of ATG9A-SBP within the Golgi, and of its release following addition of biotin, will then be

tested on relevant parameters including $\beta 1$ integrin trafficking, lamellipodia dynamics and directed cell migration.

15. ATG9A protein: a master regulator of vesicle biogenesis from the TGN?

15.1. Interaction of ATG9A with the AP complexes

A recent report demonstrated that ATG9A was required for the post-Golgi transport and maturation of lysosomal hydrolases, such as cathepsin D and L (Jia et al., 2017). This work was the first to point out a wider and non-canonical function of ATG9A, that has been proposed to function as a general regulator of vesicular trafficking. Mechanistically, Jia and colleagues found ATG9A-AP-1 interaction facilitated AP-1 association with the cathepsin receptor CIMPR, resulting in the polymerization of AP-1 and vesicle budding. Our results have demonstrated that the N-terminal AP-binding site of ATG9A was critical for the delivery of $\beta 1$ integrin at the cell front. In fact, we have demonstrated that, in ATG9A-depleted cells, overexpression of wild-type recombinant ATG9A-mCherry efficiently rescued EGF-induced delivery of $\beta 1$ integrin to the leading edge. At the contrary, a mutant ATG9A-mCherry, in which Tyrosine 8 residue of the AP-binding site was replaced by a Phenylalanine (Zhou et al., 2017), did not have the ability to rescue the relocalization of $\beta 1$ integrin toward the periphery. This result could be due to the fact that ATG9A can no longer interact with one of the two Golgi-localized AP complexes, *i.e.* AP-1 (Jia et al., 2017) or AP-4 (Ivankovic et al., 2020; Mattera et al., 2017). The use of siRNAs targeting subunits of AP-1 or AP-4 complexes, and evaluation of their effects on the exocytotic activity of ATG9A-positive vesicles at the migration front may help to answer this question.

To further understand the functional impact of the ATG9A-AP interaction, we will also try to acutely block it by the use of cell-penetrating interfering peptides. These peptides will be generated by the fusion of the AP-sorting sequence of ATG9A together with the well described cell penetrating peptide TAT (“NH₂-YGRKKRRQRRR-COOH”; (Brooks et al., 2005)). Following addition of the fusion peptide in the culture medium, we will evaluate its ability to interfere with ATG9A-pHluorin exocytotic events, lamellipodial formation and adhesion dynamics.

15.2. Interaction of ATG9A with the PI4KIII β

In addition to AP-1, it was found that ATG9A interacts with PI4KIII β , a PI4P-producing enzyme that is required for the budding of ATG9A-containing vesicles from the Golgi during autophagy induction (Judith et al., 2019). Interestingly, Golgi-localized PI4KIII β and PI4P, well-known regulators of membrane dynamics, have also been recognized as essential components of cell adhesion and migration (Bilodeau et al., 2020; Tokuda et al., 2014). Loss of the PI4KIII β pool strongly decreased cell migration and perturbed cell morphology, as well as adhesion dynamics (Bilodeau et al., 2020). Functional studies established that PI4P produced at *trans*-Golgi microdomains triggers the recruitment of *Golgi phosphoprotein 3* (GOLPH3) protein which, first, induces reorientation of the Golgi toward the leading edge and, second, the local curvature of the *trans*-Golgi membrane promoting the biogenesis of carriers and their transport to the leading edge (Buschman et al.,

2015; Rahajeng et al., 2019; Xing et al., 2016). Collectively, these data support a working model in which ATG9A, PI4KIII β and GOLPH3 may have complementary roles in the budding of pro-migratory vesicles, incorporating β 1 integrins, from the *trans*-Golgi. In order to give strength to this model, we will evaluate the impact of ATG9A knockdown on the accumulation of PI4P and recruitment of GOLPH3 at *trans*-Golgi subdomains (Figure 42).

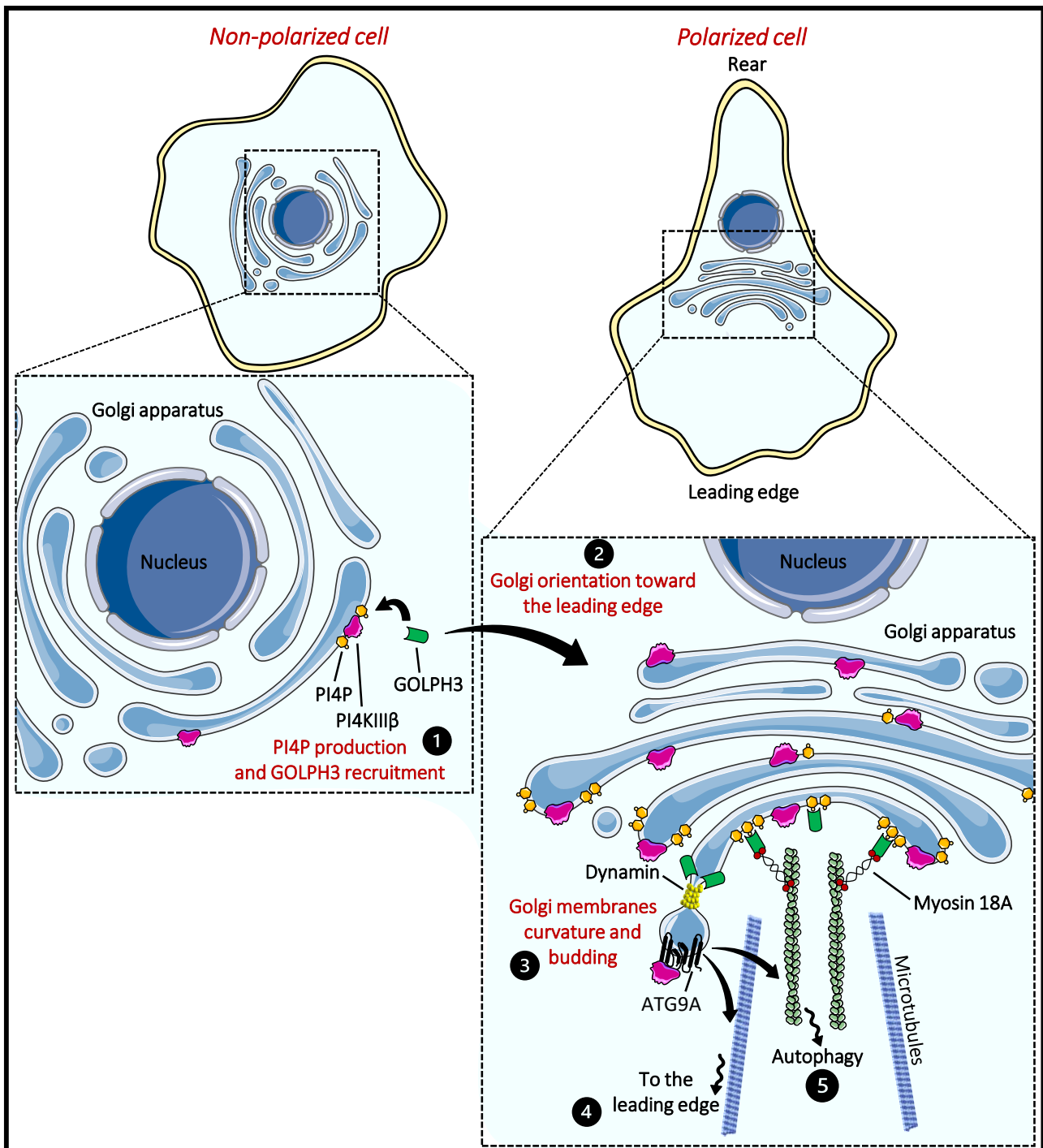


Figure 42. For caption see next page.

Figure 42. Model of ATG9A-, PI4KIII β - and GOLPH3-mediated biogenesis of vesicles from the TGN network. Interaction of ATG9A with PI4KIII β at TGN subdomains induces the production of PI4P and GOLPH3 recruitment (❶). GOLPH3 polarizes the Golgi apparatus in front the nucleus and facing the leading edge (❷) and, by inserting a hydrophobic β -loop into the bilayer, also induces curvature of the Golgi membrane (❸). Budding of vesicles, containing ATG9A, could be facilitated by other I-BAR proteins (not shown) and dynamin 2. Efficient Golgi-to-plasma membrane trafficking of ATG9A-containing vesicles may be operated by Golgi-associated fast-track microtubules (❹). ATG9A-containing vesicles may also be targeted to the phagophore *via* interaction between GOLPH3 and myosin 18A, which interacts with F-actin (❺).

It is important to take into account that GOLPH3 also plays a positive role in the regulation of autophagy. Few reports have demonstrated that depletion of GOLPH3 led to suppression of LC3B lipidation and thus autophagy inhibition. At the contrary, GOLPH3 overexpression increased LC3B lipidation and then autophagy induction (Li et al., 2016; Wang et al., 2021; Wang et al., 2019). Although the mechanistic involvement of GOLPH3 in autophagy has not been elucidated, it has been shown that GOLPH3 interacts with LC3 in different cell lines (Lu et al., 2020). It is then tempting to speculate that cooperation between ATG9A, PI4KIII β and GOLPH3 proteins may also apply for the budding of autophagic vesicles targeted to the phagophore (Figure 42). In this framework, it will be very interesting to decipher the specific mechanisms, engaged during autophagy induction or chemotactic stimulation, that may orient the trafficking of post-Golgi carriers toward the phagophore or the migration front.

15.3. Trafficking of ATG9A-positive vesicles toward the migration front: role of microtubules

Early studies have demonstrated a role for the cytoskeleton in different aspects of autophagy, especially microtubule and actin systems. For example, as described in paragraph 8.3, autophagosomes are transported along the plus-end of microtubules through an interaction between LC3 and the kinesin molecular motor, via FYCO1 and Rab7 proteins, while transport toward the minus-end of microtubules is regulated by dynactin and dynein proteins (Jordens et al., 2001; Pankiv et al., 2010; Wijdeven et al., 2016). More specifically related to our work, data from Davies and colleagues have demonstrated that RUSC2 protein facilitates the transport of ATG9A vesicles onto microtubules from the *trans*-Golgi to the cell periphery during autophagy initiation (Davies et al., 2018). They have shown that RUSC2 and ATG9A colocalize and co-precipitate, and that treatment with nocodazole prevented their peripheral localization, providing the possible mechanism by which these vesicles reach the plasma membrane (Davies et al., 2018).

Golgi-associated microtubules, as a special subgroup of microtubules, have been found to serve as fast tracks that support anterograde trafficking of post-Golgi cargoes to the leading edge (Hao et al., 2020). It has been shown that the speed of vesicles along Golgi-associated microtubules was approximately 400 nm/s (fast tracks), compared to 200 nm/s (slow tracks) for non-Golgi-associated microtubules (Hao et al., 2020). This difference relies on the fact that Golgi-associated microtubules have no intersections and directly connect the Golgi apparatus with the migration front. The non-Golgi-associated microtubules, instead, have several intersections and cover shorter distances (Hao et al., 2020). In fact, we have examined the dynamics of ATG9A-

positive vesicles, by using live-cell TIRF microscopy on cells expressing the ATG9A-mCherry fusion protein (De Pace et al., 2018). We have found that most of the motile ATG9A vesicles ($\approx 80\%$) displayed an anterograde movement from the perinuclear region toward the leading edge of polarized U87 MG cells. Although we did not estimate the trafficking speed of these vesicles, we have noticed that a very high acquisition frequency (one image every 500 millisecon) was necessary to efficiently track them. These preliminary observations suggest that ATG9A-containing vesicles preferentially use Golgi-associated microtubules for their anterograde trafficking.

What is the mechanism allowing microtubules to reach the leading edge? It has been shown that microtubules plus-ends explore the cytoplasmic area in search of cortical targets, where they can finally be stabilized. For this purpose, microtubules plus-ends interact with membrane-associated proteins, such as *microtubule-actin cross linking factor 1* (MACF1) or the *IQ-motif containing Ras GTPase-activating-like protein* (IQGAP), *via* cytoplasmic linkers which bind the microtubule tip and induce their plasma membrane “capture” (Margaron et al., 2013; Noordstra & Akhmanova, 2017; Zaoui et al., 2010). This mechanism has been demonstrated to be critical for stabilization of cell protrusions. In fact, the cytoskeleton regulator MACF1 can be recruited at the leading edge in order to capture microtubules from the perinuclear region to the plasma membrane, to form tracks on which cargos are transported (Margaron et al., 2013). Interestingly, MACF1 can also bind ELMO1 and dock180 proteins, which have been shown to have GEF activity for Rac1 in glioma and promote cell invasion (Afghani et al., 2017; Jarzynka et al., 2007). Moreover, CXCR4 activation by its ligand, CXCL12, has been reported to induce association of the receptor with ELMO1 and dock180, thus stimulating Rac1 activation at the leading edge (Li et al., 2013). Collectively, these data suggest a possible mechanism by which anterograde transport of ATG9A vesicles from the perinuclear region toward the leading edge could be governed by MACF1-dependent capture of microtubules, *via* dynamic association of MACF1 with the ELMO1:dock180:CXCR4 complex.

The IQGAP protein also represents a strong candidate that may participate to the delivery/docking of ATG9A-positive vesicles at the migration front. IQGAP, an effector of Rac1 and Cdc42, is a well-characterized cortical scaffold involved in microtubule capture at the plasma membrane during cell migration (Fukata et al., 2002). Interestingly, Claude-Taupin and colleagues have recently demonstrated the involvement of IQGAP in a non-autophagic function of ATG9A protein. They have indeed shown that ATG9A protects the plasma membrane from damage, and this function is accomplished in concert with IQGAP1 protein and components of the ESCRT system (Claude-Taupin et al., 2021). Mechanistically, the authors found that a direct interaction between IQGAP1 and ATG9A and demonstrated that depletion of IQGAP1 prevented ATG9A translocation to the plasma membrane injury site. In the context of our work, we can speculate that chemotactic stimulation may first induce the recruitment of IQGAP1 at the migration front, where it could promote the capture of Golgi-associated microtubules. Following anterograde movement of ATG9-positive vesicles along

microtubules, a specific interaction between IQGAP1 and ATG9A could ultimately facilitate the docking of the vesicles with the plasma membrane, thereby allowing exocytosis.

To better understand the mechanisms underlying the trafficking of ATG9A-positive vesicles to the leading edge, we will first perform pharmacological studies using nocodazole, a microtubule-destabilizing agent. We will then evaluate the impact of nocodazole on protrusion dynamics, as well as on the anterograde movement and the exocytosis of ATG9A-positive vesicles. The same parameters will be evaluated in a more detailed approach, by the use of interfering RNAs targeting the proteins detailed above, *i.e.* RUSC2, MACF1 and IQGAP1.

16. ATG9A and cancer cell invasion

The work done during this thesis focused on the intracellular mechanisms by which ATG9A regulates chemotactic migration in different cell lines, including highly invasive glioblastoma cells. Data obtained from this *in vitro* study may help to provide the basis for understanding how ATG9A participates in tumor invasion, *in vivo*.

Few recent reports have shown the role of ATG9A in cancer cell migration and invasion and one of these comes from Claude-Taupin and colleagues. They have shown that ATG9A is overexpressed in tissues from triple negative breast cancer, and that its loss or downregulation in the MDA-MB-231 breast cancer cell line induced inhibition of cancer cell migration and proliferation (Claude-Taupin et al., 2018). Another report described that ATG9A expression was highly induced by hypoxia in several glioblastoma cell lines, and that its depletion led to a decreased *in vitro* proliferation and delayed *in vivo* tumor growth (Rahim et al., 2017). The latest work concerns, instead, the role of ATG9B in promoting colorectal cancer invasion and metastasis, in both *in vitro* and *in vivo*, respectively. Zhong and colleagues have indeed shown that, during colorectal cancer cell migration, ATG9B transports $\beta 1$ integrin to the cell edge and promotes focal adhesions assembly by mediating an interaction between endocytosed $\beta 1$ integrin and talin 1, essential for adhesion formation (Zhong et al., 2021). Depletion of ATG9B affected $\beta 1$ integrin and talin 1 interaction and reduced focal adhesion assembly. Although they looked at ATG9B, instead of ATG9A, this study appears, surprisingly, very complementary to ours. In fact, we have shown that depletion of ATG9A totally blocked the transport of $\beta 1$ integrin toward the leading edge (Campisi et al., under revision). An important difference between Zhong's work and ours is that they did focus on vesicular trafficking and did not define where the ATG9B protein comes from. To date, the specific functions of the two orthologues of ATG9, ATG9A and ATG9B, has not been identified yet. Recent studies have reported that ATG9B is expressed in some cancers, such as cervical cancer, renal cancer and hepatocellular carcinoma (Ma et al., 2017; Tingting et al., 2019; Wang et al., 2017). Whereas, ATG9A appeared to be more expressed in breast cancer and glioblastoma (Rahim et al., 2017; Claude-Taupin et al., 2018).

General discussion and perspectives

Based on our data, several strategies could be implemented in order to evaluate the role of ATG9A during cancer cell invasion. We could first envisaged to use *cell penetrating peptides* (CPP) that have been shown to be very promising in the development of cancer treatments (Shin et al., 2014; Xie et al., 2020). These CPPs are fused to “interfering” peptide sequences, capable of blocking specific protein-protein interactions in solid tumors. By way of example, intraperitoneal administration of the TAT peptide fused to a specific domain of the connexin 43 protein, capable of interfering with the interaction between connexin 43 and the c-Src proto-oncogene, has revealed to reduce the invasiveness of GL261 glioma cells injected into the mouse brain (Jaraíz-Rodríguez et al., 2020). Based on these studies, we will generate and test, *in vivo*, the effects of chimeric “TAT-ATG9A” peptides, hoping to block the interaction of ATG9A with its different protein partners, such as subunits of the AP complexes, PI4KIII β , profilin-1, GOLPH3 or β 1 integrin. We will use a microsurgical resection xenograft model of glioblastoma (U87 MG-GFP and 42 MG-GFP) in the striatum of nude mice, a technique already widely used in our team. We will then evaluate the invasive ability of glioblastoma cells located in the resection border, by administrating a hyaluronic acid-based hydrogel containing or not the TAT-ATG9A chimeric peptide. In order to assess the ability of the TAT-ATG9A fusion peptides to cross the blood-brain barrier, we will also inject them intraperitoneally, as previously described (Jaraíz-Rodríguez et al., 2020). As bias of this strategy is that TAT-ATG9A peptides should enter the cytoplasm of all cells, both cancerous and healthy, interfering with basal levels of autophagy and thus leading to the occurrence of side effects. In order to specifically target glioblastoma cells, we will then produce and test ATG9A fusion peptides including synthetic CPPs isolated, from a screen, on their high tropism for human glioblastoma cells (data coming from the team and from COPOC Inserm Transfert, (Higa et al., 2015)).

From a clinical point of view, an analysis of data from patients with different grades of glioma obtained from *The Cancer Genome Atlas* (TCGA), allowed us to highlight the fact that strong expression of β 1 integrin, GOLPH3, profilin-1, PI4K and ATG9B proteins is a negative prognostic factor for patients (Figure 43). Although the results on ATG9A, from TCGA, are not visibly relevant, we will attempt however to confirm the interaction of the ATG9A protein with the protein partners cited above in glioblastoma cells, and we will then assess the functional impact of these interactions on lamellipodia formation and invasive mechanisms.

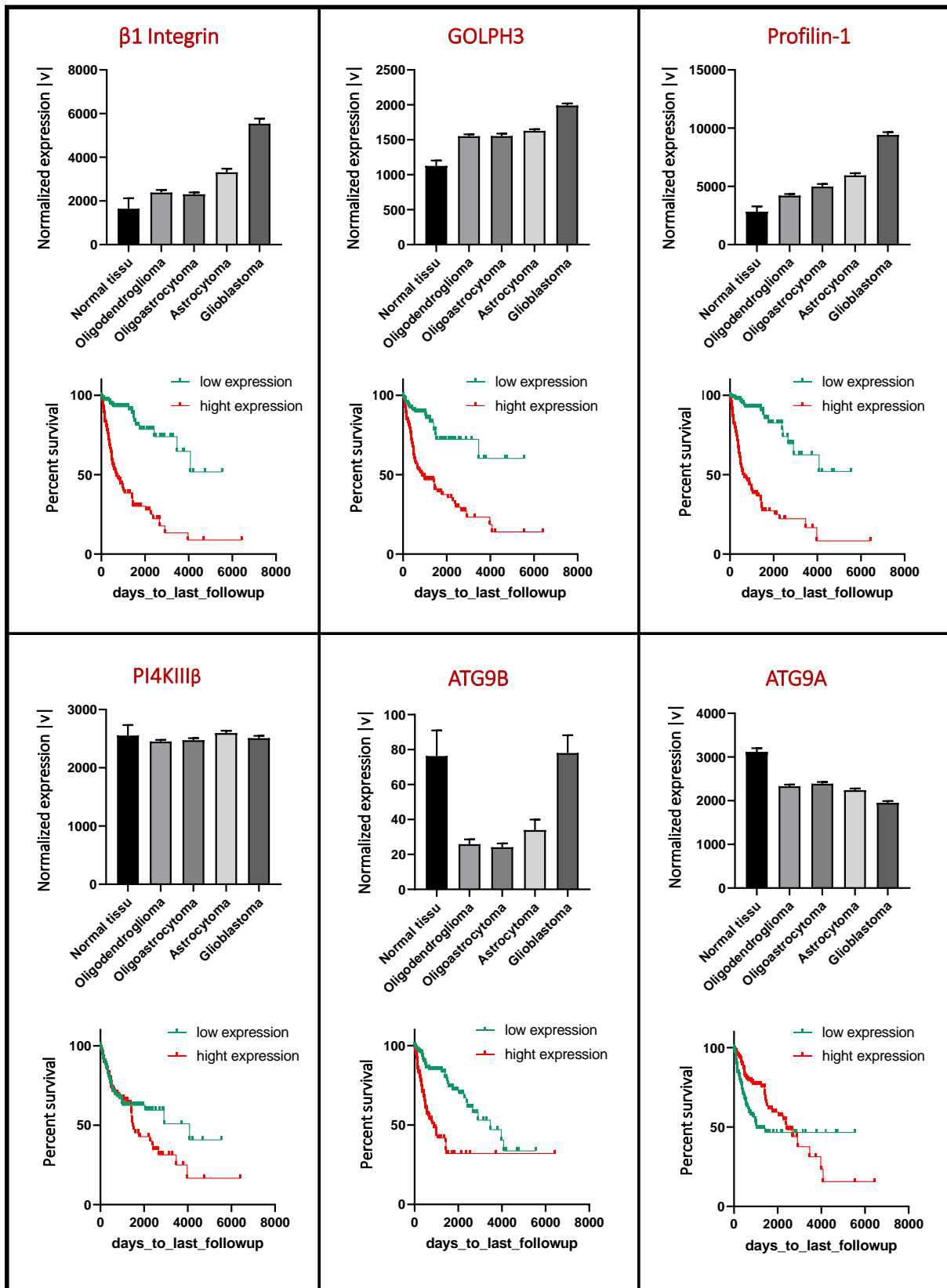


Figure 43. Clinical data from *The Cancer Genome Atlas* (TCGA). (Upper part of each panel) Gene expression levels of $\beta 1$ Integrin, GOLPH3, profilin-1, PI4KIII β , ATG9B and ATG9A in patients with different type of glioma (Oligodendroglioma, Oligoastrocytoma, Astrocytoma and Glioblastoma) compared with their expression in normal tissues. (Lower part of each panel) Survival curves of glioma patients as a function of $\beta 1$ Integrin, GOLPH3, profilin-1, PI4KIII β , ATG9B and ATG9A expression levels. These data were kindly extracted from the database and formatted by Dr. Alexandre MUTEL.

BIBLIOGRAPHICAL REFERENCES

- Abdul Rahim, S.A., A. Dirkse, A. Oudin, A. Schuster, J. Bohler, V. Barthelemy, A. Muller, L. Vallar, B. Janji, A. Golebiewska, and S.P. Niclou. 2017. Regulation of hypoxia-induced autophagy in glioblastoma involves ATG9A. *Br J Cancer*. 117:813–825. doi:10.1038/bjc.2017.263.
- Abeliovich, H., W.A. Dunn, J. Kim, and D.J. Klionsky. 2000. Dissection of autophagosome biogenesis into distinct nucleation and expansion steps. *J Cell Biol*. 151:1025–1034. doi:10.1083/jcb.151.5.1025.
- Abercrombie, M., and E.J. Ambrose. 1958. Interference microscope studies of cell contacts in tissue culture. *Experimental Cell Research*. 15:332–345. doi:10.1016/0014-4827(58)90034-X.
- Abercrombie, M., and G.A. Dunn. 1975. Adhesions of fibroblasts to substratum during contact inhibition observed by interference reflection microscopy. *Experimental Cell Research*. 92:57–62. doi:10.1016/0014-4827(75)90636-9.
- Adachi, M., T. Taki, M. Higashiyama, N. Kohno, H. Inufusa, and M. Miyake. 2000. Significance of integrin alpha5 gene expression as a prognostic factor in node-negative non-small cell lung cancer. *Clin. Cancer Res*. 6:96–101.
- Adams, A.E., D.I. Johnson, R.M. Longnecker, B.F. Sloat, and J.R. Pringle. 1990. CDC42 and CDC43, two additional genes involved in budding and the establishment of cell polarity in the yeast *Saccharomyces cerevisiae*. *J Cell Biol*. 111:131–142. doi:10.1083/jcb.111.1.131.
- Afghani, N., T. Mehta, J. Wang, N. Tang, O. Skalli, and Q.A. Quick. 2017. Microtubule actin cross-linking factor 1, a novel target in glioblastoma. *Int J Oncol*. 50:310–316. doi:10.3892/ijo.2016.3798.
- Ahmed, S., W.I. Goh, and W. Bu. 2010. I-BAR domains, IRSp53 and filopodium formation. *Semin Cell Dev Biol*. 21:350–356. doi:10.1016/j.semcdb.2009.11.008.
- Albelda, S.M., S.A. Mette, D.E. Elder, R. Stewart, L. Damjanovich, M. Herlyn, and C.A. Buck. 1990. Integrin distribution in malignant melanoma: association of the beta 3 subunit with tumor progression. *Cancer Res*. 50:6757–6764.
- Alwadej, A.H., R. Benini, A. Mahmoud, A. Alasmari, E.-J. Kamsteeg, and M. Alfadhel. 2016. Loss-of-function mutation in RUSC2 causes intellectual disability and secondary microcephaly. *Dev Med Child Neurol*. 58:1317–1322. doi:10.1111/dmcn.13250.
- Appenzeller-Herzog, C., and H.-P. Hauri. 2006. The ER-Golgi intermediate compartment (ERGIC): in search of its identity and function. *J Cell Sci*. 119:2173–2183. doi:10.1242/jcs.03019.

Bibliographical references

- Applewhite, D.A., M. Barzik, S. Kojima, T.M. Svitkina, F.B. Gertler, and G.G. Borisy. 2007. Ena/VASP proteins have an anti-capping independent function in filopodia formation. *MBoC*. 18:2579–2591. doi:10.1091/mbc.e06-11-0990.
- Arjonen, A., J. Alanko, S. Veltel, and J. Ivaska. 2012. Distinct recycling of active and inactive β 1 integrins. *Traffic*. 13:610–625. doi:10.1111/j.1600-0854.2012.01327.x.
- Ashford, T.P., and K.R. Porter. 1962. Cytoplasmic components in hepatic cell lysosomes. *J Cell Biol*. 12:198–202. doi:10.1083/jcb.12.1.198.
- Axe, E.L., S.A. Walker, M. Manifava, P. Chandra, H.L. Roderick, A. Habermann, G. Griffiths, and N.T. Ktistakis. 2008. Autophagosome formation from membrane compartments enriched in phosphatidylinositol 3-phosphate and dynamically connected to the endoplasmic reticulum. *J Cell Biol*. 182:685–701. doi:10.1083/jcb.200803137.
- Bachir, A.I., J. Zareno, K. Moissoglu, E.F. Plow, E. Gratton, and A.R. Horwitz. 2014. Integrin-associated complexes form hierarchically with variable stoichiometry in nascent adhesions. *Curr Biol*. 24:1845–1853. doi:10.1016/j.cub.2014.07.011.
- Bailly, M., F. Macaluso, M. Cammer, A. Chan, J.E. Segall, and J.S. Condeelis. 1999. Relationship between Arp2/3 complex and the barbed ends of actin filaments at the leading edge of carcinoma cells after epidermal growth factor stimulation. *J Cell Biol*. 145:331–345. doi:10.1083/jcb.145.2.331.
- Bakker, J., M. Spits, J. Neefjes, and I. Berlin. 2017. The EGFR odyssey – from activation to destruction in space and time. *J Cell Sci*. jcs.209197. doi:10.1242/jcs.209197.
- Barzik, M., T.I. Kotova, H.N. Higgs, L. Hazelwood, D. Hanein, F.B. Gertler, and D.A. Schafer. 2005. Ena/VASP proteins enhance actin polymerization in the presence of barbed end capping proteins. *J. Biol. Chem*. 280:28653–28662. doi:10.1074/jbc.M503957200.
- Bear, J.E., T.M. Svitkina, M. Krause, D.A. Schafer, J.J. Loureiro, G.A. Strasser, I.V. Maly, O.Y. Chaga, J.A. Cooper, G.G. Borisy, and F.B. Gertler. 2002. Antagonism between Ena/VASP proteins and actin filament capping regulates fibroblast motility. *Cell*. 109:509–521. doi:10.1016/S0092-8674(02)00731-6.
- Bear, J.E., Gertler, F.B. 2009. Ena/VASP: towards resolving a pointed controversy at the barbed end. *J Cell Sci*. 122(Pt 12):1947-53. doi: 10.1242/jcs.038125.
- Beckham, Y., R.J. Vasquez, J. Stricker, K. Sayegh, C. Campillo, and M.L. Gardel. 2014. Arp2/3 inhibition induces amoeboid-like protrusions in MCF10A epithelial cells by reduced cytoskeletal-membrane coupling and focal adhesion assembly. *PLoS One*. 9:e100943. doi:10.1371/journal.pone.0100943.

Bibliographical references

- Bellis, S.L., J.T. Miller, and C.E. Turner. 1995. Characterization of tyrosine phosphorylation of paxillin in vitro by focal adhesion kinase. *J Biol Chem.* 270:17437–17441. doi:10.1074/jbc.270.29.17437.
- Bello, L., M. Francolini, P. Marthyn, J. Zhang, R.S. Carroll, D.C. Nikas, J.F. Strasser, R. Villani, D.A. Cheresch, and P.McL. Black. 2001. $\alpha\beta3$ and $\alpha\beta5$ integrin expression in glioma periphery. *Neurosurgery.* 49:380–390. doi:10.1097/00006123-200108000-00022.
- Bellot, G., R. Garcia-Medina, P. Gounon, J. Chiche, D. Roux, J. Pouyssegur, and N.M. Mazure. 2009. Hypoxia-induced autophagy is mediated through hypoxia-inducible factor induction of BNIP3 and BNIP3L via their BH3 domains. *MCB.* 29:2570–2581. doi:10.1128/MCB.00166-09.
- Bhatt, A., I. Kaverina, C. Otey, and A. Huttenlocher. 2002. Regulation of focal complex composition and disassembly by the calcium-dependent protease calpain. *J Cell Sci.* 115:3415–3425.
- Bilodeau, P., D. Jacobsen, D. Law-Vinh, and J.M. Lee. 2020. Phosphatidylinositol 4-kinase III beta regulates cell shape, migration, and focal adhesion number. *MBoC.* 31:1904–1916. doi:10.1091/mbc.E19-11-0600.
- Birgisdottir, Å.B., T. Lamark, and T. Johansen. 2013. The LIR motif - crucial for selective autophagy. *J Cell Sci.* 126:3237–3247. doi:10.1242/jcs.126128.
- Bischoff, M.C., S. Lieb, R. Renkawitz-Pohl, and S. Bogdan. 2021. Filopodia-based contact stimulation of cell migration drives tissue morphogenesis. *Nat Commun.* 12:791. doi:10.1038/s41467-020-20362-2.
- Bisel, B., Y. Wang, J.-H. Wei, Y. Xiang, D. Tang, M. Miron-Mendoza, S. Yoshimura, N. Nakamura, and J. Seemann. 2008. ERK regulates Golgi and centrosome orientation towards the leading edge through GRASP65. *J Cell Biol.* 182:837–843. doi:10.1083/jcb.200805045.
- Bjorge, J.D., T.O. Chan, M. Antczak, H.J. Kung, and D.J. Fujita. 1990. Activated type I phosphatidylinositol kinase is associated with the epidermal growth factor (EGF) receptor following EGF stimulation. *Proc Natl Acad Sci USA.* 87:3816–3820. doi:10.1073/pnas.87.10.3816.
- Blagosklonny, M.V. 2010. Linking calorie restriction to longevity through sirtuins and autophagy: any role for TOR. *Cell Death Dis.* 1:e12–e12. doi:10.1038/cddis.2009.17.
- Blommaert, E.F., U. Krause, J.P. Schellens, H. Vreeling-Sindelárová, and A.J. Meijer. 1997. The phosphatidylinositol 3-kinase inhibitors wortmannin and LY294002 inhibit autophagy in isolated rat hepatocytes. *Eur J Biochem.* 243:240–246. doi:10.1111/j.1432-1033.1997.0240a.x.
- Bonifacino, J.S., and B.S. Glick. 2004. The mechanisms of vesicle budding and fusion. *Cell.* 116:153–166. doi:10.1016/S0092-8674(03)01079-1.

Bibliographical references

- Bornschlöggl, T. 2013. How filopodia pull: What we know about the mechanics and dynamics of filopodia. *Cytoskeleton*. 70:590–603. doi:10.1002/cm.21130.
- Böttcher, R.T., C. Stremmel, A. Meves, H. Meyer, M. Widmaier, H.-Y. Tseng, and R. Fässler. 2012. Sorting nexin 17 prevents lysosomal degradation of $\beta 1$ integrins by binding to the $\beta 1$ -integrin tail. *Nat Cell Biol*. 14:584–592. doi:10.1038/ncb2501.
- Bowser, D.N., and B.S. Khakh. 2007. Two forms of single-vesicle astrocyte exocytosis imaged with total internal reflection fluorescence microscopy. *Proc Natl Acad Sci USA*. 104:4212–4217. doi:10.1073/pnas.0607625104.
- Bretscher, M.S. 1996. Moving membrane up to the front of migrating cells. *Cell*. 85:465–467. doi:10.1016/S0092-8674(00)81246-5.
- Bretscher, M.S. 2008. Exocytosis provides the membrane for protrusion, at least in migrating fibroblasts. *Nat Rev Mol Cell Biol*. 9:916–916. doi:10.1038/nrm2419-c3.
- Bridgewater, R.E., J.C. Norman, and P.T. Caswell. 2012. Integrin trafficking at a glance. *J Cell Sci*. 125:3695–3701. doi:10.1242/jcs.095810.
- Brooks, H., B. Lebleu, and E. Vives. 2005. Tat peptide-mediated cellular delivery: back to basics. *Adv Drug Deliv Rev*. 57:559–577. doi:10.1016/j.addr.2004.12.001.
- Brugnera, E., L. Haney, C. Grimsley, M. Lu, S.F. Walk, A.-C. Tosello-Trampont, I.G. Macara, H. Madhani, G.R. Fink, and K.S. Ravichandran. 2002. Unconventional Rac-GEF activity is mediated through the Dock180–ELMO complex. *Nat Cell Biol*. 4:574–582. doi:10.1038/ncb824.
- Brühmann, S., D.S. Ushakov, M. Winterhoff, R.B. Dickinson, U. Curth, and J. Faix. 2017. Distinct VASP tetramers synergize in the processive elongation of individual actin filaments from clustered arrays. *Proc Natl Acad Sci USA*. 114:E5815–E5824. doi:10.1073/pnas.1703145114.
- Burke, P.M., and H.S. Wiley. 1999. Human mammary epithelial cells rapidly exchange empty EGFR between surface and intracellular pools. *J Cell Physiol*. 180:448–460. doi:10.1002/(SICI)1097-4652(199909)180:3<448::AID-JCP16>3.0.CO;2-8.
- Buschman, M.D., M. Xing, and S.J. Field. 2015. The GOLPH3 pathway regulates Golgi shape and function and is activated by DNA damage. *Front. Neurosci*. doi:10.3389/fnins.2015.00362.
- Cai, Y., N. Biais, G. Giannone, M. Tanase, G. Jiang, J.M. Hofman, C.H. Wiggins, P. Silberzan, A. Buguin, B. Ladoux, and M.P. Sheetz. 2006. Nonmuscle myosin IIA-dependent force inhibits cell spreading and drives F-actin flow. *Biophys J*. 91:3907–3920. doi:10.1529/biophysj.106.084806.

Bibliographical references

- Campellone, K.G., and M.D. Welch. 2010. A nucleator arms race: cellular control of actin assembly. *Nat Rev Mol Cell Biol.* 11:237–251. doi:10.1038/nrm2867.
- Cardoso, C.M.P., L. Groth-Pedersen, M. Høyer-Hansen, T. Kirkegaard, E. Corcelle, J.S. Andersen, M. Jäättelä, and J. Nylandsted. 2009. Depletion of Kinesin 5B affects lysosomal distribution and stability and induces perinuclear accumulation of autophagosomes in cancer cells. *PLoS ONE.* 4:e4424. doi:10.1371/journal.pone.0004424.
- Carreno, S., Å.E. Engqvist-Goldstein, C.X. Zhang, K.L. McDonald, and D.G. Drubin. 2004. Actin dynamics coupled to clathrin-coated vesicle formation at the trans-Golgi network. *J Cell Biol.* 165:781–788. doi:10.1083/jcb.200403120.
- Castellani, P., G. Viale, A. Dorcaratto, G. Nicolo, J. Kaczmarek, G. Querze, and L. Zardi. 1994. The fibronectin isoform containing the ed-b oncofetal domain: A marker of angiogenesis. *Int J Cancer.* 59:612–618. doi:10.1002/ijc.2910590507.
- Castellano, F., P. Montcourrier, J.-C. Guillemot, E. Gouin, L. Machesky, P. Cossart, and P. Chavrier. 1999. Inducible recruitment of Cdc42 or WASP to a cell-surface receptor triggers actin polymerization and filopodium formation. *Curr Biol.* 9:351–361. doi:10.1016/S0960-9822(99)80161-4.
- Caswell, P.T., and J.C. Norman. 2006. Integrin trafficking and the control of cell migration. *Traffic.* 7:14–21. doi:10.1111/j.1600-0854.2005.00362.x.
- Catalano, M., G. D'Alessandro, F. Lepore, M. Corazzari, S. Caldarola, C. Valacca, F. Faienza, V. Esposito, C. Limatola, F. Cecconi, and S. Di Bartolomeo. 2015. Autophagy induction impairs migration and invasion by reversing EMT in glioblastoma cells. *Mol Oncol.* 9:1612–1625. doi:10.1016/j.molonc.2015.04.016.
- Chan, E.Y.W., S. Kir, and S.A. Tooze. 2007. siRNA screening of the kinome identifies ULK1 as a multidomain modulator of autophagy. *J Biol Chem.* 282:25464–25474. doi:10.1074/jbc.M703663200.
- Chan, E.Y.W., A. Longatti, N.C. McKnight, and S.A. Tooze. 2009. Kinase-inactivated ULK proteins inhibit autophagy via their conserved C-terminal domains using an Atg13-independent mechanism. *Mol Cell Biol.* 29:157–171. doi:10.1128/MCB.01082-08.
- Chao, W.-T., and J. Kunz. 2009. Focal adhesion disassembly requires clathrin-dependent endocytosis of integrins. *FEBS Letters.* 583:1337–1343. doi:10.1016/j.febslet.2009.03.037.
- Chatterjee, S., B. Behnam Azad, and S. Nimmagadda. 2014. The intricate role of CXCR4 in cancer. *Adv. Cancer Res.* 124:31–82. doi:10.1016/B978-0-12-411638-2.00002-1.

Bibliographical references

- Chauhan, A.K., A. Iaconig, F.E. Baralle, and A.F. Muro. 2004. Alternative splicing of fibronectin: a mouse model demonstrates the identity of in vitro and in vivo systems and the processing autonomy of regulated exons in adult mice. *Gene*. 324:55–63. doi:10.1016/j.gene.2003.09.026.
- Chen, H., D.M. Choudhury, and S.W. Craig. 2006. Coincidence of actin filaments and talin is required to activate vinculin. *J Biol Chem*. 281:40389–40398. doi:10.1074/jbc.M607324200.
- Chen, L.-M., D. Bailey, and C. Fernandez-Valle. 2000. Association of β 1 integrin with focal adhesion kinase and paxillin in differentiating Schwann cells. *J Neurosci*. 20:3776–3784. doi:10.1523/JNEUROSCI.20-10-03776.2000.
- Chen, Z., D. Borek, S.B. Padrick, T.S. Gomez, Z. Metlagel, A.M. Ismail, J. Umetani, D.D. Billadeau, Z. Otwinowski, and M.K. Rosen. 2010. Structure and control of the actin regulatory WAVE complex. *Nature*. 468:533–538. doi:10.1038/nature09623.
- Cheng, Z.-J., J. Zhao, Y. Sun, W. Hu, Y.-L. Wu, B. Cen, G.-X. Wu, and G. Pei. 2000. β -Arrestin differentially regulates the chemokine receptor CXCR4-mediated signaling and receptor internalization, and this implicates multiple interaction sites between β -Arrestin and CXCR4. *J Biol Chem*. 275:2479–2485. doi:10.1074/jbc.275.4.2479.
- Chhabra, E.S., and H.N. Higgs. 2007. The many faces of actin: matching assembly factors with cellular structures. *Nat Cell Biol*. 9:1110–1121. doi:10.1038/ncb1007-1110.
- Chiang, H., Terlecky, C. Plant, and J. Dice. 1989. A role for a 70-kilodalton heat shock protein in lysosomal degradation of intracellular proteins. *Science*. 246:382–385. doi:10.1126/science.2799391.
- Chiang, H.L., and J.F. Dice. 1988. Peptide sequences that target proteins for enhanced degradation during serum withdrawal. *J Biol Chem*. 263:6797–6805.
- Choi, C.K., M. Vicente-Manzanares, J. Zareno, L.A. Whitmore, A. Mogilner, and A.R. Horwitz. 2008. Actin and α -actinin orchestrate the assembly and maturation of nascent adhesions in a myosin II motor-independent manner. *Nat Cell Biol*. 10:1039–1050. doi:10.1038/ncb1763.
- Clark, S.L. 1957. Cellular differentiation in the kidneys of newborn mice studies with the electron microscope. *J Biophys Biochem Cytol*. 3:349–362. doi:10.1083/jcb.3.3.349.
- Claude-Taupin, A., L. Fonderflick, T. Gauthier, L. Mansi, J.-R. Pallandre, C. Borg, V. Perez, F. Monnien, M.-P. Algros, M. Vigneron, P. Adami, R. Delage-Mourroux, P. Peixoto, M. Herfs, M. Boyer-Guittaut, and E. Hervouet. 2018. ATG9A Is overexpressed in triple negative breast cancer and its In vitro extinction leads to the inhibition of pro-cancer phenotypes. *Cells*. 7:248. doi:10.3390/cells7120248.

Bibliographical references

- Claude-Taupin, A., J. Jia, Z. Bhujabal, M. Garfa-Traoré, S. Kumar, G.P.D. da Silva, R. Javed, Y. Gu, L. Allers, R. Peters, F. Wang, L.J. da Costa, S. Pallikkuth, K.A. Lidke, M. Mauthe, P. Verlhac, Y. Uchiyama, M. Salemi, B. Phinney, S.A. Tooze, M.C. Mari, T. Johansen, F. Reggiori, and V. Deretic. 2021. ATG9A protects the plasma membrane from programmed and incidental permeabilization. *Nat Cell Biol.* 23:846–858. doi:10.1038/s41556-021-00706-w.
- Colella, B., F. Faienza, and S. Di Bartolomeo. 2019. EMT regulation by autophagy: a new perspective in glioblastoma biology. *Cancers.* 11:312. doi:10.3390/cancers11030312.
- Coly, P.-M., P. Gandolfo, H. Castel, and F. Morin. 2017. The autophagy machinery: a new player in chemotactic cell migration. *Front. Neurosci.* doi:10.3389/fnins.2017.00078.
- Coly, P.-M., N. Perzo, V. Le Joncour, C. Lecointre, M.-T. Schouft, L. Desrues, M.-C. Tonon, O. Wurtz, P. Gandolfo, H. Castel, and F. Morin. 2016. Chemotactic G protein-coupled receptors control cell migration by repressing autophagosome biogenesis. *Autophagy.* 12:2344–2362. doi:10.1080/15548627.2016.1235125.
- Conti, F.J., S.J. Monkley, M.R. Wood, D.R. Critchley, and U. Muller. 2009. Talin 1 and 2 are required for myoblast fusion, sarcomere assembly and the maintenance of myotendinous junctions. *Development.* 136:3597–3606. doi:10.1242/dev.035857.
- Cook, S., and F. McCormick. 1993. Inhibition by cAMP of Ras-dependent activation of Raf. *Science.* 262:1069–1072. doi:10.1126/science.7694367.
- Coombs, C., A. Georgantzoglou, H.A. Walker, J. Patt, N. Merten, H. Poplimont, E.M. Busch-Nentwich, S. Williams, C. Kotsi, E. Kostenis, and M. Sarris. 2019. Chemokine receptor trafficking coordinates neutrophil clustering and dispersal at wounds in zebrafish. *Nat Commun.* 10:5166. doi:10.1038/s41467-019-13107-3.
- Cuervo, A.M., and J.F. Dice. 1996. A receptor for the selective uptake and degradation of proteins by lysosomes. *Science.* 273:501–503. doi:10.1126/science.273.5274.501.
- Cuervo, A.M., and J.F. Dice. 2000. Regulation of Lamp2a levels in the lysosomal membrane. *Traffic.* 1:570–583. doi:10.1034/j.1600-0854.2000.010707.x.
- Damiano-Guercio, J., L. Kurzawa, J. Mueller, G. Dimchev, M. Schaks, M. Nemethova, T. Pokrant, S. Brühmann, J. Linkner, L. Blanchoin, M. Sixt, K. Rottner, and J. Faix. 2020. Loss of Ena/VASP interferes with lamellipodium architecture, motility and integrin-dependent adhesion. *eLife.* 9:e55351. doi:10.7554/eLife.55351.
- Damme, M., T. Suntio, P. Saftig, and E.-L. Eskelinen. 2015. Autophagy in neuronal cells: general principles and physiological and pathological functions. *Acta Neuropathol.* 129:337–362. doi:10.1007/s00401-014-1361-4.

Bibliographical references

- Davies, A.K., D.N. Itzhak, J.R. Edgar, T.L. Archuleta, J. Hirst, L.P. Jackson, M.S. Robinson, and G.H.H. Borner. 2018. AP-4 vesicles contribute to spatial control of autophagy via RUSC-dependent peripheral delivery of ATG9A. *Nat Commun.* 9:3958. doi:10.1038/s41467-018-06172-7.
- De Franceschi, N., A. Arjonen, N. Elkhatib, K. Denessiouk, A.G. Wrobel, T.A. Wilson, J. Pouwels, G. Montagnac, D.J. Owen, and J. Ivaska. 2016. Selective integrin endocytosis is driven by interactions between the integrin α -chain and AP2. *Nat Struct Mol Biol.* 23:172–179. doi:10.1038/nsmb.3161.
- De Pace, R., M. Skirzewski, M. Damme, R. Mattera, J. Mercurio, A.M. Foster, L. Cuitino, M. Jarnik, V. Hoffmann, H.D. Morris, T.-U. Han, G.M.S. Mancini, A. Buonanno, and J.S. Bonifacino. 2018. Altered distribution of ATG9A and accumulation of axonal aggregates in neurons from a mouse model of AP-4 deficiency syndrome. *PLoS Genet.* 14:e1007363. doi:10.1371/journal.pgen.1007363.
- De Tito, S., J.H. Hervás, A.R. van Vliet, and S.A. Tooze. 2020. The Golgi as an assembly line to the autophagosome. *Trends Biochem Sci.* 45:484–496. doi:10.1016/j.tibs.2020.03.010.
- Deakin, N.O., and C.E. Turner. 2008. Paxillin comes of age. *J Cell Sci.* 121:2435–2444. doi:10.1242/jcs.018044.
- Degenhardt, K., R. Mathew, B. Beaudoin, K. Bray, D. Anderson, G. Chen, C. Mukherjee, Y. Shi, C. Gélinas, Y. Fan, D.A. Nelson, S. Jin, and E. White. 2006. Autophagy promotes tumor cell survival and restricts necrosis, inflammation, and tumorigenesis. *Cancer Cell.* 10:51–64. doi:10.1016/j.ccr.2006.06.001.
- Demeter, A., M.C. Romero-Mulero, L. Csabai, M. Ölbei, P. Sudhakar, W. Haerty, and T. Korcsmáros. 2020. ULK1 and ULK2 are less redundant than previously thought: computational analysis uncovers distinct regulation and functions of these autophagy induction proteins. *Sci Rep.* 10:10940. doi:10.1038/s41598-020-67780-2.
- Dent, E.W., A.V. Kwiatkowski, L.M. Mebane, U. Philippar, M. Barzik, D.A. Rubinson, S. Gupton, J.E. Van Veen, C. Furman, J. Zhang, A.S. Alberts, S. Mori, and F.B. Gertler. 2007. Filopodia are required for cortical neurite initiation. *Nat Cell Biol.* 9:1347–1359. doi:10.1038/ncb1654.
- Deter, R.L., P. Baudhuin, and C. De Duve. 1967. Participation of lysosomes in cellular autophagy induced in rat liver by glucagon. *J Cell Biol.* 35:C11-16. doi:10.1083/jcb.35.2.c11.
- Di Bartolomeo, S., M. Corazzari, F. Nazio, S. Oliverio, G. Lisi, M. Antonioli, V. Pagliarini, S. Matteoni, C. Fuoco, L. Giunta, M. D’Amelio, R. Nardacci, A. Romagnoli, M. Piacentini, F. Cecconi, and G.M. Fimia. 2010. The dynamic interaction of AMBRA1 with the dynein motor complex regulates mammalian autophagy. *J Cell Biol.* 191:155–168. doi:10.1083/jcb.201002100.
- Di Lullo, G.A., S.M. Sweeney, J. Körkkö, L. Ala-Kokko, and J.D. San Antonio. 2002. Mapping the ligand-binding sites and disease-associated mutations on the most abundant protein in the human, type I collagen. *J Biol Chem.* 277:4223–4231. doi:10.1074/jbc.M110709200.

Bibliographical references

- Díaz, Ma.E., L. González, J.G. Miquet, C.S. Martínez, A.I. Sotelo, A. Bartke, and D. Turyn. 2012. Growth hormone modulation of EGF-induced PI3K-Akt pathway in mice liver. *Cell Signal.* 24:514–523. doi:10.1016/j.cellsig.2011.10.001.
- Dikic, I., and Z. Elazar. 2018. Mechanism and medical implications of mammalian autophagy. *Nat Rev Mol Cell Biol.* 19:349–364. doi:10.1038/s41580-018-0003-4.
- Dong, J., B. Radau, A. Otto, E.-C. Müller, C. Lindschau, and P. Westermann. 2000. Profilin I attached to the Golgi is required for the formation of constitutive transport vesicles at the trans-Golgi network. *Biochim Biophys,* 1497:253–260. doi:10.1016/S0167-4889(00)00056-2.
- Dooley, H.C., M. Razi, H.E.J. Polson, S.E. Girardin, M.I. Wilson, and S.A. Tooze. 2014. WIPI2 links LC3 conjugation with PI3P, autophagosome formation, and pathogen clearance by recruiting Atg12-5-16L1. *Mol Cell.* 55:238–252. doi:10.1016/j.molcel.2014.05.021.
- Dower, C.M., N. Bhat, E.W. Wang, and H.-G. Wang. 2017. Selective reversible inhibition of autophagy in hypoxic breast cancer cells promotes pulmonary metastasis. *Cancer Res.* 77:646–657. doi:10.1158/0008-5472.CAN-15-3458.
- Du, X., T.C. Saido, S. Tsubuki, F.E. Indig, M.J. Williams, and M.H. Ginsberg. 1995. Calpain Cleavage of the Cytoplasmic Domain of the Integrin β 2 Subunit. *J Biol Chem.* 270:26146–26151. doi:10.1074/jbc.270.44.26146.
- Dupont, N., S. Jiang, M. Pilli, W. Ornatowski, D. Bhattacharya, and V. Deretic. 2011. Autophagy-based unconventional secretory pathway for extracellular delivery of IL-1 β : Autophagy-based unconventional secretory pathway. *EMBO J.* 30:4701–4711. doi:10.1038/emboj.2011.398.
- de Duve, C. 1967. Lysosomes and phagosomes: the vacuolar apparatus. *Protoplasma.* 63:95–98. doi:10.1007/BF01248009.
- de Duve, C., B.C. Pressman, R. Gianetto, R. Wattiaux, and F. Appelmans. 1955. Tissue fractionation studies. 6. Intracellular distribution patterns of enzymes in rat-liver tissue. *Biochem J.* 60:604–617. doi:10.1042/bj0600604.
- Dyczynski, M., Y. Yu, M. Otrocka, S. Parpal, T. Braga, A.B. Henley, H. Zazzi, M. Lerner, K. Wennerberg, J. Viklund, J. Martinsson, D. Grandér, A. De Milito, and K. Pokrovskaja Tamm. 2018. Targeting autophagy by small molecule inhibitors of vacuolar protein sorting 34 (Vps34) improves the sensitivity of breast cancer cells to Sunitinib. *Cancer Letters.* 435:32–43. doi:10.1016/j.canlet.2018.07.028.
- Egan, D.F., M.G.H. Chun, M. Vamos, H. Zou, J. Rong, C.J. Miller, H.J. Lou, D. Raveendra-Panickar, C.-C. Yang, D.J. Sheffler, P. Teriete, J.M. Asara, B.E. Turk, N.D.P. Cosford, and R.J. Shaw. 2015. Small molecule inhibition of the

Bibliographical references

- autophagy kinase ULK1 and identification of ULK1 substrates. *Mol Cell*. 59:285–297. doi:10.1016/j.molcel.2015.05.031.
- Egan, D.F., D.B. Shackelford, M.M. Mihaylova, S. Gelino, R.A. Kohnz, W. Mair, D.S. Vasquez, A. Joshi, D.M. Gwinn, R. Taylor, J.M. Asara, J. Fitzpatrick, A. Dillin, B. Viollet, M. Kundu, M. Hansen, and R.J. Shaw. 2011. Phosphorylation of ULK1 (hATG1) by AMP-activated protein kinase connects energy sensing to mitophagy. *Science*. 331:456–461. doi:10.1126/science.1196371.
- Eskelinen, E.-L. 2019. Autophagy: Supporting cellular and organismal homeostasis by self-eating. *Int J Biochem Cell Biol*. 111:1–10. doi:10.1016/j.biocel.2019.03.010.
- Eskova, A., B. Knapp, D. Matelska, S. Reusing, A. Arjonen, T. Lisauskas, R. Pepperkok, R. Russell, R. Eils, J. Ivaska, L. Kaderali, H. Erfle, and V. Starkuviene. 2014. RNAi screen identifies KIF15 as a novel regulator of integrin endocytic trafficking. *J Cell Sci*. jcs.137281. doi:10.1242/jcs.137281.
- Etienne-Manneville, S. 2008. Polarity proteins in migration and invasion. *Oncogene*. 27:6970–6980. doi:10.1038/onc.2008.347.
- Ezratty, E.J., C. Bertaux, E.E. Marcantonio, and G.G. Gundersen. 2009. Clathrin mediates integrin endocytosis for focal adhesion disassembly in migrating cells. *J Cell Biol*. 187:733–747. doi:10.1083/jcb.200904054.
- Ezratty, E.J., M.A. Partridge, and G.G. Gundersen. 2005. Microtubule-induced focal adhesion disassembly is mediated by dynamin and focal adhesion kinase. *Nat Cell Biol*. 7:581–590. doi:10.1038/ncb1262.
- Faix, J., and K. Rottner. 2006. The making of filopodia. *Curr Opin Cell Biol*. 18:18–25. doi:10.1016/j.ceb.2005.11.002.
- Farré, J.-C., and S. Subramani. 2004. Peroxisome turnover by micropexophagy: an autophagy-related process. *Trends Cell Biol*. 14:515–523. doi:10.1016/j.tcb.2004.07.014.
- Feng, Y., D. He, Z. Yao, and D.J. Klionsky. 2014. The machinery of macroautophagy. *Cell Res*. 24:24–41. doi:10.1038/cr.2013.168.
- Fletcher, S.J., and J.Z. Rappoport. 2010. Moving forward: polarised trafficking in cell migration. *Trends Cell Biol*. 20:71–78. doi:10.1016/j.tcb.2009.11.006.
- Fong, A.M., R.T. Premont, R.M. Richardson, Y.-R.A. Yu, R.J. Lefkowitz, and D.D. Patel. 2002. Defective lymphocyte chemotaxis in -arrestin2- and GRK6-deficient mice. *Proc Natl Acad Sci USA*. 99:7478–7483. doi:10.1073/pnas.112198299.
- Franco, S., B. Perrin, and A. Huttenlocher. 2004. Isoform specific function of calpain 2 in regulating membrane protrusion. *Exp Cell Res*. 299:179–187. doi:10.1016/j.yexcr.2004.05.021.

Bibliographical references

- Franke, T.F., S.-I. Yang, T.O. Chan, K. Datta, A. Kazlauskas, D.K. Morrison, D.R. Kaplan, and P.N. Tsichlis. 1995. The protein kinase encoded by the Akt proto-oncogene is a target of the PDGF-activated phosphatidylinositol 3-kinase. *Cell*. 81:727–736. doi:10.1016/0092-8674(95)90534-0.
- Frieboes, H.B., J.S. Huang, W.C. Yin, and L.R. McNally. 2014. Chloroquine-mediated cell death in metastatic pancreatic adenocarcinoma through inhibition of autophagy. *JOP*. Vol 15:189-197 Pages. doi:10.6092/1590-8577/1900.
- Friedl, P., and D. Gilmour. 2009. Collective cell migration in morphogenesis, regeneration and cancer. *Nat Rev Mol Cell Biol*. 10:445–457. doi:10.1038/nrm2720.
- Fukata, M., T. Watanabe, J. Noritake, M. Nakagawa, M. Yamaga, S. Kuroda, Y. Matsuura, A. Iwamatsu, F. Perez, and K. Kaibuchi. 2002. Rac1 and Cdc42 Capture Microtubules through IQGAP1 and CLIP-170. *Cell*. 109:873–885. doi:10.1016/S0092-8674(02)00800-0.
- Funamoto, S., R. Meili, S. Lee, L. Parry, and R.A. Firtel. 2002. Spatial and temporal regulation of 3-phosphoinositides by PI 3-kinase and PTEN mediates chemotaxis. *Cell*. 109:611–623. doi:10.1016/S0092-8674(02)00755-9.
- Fuqua, J.D., C.P. Mere, A. Kronemberger, J. Blomme, D. Bae, K.D. Turner, M.P. Harris, E. Scudese, M. Edwards, S.M. Ebert, L.G.O. de Sousa, S.C. Bodine, L. Yang, C.M. Adams, and V.A. Lira. 2019. ULK2 is essential for degradation of ubiquitinated protein aggregates and homeostasis in skeletal muscle. *FASEB J*. 33:11735–11745. doi:10.1096/fj.201900766R.
- Gabel, M., and S. Chasserot-Golaz. 2016. Annexin A2, an essential partner of the exocytotic process in chromaffin cells. *J. Neurochem*. 137:890–896. doi:10.1111/jnc.13628.
- Galbraith, C.G., K.M. Yamada, and M.P. Sheetz. 2002. The relationship between force and focal complex development. *J Cell Biol*. 159:695–705. doi:10.1083/jcb.200204153.
- Galli, T., A. Zahraoui, V.V. Vaidyanathan, G. Raposo, J.M. Tian, M. Karin, H. Niemann, and D. Louvard. 1998. A novel tetanus neurotoxin-insensitive vesicle-associated membrane protein in SNARE complexes of the apical plasma membrane of epithelial cells. *MBoC*. 9:1437–1448. doi:10.1091/mbc.9.6.1437.
- Galluzzi, L., F. Pietrocola, B. Levine, and G. Kroemer. 2014. Metabolic control of autophagy. *Cell*. 159:1263–1276. doi:10.1016/j.cell.2014.11.006.
- Ganley, I.G., D.H. Lam, J. Wang, X. Ding, S. Chen, and X. Jiang. 2009. ULK1.ATG13.FIP200 complex mediates mTOR signaling and is essential for autophagy. *J Biol Chem*. 284:12297–12305. doi:10.1074/jbc.M900573200.
- García-Fernández, M., P. Karras, A. Checinska, E. Cañón, G.T. Calvo, G. Gómez-López, M. Cifdaloz, A. Colmenar, L. Espinosa-Hevia, D. Olmeda, and M.S. Soengas. 2016. Metastatic risk and resistance to BRAF inhibitors in

Bibliographical references

- melanoma defined by selective allelic loss of ATG5. *Autophagy*. 12:1776–1790. doi:10.1080/15548627.2016.1199301.
- Gardel, M.L., I.C. Schneider, Y. Aratyn-Schaus, and C.M. Waterman. 2010. Mechanical integration of actin and adhesion dynamics in cell migration. *Annu. Rev. Cell Dev. Biol.* 26:315–333. doi:10.1146/annurev.cellbio.011209.122036.
- Ge, L., D. Melville, M. Zhang, and R. Schekman. 2013. The ER–Golgi intermediate compartment is a key membrane source for the LC3 lipidation step of autophagosome biogenesis. *eLife*. 2:e00947. doi:10.7554/eLife.00947.
- Giancotti, F.G. 1999. Integrin signaling. *Science*. 285:1028–1033. doi:10.1126/science.285.5430.1028.
- Giannone, G., B.J. Dubin-Thaler, O. Rossier, Y. Cai, O. Chaga, G. Jiang, W. Beaver, H.-G. Döbereiner, Y. Freund, G. Borisy, and M.P. Sheetz. 2007. Lamellipodial actin mechanically links myosin activity with adhesion-site formation. *Cell*. 128:561–575. doi:10.1016/j.cell.2006.12.039.
- Gilmore, A.P., and K. Burridge. 1996. Regulation of vinculin binding to talin and actin by phosphatidyl-inositol-4-5-bisphosphate. *Nature*. 381:531–535. doi:10.1038/381531a0.
- Glen, H., S. Mason, H. Patel, K. Macleod, and V.G. Brunton. 2011. E7080, a multi-targeted tyrosine kinase inhibitor suppresses tumor cell migration and invasion. *BMC Cancer*. 11:309. doi:10.1186/1471-2407-11-309.
- Goh, W.I., K.B. Lim, T. Sudhakaran, K.P. Sem, W. Bu, A.M. Chou, and S. Ahmed. 2012. mDia1 and WAVE2 proteins interact directly with IRSp53 in filopodia and are involved in filopodium formation. *J. Biol. Chem.* 287:4702–4714. doi:10.1074/jbc.M111.305102.
- Gordon, P.B., and P.O. Seglen. 1988. Prelysosomal convergence of autophagic and endocytic pathways. *Biochem Biophys Res Commun*. 151:40–47. doi:10.1016/0006-291X(88)90556-6.
- Grassi, G., G. Di Caprio, L. Santangelo, G.M. Fimia, A.M. Cozzolino, M. Komatsu, G. Ippolito, M. Tripodi, and T. Alonzi. 2015. Autophagy regulates hepatocyte identity and epithelial-to-mesenchymal and mesenchymal-to-epithelial transitions promoting Snail degradation. *Cell Death Dis.* 6:e1880–e1880. doi:10.1038/cddis.2015.249.
- Grill, F.D., L.M. Ritschl, F.X. Bauer, A. Rau, D. Gau, M. Roth, M. Eblenkamp, K.-D. Wolff, and D.J. Loeffelbein. 2018. A semi-automated virtual workflow solution for the design and production of intraoral molding plates using additive manufacturing: the first clinical results of a pilot-study. *Sci Rep*. 8:11845. doi:10.1038/s41598-018-29959-6.

Bibliographical references

- Guardia, C.M., X.-F. Tan, T. Lian, M.S. Rana, W. Zhou, E.T. Christenson, A.J. Lowry, J.D. Faraldo-Gómez, J.S. Bonifacino, J. Jiang, and A. Banerjee. 2020. Structure of human ATG9A, the only transmembrane protein of the core autophagy machinery. *Cell Reports*. 31:107837. doi:10.1016/j.celrep.2020.107837.
- Guillou, H., A. Depraz-Depland, E. Planus, B. Vianay, J. Chaussy, A. Grichine, C. Albigès-Rizo, and M.R. Block. 2008. Lamellipodia nucleation by filopodia depends on integrin occupancy and downstream Rac1 signaling. *Exp Cell Res*. 314:478–488. doi:10.1016/j.yexcr.2007.10.026.
- Guo, J.Y., G. Karsli-Uzunbas, R. Mathew, S.C. Aisner, J.J. Kamphorst, A.M. Strohecker, G. Chen, S. Price, W. Lu, X. Teng, E. Snyder, U. Santanam, R.S. DiPaola, T. Jacks, J.D. Rabinowitz, and E. White. 2013. Autophagy suppresses progression of K-ras-induced lung tumors to oncocytomas and maintains lipid homeostasis. *Genes Dev*. 27:1447–1461. doi:10.1101/gad.219642.113.
- Guo, J.Y., and E. White. 2013. Autophagy is required for mitochondrial function, lipid metabolism, growth, and fate of KRAS G12D -driven lung tumors. *Autophagy*. 9:1636–1638. doi:10.4161/auto.26123.
- Gupton, S.L., and F.B. Gertler. 2007. Filopodia: The fingers that do the walking. *Science's STKE*. 2007:re5–re5. doi:10.1126/stke.4002007re5.
- Gwinn, D.M., D.B. Shackelford, D.F. Egan, M.M. Mihaylova, A. Mery, D.S. Vasquez, B.E. Turk, and R.J. Shaw. 2008. AMPK phosphorylation of raptor mediates a metabolic checkpoint. *Mol Cell*. 30:214–226. doi:10.1016/j.molcel.2008.03.003.
- Haas, P., and D. Gilmour. 2006. Chemokine signaling mediates self-organizing tissue migration in the zebrafish lateral line. *Developmental Cell*. 10:673–680. doi:10.1016/j.devcel.2006.02.019.
- Hailey, D.W., A.S. Rambold, P. Satpute-Krishnan, K. Mitra, R. Sougrat, P.K. Kim, and J. Lippincott-Schwartz. 2010. Mitochondria supply membranes for autophagosome biogenesis during starvation. *Cell*. 141:656–667. doi:10.1016/j.cell.2010.04.009.
- Hallberg, B., S.I. Rayter, and J. Downward. 1994. Interaction of Ras and Raf in intact mammalian cells upon extracellular stimulation. *J Biol Chem*. 269:3913–3916.
- Hamasaki, M., N. Furuta, A. Matsuda, A. Nezu, A. Yamamoto, N. Fujita, H. Oomori, T. Noda, T. Haraguchi, Y. Hiraoka, A. Amano, and T. Yoshimori. 2013. Autophagosomes form at ER-mitochondria contact sites. *Nature*. 495:389–393. doi:10.1038/nature11910.
- Han, J., K. Pluhackova, and R.A. Böckmann. 2017. The multifaceted role of SNARE proteins in membrane fusion. *Front. Physiol*. doi:10.3389/fphys.2017.00005.

Bibliographical references

- Hanada, T., N.N. Noda, Y. Satomi, Y. Ichimura, Y. Fujioka, T. Takao, F. Inagaki, and Y. Ohsumi. 2007. The Atg12-Atg5 conjugate has a novel E3-like activity for protein lipidation in autophagy. *J Biol Chem.* 282:37298–37302. doi:10.1074/jbc.C700195200.
- Hansen, S.D., and R.D. Mullins. 2010. VASP is a processive actin polymerase that requires monomeric actin for barbed end association. *J Cell Biol.* 191:571–584. doi:10.1083/jcb.201003014.
- Hao, H., J. Niu, B. Xue, Q.P. Su, M. Liu, J. Yang, J. Qin, S. Zhao, C. Wu, and Y. Sun. 2020. Golgi-associated microtubules are fast cargo tracks and required for persistent cell migration. *EMBO Rep.* 21. doi:10.15252/embr.201948385.
- Hara, T., K. Nakamura, M. Matsui, A. Yamamoto, Y. Nakahara, R. Suzuki-Migishima, M. Yokoyama, K. Mishima, I. Saito, H. Okano, and N. Mizushima. 2006. Suppression of basal autophagy in neural cells causes neurodegenerative disease in mice. *Nature.* 441:885–889. doi:10.1038/nature04724.
- Hartwig, J.H., K.A. Chambers, K.L. Hopcia, and D.J. Kwiatkowski. 1989. Association of profilin with filament-free regions of human leukocyte and platelet membranes and reversible membrane binding during platelet activation. *J Cell Biol.* 109:1571–1579. doi:10.1083/jcb.109.4.1571.
- Hayashi-Nishino, M., N. Fujita, T. Noda, A. Yamaguchi, T. Yoshimori, and A. Yamamoto. 2010. Electron tomography reveals the endoplasmic reticulum as a membrane source for autophagosome formation. *Autophagy.* 6:301–303. doi:10.4161/auto.6.2.11134.
- He, C., R. Sumpter, Jr., and B. Levine. 2012. Exercise induces autophagy in peripheral tissues and in the brain. *Autophagy.* 8:1548–1551. doi:10.4161/auto.21327.
- He, L., X.-S. Wu, R. Mohan, and L.-G. Wu. 2006. Two modes of fusion pore opening revealed by cell-attached recordings at a synapse. *Nature.* 444:102–105. doi:10.1038/nature05250.
- Heckman, C.A., and H.K. Plummer. 2013. Filopodia as sensors. *Cell Signal.* 25:2298–2311. doi:10.1016/j.cellsig.2013.07.006.
- Helle, S.C.J., G. Kanfer, K. Kolar, A. Lang, A.H. Michel, and B. Kornmann. 2013. Organization and function of membrane contact sites. *Biochim Biophys Acta.* 1833:2526–2541. doi:10.1016/j.bbamcr.2013.01.028.
- Herbst, R.S. 2004. Review of epidermal growth factor receptor biology. *Int J Radiat Oncol Biol Phys.* 59:S21–S26. doi:10.1016/j.ijrobp.2003.11.041.
- Higa, M., C. Katagiri, C. Shimizu-Okabe, T. Tsumuraya, M. Sunagawa, M. Nakamura, S. Ishiuchi, C. Takayama, E. Kondo, and M. Matsushita. 2015. Identification of a novel cell-penetrating peptide targeting human glioblastoma cell lines as a cancer-homing transporter. *Biochem Biophys Res Commun.* 457:206–212. doi:10.1016/j.bbrc.2014.12.089.

Bibliographical references

- Hikita, H., S. Sakane, and T. Takehara. 2018. Mechanisms of the autophagosome-lysosome fusion step and its relation to non-alcoholic fatty liver disease. *Liver Research*. 2:120–124. doi:10.1016/j.livres.2018.09.003.
- Hirata, H., H. Tatsumi, C.T. Lim, and M. Sokabe. 2014. Force-dependent vinculin binding to talin in live cells: a crucial step in anchoring the actin cytoskeleton to focal adhesions. *Am J Physiol Cell Physiol*. 306:C607–C620. doi:10.1152/ajpcell.00122.2013.
- Ho, E., and L. Dagnino. 2012. Epidermal growth factor induction of front–rear polarity and migration in keratinocytes is mediated by integrin-linked kinase and ELMO2. *MBoC*. 23:492–502. doi:10.1091/mbc.e11-07-0596.
- Honegger, A.M., R.M. Kris, A. Ullrich, and J. Schlessinger. 1989. Evidence that autophosphorylation of solubilized receptors for epidermal growth factor is mediated by intermolecular cross-phosphorylation. *Proc Natl Acad Sci USA*. 86:925–929. doi:10.1073/pnas.86.3.925.
- Hosokawa, N., T. Hara, T. Kaizuka, C. Kishi, A. Takamura, Y. Miura, S. Iemura, T. Natsume, K. Takehana, N. Yamada, J.-L. Guan, N. Oshiro, and N. Mizushima. 2009a. Nutrient-dependent mTORC1 Association with the ULK1–Atg13–FIP200 Complex Required for Autophagy. *MBoC*. 20:1981–1991. doi:10.1091/mbc.e08-12-1248.
- Hosokawa, N., T. Sasaki, S. Iemura, T. Natsume, T. Hara, and N. Mizushima. 2009b. Atg101, a novel mammalian autophagy protein interacting with Atg13. *Autophagy*. 5:973–979. doi:10.4161/auto.5.7.9296.
- Hsieh, C.-Y., P.-C. Tsai, C.-H. Tseng, Y. Chen, L.-S. Chang, and S.-R. Lin. 2013. Inhibition of EGF/EGFR activation with naphtho[1,2-b]furan-4,5-dione blocks migration and invasion of MDA-MB-231 cells. *Toxicol in Vitro*. 27:1–10. doi:10.1016/j.tiv.2012.10.001.
- Huang, C., K. Jacobson, and M.D. Schaller. 2004. MAP kinases and cell migration. *J Cell Sci*. 117:4619–4628. doi:10.1242/jcs.01481.
- Huang, X., H.-M. Bai, L. Chen, B. Li, and Y.-C. Lu. 2010. Reduced expression of LC3B-II and Beclin 1 in glioblastoma multiforme indicates a down-regulated autophagic capacity that relates to the progression of astrocytic tumors. *J Clin Neurosci*. 17:1515–1519. doi:10.1016/j.jocn.2010.03.051.
- Huet-Calderwood, C., F. Rivera-Molina, D.V. Iwamoto, E.B. Kromann, D. Toomre, and D.A. Calderwood. 2017. Novel ecto-tagged integrins reveal their trafficking in live cells. *Nat Commun*. 8:570. doi:10.1038/s41467-017-00646-w.
- Humphries, J.D., P. Wang, C. Streuli, B. Geiger, M.J. Humphries, and C. Ballestrem. 2007. Vinculin controls focal adhesion formation by direct interactions with talin and actin. *J Cell Biol*. 179:1043–1057. doi:10.1083/jcb.200703036.

Bibliographical references

- Huveneers, S., and E.H.J. Danen. 2009. Adhesion signaling - crosstalk between integrins, Src and Rho. *J Cell Sci.* 122:1059–1069. doi:10.1242/jcs.039446.
- Ichimura, Y., T. Kirisako, T. Takao, Y. Satomi, Y. Shimonishi, N. Ishihara, N. Mizushima, I. Tanida, E. Kominami, M. Ohsumi, T. Noda, and Y. Ohsumi. 2000. A ubiquitin-like system mediates protein lipidation. *Nature.* 408:488–492. doi:10.1038/35044114.
- Imai, K., F. Hao, N. Fujita, Y. Tsuji, Y. Oe, Y. Araki, M. Hamasaki, T. Noda, and T. Yoshimori. 2016. Atg9A trafficking through the recycling endosomes is required for autophagosome formation. *J Cell Sci.* 129:3781–3791. doi:10.1242/jcs.196196.
- Innocenti, M. 2018. New insights into the formation and the function of lamellipodia and ruffles in mesenchymal cell migration. *Cell Adh Migr.* 1–16. doi:10.1080/19336918.2018.1448352.
- Iozzo, R.V., and A.D. Murdoch. 1996. Proteoglycans of the extracellular environment: clues from the gene and protein side offer novel perspectives in molecular diversity and function. *FASEB j.* 10:598–614. doi:10.1096/fasebj.10.5.8621059.
- Iser, I.C., M.B. Pereira, G. Lenz, and M.R. Wink. 2017. The epithelial-to-mesenchymal transition-like process in glioblastoma: an updated systematic review and in silico investigation: EMT IN GLIOBLASTOMA. *Med. Res. Rev.* 37:271–313. doi:10.1002/med.21408.
- Itakura, E., C. Kishi-Itakura, and N. Mizushima. 2012. The hairpin-type tail-anchored SNARE Syntaxin 17 targets to autophagosomes for fusion with endosomes/lysosomes. *Cell.* 151:1256–1269. doi:10.1016/j.cell.2012.11.001.
- Ivankovic, D., J. Drew, F. Lesept, I.J. White, G. López Doménech, S.A. Tooze, and J.T. Kittler. 2020. Axonal autophagosome maturation defect through failure of ATG9A sorting underpins pathology in AP-4 deficiency syndrome. *Autophagy.* 16:391–407. doi:10.1080/15548627.2019.1615302.
- Jaber, N., and W.-X. Zong. 2013. Class III PI3K Vps34: essential roles in autophagy, endocytosis, and heart and liver function. *Ann N Y Acad Sci.* 1280:48–51. doi:10.1111/nyas.12026.
- Jaraíz-Rodríguez, M., R. Talaverón, L. García-Vicente, S.G. Pelaz, M. Domínguez-Prieto, A. Álvarez-Vázquez, R. Flores-Hernández, W.C. Sin, J. Bechberger, J.M. Medina, C.C. Naus, and A. Tabernero. 2020. Connexin43 peptide, TAT-Cx43266–283, selectively targets glioma cells, impairs malignant growth, and enhances survival in mouse models in vivo. *Neuro-Oncol.* 22:493–504. doi:10.1093/neuonc/noz243.
- Järveläinen, H., A. Sainio, M. Koulu, T.N. Wight, and R. Penttinen. 2009. Extracellular matrix molecules: potential targets in pharmacotherapy. *Pharmacol Rev.* 61:198–223. doi:10.1124/pr.109.001289.

Bibliographical references

- Jarzynka, M.J., B. Hu, K.-M. Hui, I. Bar-Joseph, W. Gu, T. Hirose, L.B. Haney, K.S. Ravichandran, R. Nishikawa, and S.-Y. Cheng. 2007. ELMO1 and Dock180, a bipartite Rac1 guanine nucleotide exchange factor, promote human glioma cell invasion. *Cancer Res.* 67:7203–7211. doi:10.1158/0008-5472.CAN-07-0473.
- Jia, S., Y. Wang, Z. You, B. Liu, J. Gao, and W. Liu. 2017. Mammalian Atg9 contributes to the post-Golgi transport of lysosomal hydrolases by interacting with adaptor protein-1. *FEBS Lett.* 591:4027–4038. doi:10.1002/1873-3468.12916.
- Jiang, F., J. Zhou, D. Zhang, M. Liu, and Y. Chen. 2018. Artesunate induces apoptosis and autophagy in HCT116 colon cancer cells, and autophagy inhibition enhances the artesunate-induced apoptosis. *Int J Mol Med.* doi:10.3892/ijmm.2018.3712.
- Jordens, I., M. Fernandez-Borja, M. Marsman, S. Dusseljee, L. Janssen, J. Calafat, H. Janssen, R. Wubbolts, and J. Neefjes. 2001. The Rab7 effector protein RILP controls lysosomal transport by inducing the recruitment of dynein-dynactin motors. *Curr Biol.* 11:1680–1685. doi:10.1016/S0960-9822(01)00531-0.
- Judith, D., H.B.J. Jefferies, S. Boeing, D. Frith, A.P. Snijders, and S.A. Tooze. 2019. ATG9A shapes the forming autophagosome through Arfaptin 2 and phosphatidylinositol 4-kinase III β . *J Cell Biol.* 218:1634–1652. doi:10.1083/jcb.201901115.
- Jung, C.H., C.B. Jun, S.-H. Ro, Y.-M. Kim, N.M. Otto, J. Cao, M. Kundu, and D.-H. Kim. 2009. ULK-Atg13-FIP200 complexes mediate mTOR signaling to the autophagy machinery. *Mol Biol Cell.* 20:1992–2003. doi:10.1091/mbc.e08-12-1249.
- Kaczmarek, J., P. Castellani, G. Nicolo, B. Spina, G. Allemanni, and L. Zardi. 1994. Distribution of oncofetal fibronectin isoforms in normal, hyperplastic and neoplastic human breast tissues. *Int J Cancer.* 59:11–16. doi:10.1002/ijc.2910590104.
- Kaksonen, M., and A. Roux. 2018. Mechanisms of clathrin-mediated endocytosis. *Nat Rev Mol Cell Biol.* 19:313–326. doi:10.1038/nrm.2017.132.
- Karanasios, E., E. Stapleton, M. Manifava, T. Kaizuka, N. Mizushima, S.A. Walker, and N.T. Ktistakis. 2013. Dynamic association of the ULK1 complex with omegasomes during autophagy induction. *J Cell Sci.* 126:5224–5238. doi:10.1242/jcs.132415.
- Kaslow, H.R., and usilla L. Burns. 1992. Pertussis toxin and target eukaryotic cells: binding, entry, and activation. *FASEB j.* 6:2684–2690. doi:10.1096/fasebj.6.9.1612292.
- Kaverina, I., O. Krylyshkina, and J.V. Small. 1999. Microtubule targeting of substrate contacts promotes their relaxation and dissociation. *J Cell Biol.* 146:1033–1044. doi:10.1083/jcb.146.5.1033.

Bibliographical references

- Kawabata, T., and T. Yoshimori. 2020. Autophagosome biogenesis and human health. *Cell Discov.* 6:33. doi:10.1038/s41421-020-0166-y.
- Ke, P.-Y. 2018. The multifaceted roles of autophagy in Flavivirus-host interactions. *IJMS.* 19:3940. doi:10.3390/ijms19123940.
- Kean, M.J., K.C. Williams, M. Skalski, D. Myers, A. Burtnik, D. Foster, and M.G. Coppelino. 2009. VAMP3, syntaxin-13 and SNAP23 are involved in secretion of matrix metalloproteinases, degradation of the extracellular matrix and cell invasion. *J Cell Sci.* 122:4089–4098. doi:10.1242/jcs.052761.
- Kenific, C.M., S.J. Stehbens, J. Goldsmith, A.M. Leidal, N. Faure, J. Ye, T. Wittmann, and J. Debnath. 2016. NBR1 enables autophagy-dependent focal adhesion turnover. *J Cell Biol.* 212:577–590. doi:10.1083/jcb.201503075.
- Kim, E., P. Goraksha-Hicks, L. Li, T.P. Neufeld, and K.-L. Guan. 2008. Regulation of TORC1 by Rag GTPases in nutrient response. *Nat Cell Biol.* 10:935–945. doi:10.1038/ncb1753.
- Kimmey, J.M., J.P. Huynh, L.A. Weiss, S. Park, A. Kambal, J. Debnath, H.W. Virgin, and C.L. Stallings. 2015. Unique role for ATG5 in neutrophil-mediated immunopathology during *M. tuberculosis* infection. *Nature.* 528:565–569. doi:10.1038/nature16451.
- Kimura, T., J. Jia, S. Kumar, S.W. Choi, Y. Gu, M. Mudd, N. Dupont, S. Jiang, R. Peters, F. Farzam, A. Jain, K.A. Lidke, C.M. Adams, T. Johansen, and V. Deretic. 2017. Dedicated SNAREs and specialized TRIM cargo receptors mediate secretory autophagy. *EMBO J.* 36:42–60. doi:10.15252/embj.201695081.
- Kimura, T., Y. Takabatake, A. Takahashi, and Y. Isaka. 2013. Chloroquine in cancer therapy: a double-edged sword of autophagy. *Cancer Res.* 73:3–7. doi:10.1158/0008-5472.CAN-12-2464.
- King, D., D. Yeomanson, and H.E. Bryant. 2015. PI3King the lock: targeting the PI3K/Akt/mTOR pathway as a novel therapeutic strategy in neuroblastoma. *J Pediatr Hematol Oncol.* 37:245–251. doi:10.1097/MPH.0000000000000329.
- Kirisako, T., Y. Ichimura, H. Okada, Y. Kabeya, N. Mizushima, T. Yoshimori, M. Ohsumi, T. Takao, T. Noda, and Y. Ohsumi. 2000. The reversible modification regulates the membrane-binding state of Apg8/Aut7 essential for autophagy and the cytoplasm to vacuole targeting pathway. *J Cell Biol.* 151:263–276. doi:10.1083/jcb.151.2.263.
- Kirkpatrick, C.A., and S.B. Selleck. 2007. Heparan sulfate proteoglycans at a glance. *J Cell Sci.* 120:1829–1832. doi:10.1242/jcs.03432.
- Kiss, V., A. Jipa, K. Varga, S. Takáts, T. Maruzs, P. Lőrincz, Z. Simon-Vecsei, S. Szikora, I. Földi, C. Bajusz, D. Tóth, P. Vilmos, I. Gáspár, P. Ronchi, J. Mihály, and G. Juhász. 2020. *Drosophila* Atg9 regulates the actin cytoskeleton via interactions with profilin and Ena. *Cell Death Differ.* 27:1677–1692. doi:10.1038/s41418-019-0452-0.

Bibliographical references

Kiyokawa, E., Y. Hashimoto, T. Kurata, H. Sugimura, and M. Matsuda. 1998. Evidence that DOCK180 up-regulates signals from the CrkII-p130Cas complex. *J Biol Chem.* 273:24479–24484. doi:10.1074/jbc.273.38.24479.

Klionsky, D.J., A.K. Abdel-Aziz, S. Abdelfatah, M. Abdellatif, A. Abdoli, S. Abel, H. Abeliovich, M.H. Abildgaard, Y.P. Abudu, A. Acevedo-Arozena, I.E. Adamopoulos, K. Adeli, T.E. Adolph, A. Adornetto, E. Aflaki, G. Agam, A. Agarwal, B.B. Aggarwal, M. Agnello, P. Agostinis, J.N. Agrewala, A. Agrotis, P.V. Aguilar, S.T. Ahmad, Z.M. Ahmed, U. Ahumada-Castro, S. Aits, S. Aizawa, Y. Akkoc, T. Akoumianaki, H.A. Akpinar, A.M. Al-Abd, L. Al-Akra, A. Al-Gharaibeh, M.A. Alaoui-Jamali, S. Alberti, E. Alcocer-Gómez, C. Alessandri, M. Ali, M.A. Alim Al-Bari, S. Aliwaini, J. Alizadeh, E. Almacellas, A. Almasan, A. Alonso, G.D. Alonso, N. Altan-Bonnet, D.C. Altieri, É.M.C. Álvarez, S. Alves, C. Alves da Costa, M.M. Alzaharna, M. Amadio, C. Amantini, C. Amaral, S. Ambrosio, A.O. Amer, V. Ammanathan, Z. An, S.U. Andersen, S.A. Andrabi, M. Andrade-Silva, A.M. Andres, S. Angelini, D. Ann, U.C. Anozie, M.Y. Ansari, P. Antas, A. Antebi, Z. Antón, T. Anwar, L. Apetoh, N. Apostolova, T. Araki, Y. Araki, K. Arasaki, W.L. Araújo, J. Araya, C. Arden, M.-A. Arévalo, S. Arguelles, E. Arias, J. Arikath, H. Arimoto, A.R. Ariosa, D. Armstrong-James, L. Arnauné-Pelloquin, A. Aroca, D.S. Arroyo, I. Arsov, R. Artero, D.M.L. Asaro, M. Aschner, M. Ashrafizadeh, O. Ashur-Fabian, A.G. Atanasov, A.K. Au, P. Auberger, et al. 2021. Guidelines for the use and interpretation of assays for monitoring autophagy (4th edition) 1. *Autophagy.* 17:1–382. doi:10.1080/15548627.2020.1797280.

Klionsky, D.J., J.M. Cregg, W.A. Dunn, S.D. Emr, Y. Sakai, I.V. Sandoval, A. Sibirny, S. Subramani, M. Thumm, M. Veenhuis, and Y. Ohsumi. 2003. A unified nomenclature for yeast autophagy-related genes. *Dev Cell.* 5:539–545. doi:10.1016/S1534-5807(03)00296-X.

Kodama, Y., and C.-D. Hu. 2012. Bimolecular fluorescence complementation (BiFC): A 5-year update and future perspectives. *Biotech.* 53. doi:10.2144/000113943.

Koga, H., M. Martinez-Vicente, F. Macian, V.V. Verkhusha, and A.M. Cuervo. 2011. A photoconvertible fluorescent reporter to track chaperone-mediated autophagy. *Nat Commun.* 2:386. doi:10.1038/ncomms1393.

Kolch, W. 2000. Meaningful relationships: the regulation of the Ras/Raf/MEK/ERK pathway by protein interactions. *Biochem J.* 351 Pt 2:289–305.

Komatsu, M., T. Ueno, S. Waguri, Y. Uchiyama, E. Kominami, and K. Tanaka. 2007. Constitutive autophagy: vital role in clearance of unfavorable proteins in neurons. *Cell Death Differ.* 14:887–894. doi:10.1038/sj.cdd.4402120.

Bibliographical references

- Komatsu, M., S. Waguri, T. Chiba, S. Murata, J. Iwata, I. Tanida, T. Ueno, M. Koike, Y. Uchiyama, E. Kominami, and K. Tanaka. 2006. Loss of autophagy in the central nervous system causes neurodegeneration in mice. *Nature*. 441:880–884. doi:10.1038/nature04723.
- Komatsu, M., S. Waguri, T. Ueno, J. Iwata, S. Murata, I. Tanida, J. Ezaki, N. Mizushima, Y. Ohsumi, Y. Uchiyama, E. Kominami, K. Tanaka, and T. Chiba. 2005. Impairment of starvation-induced and constitutive autophagy in Atg7-deficient mice. *J Cell Biol*. 169:425–434. doi:10.1083/jcb.200412022.
- Korolchuk, V.I., S. Saiki, M. Lichtenberg, F.H. Siddiqi, E.A. Roberts, S. Imarisio, L. Jahreiss, S. Sarkar, M. Futter, F.M. Menzies, C.J. O’Kane, V. Deretic, and D.C. Rubinsztein. 2011. Lysosomal positioning coordinates cellular nutrient responses. *Nat Cell Biol*. 13:453–460. doi:10.1038/ncb2204.
- Kourouniotis, G., Y. Wang, S. Pennock, X. Chen, and Z. Wang. 2016. Non-ligand-induced dimerization is sufficient to initiate the signalling and endocytosis of EGF receptor. *IJMS*. 17:1200. doi:10.3390/ijms17081200.
- Krick, R., Y. Muehe, T. Prick, S. Bremer, P. Schlotterhose, E.-L. Eskelinen, J. Millen, D.S. Goldfarb, and M. Thumm. 2008. Piecemeal microautophagy of the nucleus requires the core macroautophagy genes. *MBoC*. 19:4492–4505. doi:10.1091/mbc.e08-04-0363.
- Krishnan, K., and P.D.J. Moens. 2009. Structure and functions of profilins. *Biophys Rev*. 1:71–81. doi:10.1007/s12551-009-0010-y.
- Krueger, K.M., Y. Daaka, J.A. Pitcher, and R.J. Lefkowitz. 1997. The role of sequestration in G protein-coupled receptor resensitization. *J Biol Chem*. 272:5–8. doi:10.1074/jbc.272.1.5.
- Krupnick, J.G., and J.L. Benovic. 1998. The role of receptor kinases and arrestins in G protein-coupled receptor regulation. *Annu Rev Pharmacol Toxicol*. 38:289–319. doi:10.1146/annurev.pharmtox.38.1.289.
- Kupfer, A., G. Dennert, and S.J. Singer. 1983. Polarization of the Golgi apparatus and the microtubule-organizing center within cloned natural killer cells bound to their targets. *Proc Natl Acad Sci USA*. 80:7224–7228. doi:10.1073/pnas.80.23.7224.
- Kural, C., A.A. Akatay, R. Gaudin, B.-C. Chen, W.R. Legant, E. Betzig, and T. Kirchhausen. 2015. Asymmetric formation of coated pits on dorsal and ventral surfaces at the leading edges of motile cells and on protrusions of immobile cells. *MBoC*. 26:2044–2053. doi:10.1091/mbc.E15-01-0055.
- Kuchitsu, Y., Fukuda, M. 2018. Revisiting Rab7 Functions in Mammalian Autophagy: Rab7 Knockout Studies. *Cells*. 19;7(11):215. doi: 10.3390/cells7110215.
- Kvam, E. 2004. Nvj1p is the outer-nuclear-membrane receptor for oxysterol-binding protein homolog Osh1p in *Saccharomyces cerevisiae*. *J Cell Sci*. 117:4959–4968. doi:10.1242/jcs.01372.

Bibliographical references

- Lai, F.P.L., M. Szczodrak, J.M. Oelkers, M. Ladwein, F. Acconcia, S. Benesch, S. Auinger, J. Faix, J.V. Small, S. Polo, T.E.B. Stradal, and K. Rottner. 2009. Cortactin promotes migration and platelet-derived growth factor-induced actin reorganization by signaling to Rho-GTPases. *MBoC*. 20:3209–3223. doi:10.1091/mbc.e08-12-1180.
- Lai, L.T.F., C. Yu, J.S.K. Wong, H.S. Lo, S. Benlekbir, L. Jiang, and W.C.Y. Lau. 2019. Subnanometer resolution cryo-EM structure of Arabidopsis thaliana ATG9. *Autophagy*. 16:575–583. doi:10.1080/15548627.2019.1639300.
- Lambrechts, A., V. Jonckheere, D. Dewitte, J. Vandekerckhove, and C. Ampe. 2002. Mutational analysis of human profilin I reveals a second PI(4,5)-P2 binding site neighbouring the poly(L-proline) binding site. *BMC Biochem*. 3:12. doi:10.1186/1471-2091-3-12.
- Lauffenburger, D.A., and A.F. Horwitz. 1996. Cell Migration: A physically integrated molecular process. *Cell*. 84:359–369. doi:10.1016/S0092-8674(00)81280-5.
- Laukaitis, C.M., D.J. Webb, K. Donais, and A.F. Horwitz. 2001. Differential Dynamics of $\alpha 5$ Integrin, Paxillin, and α -actinin during formation and disassembly of adhesions in migrating cells. *J Cell Biol*. 153:1427–1440. doi:10.1083/jcb.153.7.1427.
- Lawson, M.A., and F.R. Maxfield. 1995. Ca²⁺- and calcineurin-dependent recycling of an integrin to the front of migrating neutrophils. *Nature*. 377:75–79. doi:10.1038/377075a0.
- Lazarini, F., T.N. Tham, P. Casanova, F. Arenzana-Seisdedos, and M. Dubois-Dalcq. 2003. Role of the γ -chemokine stromal cell-derived factor (SDF-1) in the developing and mature central nervous system. *Glia*. 42:139–148. doi:10.1002/glia.10139.
- Le Clainche, C., and M.-F. Carlier. 2008. Regulation of actin assembly associated with protrusion and adhesion in cell migration. *Physiol Rev*. 88:489–513. doi:10.1152/physrev.00021.2007.
- Lecointre, C., L. Desrues, J.E. Joubert, N. Perzo, P.-O. Guichet, V. Le Joncour, C. Brulé, M. Chabbert, R. Leduc, L. Prézeau, A. Laquerrière, F. Proust, P. Gandolfo, F. Morin, and H. Castel. 2015. Signaling switch of the urotensin II vasosactive peptide GPCR: prototypic chemotaxic mechanism in glioma. *Oncogene*. 34:5080–5094. doi:10.1038/onc.2014.433.
- Lee, E.-J., and C. Tournier. 2011. The requirement of uncoordinated 51-like kinase 1 (ULK1) and ULK2 in the regulation of autophagy. *Autophagy*. 7:689–695. doi:10.4161/auto.7.7.15450.
- Lee, J.-A., A. Beigneux, S.T. Ahmad, S.G. Young, and F.-B. Gao. 2007. ESCRT-III dysfunction causes autophagosome accumulation and neurodegeneration. *Curr Biol*. 17:1561–1567. doi:10.1016/j.cub.2007.07.029.

Bibliographical references

- Lee, Y.-K., and J.-A. Lee. 2016. Role of the mammalian ATG8/LC3 family in autophagy: differential and compensatory roles in the spatiotemporal regulation of autophagy. *BMB Reports*. 49:424–430. doi:10.5483/BMBRep.2016.49.8.081.
- Lefkowitz, R.J., K. Rajagopal, and E.J. Whalen. 2006. New roles for β -arrestins in cell signaling: not just for seven-transmembrane receptors. *Mol Cell*. 24:643–652. doi:10.1016/j.molcel.2006.11.007.
- Lemasters, J.J. 2014. Variants of mitochondrial autophagy: Types 1 and 2 mitophagy and micromitophagy (Type 3). *Redox Biol*. 2:749–754. doi:10.1016/j.redox.2014.06.004.
- Letinic, K., R. Sebastian, D. Toomre, and P. Rakic. 2009. Exocyst is involved in polarized cell migration and cerebral cortical development. *Proc Natl Acad Sci USA*. 106:11342–11347. doi:10.1073/pnas.0904244106.
- Li, H., L. Yang, H. Fu, J. Yan, Y. Wang, H. Guo, X. Hao, X. Xu, T. Jin, and N. Zhang. 2013. Association between Gai2 and ELMO1/Dock180 connects chemokine signalling with Rac activation and metastasis. *Nat Commun*. 4:1706. doi:10.1038/ncomms2680.
- Li, P., A.T. Bademosi, J. Luo, and F.A. Meunier. 2018. Actin remodeling in regulated exocytosis: toward a mesoscopic view. *Trends Cell Biol*. 28:685–697. doi:10.1016/j.tcb.2018.04.004.
- Li, T., H. You, X. Mo, W. He, X. Tang, Z. Jiang, S. Chen, Y. Chen, J. Zhang, and Z. Hu. 2016. GOLPH3 mediated Golgi stress response in modulating N2A cell death upon oxygen-glucose deprivation and reoxygenation Injury. *Mol Neurobiol*. 53:1377–1385. doi:10.1007/s12035-014-9083-0.
- Li, W., J. Li, and J. Bao. 2012. Microautophagy: lesser-known self-eating. *Cell. Mol. Life Sci*. 69:1125–1136. doi:10.1007/s00018-011-0865-5.
- Li, Y., P.-S. Wang, G. Lucas, R. Li, and L. Yao. 2015. ARP2/3 complex is required for directional migration of neural stem cell-derived oligodendrocyte precursors in electric fields. *Stem Cell Res Ther*. 6:41. doi:10.1186/s13287-015-0042-0.
- Li, Z., M. Hannigan, Z. Mo, B. Liu, W. Lu, Y. Wu, A.V. Smrcka, G. Wu, L. Li, M. Liu, C.-K. Huang, and D. Wu. 2003. Directional sensing requires G β γ -mediated PAK1 and PIX α -dependent activation of Cdc42. *Cell*. 114:215–227. doi:10.1016/S0092-8674(03)00559-2.
- Liang, C., J. Lee, K.-S. Inn, M.U. Gack, Q. Li, E.A. Roberts, I. Vergne, V. Deretic, P. Feng, C. Akazawa, and J.U. Jung. 2008. Beclin1-binding UVRAG targets the class C Vps complex to coordinate autophagosome maturation and endocytic trafficking. *Nat Cell Biol*. 10:776–787. doi:10.1038/ncb1740.
- Liang, X.H., S. Jackson, M. Seaman, K. Brown, B. Kempkes, H. Hibshoosh, and B. Levine. 1999. Induction of autophagy and inhibition of tumorigenesis by beclin 1. *Nature*. 402:672–676. doi:10.1038/45257.

Bibliographical references

- Lidke, D.S., K.A. Lidke, B. Rieger, T.M. Jovin, and D.J. Arndt-Jovin. 2005. Reaching out for signals. *J Cell Biol.* 170:619–626. doi:10.1083/jcb.200503140.
- Lin, Y.-C., J.-F. Lin, S.-I. Wen, S.-C. Yang, T.-F. Tsai, H.-E. Chen, K.-Y. Chou, and T.I.-S. Hwang. 2017. Chloroquine and hydroxychloroquine inhibit bladder cancer cell growth by targeting basal autophagy and enhancing apoptosis. *Kaohsiung J Med Sci.* 33:215–223. doi:10.1016/j.kjms.2017.01.004.
- Liu, S., D.A. Calderwood, and M.H. Ginsberg. 2000. Integrin cytoplasmic domain-binding proteins. *J Cell Sci* 113 (Pt 20):3563–3571.
- Liu, Z., X. Yang, C. Chen, B. Liu, B. Ren, L. Wang, K. Zhao, S. Yu, and H. Ming. 2013. Expression of the Arp2/3 complex in human gliomas and its role in the migration and invasion of glioma cells. *Oncol Rep.* 30:2127–2136. doi:10.3892/or.2013.2669.
- Lobert, V.H., and H. Stenmark. 2012. The ESCRT machinery mediates polarization of fibroblasts through regulation of myosin light chain. *J Cell Sci.* 125:29–36. doi:10.1242/jcs.088310.
- Locher, R., P.A. Erba, B. Hirsch, E. Bombardieri, L. Giovannoni, D. Neri, H. Dürkop, and H.D. Menssen. 2014. Abundant in vitro expression of the oncofetal ED-B-containing fibronectin translates into selective pharmacodelivery of ¹³¹I-L19SIP in a prostate cancer patient. *J Cancer Res Clin Oncol.* 140:35–43. doi:10.1007/s00432-013-1538-6.
- Long, W., P. Yi, L. Amazit, H.L. LaMarca, F. Ashcroft, R. Kumar, M.A. Mancini, S.Y. Tsai, M.-J. Tsai, and B.W. O'Malley. 2010. SRC-3Δ4 mediates the interaction of EGFR with FAK to promote cell migration. *Mol Cell.* 37:321–332. doi:10.1016/j.molcel.2010.01.004.
- Lowenstein, E.J., R.J. Daly, A.G. Batzer, W. Li, B. Margolis, R. Lammers, A. Ullrich, E.Y. Skolnik, D. Bar-Sagi, and J. Schlessinger. 1992. The SH2 and SH3 domain-containing protein GRB2 links receptor tyrosine kinases to ras signaling. *Cell.* 70:431–442. doi:10.1016/0092-8674(92)90167-B.
- Lu, L., M. Tang, Z. Qi, S. Huang, Y. He, D. Li, L. Li, and L. Chen. 2020. Regulation of the Golgi apparatus via GOLPH3-mediated new selective autophagy. *Life Sci.* 253:117700. doi:10.1016/j.lfs.2020.117700.
- Lum, J.J., D.E. Bauer, M. Kong, M.H. Harris, C. Li, T. Lindsten, and C.B. Thompson. 2005. Growth factor regulation of autophagy and cell survival in the absence of apoptosis. *Cell.* 120:237–248. doi:10.1016/j.cell.2004.11.046.
- Luttrell, L.M., F.L. Roudabush, E.W. Choy, W.E. Miller, M.E. Field, K.L. Pierce, and R.J. Lefkowitz. 2001. Activation and targeting of extracellular signal-regulated kinases by β-arrestin scaffolds. *Proc Natl Acad Sci USA.* 98:2449–2454. doi:10.1073/pnas.041604898.

Bibliographical references

- Ma, Z., Z. Qi, Z. Shan, J. Li, J. Yang, and Z. Xu. 2017. The role of CRP and ATG9B expression in clear cell renal cell carcinoma. *Biosci Rep.* 37:BSR20171082. doi:10.1042/BSR20171082.
- MacDonald, P.E., M. Braun, J. Galvanovskis, and P. Rorsman. 2006. Release of small transmitters through kiss-and-run fusion pores in rat pancreatic β cells. *Cell Metab.* 4:283–290. doi:10.1016/j.cmet.2006.08.011.
- Machacek, M., and G. Danuser. 2006. Morphodynamic profiling of protrusion phenotypes. *Biophys J.* 90:1439–1452. doi:10.1529/biophysj.105.070383.
- Machesky, L.M., and A. Li. 2010. Fascin: invasive filopodia promoting metastasis. *Commun Integr Biol.* 3:263–270. doi:10.4161/cib.3.3.11556.
- Mack, H.I.D., B. Zheng, J.M. Asara, and S.M. Thomas. 2012. AMPK-dependent phosphorylation of ULK1 regulates ATG9 localization. *Autophagy.* 8:1197–1214. doi:10.4161/auto.20586.
- Maeda, S., H. Yamamoto, L.N. Kinch, C.M. Garza, S. Takahashi, C. Otomo, N.V. Grishin, S. Forli, N. Mizushima, and T. Otomo. 2020. Structure, lipid scrambling activity and role in autophagosome formation of ATG9A. *Nat Struct Mol Biol.* 27:1194–1201. doi:10.1038/s41594-020-00520-2.
- Maghazachi, A.A. 1997. Role of the heterotrimeric G proteins in stromal-derived factor-1 α -induced natural killer cell chemotaxis and calcium mobilization. *Biochem Biophys Res Commun.* 236:270–274. doi:10.1006/bbrc.1997.6937.
- Magnuson, V.L., M. Young, D.G. Schattenberg, M.A. Mancini, D.L. Chen, B. Steffensen, and R.J. Klebe. 1991. The alternative splicing of fibronectin pre-mRNA is altered during aging and in response to growth factors. *J. Biol. Chem.* 266:14654–14662.
- Mahalingam, D., M. Mita, J. Sarantopoulos, L. Wood, R.K. Amaravadi, L.E. Davis, A.C. Mita, T.J. Curiel, C.M. Espitia, S.T. Nawrocki, F.J. Giles, and J.S. Carew. 2014. Combined autophagy and HDAC inhibition: A phase I safety, tolerability, pharmacokinetic, and pharmacodynamic analysis of hydroxychloroquine in combination with the HDAC inhibitor vorinostat in patients with advanced solid tumors. *Autophagy.* 10:1403–1414. doi:10.4161/auto.29231.
- Maisel, S., D. Broka, and J. Schroeder. 2018. Intravesicular epidermal growth factor receptor subject to retrograde trafficking drives epidermal growth factor-dependent migration. *Oncotarget.* 9:6463–6477. doi:10.18632/oncotarget.23766.
- Margadant, C., H.N. Monsuur, J.C. Norman, and A. Sonnenberg. 2011. Mechanisms of integrin activation and trafficking. *Curr Opin Cell Biol.* 23:607–614. doi:10.1016/j.ceb.2011.08.005.

Bibliographical references

- Margaron, Y., N. Fradet, and J.-F. Côté. 2013. ELMO recruits actin cross-linking family 7 (ACF7) at the cell membrane for microtubule capture and stabilization of cellular protrusions. *J Biol Chem.* 288:1184–1199. doi:10.1074/jbc.M112.431825.
- Mari, M., J. Griffith, E. Rieter, L. Krishnappa, D.J. Klionsky, and F. Reggiori. 2010. An Atg9-containing compartment that functions in the early steps of autophagosome biogenesis. *J Cell Biol.* 190:1005–1022. doi:10.1083/jcb.200912089.
- Martel, V., L. Vignoud, S. Dupe, P. Frachet, M.R. Block, and C. Albiges-Rizo. 2000. Talin controls the exit of the integrin alpha 5 beta 1 from an early compartment of the secretory pathway. *J Cell Sci.* 113:1951–1961. doi:10.1242/jcs.113.11.1951.
- Marzella, L., J. Ahlberg, and H. Glaumann. 1980. In vitro uptake of particles by lysosomes. *Exp Cell Res.* 129:460–466. doi:10.1016/0014-4827(80)90515-7.
- Matoba, K., T. Kotani, A. Tsutsumi, T. Tsuji, T. Mori, D. Noshiro, Y. Sugita, N. Nomura, S. Iwata, Y. Ohsumi, T. Fujimoto, H. Nakatogawa, M. Kikkawa, and N.N. Noda. 2020. Atg9 is a lipid scramblase that mediates autophagosomal membrane expansion. *Nat Struct Mol Biol.* 27:1185–1193. doi:10.1038/s41594-020-00518-w.
- Matsuda, S., E. Miura, K. Matsuda, W. Kakegawa, K. Kohda, M. Watanabe, and M. Yuzaki. 2008. Accumulation of AMPA receptors in autophagosomes in neuronal axons lacking adaptor protein AP-4. *Neuron.* 57:730–745. doi:10.1016/j.neuron.2008.02.012.
- Matsunaga, K., E. Morita, T. Saitoh, S. Akira, N.T. Ktistakis, T. Izumi, T. Noda, and T. Yoshimori. 2010. Autophagy requires endoplasmic reticulum targeting of the PI3-kinase complex via Atg14L. *J Cell Biol.* 190:511–521. doi:10.1083/jcb.200911141.
- Matsunaga, K., T. Saitoh, K. Tabata, H. Omori, T. Satoh, N. Kurotori, I. Maejima, K. Shirahama-Noda, T. Ichimura, T. Isobe, S. Akira, T. Noda, and T. Yoshimori. 2009. Two Beclin 1-binding proteins, Atg14L and Rubicon, reciprocally regulate autophagy at different stages. *Nat Cell Biol.* 11:385–396. doi:10.1038/ncb1846.
- Matsuoka, S., and M. Ueda. 2018. Mutual inhibition between PTEN and PIP3 generates bistability for polarity in motile cells. *Nat Commun.* 9:4481. doi:10.1038/s41467-018-06856-0.
- Matsuura, A., M. Tsukada, Y. Wada, and Y. Ohsumi. 1997. Apg1p, a novel protein kinase required for the autophagic process in *Saccharomyces cerevisiae*. *Gene.* 192:245–250. doi:10.1016/S0378-1119(97)00084-X.
- Mattera, R., S.Y. Park, R. De Pace, C.M. Guardia, and J.S. Bonifacino. 2017. AP-4 mediates export of ATG9A from the trans-Golgi network to promote autophagosome formation. *Proc Natl Acad Sci USA.* 114:E10697–E10706. doi:10.1073/pnas.1717327114.

Bibliographical references

- Mattila, P.K., and P. Lappalainen. 2008. Filopodia: molecular architecture and cellular functions. *Nat Rev Mol Cell Biol.* 9:446–454. doi:10.1038/nrm2406.
- McAfee, Q., Z. Zhang, A. Samanta, S.M. Levi, X.-H. Ma, S. Piao, J.P. Lynch, T. Uehara, A.R. Sepulveda, L.E. Davis, J.D. Winkler, and R.K. Amaravadi. 2012. Autophagy inhibitor Lys05 has single-agent antitumor activity and reproduces the phenotype of a genetic autophagy deficiency. *Proc Natl Acad Sci USA.* 109:8253–8258. doi:10.1073/pnas.1118193109.
- Meisenhelder, J., P.-G. Suh, S.G. Rhee, and T. Hunter. 1989. Phospholipase C- γ is a substrate for the PDGF and EGF receptor protein-tyrosine kinases in vivo and in vitro. *Cell.* 57:1109–1122. doi:10.1016/0092-8674(89)90048-2.
- Melia, T.J., A.H. Lystad, and A. Simonsen. 2020. Autophagosome biogenesis: From membrane growth to closure. *J Cell Biol.* 219:e202002085. doi:10.1083/jcb.202002085.
- Mellor, H. 2010. The role of formins in filopodia formation. *Biochim Biophys Acta.* 1803:191–200. doi:10.1016/j.bbamcr.2008.12.018.
- Menon, M.B., and S. Dhamija. 2018. Beclin 1 Phosphorylation – at the Center of Autophagy Regulation. *Front. Cell Dev. Biol.* 6:137. doi:10.3389/fcell.2018.00137.
- Mercer, C.A., A. Kaliappan, and P.B. Dennis. 2009. A novel, human Atg13 binding protein, Atg101, interacts with ULK1 and is essential for macroautophagy. *Autophagy.* 5:649–662. doi:10.4161/auto.5.5.8249.
- Merlot, S., and R.A. Firtel. 2003. Leading the way: directional sensing through phosphatidylinositol 3-kinase and other signaling pathways. *J Cell Sci.* 116:3471–3478. doi:10.1242/jcs.00703.
- Midulla, M., R. Verma, M. Pignatelli, M.A. Ritter, N.S. Courtenay-Luck, and A.J. George. 2000. Source of oncofetal ED-B-containing fibronectin: implications of production by both tumor and endothelial cells. *Cancer Res.* 60:164–169.
- Mijaljica, D., M. Prescott, and R.J. Devenish. 2011. Microautophagy in mammalian cells: Revisiting a 40-year-old conundrum. *Autophagy.* 7:673–682. doi:10.4161/auto.7.7.14733.
- Miklavc, P., E. Hecht, N. Hobi, O.H. Wittekindt, P. Dietl, C. Kranz, and M. Frick. 2012. Actin coating and compression of fused secretory vesicles are essential for surfactant secretion: a role for Rho, formins and myosin II. *J Cell Sci.* doi:10.1242/jcs.105262.
- Mizushima, N. 2018. A brief history of autophagy from cell biology to physiology and disease. *Nat Cell Biol.* 20:521–527. doi:10.1038/s41556-018-0092-5.

Bibliographical references

- Mizushima, N., A. Kuma, Y. Kobayashi, A. Yamamoto, M. Matsubae, T. Takao, T. Natsume, Y. Ohsumi, and T. Yoshimori. 2003. Mouse Apg16L, a novel WD-repeat protein, targets to the autophagic isolation membrane with the Apg12-Apg5 conjugate. *J Cell Sci.* 116:1679–1688. doi:10.1242/jcs.00381.
- Mizushima, N., T. Noda, and Y. Ohsumi. 1999. Apg16p is required for the function of the Apg12p-Apg5p conjugate in the yeast autophagy pathway. *EMBO J.* 18:3888–3896. doi:10.1093/emboj/18.14.3888.
- Mizushima, N., H. Sugita, T. Yoshimori, and Y. Ohsumi. 1998. A New Protein Conjugation System in Human. *J Biol Chem.* 273:33889–33892. doi:10.1074/jbc.273.51.33889.
- Moreau, K., B. Ravikumar, C. Puri, and D.C. Rubinsztein. 2012. Arf6 promotes autophagosome formation via effects on phosphatidylinositol 4,5-bisphosphate and phospholipase D. *J Cell Biol.* 196:483–496. doi:10.1083/jcb.201110114.
- Morgan, M.R., A. Byron, M.J. Humphries, and M.D. Bass. 2009. Giving off mixed signals-Distinct functions of $\alpha 5 \beta 1$ and $\alpha v \beta 3$ integrins in regulating cell behaviour. *IUBMB Life.* 61:731–738. doi:10.1002/iub.200.
- Moriki, T., H. Maruyama, and I.N. Maruyama. 2001. Activation of preformed EGF receptor dimers by ligand-induced rotation of the transmembrane domain¹¹Edited by B. Holland. *J Mol Biol.* 311:1011–1026. doi:10.1006/jmbi.2001.4923.
- Morita, H., A. Yoshimura, K. Inui, T. Ideura, H. Watanabe, L. Wang, R. Soininen, and K. Tryggvason. 2005. Heparan sulfate of perlecan is involved in glomerular filtration. *JASN.* 16:1703–1710. doi:10.1681/ASN.2004050387.
- Mousavi, S.A., L. Malerød, T. Berg, and R. Kjekshus. 2004. Clathrin-dependent endocytosis. *Biochem J.* 377:1–16. doi:10.1042/bj20031000.
- Mulcahy Levy, J.M., and A. Thorburn. 2020. Autophagy in cancer: moving from understanding mechanism to improving therapy responses in patients. *Cell Death Differ.* 27:843–857. doi:10.1038/s41418-019-0474-7.
- Müller, O., T. Sattler, M. Flötenmeyer, H. Schwarz, H. Plattner, and A. Mayer. 2000. Autophagic tubes. *J Cell Biol.* 151:519–528. doi:10.1083/jcb.151.3.519.
- Nakamura, K., H. Yano, H. Uchida, S. Hashimoto, E. Schaefer, and H. Sabe. 2000. Tyrosine phosphorylation of paxillin α is involved in temporospatial regulation of paxillin-containing focal adhesion formation and F-actin organization in motile cells. *J Biol Chem.* 275:27155–27164. doi:10.1016/S0021-9258(19)61492-4.
- Nakatogawa, H., J. Ishii, E. Asai, and Y. Ohsumi. 2012. Atg4 recycles inappropriately lipidated Atg8 to promote autophagosome biogenesis. *Autophagy.* 8:177–186. doi:10.4161/auto.8.2.18373.

Bibliographical references

- Nakatogawa, H., K. Suzuki, Y. Kamada, and Y. Ohsumi. 2009. Dynamics and diversity in autophagy mechanisms: lessons from yeast. *Nat Rev Mol Cell Biol.* 10:458–467. doi:10.1038/nrm2708.
- Nam, J.-M., Y. Onodera, M.J. Bissell, and C.C. Park. 2010. Breast cancer cells in three-dimensional culture display an enhanced radioresponse after coordinate targeting of integrin $\alpha 5\beta 1$ and fibronectin. *Cancer Res.* 70:5238–5248. doi:10.1158/0008-5472.CAN-09-2319.
- Nejedla, M., Said, S., Sulimenko, V., de Almeida, FN., Blom, H., Draber, P., Aspenström, P., Karlsson, R. 2016. Profilin connects actin assembly with microtubule dynamics. *Mol Biol Cell.* 27(15):2381-93. doi:10.1091/mbc.E15-11-0799.
- Nieswandt, B., M. Moser, I. Pleines, D. Varga-Szabo, S. Monkley, D. Critchley, and R. Fässler. 2007. Loss of talin1 in platelets abrogates integrin activation, platelet aggregation, and thrombus formation in vitro and in vivo. *J Exp Med.* 204:3113–3118. doi:10.1084/jem.20071827.
- Nieves, B., C.W. Jones, R. Ward, Y. Ohta, C.G. Reverte, and S.E. LaFlamme. 2010. The NPIY motif in the integrin 1 tail dictates the requirement for talin-1 in outside-in signaling. *J Cell Sci.* 123:1216–1226. doi:10.1242/jcs.056549.
- Nightingale, T.D., D.F. Cutler, and L.P. Cramer. 2012. Actin coats and rings promote regulated exocytosis. *Trends Cell Biol.* 22:329–337. doi:10.1016/j.tcb.2012.03.003.
- Nightingale, T.D., I.J. White, E.L. Doyle, M. Turmaine, K.J. Harrison-Lavoie, K.F. Webb, L.P. Cramer, and D.F. Cutler. 2011. Actomyosin II contractility expels von Willebrand factor from Weibel–Palade bodies during exocytosis. *J Cell Biol.* 194:613–629. doi:10.1083/jcb.201011119.
- Nilsson, P., K. Loganathan, M. Sekiguchi, Y. Matsuba, K. Hui, S. Tsubuki, M. Tanaka, N. Iwata, T. Saito, and T.C. Saïdo. 2013. A β secretion and plaque formation depend on autophagy. *Cell Rep.* 5:61–69. doi:10.1016/j.celrep.2013.08.042.
- Nishimura, T., and K. Kaibuchi. 2007. Numb controls integrin endocytosis for directional cell migration with aPKC and PAR-3. *Dev Cell.* 13:15–28. doi:10.1016/j.devcel.2007.05.003.
- Nishimura, T., and S.A. Tooze. 2020. Emerging roles of ATG proteins and membrane lipids in autophagosome formation. *Cell Discov.* 6:32. doi:10.1038/s41421-020-0161-3.
- Nobes, C.D., and A. Hall. 1995. Rho, Rac, and Cdc42 GTPases regulate the assembly of multimolecular focal complexes associated with actin stress fibers, lamellipodia, and filopodia. *Cell.* 81:53–62. doi:10.1016/0092-8674(95)90370-4.
- Noordstra, I., and A. Akhmanova. 2017. Linking cortical microtubule attachment and exocytosis. *F1000Res.* 6:469. doi:10.12688/f1000research.10729.1.

Bibliographical references

- Novikoff, A.B., H. Beaufay, and C. de Duve. 1956. ELECTRON MICROSCOPY OF LYSOSOME-RICH FRACTIONS FROM RAT LIVER. *J Biophys Biochem Cytol.* 2:179–184. doi:10.1083/jcb.2.4.179.
- Novikoff, A.B., and E. Essner. 1962. CYTOLYSOMES AND MITOCHONDRIAL DEGENERATION. *J Cell Biol.* 15:140–146. doi:10.1083/jcb.15.1.140.
- Ohsumi, Y. 2014. Historical landmarks of autophagy research. *Cell Res.* 24:9–23. doi:10.1038/cr.2013.169.
- Ohta, Y., J.H. Hartwig, and T.P. Stossel. 2006. FilGAP, a Rho- and ROCK-regulated GAP for Rac binds filamin A to control actin remodelling. *Nat Cell Biol.* 8:803–814. doi:10.1038/ncb1437.
- Orsi, A., M. Razi, H.C. Dooley, D. Robinson, A.E. Weston, L.M. Collinson, and S.A. Tooze. 2012. Dynamic and transient interactions of Atg9 with autophagosomes, but not membrane integration, are required for autophagy. *MBoC.* 23:1860–1873. doi:10.1091/mbc.e11-09-0746.
- Osmani, N., F. Peglion, P. Chavrier, and S. Etienne-Manneville. 2010. Cdc42 localization and cell polarity depend on membrane traffic. *J Cell Biol.* 191:1261–1269. doi:10.1083/jcb.201003091.
- Padman, B.S., T.N. Nguyen, L. Uoselis, M. Skulsupaisarn, L.K. Nguyen, and M. Lazarou. 2019. LC3/GABARAPs drive ubiquitin-independent recruitment of Optineurin and NDP52 to amplify mitophagy. *Nat Commun.* 10:408. doi:10.1038/s41467-019-08335-6.
- Pankiv, S., E.A. Alemu, A. Brech, J.-A. Bruun, T. Lamark, A. Øvervatn, G. Bjørkøy, and T. Johansen. 2010. FYCO1 is a Rab7 effector that binds to LC3 and PI3P to mediate microtubule plus end-directed vesicle transport. *J Cell Biol.* 188:253–269. doi:10.1083/jcb.200907015.
- Park, H.-O., and E. Bi. 2007. Central roles of small GTPases in the development of cell polarity in yeast and beyond. *MMBR.* 71:48–96. doi:10.1128/MMBR.00028-06.
- Park, S.Y., and X. Guo. 2014. Adaptor protein complexes and intracellular transport. *Biosci Rep.* 34:e00123. doi:10.1042/BSR20140069.
- Parri, M., and P. Chiarugi. 2010. Rac and Rho GTPases in cancer cell motility control. *Cell Commun. Signal.* 8:23. doi:10.1186/1478-811X-8-23.
- Parsons, J.T., A.R. Horwitz, and M.A. Schwartz. 2010. Cell adhesion: integrating cytoskeletal dynamics and cellular tension. *Nat Rev Mol Cell Biol.* 11:633–643. doi:10.1038/nrm2957.
- Parsons, M., J. Monypenny, S.M. Ameer-Beg, T.H. Millard, L.M. Machesky, M. Peter, M.D. Keppler, G. Schiavo, R. Watson, J. Chernoff, D. Zicha, B. Vojnovic, and T. Ng. 2005. Spatially distinct binding of Cdc42 to PAK1 and N-WASP in breast carcinoma cells. *MCB.* 25:1680–1695. doi:10.1128/MCB.25.5.1680-1695.2005.

Bibliographical references

- Pasic, L., T. Kotova, and D.A. Schafer. 2008. Ena/VASP proteins capture actin filament barbed ends. *J Biol Chem.* 283:9814–9819. doi:10.1074/jbc.M710475200.
- Pattingre, S., A. Tassa, X. Qu, R. Garuti, X.H. Liang, N. Mizushima, M. Packer, M.D. Schneider, and B. Levine. 2005. Bcl-2 antiapoptotic proteins inhibit Beclin 1-dependent autophagy. *Cell.* 122:927–939. doi:10.1016/j.cell.2005.07.002.
- Paul, N.R., G. Jacquemet, and P.T. Caswell. 2015. Endocytic trafficking of integrins in cell migration. *Curr Biol.* 25:R1092-1105. doi:10.1016/j.cub.2015.09.049.
- Peach, R., D. Hollenbaugh, I. Stamenkovic, and A. Aruffo. 1993. Identification of hyaluronic acid binding sites in the extracellular domain of CD44. *J Cell Biol.* 122:257–264. doi:10.1083/jcb.122.1.257.
- Peng, J., B.J. Wallar, A. Flanders, P.J. Swiatek, and A.S. Alberts. 2003. Disruption of the diaphanous-related formin Drf1 gene encoding mDia1 reveals a role for Drf3 as an effector for Cdc42. *Curr Biol.* 13:534–545. doi:10.1016/S0960-9822(03)00170-2.
- Petiot, A., E. Ogier-Denis, E.F. Blommaart, A.J. Meijer, and P. Codogno. 2000. Distinct classes of phosphatidylinositol 3'-kinases are involved in signaling pathways that control macroautophagy in HT-29 cells. *J Biol Chem.* 275:992–998. doi:10.1074/jbc.275.2.992.
- Petrini, I., S. Barachini, V. Carnicelli, S. Galimberti, L. Modeo, R. Boni, M. Sollini, and P.A. Erba. 2017. ED-B fibronectin expression is a marker of epithelial-mesenchymal transition in translational oncology. *Oncotarget.* 8:4914–4921. doi:10.18632/oncotarget.13615.
- Pfaff, M., X. Du, and M.H. Ginsberg. 1999. Calpain cleavage of integrin β cytoplasmic domains. *FEBS Letters.* 460:17–22. doi:10.1016/S0014-5793(99)01250-8.
- Pfeifer, U. 1977. Inhibition by insulin of the physiological autophagic breakdown of cell organelles. *Acta Biol Med Ger.* 36:1691–1694.
- Pimm, M.L., J. Hotaling, and J.L. Henty-Ridilla. 2020. Profilin choreographs actin and microtubules in cells and cancer. *Int Rev Cell Mol Biol.* Elsevier. 155–204.
- Pollard, T.D., and G.G. Borisy. 2003. Cellular motility driven by assembly and disassembly of actin filaments. *Cell.* 112:453–465. doi:10.1016/S0092-8674(03)00120-X.
- Ponti, A. 2004. Two distinct actin networks drive the protrusion of migrating cells. *Science.* 305:1782–1786. doi:10.1126/science.1100533.
- Presley, J.F., N.B. Cole, T.A. Schroer, K. Hirschberg, K.J.M. Zaal, and J. Lippincott-Schwartz. 1997. ER-to-Golgi transport visualized in living cells. *Nature.* 389:81–85. doi:10.1038/38001.

Bibliographical references

- Proux-Gillardeaux, V., J. Gavard, T. Irinopoulou, R.-M. Mege, and T. Galli. 2005. Tetanus neurotoxin-mediated cleavage of cellubrevin impairs epithelial cell migration and integrin-dependent cell adhesion. *Proc Natl Acad Sci USA*. 102:6362–6367. doi:10.1073/pnas.0409613102.
- Puri, C., M. Renna, C.F. Bento, K. Moreau, and D.C. Rubinsztein. 2013. Diverse autophagosome membrane sources coalesce in recycling endosomes. *Cell*. 154:1285–1299. doi:10.1016/j.cell.2013.08.044.
- Puri, C., M. Vicinanza, A. Ashkenazi, M.J. Gratian, Q. Zhang, C.F. Bento, M. Renna, F.M. Menzies, and D.C. Rubinsztein. 2018. The RAB11A-positive compartment is a primary platform for autophagosome assembly mediated by WIPI2 recognition of PI3P-RAB11A. *Dev Cell*. 45:114-131.e8. doi:10.1016/j.devcel.2018.03.008.
- Pytela, R., M.D. Pierschbacher, and E. Ruoslahti. 1985. Identification and isolation of a 140 kd cell surface glycoprotein with properties expected of a fibronectin receptor. *Cell*. 40:191–198. doi:10.1016/0092-8674(85)90322-8.
- Qiang, L., B. Zhao, M. Ming, N. Wang, T.-C. He, S. Hwang, A. Thorburn, and Y.-Y. He. 2014. Regulation of cell proliferation and migration by p62 through stabilization of Twist1. *Proc Natl Acad Sci USA*. 111:9241–9246. doi:10.1073/pnas.1322913111.
- Qu, X., J. Yu, G. Bhagat, N. Furuya, H. Hibshoosh, A. Troxel, J. Rosen, E.-L. Eskelinen, N. Mizushima, Y. Ohsumi, G. Cattoretti, and B. Levine. 2003. Promotion of tumorigenesis by heterozygous disruption of the beclin 1 autophagy gene. *J Clin Invest*. 112:1809–1820. doi:10.1172/JCI20039.
- Rabanal-Ruiz, Y., E.G. Otten, and V.I. Korolchuk. 2017. mTORC1 as the main gateway to autophagy. *Essays Biochem*. 61:565–584. doi:10.1042/EBC20170027.
- Ragusa, M.J., R.E. Stanley, and J.H. Hurley. 2012. Architecture of the Atg17 complex as a scaffold for autophagosome biogenesis. *Cell*. 151:1501–1512. doi:10.1016/j.cell.2012.11.028.
- Rahajeng, J., R.S. Kuna, S.L. Makowski, T.T.T. Tran, M.D. Buschman, S. Li, N. Cheng, M.M. Ng, and S.J. Field. 2019. Efficient Golgi forward trafficking requires GOLPH3-driven, PI4P-dependent membrane curvature. *Dev Cell*. 50:573-585.e5. doi:10.1016/j.devcel.2019.05.038.
- Rahmeh, R., M. Damian, M. Cottet, H. Orcel, C. Mendre, T. Durroux, K.S. Sharma, G. Durand, B. Pucci, E. Trinquet, J.M. Zwier, X. Deupi, P. Bron, J.-L. Baneres, B. Mouillac, and S. Granier. 2012. Structural insights into biased G protein-coupled receptor signaling revealed by fluorescence spectroscopy. *Proc Natl Acad Sci USA*. 109:6733–6738. doi:10.1073/pnas.1201093109.
- Rao, Y., M.G. Perna, B. Hofmann, V. Beier, and T. Wollert. 2016. The Atg1–kinase complex tethers Atg9-vesicles to initiate autophagy. *Nat Commun*. 7:10338. doi:10.1038/ncomms10338.

Bibliographical references

- Rappoport, J.Z., and S.M. Simon. 2003. Real-time analysis of clathrin-mediated endocytosis during cell migration. *J Cell Sci.* 116:847–855. doi:10.1242/jcs.00289.
- Rappoport, J.Z., and S.M. Simon. 2009. Endocytic trafficking of activated EGFR is AP-2 dependent and occurs through preformed clathrin spots. *J Cell Sci.* 122:1301–1305. doi:10.1242/jcs.040030.
- Ravikumar, B., K. Moreau, L. Jahreiss, C. Puri, and D.C. Rubinsztein. 2010. Plasma membrane contributes to the formation of pre-autophagosomal structures. *Nat Cell Biol.* 12:747–757. doi:10.1038/ncb2078.
- Rebecca, V.W., and R.K. Amaravadi. 2016. Emerging strategies to effectively target autophagy in cancer. *Oncogene.* 35:1–11. doi:10.1038/onc.2015.99.
- Rebecca, V.W., M.C. Nicastri, C. Fennelly, C.I. Chude, J.S. Barber-Rotenberg, A. Ronghe, Q. McAfee, N.P. McLaughlin, G. Zhang, A.R. Goldman, R. Ojha, S. Piao, E. Noguera-Ortega, A. Martorella, G.M. Alicea, J.J. Lee, L.M. Schuchter, X. Xu, M. Herlyn, R. Marmorstein, P.A. Gimotty, D.W. Speicher, J.D. Winkler, and R.K. Amaravadi. 2019. PPT1 promotes tumor growth and is the molecular target of chloroquine derivatives in cancer. *Cancer Discov.* 9:220–229. doi:10.1158/2159-8290.CD-18-0706.
- Rebecca, V.W., M.C. Nicastri, N. McLaughlin, C. Fennelly, Q. McAfee, A. Ronghe, M. Nofal, C.-Y. Lim, E. Witze, C.I. Chude, G. Zhang, G.M. Alicea, S. Piao, S. Murugan, R. Ojha, S.M. Levi, Z. Wei, J.S. Barber-Rotenberg, M.E. Murphy, G.B. Mills, Y. Lu, J. Rabinowitz, R. Marmorstein, Q. Liu, S. Liu, X. Xu, M. Herlyn, R. Zoncu, D.C. Brady, D.W. Speicher, J.D. Winkler, and R.K. Amaravadi. 2017. A unified approach to targeting the lysosome's degradative and growth signaling roles. *Cancer Discov.* 7:1266–1283. doi:10.1158/2159-8290.CD-17-0741.
- Reggiori, F., T. Shintani, H. Chong, U. Nair, and D.J. Klionsky. 2005. Atg9 cycles between mitochondria and the pre-autophagosomal structure in yeasts. *Autophagy.* 1:101–109. doi:10.4161/auto.1.2.1840.
- Ren, G., M.S. Crampton, and A.S. Yap. 2009. Cortactin: Coordinating adhesion and the actin cytoskeleton at cellular protrusions. *Cell Motil. Cytoskeleton.* 66:865–873. doi:10.1002/cm.20380.
- van Rheenen, J., J. Condeelis, and M. Glogauer. 2009. A common cofilin activity cycle in invasive tumor cells and inflammatory cells. *J Cell Sci.* 122:305–311. doi:10.1242/jcs.031146.
- Ridley, A.J. 2011. Life at the leading edge. *Cell.* 145:1012–1022. doi:10.1016/j.cell.2011.06.010.
- Ridley, A.J., M.A. Schwartz, K. Burridge, R.A. Firtel, M.H. Ginsberg, G. Borisy, J.T. Parsons, and A.R. Horwitz. 2003. Cell migration: integrating signals from front to back. *Science.* 302:1704–1709. doi:10.1126/science.1092053.
- Riggs, K.A., N. Hasan, D. Humphrey, C. Raleigh, C. Nevitt, D. Corbin, and C. Hu. 2012. Regulation of integrin endocytic recycling and chemotactic cell migration by syntaxin 6 and VAMP3 interaction. *J Cell Sci.* 125:3827–3839. doi:10.1242/jcs.102566.

Bibliographical references

- Ripamonti, M., N. Liaudet, L. Azizi, D. Bouvard, V.P. Hytönen, and B. Wehrle-Haller. 2021. Structural and functional analysis of LIM domain-dependent recruitment of paxillin to $\alpha\beta 3$ integrin-positive focal adhesions. *Commun Biol.* 4:380. doi:10.1038/s42003-021-01886-9.
- Rizzoli, S.O., and R. Jahn. 2007. Kiss-and-run, collapse and 'readily retrievable' vesicles. *Traffic.* 8:1137–1144. doi:10.1111/j.1600-0854.2007.00614.x.
- Robinson, M.S. 2015. Forty years of clathrin-coated vesicles. *Traffic.* 16:1210–1238. doi:10.1111/tra.12335.
- Rogers, S.L., P.C. Letourneau, S.L. Palm, J. McCarthy, and L.T. Furcht. 1983. Neurite extension by peripheral and central nervous system neurons in response to substratum-bound fibronectin and laminin. *Developmental Biology.* 98:212–220. doi:10.1016/0012-1606(83)90350-0.
- Rohatgi, R., H.H. Ho, and M.W. Kirschner. 2000. Mechanism of N-Wasp activation by Cdc42 and phosphatidylinositol 4,5-bisphosphate. *J Cell Biol.* 150:1299–1310. doi:10.1083/jcb.150.6.1299.
- Rosenfeld, M.R., X. Ye, J.G. Supko, S. Desideri, S.A. Grossman, S. Brem, T. Mikkelsen, D. Wang, Y.C. Chang, J. Hu, Q. McAfee, J. Fisher, A.B. Troxel, S. Piao, D.F. Heitjan, K.-S. Tan, L. Pontiggia, P.J. O'Dwyer, L.E. Davis, and R.K. Amaravadi. 2014. A phase I/II trial of hydroxychloroquine in conjunction with radiation therapy and concurrent and adjuvant temozolomide in patients with newly diagnosed glioblastoma multiforme. *Autophagy.* 10:1359–1368. doi:10.4161/auto.28984.
- Rottner, K., A. Hall, and J.V. Small. 1999. Interplay between Rac and Rho in the control of substrate contact dynamics. *Curr Biol.* 9:640-51. doi:10.1016/S0960-9822(99)80286-3.
- Rotty, J.D. 2020. Actin cytoskeleton: Profilin gives cells an edge. *Curr Biol.* 30:R807–R809. doi:10.1016/j.cub.2020.05.041.
- Rotty, J.D., C. Wu, and J.E. Bear. 2013. New insights into the regulation and cellular functions of the ARP2/3 complex. *Nat Rev Mol Cell Biol.* 14:7–12. doi:10.1038/nrm3492.
- Rozario, T., and D.W. DeSimone. 2010. The extracellular matrix in development and morphogenesis: A dynamic view. *Dev Biol.* 341:126–140. doi:10.1016/j.ydbio.2009.10.026.
- Rubin, J.B. 2009. Chemokine signaling in cancer: One hump or two? *Semin Cancer Biol.* 19:116–122. doi:10.1016/j.semcancer.2008.10.001.
- Russell, R.C., Y. Tian, H. Yuan, H.W. Park, Y.-Y. Chang, J. Kim, H. Kim, T.P. Neufeld, A. Dillin, and K.-L. Guan. 2013. ULK1 induces autophagy by phosphorylating Beclin-1 and activating VPS34 lipid kinase. *Nat Cell Biol.* 15:741–750. doi:10.1038/ncb2757.

Bibliographical references

- Russell, R.C., H.-X. Yuan, and K.-L. Guan. 2014. Autophagy regulation by nutrient signaling. *Cell Res.* 24:42–57. doi:10.1038/cr.2013.166.
- Ryan, T.A. 2003. Kiss-and-run, fuse-pinch-and-linger, fuse-and-collapse: The life and times of a neurosecretory granule. *Proc Natl Acad Sci USA.* 100:2171–2173. doi:10.1073/pnas.0530260100.
- Saitoh, T., N. Fujita, M.H. Jang, S. Uematsu, B.-G. Yang, T. Satoh, H. Omori, T. Noda, N. Yamamoto, M. Komatsu, K. Tanaka, T. Kawai, T. Tsujimura, O. Takeuchi, T. Yoshimori, and S. Akira. 2008. Loss of the autophagy protein Atg16L1 enhances endotoxin-induced IL-1 β production. *Nature.* 456:264–268. doi:10.1038/nature07383.
- Sakai, M., N. Araki, and K. Ogawa. 1989. Lysosomal movements during heterophagy and autophagy: With special reference to nematolysosome and wrapping lysosome. *J. Elec. Microsc. Tech.* 12:101–131. doi:10.1002/jemt.1060120206.
- Sancak, Y., L. Bar-Peled, R. Zoncu, A.L. Markhard, S. Nada, and D.M. Sabatini. 2010. Ragulator-Rag complex targets mTORC1 to the lysosomal surface and is necessary for its activation by amino acids. *Cell.* 141:290–303. doi:10.1016/j.cell.2010.02.024.
- Sancak, Y., T.R. Peterson, Y.D. Shaul, R.A. Lindquist, C.C. Thoreen, L. Bar-Peled, and D.M. Sabatini. 2008. The Rag GTPases bind Raptor and mediate amino acid signaling to mTORC1. *Science.* 320:1496–1501. doi:10.1126/science.1157535.
- Sawa-Makarska, J., V. Baumann, N. Coudeville, S. von Bülow, V. Nogellova, C. Abert, M. Schuschnig, M. Graef, G. Hummer, and S. Martens. 2020. Reconstitution of autophagosome nucleation defines Atg9 vesicles as seeds for membrane formation. *Science.* 369:eaaz7714. doi:10.1126/science.aaz7714.
- Schaefer, L., and R.M. Schaefer. 2010. Proteoglycans: from structural compounds to signaling molecules. *Cell Tissue Res.* 339:237–246. doi:10.1007/s00441-009-0821-y.
- Schaller, M.D., C.A. Otey, J.D. Hildebrand, and J.T. Parsons. 1995. Focal adhesion kinase and paxillin bind to peptides mimicking beta integrin cytoplasmic domains. *J Cell Biol.* 130:1181–1187. doi:10.1083/jcb.130.5.1181.
- Schlaepfer, D.D., S.K. Mitra, and D. Ilic. 2004. Control of motile and invasive cell phenotypes by focal adhesion kinase. *Biochim Biophys Acta.* 1692:77–102. doi:10.1016/j.bbamcr.2004.04.008.
- Schlessinger, J. 2000. Cell signaling by receptor tyrosine kinases. *Cell.* 103:211–225. doi:10.1016/S0092-8674(00)00114-8.
- Schmoranzler, J. 2003. Migrating fibroblasts perform polarized, microtubule-dependent exocytosis towards the leading edge. *J Cell Sci.* 116:4513–4519. doi:10.1242/jcs.00748.

Bibliographical references

- Schütter, M., P. Giavalisco, S. Brodesser, and M. Graef. 2020. Local fatty acid channeling into phospholipid synthesis drives phagophore expansion during autophagy. *Cell*. 180:135-149.e14. doi:10.1016/j.cell.2019.12.005.
- Scita, G., and P.P. Di Fiore. 2010. The endocytic matrix. *Nature*. 463:464–473. doi:10.1038/nature08910.
- Ségaliny, A.I., M. Tellez-Gabriel, M.-F. Heymann, and D. Heymann. 2015. Receptor tyrosine kinases: Characterisation, mechanism of action and therapeutic interests for bone cancers. *J Bone Oncol*. 4:1–12. doi:10.1016/j.jbo.2015.01.001.
- SenGupta, S., C.A. Parent, and J.E. Bear. 2021. The principles of directed cell migration. *Nat Rev Mol Cell Biol*. 22:529–547. doi:10.1038/s41580-021-00366-6.
- Serrano, K., and D.V. Devine. 2004. Vinculin is proteolyzed by calpain during platelet aggregation: 95 kDa cleavage fragment associates with the platelet cytoskeleton. *Cell Motil. Cytoskeleton*. 58:242–252. doi:10.1002/cm.20011.
- Servant, G., O.D. Weiner, E.R. Neptune, J.W. Sedat, and H.R. Bourne. 1999. Dynamics of a chemoattractant receptor in living neutrophils during chemotaxis. *MBoC*. 10:1163–1178. doi:10.1091/mbc.10.4.1163.
- Shafaq-Zadah, M., C.S. Gomes-Santos, S. Bardin, P. Maiuri, M. Maurin, J. Iranzo, A. Gautreau, C. Lamaze, P. Caswell, B. Goud, and L. Johannes. 2016. Persistent cell migration and adhesion rely on retrograde transport of β 1 integrin. *Nat Cell Biol*. 18:54–64. doi:10.1038/ncb3287.
- Sharifi, M.N., E.E. Mowers, L.E. Drake, C. Collier, H. Chen, M. Zamora, S. Mui, and K.F. Macleod. 2016. Autophagy promotes focal adhesion disassembly and cell motility of metastatic tumor cells through the direct interaction of Paxillin with LC3. *Cell Reports*. 15:1660–1672. doi:10.1016/j.celrep.2016.04.065.
- Shattil, S.J., C. Kim, and M.H. Ginsberg. 2010. The final steps of integrin activation: the end game. *Nat Rev Mol Cell Biol*. 11:288–300. doi:10.1038/nrm2871.
- Shin, M.C., J. Zhang, K.A. Min, K. Lee, Y. Byun, A.E. David, H. He, and V.C. Yang. 2014. Cell-penetrating peptides: Achievements and challenges in application for cancer treatment. *J Biomed Mater Res*. 102:575–587. doi:10.1002/jbm.a.34859.
- Shinojima, N., K. Tada, S. Shiraishi, T. Kamiryo, M. Kochi, H. Nakamura, K. Makino, H. Saya, H. Hirano, J.-I. Kuratsu, K. Oka, Y. Ishimaru, and Y. Ushio. 2003. Prognostic value of epidermal growth factor receptor in patients with glioblastoma multiforme. *Cancer Res*. 63:6962–6970.
- Sigismund, S., T. Woelk, C. Puri, E. Maspero, C. Tacchetti, P. Transidico, P.P. Di Fiore, and S. Polo. 2005. Clathrin-independent endocytosis of ubiquitinated cargos. *Proc Natl Acad Sci USA*. 102:2760–2765. doi:10.1073/pnas.0409817102.

Bibliographical references

- Simonson, W.T.N., S.J. Franco, and A. Huttenlocher. 2006. Talin1 regulates TCR-mediated LFA-1 function. *J Immunol.* 177:7707–7714. doi:10.4049/jimmunol.177.11.7707.
- Simunovic, M., G.A. Voth, A. Callan-Jones, and P. Bassereau. 2015. When physics takes over: BAR proteins and membrane curvature. *Trends Cell Biol.* 25:780–792. doi:10.1016/j.tcb.2015.09.005.
- Skruber, K., P.V. Warp, R. Shklyarov, J.D. Thomas, M.S. Swanson, J.L. Henty-Ridilla, T.-A. Read, and E.A. Vitriol. 2020. Arp2/3 and Mena/VASP require Profilin 1 for actin network assembly at the leading edge. *Curr Biol.* 30:2651–2664.e5. doi:10.1016/j.cub.2020.04.085.
- Small, J.V., B. Geiger, I. Kaverina, and A. Bershadsky. 2002. How do microtubules guide migrating cells? *Nat Rev Mol Cell Biol.* 3:957–964. doi:10.1038/nrm971.
- Smith, J.S., I. Tachibana, S.M. Passe, B.K. Huntley, T.J. Borell, N. Iturria, J.R. O’Fallon, P.L. Schaefer, B.W. Scheithauer, C.D. James, J.C. Buckner, and R.B. Jenkins. 2001. PTEN mutation, EGFR amplification, and outcome in patients with anaplastic astrocytoma and glioblastoma multiforme. *J Natl Cancer Inst.* 93:1246–1256. doi:10.1093/jnci/93.16.1246.
- Sneeggen, M., N.M. Pedersen, C. Campsteijn, E.M. Haugsten, H. Stenmark, and K.O. Schink. 2019. WDFY2 restrains matrix metalloproteinase secretion and cell invasion by controlling VAMP3-dependent recycling. *Nat Commun.* 10:2850. doi:10.1038/s41467-019-10794-w.
- Sjøreng, K., M.J. Munson, C.A. Lamb, G.T. Bjørndal, S. Pankiv, S.R. Carlsson, S.A. Tooze, and A. Simonsen. 2018. SNX18 regulates ATG9A trafficking from recycling endosomes by recruiting Dynamin-2. *EMBO Rep.* 19. doi:10.15252/embr.201744837.
- Sotelo, J., E. Briceño, and M.A. López-González. 2006. Adding chloroquine to conventional treatment for glioblastoma multiforme: a randomized, double-blind, placebo-controlled trial. *Ann Intern Med.* 144:337. doi:10.7326/0003-4819-144-5-200603070-00008.
- Srinivasan, S., F. Wang, S. Glavas, A. Ott, F. Hofmann, K. Aktories, D. Kalman, and H.R. Bourne. 2003. Rac and Cdc42 play distinct roles in regulating PI(3,4,5)P3 and polarity during neutrophil chemotaxis. *J Cell Biol.* 160:375–385. doi:10.1083/jcb.200208179.
- Steven Wiley, H. 2003. Computational modeling of the EGF-receptor system: a paradigm for systems biology. *Trends in Cell Biol.* 13:43–50. doi:10.1016/S0962-8924(02)00009-0.
- Stevens, C.F., and J.H. Williams. 2000. “Kiss and run” exocytosis at hippocampal synapses. *Proc Natl Acad Sci USA.* 97:12828–12833. doi:10.1073/pnas.230438697.

Bibliographical references

- Su, H., F. Yang, Q. Wang, Q. Shen, J. Huang, C. Peng, Y. Zhang, W. Wan, C.C.L. Wong, Q. Sun, F. Wang, T. Zhou, and W. Liu. 2017. VPS34 acetylation controls its lipid kinase activity and the initiation of canonical and non-canonical autophagy. *Mol Cell*. 67:907-921.e7. doi:10.1016/j.molcel.2017.07.024.
- Sun, T., X. Li, P. Zhang, W.-D. Chen, H. Zhang, D.-D. Li, R. Deng, X.-J. Qian, L. Jiao, J. Ji, Y.-T. Li, R.-Y. Wu, Y. Yu, G.-K. Feng, and X.-F. Zhu. 2015. Acetylation of Beclin 1 inhibits autophagosome maturation and promotes tumour growth. *Nat Commun*. 6:7215. doi:10.1038/ncomms8215.
- Sun, Y., Z. Cheng, L. Ma, and G. Pei. 2002. β -Arrestin2 is critically involved in CXCR4-mediated chemotaxis, and this is mediated by its enhancement of p38 MAPK activation. *J Biol Chem*. 277:49212–49219. doi:10.1074/jbc.M207294200.
- Suraneni, P., B. Fogelson, B. Rubinstein, P. Noguera, N. Volkmann, D. Hanein, A. Mogilner, and R. Li. 2015. A mechanism of leading-edge protrusion in the absence of Arp2/3 complex. *MBoC*. 26:901–912. doi:10.1091/mbc.E14-07-1250.
- Suraneni, P., B. Rubinstein, J.R. Unruh, M. Durnin, D. Hanein, and R. Li. 2012. The Arp2/3 complex is required for lamellipodia extension and directional fibroblast cell migration. *J Cell Biol*. 197:239–251. doi:10.1083/jcb.201112113.
- Suzuki, K., T. Kirisako, Y. Kamada, N. Mizushima, T. Noda, and Y. Ohsumi. 2001. The pre-autophagosomal structure organized by concerted functions of APG genes is essential for autophagosome formation. *EMBO J*. 20:5971–5981. doi:10.1093/emboj/20.21.5971.
- Svitkina, T.M., and G.G. Borisy. 1999. Arp2/3 complex and actin depolymerizing factor/cofilin in dendritic organization and treadmilling of actin filament array in lamellipodia. *J Cell Biol*. 145:1009–1026. doi:10.1083/jcb.145.5.1009.
- Tadokoro, S. 2003. Talin Binding to integrin tails: a final common step in integrin activation. *Science*. 302:103–106. doi:10.1126/science.1086652.
- Taeger, J., C. Moser, C. Hellerbrand, M.E. Mycielska, G. Glockzin, H.J. Schlitt, E.K. Geissler, O. Stoeltzing, and S.A. Lang. 2011. Targeting FGFR/PDGFR/VEGFR impairs tumor growth, angiogenesis, and metastasis by effects on tumor cells, endothelial cells, and pericytes in pancreatic cancer. *Mol Cancer Ther*. 10:2157–2167. doi:10.1158/1535-7163.MCT-11-0312.
- Takahashi, Y., X. Liang, T. Hattori, Z. Tang, H. He, H. Chen, X. Liu, T. Abraham, Y. Imamura-Kawasawa, N.J. Buchkovich, M.M. Young, and H.-G. Wang. 2019. VPS37A directs ESCRT recruitment for phagophore closure. *J Cell Biol*. 218:3336–3354. doi:10.1083/jcb.201902170.

Bibliographical references

- Takahashi, Y., C.L. Meyerkord, T. Hori, K. Runkle, T.E. Fox, M. Kester, T.P. Loughran, and H.-G. Wang. 2011. Bif-1 regulates Atg9 trafficking by mediating the fission of Golgi membranes during autophagy. *Autophagy*. 7:61–73. doi:10.4161/auto.7.1.14015.
- Takahashi, Y., N. Tsotakos, Y. Liu, M.M. Young, J. Serfass, Z. Tang, T. Abraham, and H.-G. Wang. 2016. The Bif-1-Dynamin 2 membrane fission machinery regulates Atg9-containing vesicle generation at the Rab11-positive reservoirs. *Oncotarget*. 7:20855–20868. doi:10.18632/oncotarget.8028.
- Takamura, A., M. Komatsu, T. Hara, A. Sakamoto, C. Kishi, S. Waguri, Y. Eishi, O. Hino, K. Tanaka, and N. Mizushima. 2011. Autophagy-deficient mice develop multiple liver tumors. *Genes Dev*. 25:795–800. doi:10.1101/gad.2016211.
- Takehige, K., M. Baba, S. Tsuboi, T. Noda, and Y. Ohsumi. 1992. Autophagy in yeast demonstrated with proteinase-deficient mutants and conditions for its induction. *J Cell Biol*. 119:301–311. doi:10.1083/jcb.119.2.301.
- Tanaka, M., T. Kikuchi, H. Uno, K. Okita, T. Kitanishi-Yumura, and S. Yumura. 2017. Turnover and flow of the cell membrane for cell migration. *Sci Rep*. 7:12970. doi:10.1038/s41598-017-13438-5.
- Tayeb, M., M. Skalski, M. Cha, M. Kean, M. Scaife, and M. Coppolino. 2005. Inhibition of SNARE-mediated membrane traffic impairs cell migration. *Exp Cell Res*. 305:63–73. doi:10.1016/j.yexcr.2004.12.004.
- Teicher, B.A., and S.P. Fricker. 2010. CXCL12 (SDF-1)/CXCR4 Pathway in Cancer. *Clin Cancer Res*. 16:2927–2931. doi:10.1158/1078-0432.CCR-09-2329.
- Tekirdag, K., and A.M. Cuervo. 2018. Chaperone-mediated autophagy and endosomal microautophagy: Jointed by a chaperone. *J Biol Chem*. 293:5414–5424. doi:10.1074/jbc.R117.818237.
- Tingting, C., Y. Shizhou, Z. Songfa, X. Junfen, L. Weiguo, C. Xiaodong, and X. Xing. 2019. Human papillomavirus 16E6/E7 activates autophagy via Atg9B and LAMP1 in cervical cancer cells. *Cancer Med*. 8:4404–4416. doi:10.1002/cam4.2351.
- Titorenko, V.I., I. Keizer, W. Harder, and M. Veenhuis. 1995. Isolation and characterization of mutants impaired in the selective degradation of peroxisomes in the yeast *Hansenula polymorpha*. *J bacteriol*. 177:357–363. doi:10.1128/JB.177.2.357-363.1995.
- Tokuda, E., T. Itoh, J. Hasegawa, T. Ijuin, Y. Takeuchi, Y. Irino, M. Fukumoto, and T. Takenawa. 2014. Phosphatidylinositol 4-phosphate in the Golgi apparatus regulates cell–cell adhesion and invasive cell migration in human breast cancer. *Cancer Res*. 74:3054–3066. doi:10.1158/0008-5472.CAN-13-2441.

Bibliographical references

- Totsukawa, G., Y. Wu, Y. Sasaki, D.J. Hartshorne, Y. Yamakita, S. Yamashiro, and F. Matsumura. 2004. Distinct roles of MLCK and ROCK in the regulation of membrane protrusions and focal adhesion dynamics during cell migration of fibroblasts. *J Cell Biol.* 164:427–439. doi:10.1083/jcb.200306172.
- Trepat, X., Z. Chen, and K. Jacobson. 2012. Cell migration. In *comprehensive physiology*. 2(4):2369-92. doi: 10.1002/cphy.c110012.
- Tseng, H.-Y., N. Thorausch, T. Ziegler, A. Meves, R. Fässler, and R.T. Böttcher. 2014. Sorting nexin 31 binds multiple β integrin cytoplasmic domains and regulates β 1 Integrin surface levels and stability. *J Mol Biol.* 426:3180–3194. doi:10.1016/j.jmb.2014.07.003.
- Tsuboyama, K., I. Koyama-Honda, Y. Sakamaki, M. Koike, H. Morishita, and N. Mizushima. 2016. The ATG conjugation systems are important for degradation of the inner autophagosomal membrane. *Science.* 354:1036–1041. doi:10.1126/science.aaf6136.
- Tsukada, M., and Y. Ohsumi. 1993. Isolation and characterization of autophagy-defective mutants of *Saccharomyces cerevisiae*. *FEBS Letters.* 333:169–174. doi:10.1016/0014-5793(93)80398-E.
- Tuloup-Minguez, V., ahmed Hamai, A. Greffard, V. Nicolas, P. Codogno, and J. Botti. 2013. Autophagy modulates cell migration and β 1 integrin membrane recycling. *Cell Cycle.* 12:3317–3328. doi:10.4161/cc.26298.
- Turner, C.E. 2000. Paxillin and focal adhesion signalling. *Nat Cell Biol.* 2:E231–E236. doi:10.1038/35046659.
- Turner, C.E., J.R. Glenney, and K. Burridge. 1990. Paxillin: a new vinculin-binding protein present in focal adhesions. *J Cell Biol.* 111:1059–1068. doi:10.1083/jcb.111.3.1059.
- Ullrich, A., and J. Schlessinger. 1990. Signal transduction by receptors with tyrosine kinase activity. *Cell.* 61:203–212. doi:10.1016/0092-8674(90)90801-K.
- Umbrecht-Jenck, E., V. Demais, V. Calco, Y. Bailly, M.-F. Bader, and S. Chasserot-Golaz. 2010. S100A10-mediated translocation of annexin-A2 to SNARE proteins in adrenergic chromaffin cells undergoing exocytosis. *Traffic.* 11:958–971. doi:10.1111/j.1600-0854.2010.01065.x.
- Umekawa, M., and D.J. Klionsky. 2012. The cytoplasm-to-vacuole targeting pathway: a historical perspective. *Int J Cell Biol.* 2012:1–8. doi:10.1155/2012/142634.
- van der Vaart, A., J. Griffith, and F. Reggiori. 2010. Exit from the Golgi is required for the expansion of the autophagosomal phagophore in yeast *Saccharomyces cerevisiae*. *MBoC.* 21:2270–2284. doi:10.1091/mbc.e09-04-0345.

Bibliographical references

- Van Keymeulen, A., K. Wong, Z.A. Knight, C. Govaerts, K.M. Hahn, K.M. Shokat, and H.R. Bourne. 2006. To stabilize neutrophil polarity, PIP3 and Cdc42 augment RhoA activity at the back as well as signals at the front. *J Cell Biol.* 174:437–445. doi:10.1083/jcb.200604113.
- Vats, S., and T. Galli. 2021. Introducing secretory reticulophagy/ER-phagy (SERP), a VAMP7-dependent pathway involved in neurite growth. *Autophagy.* 17:1037–1039. doi:10.1080/15548627.2021.1883886.
- Veale, K.J., C. Offenhäuser, and R.Z. Murray. 2011. The role of the recycling endosome in regulating lamellipodia formation and macrophage migration. *Commun Integr Biol.* 4:44–47. doi:10.4161/cib.4.1.13569.
- Veale, K.J., C. Offenhäuser, S.P. Whittaker, R.P. Estrella, and R.Z. Murray. 2010. Recycling endosome membrane incorporation into the leading edge regulates lamellipodia formation and macrophage migration. *Traffic.* 11:1370–1379. doi:10.1111/j.1600-0854.2010.01094.x.
- Verbeek, B.S., S.S. Adriaansen-Slot, T.M. Vroom, T. Beckers, and G. Rijksen. 1998. Overexpression of EGFR and c-erbB2 causes enhanced cell migration in human breast cancer cells and NIH3T3 fibroblasts. *FEBS Letters.* 425:145–150. doi:10.1016/S0014-5793(98)00224-5.
- Vitorino, P., and T. Meyer. 2008. Modular control of endothelial sheet migration. *Genes & Development.* 22:3268–3281. doi:10.1101/gad.1725808.
- Vitriol, E.A., L.M. McMillen, M. Kapustina, S.M. Gomez, D. Vavylonis, and J.Q. Zheng. 2015. Two functionally distinct sources of actin monomers supply the leading edge of lamellipodia. *Cell Reports.* 11:433–445. doi:10.1016/j.celrep.2015.03.033.
- Vogel, G., L. Thilo, H. Schwarz, and R. Steinhart. 1980. Mechanism of phagocytosis in dictyostelium discoideum: phagocytosis is mediated by different recognition sites as disclosed by mutants with altered phagocytotic properties. *J Cell Biol.* 86:456–465. doi:10.1083/jcb.86.2.456.
- Wang, J., and K.E. Howell. 2000. The luminal domain of TGN38 interacts with integrin β 1 and is involved in its trafficking. *Traffic.* 1:713–723. doi:10.1034/j.1600-0854.2000.010904.x.
- Wang, K., Y. Qi, X. Wang, Y. Liu, M. Zhao, D. Zhou, Y. Zhang, Y. Wang, R. Yu, and X. Zhou. 2021. GOLPH3 promotes glioma progression by enhancing PHB2-mediated autophagy. *Am J Cancer Res.* 11:2106–2123.
- Wang, L., K. Zhao, B. Ren, M. Zhu, C. Zhang, P. Zhao, H. Zhou, L. Chen, S. Yu, and X. Yang. 2015. Expression of cortactin in human gliomas and its effect on migration and invasion of glioma cells. *Oncol Rep.* 34:1815–1824. doi:10.3892/or.2015.4156.
- Wang, N., H.-Y. Tan, S. Li, and Y. Feng. 2017. Atg9b deficiency suppresses autophagy and potentiates endoplasmic reticulum stress-associated hepatocyte apoptosis in hepatocarcinogenesis. *Theranostics.* 7:2325–2338. doi:10.7150/thno.18225.

Bibliographical references

- Wang, X., Z. Wang, Y. Zhang, Y. Wang, H. Zhang, S. Xie, P. Xie, R. Yu, and X. Zhou. 2019. Golgi phosphoprotein 3 sensitizes the tumour suppression effect of gefitinib on gliomas. *Cell Prolif.* 52. doi:10.1111/cpr.12636.
- Wang, Z., G. Miao, X. Xue, X. Guo, C. Yuan, Z. Wang, G. Zhang, Y. Chen, D. Feng, J. Hu, and H. Zhang. 2016. The Vici syndrome protein EPG5 is a Rab7 effector that determines the fusion specificity of autophagosomes with late endosomes/lysosomes. *Mol Cell.* 63:781–795. doi:10.1016/j.molcel.2016.08.021.
- Wei, Y., Z. Zou, N. Becker, M. Anderson, R. Sumpter, G. Xiao, L. Kinch, P. Koduru, C.S. Christudass, R.W. Veltri, N.V. Grishin, M. Peyton, J. Minna, G. Bhagat, and B. Levine. 2013. EGFR-mediated Beclin 1 phosphorylation in autophagy suppression, tumor progression, and tumor chemoresistance. *Cell.* 154:1269–1284. doi:10.1016/j.cell.2013.08.015.
- Weidberg, H., E. Shvets, T. Shpilka, F. Shimron, V. Shinder, and Z. Elazar. 2010. LC3 and GATE-16/GABARAP subfamilies are both essential yet act differently in autophagosome biogenesis. *EMBO J.* 29:1792–1802. doi:10.1038/emboj.2010.74.
- Weiner, O.D. 2002a. Regulation of cell polarity during eukaryotic chemotaxis: the chemotactic compass. *Curr Opin Cell Biol.* 14:196–202. doi:10.1016/S0955-0674(02)00310-1.
- Weiner, O.D. 2002b. Rac activation: P-Rex1 - a convergence point for PIP(3) and Gbetagamma? *Curr. Biol.* 12:R429-431. doi:10.1016/s0960-9822(02)00917-x.
- Weiner, O.D., P.O. Nielsen, G.D. Prestwich, M.W. Kirschner, L.C. Cantley, and H.R. Bourne. 2002. A ptdInsP3- and Rho GTPase-mediated positive feedback loop regulates neutrophil polarity. *Nat Cell Biol.* 4:509–513. doi:10.1038/ncb811.
- Wen, J.-K., Y.-T. Wang, C.-C. Chan, C.-W. Hsieh, H.-M. Liao, C.-C. Hung, and G.-C. Chen. 2017. Atg9 antagonizes TOR signaling to regulate intestinal cell growth and epithelial homeostasis in *Drosophila*. *eLife.* 6:e29338. doi:10.7554/eLife.29338.
- Wen, P.J., S. Grenklo, G. Arpino, X. Tan, H.-S. Liao, J. Heureaux, S.-Y. Peng, H.-C. Chiang, E. Hamid, W.-D. Zhao, W. Shin, T. Näreoja, E. Evergren, Y. Jin, R. Karlsson, S.N. Ebert, A. Jin, A.P. Liu, O. Shupliakov, and L.-G. Wu. 2016. Actin dynamics provides membrane tension to merge fusing vesicles into the plasma membrane. *Nat Commun.* 7:12604. doi:10.1038/ncomms12604.
- Westhoff, M.A., B. Serrels, V.J. Fincham, M.C. Frame, and N.O. Carragher. 2004. Src-mediated phosphorylation of focal adhesion kinase couples actin and adhesion dynamics to survival signaling. *Mol Cell Biol.* 24:8113–8133. doi:10.1128/MCB.24.18.8113-8133.2004.

Bibliographical references

- White, D.P., P.T. Caswell, and J.C. Norman. 2007. $\alpha\beta3$ and $\alpha5\beta1$ integrin recycling pathways dictate downstream Rho kinase signaling to regulate persistent cell migration. *J Cell Biol.* 177:515–525. doi:10.1083/jcb.200609004.
- Wijdeven, R.H., H. Janssen, L. Nahidiazar, L. Janssen, K. Jalink, I. Berlin, and J. Neefjes. 2016. Cholesterol and ORP1L-mediated ER contact sites control autophagosome transport and fusion with the endocytic pathway. *Nat Commun.* 7:11808. doi:10.1038/ncomms11808.
- Williamson, R.C., and M.D. Bass. 2015. Comparing the affinity of GTPase-binding proteins using competition assays. *JoVE.* 53254. doi:10.3791/53254.
- Wise, S.G., and A.S. Weiss. 2009. Tropoelastin. *Int J Biochem Cell Biol.* 41:494–497. doi:10.1016/j.biocel.2008.03.017.
- Wixler, V., D. Geerts, E. Laplantine, D. Westhoff, N. Smyth, M. Aumailley, A. Sonnenberg, and M. Paulsson. 2000. The LIM-only protein DRAL/FHL2 binds to the cytoplasmic domain of several α and β integrin chains and is recruited to adhesion complexes. *J Biol Chem.* 275:33669–33678. doi:10.1074/jbc.M002519200.
- Wojnacki, J., S. Nola, P. Bun, B. Cholley, F. Filippini, M.T. Pressé, J. Lipecka, S. Man Lam, J. N'guyen, A. Simon, A. Ouslimani, G. Shui, C.M. Fader, M.I. Colombo, I.C. Guerrero, and T. Galli. 2020. Role of VAMP7-dependent secretion of reticulon 3 in neurite growth. *Cell Reports.* 33:108536. doi:10.1016/j.celrep.2020.108536.
- Wolfman, A., and I. Macara. 1990. A cytosolic protein catalyzes the release of GDP from p21ras. *Science.* 248:67–69. doi:10.1126/science.2181667.
- Wong, P.-M., C. Puente, I.G. Ganley, and X. Jiang. 2013. The ULK1 complex: sensing nutrient signals for autophagy activation. *Autophagy.* 9:124–137. doi:10.4161/auto.23323.
- Worby, C.A., and J.E. Dixon. 2014. PTEN. *Annu. Rev. Biochem.* 83:641–669. doi:10.1146/annurev-biochem-082411-113907.
- Wu, C., S.B. Asokan, M.E. Berginski, E.M. Haynes, N.E. Sharpless, J.D. Griffith, S.M. Gomez, and J.E. Bear. 2012. Arp2/3 is critical for lamellipodia and response to extracellular matrix cues but is dispensable for chemotaxis. *Cell.* 148:973–987. doi:10.1016/j.cell.2011.12.034.
- Wu, X., M.J. Bradley, Y. Cai, D. Kummel, E.M. De La Cruz, F.A. Barr, and K.M. Reinisch. 2011. Insights regarding guanine nucleotide exchange from the structure of a DENN-domain protein complexed with its Rab GTPase substrate. *Proc Natl Acad Sci USA.* 108:18672–18677. doi:10.1073/pnas.1110415108.
- Wu, Y.I., D. Frey, O.I. Lungu, A. Jaehrig, I. Schlichting, B. Kuhlman, and K.M. Hahn. 2009. A genetically encoded photoactivatable Rac controls the motility of living cells. *Nature.* 461:104–108. doi:10.1038/nature08241.

Bibliographical references

- Xiao, Z., N. Zhang, D.B. Murphy, and P.N. Devreotes. 1997. Dynamic distribution of chemoattractant receptors in living cells during chemotaxis and persistent stimulation. *J Cell Biol.* 139:365–374. doi:10.1083/jcb.139.2.365.
- Xie, J., Y. Bi, H. Zhang, S. Dong, L. Teng, R.J. Lee, and Z. Yang. 2020. Cell-penetrating peptides in diagnosis and treatment of human diseases: from preclinical research to clinical application. *Front. Pharmacol.* 11:697. doi:10.3389/fphar.2020.00697.
- Xie, Z., U. Nair, and D.J. Klionsky. 2008. Atg8 controls phagophore expansion during autophagosome formation. *MBoC.* 19:3290–3298. doi:10.1091/mbc.e07-12-1292.
- Xing, M., M.C. Peterman, R.L. Davis, K. Oegema, A.K. Shiau, and S.J. Field. 2016. GOLPH3 drives cell migration by promoting Golgi reorientation and directional trafficking to the leading edge. *MBoC.* 27:3828–3840. doi:10.1091/mbc.E16-01-0005.
- Yadav, S., S. Puri, and A.D. Linstedt. 2009. A primary role for Golgi positioning in directed secretion, cell polarity, and wound healing. *MBoC.* 20:1728–1736. doi:10.1091/mbc.e08-10-1077.
- Yamaguchi, J., C. Suzuki, T. Nanao, S. Kakuta, K. Ozawa, I. Tanida, T. Saitoh, T. Sunabori, M. Komatsu, K. Tanaka, S. Aoki, K. Sakimura, and Y. Uchiyama. 2018. Atg9a deficiency causes axon-specific lesions including neuronal circuit dysgenesis. *Autophagy.* 14:764–777. doi:10.1080/15548627.2017.1314897.
- Yang, C., L. Czech, S. Gerboth, S. Kojima, G. Scita, and T. Svitkina. 2007. Novel roles of formin mDia2 in lamellipodia and filopodia formation in motile cells. *PLoS Biol.* 5:e317. doi:10.1371/journal.pbio.0050317.
- Yang, C., and T. Svitkina. 2011. Filopodia initiation: Focus on the Arp2/3 complex and formins. *Cell Adh Migr.* 5:402–408. doi:10.4161/cam.5.5.16971.
- Ye, H., Y. Zhang, L. Geng, and Z. Li. 2015. Cdc42 expression in cervical cancer and its effects on cervical tumor invasion and migration. *Int J Oncol.* 46:757–763. doi:10.3892/ijo.2014.2748.
- Ylä-Anttila, P., H. Vihinen, E. Jokitalo, and E.-L. Eskelinen. 2009. 3D tomography reveals connections between the phagophore and endoplasmic reticulum. *Autophagy.* 5:1180–1185. doi:10.4161/auto.5.8.10274.
- Young, A.R.J., E.Y.W. Chan, X.W. Hu, R. Köchl, J. Lippincott-Schwartz, and S.A. Tooze. 2006. Starvation and ULK1-dependent cycling of mammalian Atg9 between the TGN and endosomes. *J Cell Sci.* 119:3888–3900. doi:10.1242/jcs.03172.
- Yuan, W., P.E. Strømhaug, and W.A. Dunn. 1999. Glucose-induced autophagy of peroxisomes in *Pichia pastoris* requires a unique E1-like protein. *MBoC.* 10:1353–1366. doi:10.1091/mbc.10.5.1353.
- Yun, C., and S. Lee. 2018. The roles of autophagy in cancer. *IJMS.* 19:3466. doi:10.3390/ijms19113466.

Bibliographical references

- Zaarour, R.F., B. Azakir, E.Y. Hajam, H. Nawafleh, N.A. Zeinelabdin, A.S.T. Engelsen, J. Thiery, C. Jamora, and S. Chouaib. 2021. Role of hypoxia-mediated autophagy in tumor cell death and survival. *Cancers*. 13:533. doi:10.3390/cancers13030533.
- Zahedi, S., B.E. Fitzwalter, A. Morin, S. Grob, M. Desmarais, A. Nellan, A.L. Green, R. Vibhakar, T.C. Hankinson, N.K. Foreman, and J.M. Mulcahy Levy. 2019. Effect of early-stage autophagy inhibition in BRAFV600E autophagy-dependent brain tumor cells. *Cell Death Dis.* 10:679. doi:10.1038/s41419-019-1880-y.
- Zaidel-Bar, R. 2003. Early molecular events in the assembly of matrix adhesions at the leading edge of migrating cells. *J Cell Sci.* 116:4605–4613. doi:10.1242/jcs.00792.
- Zamir, E., B.Z. Katz, S. Aota, K.M. Yamada, B. Geiger, and Z. Kam. 1999. Molecular diversity of cell-matrix adhesions. *J. Cell. Sci.* 112 (Pt 11):1655–1669.
- Zaoui, K., K. Benseddik, P. Daou, D. Salaun, and A. Badache. 2010. ErbB2 receptor controls microtubule capture by recruiting ACF7 to the plasma membrane of migrating cells. *Proc Natl Acad Sci USA.* 107:18517–18522. doi:10.1073/pnas.1000975107.
- Zhang, H., M. Bosch-Marce, L.A. Shimoda, Y.S. Tan, J.H. Baek, J.B. Wesley, F.J. Gonzalez, and G.L. Semenza. 2008. Mitochondrial autophagy is an HIF-1-dependent adaptive metabolic response to hypoxia. *J Biol Chem.* 283:10892–10903. doi:10.1074/jbc.M800102200.
- Zhao, L., P. Liu, G. Boncompain, F. Loos, S. Lachkar, L. Bezu, G. Chen, H. Zhou, F. Perez, O. Kepp, and G. Kroemer. 2018. Identification of pharmacological inhibitors of conventional protein secretion. *Sci Rep.* 8:14966. doi:10.1038/s41598-018-33378-y.
- Zhong, Y., T. Long, C.-S. Gu, J.-Y. Tang, L.-F. Gao, J.-X. Zhu, Z.-Y. Hu, X. Wang, Y.-D. Ma, Y.-Q. Ding, Z.-G. Li, and X.-Y. Wang. 2021. MYH9-dependent polarization of ATG9B promotes colorectal cancer metastasis by accelerating focal adhesion assembly. *Cell Death Differ.* doi:10.1038/s41418-021-00813-z.
- Zhou, C., K. Ma, R. Gao, C. Mu, L. Chen, Q. Liu, Q. Luo, D. Feng, Y. Zhu, and Q. Chen. 2017. Regulation of mATG9 trafficking by Src- and ULK1-mediated phosphorylation in basal and starvation-induced autophagy. *Cell Res.* 27:184–201. doi:10.1038/cr.2016.146.
- Zhou, F., Z. Wu, M. Zhao, R. Murtazina, J. Cai, A. Zhang, R. Li, D. Sun, W. Li, L. Zhao, Q. Li, J. Zhu, X. Cong, Y. Zhou, Z. Xie, V. Gyurkovska, L. Li, X. Huang, Y. Xue, L. Chen, H. Xu, H. Xu, Y. Liang, and N. Segev. 2019. Rab5-dependent autophagosome closure by ESCRT. *J Cell Biol.* 218:1908–1927. doi:10.1083/jcb.201811173.

SUPPLEMENTARY PUBLICATION



Targeting the Urotensin II/UT G Protein-Coupled Receptor to Counteract Angiogenesis and Mesenchymal Hypoxia/Necrosis in Glioblastoma

OPEN ACCESS

Edited by:

Lucas Treppe,
 VIB-KU Leuven Center for Cancer
 Biology, Belgium

Reviewed by:

Michele Caraglia,
 University of Campania Luigi Vanvitelli,
 Italy
 Yu Gan,
 Shanghai Cancer Institute, China

*Correspondence:

Hélène Castel
 helene.castel@univ-rouen.fr

† These authors share last authorship

Specialty section:

This article was submitted to
 Molecular and Cellular Oncology,
 a section of the journal
 Frontiers in Cell and Developmental
 Biology

Received: 12 January 2021

Accepted: 11 March 2021

Published: 14 April 2021

Citation:

Le Joncour V, Guichet P-O,
 Dembélé K-P, Mutel A, Campisi D,
 Perzo N, Desrués L, Modzelewski R,
 Couraud P-O, Honnorat J,
 Ferracci F-X, Marguet F,
 Laquerrière A, Vera P, Bohn P,
 Langlois O, Morin F, Gandolfo P and
 Castel H (2021) Targeting
 the Urotensin II/UT G Protein-Coupled
 Receptor to Counteract Angiogenesis
 and Mesenchymal Hypoxia/Necrosis
 in Glioblastoma.
 Front. Cell Dev. Biol. 9:652544.
 doi: 10.3389/fcell.2021.652544

Vadim Le Joncour¹, Pierre-Olivier Guichet¹, Kleouforo-Paul Dembélé¹,
 Alexandre Mutel¹, Daniele Campisi¹, Nicolas Perzo¹, Laurence Desrués¹,
 Romain Modzelewski², Pierre-Olivier Couraud³, Jérôme Honnorat^{4,5,6},
 François-Xavier Ferracci^{1,7}, Florent Marguet⁸, Annie Laquerrière⁹, Pierre Vera²,
 Pierre Bohn², Olivier Langlois^{1,7}, Fabrice Morin¹, Pierrick Gandolfo^{1†} and
 Hélène Castel^{1*†}

¹ UNIROUEN, INSERM U1239, DC2N, Institute for Research and Innovation in Biomedicine (IRIB), Normandie Rouen
 Université, Rouen, France, ² EA 4108, Laboratoire d'Informatique, de Traitement de l'Information et des Systèmes (LITIS),
 University of Rouen, Mont-Saint-Aignan, France, ³ Université de Paris, Institut Cochin, Inserm U1016, CNRS UMR 8104,
 Paris, France, ⁴ Neuro-Oncology Department, Hospices Civils de Lyon, Hôpital Neurologique, Bron, France, ⁵ Institute
 NeuroMyoGène, INSERM U1217/CNRS UMR 5310, Lyon, France, ⁶ University Claude Bernard Lyon 1, Université de Lyon,
 Lyon, France, ⁷ Neurosurgery Service, Rouen CHU Hospital, Rouen, France, ⁸ Anathomocytopathology Service, Rouen CHU
 Hospital, Rouen, France

Glioblastomas (GBMs) are the most common primary brain tumors characterized by strong invasiveness and angiogenesis. GBM cells and microenvironment secrete angiogenic factors and also express chemoattractant G protein-coupled receptors (GPCRs) to their advantage. We investigated the role of the vasoactive peptide urotensin II (Ull) and its receptor UT on GBM angiogenesis and tested potential ligand/therapeutic options based on this system. On glioma patient samples, the expression of Ull and UT increased with the grade with marked expression in the vascular and peri-necrotic mesenchymal hypoxic areas being correlated with vascular density. *In vitro* human Ull stimulated human endothelial HUV-EC-C and hCMEC/D3 cell motility and tubulogenesis. In mouse-transplanted Matrigel sponges, mouse (mUll) and human Ull markedly stimulated invasion by macrophages, endothelial, and smooth muscle cells. In U87 GBM xenografts expressing Ull and UT in the glial and vascular compartments, Ull accelerated tumor development, favored hypoxia and necrosis associated with increased proliferation (Ki67), and induced metalloproteinase (MMP)-2 and -9 expression in Nude mice. Ull also promoted a "tortuous" vascular collagen-IV expressing network and integrin expression mainly in the vascular compartment. GBM angiogenesis and integrin $\alpha\beta3$ were confirmed by *in vivo* ^{99m}Tc-RGD tracer imaging and tumoral capture in the non-necrotic area of U87 xenografts in Nude mice. Peptide analogs of Ull and UT antagonist were also tested as potential tumor repressor. Urotensin II-related peptide URP inhibited angiogenesis *in vitro* and failed

to attract vascular and inflammatory components in Matrigel *in vivo*. Interestingly, the UT antagonist/biased ligand urantide and the non-peptide UT antagonist palosuran prevented Ull-induced tubulogenesis *in vitro* and significantly delayed tumor growth *in vivo*. Urantide drastically prevented endogenous and Ull-induced GBM angiogenesis, MMP, and integrin activations, associated with GBM tumoral growth. These findings show that Ull induces GBM aggressiveness with necrosis and angiogenesis through integrin activation, a mesenchymal behavior that can be targeted by UT biased ligands/antagonists.

Keywords: glioblastoma, urotensin II, UT receptor, angiogenesis, necrosis, biased ligand

INTRODUCTION

Malignant gliomas and mainly glioblastomas (GBMs) are the most common group of primary brain tumors with an incidence of 8.9 cases per 100,000 persons/year in the United States (CBTRUS 2008–2012). According to the WHO classification of 2016, three major diagnostic subtypes of gliomas are individualized in three groups: (i) IDH-mutant, (ii) IDH-wildtype for most comprising GBM, and (iii) IDH not otherwise specified (Louis et al., 2016). GBMs are also characterized by common histopathological features including heterogeneity with regional high abnormal vascularized networks with necrotic foci, surrounded by hyper-cellular areas of “pseudopalisading” cells (Karsy et al., 2012; Alifieris and Trafalis, 2015), correlated with response to treatment (Stupp et al., 2005; Wen and Brandes, 2009). This GBM inter- and intra- heterogeneity was highlighted by the identification of major transcriptomic subgroups including the proneural (PN), neural (N), classical (CL), and mesenchymal (MES) GBM subgroups (Verhaak et al., 2010), potentially recapitulated within a GBM resection fragment (Wick and Kessler, 2018), strongly supporting the heterogeneous and constantly metamorphosing nature of GBM (Aubry et al., 2015).

The pronounced vascularization of GBM exhibits aberrant, malfunctioning, and leaky features resulting in vasogenic edema and increased tissue hypoxia sustaining the increased tumor malignancy (Takano, 2012; Bougnaud et al., 2016; Cavazos and Brenner, 2016). Angiogenic regulators are secreted by GBM cells but also infiltrating myeloid cells such as tumor-associated macrophages (TAMs) and Tie-expressing monocytes via ligands expressed by the tumor and/or stromal cells and targets present at the endothelial level (Eelen et al., 2020). The well-known anti-human VEGFA antibody bevacizumab has been shown not only to reduce tumor edema, angiogenesis, and disease burden but also to provoke adaptive escape mechanisms involving hypoxia by pruning tumor blood vessels, switching to a glycolytic metabolism, neo-vascularization, and/or infiltrative tumor growth (Norden et al., 2008; Eelen et al., 2020). Tumor relapse is associated with cell invasion of brain parenchyma likely involving chemotactic factors (Xie et al., 2014), such as cytokines, growth factors, chemokines, or vasoactive peptides activating G protein-coupled receptors (GPCRs) (Hembruff and Cheng, 2009; Borsig et al., 2014). Glioma cells but also macrophages are a major source of chemoattractants and they express one or more chemoattractant GPCRs to their advantage

(Cherry and Stella, 2014; Gagliardi et al., 2014; Zhou et al., 2014), allowing leukocyte attraction or exacerbating angiogenesis (Glass and Synowitz, 2014). Some vasoactive peptides and their GPCRs, conventionally involved in the angiogenic and inflammatory processes, constitute promising therapeutic targets in angiogenic and invasive tumors. The selective blockade of the angiotensin II (Ang-II) receptor AT1 by losartan inhibits the development of murine glioma and decreases tumor neo-angiogenesis (Rivera et al., 2001; Arrieta et al., 2005). The antagonism of endothelin-1 (ET-1) receptor by atrasentan in a phase I clinical study showed partial responses, lasting stabilization, or even absence of progression of GBM (Phuphanich et al., 2008). The immunoneutralization of adrenomedullin (ADM) caused a dramatic inhibition of prostate and GBM tumor development in Nude mice, accompanied by a drastic diminution of intratumoral vascular density (Kaafarani et al., 2009; Metellus et al., 2011).

Human urotensin II (Ull) (Coulouarn et al., 1998) and its peptide paralog Ull-related peptide (URP) (Sugo et al., 2003) are cyclic neuropeptides of 11 and 8 amino acids in human, respectively, and exhibit a fully conserved C-terminal cyclic hexapeptide (CFWKYC) core that plays a major role in biological activity (Brulé et al., 2014; Table 1). Ull and URP are considered the most potent endogenous vasoactive molecules known so far acting through a common GPCR called UT, being evolutionary linked to chemokine GPCRs (Ames et al., 1999; Brulé et al., 2014; Castel et al., 2017).

TABLE 1 | Names, sequences, and characteristics of the different urotensinergic peptide and non-peptide ligands used in the study.

UT ligand	Known function	Sequence
Human Ull (Ull)	Endogenous agonist	HTPD[CFWKYC]V
Murine Ull (mUll)		pEHGAAP[CFWLYC]I
Ull-related peptide (URP)		HA[CFWKYC]V
Ull _{4–11}	Synthetic agonist	HD[CFWKYC]V
Urantide	Peptide antagonist/biased ligand	D[Pen-F _D -W-Orn-YC]V
Palosuran	Non-peptide antagonist	1-[2-(4-benzyl-4-hydroxy-piperidin-1-yl)-ethyl]-3-(2-methyl-quinolin-4-yl)-urea sulfate salt

Cyclic core domain (disulfide bonds between two C residues) is represented by brackets. Unnatural amino acids: Orn, ornithine; Pen, penicillamine.

First studies established that the urotensinergic system is involved in migration of rat fibroblasts (Zhang et al., 2008), rat endothelial progenitor cells (Xu et al., 2009), human monocytes (Segain et al., 2007), and *in vitro* angiogenesis (Spinazzi et al., 2006), therefore stressing on the potential chemokine and pro-angiogenic status of UII in cancer. Indeed, UT receptor was shown to regulate migration of prostatic (Grieco et al., 2011), bladder (Franco et al., 2014), and colon (Federico et al., 2014) cancer cell lines. More recently, we and others proposed UII as an original chemokine (Castel et al., 2017; Sun and Liu, 2019), stimulating lung or colorectal cancer cell proliferation and metalloproteinase-9 (MMP-9) activation (Zhou et al., 2012). In the central nervous system (CNS), UT was detected in the vascular compartment (Clavier et al., 2018), in astroglial processes, and in human native astrocytes and GBM cell lines (Castel et al., 2006; Jarry et al., 2010; Desrués et al., 2012). In GBM cells, UII induces chemotactic migration/adhesion *via* G13/Rho/ROCK/actin polymerization and partially the Gi/o/PI3K pathways involving inhibition of the autophagy process (Lecointre et al., 2015; Coly et al., 2016). The chemoattractant activity of the UII-UT system may play multiple roles during glioma invasion or on microenvironmental cells leading to angiogenesis. In the present study, we characterized the expression of UII peptides and their receptor UT in a series of human glioma biopsies compared with normal brain tissue by immunohistochemistry and from transcriptome array analyses of gliomas from The Cancer Genome Atlas (TCGA) database as well as by quantitative-PCR (qPCR) in glioma cell lines. We found marked increased expression of UII and UT in high malignancy gliomas associated with the vascular component in GBM. The native UII and no other urotensin analog stimulates endothelial tube formation *in vitro* and promotes the *in vivo* recruitment of pro-angiogenic cells in matrices' sponges. In heterotopic U87 GBM cells xenografted in Nude mice, intratumoral injections of UII accelerated proliferation and GBM growth and exacerbated abnormal angiogenesis associated with hypoxia and necrotic features confirmed by *in vivo* ^{99m}Tc-RGD tracer imaging and tumoral capture in non-necrotic areas. The UT antagonist/biased ligand urantide and the non-peptide UT antagonist palosuran prevented UII-induced tubulogenesis *in vitro* and significantly delayed tumor growth *in vivo*. Urantide drastically prevented UII-induced GBM angiogenesis, MMP-2 and MMP-9 expression, and integrin activation associated with GBM growth. The specific blockade of UT receptor signaling should constitute a new multicellular targeting option in the therapeutic arsenal against GBM.

MATERIALS AND METHODS

Tumor Patient Samples

Non-tumoral brain tissues and brain glioma tumors were obtained from patients cared at the Rouen CHU Hospital in France from 2008 to 2014. Sixty-six tumors were taken from the Center of Biological Resources located in the Department of Pathology, Rouen University Hospital. The selection criteria were a diagnosis of glial tumor, surgical resection or biopsy, treated by surgery alone, surgery plus radiotherapy, surgery

plus radiotherapy and Temozolomide chemotherapy, or surgery plus radiotherapy and PCV (Procarbazine, Lomustine, and Vincristine) chemotherapy (Stupp protocol), and patients with completed clinical information (see Table 2 for detailed information). All patients provided written informed consent for the study. The age of patients, their clinical outcomes, and tumor histopathologic classifications were typical of the category of adult with diffuse glioma (Verhaak et al., 2010; Brennan et al., 2013).

Immunohistochemistry

Four-micrometer sections were obtained from formalin-fixed paraffin-embedded tissues. Before antibody staining, heat-induced antigen retrieval was performed in a sodium citrate buffer solution at 95°C for 45 min. Immunohistochemistry was performed using Envision G12 Doublestain System Rabbit/Mouse kit (Dako, K5361) according to the manufacturer's protocol. Primary antibodies against Urotensin II (Sigma-Aldrich, HPA017000, 1:50), urotensin II receptor (Santa Cruz, sc20940, 1:50), CD34 (Novocastra, RTU-END, 1:1), CA9 (Abcam, ab15086, 1:1000), and α -SMA (Sigma-Aldrich, A2547, 1:500) were used and incubated overnight at 4°C. Rabbit polyclonal and mouse monoclonal antibodies were revealed with DAB and Permanent red, respectively. Nuclei were counterstained with hematoxylin. For each tumor series, a consecutive section was stained using hematoxylin-eosin (H&E) for structural information.

Scoring of UII/UT Staining in Human Biopsies

Tissue samples were independently scored by two pathologists (AL and FM) and one scientist (POG). The percentage of positive cells (P) was determined as follows: $P = 0$, no positive cells; $P = 1$, <10% of positive cells; $P = 2$, 11–50% of positive cells; $P = 3$, >50% of positive cells. Semi-quantitative evaluation of immunolabeling intensity (I) was determined as follows: $I = 0$, no staining; $I = 1$, weak expression; $I = 2$, moderate expression; $I = 3$, strong expression. The score was expressed as the sum of $(P + I)$ comprised between 0 and 6. For each sample, we scored the expression of UII and UT in three different tumor locations: parenchyma, vascular, and perinecrotic components. The total score was the sum of each score.

Culture of Cell Lines

The human glioma SW1088 and U87 cell lines were obtained from ATCC (LGC Standards, Molsheim, France) and 8MG, 42MG, and U251 cell lines were provided by Pr. J. Honnorat (CRNL, Lyon, France). Culture media components were purchased from Life Technologies (Thermo Fisher Scientific, Saint-Aubin, France) or Lonza (Levallois-Perret, France). U87 cells were maintained in minimum essential medium (DMEM) supplemented with sodium pyruvate (1%), non-essential amino acids (1%), and antibiotics (1%) all from Fischer Scientific (Illkirch, France) and heat-inactivated fetal bovine serum (FBS, 10%). Human umbilical vein (HUV-EC-C, from ATCC) and human cerebral microvascular (hCMEC/D3) (Weksler et al., 2005, 2013) endothelial cell lines were maintained in endothelial

TABLE 2 | Clinico-demographical parameters of the different glioma groups studied retrospectively and prospectively.

CNS tissues	Grade WHO 2016	Grade WHO 2008	Subtype	N	Median age	Gender (M/F)	Localization	Treatment
Gliomas	I		Pilocytic astrocytoma	8	16 (2–25)	4/4	CH (n = 6), V (n = 2)	CR
			II	13	36 (26–60)	8/5	SC (n = 11), BG (n = 1), BS (n = 1)	CR alone (n = 4), T (n = 5), RT (n = 4)
			AII	Diffuse astrocytoma, IDH1-mutant	3			
			AII	Diffuse astrocytoma, IDH1-wildtype	3			
			OII	Oligodendroglioma, IDH1-mutant and 1p/19q-codeleted	3			
			OIII	Oligodendroglioma, IDH1-wildtype and 1p/19q-codeleted	1			
			OAI	Oligoastrocytoma, NOS	3			
		III		15	52 (24–71)	11/4	SC (n = 15)	CR alone (n = 1), STUPP (n = 6), RT + PCV (n = 1), RT alone (n = 6), T alone (n = 1)
			AIII	Anaplastic astrocytoma, IDH1-mutant	1			
			AIII	Anaplastic astrocytoma, IDH1-wildtype	6			
			OIII	Anaplastic oligodendroglioma, IDH1-mutant and 1p/19q-codeleted	4			
			OAI	Anaplastic oligoastrocytoma, NOS	4			
		IV		24	56 (23–75)	16/8	SC (n = 23), M (n = 1)	STUPP (n = 23), RT alone (n = 1)
		GBM	Glioblastoma, IDH1-mutant	5				
		GBM	Glioblastoma, IDH1-wildtype	19				
Non-tumoral			6	45 (32–49)	1/4	–	–	
			Hippocampal sclerosis	4				
			Focal cortical dysplasia	1				
			Normal cerebellum	1				

Grading is indicated along histopathological classification (see **Figure 1**) and according to the WHO classification 2016 from last information available in 2017. BG, basal ganglia; BS, brainstem; CH, cerebellar hemisphere; CR, chiralurgical resection; IDH1mut, IDH1 (R132H) positive (immunohistochemistry); IDH1wt, IDH1 (R132H) negative (immunohistochemistry); M, medullary; N, number of samples; NOS, not otherwise specified; PCV, procarbazine, lomustine (CCNU) and vincristine; RT, radiotherapy; SC, supratentorial cortex; STUPP, therapy protocol involving radiotherapy plus concomitant and adjuvant Temozolomide; T, Temozolomide; V, vermis. Bold values correspond to the total of samples per/grade in the table.

basal medium-2 (Lonza, Bâle, Switzerland) containing chemically defined concentrated lipids (1%, Fischer Scientific), HEPES (1%, Fischer Scientific), hydrocortisone (0.2 µg/ml, Sigma-Aldrich), bFGF-2 (50 ng/ml, Eurobio Abcys, Courtaboeuf Les Ulis, France), ascorbic acid (1 µg/ml, Fischer Scientific), and gold-defined FBS (5%, PAA Laboratories). When cultures reached 90% of confluence, cells were harvested and prepared for *in vitro* experiments according to the following procedures or were just rinsed in PBS for transplantation in Nude mice.

Vascular Characteristic of Malignant Glioma Patient Samples

For each patient sampled tumor, at least three microphotographs were taken (Nikon I widefield microscope) from slices stained with an anti-CD34, and saved as 2560 × 1920 pixels pictures.

Three different vascular properties were analyzed on vascular CD34+ structures with vascular histological characteristics by using ImageJ software (NIH, Bethesda, MD, United States). First, the vascular density was quantified by manually isolating each microvessel in the field and summed, and then microvessel coverage area was normalized to the whole tumoral area. Vessel diameter was quantified from transversal vessel sections, after manual selections, and the highest radius value was used for the quantification by using ImageJ shape descriptors feature. Vessel circularity was quantified on transversal sections to estimate vessel irregularities, after manual selections, and measured by using the following equation:

$$\frac{4\pi[\text{Area}]}{[\text{Perimeter}]^2}$$

Quantitative Real-Time PCR Analysis

Total RNA was isolated from tumor cell line extracts using TRIzol reagent according to the manufacturer's protocol (Sigma-Aldrich, Saint-Quentin-Fallavier, France). First-strand cDNA were transcribed from 1 µg of total RNA in quadruplicates using the Superscript II reverse transcriptase (random primers method, Promega, Charbonnières-les-bains, France). For quantitative RT-PCR, cDNA amplification was monitored using SYBR Green (Thermo Fisher Scientific, Illkirch, France) chemistry on the real-time PCR system (QuantStudio3, Applied Biosystems, Zug, Switzerland). Primers were designed by retrieving nucleotide sequence from NCBI gene database and using the Primer3Plus program¹. The specific primers targeting UTS2 (encoding UII), UTS2D (encoding URP), UTS2R (encoding UT), and MMP9 and ITGAV (encoding integrin αv) mRNA were synthesized by Eurofins genomics (Les Ulis, France), and their sequences are listed in **Supplementary Table 1**. The conditions for PCR reactions were 45 cycles, 95°C/1 s, 60°C/20 s, a step specific for UII mRNA (73°C/5 s), and 95°C/1 s using the primers specified in **Supplementary Table 1**. Minus-reverse transcription ("–RT") controls were systematically performed, and the quality of PCR products was evaluated by generating a melting curve, which was also used to verify the absence of PCR artifacts (primer dimers) or non-specific PCR products. Samples were amplified in triplicates (three different culture flasks and three different RT) and relative mRNA copy levels were determined using the comparative $\Delta\Delta Ct$ method. Glyceraldehyde-3-phosphate dehydrogenase (GAPDH) or ubiquitin C (UBC) transcript levels were used as a reference to control mRNA levels and stability within each cell line. Results were analyzed by using the Quantstudio design and analysis software (Applied Biosystems) and are expressed as mean of gene of interest expression relative to GAPDH or UBC reference gene.

Tumor Data Base Analysis

The clinical and molecular data on low-grade glioma and GBM samples for this study were downloaded from The Cancer Genome Atlas database² firstly in 2014, and the molecular information was again downloaded in February 2016. The clinical information used was the overall patient survival. The molecular data used were mRNA expression levels of UTS2, UTS2D, and UTS2R obtained from RNA-seq information by means of Illumina TruSeq Kit Paired-end Sequencing on Illumina HiSeq2000 (Cancer Genome Atlas Research Network, 2008), and the gene expression level within the GBM subgroups of the Verhaak classification was obtained from different microarray platforms previously processed and summarized (Verhaak et al., 2010; Brennan et al., 2013). Detection of somatic variants (IDHmut) from the TCGA Whole-Exome Sequencing and RNA-Seq data was done using RADIA. RADIA is a computational method combining the patient-matched normal and tumor DNA with the tumor RNA (Lecointre et al., 2015; Coly et al., 2016). The mRNA levels were represented as "normalized count" corresponding to a transformation of the "raw_count." For each

gene of interest, all "raw_count" values were divided by the 75th percentile of the column patient (after removing zeros) and multiplied by 1,000. For the gene-level survival analysis, we divided the corresponding cohorts (all glioma) by the mean gene expression level (low or high) of UTS2, UTS2D, or UTS2R. We then used a log rank (Mantel–Cox) test to compare the survival durations between the two groups.

Western Blot of Pre-Pro UII and UT

Glioblastoma cell lines and hCMEC/D3 cells were treated during 24 h in the absence of FBS and in the absence or the presence of UII (10^{-9} M). Cell lysates (20 µg total proteins) were prepared in ice-cold Lysis Buffer (25 mM Tris–HCl, pH 7.6, 150 mM NaCl, 1% NP40, 1% sodium deoxycholate, and 0.1% SDS), mixed with Laemmli buffer and loaded onto 4–12% polyacrylamide gels (CliniSciences, Nanterre, France). Proteins were transferred onto PVDF membranes, blocked with 5% non-fat milk and 5% bovine serum albumin, and incubated with the anti-pre-pro UII (Sigma, HPA-01700), UT (H-90) (Santa-Cruz, sc-20940), or β -tubulin (Santa-Cruz, sc-9104) overnight at 4°C and then with horseradish peroxidase-conjugated secondary antibodies (Santa-Cruz) for 2 h at room temperature. Immunoreactive bands were visualized by using the ECL Western blotting substrate (GE Healthcare, Aulnay-sous-Bois, France) and their molecular weight were determined by using PageRuler Plus prestained protein ladder (10–250 kDa) markers (Fisher Scientific).

Cell Migration Assay

Transwell membranes (24 wells, Corning, Fisher Scientific) with 8-µm pores were coated with 25 µg/ml collagen I (Invitrogen) (4°C, 12 h). Endothelial and glioma cells (5×10^4) suspended in 100 µl of culture medium (with 1% gold-defined FBS for endothelial cells) were added onto the upper chamber of the Transwell and UT ligands (600 µl) were added in the bottom chamber. After 24-h incubation at 37°C, cells were rinsed with PBS and the non-migrating cells were removed using a cotton swab from the upper chamber. Migrating cells were fixed in successive methanol baths and stained with H&E, and then membranes were mounted on glass slides with Mowiol (Calbiochem, Molsheim, France). Random phase contrast images were acquired using a digital camera (Nikon D-600), and image analysis was carried out using *ImageJ*'s Cell Counter plugin (NIH, Bethesda, United States).

In vitro Tubulogenesis Assay

Growth factor-reduced Matrigel (Beckon Dickinson, Le Pont-de-Claix, France) was thawed on ice overnight and spread homogeneously (100 µl) in 24-well plates for 30 min at 37°C to allow Matrigel polymerization. Endothelial cells (5×10^4 cells/cm²) were seeded in basal medium and incubated for 24 h in the absence or the presence of UT agonists (Phoenix Pharmaceuticals, Inc) (UII, mUII, URP, UII_{4–11}, **Table 1**) at 10^{-12} to 10^{-7} M, the UT antagonist/biased ligand urantide (Peptides International, Louisville, KY, United States, **Table 1**), or the UT antagonist palosuran (Actelion Pharmaceuticals, Allschwil, Switzerland, **Table 1**) from 10^{-10} to 10^{-7} M. Phase contrast image analysis was carried out using *ImageJ* software.

¹<http://www.bioinformatics.nl/cgi-bin/primer3plus/primer3plus.cgi/>

²<https://www.cancer.gov/about-nci/organization/ccg/research/structural-genomics/tcga>

Animal Studies

All procedures were performed in accordance with the French Ethical Committee as well as the guidelines of European Parliament directive 2010/63/EU and the Council for the Protection of Animals Used for Scientific Purposes. This project was approved by the “Comité d’Ethique Normandie en Matière d’Expérimentation Animale” CENOMEXA under the National Committee on Animal Experimentation and received the following number N/13-11-12/36/11-17. Animal manipulations were carried out under the supervision of an authorized investigator (H. Castel; authorization no. 76.98 from the Ministère de l’Alimentation, de l’Agriculture et de la Pêche and surgery agreement). For the tumorigenesis studies, 6-week-old male athymic *Swiss (nu/nu)* mice (Charles River Laboratories, L’Arbresle, France) were used. For the *in vivo* chemoattraction assay, 3- to 6-week-old male C57Bl/6 mice (Janvier Labs, Saint-Berthevin, France) were used. Mice were housed in sterile cages, in a temperature-controlled room with a 12-h light/12-h dark schedule and fed with autoclaved food and water *ad libitum*.

In vivo Chemoattraction Assay

Male C57Bl/6 mice were injected subcutaneously above the pelvis area with 200 μ l of liquid growth factor-reduced Matrigel combined either with EG-VEGF (Miltenyi Biotechnologies, Paris, France) or with human recombinant EGF (R&D Systems, Metz, France) (500 ng/ml, each), UT agonists (UII, mUII, URP, and UII₄₋₁₁) at 50 ng/ml, UT antagonists/biased ligand palosuran or urantide at 1 μ g/ml, or alone as a negative control. Subcutaneous plug incubation continued for 21 days or until mice had to be sacrificed following institutional ethical guidelines criteria. Matrigel plugs were resected and immediately frozen in a -40° C isopentane solution until immunohistochemistry.

Xenograft Studies

U87 cells were injected subcutaneously into the right flank (3×10^7) of 6-week-old male athymic mice. Mice were randomized into treatment groups after tumors were developed (mean s.c. volume = 100 mm³, 400–600 mm³). UT agonists (UII, mUII, URP, and UII₄₋₁₁; 2.9 ng/kg, each) or UT antagonists/biased ligand (palosuran, 29 ng/kg; urantide 290 ng/kg) or saline solution (vehicle) was administered intratumorally every day. Subcutaneous tumor volumes were measured with a caliper every 2 days, by using the following formula: width \times length \times height \times 0.52. Treatment continued until mice had to be sacrificed (i.e., 2-cm³ maximal tumor dimension, cutaneous ulceration, or symptoms) or study end. In some experiments, 30 min before euthanasia, pimonidazole (60 mg/kg, HypoxyprobeTM-1 Omni Kit, Burlington, United States) was administered intravenously, and glioma tissues were collected and immediately frozen in a -40° C isopentane solution until immunohistochemistry.

Animal Immunohistochemistry

Cryostat sections of Matrigel plugs (10 μ m) were processed in a Leica CM1900 cryostat, or xenograft sections (9 μ m) were processed in a Leica CM1950 cryostat, mounted directly on slides,

and then fixed in 4% paraformaldehyde. Non-specific binding sites were blocked with normal serum (10%) from the animal source of the appropriate corresponding secondary antibody. Immunolabeling was conducted using primary antibodies against UT receptor, F4/80 (Santa Cruz Biotechnologies, Heidelberg, Germany), collagen-IV (Coll-IV, Merck-Millipore, Molsheim, France), α -smooth muscle cell actin (α -SMA) and Prestige-Graded UII (Sigma-Aldrich, Saint-Quentin Fallavier, France), or α v integrin, MMP-2 and MMP-9, and CD31 and CD34 (Abcam, Paris, France), diluted according to the manufacturer’s technical specifications in the incubation media [0.1 M Tris (pH 7.5), 0.15 M NaCl, 10% normal serum, and 0.03% Triton X-100] and then incubated overnight at 4°C. Signal amplification utilized fluorochrome (Alexa 488 or Alexa 594)-conjugated secondary antibodies (Life Technologies, Saint Aubin, France), and cell nuclei DNA was stained with 4’,6-diamidino-2-phenylindole (DAPI, Sigma-Aldrich). Control sections were incubated in the absence of the primary antibodies.

Micro-SPECT Imaging and ^{99m}Tc RGD Radioligand

Cyclo(RGD_DY[K-HYNIC]) (HYNIC-RGD) was synthesized on a solid support using standard solid-phase synthesis and was purchased from the PolyPeptide Group (Strasbourg, France). The labeling method following the previously described protocol (Becker et al., 2015) is more detailed in the **Supplementary Material**, and chemical structures are shown in **Supplementary Figure 6A**. Other reagents were purchased from Sigma-Aldrich (Saint-Quentin-Fallavier, France). Na^{99m}TcO₄ was obtained by elution, with 0.9% saline, from a commercial ⁹⁹Mo/^{99m}Tc generator (Ultra-TechneKow; Covidien, Petten, Netherlands). The RGD-derived peptide purity was greater than 95% as analyzed by reverse-phase high-performance liquid chromatography and mass spectroscopy, and the net peptide content was estimated by elemental analysis.

SPECT imaging was performed using a small animal imaging system with parallel collimators and a 140 keV \pm 10% photopeak energy window (Triumph SPECT/CT; GMI, Los Angeles, CA, United States) and GE Healthcare (Fairfield, CT, United States). U87-xenografted Nude mice were injected through the tail vein with \sim 30 MBq (in about 0.1 ml) of [^{99m}Tc]-HYNIC-RGD under continuous isoflurane anesthesia (2.5% in O₂, 1 l/min). [^{99m}Tc]-HYNIC-RGD dynamic imaging was carried out 1 h after injection and planar images were recorded every minute. [^{99m}Tc]-HYNIC-RGD SPECT imaging was carried out 2 h after injection. Treatment of the dynamic imaging is detailed in **Supplementary Methods**.

Ex vivo Micro-SPECT Imaging of Tumors

In tumor samples examined *ex vivo*, 30 MBq was precisely measured and diluted by a factor of 1000 to obtain a dose calibrator. Background counts were subtracted, and the radioactive decay was corrected to the time of injection. The radioactivity concentration that had accumulated in the tissue samples over the 2-h period following the [^{99m}Tc]HYNIC-RGD injection was expressed as a percentage of the injected

dose (%ID) and normalized per gram of tissue (%ID/g). For *ex vivo* biodistribution, samples of various tissues were collected 120 min after injection and weighed, and radioactivity was measured using an automatic gamma counter (1470–001 Wizard Gamma Counter; PerkinElmer and Wallac, Turku, Finland) calibrated with a gamma peak calibrator (^{129}I). A $^{99\text{m}}\text{Tc}$ sample was measured using an activity calibrator (MEDI404; Medisystem, Guyancourt, France). Detailed methods of visualization and quantification of radioactivity were provided in the **Supplementary Methods**.

Statistical Analyses

Data were expressed as mean \pm SEM and GraphPad Prism (version 5; GraphPad Software, Inc., La Jolla, United States) was used for statistical analyses. Student *t*-test was used for parametric comparisons between paired variables, the Mann–Whitney *U* test was used for non-parametric pairwise comparisons, multivariate analyses were done with ANOVA with *post hoc* Dunnett (*in vitro* analyses) or Bonferroni tests (e.g., *in vivo* studies) as appropriate, the vascular property multivariate analyses were done with Kruskal–Wallis and Dunn's post-test, and survival curves were generated by the Kaplan–Meier method. Correlation is considered significant when $P < 0.05$, and r represents the Pearson correlation coefficient. All reported P -values were two-sided and considered to be statistically significant at $P < 0.05$.

RESULTS

UII and UT Expression in Patient Gliomas and Human Glioma Cell Lines

The UII/UT system was first characterized on different glial tumors from patient tumor samples obtained after a first tumor resection or a small size biopsy (tumor bank of Haute-Normandie, France) by immunohistochemistry. These glial tumors were presented according to WHO 2008 histopathological classification, ranging from astrocytoma (AII/III), oligodendroglioma (OII/III), or oligoastrocytoma (OAI/III) to highly aggressive glioblastoma multiform (GBM, IV) based on morphological features and associated with a very poor prognosis (Xu et al., 2015). Since 2016, grade II diffuse and grade II anaplastic astrocytoma have been divided into mutated and wild-type IDH1/2 even if the great majority falls into IDHmut; astrocytomas, grade II oligodendroglioma are IDHmut and 1p/19q codeleted while GBMs are most often represented by GBM IDHwt (90% of cases) (Louis et al., 2016). Sixty patients were included retrospectively and prospectively, and tumor grades and molecular signatures were described according to the WHO 2016 classification in **Table 2**. The anatomic sites of the tumors were supratentorial cortex (49/60, 81%), basal ganglia (1/60, 2%), brainstem (1/60, 2%), intramedullary (1/60, 2%), cerebellar hemisphere (6/60, 10%), and vermis (2/60, 3%) (**Table 2**). Immunohistochemical analysis showed a higher expression of the UII/UT couple in astrocytomas (AII/III) compared with oligodendrogliomas (OII/III) when positive cells were $> 50\%$ (**Figure 1A**). In GBMs, strong localized expression of UII and UT was observed in vascular and perinecrotic areas,

in immunoreactive zones for respectively, the mesenchymal marker α -SMA-positive cells and for the carbonic anhydrase 9 (CA9) (**Figure 1B**), suggesting links between tumoral pericytes and hypoxia. From consecutive sections of non-tumor CNS tissue, the UII and UT immunostaining appeared in gray matter (GM), in particular in neurons instead of oligodendrocytes (peri-neuronal satellitosis) and in the white matter (WM) (**Figure 1C**). Score analysis of the UII and UT staining indicated a gradual increased expression with the grade, from grade I (PA) to grade IV (GBM), and also from OII/OIII, OAI/III, and AII/III (**Figures 1A,D**) reaching significant scores in GBM compared with PA (**Figure 1D**). As shown in **Figure 1E**, the vascular density and diameter were significantly increased in anaplastic astrocytoma and GBM while vessel defaults in circularity were shown altered in GBM. The expression levels of UII and UT were significantly correlated with increased vascular density, mainly in high-grade tumors (**Figure 1E**) and UII was also correlated with UT (**Figure 1F**) (Pearson coefficient, $P < 0.001$). Progression-free survival curves of 20 patients with primary GBM indicated that high expression of the urotensinergic components were significantly correlated with early recurrence (UII, score $> 11.5/18$; UT, score $> 12.5/18$) and were correlated with a median survival of 224 days when any of the UII and UT are highly expressed (**Figure 1F**). Expression mRNA level of UTS2 encoding UII, UTS2R encoding UT, and UTS2D encoding URP was also tested from TCGA (**Figure 2**). For each gene, profiles of normalized expression were extracted from 66 glioma samples presented in **Figure 2A** according to the grading classification. UTS2 was found to be significantly more expressed in astrocytoma and mostly GBM, suggesting an association with high-grade gliomas. As observed in the histopathological classification, UTS2R and UTS2D were equally expressed in IDHwt or IDHmut tumors, whereas UTS2 displayed a higher expression in IDHwt gliomas, suggesting an association with malignancy (**Figure 2B**). Within the four groups of GBM along with the Verhaak classification (Verhaak et al., 2010), UTS2R (UT) and UTS2D (URP) were expressed in all groups of GBM, but importantly, UTS2 (UII) exhibited a net higher expression in the mesenchymal subgroup, suggesting that UII may be associated with glioma prognosis (**Figure 2C**). UTS2R and UTS2 mRNA levels from TCGA showed that patients having high UTS2R or UTS2 expression exhibit significantly lower mean survival probability, while no difference was observed for UTS2D (**Figure 2D**). These data establish a relationship between UII, and also UT expression in GBM, mainly with the hypoxic/vascularized state of the more aggressive GBM. QPCR analyses of mRNAs encoding UII, URP, and UT in the SW1088 (anaplastic astrocytoma) and in U87, U251, 8MG, and 42MG GBM cell lines here established that expression levels were non-homogeneous and higher for UTS2R in 8MG and 42MG, UTS2 in U87, and UTS2D in SW1088 (**Figure 3A**). To verify a possible autocrine/paracrine mechanism in which UII may in turn induce UTS2 or UTS2R expression encoding UII and UT, we evaluate 24-h GBM cells as well as a human EC line hCMEC/D3 exposed to UII (10^{-9} M). UII stimulated the expression of UII at least in part by U87 and 8MG as confirmed by the qPCR and Western blot

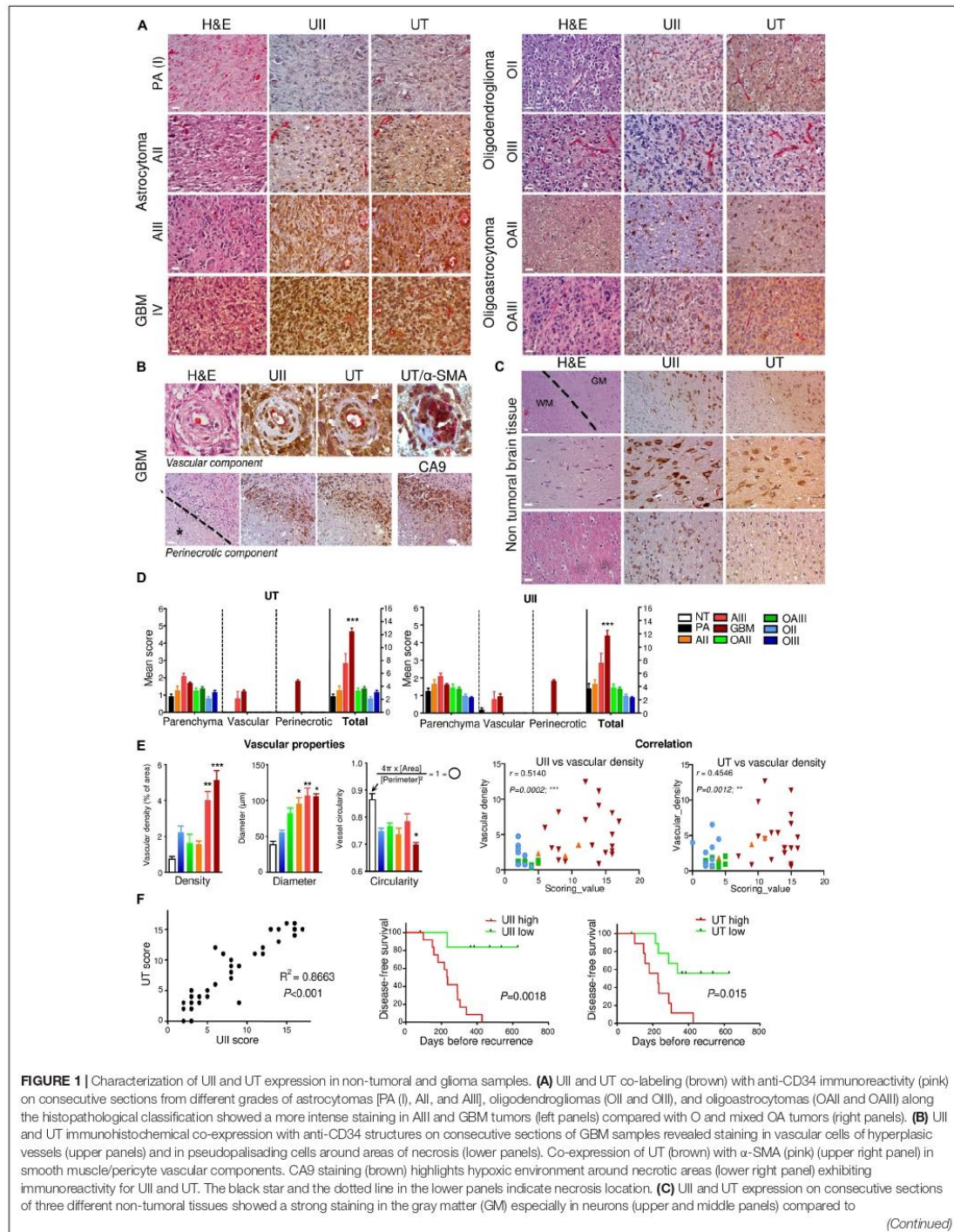


FIGURE 1 | Continued
 oligodendrocytes from the GM (peri-neuronal satellitosis) and in the white matter (WM) (upper and lower panels). The dotted line delineates the frontier between GM and WM. **(D)** Quantification of experiments presented in **(A,B)** and represented as the mean \pm SEM of UT (left panel) and UII (right panel) scores (see section "Materials and Methods"). * $P < 0.05$; ** $P < 0.01$; *** $P < 0.001$ (one-way ANOVA and multiple comparison test with Tukey's correction). **(E)** Vascular density, diameter, and circularity quantified from NT and malignant glioma (All/Oll to GBM) samples based on the CD34-positive structures and histological characteristics from, at least in part, three different images per patient tumor slice. *Left*, Histograms of mean \pm SEM (Kruskal–Wallis and Dunn's post-test: *** $P < 0.001$). *Right*, Scatter plot of the correlation between UII scoring value versus vascular density (left) and UT scoring value versus vascular density (right). Score correlation in glioma showed a significant correlation between UII and UT and vascular density more particular within All and GBM samples. **(F)** Total score correlation in glioma samples showed a significant correlation between UII and its receptor UT. Disease-free survival curves of 20 primary GBM for UII (left panel) and UT (right panel). In **(E,F)**, the correlation is considered significant when $P < 0.05$, r represents the Pearson correlation coefficient. H/E: Hematoxylin–Eosin staining. Scale bar = 10 μm for **(A,B)**, and **(C)**, middle and lower panels), and 20 μm for **(C)**, upper panel).

analysis, but not in EC constitutively expressing UII and UT (Figures 3B,C).

UT Mediates Motility of GBMs and Endothelial Cells and Stimulates Tubulogenesis *in vitro*

To examine the role of UII on glioma tumorigenesis, we used U87 GBM cells, endogenously expressing UII and functional UT (Figure 4A). We confirmed that UT activation by UII (10^{-9} and 10^{-8} M) leads to chemotactic migration in Boyden's chamber assay (Figure 4B) and did not alter cell density after a 48-h treatment (Supplementary Figure 1A). We confirmed that hCMEC/D3 expressed UT at the plasma membrane and UII in the cytoplasmic and perinuclear compartments (Figure 4A). UII (10^{-10} and 10^{-9} M) stimulated hCMEC/D3 cell migration (Figure 4B) with no measurable effects on hCMEC/D3 or HU-VEC-C cell density/proliferation (Supplementary Figures 1B,C). These observations were suggestive of proinvasive and angiogenic capacities of the UII/UT system. We then tested the ability of the UT endogenous agonists UII and URP, the shorter synthetic peptide analog referred to as a full agonist UII_{4–11}, the UT antagonist/biased ligand urantide (Camarda et al., 2004; Brulé et al., 2014), and the UT antagonist palosuran (Clozel et al., 2004; Table 1) to promote tubular organization of hCMEC/D3 and HUV-EC-C cells (Figure 4C). Only UII was able to enhance the endothelial network complexity in both hCMEC/D3 and HUV-EC-C, whereas URP and UII_{4–11} (10^{-7} M) disrupted EC associations (Figure 4D). The proangiogenic properties of UII were mainly relayed by EC collective motility, as demonstrated by significant increased amount of endothelial junctions and branches, resulting in a much more intensified and complex tubular structure of hCMEC/D3 and HUV-EC-C (Figures 4C,D) and increased segments and polygons of hCMEC/D3 (Figure 4D). Urantide (10^{-6} M) drastically counteracted these endothelial associations and branch length mainly in hCMEC/D3, whereas palosuran (10^{-6} M) did not significantly modify basal tubulogenesis (Figure 4D). Urantide and palosuran systematically prevented UII-induced tubulogenic effects (Figure 4D).

Chemoattractant Function of UII Toward Proangiogenic Cells *in vivo*

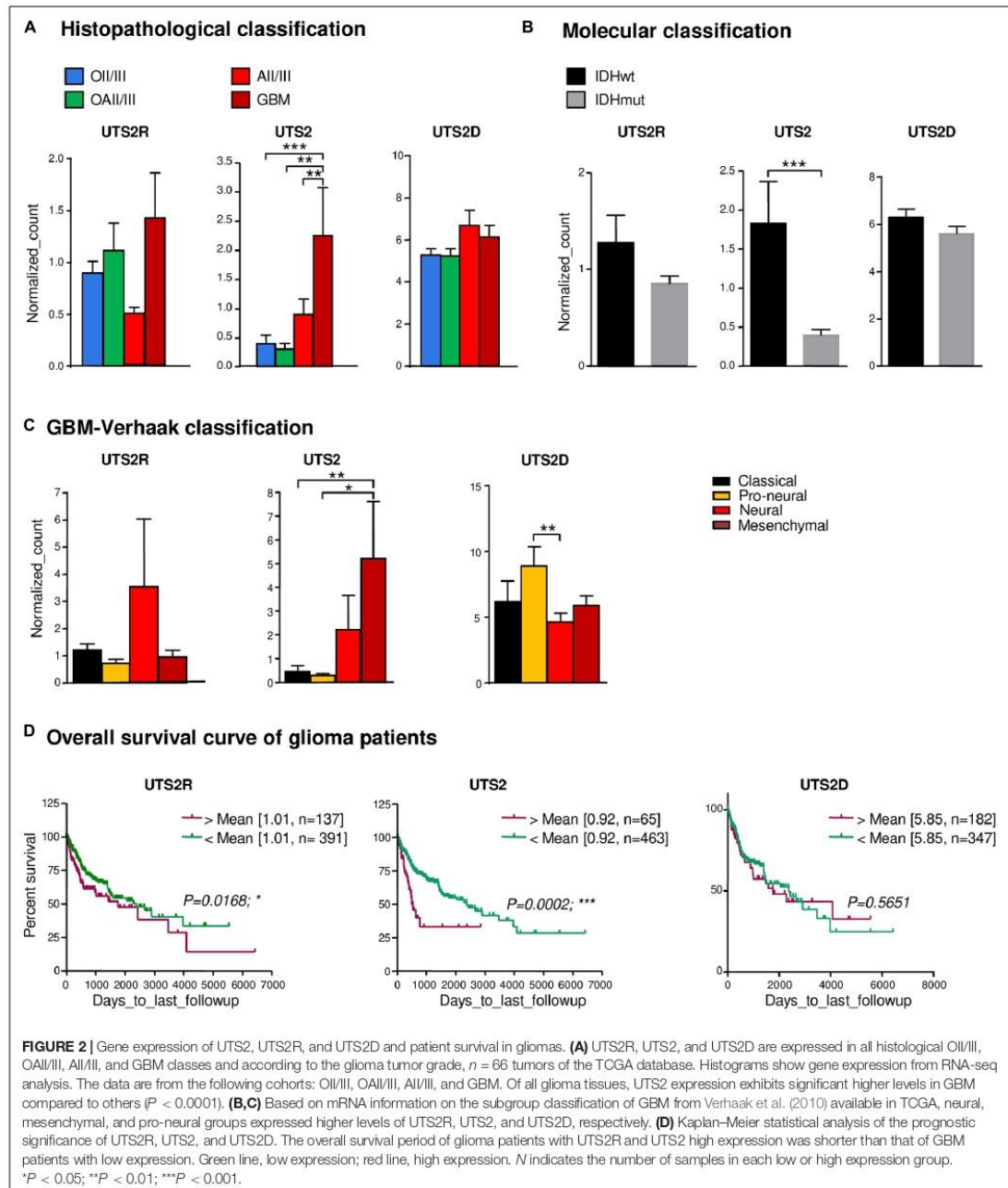
The potential proangiogenic properties of the urotensineric system were then investigated *in vivo*, via Matrigel plugs subcutaneously implanted in C57B/16 mice. To validate

the assay, liquid Matrigel containing either EG-VEGF or EGF (500 ng/ml, each) was injected in mice for 3 weeks. Resected sponges revealed blood drops or fully formed blood vessels (Figure 5A) and immunopositive cells for the macrophage F4/80, endothelial basal membrane collagen-IV (COLL-IV), and α -SMA markers (Figure 5A). Matrigel sponges containing UII or the murine sequence of the peptide (mUII) (50 ng/ml, each) exhibited similar hemorrhagic drops (Figure 5B). Quantification showed a marked stimulation of macrophage invasion and of capillary-like structures, formed by the association of endothelial and smooth muscle cells (Figure 5B). URP and UII_{4–11} (50 ng/ml, each) or urantide and palosuran (50 ng/ml, each) failed to chemoattract cells into the plugs (Figure 5B). These results indicate that the urotensineric system is involved in angiogenesis *in vivo* and that available drugs may constitute anti-angiogenic compounds targeting UT.

The Urotensineric System Is Required for GBM Growth Interfering With Mouse Survival

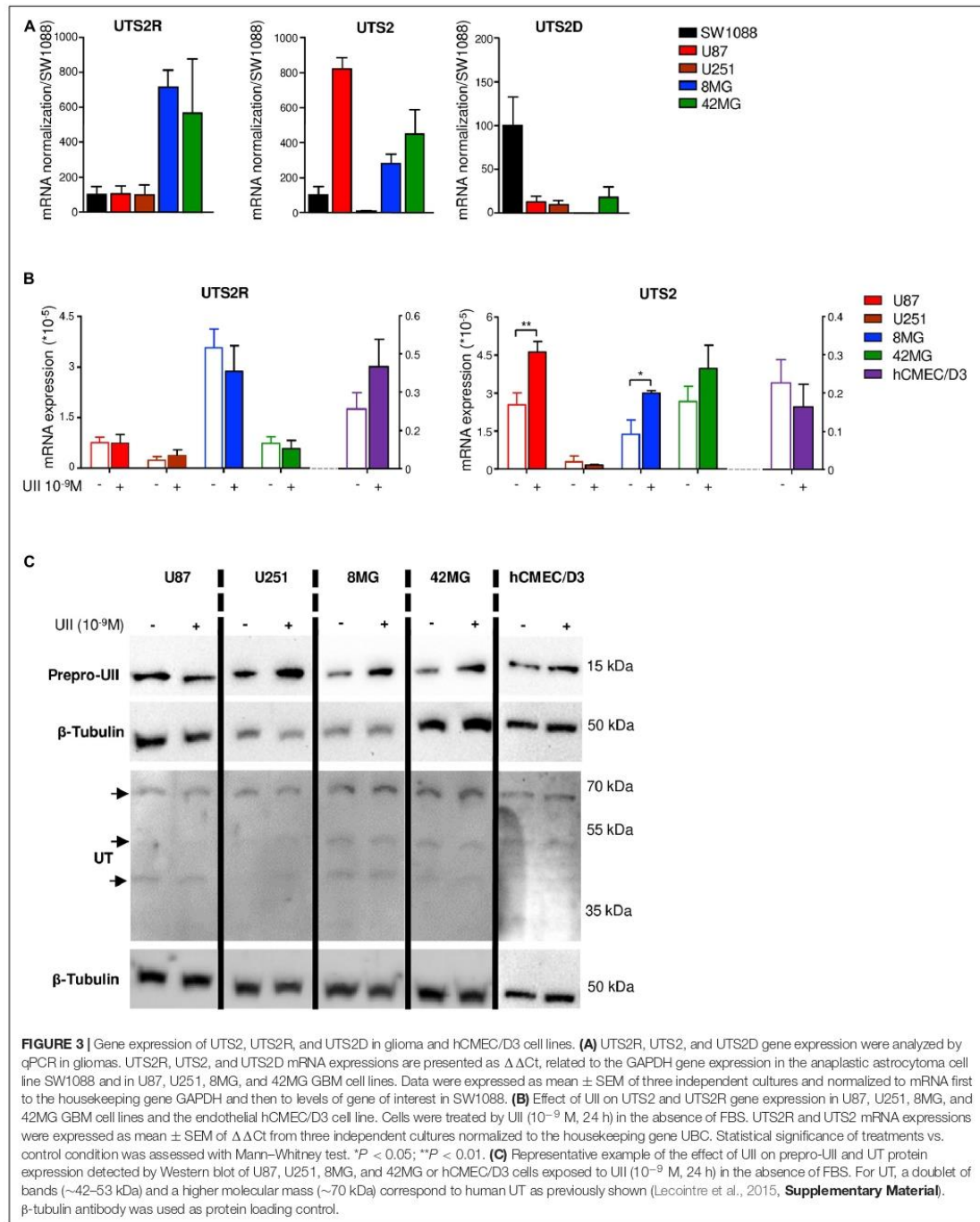
To investigate the involvement of the urotensineric system in angiogenesis and tumorigenic process in GBM, daily intratumoral injections of UII on U87 xenograft tumors were performed when tumors reached $\approx 100 \text{ mm}^3$. Exogenous administration of UII (2.9 ng/kg) significantly accelerated tumor growth (Figures 6A,D) without affecting the body weight (Supplementary Figure 2). The median survival of animals receiving intratumoral injections of UII decreased compared with vehicle (Figures 6A,D). Vehicle or UII-tumor xenografts expressed UII and mostly UT in perinecrotic areas (pseudopalisadic area) and in vascular components (Figure 6B). URP (2.9 ng/kg) and UII_{4–11} (2.9 ng/kg) did not significantly modify GBM tumorigenic growth as well as mouse median survival (Figure 6C).

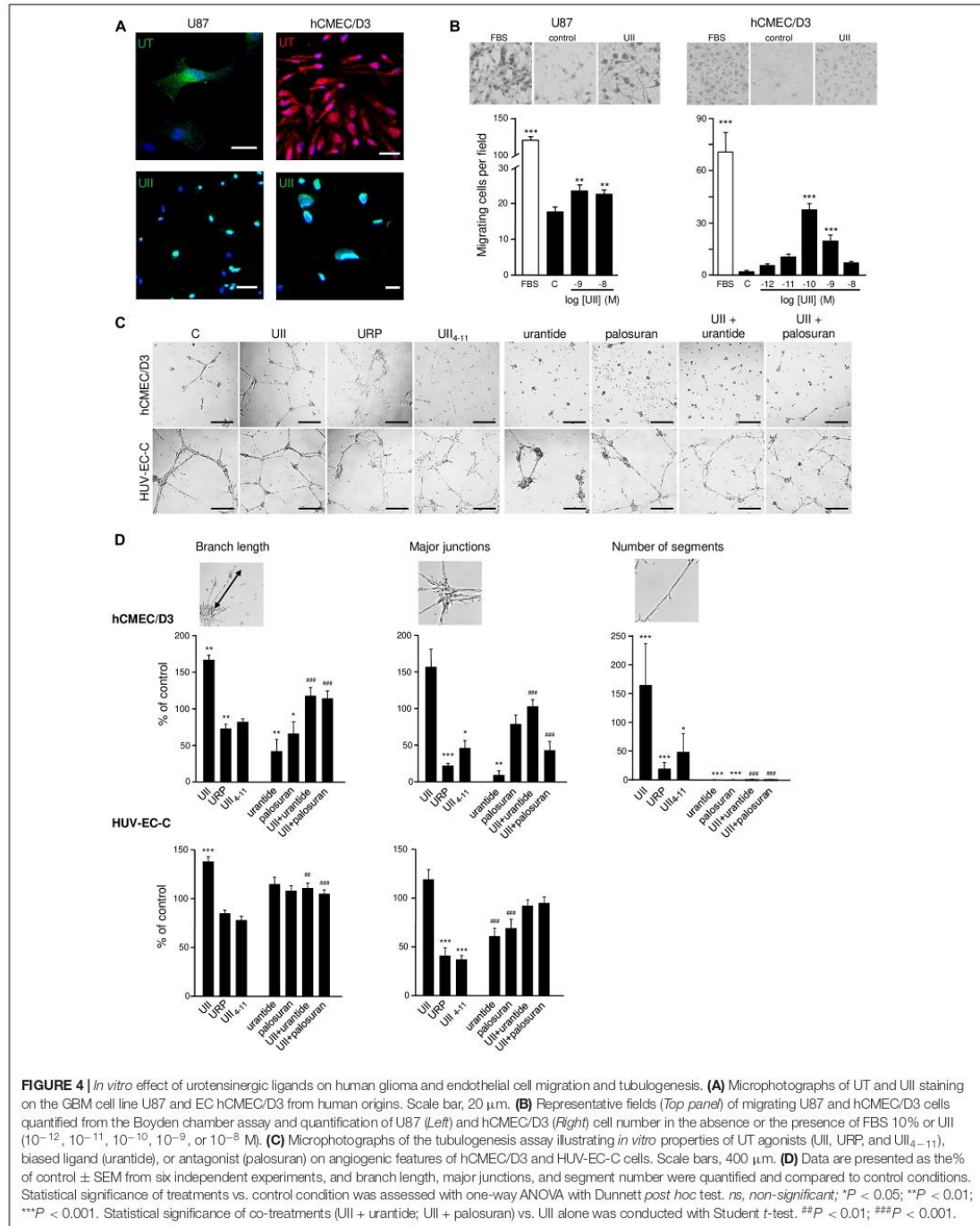
Animals receiving intratumoral administration of palosuran featured diminished tumor growth but no significant extended survival (Figure 6D, $P = 0.2922$). Co-administered with UII, palosuran partially prevented the UII-evoked stimulation of tumor growth (Figure 6D). The biased UT ligand urantide showed a strong inhibitory effect on tumor growth by maintaining significantly smaller tumor volumes for an extended period (Figure 6D), whereas the animal survival was markedly increased. When added at a 10-fold higher dose (Supplementary Figure 3A), or when

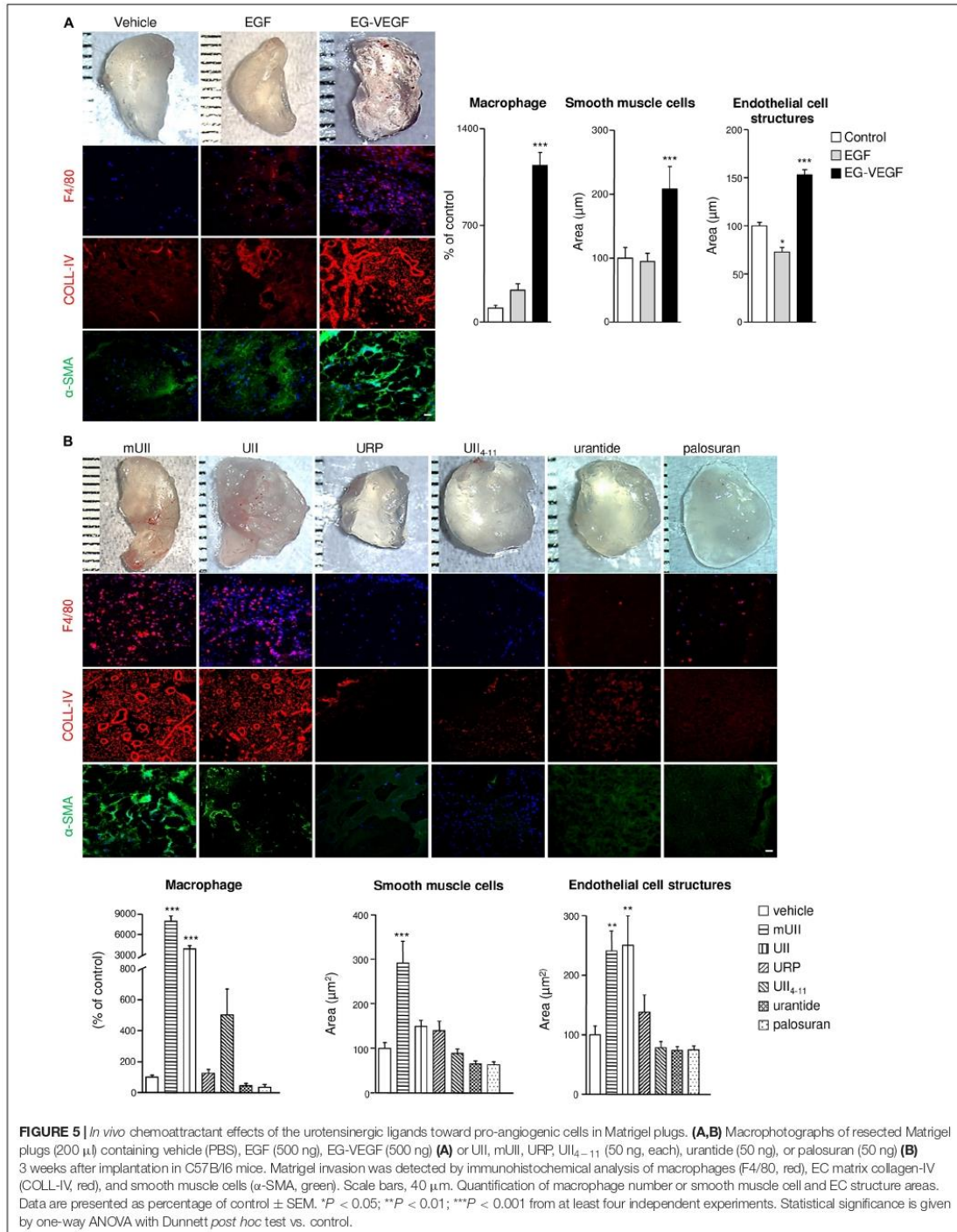


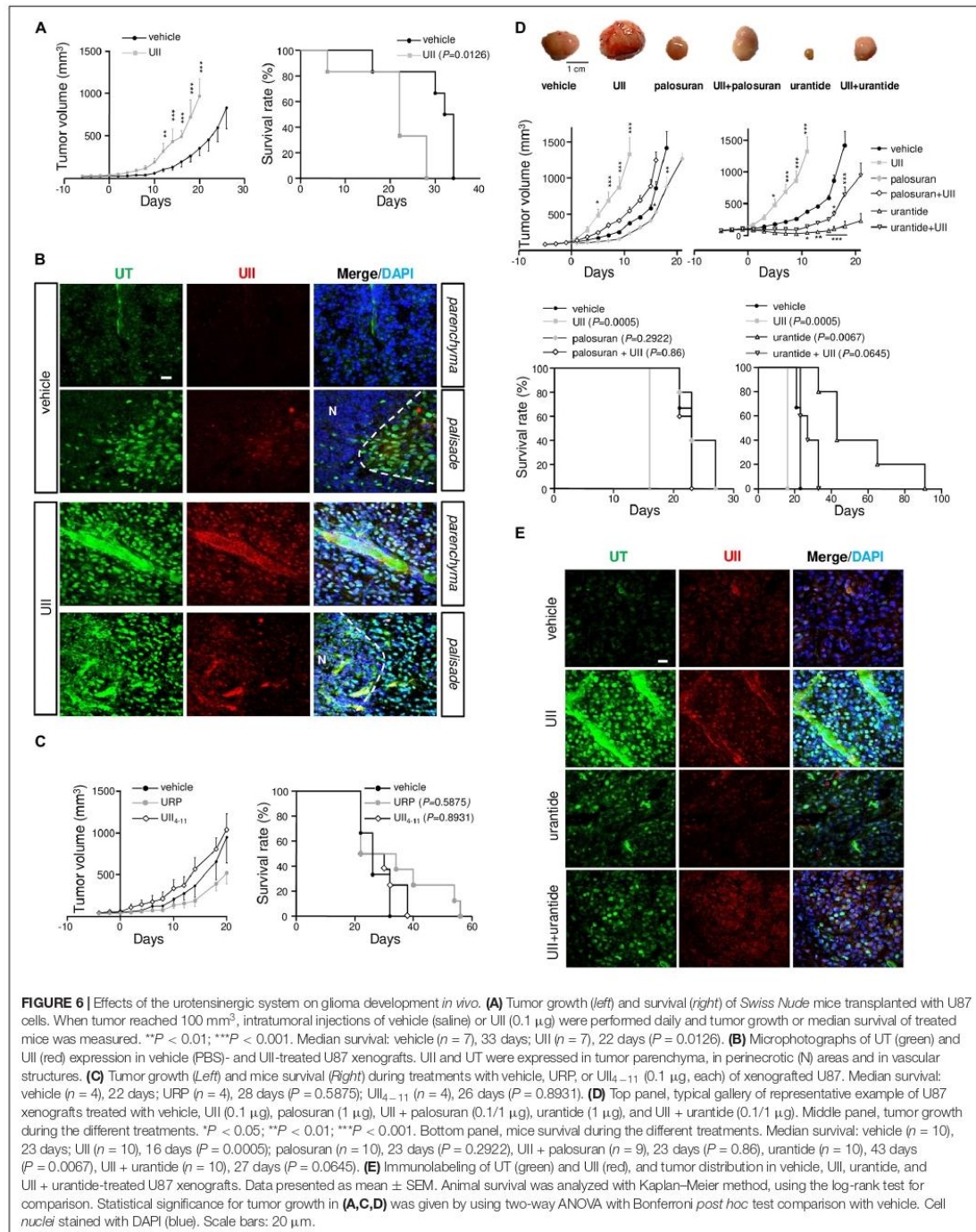
tumors reached a large volume ($>500 \text{ mm}^3$, **Supplementary Figure 3B**), urantide exhibited a significant anti-tumoral effect. Also, UII-treated xenografts expressed UII and

UT in GBM and in vascular components (**Figure 6E**), while urantide prevented UII-promoting UII and UT expression (**Figure 6E**).









The Urotensinergic System Is Involved in GBM Cell Proliferation, Necrosis, and MMP-2/9 Activation *in vivo*

We next tested whether U87 xenograft treatments result in UT-regulating GBM proliferation. After a 15-day treatment, UII significantly increased the proliferation index, measured by the immunostaining of the proliferation marker Ki67 (Figure 7A). Palosuran and urantide significantly diminished endogenous cell proliferation by themselves, and UII-induced proliferation was also prevented by palosuran or urantide (Figure 7A, bottom left). Accordingly, a significant correlation (Pearson's $r = 0.6579$, $R^2 = 0.4328$, $P < 0.0001$) between the proliferation index and tumor volume was found at 15 days (Figure 7A, bottom right).

Rapid proliferation within glioma outstrips their blood supply likely leading to intratumoral necrosis and induction of hypoxia likely involving HIF-1 α and HIF-2 α overexpression (Supplementary Figure 4). We then investigated the distribution of the hypoxic marker pimonidazole in U87 xenografts after a 15-day treatment or when tumors reached 1,000 mm³. In UII-treated tumors, the size of hypoxic areas (green) was strongly increased, indicating the hypoxic status of UII-treated tumors (Figure 7B). After urantide treatment, a similar tendency can be observed without significance. In GBM, the sustained hypoxia is classically followed by necrosis. The size of necrotic area was quantified after H&E coloration on 15-day-treated and on large tumors (>1,000 mm³). UII strongly increased the size of necrotic areas (Figure 7C), whereas urantide evoked a significant decrease of necrosis at day 15, and finally showed a necrotic index resembling those of the UII-treated tumors after tumor relapse (Figure 7C).

In UII-treated tumors, capillaries appeared co-stained with anti-UII and anti-CD31, suggesting that endothelial compartment also serve as a reservoir of UII production (Figure 8A, left panel). UT was highly expressed in both glioma and EC, but not in α -SMA-positive structures (Figure 8A, right panel). The angiogenic status of xenografts under UII, urantide, or palosuran treatment after 15 days of daily injections and when tumors have reached 1,000 to 1,500 mm³ was investigated. At 15 days, exogenous UII strongly altered the blood vessel architecture, with tortuous and disorganized vascular networks (Figure 8B, left). Palosuran or urantide markedly diminished the blood vessel density (Figure 8B, left). In >1,000 mm³ tumors, UII maintained a strong angiogenic status whereas palosuran but mostly urantide decreased the basal vascular density and number of branches (Figure 8B, right), only urantide being able to reduce capillary-like structure diameter (Figure 8B, right). These suggest that urantide acts as a potent antagonist of the murine UT expressed on vascular components of host mice, to evoke a strong angiogenic activity.

Glioblastoma growth, hypoxia, and angiogenesis have been shown to be associated with mesenchymal marker expression including MMPs, and more especially MMP-2 during blood vessel reorganization and MMP-9 during invasion (Xu et al., 2015). As illustrated in Figure 9A, MMP-2 was mainly localized in large capillary-like structures and showed significant higher surface covered after treatment with UII. The proinvasive MMP-9 is also observed in large blood vessels and surrounding

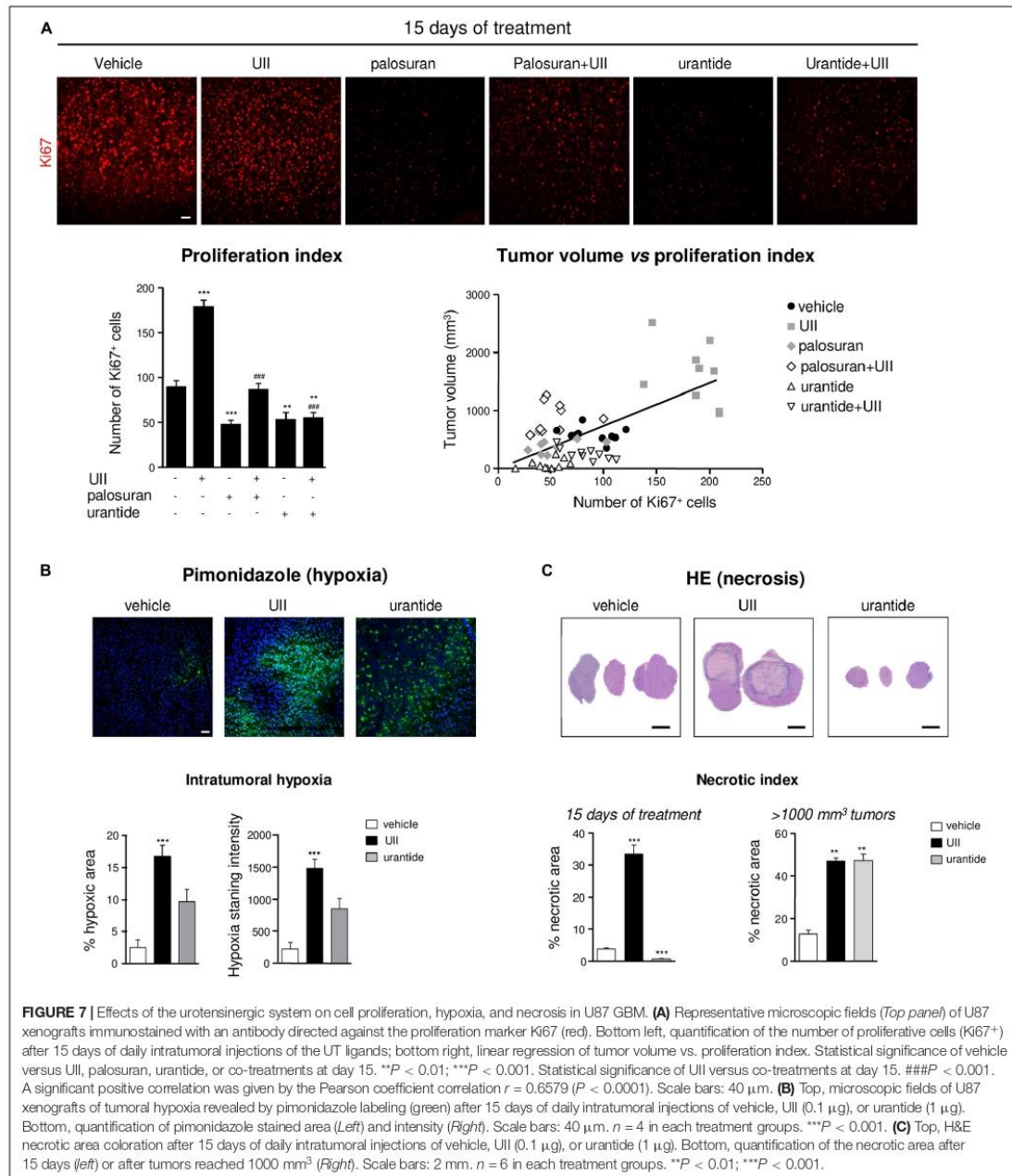
tumor cells, with intense immunofluorescence in UII-treated xenografts (Figure 9B). A similar trend was found *in vitro*, in hCMEC/D3 with higher MMP9 gene expression upon UII treatment (Supplementary Figure 5). Palosuran and, more efficiently, urantide markedly prevented MMP-2 and MMP-9 expression whereas urantide significantly counteracted the UII-evoked MMP-2 and MMP-9 activations (Figures 9A,B). These observations suggest endogenous UII-induced hypoxic and proliferative mechanisms in GBM, likely stimulating mesenchymal phenotype associated with angiogenic features.

UII Stimulates $\alpha\text{v}\beta$ Integrin Expression and ^{99m}Tc-RGD Binding in U87 GBM Xenografts

Angiogenesis and mesenchymal phenotype are accompanied by integrin reactivation. At 15 days, it was observed that αv -immunolabeled structures expressed the EC progenitor CD34 marker, more specifically in UII-treated tumors (Figures 10A,B, left). *In vitro*, UII favored the expression of the ITGAV gene mRNA encoding αv integrin from at least in part U87 and 8MG GBM cells (Supplementary Figure 5). The $\alpha\text{v}\beta 3$ integrins were previously investigated as targets for direct molecular imaging of tumor angiogenesis with SPECT as they are considered as a key marker of activated EC (Schnell et al., 2009). Here, we used a ^{99m}Tc tracer containing the RGD (arginine, glycine, aspartate, ^{99m}Tc-RGD) binding motif already validated (Rylova et al., 2014) to image $\alpha\text{v}\beta 3$ expression in GBM *in vivo* (Supplementary Material and Supplementary Figure 6). In U87 xenografts, UII stimulated tumor growth (Figures 10B,C) but paradoxically provoked a decrease of RGD tumor uptake after 15 days of treatment (Figure 10C). The *ex vivo* γ -ray quantification of the total tumor showed ^{99m}Tc-RGD capture enhanced in UII- and reduced in urantide-treated tumors, respectively, mainly due to the tumor size. From merged H&E staining and the ^{99m}Tc-RGD distribution, it was observable that 10% of the control tumors and whole UII-treated tumors were necrotic, respectively. Analysis of the ^{99m}Tc-RGD capture in the tumor (T), the necrotic tumor (NT), or the non-necrotic tumor (NNT) revealed that UII-treated tumors exhibited more RGD binding around the necrotic area (Figure 10D), suggesting increase of integrin expression and potentially tumor angiogenesis.

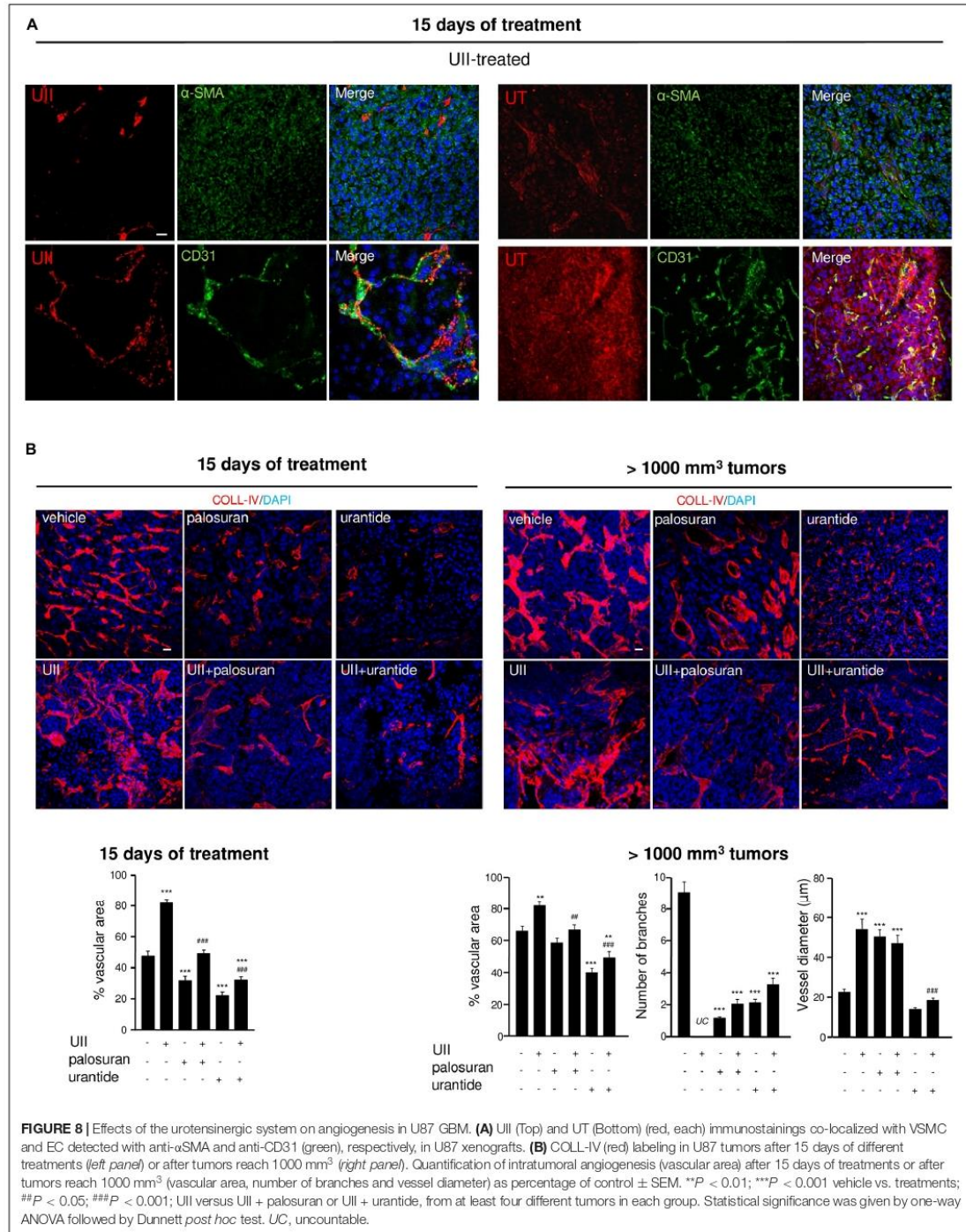
DISCUSSION

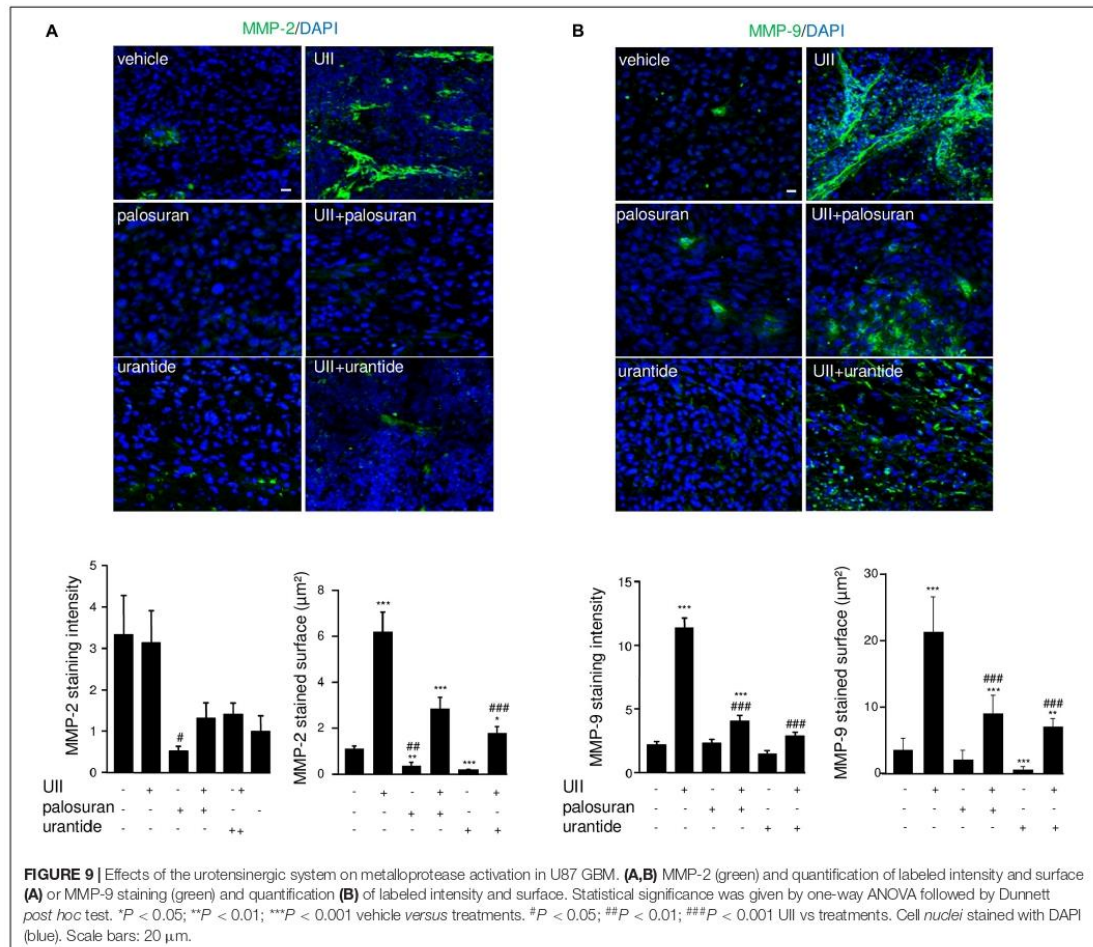
Angiogenesis has been shown to play a key role in the multi-step formation of GBM and results from a complex multicellular communication between glioma, endothelial, inflammatory, and/or reactive glial cells (Hanahan and Coussens, 2012). However, anti-angiogenics including bevacizumab can prolong the progression-free survival in patient with recurrent GBM (Lai et al., 2011) but led to a dramatic progression likely *via* exacerbated hypoxic and mesenchymal acquired status (Bergers and Hanahan, 2008; Keunen et al., 2011). Therefore, targeting vasoactive peptide receptor behaving as angiogenic chemokines involved in angiogenesis, inflammatory cell attraction, and



invasion of GBM cell lines should constitute an original and promising target system. Here, we report that the peptide UII and its receptor UT, expressed in malignant high-grade gliomas, promote angiogenesis and tumor vascular abnormal phenotype

via up-regulation of mesenchymal factors including $\alpha\text{v}\beta$ integrins and MMP-9, accompanying tumor growth, proliferation, and hypoxia/necrosis. This UII/UT system expressed in the U87-xenografted GBM model is shown to be efficiently targeted by





biased/antagonist UT ligands leading to tumor growth inhibition by, at least in part, reducing angiogenesis.

From TCGA, we show that UTS2 encoding Ull is more expressed in high-grade astrocytic gliomas including GBMs and, within GBM, appears to be upregulated in the mesenchymal subclass of the Verhaak classification. A significant positive correlation between UT and Ull expression in glioma samples also suggest paracrine/autocrine mechanisms within the GBM tumor bulk. Interestingly, glioma patients expressing the highest levels of UT and mainly Ull mRNA had significantly shorter survival durations than cases with lower expressions; this prognostic cue can be associated with the strong expression of Ull and UT in the hypoxic/vascular area of GBM samples, the positive correlation found between Ull and UT expression, and the density of the abnormal vascularization. Indeed, inflammatory processes and/or hypoxic microenvironment within the tumor or neighboring normal tissues likely

result in secretion by GBM cells of immunomodulatory cytokines and other factors such as CSF1 (colony-stimulating factor 1), C-C/CXC motif chemokines, or GDNF (glial cell-derived neurotrophic factor), which polarize TAMs toward an immunosuppressive M2 phenotype (Chang et al., 2016; Chen et al., 2017; Wang et al., 2019). TAM may in turn induce growth factor release triggering specific transcription factors important for mesenchymal transition associated with angiogenesis (Bogoch et al., 2017). Indeed, mesenchymal GBMs are characterized by expression of chemokine ligand/GPCRs such CXCL12/CXCR4, thrombin/PAR-1, or IL-8/CXCR2-associated signaling stimulating angiogenesis (Rollins, 2006; Albin et al., 2018) or factors supporting tissue remodeling and angiogenesis such as MMP-2 or MMP-9 (Gabrusiewicz et al., 2011). While GBM expressed Ull and UT more specifically in mesenchymal tumor areas, the previous description of UT expression in a majority of monocytes/macrophages and the

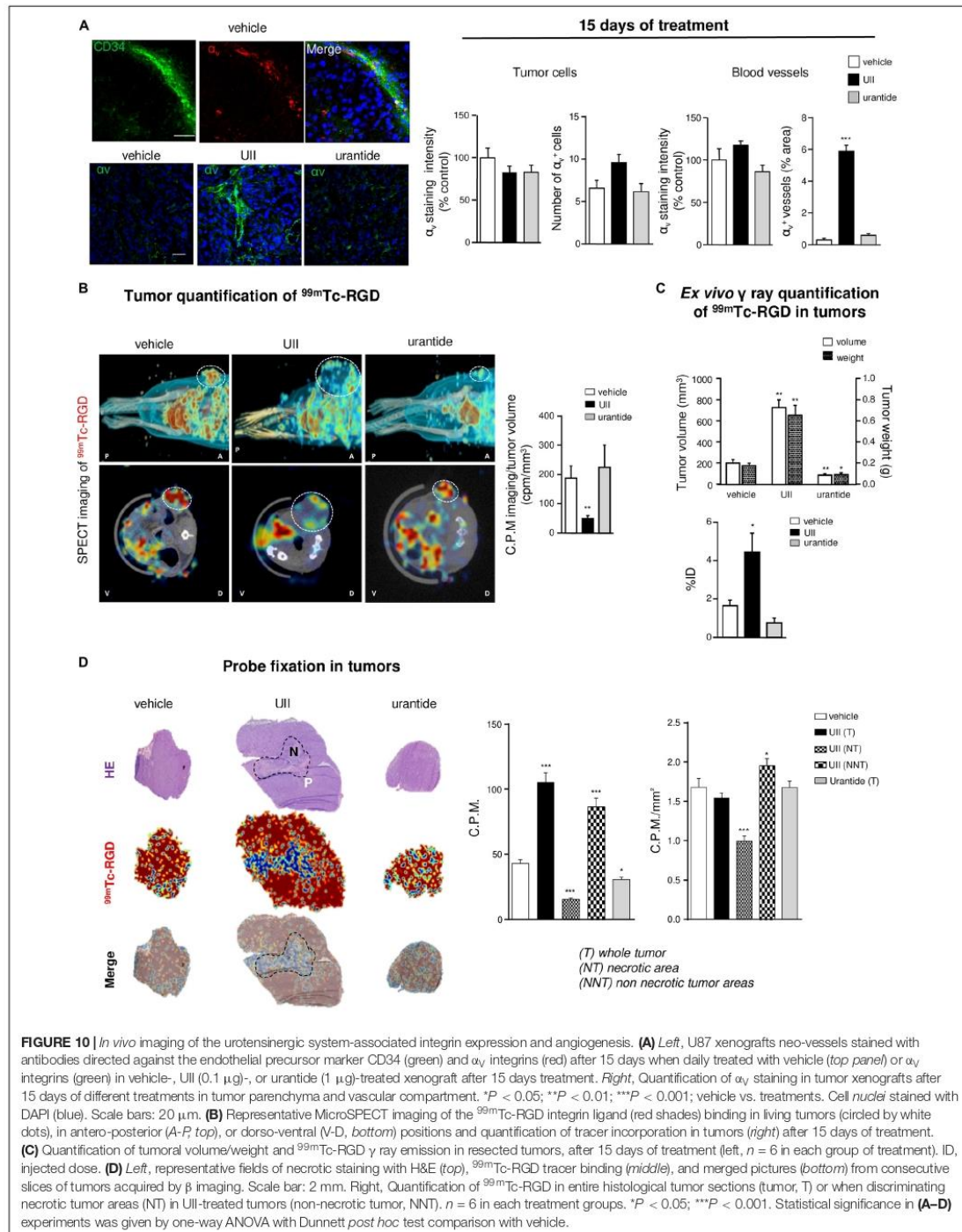


FIGURE 10 | *In vivo* imaging of the urotensinergic system-associated integrin expression and angiogenesis. **(A)** Left, U87 xenografts neo-vessels stained with antibodies directed against the endothelial precursor marker CD34 (green) and α_v integrins (red) after 15 days when daily treated with vehicle (top panel) or α_v integrins (green) in vehicle-, UII (0.1 μg)-, or urantide (1 μg)-treated xenograft after 15 days treatment. Right, Quantification of α_v staining in tumor xenografts after 15 days of different treatments in tumor parenchyma and vascular compartment. * $P < 0.05$; ** $P < 0.01$; *** $P < 0.001$; vehicle vs. treatments. Cell nuclei stained with DAPI (blue). Scale bars: 20 μm . **(B)** Representative MicroSPECT imaging of the ^{99m}Tc -RGD integrin ligand (red shades) binding in living tumors (circled by white dots), in antero-posterior (A-P; top), or dorso-ventral (V-D, bottom) positions and quantification of tracer incorporation in tumors (right) after 15 days of treatment. **(C)** Quantification of tumoral volume/weight and ^{99m}Tc -RGD γ ray emission in resected tumors, after 15 days of treatment (left, $n = 6$ in each group of treatment), ID, injected dose. **(D)** Left, representative fields of necrotic staining with H&E (top), ^{99m}Tc -RGD tracer binding (middle), and merged pictures (bottom) from consecutive slices of tumors acquired by β imaging. Scale bar: 2 mm. Right, Quantification of ^{99m}Tc -RGD in entire histological tumor sections (tumor, T) or when discriminating necrotic tumor areas (NT) in UII-treated tumors (non-necrotic tumor, NNT). $n = 6$ in each treatment groups. * $P < 0.05$; *** $P < 0.001$. Statistical significance in **(A–D)** experiments was given by one-way ANOVA with Dunnett *post hoc* test comparison with vehicle.

UII-induced TAM infiltration promoting an inflammatory environment in lung cancer (Segain et al., 2007; Zhou et al., 2012) strongly support a key role of the UII/UT system in hypoxia/inflammation-induced mesenchymal transition, TAM infiltration, angiogenesis, and, as a consequence, resistance to treatment.

The pro-inflammatory cytokine function of the UII/UT system at the vascular compartment has been suggested by the UII-induced synthesis of pro-thrombotic and inflammatory markers such as PAI-1, in cultured smooth muscle cells or EC (Djordjevic et al., 2005; Cirillo et al., 2008). Here, we confirmed the expression of UT and UII by glioma cells and showed that UII induces chemotactic migration and tubulogenesis of human hCMEC/D3 and HUV-EC-C, without main impact on cell proliferation. The observed chemoattractant effects of UII on brain and umbilical ECs are in a good agreement with the first study of Spinazzi et al. (2006) establishing *in vivo* tubulogenic properties and sustains a UII-induced initiation of vessel sprouting during co-optation. These angiogenic properties were validated *in vivo* by means of the matrigel plugs, in which angiogenic compounds such as EG-VEGF allowed penetration by host cells and formation of new blood vessels. Matrigels containing urotensinergic ligands chemoattract and capture host cells, e.g., macrophages, vascular smooth muscle cells, or EC (Matsusaka and Wakabayashi, 2006; Segain et al., 2007; Park et al., 2013) signs of pro-inflammatory and pro-angiogenic properties of UII toward murine cells. Interestingly, the presupposed UT agonists URP or the short sequence peptide UII_{4–11} failed to promote recruitment of vascular cells *in vitro* (Table 1). Also, we describe the angiogenic potential of UT on EC *in vivo* when activated by UII but not URP or hUII_{4–11}. Originally observed here, URP and shorter UII-derived sequences exhibit antagonistic/inhibitory properties on tubulogenesis *in vitro*, suggesting a potential endogenous biased activity of URP on UT, antagonizing UII-induced migratory function. Some distinct activities on vascular and glial functions (Prosser et al., 2008; Hirose et al., 2009; Jarry et al., 2010) would at least in part reside in the UII-mediated long-lasting effects through insurmountable binding on UT, whereas URP usually induces transient responses (Hirose et al., 2009; Desrues et al., 2012). Both URP and hUII_{4–11} were used as lead sequence for the design of UT synthetic drugs including antagonists. The first “peptide antagonists” of rodent UT were obtained by focusing on Lys8 of UII to develop urantide (Table 1; Patacchini et al., 2003) exhibiting on CHO or HEK cells expressing recombinant human UT residual agonist (Camarda et al., 2004) or biased activity (Brulé et al., 2014). Here, when urantide was directly tested on EC-forming tubulogenesis, a marked constitutive inhibition is observed whereas the antagonist palosuran (Table 1) remained inactive on tube formation, both preventing UII-induced angiogenesis. The urantide-inhibitory function raises the possibility of a biased function negatively regulating the UT-signaling cascades, e.g., partially Gq and internalization as previously shown (Brulé et al., 2014), specifically involved in tubulogenesis. Diebold et al. (2012) demonstrated a NOX2-containing NADPH oxidase as a source of ROS responsible for UII-induced angiogenesis (Patacchini et al., 2003), supporting the idea that UII recruits NOX2 through a

mechanism involving at least in part Gq and/or internalization of UT. To dissect the involvement of the urotensinergic system in GBM growth and angiogenesis, U87 heterotopic xenografts in *Nude* mice were injected with UT “agonists” (UII or URP or hUII_{4–11}), biased ligand (urantide) or antagonist (palosuran) alone, or in combination with UII. UII dramatically accelerates GBM growth, correlated with a significant reduced animal survival, while URP or hUII_{4–11} remained inactive at the same tested doses and/or exhibit tumor repressor function at a higher dose, reinforcing the notion that URP may be a naturally produced biased/competitive ligand of UT. In the same line, the short peptide urantide drastically inhibited GBM growth and promoted long-lasting survival. By comparison, the most well-studied primate UT antagonist palosuran only delayed gliomagenesis and animal death. It can be explained by the low antagonist behavior of palosuran toward rodent UT present in host cells, compared with the antagonist activity of urantide toward murine UT (Patacchini et al., 2003) combined with its biased activity on human UT (Brulé et al., 2014). As recently validated with the design of a radiolabeled DOTA-urantide binding UT injectable *in vivo* (Poret et al., 2020), UT expressed in GBM cells as well as in vascular/myeloid compartments would constitute a key pharmacological target for the design of therapeutic molecules based on the structure of urantide.

Detection of the key markers of the high-grade GBM as well as measurement of the proliferation index and hypoxic–necrotic areas provide cues of the impact of the urotensinergic system on glioma malignancy. We show that UII enhanced cell proliferation within GBM tumors, whereas palosuran and urantide inhibited this mitogenic activity, even in the presence of exogenous UII. This UII-promoting mitogenic mechanism should not result from a direct activation of glioma cells (Lecointre et al., 2015). However, anti-angiogenic treatment leads to tumoral hypoxic features and mesenchymal phenotype associated with increased proliferative capacity (Xu et al., 2015). Here, UII similarly exacerbates hypoxia surrounding large central necrotic areas, likely mimicking the adverse events of anti-angiogenics. Despite a report suggesting that UT relays activation of HIF-1 α through NOX2 in endothelial cells controlling tubulogenesis *in vitro* (Diebold et al., 2012), we did not observe UII-evoked induction of HIF-1/2 in normo- or hypoxic conditions in GBM or EC *in vitro*. UII may rather configure the tumor microenvironment composed of endothelial, perivascular, and/or inflammatory cells, promoting tumor progression by mediating hypoxia, abnormal angiogenesis, desmoplasia, and/or mesenchymal characteristics. The mesenchymal components including MMP-2 and MMP-9 can contribute to tumor invasion through breaking down of basement membrane including Coll-IV (Fan et al., 2012). In agreement, the production of MMP-9 after UII treatment of lung adenocarcinoma in mice (Zhou et al., 2012) was previously described. We show that UII treatment of GBM xenografts evoked MMP-2 and MMP-9 overexpression mainly in the vascular and glioma cell compartments, respectively, and that UII stimulates MMP9 gene expression in hCMEC/D3 *in vitro*. Again, palosuran and urantide diminished and prevented UII-evoked MMPs expression, indicating that the urotensinergic system activates the vascular network during tumor progression.

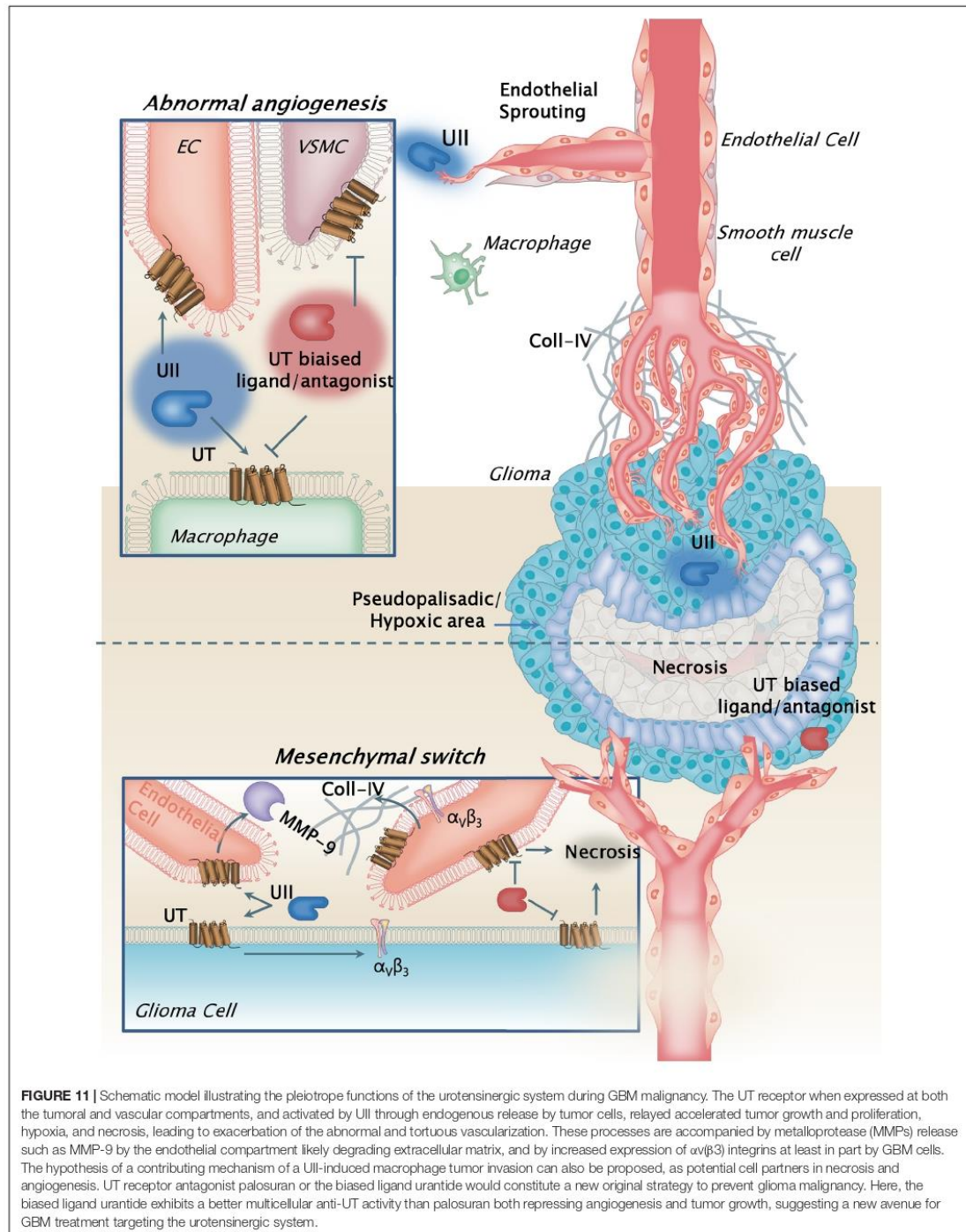


FIGURE 11 | Schematic model illustrating the pleiotropic functions of the urotensinergic system during GBM malignancy. The UT receptor when expressed at both the tumoral and vascular compartments, and activated by UII through endogenous release by tumor cells, relayed accelerated tumor growth and proliferation, hypoxia, and necrosis, leading to exacerbation of the abnormal and tortuous vascularization. These processes are accompanied by metalloprotease (MMPs) release such as MMP-9 by the endothelial compartment likely degrading extracellular matrix, and by increased expression of $\alpha_v\beta_3$ integrins at least in part by GBM cells. The hypothesis of a contributing mechanism of a UII-induced macrophage tumor invasion can also be proposed, as potential cell partners in necrosis and angiogenesis. UT receptor antagonist palosuran or the biased ligand urantide would constitute a new original strategy to prevent glioma malignancy. Here, the biased ligand urantide exhibits a better multicellular anti-UT activity than palosuran both repressing angiogenesis and tumor growth, suggesting a new avenue for GBM treatment targeting the urotensinergic system.

Extracellular Coll-IV and membrane α_V integrins are known to be scaffolding adhesion molecules for angiogenesis and tumoral infiltration correlated with progression of numerous cancers (Mammoto et al., 2013). We describe and quantify α_V integrin patterns in glioma cells or vessels and establish a marked increased expression in endothelium and glioma cells during the course of GBM malignancy when treated with UII. These $\alpha_V\beta_3$ integrins were previously investigated as targets for molecular SPECT imaging of tumor angiogenesis *in vivo* while they are also expressed by glioma cells (Schnell et al., 2009). We observe increased GBM uptake of ^{99}Tc -RGD in the periphery of the tumor surrounding the necrotic area after UII treatment. However, *in vivo* radio-counting showed decreased incorporation within the tumor. As recently previously proposed for bevacizumab-treated GBM in mice (Rylova et al., 2014), delayed necrosis explains the decrease of RGD uptake *in vivo*. We believe UII sets up tortuous angiogenesis with enhanced integrin expression, associated with chaotic blood flow and/or interstitial pressure reducing perfusion, thereby confining RGD probe capture to the tumor peripheral ring.

Altogether, our study emphasizes that UII and its receptor UT are more expressed in GBMs than in low-grade gliomas, specifically in vascular and hypoxia mesenchymal areas, and play a major role in gliomagenesis *via*, at least in part, angiogenesis, promoting MMP-2/-9 and α_V integrin expression within the tumor bulk. Because UT may also relay glioma cell migration, this work shows the interesting opportunity provided by new class of vasoactive and chemokine peptide receptor targets controlling multicellular functions within the GBM microenvironment and involved in the mesenchymal transformation (Figure 11).

DATA AVAILABILITY STATEMENT

The original contributions presented in the study are included in the article/Supplementary Material, further inquiries can be directed to the corresponding author/s.

ETHICS STATEMENT

The animal study was reviewed and approved by the "Comité d'Ethique Normandie en Matière d'Expérimentation Animale" CENOMEXA under the National Committee on Animal Experimentation, and received the following number N/13-11-12/36/11-17.

AUTHOR CONTRIBUTIONS

VLJ performed main experiments, quantifications and analyses on glioma cells and endothelial cells *in vitro* (cell migration,

tubulogenesis) and *in vivo* (matrigel plugs, tumor xenografts and ligand injections, animal immunohistochemistry, MicroSpect imaging). P-OG and K-PD carried out immunohistochemistry, analysis, scoring from patient clinical information, and quantitative PCR on glioma biopsies and glioma cell lines. AM analyzed *in silico* mRNA expression levels from the TCGA database and vascular characteristics from glioma patient biopsies. NP, DC, and LD maintained culture of glioma and endothelial cell lines, and performed cell proliferation studies, and Western blot for hypoxic marker expression. P-OC established and provided the hCMEC/D3 human microendothelial cell line. JH contributed to the studies on the GBM cell xenografts and intratumoral administration of urantide. F-XF, OL, AL, and FMa provided GBM biopsies and all clinical information from the Haute-Normandie tumorbank, France. RM, PB, and PV established the angiogenic RGD tracer and allowed the *in vivo* microSPECT imaging and analysis. FMO contributed to the analysis of the data and provided critical comments. PG and HC supervised the study, provided all critical analyses, and wrote the manuscript. All authors contributed to the article and approved the submitted version.

FUNDING

This work was supported by INSERM, Géfluc, TC2N network, Ligue Régionale Contre le Cancer, the Regional Council of Normandy and the European Community FEDER program (Europe gets involved in regional development through the ERDF program) (Grants DO-IT, PACT-PACT-PACBS and PHEDERCPG), Institute on Innovative and Biomedical Research (IRIB), and University of Rouen. VLJ, P-OG, K-PD, AM, and DC were recipients of a fellowship from the Région Normandie or French ministry.

ACKNOWLEDGMENTS

We gratefully acknowledge the PRIMACEN platform (University of Rouen, France) for imaging equipment and Mr. Arnaud Arabo and Mrs. Huguette Lemonnier for skillful technical assistance.

SUPPLEMENTARY MATERIAL

The Supplementary Material for this article can be found online at: <https://www.frontiersin.org/articles/10.3389/fcell.2021.652544/full#supplementary-material>

REFERENCES

Albini, A., Bruno, A., Noonan, D. M., and Mortara, L. (2018). Contribution to tumor angiogenesis from innate immune cells within the tumor microenvironment: implications for immunotherapy. *Front. Immunol.* 9:527. doi: 10.3389/fimmu.2018.00527

Aliferis, C., and Trafalis, D. T. (2015). Glioblastoma multiforme: pathogenesis and treatment. *Pharmacol. Ther.* 152, 63–82. doi: 10.1016/j.pharmthera.2015.05.005

Ames, R. S., Sarau, H. M., Chambers, J. K., Willette, R. N., Aiyar, N. V., Romanic, A. M., et al. (1999). Human urotensin-II is a potent vasoconstrictor and agonist for the orphan receptor GPR14. *Nature* 401, 282–286. doi: 10.1038/45809

- Arrieta, O., Guevara, P., Escobar, E., García-Navarrete, R., Pineda, B., and Sotelo, J. (2005). Blockage of angiotensin II type I receptor decreases the synthesis of growth factors and induces apoptosis in C6 cultured cells and C6 rat glioma. *Br. J. Cancer* 92, 1247–1252. doi: 10.1038/sj.bjc.6602483
- Aubry, M., de Tayrac, M., Etcheverry, A., Clavreul, A., Saikali, S., Menei, P., et al. (2015). From the core to beyond the margin: a genomic picture of glioblastoma intratumor heterogeneity. *Oncotarget* 6, 12094–12109. doi: 10.18632/oncotarget.3297
- Becker, S., Bohn, P., Bouyeure-Petit, A.-C., Modzelewski, R., Gensanne, D., Picquenot, J.-M., et al. (2015). Bevacizumab enhances efficiency of radiotherapy in a lung adenocarcinoma rodent model: role of $\alpha v \beta 3$ imaging in determining optimal window. *Nucl. Med. Biol.* 42, 923–930. doi: 10.1016/j.nucmedbio.2015.08.002
- Bergers, G., and Hanahan, D. (2008). Modes of resistance to anti-angiogenic therapy. *Nat. Rev. Cancer* 8, 592–603. doi: 10.1038/nrc2442
- Bogoch, Y., Friedlander-Malik, G., Lupu, L., Bondar, E., Zohar, N., Langier, S., et al. (2017). Augmented expression of RUNX1 deregulates the global gene expression of U87 glioblastoma multiforme cells and inhibits tumor growth in mice. *Tumour Biol.* 39:1010428317698357. doi: 10.1177/1010428317698357
- Borsig, L., Wolf, M. J., Roblek, M., Lorentzen, A., and Heikenwalder, M. (2014). Inflammatory chemokines and metastasis—tracing the accessory. *Oncogene* 33, 3217–3224. doi: 10.1038/onc.2013.272
- Bougnaud, S., Golebiewska, A., Oudin, A., Keunen, O., Harter, P. N., Mäder, L., et al. (2016). Molecular crosstalk between tumour and brain parenchyma instructs histopathological features in glioblastoma. *Oncotarget* 7, 31955–31971. doi: 10.18632/oncotarget.7454
- Brennan, C. W., Verhaak, R. G. W., McKenna, A., Campos, B., Nounshmehr, H., Salama, S. R., et al. (2013). The somatic genomic landscape of glioblastoma. *Cell* 155, 462–477. doi: 10.1016/j.cell.2013.09.034
- Brulé, C., Perzo, N., Joubert, J.-E., Sainsily, X., Leduc, R., Castel, H., et al. (2014). Biased signaling regulates the pleiotropic effects of the urotensin II receptor to modulate its cellular behaviors. *FASEB J.* 28, 5148–5162. doi: 10.1096/fj.14-249771
- Camarda, V., Song, W., Marzola, E., Spagnol, M., Guerrini, R., Salvadori, S., et al. (2004). Urotensin II mimics urotensin-II induced calcium release in cells expressing recombinant UT receptors. *Eur. J. Pharmacol.* 498, 83–86. doi: 10.1016/j.ejphar.2004.07.089
- Cancer Genome Atlas Research Network. (2008). Comprehensive genomic characterization defines human glioblastoma genes and core pathways. *Nature* 455, 1061–1068. doi: 10.1038/nature07385
- Castel, H., Desrués, L., Joubert, J.-E., Tonon, M.-C., Prêzeau, L., Chabbert, M., et al. (2017). The G protein-coupled receptor UT of the neuropeptide urotensin II displays structural and functional chemokine features. *Front. Endocrinol.* 8:76. doi: 10.3389/fendo.2017.00076
- Castel, H., Diallo, M., Chatenet, D., Leprince, J., Desrués, L., Schouff, M.-T., et al. (2006). Biochemical and functional characterization of high-affinity urotensin II receptors in rat cortical astrocytes. *J. Neurochem.* 99, 582–595. doi: 10.1111/j.1471-4159.2006.04130.x
- Cavazos, D. A., and Brenner, A. J. (2016). Hypoxia in astrocytic tumors and implications for therapy. *Neurobiol. Dis.* 85, 227–233. doi: 10.1016/j.nbd.2015.06.007
- Chang, A. L., Miska, J., Wainwright, D. A., Dey, M., Rivetta, C. V., Yu, D., et al. (2016). CCL2 produced by the glioma microenvironment is essential for the recruitment of regulatory T cells and myeloid-derived suppressor cells. *Cancer Res.* 76, 5671–5682. doi: 10.1158/0008-5472.CAN-16-0144
- Chen, Z., Feng, X., Herting, C. J., García, V. A., Nie, K., Pong, W. W., et al. (2017). Cellular and molecular identity of tumor-associated macrophages in glioblastoma. *Cancer Res.* 77, 2266–2278. doi: 10.1158/0008-5472.CAN-16-2310
- Cherry, A. E., and Stella, N. (2014). G protein-coupled receptors as oncogenic signals in glioma: emerging therapeutic avenues. *Neuroscience* 278, 222–236. doi: 10.1016/j.neuroscience.2014.08.015
- Cirillo, P., De Rosa, S., Pacileo, M., Gargiulo, A., Angri, V., Fiorentino, I., et al. (2008). Human urotensin II induces tissue factor and cellular adhesion molecules expression in human coronary endothelial cells: an emerging role for urotensin II in cardiovascular disease. *J. Thromb. Haemost.* 6, 726–736. doi: 10.1111/j.1538-7836.2008.02923.x
- Clavier, T., Mutel, A., Desrués, L., Lefevre-Scelles, A., Gastaldi, G., Amki, M. E., et al. (2018). Association between vasoactive peptide urotensin II in plasma and cerebral vasospasm after aneurysmal subarachnoid hemorrhage: a potential therapeutic target. *J. Neurosurg.* doi: 10.3171/2018.4.JNSI.172313 Online ahead of print
- Clozel, M., Binkert, C., Birker-Robaczewska, M., Boukhadra, C., Ding, S.-S., Fischli, W., et al. (2004). Pharmacology of the urotensin-II receptor antagonist palosuran (ACT-058362; 1-[2-(4-benzyl-4-hydroxy-piperidin-1-yl)-ethyl]-3-(2-methyl-quinolin-4-yl)-urea sulfate salt): first demonstration of a pathophysiological role of the urotensin system. *J. Pharmacol. Exp. Ther.* 311, 204–212. doi: 10.1124/jpet.104.068320
- Coly, P.-M., Perzo, N., Le Joncour, V., Lecointre, C., Schouff, M.-T., Desrués, L., et al. (2016). Chemotactic G protein-coupled receptors control cell migration by repressing autophagosome biogenesis. *Autophagy* 12, 2344–2362. doi: 10.1080/15548627.2016.1235125
- Coulouarn, Y., Lührmann, I., Jegou, S., Anouar, Y., Tostivint, H., Beauvillain, J. C., et al. (1998). Cloning of the cDNA encoding the urotensin II precursor in frog and human reveals intense expression of the urotensin II gene in motoneurons of the spinal cord. *Proc. Natl. Acad. Sci. U.S.A.* 95, 15803–15808.
- Desrués, L., Lefebvre, T., Lecointre, C., Schouff, M.-T., Leprince, J., Compère, V., et al. (2012). Down-regulation of GABA(A) receptor via promiscuity with the vasoactive peptide urotensin II receptor. Potential involvement in astrocyte plasticity. *PLoS One* 7:e36319. doi: 10.1371/journal.pone.0036319
- Diebold, I., Petry, A., Sabrane, K., Djordjevic, T., Hess, J., and Görlach, A. (2012). The HIF1 target gene NOX2 promotes angiogenesis through urotensin-II. *J. Cell Sci.* 125, 956–964. doi: 10.1242/jcs.094060
- Djordjevic, T., BelAiba, R. S., Bonello, S., Pfeilschifter, J., Hess, J., and Görlach, A. (2005). Human urotensin II is a novel activator of NADPH oxidase in human pulmonary artery smooth muscle cells. *Arterioscler. Thromb. Vasc. Biol.* 25, 519–525. doi: 10.1161/01.ATV.0000154279.98244.eb
- Eelen, G., Treps, L., Li, X., and Carmeliet, P. (2020). Basic and therapeutic aspects of angiogenesis updated. *Circ. Res.* 127, 310–329. doi: 10.1161/CIRCRESAHA.120.316851
- Fan, H.-X., Li, H.-X., Chen, D., Gao, Z.-X., and Zheng, J.-H. (2012). Changes in the expression of MMP2, MMP9, and ColIV in stromal cells in oral squamous tongue cell carcinoma: relationships and prognostic implications. *J. Exp. Clin. Cancer Res.* 31:90. doi: 10.1186/1756-9966-31-90
- Federico, A., Zappavigna, S., Romano, M., Grieco, P., Luce, A., Marra, M., et al. (2014). Urotensin-II receptor is over-expressed in colon cancer cell lines and in colon carcinoma in humans. *Eur. J. Clin. Invest.* 44, 285–294. doi: 10.1111/eci.12231
- Franco, R., Zappavigna, S., Gigantino, V., Luce, A., Cantile, M., Cerrone, M., et al. (2014). Urotensin II receptor determines prognosis of bladder cancer regulating cell motility/invasion. *J. Exp. Clin. Cancer Res.* 33:48. doi: 10.1186/1756-9966-33-48
- Gabrusiewicz, K., Ellert-Miklaszewska, A., Lipko, M., Sielska, M., Frankowska, M., and Kaminska, B. (2011). Characteristics of the alternative phenotype of microglia/macrophages and its modulation in experimental gliomas. *PLoS One* 6:e23902. doi: 10.1371/journal.pone.0023902
- Gagliardi, F., Narayanan, A., Reni, M., Franzin, A., Mazza, E., Boari, N., et al. (2014). The role of CXCR4 in highly malignant human gliomas biology: current knowledge and future directions. *Glia* 62, 1015–1023. doi: 10.1002/glia.22669
- Glass, R., and Synowitz, M. (2014). CNS macrophages and peripheral myeloid cells in brain tumours. *Acta Neuropathol.* 128, 347–362. doi: 10.1007/s00401-014-1274-2
- Grieco, P., Franco, R., Bozzuto, G., Toccaceli, L., Sgambato, A., Marra, M., et al. (2011). Urotensin II receptor predicts the clinical outcome of prostate cancer patients and is involved in the regulation of motility of prostate adenocarcinoma cells. *J. Cell. Biochem.* 112, 341–353. doi: 10.1002/jcb.22933
- Hanahan, D., and Coussens, L. M. (2012). Accessories to the crime: functions of cells recruited to the tumor microenvironment. *Cancer Cell* 21, 309–322. doi: 10.1016/j.ccr.2012.02.022
- Hembruff, S. L., and Cheng, N. (2009). Chemokine signaling in cancer: implications on the tumor microenvironment and therapeutic targeting. *Cancer Ther.* 7, 254–267.

- Hirose, T., Takahashi, K., Mori, N., Nakayama, T., Kikuya, M., Ohkubo, T., et al. (2009). Increased expression of urotensin II, urotensin II-related peptide and urotensin II receptor mRNAs in the cardiovascular organs of hypertensive rats: comparison with endothelin-1. *Peptides* 30, 1124–1129. doi: 10.1016/j.peptides.2009.02.009
- Jarry, M., Diallo, M., Lecointre, C., Desrues, L., Tokay, T., Chatenet, D., et al. (2010). The vasoactive peptides urotensin II and urotensin II-related peptide regulate astrocyte activity through common and distinct mechanisms: involvement in cell proliferation. *Biochem. J.* 428, 113–124. doi: 10.1042/BJ20090867
- Kaafarani, I., Fernandez-Sauze, S., Berenguer, C., Chinot, O., Delfino, C., Dussert, C., et al. (2009). Targeting adrenomedullin receptors with systemic delivery of neutralizing antibodies inhibits tumor angiogenesis and suppresses growth of human tumor xenografts in mice. *FASEB J.* 23, 3424–3435. doi: 10.1096/fj.08.12.7852
- Karsy, M., Gelbman, M., Shah, P., Balumbu, O., Moy, F., and Arslan, E. (2012). Established and emerging variants of glioblastoma multiforme: review of morphological and molecular features. *Folia Neuropathol.* 50, 301–321.
- Keunen, O., Johansson, M., Oudin, A., Sanzey, M., Rahim, S. A. A., Fack, F., et al. (2011). Anti-VEGF treatment reduces blood supply and increases tumor cell invasion in glioblastoma. *Proc. Natl. Acad. Sci. U.S.A.* 108, 3749–3754. doi: 10.1073/pnas.1014480108
- Lai, A., Tran, A., Nghiemphu, P. L., Pope, W. B., Solis, O. E., Selch, M., et al. (2011). Phase II study of bevacizumab plus temozolomide during and after radiation therapy for patients with newly diagnosed glioblastoma multiforme. *J. Clin. Oncol.* 29, 142–148. doi: 10.1200/JCO.2010.30.2729
- Lecointre, C., Desrues, L., Joubert, J. E., Perzo, N., Guichet, P.-O., Le Joncour, V., et al. (2015). Signaling switch of the urotensin II vasoactive peptide GPCR: prototypic chemotactic mechanism in glioma. *Oncogene* 34, 5080–5094. doi: 10.1038/ncr.2014.433
- Louis, D. N., Perry, A., Reifenberger, G., von Deimling, A., Figarella-Branger, D., Cavenee, W. K., et al. (2016). The 2016 world health organization classification of tumors of the central nervous system: a summary. *Acta Neuropathol.* 131, 803–820. doi: 10.1007/s00401-016-1545-1
- Mammoto, T., Jiang, A., Jiang, E., Panigrahy, D., Kieran, M. W., and Mammoto, A. (2013). Role of collagen matrix in tumor angiogenesis and glioblastoma multiforme progression. *Am. J. Pathol.* 183, 1293–1305. doi: 10.1016/j.ajpath.2013.06.026
- Matsusaka, S., and Wakabayashi, I. (2006). Enhancement of vascular smooth muscle cell migration by urotensin II. *Naunyn. Schmiedeberg's Arch. Pharmacol.* 373, 381–386. doi: 10.1007/s00210-006-0086-x
- Metellus, P., Voutsinos-Porche, B., Nanni-Metellus, I., Colin, C., Fina, F., Berenguer, C., et al. (2011). Adrenomedullin expression and regulation in human glioblastoma, cultured human glioblastoma cell lines and pilocytic astrocytoma. *Eur. J. Cancer* 47, 1727–1735. doi: 10.1016/j.ejca.2011.02.021
- Norden, A. D., Drappatz, J., and Wen, P. Y. (2008). Novel anti-angiogenic therapies for malignant gliomas. *Lancet Neurol.* 7, 1152–1160. doi: 10.1016/S1474-4422(08)70260-6
- Park, S. L., Lee, B. K., Kim, Y.-A., Lee, B. H., and Jung, Y.-S. (2013). Inhibitory effect of an urotensin II receptor antagonist on proinflammatory activation induced by urotensin II in human vascular endothelial cells. *Biomol. Ther.* 21, 277–283. doi: 10.4062/biomolther.2013.051
- Patacchini, C., Masci, S., D'Ovidio, R., and Lafiandra, D. (2003). Heterologous expression and purification of native and mutated low molecular mass glutenin subunits from durum wheat. *J. Chromatogr. B Analyt. Technol. Biomed. Life. Sci.* 786, 215–220.
- Phuphanich, S., Carson, K. A., Grossman, S. A., Lesser, G., Olson, J., Mikkelsen, T., et al. (2008). Phase I safety study of escalating doses of atrasentan in adults with recurrent malignant glioma. *Neuro Oncol.* 10, 617–623. doi: 10.1215/15228517-2008-013
- Poret, B., Desrues, L., Bonin, M.-A., Pedard, M., Dubois, M., Leduc, R., et al. (2020). Development of novel 111-In-labelled DOTA urotensin II analogues for targeting the UT receptor overexpressed in solid tumours. *Biomolecules* 10:471. doi: 10.3390/biom10030471
- Prosser, H. C. G., Forster, M. E., Richards, A. M., and Pemberton, C. J. (2008). Urotensin II and urotensin II-related peptide (URP) in cardiac ischemia-reperfusion injury. *Peptides* 29, 770–777. doi: 10.1016/j.peptides.2007.08.013
- Rivera, E., Arrieta, O., Guevara, P., Duarte-Rojo, A., and Sotelo, J. (2001). AT1 receptor is present in glioma cells; its blockage reduces the growth of rat glioma. *Br. J. Cancer* 85, 1396–1399. doi: 10.1054/bjoc.2001.2102
- Rollins, B. J. (2006). Inflammatory chemokines in cancer growth and progression. *Eur. J. Cancer* 42, 760–767. doi: 10.1016/j.ejca.2006.01.002
- Rylova, S. N., Barnucz, E., Fani, M., Braun, F., Werner, M., Lassmann, S., et al. (2014). Does imaging $\alpha\beta3$ integrin expression with PET detect changes in angiogenesis during bevacizumab therapy? *J. Nucl. Med.* 55, 1878–1884. doi: 10.2967/jnumed.114.137570
- Schnell, O., Krebs, B., Carlsen, J., Miederer, I., Goetz, C., Goldbrunner, R. H., et al. (2009). Imaging of integrin $\alpha(v)\beta(3)$ expression in patients with malignant glioma by [^{18}F] Galacto-RGD positron emission tomography. *Neuro Oncol.* 11, 861–870. doi: 10.1215/15228517-2009-024
- Segain, J.-P., Rolli-Derkinderen, M., Gervois, N., Raingeard de la Blétière, D., Loirand, G., and Pacaud, P. (2007). Urotensin II is a new chemotactic factor for UT receptor-expressing monocytes. *J. Immunol.* 179, 901–909.
- Spinazzi, R., Albertin, G., Nico, B., Guidolin, D., Di Liddo, R., Rossi, G. P., et al. (2006). Urotensin-II and its receptor (UT-R) are expressed in rat brain endothelial cells, and urotensin-II via UT-R stimulates angiogenesis in vivo and in vitro. *Int. J. Mol. Med.* 18, 1107–1112.
- Stupp, R., Mason, W. P., van den Bent, M. J., Weller, M., Fisher, B., Taphoorn, M. J. B., et al. (2005). Radiotherapy plus concomitant and adjuvant temozolomide for glioblastoma. *N. Engl. J. Med.* 352, 987–996. doi: 10.1056/NEJMoa043330
- Sugo, T., Murakami, Y., Shimomura, Y., Harada, M., Abe, M., Ishibashi, Y., et al. (2003). Identification of urotensin II-related peptide as the urotensin II-immunoreactive molecule in the rat brain. *Biochem. Biophys. Res. Commun.* 310, 860–868.
- Sun, S.-L., and Liu, L.-M. (2019). Urotensin II: an inflammatory cytokine. *J. Endocrinol.* doi: 10.1530/JOE-18-0505 Online ahead of print.
- Takano, S. (2012). Glioblastoma angiogenesis: VEGF resistance solutions and new strategies based on molecular mechanisms of tumor vessel formation. *Brain Tumor Pathol.* 29, 73–86. doi: 10.1007/s10014-011-0077-6
- Verhaak, R. G. W., Hoadley, K. A., Purdom, E., Wang, V., Qi, Y., Wilkerson, M. D., et al. (2010). Integrated genomic analysis identifies clinically relevant subtypes of glioblastoma characterized by abnormalities in PDGFRA, IDH1, EGFR, and NF1. *Cancer Cell* 17, 98–110. doi: 10.1016/j.ccr.2009.12.020
- Wang, X., Guo, G., Guan, H., Yu, Y., Lu, J., and Yu, J. (2019). Challenges and potential of PD-1/PD-L1 checkpoint blockade immunotherapy for glioblastoma. *J. Exp. Clin. Cancer Res.* 38:87. doi: 10.1186/s13046-019-1085-3
- Weksler, B., Romero, I. A., and Couraud, P.-O. (2013). The hCMEC/D3 cell line as a model of the human blood brain barrier. *Fluids Barriers CNS* 10:16. doi: 10.1186/2045-8118-10-16
- Weksler, B. B., Subileau, E. A., Perrière, N., Charneau, P., Holloway, K., Leveque, M., et al. (2005). Blood-brain barrier-specific properties of a human adult brain endothelial cell line. *FASEB J.* 19, 1872–1874. doi: 10.1096/fj.04-34.58fj
- Wen, P. Y., and Brandes, A. A. (2009). Treatment of recurrent high-grade gliomas. *Curr. Opin. Neurol.* 22, 657–664. doi: 10.1097/WCO.0b013e32833229e3
- Wick, W., and Kessler, T. (2018). Drug repositioning meets precision in glioblastoma. *Clin. Cancer Res.* 24, 256–258. doi: 10.1158/1078-0432.CCR-17-2989
- Xie, Q., Mittal, S., and Berens, M. E. (2014). Targeting adaptive glioblastoma: an overview of proliferation and invasion. *Neuro Oncol.* 16, 1575–1584. doi: 10.1093/neuonc/nou147
- Xu, H., Rahimpour, S., Nesvick, C. L., Zhang, X., Ma, J., Zhang, M., et al. (2015). Activation of hypoxia signaling induces phenotypic transformation of glioma cells: implications for bevacizumab antiangiogenic therapy. *Oncotarget* 6, 11882–11893. doi: 10.18632/oncotarget.3592
- Xu, S., Jiang, H., Wu, B., Yang, J., and Chen, S. (2009). Urotensin II induces migration of endothelial progenitor cells via activation of the RhoA/Rho kinase pathway. *Tohoku J. Exp. Med.* 219, 283–288.

- Zhang, Y.-G., Li, J., Li, Y.-G., and Wei, R.-H. (2008). Urotensin II induces phenotypic differentiation, migration, and collagen synthesis of adventitial fibroblasts from rat aorta. *J. Hypertens.* 26, 1119–1126. doi: 10.1097/HJH.0b013e3282fa1412
- Zhou, C.-H., Wan, Y.-Y., Chu, X.-H., Song, Z., Xing, S.-H., Wu, Y.-Q., et al. (2012). Urotensin II contributes to the formation of lung adenocarcinoma inflammatory microenvironment through the NF- κ B pathway in tumor-bearing nude mice. *Oncol. Lett.* 4, 1259–1263. doi: 10.3892/ol.2012.932
- Zhou, J., Xiang, Y., Yoshimura, T., Chen, K., Gong, W., Huang, J., et al. (2014). The role of chemoattractant receptors in shaping the tumor microenvironment. *BioMed Res. Int.* 2014:751392. doi: 10.1155/2014/751392

Conflict of Interest: The authors declare that the research was conducted in the absence of any commercial or financial relationships that could be construed as a potential conflict of interest.

Copyright © 2021 Le Joncour, Guichet, Dembélé, Mutel, Campisi, Perzo, Desrues, Modzelewski, Couraud, Honnorat, Ferracci, Marguet, Laquerrière, Vera, Bohn, Langlois, Morin, Gandolfo and Castel. This is an open-access article distributed under the terms of the Creative Commons Attribution License (CC BY). The use, distribution or reproduction in other forums is permitted, provided the original author(s) and the copyright owner(s) are credited and that the original publication in this journal is cited, in accordance with accepted academic practice. No use, distribution or reproduction is permitted which does not comply with these terms.